

RICE UNIVERSITY

**Composition, Turnover, and Mechanics of Extracellular
Matrix in Developing, Aging, and Pathological Valves**

for application in the design of age-specific tissue engineered heart valves

by
Elizabeth Humes Stephens

May 2010

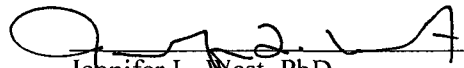
THESIS SUBMITTED IN PARTIAL FULFILLMENT OF THE
REQUIREMENTS FOR THE DEGREE

Doctor of Philosophy in Bioengineering

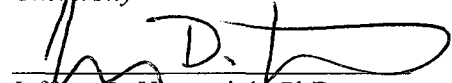
APPROVED, THESIS COMMITTEE:



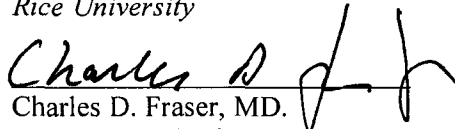
K. Jane Grande-Allen, PhD. (chair)
*Associate Professor, Department of
Bioengineering, Rice University*



Jennifer L. West, PhD.
*Chair, Department of Bioengineering, Rice
University*



Jeffrey D. Hartgerink, PhD.
*Associate Professor, Department of Chemistry,
Rice University*



Charles D. Fraser, MD.
*Surgeon-in-Chief, Chief, Cardiac Surgery and
Division of Congenital Heart Surgery, Texas
Children's Hospital*

UMI Number: 3421197

All rights reserved

INFORMATION TO ALL USERS

The quality of this reproduction is dependent upon the quality of the copy submitted.

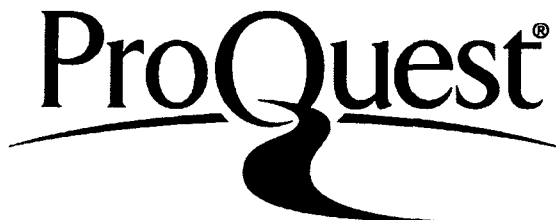
In the unlikely event that the author did not send a complete manuscript and there are missing pages, these will be noted. Also, if material had to be removed, a note will indicate the deletion.



UMI 3421197

Copyright 2010 by ProQuest LLC.

All rights reserved. This edition of the work is protected against unauthorized copying under Title 17, United States Code.



ProQuest LLC
789 East Eisenhower Parkway
P.O. Box 1346
Ann Arbor, MI 48106-1346

Abstract

Extracellular Matrix in Developing, Aging, and Pathological Valves

for application in the design of age-specific tissue engineered heart valves

by

Elizabeth Humes Stephens

Debilitating valve disease necessitating valve replacement affects patients of all ages, all of whom would benefit from a tissue engineered heart valve with immunocompatibility, the ability of the valve to remodel in response to altered hemodynamics or patient growth, and physiologic mechanics. However, there may be age-specific requirements for such a valve. The overarching goal of this thesis was to characterize the extracellular matrix in developing, aging, and pathological mitral and aortic valves (MV, AV) in order to provide design criteria for an age-specific tissue engineered heart valve. The extracellular matrix plays a vital role in valve function; not only does it comprise the bulk of the valve tissue, but it determines the material properties of the valve, is integrally involved in biological signaling processes, and is altered in a number of valve pathologies. To this end, the composition, structure, and material properties of normal MV and AV were characterized with particular attention paid to valve heterogeneity and aging-related changes. Valves from disease states such as functional mitral regurgitation, dilated cardiomyopathy, iatrogenic valve wounds, calcific aortic valve disease, and myxomatous mitral valve disease were also analyzed to

provide negative design criteria for a tissue engineered heart valve. Lastly, preliminary work was performed in developing a tissue engineered heart valve using poly(ethylene) glycol (PEG) hydrogels and valve cells of different ages. In sum, this body of work provides necessary design criteria for an age-specific tissue engineered heart valve, but in the process of analyzing various aspects of normal and diseased MV and AV, this thesis additionally provides insight into a variety of aspects of normal valve physiology, such as the relationship between valve composition and material properties and the mechanical environment, as well as insight into various valve diseases, such as the role of MV remodeling in functional mitral regurgitation and disease progression, with potential clinical implications for patients with these diseases.

Acknowledgements

To my advisor, Dr. K. Jane Grande-Allen, for the opportunity to work in her lab and her contagious enthusiasm for valve research. To my committee members, Dr. Jennifer West, Dr. Jeffrey Hartgerink, and Dr. Charles Fraser for their guidance and support. In particular, to Dr. West for her sponsorship of my F30 grant and expert guidance in the PEG project and to Dr. Fraser for his encouragement and guidance in my clinical career.

To my undergraduates who not only contributed much to the experimental work and analysis, but taught me how to be a better mentor. These include Ashley Smith, Luis Lazaro, Indrajit Nandi, Jennifer Shangkuan, Nicky de Jonge, Mark Mendenhall, Joshua Carroll, Joyce Kuo, Aaron Patton, Allison Post, Kai Chu, Meaghan McNeill, and Daniel Laucirica.

To my lab mates, especially Dr. Tracy Blevins, Dr. Jerome Saltarelli, Dr. Vishal Gupta, Dr. Zannatul Ferdous, Dr. David Allison, Dr. Janet Barzilla, Chris Durst, Hubert Tseng, and Nikhil Gheewala, whose contributions ranged from training in experimental techniques and guidance in experimental design, to collaborating on manuscripts and discussing potential implications of my work. Special thanks to Chris Durst for his collaboration on multiple projects.

To students in other Rice labs whose consultation was vital, including Michael Cuchiara, Maude Rowland, Stephanie Nemir, Dr. Jean Altus, and Dr. Melissa McHale in the West lab. Also to Rice staff scientists Nancy Turner, John Wright, Dr. L. Scott Baggett, Dr. Sean Moran, and Dr. Bill Deery whose expertise was invaluable.

To my collaborators at Stanford, including Dr. D. Craig Miller, Dr. Neil Ingels, Jr., Dr. Tom Nguyen, Dr. Tomasz Timek, Dr. Julia Swanson, Dr. Aki Itoh, and Dr. Wolf Bothe. To Dr. D. Craig Miller and Dr. Neil Ingels in particular for their keen insight, many stimulating discussions, and key contributions in preparing manuscripts and presentations. Especially to Dr. D. Craig Miller for acting as my mentor for my AATS summer scholarship, enabling me to attend several conferences, and encouraging me both in my research and as I embark upon my clinical career.

To my collaborators at Texas Children's Hospital, including Dr. Debra Kearney for her expertise and patient teaching with respect to congenital valve disease, and Kathy Carberry and Karol Arrington who made the congenital valve project possible.

To my family, for making me who I am. For stressing the importance of character, hard work and discipline, as well as creativity and ingenuity. For valuing education and scientific enquiry, as well as compassion and service. For encouraging me through disappointments and celebrating with me during successes. For believing in me when I didn't believe in myself. For being there for me through it all.

With special tribute to Emily Clark Holcomb (b., d. March 27, 2007), victim of congenital heart disease, who has provided added inspiration and motivation, and brought the gravity of the disease painfully close to home.

Table of Contents

VOLUME 1

Abstract	ii
Acknowledgements.....	iv
List of Tables and Figures	xxxix
List of Abbreviations	liv
I. Chapter 1: Background.....	1
A. Congenital Valve Disease	1
i. Epidemiology.....	1
ii. Types of Congenital Valve Disease	1
iii. Current Treatments.....	2
B. Heart Valve Anatomy	4
i. The Four Valves.....	4
ii. Mitral Valve.....	5
iii. Aortic and Pulmonic Valves.....	6
iv. Histological Valve Layers	7
C. Extracellular Matrix.....	7
i. Collagen.....	8
ii. Elastic Fibers.....	9
iii. Proteoglycans and Glycosaminoglycans	10

iv. Matrix Metalloproteinases	13
D. Characterization of Adult Valves in Health and	
Disease	14
i. Valvular Interstitial Cells (VICs) and Cell Phenotype	14
ii. Mechanical Characterization of Valves.....	17
iii. Valve Composition and its Mechanical Environment.....	18
iv. Valve Changes in Mitral Regurgitation.....	20
v. Valve Response to Acute Injury.....	21
E. Changes in Valves with Development and Aging	22
i. Histology and Biochemistry	22
ii. Mechanical Properties	25
F. Tissue Engineering Heart Valves	25
i. Design Criteria	25
ii. Cell Sources	26
iii. Scaffolds and PEG Hydrogels	27
iv. Challenges.....	30
G. Summary	32
i. Synopsis of Previous Work.....	32
ii. Thesis Motivation, Scope, and Structure.....	33

II. Studies

A. METHODS

Chapter 2: The Use of Collagenase III for the

Isolation of Porcine Aortic Valvular Interstitial

Cells: Rationale and Optimization48

A. Introduction 50

B. Methods..... 53

i. General Procedure.....53

ii. Assessment of Cell Number55

iii. Experimental Conditions.....56

iv. Statistical and Cost Benefit Analyses.....56

C. Results 57

i. Valvular Interstitial Cell Isolation from 6-Month-Old Pig.....57

ii. Valvular Interstitial Cell Isolation from 6-Week-Old Pig.....60

D. Discussion 65

E. Conclusions 68

B. CHARACTERIZATION OF NORMAL VALVES

i. Aging: Composition and Structure

Chapter 3: Age-Related Changes in Collagen

Synthesis and Turnover in Porcine Heart Valves.....72

A. Introduction74

B. Methods.....75

i. General Procedure75

ii. Histology and Immunohistochemistry75

iii. Cell Density Assessment79

iv. Statistical Analysis79

C. Results79

i. Cellular Density79

ii. Movat Tissue Organization.....80

iii. Fetal Valve Immunohistochemistry84

iv. Matrix Turnover and the “Activated” Cell Phenotype84

v. Common Findings between Aortic and Mitral Valves.....87

vi. Differences between Aortic and Mitral Valves.....89

vii. Postnatal Aging Changes in Aortic and Mitral Valves91

viii. Novel Finding of SMaA Expression93

D. Discussion94

i. Relevance to Human Valves.....96

ii. Limitations.....	96
E. Conclusions	97
<i>Chapter 4: Valve Proteoglycan Content and Glycosaminoglycan Fine Structure are Unique to Microstructure, Mechanical Load, and Age: Relevance to an Age-Specific Tissue Engineered Heart Valve</i>	<i>102</i>
A. Introduction	104
B. Methods.....	106
i. General Procedure.....	106
ii. Histology and Histochemistry	106
iii. Fluorophore-Assisted Carbohydrate Electrophoresis (FACE).....	107
iv. Statistical Analysis	109
C. Results	110
i. Proteoglycan Distribution.....	110
ii. Hyaluronan Distribution.....	114
iii. Distribution of Other Matrix Components and Co-localization with PGs.....	114
iv. Hydration.....	116
v. GAG Compositional Analysis	119

vi. Chain Length.....	122
D. Discussion	123
i. PGs and GAGs Vary in Distribution between Layers and Loading	
Regions.....	123
ii. Valve PG and GAG Composition Reflects Mechanical	
Requirements.....	125
iii. Aging Transforms AV Composition from Compressive to Tensile	126
iv. Interplay of PGs with Elastin and Fibrillin.....	126
v. Implications for Valve Disease and Tissue Engineered Heart	
Valves	127
vi. Limitations.....	128
E. Conclusions	130

Chapter 5: Perinatal Changes in Mitral and Aortic

<i>Valve Composition</i>	<i>137</i>
A. Introduction	139
B. Methods.....	141
i. Tissue Procurement and Sample Preparation	141
ii. Histology and Immunohistochemistry	141
iii. Statistical Analysis.....	143
C. Results	144
i. Perinatal Changes in Valve Structure.....	144

ii. Perinatal Changes in Valve Composition.....	147
iii. Perinatal Changes in Relative Composition of AV and MV	149
iv. Location and Co-localization of Matrix Components	151
D. Discussion	155
i. Perinatal Changes in AV and MV Structure and Composition	155
ii. Regional Heterogeneity in Perinatal Changes in Valve Composition	157
iii. Localization of Matrix Components within AV and MV	157
iv. Proposed Functional Consequences of Valve Structural and Compositional Changes	160
v. Implications.....	161
vi. Limitations.....	163
E. Conclusions	164

Chapter 6: Regional Heterogeneity in Aortic Valve

<i>GAG Composition</i>	<i>172</i>
A. Introduction	175
B. Methods.....	177
i. General Procedure.....	177
ii. Fluorophore-Assisted Carbohydrate Electrophoresis (FACE)	177
iii. Statistical Analysis.....	178
C. Results	178

D. Discussion	182
i. Regional Heterogeneity in AV Composition.....	183
ii. Potential Relationship between Regional Heterogeneity in AV Mechanics and GAG Composition.....	184
iii. Nodule of Arantius: Structure and Function.....	185
iv. Limitations and Future Studies	186
E. Conclusions	187

i. Aging: Material Properties

Chapter 7: Age-Related Changes in Material

Behavior of Porcine Mitral and Aortic Valves and

Correlation to Matrix Composition 191

A. Introduction	193
B. Methods.....	194
i. Tissue Sample Procurement.....	194
ii. Mechanical Testing	196
iii. Data Analysis.....	196
iv. Histology and Immunohistochemistry	198
v. Statistical Analysis	199
C. Results	199
i. Thickness	199

ii. Post-Transition and Pre-Transition Stiffnesses.....	200
iii. Stress Relaxation.....	201
iv. Extensibility	203
v. Radius of Transition Curvature.....	204
vi. Differences between AV Leaflets	205
vii. Differences in Valve Matrix Composition	206
D. Discussion	208
E. Conclusions	213

VOLUME 2

ii. Valve Heterogeneity: Composition and Motion

Chapter 8: Cellular and Extracellular Matrix Basis

for Heterogeneity in Mitral Annular Contraction222

A. Introduction	225
B. Methods.....	226
i. Animal Protocol	226
ii. Histology and Immunohistochemistry	227
iii. Statistical Analysis.....	230
C. Results	230
i. Heterogeneity of Annular Segment Contraction.....	230
ii. Differences in Leaflet Insertion Structure	231

iii. Compositional Heterogeneity between Septal and Lateral Segments and between Commissures	232
iv. Compositional Heterogeneity among Septal, Lateral, and Commissural Segments.....	235
v. Correlations between Expression of Different Proteins	236
D. Discussion	237
i. Functional Implication of Heterogeneous Valve Insertion Structure.....	237
ii. Annular Compositional Heterogeneity and Relation to Contraction.....	238
iii. Potential Functional Contributions of Myofibroblasts.....	239
iv. Implications.....	240
v. Limitations	241
E. Conclusions	241

Chapter 9: Relationship of Mitral Leaflet

Compositional Heterogeneity to Leaflet

<i>Deformation</i>	<i>245</i>
A. Introduction	247
B. Methods.....	248
i. Animal Protocol	248
ii. Histology and Immunohistochemistry	249
iii. Statistical Analysis.....	250
C. Results	251

i. Differences in Leaflet Length Changes across Annular Segments.....	251
ii. Differences in Leaflet Structure across Annular Segments.....	252
iii. Compositional Heterogeneity between Septal and Lateral Segments and between Commissures	253
iv. Compositional Heterogeneity across MV Segments.....	256
v. Correlations between Proteins within Leaflet Regions	258
D. Discussion	258
i. Characterization of Commissural Leaflets	259
ii. Differences in Leaflet Structure.....	260
iii. Relation between Leaflet Composition, Leaflet Deformation, and the Role of the Myofibroblast	260
iv. Implications.....	262
v. Limitations	262
E. Conclusions	263

ii. Valve Heterogeneity: Valvular Interstitial Cells and Myofibroblasts

<i>Chapter 10: Fibronectin-Based Isolation of Valvular Interstitial Cell Subpopulations: Relevance to Valve Disease.....</i>	267
A. Introduction	269

B. Methods	271
i. Isolation of Valvular Interstitial Cells.....	271
ii. Isolation of Subpopulations.....	272
iii. Adhesion of Subpopulations to TCP.....	274
iv. Flow Cytometry.....	274
v. Immunocytochemistry.....	276
vi. Preliminary Analysis of Human Myxomatous Valves and VICs.....	277
vii. Statistical Analysis.....	278
C. Results	279
i. Confirmation of FAST and SLOW Subpopulation Adhesion Rate.....	279
ii. Flow Cytometry-Porcine VICs.....	280
iii. Flow Cytometry and Immunohistochemistry-Human Myxomatous Valves.....	282
iv. Immunocytochemistry.....	283
D. Discussion	286
E. Conclusions	290

<i>Chapter 11: Functional Characterization of Fibronectin-Separated Valvular Interstitial Cell Subpopulations: Application to Study of Valve Disease</i>	297
---	------------

A. Introduction	299
B. Methods.....	300
i. VIC Isolation.....	300
ii. Isolation of VIC Subpopulations.....	301
iii. Collagen Constructs	301
iv. Mechanical Testing	303
v. Statistical Analysis	303
C. Results	304
i. Collagen Construct Contraction.....	304
ii. Material Properties of Collagen Constructs.....	306
D. Discussion	308
E. Conclusions	312

iii. Cell-Matrix Coupling

Chapter 12: Functional Coupling of Valvular

Interstitial Cells and Collagen in the Mitral Leaflet..... 317

A. Introduction	320
B. Methods.....	321
i. Immunofluorescence	321
ii. Confocal Microscopy	322
iii. Custom-Built Strain-Load Device	324

iv. Force Generation Studies.....	325
v. Statistical Analysis	327
C. Results	327
i. VICs Aligned and Integrated with Collagen Fibers.....	327
ii. VIC Alpha ₂ Beta ₁ Integrins Localized to Collagen Fibers.....	328
iii. Blocking Alpha ₂ Beta ₁ Integrins or Actin Polymerization Prevented Force Generation.....	333
D. Discussion	334
i. Structural Interaction between VICs, Integrins, and Collagen Fibers.....	334
ii. VIC-Integrin-Collagen Functional Unit	336
iii. VIC-Integrin-Collagen in Stiffness Modulation	336
iv. Valve Force Generation in an Isometric Setting.....	339
v. Implications.....	340
vi. Limitations and Future Studies	342
E. Conclusions	343

C. VALVE INJURY AND DISEASE

i. Congenital Valve Disease

Chapter 13: Insight into Histological and Pathological Abnormalities in Congenitally

<i>Diseased Valves Based on Advances in</i>	
<i>Understanding Normal Valve Microstructure and</i>	
<i>Extracellular Matrix</i>	348
A. Introduction	350
B. Spectrum of Congenital Semilunar Valve Disease	351
C. Normal Semilunar Valve Structure.....	355
i. Valve Macrostructure	355
ii. Valve Changes with Age and Altered Hemodynamics	356
D. Macroscopic Characterization of Congenital	
Semilunar Valve Disease.....	357
i. Bicuspid Aortic Valve.....	358
ii. Dysplastic Semilunar Valves.....	359
iii. Acquired Macroscopic Valve Changes	360
E. Microscopic Characterization of Congenital	
Semilunar Valve Disease.....	361
i. CSVD Microstructure.....	361
ii. Mechanical Implications of CSVD Microstructure	363
iii. Insight into Possible Pathogenesis of CSVD.....	365
iv. Role of Hemodynamics in CSVD.....	367
F. Microstructural Characterization of Bicuspid Aortic	
Valve (BAV) and its Implications	369

i. Possible Pathogenesis of BAV.....	369
ii. Proteoglycans and Glycosaminoglycans in BAV	370
iii. Dysregulation of Fibrillar-Related Proteins in BAV	371
iv. Associated Aortic Wall Abnormalities in BAV.....	372
v. Insight BAV Provides into other Congenital Valve Diseases	373

G. Importance of Valves in Broader Diseases'

Pathogenesis and Progression	374
---	------------

H. Conclusions.....	374
----------------------------	------------

Chapter 14: Extracellular Matrix Remodeling and

Cell Phenotypic Changes in Dysplastic and

Hemodynamically Altered Semilunar Heart Valves..... 383

A. Introduction	386
------------------------------	------------

B. Methods.....	387
------------------------	------------

i. Sample Set.....	387
--------------------	-----

ii. Histology and Immunohistochemistry	388
--	-----

iii. Flow Cytometry	389
---------------------------	-----

iv. Statistical Analysis	390
--------------------------------	-----

C. Results	391
-------------------------	------------

i. Age-Related Changes in Matrix Composition of Semilunar Valves	391
--	-----

ii. Matrix Changes in Pathological Semilunar Valves	392
---	-----

iii. Remodeling of Leaflet Layers in Pathological Semilunar Valves.....	395
iv. Correlations between Matrix Components in Pathological Semilunar Valves.....	399
v. Differences between AV and PV VICs	400
vi. Changes in VICs from Pathological Semilunar Valves	403
C. Discussion	404
i. Previous Studies of Matrix Composition in Congenitally Diseased Valves	404
ii. Altered Matrix Composition and VIC Cell Phenotype in Pathological Valves	408
iii. Age-Related Changes in Differences between AV and PV among CTRL Samples	408
iv. Implications.....	409
v. Limitations and Future Studies	410
E. Conclusions	411

ii. Dilated Cardiomyopathy and “Functional” Mitral

Regurgitation

Chapter 15: The Effects of Hemodynamics of

Regurgitation Alone are Sufficient for Mitral Valve

Leaflet Remodeling **414**

A. Introduction	416
B. Methods.....	417
i. Surgical Protocol.....	417
ii. Histology and Immunohistochemistry	419
iii. Statistical Analysis.....	422
C. Results	422
D. Discussion	427
i. Anterior Leaflet Remodeling and Functional Consequences	427
ii. Potential Mechanism for Observed Changes.....	429
iii. Pathological versus Adaptive Leaflet Remodeling.....	430
iv. Potential Mechanism for “MR Begets MR”	431
v. Limitations.....	432
E. Conclusions	433

Chapter 16: Significant Changes in Mitral Valve

Leaflet Matrix Composition and Turnover with

Tachycardia-Induced Cardiomyopathy.....438

A. Introduction	440
B. Methods.....	440
i. Animal Protocol	441
ii. Histology and Immunohistochemistry	443

iii. Statistical Analysis.....	444
C. Results	445
i. Dynamic Leaflet Changes after the Development of Dilated Cardiomyopathy	445
ii. Structural Changes in TIC Leaflets.....	446
iii. Greater Collagen Turnover in TIC Leaflets	448
iv. Greater Elastic Turnover in TIC Leaflets	450
v. Proteoglycans and Glycosaminoglycans in TIC Leaflets.....	451
vi. Greater Valve Cell Activation in TIC Leaflets.....	451
vii. Cell Activation and Correlations between Proteins within Leaflet Regions and Layers.....	452
viii. Relationship of LV Remodeling to Observed Leaflet Changes	452
D. Discussion	453
i. Changes in Matrix Composition are Heterogeneous.....	454
ii. Influence of Mitral Regurgitation and Left Ventricular Remodeling	456
iii. Changes in Phenotype and Matrix Markers Implicate Role of Myofibroblasts.....	457
iv. Implications for Human DCM.....	457
v. Limitations	458
E. Conclusions	460

Chapter 17: Mitral Annular Region Ultrastructural Changes in Dilated Cardiomyopathy Correlate with Regional Remodeling465

A. Introduction467

B. Methods.....467

 i. Animal Protocol468

 ii. Histology and Immunohistochemistry469

 iii. Statistical Analysis471

C. Results472

 i. Development of Dilated Cardiomyopathy and Changes in Annular Dimensions.....472

 ii. Greater Collagen Turnover in TIC Annular Region472

 iii. Greater Elastic Fiber Turnover in TIC Annular Region.....475

 iv. Greater Cell Activation in TIC Annular Region.....475

 v. Relative Changes in Composition between Annular Segments.....475

 vi. Correlations between Expression of Proteins in Annular Segments476

 vii. Relationship between Expression of Proteins and LV Remodeling.....477

D. Discussion477

 i. Changes in Annular Composition with TIC in Relation to Changes in Annular Dimensions478

 ii. Implicated Role of Myofibroblasts478

iii. Role of Specific Layers in Annular Remodeling with TIC.....	479
iv. Annular Compositional Changes with TIC in the Context of LV Remodeling	480
v. Implications.....	480
vi. Limitations.....	481
E. Conclusions	482

VOLUME 3

iii. Valve Wound Injury

Chapter 18: Extracellular Matrix Remodeling in

Response to Mitral Leaflet Injury.....486

A. Introduction	488
B. Methods.....	490
i. Experimental Animal Protocol	490
ii. Histology and Immunohistochemistry	490
iii. Assessment of Cell Density, Leaflet Thickness, and Hole Closure.....	492
iv. Statistical Analysis	493
C. Results	493
i. Remodeling in Thickened, Cell-Dense Areas Reduced Hole Diameter.....	493
ii. Matrix Turnover and Cell Activation.....	497
iii. Patterns of Remodeling	497

iv. Structural and Global Leaflet Changes.....	499
D. Discussion	500
i. Increased Collagen Turnover in Hole-Punch Region	500
ii. Cells in Remodeling Tissue Show an Activated Phenotype.....	501
iii. Distinct Areas of Remodeling Surrounding Hole-Punch.....	502
iv. Characteristics of Greater Wound Closure.....	503
v. Limitations	503
E. Conclusions	504

iv. Myxomatous Mitral Valve Disease

Chapter 19: MAPK Pathway in Myxomatous Mitral

Valve Disease 510

A. Introduction	513
B. Methods.....	514
i. Sample Set	514
ii. Histology and Immunohistochemistry	515
C. Results	516
i. Distribution of SMaA.....	516
ii. Co-localization of SMaA and NMM.....	517
iii. Co-localization of MAPK Markers, TGF β , and Myofibroblast Markers	519
iv. Distribution of MAPK Markers Relative to Histological Layers	521

v. Distribution of MAPK Markers Relative to Proteoglycans.....	524
D. Discussion	524
i. MAPK Pathway in Myofibroblast Activation	525
ii. MAPK Pathway in VICs	526
iii. MAPK Pathway in Myxomatous Mitral Valve Disease	527
iv. Myofibroblast Phenotype and Compositional Changes in Myxomatous Mitral Valve Disease	527
v. Myofibroblast Phenotype in Valvulopathies	528
vi. Implications.....	529
vii. Limitations and Future Studies	530
E. Conclusions	530

v. Calcified Aortic Valve Disease

Chapter 20: Differential Proteoglycan and

Hyaluronan Distribution in Calcified Aortic Valves..... 536

A. Introduction	538
B. Methods.....	540
i. Tissue Procurement and Decalcification.....	540
ii. Histology and Immunohistochemistry	541
iii. Analysis of Immunohistochemical Staining.....	542
iv. Statistical Analysis	542
C. Results	543

D. Discussion	548
E. Conclusions	553

Chapter 21: Hyaluronan Turnover and Hypoxic

Brown Adipocytes are Co-localized with

Endochondral Ossification in Calcified Aortic

Valves **560**

A. Introduction **563**

B. Methods..... **565**

i. Tissue Procurement and Decalcification.....565

ii. Histology and Immunohistochemistry565

iii. Analysis of Immunohistochemical Staining.....566

iv. Statistical Analysis567

C. Results **568**

i. Co-localizations between Markers.....568

ii. Correlations within Mechanistic Families.....570

iii. Correlations between Mechanistic Families.....571

D. Discussion **575**

i. Role for Hypoxia in Calcification.....575

ii. Role for HA Regulation in Calcification.....577

iii. Distinctions among Nodule Regions and Prenodules580

iv. Limitations	581
E. Conclusions	581

D. TISSUE ENGINEERING

Chapter 22: Age- and Valve-Region-Specific

Responses of Mitral Valvular Interstitial Cells to

Substrate Stiffness 584

A. Introduction 588

B. Methods..... 590

i. Preparation and Purification of PEG-Diacrylate (PEG-DA).....590

ii. Preparation and Purification of PEG-RGDS and PEG-WRGDS593

iii. Preparation and Purification of Methacrylated Heparin.....594

iv. Polymerization of Functionalized PEG Hydrogels597

v. Quantification of Methacrylated Heparin in Functionalized PEG

Hydrogels597

vi. Quantification of PEG-RGDS in Functionalized PEG Hydrogels.....598

vii. Optimization of Functionalized PEG Hydrogels598

viii. Determination of Elastic Modulus of Functionalized PEG

Hydrogels600

ix. Cell Culture and Cell Seeding onto PEG.....601

x. Immunocytochemistry601

xi. Statistical Analysis	602
C. Results	603
i. Stiffness of Different Weight-Volume Fraction Functionalized PEG Hydrogels.....	603
ii. SMaA Expression of VICs on Gels of Different Stiffnesses.....	603
iii. P4H Expression of VICs on Gels of Different Stiffnesses.....	605
iv. HSP47 Expression of VICs on Gels of Different Stiffnesses.....	606
v. VIC Morphology on Gels of Different Stiffnesses	607
D. Discussion	609
i. Previous Studies of VICs and Substrate Stiffness	609
ii. Age-Specific and Valve-Region Specific Responses of VICs to Substrate Stiffness	611
iii. VIC Subpopulations.....	615
iv. Implications.....	615
v. Limitations and Future Studies	616
E. Conclusions	617
 IV. Chapter 23: Conclusions	622
A. Summary of Principal Findings and their Implications.....	622
i. Age-Related Changes in Valves	622
ii. Valve And Valve-Region Heterogeneity.....	623

iii. Normal Valve Physiology	624
iv. Involvement of Valves in Acquired Cardiac Diseases	625
v. Acquired Valve Disease	626
vi. Congenital Valve Disease	627
vii. Structure-Function Relationship in the Valve.....	628
viii. Valvular Interstitial Cells.....	629
ix. Methods	630
B. Unique Contributions to the Literature	631
i. Age-Related Changes in Valves	631
ii. Valve and Valve-Region Heterogeneity.....	632
iii. Normal Valve Physiology	633
iv. Involvement of Valves in Acquired Cardiac Diseases	633
v. Acquired Valve Disease	634
vi. Congenital Valve Disease	635
vii. Structure-Function Relationship in the Valve.....	635
viii. Valvular Interstitial Cells.....	636
ix. Methods	637
C. Unifying Themes	637
i. Importance of the Extracellular Matrix	638
ii. Importance of Valvular Interstitial Cells.....	640
iii. Importance of the Valve Mechanical Environment	641
iv. Structure-Function Relationship	641
v. Valve Heterogeneity	642

D. Future Directions	643
i. Age-Related Changes in Valves	643
ii. Valve and Valve-Region Heterogeneity.....	644
iii. Involvement of Valves in Acquired Cardiac Diseases.....	644
iv. Acquired Valve Disease	645
v. Congenital Valve Disease.....	645
vi. Structure-Function Relationship in the Valve.....	646
vii. Valvular Interstitial Cells.....	646
viii. Methods	647
E. Design Criteria for a Tissue Engineered Heart Valve.....	648
i. Overview.....	648
ii. Insight of Thesis Work into Tissue Engineered Heart Valve	
Characteristics	648
A. Age-Specific, Valve-Specific Design Criteria for Tissue	
Engineered Heart Valves.....	649
B. Cellular Component of a Tissue Engineered Heart Valve	649
C. Material Properties of a Tissue Engineered Heart Valve	650
D. Macrostructure and Matrix Composition of a Tissue	
Engineered Heart Valve	650
E. Heterogeneity within a Tissue Engineered Heart Valve.....	652
iii. Different Approaches for Constructing a Tissue Engineered Heart	
Valve.....	653

A. Macrostructure and Material Properties for Physiologic Function.....	653
B. Capability for Growth and Remodeling	656
C. Immunocompatibility	657
iv. Application of Thesis Work in Relation to Different Tissue Engineered Heart Valve Approaches.....	659
A. Insights into Different Approaches for Obtaining Macrostructure and Material Properties for Physiologic Function.....	659
B. Capability for Growth and Remodeling	661
C. Immunocompatibility	661
v. Remaining Data Required.....	663
A. Cellular Component of a Tissue Engineered Heart Valve	663
B. Growth and Remodeling in a Tissue Engineered Heart Valve	665
C. Macrostructure and Material Properties of a Tissue Engineered Heart Valve	665
D. Different Approaches for Constructing a Tissue Engineered Heart Valve	667
E. General Considerations.....	667
F. Conclusion	668

<i>V. Appendix.....</i>	673
--------------------------------	------------

**Chapter 24: Abundance and Location of
Hyaluronan and Proteoglycans within**

Myxomatous Mitral Valves674

A. Introduction676

B. Methods.....678

 i. Tissue Procurement.....678

 ii. Histochemistry679

 iii. Localization680

 iv. Statistical Analysis681

C. Results681

 i. IHC for Decorin, Biglycan, and Versican681

 ii. IHC for HA and HARE683

 iii. Co-localization of Specific PGs and Other Extracellular Matrix
 Components.....684

 iv. Effect of Gender and Age on Abundance of PGs686

D. Discussion686

E. Conclusions690

E. MYOCARDIAL MECHANICS

Chapter 25: The Myocardium Overlying the

Papillary Muscle Contributes to the Antero-Lateral

Left Ventricular Wall Deformation Continuum694

A. Introduction697

B. Methods.....698

i. Surgical Transmural Beadset Placement699

ii. *In Vivo* Marker Data Acquisition.....702

iii. Quantitative Analysis of Myofiber Angle702

iv. Analysis of Strains.....703

v. Statistical Analysis705

C. Results705

D. Discussion711

i. LV Myocardium Overlying Antero-Lateral Papillary is Not Unique.....712

ii. Antero-Lateral Continuum of LV Transmural Strains Despite

 Similarities in Myofibers714

iii. Transmural Gradients Evident throughout Regions.....715

iv. Transmural Strains of Myocardium Overlying Papillary Implicate

 Robust Cardiac Structure717

v. Implications.....717

vi. Limitations.....718

E. Conclusions	720
<i>Chapter 26: Temporal and Regional Heterogeneity in Left Ventricular Deformation: Implications for Myofiber Coupling.....</i>	727
A. Introduction	730
B. Methods.....	730
i. Analysis of Strain Development Throughout the Cardiac Cycle.....	731
ii. Statistical Analysis.....	731
C. Results	731
i. Transmural Thickening (Radial Normal Strain).....	731
ii. Longitudinal Normal Strain.....	733
iii. Circumferential Normal Strain	737
iv. Myofiber Fiber and Cross-fiber Strains.....	737
D. Discussion	743
i. Temporal and Regional Heterogeneity in Transmural Thickening.....	743
ii. Temporal and Regional Heterogeneity in Longitudinal Strain.....	744
iii. Temporal and Regional Heterogeneity in Circumferential Strain	745
iv. Temporal and Regional Strain Heterogeneity Despite Similarities in Myofibers	745
v. Components Contributing to Early Rise in LV Pressure.....	747

vi. Relationship of Results to Previous Studies of End Systole LV	
Transmural Strain Heterogeneity	748
vii. Implications	749
viii. Limitations.....	750
E. Conclusions	751

List of Tables and Figures

VOLUME 1

I. Chapter 1: Background

Fig. 1-1: Bioprosthetic valve with calcification

Fig. 1-2: Typical tension-strain curve

Fig. 1-3: Structure of PGs and GAGs

Table 1-1: MMP 1, 2, 9, and 13 specificity

Table 1-2: Pros and cons of different cell sources used in tissue engineering

Table 1-3: Pros and cons of different scaffolds used in tissue engineering

Table 1-4: Examples of different scaffolds and cells used in tissue engineering

II. Studies

A. METHODS

Chapter 2: The Use of Collagenase III for the Isolation of Porcine Aortic Valvular Interstitial Cells: Rationale and Optimization

Table 2-1: Reported enzymatic VIC isolation techniques

Table 2-2: Experimental conditions

Fig. 2-1: Optimization of collagenase III concentration for 6-month-old valves

Fig. 2-2: Cost benefit analysis

Fig. 2-3: Optimization of additional enzymes for 6-month-old valves

Fig. 2-4: Optimization of digestion duration and collagenase III concentration for
6-week-old valves

Fig. 2-5: Optimization of additional enzymes for 6-week-old valves

Fig. 2-6: Fresh versus frozen enzymatic cocktail

Table 2-3: Optimized enzymatic digestion mixtures for 6-week-old and 6-month-old porcine heart valves

Table 2-4: Human and porcine age equivalencies

Table 2-5: Activities of enzymes in crude collagenase III preparation

B. CHARACTERIZATION OF NORMAL VALVES

i. Aging: Composition and Structure

Chapter 3: Age-Related Changes in Collagen Synthesis and Turnover in Porcine Heart Valves

Table 3-1: Sample size

Table 3-2: Collection of antibodies used in immunohistochemistry

Fig. 3-1A: Diagram of layers of MV and AV

Fig. 3-1B: Grading rubric

Fig. 3-2: Decrease in cell density with aging

Fig. 3-3: Differential protein expression in 1st trimester MV compared to 2nd trimester MV

Fig. 3-4: Picrosirius red stain of 3rd trimester MV

Fig. 3-5: Tissue organization of various aged AVs

Fig. 3-6: Co-localization of P4H, MMP13, HSP47, and SMaA

Fig. 3-7: SMaA in fetal valves

Fig. 3-8: Collagen remodeling maximum around fibrosa

Fig. 3-9: Picrosirius red stain of fibrosa

Table 3-3: Differential protein expression between layers

Table 3-4: Comparison of protein expression between MV and AV

Fig. 3-10: Col III in AV and MV

Fig. 3-11: Anatomical distribution of SMaA

Chapter 4: Valve Proteoglycan Content and Glycosaminoglycan Fine Structure are Unique to Microstructure, Mechanical Load, and Age: Relevance to an Age-Specific Tissue Engineered Heart Valve

Fig. 4-1: Differentiation of PGs in fetal valves

Table 4-1A: IHC differential protein expression between layers of postnatal valves

Table 4-1B: IHC changes in protein expression in postnatal valves with aging

Table 4-1C: IHC differences in protein expression between postnatal MV and AV

Fig. 4-2: Elastin and VC distribution

Fig. 4-3: Percent hydration and HA in valves of different ages

Fig. 4-4: Proportion of GAGs in valves of different ages

Table 4-2: Ratio of GAG components of valves of different ages

Table 4-3: Comparison of GAG compositions between valves

Fig. 4-5: GAG composition in valves of different ages

Fig. 4-6: GAG chain length in valves of different ages

Chapter 5: Perinatal Changes in Mitral and Aortic Valve Composition

Fig. 5-1A: Photographs of 3rd trimester valves

Fig. 5-1B: Structure of 3rd trimester and 2 day-old MV and AV

Fig. 5-2: Delineation and saffron-staining collagen in AV and MV

Fig. 5-3: Elastin and VC in AV

Fig. 5-4: HA and HARE in AV

Fig. 5-5: Collagen-related proteins in AV

Fig. 5-6: Differences between AV and MV in 3rd trimester and 2 day-old pigs

Fig. 5-7: Co-localization of proteins in AV and MV

Fig. 5-8: HARE staining in 3rd trimester and 2 day-old valves

Fig. 5-9: CD44 and TGF β staining in representative 2 day-old MV

Fig 5-10: Example of congenitally diseased human AV

Chapter 6: Regional Heterogeneity in Aortic Valve GAG Composition

Fig. 6-1: Regions of AV analyzed

Table 6-1: Wet and dry weights for samples

Fig. 6-2: Amount of GAGs in different regions of AV

Fig. 6-3: Average GAG content in different regions of AV

Fig. 6-4: Proportional GAG content in different regions of AV

Fig. 6-5: Percent hydration of different regions of AV

i. Aging: Material Properties

Chapter 7: Age-Related Changes in Material Behavior of Porcine Mitral and Aortic Valves and Correlation to Matrix Composition

Table 7-1: Sample set

Fig. 7-1A: Orientation of MV tissue strips

Fig. 7-1B: Mechanical testing set-up

Fig. 7-2: Thickness AV, MV of different ages

Fig. 7-3: Post-transition stiffness of AV, MV of different ages

Fig. 7-4: Pre-transition stiffness of AV, MV of different ages

Table 7-2: Stress relaxation time constants

Fig. 7-5: Total percent stress relaxation of AV, MV of different ages

Fig. 7-6: Extensibility of AV, MV of different ages

Fig. 7-7: Radius of transition curvature of AV, MV of different ages

Fig. 7-8: Movat-stained samples of 6-week-old and 6-year-old AV, MV radial sections

Fig. 7-9: Movat-stained samples of AV, MV circumferential sections of different ages

Fig. 7-10: Col III and NMM in 6-month-old and 6-year-old MVAC sample sections

VOLUME 2

ii. Valve Heterogeneity: Composition and Motion

Chapter 8: Cellular and Extracellular Matrix Basis for Heterogeneity in Mitral Annular Contraction

Fig. 8-1: Location of different annular segments analyzed

Table 8-1: Panel of antibodies used in IHC

Fig. 8-2A: Histologically stained sample relative to implanted radiopaque marker

Fig. 8-2B: Grading rubric for degree of insertion

Table 8-2: Percent contraction of annular segments

Fig. 8-3: Differences in insertion structure between MV annular segments

Fig. 8-4: Col I and Col III in different annular segments

Fig. 8-5: MMP13 and SMaA in different annular segments

Fig. 8-6: Elastin in different annular segments

Chapter 9: Relationship of Mitral Leaflet Compositional Heterogeneity to Leaflet Deformation

Fig. 9-1: Location of implanted radiopaque markers

Fig. 9-2: Locations of leaflet regions and histological layers

Table 9-1: Minimum and maximum leaflet segment lengths

Fig. 9-3: Degree of delineation between leaflet layers

Fig. 9-4: Examples of chordae tendinae insertion in different annular segments

Fig. 9-5: Col I and Col III in mid-leaflet region of different annular segments

Fig. 9-6: MMP13 and SMaA in mid-leaflet region of different annular segments

Fig. 9-7: Elastin in mid-leaflet region of different annular segments

ii. Valve Heterogeneity: Valvular Interstitial Cells and Myofibroblasts

Chapter 10: Fibronectin-Based Isolation of Valvular Interstitial Cell

Subpopulations: Relevance to Valve Disease

Fig. 10-1: Process of isolating VIC subpopulations

Fig. 10-2: Adhesion of VIC subpopulation to TCP and FN over time

Fig. 10-3: Flow cytometry marker fluorescence of FN and TCP subpopulations

Fig. 10-4A: Ratio of FN FAST to FN SLOW flow cytometry marker mean
fluorescence for human myxomatous MV

Fig. 10-4B: FN immunohistochemical staining in normal and myxomatous MV

Fig. 10-5: Immunocytochemistry marker integrated optical density of FN and
TCP subpopulations

Fig. 10-6: Representative images of immunocytochemistry of TCP
subpopulations

Chapter 11: Functional Characterization of Fibronectin-Separated Valvular

Interstitial Cell Subpopulations: Application to Study of Valve Disease

Fig. 11-1: Collagen constructs in silicon wells

Fig. 11-2: Contraction of collagen constructs by VIC subpopulations

Fig. 11-3: Elastic modulus of collagen constructs seeded by different VIC
subpopulations

Fig. 11-4: Failure stress of collagen constructs seeded by different VIC subpopulations

iii. Cell-Matrix Coupling

Chapter 12: Functional Coupling of Valvular Interstitial Cells and Collagen in the Mitral Leaflet

Fig. 12-1: Custom-built strain-load device

Fig. 12-2: VIC alignment relative to collagen fibers

Fig. 12-3: VIC cytoplasm in relation to crimped collagen fibers

Fig. 12-4: VIC actin in relation to collagen fibers

Fig. 12-5: VIC actin in region in which collagen fibers are not aligned

Fig. 12-6: Alpha₂beta₁ integrins on VIC membrane

Fig. 12-7: Alpha₂beta₁ integrins on collagen fibers

Fig. 12-8: VIC alignment relative to collagen fibers after blocking alpha₂beta₁ integrins

Fig. 12-9: Force generated by MV leaflets exposed to various treatments

Fig. 12-10: Diagram illustrating the proposed VIC-integrin-collagen functional unit

Fig. 12-11: Diagram conceptualizing different means of force generation in MV

C. VALVE INJURY AND DISEASE

i. Congenital Valve Disease

Chapter 13: Insight into Histological and Pathological Abnormalities in Congenitally Diseased Valves Based on Advances in Understanding Normal Valve Microstructure and Extracellular Matrix

Fig. 13-1: Gross photograph of an atretic PV

Fig. 13-2A,B: Gross photographs of normal AVs

Fig. 13-3: Gross photograph of a bicuspid stenotic AV with diffuse fibrosis

Fig. 13-4: Gross photograph of a severely dysplastic AV with associated left ventricular hypertrophy

Fig. 13-5: Gross photograph of a mildly dysplastic AV

Fig. 13-6: Movat pentachrome stained section of a dysplastic PV compared to a normal PV

Fig. 13-7: Movat pentachrome stained section of a PV with insufficiency

Chapter 14: Extracellular Matrix Remodeling and Cell Phenotypic Changes in Dysplastic and Hemodynamically Altered Semilunar Heart Valves

Table 15-1: Antibodies used in flow cytometry and immunohistochemistry

Fig. 14-1: Expression of PGs and HA in different aged CTRL AVs

Fig. 14-2: Expression of collagen turnover and cell activation markers in different aged CTRL AVs

Fig. 14-3: Expression of matrix components in HEMO AVs and PVs compared to CTRLs

Fig. 14-4: Expression of matrix components in HEMO, HEMO/DYSP, and CTRL AVs

Fig. 14-5: Expression of matrix components in HEMO and HEMO/DYSP plaques and the regions underlying plaques compared to CTRLs

Fig. 14-6: Plaque in a HEMO/DYSP BAV displaying decreased HA

Fig. 14-7: CTRL valve displaying normal leaflet layer delineation and layer-specific protein expression

Fig. 14-8: HEMO/DYSP AV demonstrating lack of leaflet layer delineation and marbling of matrix components

Fig. 14-9: HEMO/DYSP PV displaying remodeling in the spongiosa

Fig. 14-10: HEMO/DYSP AV demonstrating variability in loss of leaflet layered
microstructure along the length of the leaflet

Fig. 14-11: SMaA staining and co-localization with other markers in
HEMO/DYSP AV with plaque

Fig. 14-12: Marker expression in VICs from AV compared to PV for different
ages

Fig. 14-13A: Cell morphology of VICs from HEMO PV compared to CTRL PV

Fig. 14-13B: Cell morphology of VICs from HEMO/DYSP AV, PV compared to
CTRLs

Fig. 14-14A: Marker expression in VICs from Ross valves compared to CTRL
AVs and PVs

Fig. 14-14B: Cell morphology of VICs from Ross valves compared to CTRL
AVs and PVs

ii. Dilated Cardiomyopathy and “Functional” Mitral Regurgitation

Chapter 15: The Effects of Hemodynamics of Regurgitation Alone are Sufficient for Mitral Valve Leaflet Remodeling

Fig. 15-1: Intraoperative picture of hole-punch made in PML

Fig. 15-2: Location from which AML samples were taken

Table 15-1: Antibodies used in immunohistochemistry

Fig. 15-3A: Histology of MV

Fig. 15-3B: Rubrics for grading immunohistochemical staining

Fig. 15-4A: MR grade over time

Fig. 15-4B: Sample echo image of regurgitant jet

Fig. 15-5: Collagen-related markers in HOLE and CTRL

Fig. 15-6: MMP9, MMP1 in HOLE and CTRL

Fig. 15-7: Elastin in HOLE and CTRL

Chapter 16: Significant Changes in Mitral Valve Leaflet Matrix Composition and Turnover with Tachycardia-Induced Cardiomyopathy

Fig. 16-1: Locations of implanted radiopaque markers and tissue sections analyzed

Table 16-1: Panel of antibodies used in immunohistochemistry

Fig. 16-2: Pre-TIC and post-TIC MR

Table 16-2: Pre-TIC and TIC maximum leaflet segment lengths

Fig. 16-3A,B: Delineation between leaflet layers in TIC and CTRL

Fig. 16-3C: Examples of muscle found in TIC leaflets

Fig. 16-4: MMP13 in TIC and CTRL

Fig. 16-5: Col I in TIC and CTRL

Fig. 16-6: MMP9 in TIC and CTRL

Fig. 16-7: SMaA in TIC and CTRL

Chapter 17: Mitral Annular Region Ultrastructural Changes in Dilated Cardiomyopathy Correlate with Regional Remodeling

Fig. 17-1: Location of different annular segments

Fig. 17-2: Histologically stained leaflet in relation to implanted radiopaque marker, increased collagen in TIC

Table 17-1: Panel of antibodies used in immunohistochemistry

Table 17-2: Annular segment length changes with TIC

Fig. 17-3: Col I in TIC and CTRL

Fig. 17-4: MMP9, NMM in TIC and CTRL

Fig. 17-5: SMaA in TIC and CTRL

VOLUME 3

iii. Valve Wound Injury

Chapter 18: Extracellular Matrix Remodeling in Response to Mitral Leaflet Injury

Fig. 18-1A: Locations from which analyzed tissue samples were taken

Fig. 18-1B: Normal MV posterior leaflet

Fig. 18-1C: Grading rubrics for IHC staining intensity

Fig. 18-2: Remodeling reducing hole diameter, neovascularization and fibrin accumulation

Fig. 18-3A: Initial and final hole diameter

Fig. 18-3B: Cell density of HOLE and CTRL

Fig. 18-4A,B: PG, GAG, and markers of matrix turnover in HOLE and CTRL

Fig. 18-4C: Delineation of matrix components

Fig. 18-5A: Two regions of matrix remodeling

Fig. 18-5B: Decreased delineation in HOLE compared to CTRL

Fig. 18-5C: Picosirius red staining of HOLE and CTRL

iv. Myxomatous Mitral Valve Disease

Chapter 19: MAPK Pathway in Myxomatous Mitral Valve Disease

Table 19-1: Subject demographics

Table 19-2: Antibodies used in immunohistochemistry

Fig. 19-1: SMaA and NMM in normal and myxomatous MVs

Fig. 19-2: Co-localization of MAPK pathway markers and TGF β in the myxomatous MV

Fig. 19-3: Co-localization of myofibroblast markers, MAPK pathway markers, and TGF β in the myxomatous MV

Fig. 19-4: Localization of ERK2 to areas of matrix remodeling in the myxomatous MV

Fig. 19-5: Localization of NMM to areas of matrix remodeling in the myxomatous MV

v. Calcified Aortic Valve Disease

Chapter 20: Differential Proteoglycan and Hyaluronan Distribution in Calcified Aortic Valves

Fig. 20:1: Nodules and prenodules in calcified AVs stained with Movat pentachrome, HA, and versican

Fig. 20:2: Intensities of PGs and HA in different regions of calcified AVs

Fig. 20:3: Calcified AV stained with Movat pentachrome, PGs, and HA

Fig. 20:4: Calcified AV stained with Movat pentachrome, DCN, and BGN

Chapter 21: Hyaluronan Turnover and Hypoxic Brown Adipocytes are Co-localized with Endochondral Ossification in Calcified Aortic Valves

Table 21-1: Antibodies used in immunohistochemistry

Fig. 21-1: Location of various regions analyzed

Fig. 21-2: Co-localization of BMP-2, Hyal-1, HAS-2, and CD168 in calcified AVs

Fig. 21-3: Co-localization of BMP-2, PGC-1 α , UCP-1, and HIF-1 α in calcified AVs

Fig. 21-4: Localization of periostin staining in calcified AVs

Table 21-2: Correlations within mechanistic families

Table 21-3: Correlations between different mechanistic families

Fig. 21-5: Mechanism of calcification at nodule edge relative to outside of nodule

D. TISSUE ENGINEERING

Chapter 22: Age- and Valve-Region-Specific Responses of Mitral Valvular Interstitial Cells to Substrate Stiffness

Fig. 22-1: PEG-DA reaction schematic

Fig. 22-2: ^1H NMR of PEG-DA

Fig. 22-3: PEG-RGDS reaction schematic

Fig. 22-4: Gel permeation chromatography of PEG-RGDS

Fig. 22-5: Gel permeation chromatography of PEG-WRGDS

Fig. 22-6: ^1H NMR of methacrylated heparin

Fig. 22-7: Concentration of methacrylated heparin in different weight-volume fraction PEG hydrogels

Fig. 22-8: Optimization of PEG-WGRDS in different weight-volume fraction PEG hydrogels

Fig. 22-9: Stiffnesses of different weight-volume fraction functionalized PEG hydrogels

Fig. 22-10: Percent VICs displaying positive SMaA staining on gels of different stiffnesses

Fig. 22-11: SMaA staining intensity for positive SMaA staining VICs on gels of different stiffnesses

Fig. 22-12: P4H staining intensity of VICs on gels of different stiffnesses

Fig. 22-13: HSP47 staining intensity of VICs on gels of different stiffnesses

Fig. 22-14: Distinct morphologic subpopulations of VICs on gels of different stiffnesses

Fig. 22-15: Schematic of hypothetical marker expression-substrate stiffness curves

IV. Chapter 23: Conclusions

Fig. 23-1: Schematic of themes underlying thesis work

V. Appendix

Chapter 24: Abundance and Location of Hyaluronan and Proteoglycans within Myxomatous Mitral Valves

Table 24-1: Subject demographics

Fig. 24-1: Sample IHC images of PGs in normal and myxomatous MV

Fig. 24-2: Abundance of PGs in normal and myxomatous MV

Fig. 24-3: Sample IHC images of HA and HARE in normal and myxomatous MV

Fig. 24-4: Abundance of HA and HARE in normal and myxomatous MV

E. MYOCARDIAL MECHANICS

Chapter 25: The Myocardium Overlying the Papillary Muscle Contributes to the Antero-Lateral Left Ventricular Wall Deformation Continuum

Fig. 25-1: Transmural beadsets

Table 25-1: Hemodynamic data

Table 25-2: Normal strains

Table 25-3: Shear strains

Table 25-4: Principal strains

Fig. 25-2: Myofiber angles

Table 25-5: Fiber and cross-fiber strains

Chapter 26: Temporal and Regional Heterogeneity in Left Ventricular Deformation: Implications for Myofiber Coupling

Fig. 26-1: E_{RR} in ANT, PAP, and LAT regions throughout the cardiac cycle

Fig. 26-2: E_{LL} in ANT, PAP, and LAT regions throughout the cardiac cycle

Fig. 26-3: E_{CC} in ANT, PAP, and LAT regions throughout the cardiac cycle

Fig. 26-4: E_f in ANT, PAP, and LAT regions throughout the cardiac cycle

Fig. 26-5: E_{cross} in ANT, PAP, and LAT regions throughout the cardiac cycle

Fig. 26-6: E_f and E_{cross} during IVC in ANT and LAT regions

Fig. 26-7: E_{cross} and E_{RR} in LAT throughout the cardiac cycle

List of Abbreviations

α =myofiber angle
ABAM=antibiotic/antimycotic
AML=anterior mitral leaflet
ANOVA=analysis of variance
ANT=anterior myocardium of LV
ANT-C=anterior commissure
APM=antero-lateral papillary muscle
AV=aortic valve
BAV=bicuspid aortic valve
BCM=Baylor College of Medicine
BGN=biglycan
BMP-2=bone morphogenic protein-2
BGS=bovine growth serum
BL=basal leaflet
CHD=congenital heart disease
CHTN=Cooperative Human Tissue Network
Col=collagen
CAVD=calcific aortic valve disease
CPVD=congenital polyvalvular disease
CS=chondroitin sulfate
CSVD=congenital semilunar valve disease
CVD=congenital valve disease
CTRL=control
DCM=dilated cardiomyopathy
DMSO=dimethyl sulfoxide
DS=dermatan sulfate
DCN=decorin
 E_1 =principal strain
ECG=electrocardiography
ECM=extracellular matrix
 E_{CC} =circumferential normal strain
 E_{CL} =circumferential-longitudinal shear strain
 E_{CR} =circumferential-radial shear strain
ED=end diastole
ED-A=extra domain-A
EDV=end-diastolic volume
EDVI=end-diastolic volume index
EF=ejection fraction
 E_{LL} =longitudinal normal strain
 E_{LR} =longitudinal-radial shear strain
 E_{RR} =radial normal strain
ERK=extracellular signal-regulated kinase
ES=end systole
ESLVP=end systolic LV pressure
ESV=end-systolic volume
ESVI=end-systolic volume index
ERK=extracellular-related signaling kinase
FACE=fluorophore-assisted carbohydrate electrophoresis

FC=flow cytometry
 FSC=forward scatter in flow cytometry
 FGF=fibroblast growth factor
 FN=fibronectin
 G0S,4S,6S=unsulfated, 4-sulfated, 6-sulfated glucuronate
 GAG=glycosaminoglycan
 galNAC=N-acetylgalatosamine
 HA=hyaluronan
 HARE=hyaluronan receptor for endocytosis
 HAS-2=hyaluronan synthase-2
 HEMO=hemodynamically altered valves
 HEMO/DYSP=dysplastic valves with hemodynamic pathologic changes
 HIF-1 α =Hypoxia inducible factor-1 α
 Hyase=hyaluronidase
 HSP=heat shock protein
 Hyal-1=hyaluronidase-1
 I0S,4S,6S=unsulfated, 4-sulfated, 6-sulfated iduronate
 ICC=immunocytochemistry
 IHC=immunohistochemistry
 IVC=isovolumic contraction
 JNK=c-Jun N-terminal kinase
 LAT=lateral MV, or in Ch. 25 and 26 lateral LV myocardium
 LOX=lysyl oxidase
 LV=left ventricle
 LVESV=LV end systolic volume
 LVEDV=LV end diastolic volume
 MAP=mitogen-activated protein
 MAPK=mitogen-activated protein kinase
 MHC=myosin heavy chain
 ML=mid-leaflet
 MMP=matrix metalloprotease
 MR=mitral regurgitation
 MV=mitral valve
 MVAC=mitral valve anterior center
 MVF=mitral valve free edge
 MTT=3-(4,5-dimethylthiazol-2-yl)-2,5-diphenyl tetrazolium bromide
 NC=non-coronary AV leaflet
 NMM=non-muscle myosin
 NodCtr=center region of calcified nodule
 NodEdge=region at edge of calcified nodule
 NodSurr=region surrounding calcified nodule
 NMR=nuclear magnetic resonance
 PAP=region of LV myocardium overlying the antero-lateral papillary muscle
 PCNA=proliferating cell nuclear antigen
 P4H=prolyl 4-hydroxylase
 PBS=phosphate buffered saline
 PCNA=proliferating cell nuclear antigen
 PEG=poly(ethylene) glycol
 PEG-DA=poly(ethylene) glycol-diacrylate
 PEG-RGDS=PEG conjugated with an RGDS peptide
 PEG-SCM=hetero bifunctional PEG

PEG-WRGDS=PEG conjugated with a WRGDS peptide
pERK=phosphorylated ERK
PG=proteoglycan
PGA=poly(glycolic acid)
PGC-1 α =peroxisome proliferator-activated receptor γ , co-activator 1 α
PHA=poly(hydroxyalkanoate)
PLGA=polylactide-co-glycolide
PML=posterior mitral leaflet
PPM=postero-medial papillary muscle
POST-C=posterior commissure
PreNod=central region of calcified prenodule
PreNodSurr=region surrounding prenodule
PV=pulmonary valve
PVA=poly(vinyl alcohol)
PEUU=poly(ester urethane) urea.
OPF=oligo (PEG) fumarate
R1,2=region 1, 2
RGDS=Arg-Gly-Asp-Ser peptide
RHAMM=receptor for HA-mediated motility
RM ANOVA=repeat measures ANOVA
RTC=radius of transition curvature
RV=right ventricle
SEM=standard error of the mean
SEPT=septal MV
SMaA=smooth muscle alpha-actin
Smem=non-muscle myosin
SMM=smooth muscle myosin
SSC=side scatter in flow cytometry
Subepi=subepicardium
Subendo=subendocardium
TCP=tissue culture plastic
TCPS=tissue culture polystyrene
TEHV=tissue engineered heart valve
TGF β =transforming growth factor-beta
TIC=tachycardia-induced cardiomyopathy
TNF- α =tumor necrosis factor- α
TSG-6=TNF- α stimulated gene-6
tPG=total PG
tPMH=total P4H, MMP13, HSP47
UCP-1=uncoupling protein-1
VIC=valvular interstitial cells
VC=versican
XS=di- and tri-sulfated glucuronate/iduronate
WRGDS=Tryp-Arg-Gly-Asp-Ser peptide

Chapter 1: Background

A. Congenital Valve Disease

i. Epidemiology

Approximately 1 million Americans are diagnosed with a congenital heart defect (CHD).¹ CHD is the most common congenital defect, occurring in one out of every 100 live births.² Of the 36,000 babies born with congenital heart defects in the US each year, 9200 require invasive treatment or die in the first year of life.³ In 2000 alone 213,000 life years were lost before age 65 because of CHD, nearly equal to the sum of leukemia, prostate cancer, and Alzheimer's disease.⁴ Of the many abnormalities seen in CHD, the majority involve the valves and/or septa.⁵ Clearly congenital valve disease produces a great burden on our society both in terms of resources and loss of life. Congenital valve disease is both prevalent and deadly and as such presents an important challenge for biomedical science to overcome.

ii. Types of Congenital Valve Disease

The wide range of congenital valve disease types adds to the difficulty of treating the disease. Diseased valves can be divided into four categories: those that affect the 1) valve leaflet, 2) commissures, 3) chordae tendinae, and/or 4) papillary muscle.⁶ These abnormal valves can occur in isolation or within a complex of cardiac defects. When the valve malformation is the result of a developmental defect, tissues derived from the same cells as the valves, or reliant on the same factor (be it gene, protein, transcription factor),

will be malformed as well, accounting for some of the complex malformations. Furthermore, systemic diseases including connective tissue diseases, metabolic diseases, and various storage diseases may present with a dysmorphic heart and valves. In addition to isolated cases of valve disease and those that are part of more extensive disease, there is congenital polyvalvular disease in which multiple valves are malformed but not in conjunction with broader disease.⁷

Systemic congenital diseases that affect the heart may be considered outside of the above classification. These include metabolic disorders such as Hurler's syndrome and connective tissue diseases such as Marfan's syndrome.⁸ Children can also have valve disease that is acquired. In the past, the majority of acquired heart disease was secondary to rheumatic fever, however this is much less common today. Valve disease may also be acquired secondary to infection,⁸ but this research focuses on congenital disease and its treatment methods.

iii. Current Treatments

Current treatment for congenital valve disease is suboptimal at best. Patients require 4-6 open-heart operations before they reach adulthood to replace valves that have become too small as the child grows. Operations continue in their adult years.⁹ Current valves have an average durability of 10-15 years,¹⁰ making re-operation unavoidable. However re-operation carries significantly increased surgical risk.¹¹ Adhesions have formed from previous operations making access to the heart more difficult and the risk of heart rupture greater. The old valve, now ingrown to the native tissue, must be painstakingly dissected leaving enough tissue to anchor the new valve. Lastly, the tissue to which the new valve must be sewn is weakened because of previous sutures and the

aforementioned dissection.¹¹ Not only does this bring higher risk to the operation but it substantially increases the duration of time that the patient must be supported by the cardiopulmonary bypass machine. Cardiopulmonary bypass, of course, carries its own risks including brain injury from lack of cerebral blood flow and an often fatal syndrome in which the body reacts to antigens on the tubing of the cardiopulmonary bypass machine.

Even if these surgical risks could be eliminated, there still is no satisfactory treatment for congenital valve disease. The two current, effective treatments for adult valve disease, mechanical and bioprosthetic, are problematic in children. Mechanical valves, usually made of pyrolytic carbon, require continual anticoagulation therapy that is often not compatible with a child's active lifestyle.¹¹ Warfarin therapy is further complicated by a variety of circumstances which alter its metabolism and prothrombin time, such as the rate of growth and nutritional status of the patient and antibiotics that the patient is given for infection.¹¹ Complications of warfarin therapy include bruising, excessive bleeding, stroke, and infarct.¹¹ Furthermore, warfarin requires strict daily dosing and frequent hospital visits to check coagulation status.¹¹ As these children mature, anti-coagulation during pregnancy becomes an additional problem. Warfarin is teratogenic, so pregnant mothers must use injectable heparin and face major complications upon delivery.¹¹ While a mechanical valve is not practical because of the need for anti-coagulation, porcine replacement valves have the difficulty of rapid calcification and mechanical failure. In children this calcification is on the order of a few years and in infants on the order of months (Fig. 1-1).¹²

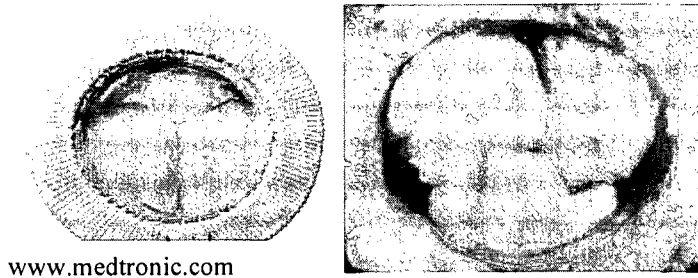


Fig. 1-1: Bioprosthetic valve: Left shows valve before implantation, Right panel shows valve after explantation with severe calcification.

This lack of treatment options would be solved with a tissue engineered heart valve made of a patient's own (autologous) cells. Implanted when the patient is an infant, the valve would grow with the child. Because it would be made out of the patient's own cells, neither an immune reaction nor coagulation would be problematic. Furthermore, such a valve would be able to remodel to adapt to its hemodynamic environment as well as regenerate and repair itself.

B. Heart Valve Anatomy

i. The Four Valves

There are four valves found in the heart. The mitral and tricuspid valves are known as atrioventricular valves, as they separate the atria and ventricle of the left and right side of the heart respectively. The two other valves, the aortic and pulmonic, are known as semilunar valves. The pulmonic valve controls flow between the right ventricle and the pulmonary circulation, while the aorta controls flow from the left ventricle to the systemic circulation (via the aorta). Each of these valves exists in a distinct environment and has a unique structure and function. The tricuspid and pulmonic

valves function within the low pressure environments of the right ventricle and pulmonary circulation, and therefore are thinner. The mitral and aortic valves, however, experience high pressure blood flow on its way to systemic circulation, and therefore are considerably thicker, among other differences. Another obvious difference between the four valves is chordae tendinae. Chordae tendinae are fibrous strings that attach to the edges of the atrioventricular valves and secure them to the heart via papillary muscles. Another obvious difference between the four valves is the number of valve leaflets. The mitral valve consists of two leaflets, the anterior and posterior, while the tricuspid and semilunar valves consist of three leaflets. The tricuspid valve will not be covered in depth in this Background section, as it is not a subject of this research.

ii. Mitral Valve

On closer examination more unique features of the mitral valve are noted. The mitral valve leaflets are not identical. The posterior leaflets is considerably smaller in radial depth (measured from annulus to free edge) than the anterior with a number of scallops in its leaflet; usually there are three scallops and the middle scallop is the largest.¹³ These scallops and the lack of clear landmarks has made identifying portions of the posterior leaflet difficult.¹⁴ According to Ranganathan et al., the posterior leaflet includes all tissue posterior to the two anterior leaflet commissures, which usually are clearly distinguishable and defined by chordal attachments.¹⁴ Three zones are distinguished in the posterior leaflet: the rough zone from the line of leaflet closure to the free edge, the membranous or clear zone, which is clear upon transillumination, and the basal zone which spans the region from the clear zone to the annulus.¹⁴

The anterior leaflet similarly has distinct regions that can be identified upon gross examination. The atrial surface of the anterior leaflet has a distinct ridge 0.8 to 1.0 cm from the free edge that is the line of leaflet closure.¹⁴ Distal to the ridge is a region rough to palpation, appropriately called the rough zone. Upon closure the rough zone of the anterior leaflet apposes the similar rough zone on the posterior leaflet. The greater thickness of this region of the anterior leaflet, in part, is due to the numerous chordal insertions in that area.¹⁴ The area between the rough zone and the valve annulus is called the clear zone, because it is clear on transillumination, or “anterior center.”¹⁴ This area is about twice the height of the rough zone and is free from chordal insertions.¹⁴

iii. Aortic and Pulmonic Valves

The aortic and pulmonic valves have three leaflets (a.k.a “cusps”) of equal size and shape, without chordae. The aortic valve additionally has the sinuses of Valsalva, which are pockets formed by localized dilatations in the aortic wall on one side and the aortic leaflets on the other side. Behind the right coronary leaflet and left coronary cusps, at the center of these pockets are the ostia for the right and left coronary arteries respectively. Vortices that form within these sinuses are thought to be important in facilitating cusp closure.¹⁵ After the heart contracts, blood flow enters these sinuses and provides blood flow to the heart muscle itself. The presence of the coronary arteries and their blood flow creates distinct hemodynamic environments for the right and left aortic valve cusps as compared to the non-coronary cusp. The aortic valve also has unique localized thickenings in the center near the free edge of each cusp, known as the nodules of Arantius.

iv. Histological Valve Layers

Macroscopically the heart valves are formed by layers of tissue with distinct compositions, mechanical properties, and functional roles. For the atrioventricular valves there are four layers named atrialis, spongiosa, fibrosa, and ventricularis, aptly named as the atrialis faces the atrium and the ventricularis faces the ventricle.¹⁶ Each of these layers has a different composition. The fibrosa is dominated by collagen, the atrialis and ventricularis are dominated by elastic fibers, while the spongiosa contains many proteoglycans and hyaluronan (see explanation of proteoglycans below).¹⁶ The relative thickness of these layers throughout portions of the valve also varies.¹⁷

Similar to the atrioventricular valves, in the semilunar valves there are three layers, the fibrosa, spongiosa, and ventricularis, with again the ventricularis facing the ventricle.¹⁸ In the aortic valve the fibrosa faces the aorta and, similar to the fibrosa of the atrioventricular valves, is principally composed of circumferential collagen in a crimped configuration which stretches out during valve closure.¹¹ The ventricularis is much thinner than the fibrosa and is composed of a sheet of predominantly elastic fibers arranged radially with some collagen.^{11, 19} The intermediate layer, the spongiosa, has very loosely arranged collagen with an abundance of glycosaminoglycans, as evident in the atrioventricular valves.¹¹

C. Extracellular Matrix

In recent years the importance of the extracellular matrix (ECM) in tissue formation, maintenance, and function has become increasingly evident. Previously

thought to merely fill in the spaces between cells, it has become clear that the extracellular matrix is vital to healthy tissue of all types. Besides this, research shows that the extracellular matrix plays an active role in multiple important processes including cell migration, proliferation, differentiation, and regeneration. The extracellular matrix is actively involved in these processes through the expression of different receptors and the binding and controlled release of growth factors and other cytokines. The contents of the extracellular matrix include collagen and elastic fibers, proteoglycans (PGs) and glycosaminoglycans (GAGs), and various receptors and adhesion molecules, which are covered in the subsequent sections.

i. Collagen

Collagen provides the valve with the tensile strength necessary to withstand its hemodynamic environment. The dominant collagen type in the adult aortic valve is collagen I (74%) with some type III (24%) and a small amount of collagen type V (2%).²⁰ Collagen type I is concentrated in the fibrosa layer.²¹ The crimped configuration of the collagen fibers is critical to the material properties of the valve. As tension is applied to heart valves the collagen fibers uncrimp and then begin to bear load.²² The uncrimping of the collagen fibers creates the pre-transition region and extensibility evident within the valve stress-strain or tension-strain curves (Fig. 1-2).²² The modulus of the post-transition region of the valve stress-strain curve (calculated as the slope of that region of the curve) is then believed to be mainly determined by the stiffness of the uncrimped collagen.²² The alignment of collagen I fibers, at least in part, creates the anisotropic properties of the valve. For example, in the aortic valve collagen I fibers are primarily

aligned in the circumferential direction,²³ which gives aortic valves a much stiffer modulus in the circumferential direction as compared to the radial direction.²⁴

Collagen III, the second main collagen type seen in valves, is known as “reticular” collagen. Collagen type III has qualities of flexibility that collagen I does not possess. At the microstructural level collagen III is also different. Instead of forming bundles of fibrils to within a thick fiber like collagen type I, collagen III forms networks,^{25, 26} thereby explaining its mechanical role in flexibility. Collagen III distribution within the valve is also different from that of collagen I in that it is considerably more ubiquitous.²⁷

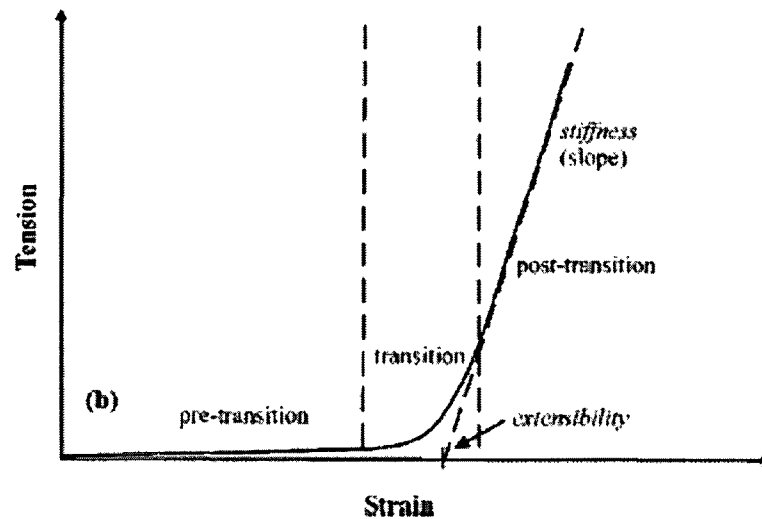


Fig. 1-2: Typical tension-strain curve of a valve.²⁸

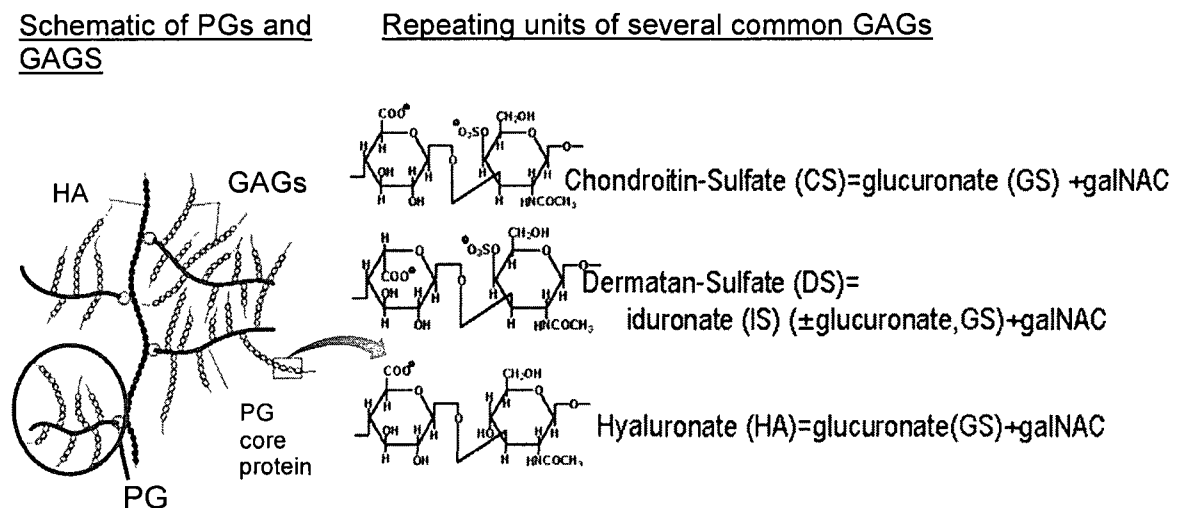
ii. Elastic Fibers

Elastic fibers are predominantly found in the atrialis and ventricularis of the mitral valve, and the ventricularis of the AV. They are formed by an amorphous core of elastin protein surrounded by fibrillin.²⁹ In the process of elastic fiber formation, fibrillin is

present first and acts as a scaffold on which the elastin is then deposited.²⁹ Elastic fibers provide recoil to valves so that after each heart beat the valve returns to its original configuration.²² Within the valve tension-strain curve, elastic fibers are thought to create the slope within the “toe” or transition regions of the curve (Fig. 1-2).²² Lysyl oxidase, a crosslinking enzyme in collagen fiber formation, is also involved in crosslinking elastic fibers.²⁹

iii. Proteoglycans and Glycosaminoglycans

PGs and GAGs have multiple roles in connective tissues including providing hydration, compliance, viscosity, regulation of collagen fibrillogenesis, and prevention of calcification and thrombogenicity.³⁰⁻³² PGs contain a core chain of protein and chains of GAGs covalently attached to that core protein like the bristles of a bottle brush (Fig. 1-3).³²



Pearson Education, Inc.; www.dentistry.leeds.ac.uk/~thcme/glycans.html

Fig. 1-3: Structure of PGs and GAGs. The nomenclature to describe GAGs is complex. The terms “iduronate” and “glucuronate” are based on the susceptibility to digestion by various enzymes. The term dermatan sulfate is used whenever there is any iduronate present. If the GAG contains glucuronate alone, it is referred to as chondroitin sulfate.

PGs as a family are quite diverse. The protein cores size range from 10 kDa to 400,000 kDa.³³ Some are soluble, others are insoluble, some are membrane-spanning, others lipid-tailed, and others secreted.³³ Even the number of GAG chains can vary substantially, from one to one hundred.³³ PGs are divided into many different families. The small, leucine-rich interstitial matrix PGs include decorin, biglycan, fibromodulin, and lumican, among others. The large CS PGs include aggrecan, versican, neurocan, and brevican, and the cell surface PGs include syndecans and glypicans. There are also the basement membrane PGs perlecan and agrin.³³ However, the predominant PGs found in heart valves are versican, decorin, and biglycan; therefore, these PGs are discussed in more detail in the following sections.

Versican, with its large hydrodynamic domains, contributes to tissue's material properties of viscoelasticity and turgidity (including providing resistance to compression).^{34, 35} Versican remains at the cell surface via interaction with HA³⁶ where it contributes to the pericellular matrix and plays a role in cellular interactions.³⁴ Versican appears to play a critical role in cell migration during development and diseased states by creating an expanded nonfibrillar extracellular space.³⁴ Evidence also suggests that versican plays an active role in elastin formation by its interaction with the microfibril components fibulin and fibrillin-1.^{37,38}

Decorin was identified years ago “decorating” collagen at the d band.^{39, 40} It is now known that decorin and biglycan play key roles in collagen fiber formation, as evidenced by mutant animals showing severe defects in collagen fiber formation and packing.⁴¹ Indeed decorin shows strong association with collagen type I/III in the collagen bundles.³⁵ Both decorin and biglycan are from the same family of small leucine

rich PGs, and both are seen widely in connective tissues.³⁴ The leucine rich repeat regions that make decorin and biglycan unique are important in mediating protein-protein interactions, specifically interactions with other matrix proteins, including collagens, fibronectin, elastin, and thrombospondin, as well as play a part in matrix assembly and fibrillogenesis.³⁴ Evidence also suggests that both decorin and biglycan can modify the response of cells to growth factors, like transforming growth factor-beta (TGF β) and epidermal growth factor.³⁴ Despite the similar roles and structures of decorin and biglycan, each is unique. Decorin is found more extracellularly attached to collagen I, while biglycan is found closer to the cell.⁴² Not only do they show different expression patterns, but they are differentially regulated.³⁴ For example, TGF β tends to downregulate decorin in a number of cell types while it strongly upregulates biglycan.⁴³⁻⁴⁹ It has been suggested that decorin may play an important role in interacting with versican to produce the ultrastructure of collagen within soluble ECM.³⁵

The basic structure of GAGs is relatively simple. GAGs are composed of repeating disaccharides of uronic acid and an amino sugar. GAGs become complex and diverse in their post-translational modifications that occur throughout the GAG chain. Hyaluronan (HA), as a GAG, is unique in that it does not attach to a protein core and has no modifications.⁵⁰ HA polymers can be extremely long, with molecular masses in the millions.⁵⁰ Although HA does not attach to a core protein, it can aggregate with other PGs.⁵⁰ HA is prevalent in the heart valve where it is primarily localized to the spongiosa layer. HA has many roles in a variety of areas, including in embryonic development, tissue organization, wound healing, angiogenesis, tumorigenesis, and cell adhesion and mobility.⁵¹⁻⁶² HA also has important mechanical functions. HA bears compression as

well as lubricates articulating surfaces in the body.⁶³ The role of HA in tissue organization is via cell-surface receptors CD44 and “receptor for HA mediated motility” RHAMM.⁶³ More recent studies in HA metabolism show that there is a receptor involved in HA clearance named “HARE” (HA receptor for endocytosis), which among other locations in the body, is expressed in heart valves.⁶⁴

iv. Matrix Metalloproteinases

The matrix metalloproteinases (MMPs) are a family of enzymes predominantly responsible for matrix degradation. The specificity of each MMP is unique, although there is a large amount of overlap; a partial compilation of MMPs, those relevant to this thesis, and their substrates are included in Table 1-1. MMPs have been found to have a number of important roles in health and disease in a variety of tissues. Pressure induced heart failure has been linked with a number of MMPs including 1, 2, 3, 9, 13, and 14, and expression increases as heart failure worsens.⁶⁵ Similarly in aortic stenosis studies have demonstrated an increase in MMP2, 3 and 9, and tissue inhibitor of MMP2.^{66,67}

Table 1-1: MMP 1, 2, 9, and 13 Specificity.

MMP	Alternate Name	ECM Substrates
MMP1	Interstitial collagenase	Collagens I, II, III, VII, X, XI; versican, aggrecan, fibronectin, vitronectin, laminin, entactin, tenascin, gelatin, myelin basic protein, link protein
MMP2	Gelatinase A	Collagens I, II, III, IV, V, VII, X, XI; versican, aggrecan, fibronectin, vitronectin, laminin, entactin, tenascin, gelatin, elastin, myelin basic protein, link protein, SPARC, galectin-3
MMP9	Gelatinase B	Collagens IV, V, XI, XIV; versican, decorin, aggrecan, vitronectin, laminin, gelatin, elastin, myelin basic protein, link protein, SPARC, galectin-3
MMP13	Collagenase 3	Collagens I, II, III, IV, VI, IX, X, XIV, collagen telopeptides; aggrecan, fibronectin, large tenascin-C, gelatin, perlecan

Adapted from Crit Rev Oral Biol Med 12(5): 373-398.⁶⁸ Highlighted and bolded substrates indicate matrix components that have been stained for in the studies that comprise this thesis.

D. Characterization of Adult Valves in Health and Disease

i. Valvular Interstitial Cells (VICs) and Cell Phenotype

It was not until recently that researchers discovered the importance of the cells within these histologically defined valve layers, cells called “valvular interstitial cells” or VICs. Not only do the VICs produce the collagen, elastin, PGs, and GAGs that comprise the extracellular matrix, but they produce cytokines and chemokines, modulate the immune response, and produce matrix MMPs that break down and remodel the matrix, and in so doing release growth factors within the matrix.⁶⁹

VICs are a heterogeneous population comprised of cells with a range of cell phenotypes, some of which appear more fibroblast-like and some of which appear more myofibroblast-like.⁷⁰ The more fibroblast-like cell population consists of spindle-shaped, elongated cells, that once confluent exhibit a swirling pattern and pile on top of each other, features characteristic of fibroblasts.⁶⁹ These cells contain organelles predominantly for matrix synthesis and secretion.⁶⁹ Correspondingly, they express prolyl 4-hydroxylase (P4H), which indicates active collagen synthesis.⁶⁹ Another VIC population consists of cuboidal cells that displays prominent stress fibers, and accordingly expresses smooth muscle alpha-actin (SMaA).⁶⁹ Besides these two groups of VICs, smooth muscle cells are found within valves either alone or in small bundles.⁶⁹ It is not clear how or by what means these phenotypes are genetically or otherwise determined by the body.

Understanding the unique phenotype of VICs is important with respect to understanding valve disease, as well as manipulation of cell sources for use in tissue

engineering (the topic of cell sources in tissue engineering is discussed below). There are a number of methods for studying cell phenotype, the most common being immunocytochemistry (ICC) and flow cytometry (FC). One of the challenges of investigating cell phenotype in VICs is that these techniques require some period of time in cell culture before testing can occur. Depending on the different environments these cells are put in, their phenotype may be altered during this time.

With these limitations on the techniques in mind, much has been reported regarding cell phenotype, although the results often do not agree. Latif et al. took valve cells from three humans (ages 50-60 years old) and tested these cells (all four valves together) using ICC.⁷¹ Those authors found a >90% prevalence of fibroblast surface antigen (FSA) expression, 50-100% SMAA expression, <2% desmin expression, and highly variable expression of smooth muscle myosin (SMM) expression.⁷¹ In a second study Latif et al. reported on a number of additional markers on these set of valve cells.⁷² By ICC they reported myosin heavy chain (MHC) I expression in almost all VICs, while variable expression of MHCII.⁷² SMM and desmin were expressed by low numbers of cells, while vimentin showed strong, uniform expression.⁷² Fibronectin was found to stain strongly surrounding the cells.⁷² In a similar study Rabkin et al. looked at the cell phenotype of human valves (all four valves considered together) using ICC.⁷³ Those authors found that normal human VICs were negative for expression of SMAA, SMM, vimentin, and MMP13.⁷³ These results clearly contradict those of Latif et al.

Dreger et al. compared the four different valves' cell phenotype in human VICs.⁷⁴ They found that MMP2 was expressed only in the AV and PV, MMP3 and 9 were not expressed in any valves, TIMP1 and 2 were expressed in all valves, and TIMP3 was only

expressed in the TV.⁷⁴ In a similar study in which Della Rocca et al. used immunohistochemistry (IHC) and western blot analysis to compare AV and PV cell phenotypes, they reported increased vimentin and expression in AV compared to PV detected by IHC.⁷⁵ They also reported a sparse population of SMaA and SMM positive cells only on the outer edge of the fibrosa.⁷⁵ Analysis by western blot showed that AV and PV had equal amounts of vimentin and non-muscle myosin, while AV had increased amounts of SM α A and both AV and PV were negative for SMM and the related smooth muscle specific protein 22.⁷⁵ In a third study, Taylor et al. used ICC and IHC to look at human VICs from each valve.⁷⁶ They found that vimentin was expressed by almost all VICs, desmin by 1.3 \pm 2.3% of AV, and SMaA by 78 \pm 28% of AV and 66 \pm 33% of MV.⁷⁶ Expression of SMM was found to be 4 \pm 6%, with no detectable difference between valves.⁷⁶ Their results using IHC showed SMM, SMaA, FSA, and vimentin expressed by almost all VICs, while P4H and desmin expressed by few.⁷⁶ The VICs in culture were found to express less SMM, P4H, and FSA.⁷⁶

While these studies have not come to a consensus as to the specific expression profiles of VICs from different valves, as a whole this body of work supports the notion of multiple subpopulations of VICs within valves. Studies in diseased valves have demonstrated enrichment of certain VIC subpopulations, such as the VIC myofibroblast,⁷³ that are thought to play a role in pathogenesis of these valve diseases. Future studies further elucidating these VIC subpopulations and their expression profiles both in normal and diseased valves, as well as techniques allowing the isolation of these subpopulations, will likely yield insight into the pathogenesis of these valve diseases.

ii. Mechanical Characterization of Valves

Different parts of the valves experience different loading patterns and appear to have different functional roles. For example, in the mitral valve the chordae and central region of the anterior leaflet experience tension, while the free edge of the anterior leaflet and the majority of the posterior leaflet predominantly experience compression.¹⁶ The physical loads on the three layers are complex. In the aortic valve the fibrosa and ventricularis are inherently preloaded, due to their attachment to each other.¹⁹ The fibrosa is under compression and the ventricularis under tension.¹⁹ Studies suggest that in the aortic valve the collagen in the belly of the cusp experiences the membrane stresses, “collects” them, and distributes them to the aortic wall via branching chords of collagen.¹¹ The belly of the cusp contains a nearly isotropic mesh of collagen that is held in a crimped conformation via connections to the ventricularis, causing the collagen to be under axial compression.¹¹ Vesely et al., in analyzing the collagen bundles, found that about half of these collagen bundles are highly branched, contributing to stress distribution, while the other half span the entire length of the cusp without branching.¹¹ Elastin is found within the aortic valve in the form of a continuous amorphous sheet that often transitions to a network of fibers.¹¹ This elastin appears to store energy during diastolic loading, and then uses the stored energy to return the collagen, when unloaded, to its crimped conformation.¹¹ It is believed that the spongiosa acts as a buffer zone and enables shearing between the ventricularis and fibrosa as the valves open and close.¹¹ In modeling the forces and stresses on the valves and the mechanical responses of valves, it is clear that the unique properties of valves are, in part, due to the multilayered nature of the valve and the crimped collagen configuration within the fibrosa layer.⁷⁷

The material properties of valves, such as ultimate tensile strength, Young's modulus, and viscoelasticity, have been predominantly assessed using either biaxial or uniaxial tensile testing of tissue. This mechanical testing has revealed a number of differences between the material properties of the different valves and valve regions. In pig, Christie et al. found that PV and AV had similar mechanical properties in the circumferential direction, but that the PV was more extensible in the radial direction.⁷⁸ In human valves, Stradins et al. found that the ultimate stress in the radial direction for AV and PV were nearly equal, while ultimate stress in the circumferential direction was higher in PV.⁷⁹ Comparison of AV and PV mechanical properties has also been assessed within a pulsatile flow simulator.⁸⁰ In this study PV were found to be more compliant than AV under systemic pressures, as well as had a smaller pressure drop, suggesting that PV can mechanically withstand systemic pressures and under those conditions may even perform better.⁸⁰ Others have exposed porcine PV to aortic pressures to see how the tissue would respond and found that PV responded by increasing collagen content as well as sulfated GAGs.⁸¹ Differences in the mechanical properties between the different leaflets of the MV have also been demonstrated. Using uniaxial tensile testing Kunzelman et al. demonstrated that the posterior leaflet of the MV was not as stiff circumferentially or radially compared to the anterior leaflet.⁸²

iii. Valve Composition and its Mechanical Environment

The valve undergoes dynamic, regionally heterogeneous mechanical loading, and studies have demonstrated that regional valve composition appears to be related to that local mechanical environment. For instance, the mitral valve is known to have distinct

loading patterns among the different valve regions. When the valve is closed, the central region of the anterior leaflet and chordae experience tension, while the free edge of the anterior leaflet and most of the posterior leaflet are under compression.¹⁶ Appropriately, the chordae and anterior center region of the anterior leaflet contain the most collagen.¹⁷ In the compressive regions, the free edge of the anterior leaflet and the majority of the posterior leaflet, the collagenous layer is thinner and the spongiosa layer is thicker.¹⁶ Furthermore, these regions differ in collagen fiber alignment. The center of the anterior leaflet of the mitral valve and the chordae tendinae contains more highly aligned collagen,^{83, 84} whereas the posterior leaflet and free edge of the anterior leaflet demonstrate less collagen fiber alignment.¹⁷ These different regions were also found to have different PG and GAG content. The regions of tension were found to contain less water, less hyaluronan, and iduronate.¹⁶ These GAGs likely are part of the small PGs decorin and biglycan, which were found to be prominent in these regions.¹⁶ In contrast, areas of compression, such as posterior leaflet and the free edge of the anterior leaflet, had significantly more water, more hyaluronan, and more glucuronate.¹⁶ These GAGs are likely part of versican, a large PG that binds a particularly large amount of water.¹⁶ This study also demonstrated a significant decrease in GAGs with age.¹⁶

GAG composition in the MV has also been shown to change during disease. Studies of myxomatous mitral valves found that the chordae in particular had a different biochemical composition as compared to those of healthy mitral valves.³¹ The chordae were found to have 3-9% more water content and 30-159% higher concentrations of GAGs mostly due to increased hyaluronan and chondroitin-6-sulfate.³¹ It is thought that this elevation in GAGs and deficiency in elastin in the chordae may cause the mechanical

weakness of the valves that results in valve prolapse in myxomatous mitral valve disease.³¹

iv. Valve Changes in Mitral Regurgitation

Mitral regurgitation (MR) has been the subject of many adult valve studies. However, this disease often appears in the context of dilated cardiomyopathy and heart failure which has made understanding MR and the role of the valve in MR quite complex. For many years MR in the context of heart failure has been considered a functional problem. That is, the valve is thought to be normal, but the ventricle has been distorted in such a way as to prevent adequate valve coaptation. However, Timek et al. found changes in the MV in an animal model of dilated cardiomyopathy, a type of functional MR.⁸⁵ The anterior leaflet lengthened significantly in the free-edge region.⁸⁵ The posterior leaflet showed a significant decrease in curvature once functional MR was created.⁸⁵ In a related study, MVs from patients with functional MR and heart failure were found to have greater DNA and collagen content, particularly in the free edge, compared to controls.⁸⁶ Altered material properties were also demonstrated in these valves, including a 61% decrease in stiffness in the radial direction and 50% decrease in stiffness in the circumferential direction compared to control valves.⁸⁶ In total these studies show that the valve itself is altered in functional MR.

Similarly, Kunzelman and Quick specifically looked at collagen concentration in hearts with coronary ligation (“ischemic controls”) and papillary infarct which created ischemic regurgitation.⁸⁷ Collagen content was then analyzed and found to be the greatest percentage of dry weight in the normal leaflets, lower in the ischemic controls,

and further lowered in the papillary infarct group.⁸⁷ The collagen content was also found to be the highest in the center of the leaflet and decrease towards the commissures.⁸⁷

v. Valve Response to Acute Injury

Studies examining the response of the valve to acute injury have been largely limited to pathological characterization of the wound area. In a study of a slice wound in the free edge of the MV, Tamura et al. characterized two types of granulation tissue, one which was myxoid and one which was fibrous.⁸⁸ During the wound healing process they reported that fibroblasts first migrate into the wounded region and then differentiate into myofibroblasts with SMaA expression.⁸⁸ In this study Movat, Masson, and hemotoxylin and eosin stains were used to analyze the changes in the tissue during the wound healing process, along with immunohistochemistry for SMaA.⁸⁸ In a second study Tamura et al. looked at the response of the mitral valve to sutures.⁸⁹ In this study they found thrombi covering the atrial surface and a fibrous neointima covering the ventricular surface starting at 2 weeks.⁸⁹ They reported that healing was slow, particularly at the free edge in which it took 12-16 weeks for a fibrous sheath to cover the sutures (vs. 4 weeks in the basal region).⁸⁹ Two other studies worth mentioning related to wound healing in the valve are studies by Durbin and Lester. Durbin et al. studied valve injury using an *in vitro* model in which they scraped a line through a monolayer of VICs in culture, and then measured migration of the different VIC subtypes.⁹⁰ In this experiment they found that the spindle-shaped VICs tended to migrate the most quickly while the cobble-stone shaped cells acted to synthesize matrix for the “wound.”⁹⁰ Durbin and others have also researched the cell signaling involved in the healing process, including the importance of nitric oxide.⁹¹ Lester et al. specifically looked at the response of the anterior leaflet of the

MV to denudation injury using pieces of valve incubated in a Petri dish for 6 days.⁹² In this study the authors found that valve cells on the ventricular side of the injured leaflet grew into the wound more rapidly than those on the atrial side, for reasons that are unknown.⁹² The role of inflammation and valve injury has also been extensively investigated in the context of chronic valve diseases, for instance inflammation has been implicated to be important in the development of calcific aortic stenosis.⁹³⁻⁹⁵

E. Changes in Valves with Development and Aging

i. Histology and Biochemistry

Aikawa et al. has done the most work on characterizing the human heart valve matrix from the fetus to the adult. In their work they studied semilunar valve structure, the phenotype of valvular interstitial and endothelial cells, and histology for a number of matrix components.⁹⁶ They documented a transition from a largely amorphous GAG-rich matrix to a trilaminar structure at 36 weeks.⁹⁶ Valves at birth appeared rudimentary compared to adult valves, indicating that significant postnatal development occurs. Collagen content increased through fetal development, but then was found to remain relatively constant during the postnatal period. During postnatal development there was a decrease in thin collagen fibers, an increase in thick collagen fibers, and an increase in collagen fiber alignment. Elastin content was found to increase postnatally. VIC cell density was found to decrease rapidly from fetal to adult valves. The fetal VIC cell phenotype was more myofibroblast-like with more activation (seen by expression of SMAA and embryonic myosin heavy chain) and expression of proteolytic enzymes

(including MMP13) relative to postnatal VICs. Analysis of the neonatal valve showed an increase in cell activation of AV cells compared to PV, as the AV adjusted to the higher pressures of the postnatal circulatory system.⁹⁶

Valve development has been studied in depth in both the mouse and avian animal model. Kruithof et al. observed endocardial cushion growth, valve formation, and valve condensation in the mouse.⁹⁷ Changes that were apparent during the perinatal time period include a decrease in alcian blue staining mucopolysaccharides and a decrease in the PG versican.⁹⁷ Specifically, versican was observed homogenously throughout the leaflet before becoming restricted to the atrialis starting at in the early postnatal period.⁹⁷ Collagen I and V staining was diffuse in the embryonic period and became localized to the ventricularis after birth.⁹⁷ In contrast, collagen VI was constant in the entire leaflet with age.⁹⁷ Others have demonstrated that the two most abundant components of endocardial cushions are versican and hyaluronan,^{98, 99} and in fact that versican is necessary for endocardial cushion formation.⁹⁹

In the studies of valve development in the avian model by Hinton et al., they found elastin appearing late during cusp remodeling, along with collagen in the fibrosa and elastic fiber fragments in the ventricularis.¹⁰⁰ The PG aggrecan was expressed during cushion elongation, and present in the fibrosa and spongiosa during cusp remodeling.¹⁰⁰ Distinction of the fibrosa and spongiosa layers was evident late in the embryonic period just before birth.¹⁰⁰

While histology of matrix components has been looked at to some degree in human semilunar valves⁹⁶ they have not been examined in the pig, a common animal model for human heart valve biology and disease. Furthermore, the studies in valve

development performed in other species concentrated on aspects of valve development distinct from the aspects in this proposal. Kruithof et al. concentrated on endocardial growth, valve formation and valve condensation, all events very early in valve development.⁹⁷ The mouse studies of Hinton et al. also focused on valve condensation along with valve remodeling that occurs later in fetal development.¹⁰⁰ Beyond these studies in semilunar valves, little has been done in the atrioventricular valves during development.

Early investigations into changes in valves with aging depended on basic histology and biochemistry. While the results have not been unanimous, certain age-related changes have been agreed upon. Multiple studies have found an increase in collagen crosslinking with age, first detected by increased digestion time.^{101, 102} Fibrosity has been found to increase with age but so does collagen fiber degeneration.²⁷ Some have described aged collagen fibers as more “smudgy,” swollen, and disoriented.¹⁰³ More recent studies reported that large diameter collagen fibers become larger with age.⁹⁶ A consensus as to the total amount of collagen changing with age has not been made. Keller and Angrist reported an increase in the total amount of collagen fibers,^{21, 102} while Bashey et al. demonstrated reduced collagen concentration accompanied by a reduction in the total amount of protein.¹⁰¹ Elastin content has generally been reported as increasing with age,^{27, 96, 103} although some have reported this increase to be slight, and even negligent in the AV.¹⁰¹ In terms of GAG content, Sell and Scully reported a decrease in acid mucopolysaccharides from the 3rd to 5th decade,¹⁰³ while McDonald et al. reported an increase with age, specifically in the spongiosa, especially the distal portion.²⁷

ii. Mechanical Properties

Assessment of age-related changes in the mechanical properties of valves has largely been overlooked, with the exception of a study by Christie et al. in which failure strain was measured for different aged human AV.¹⁰⁴ In this study they found that the radial failure strain in AV was ~80% in the 15 years-old young adult, but that failure strain decreased by ~4% per year such that at 25 years-old the stretch was 40%.¹⁰⁴ From there the extensibility remained constant until age 40 years-old at which the stretch began to decrease by 1% per year at least until age 58 years-old.¹⁰⁴ The authors attributed the decrease in stretch from age 16 years-old to 25 years-old to the fact that the area of the leaflets is not changing, but there is an increase in the luminal diameter.¹⁰⁴ The authors reasoned that the leaflets respond by remaining more stretched.¹⁰⁴ However, other than this study, age-related changes in mechanical properties of valves have not been addressed.

F. Tissue Engineering Heart Valves

i. Design Criteria

The characteristics desired of a tissue engineered valve include: 1) simulate native valve motion as closely as possible, most importantly not obstructing blood flow during opening and closing quickly after blood entry without leaking; 2) not adversely interact with the blood, such as inducing infection or thrombosis, or lysing red blood cells; 3) demonstrate structural and material stability, i.e., a durable, long-lasting, chemically inert

device that integrates with native tissue; 4) easily implantable; 5) remodel in response to changing mechanical demands, including growth for tissue engineered heart valves used in pediatric patients.¹⁰⁵ In order to accomplish this several general strategies are being used. Some have tried using cells that are not cardiac derived and using biological and mechanical stimuli to induce proper differentiation and organization into valves. Others propose using only the native valve cells in the tissue engineered valve, and speculate that by their inherent nature these cells will properly organize themselves. Still others propose simply inserting a scaffold and allowing the patient's own cells to seed the scaffold and form a valve *in vivo*. This has been done with acellularized human valves.¹⁰⁶ Proposals addressing the layered complexity of valves include assembling building blocks such as branched collagen, elastin sheets and tubes, and hydrated GAG matrix.¹¹

ii. Cell Sources

While some scientists focus on recreating the mechanical environment in which valves reside via complex bioreactors, others focus on potential cell sources (Table 1-3). As mentioned above, some scientists are proponents for using valve cells, while others have searched for other cell types that can be easily manipulated to behave like valve cells. A wide variety of cell types have been assessed for their potential use in a tissue engineered heart valve and include mesenchymal stem cells,¹⁰⁷ radial artery cells,¹⁰⁸ stromal cells,¹⁰⁹ bone marrow cells,¹⁰⁹ valve cells,¹¹⁰ chorionic villi-derived cells,¹¹¹ and femoral artery myofibroblasts.¹¹² A number of other cell types have been used for vascular engineered tissues, and have the potential to be used in a tissue engineered heart valve.¹¹³ An additional complexity to the cell source problem is the heterogeneity of

cells within the native valve; the native valve contains VICs (including subpopulations that are myofibroblast-like), endothelial cells, as well as smaller populations of smooth muscle, cardiac muscle, and nerve cells.¹¹⁴ Methods such as sequential seeding can be used to partially re-create the cellular heterogeneity present in native valves. For example, Rothenburger seeded myofibroblasts on scaffolds and then added endothelial cells.¹¹⁵

Table 1-2. Pros and Cons of Different Cell Sources Used in Tissue Engineering.

Cell Sources	Pros	Cons
VICs	Inherent properties to create proper matrix	Autologous VICs couldn't be used in CVD patients; difficult to harvest
Dermal fibroblasts	Autologous cells could be used in CVD patients; easy to harvest	Require conditioning to create proper valve matrix; concern long-term maintenance of proper phenotype
Stem Cells	Autologous cells could be used in CVD patients	Require conditioning to create proper valve matrix; tumorigenic potential; concern long-term maintenance of proper phenotype; bone marrow stem cell harvest painful

Adapted from J Biomed Mater Res B Appl Biomater 83(1): 16-43.¹¹⁶

iii. Scaffolds and PEG Hydrogels

The scaffold in engineered tissues has several functions. First it provides a means for transplantation of a large number of cells. This type of cell delivery can be considered, in and of itself, a “drug delivery” system,¹¹⁷ but growth factors or other biologically active agents can also be attached and/or released from the scaffold. Secondly, the scaffold acts as a three dimensional space in which the cells can grow. As such it can also provide structural cues for directed growth.¹¹⁷

The material composition of the scaffold is particularly important (Table 1-3). Some propose an acellular scaffold with or without fixation,¹¹ however one of the challenges with these acellular scaffolds is the complete and non-destructive removal of all cells to minimize the immunogenicity of the scaffold. The main disadvantage with this approach is that because the result scaffold is acellular, it does not allow for cell-mediated remodeling or repair.¹¹⁸ Others propose a natural scaffold, such as a scaffold constructed from collagen, i.e., a collagen “sponge,”¹¹⁹ or even dura mater¹²⁰ or small intestinal submucosa.¹²¹ Others propose using natural components formed into a tissue engineered construct; hyaluronan,¹²² fibrin,¹²³ and collagen¹²⁴ have been utilized in this manner. Some propose a degradable scaffold, made of either natural or synthetic components, so that the scaffold is gradually replaced by the patient’s own tissue.¹¹ This

Table 1-3. Pros and Cons of Different Scaffolds Used in Tissue Engineering.

Scaffolds	Pros	Cons
Natural Matrices	3D matrix architecture, anisotropic material properties, bioactive cues	Variability, ill-defined, tuning properties difficult, immune concerns
Natural Components	More control over composition, reproducibility than natural matrices	Lack inherent 3D matrix structure, endogenous bioactive cues, regional heterogeneity, anisotropy, difficult to control degradation rate
Synthetic	Reproducible; tunable material properties, bioactive components, degradation rate; can be made responsive to environment	Lack inherent 3D matrix structure, endogenous bioactive cues, regional heterogeneity, anisotropy, potential toxic metabolites with degradation

Adapted from J Biomed Mater Res B Appl Biomater 83(1):16-43.¹¹⁶

decreases the time the immune system must battle a foreign object as well as allows for growth and remodeling.¹¹⁹

Hydrogels are an expanding topic in the field of tissue engineered scaffolds with numerous advances making them an increasingly more attractive option. Poly(ethylene glycol) (PEG) hydrogel scaffolds are extremely hydrophilic, which prevents protein adsorption, a critical step in the immunogenicity and degradation of bioprosthesis.¹²⁵ Furthermore, these scaffolds are also highly permeable allowing the exchange of nutrients and waste materials.¹²⁶ One of the factors that makes these gels particularly attractive is the ability to custom tailor them by conjugating various peptides, including cell ligands and growth factors, to the PEG backbone. This capability can allow for selective adhesion of particular cell types, manipulation of cell phenotype, as well as enhancement of various tissue processes such as angiogenesis or tissue remodeling. This “biofunctionality” makes PEG hydrogels ideal for the tissue engineering of heart valves. In the case of valves, this technology would be optimal if a ligand for VICs was attached to these hydrogels, allowing VICs to populate the scaffolds without other proteins or cells invading. Different growth factors could also be attached in order to encourage both growth and a specific cell phenotype. Furthermore, these hydrogels can be made with enzyme degradable sequences in their polymer backbone allowing the scaffold to be degraded as the scaffold becomes populated (and as the cells’ own secreted enzymes degrade the scaffold).¹²⁷ With careful design the number of degradable sequences within the hydrogel could be generated such that the scaffold would only begin to be degraded once the seeded cells produced enough matrix to withstand its mechanical environment on its own. In that manner a patient would have foreign material in his or her body for a

limited amount of time, decreasing any immune response. A recent advance in this area is the encapsulation of cells within the PEG scaffold¹²⁸ utilizing a polymerization method that does not damage the cells.¹²⁹ The key advantage here is the homogeneous distribution of cells throughout the scaffold. In the traditional technique of seeding cells onto scaffolds, the ultimate cell density throughout the scaffold is highly variable. Various techniques, such as serum deprivation¹³⁰ and bioreactors,¹³¹ have been used to improve these results, but using encapsulated cells ensures a homogeneous distribution of cells.

Various combinations of cell sources and scaffolds have been tested, both within *in vitro* and *in vivo* settings, in tissue engineering. A few, with particular attention paid to tissue engineered heart valve applications, are outlined in Table 1-4.

iv. Challenges

Heart valves are among the most complex connective tissue structures in the entire body.¹⁶ As the field of tissue engineering works to create valves, it faces the difficulties presented by this complexity on multiple levels. At a macroscopic, tissue level, it is believed that the spongiosa acts as a buffer zone and enables shearing between the ventricularis and fibrosa as the valves open and close.¹¹ In modeling the forces and stresses on the valves and the valves mechanical responses, it is clear that the unique properties of valves are, in part, due to its multilayered nature and the folded configuration of the fibrosa.⁷⁷ Therefore, it appears including this macroscopic heterogeneity in a tissue engineered heart valve would be important for proper valve mechanics.

Table 1-4. Examples of Different Scaffolds and Cells Used in Tissue Engineering.

<u>Natural Components</u>				
	<u>Reference</u>	<u>in vivo?</u>	<u>TEHV?</u>	<u>Cell Source</u>
Hyaluronan	Masters, 2004 ¹²²	no	yes	Porcine VICs
Fibrin	Robinson, 2008 ¹²³	no	yes	Human dermal fibroblasts
Collagen	Butcher, 2004 ¹²⁴	no	yes	Porcine VICs
Combination, i.e., Collagen-HA	Hahn, 2006 ¹³²	no	no	Porcine vocal fold fibroblast cells
<u>Natural Matrices</u>				
	<u>Reference</u>	<u>in vivo?</u>	<u>TEHV?</u>	<u>Cell Source</u>
Small intestinal submucosa (SIS)	Cimini, 2005 ¹²¹	no	yes	Human neonatal dermal fibroblasts
Decellularized valves	Steinhoff, 2000 ¹³³	yes (ovine PV)	yes	Ovine carotid artery endothelial cells and myofibroblasts
Collagen sponge	Taylor, 2002 ⁷⁶	no	yes	Human VICs
<u>Synthetic</u>				
	<u>Reference</u>	<u>in vivo?</u>	<u>TEHV?</u>	<u>Cell Source</u>
PEG (-meth HA)	Cushing, 2007 ¹³⁴	no	yes	Porcine VICs
PVA	Martens, 2003 ¹³⁵	no	no (cartilage)	Bovine chondrocytes
PHA	Sodian, 2000 ¹³⁶	yes (ovine PV)	yes	Ovine jugular vein and endothelial cells
PGA	Hoerstrup, 2000 ¹³⁷	yes (ovine PV)	yes	Ovine carotid artery and endothelial cells
PGA, PLGA	Sutherland, 2005 ¹³⁸	yes	yes	Ovine BMSC
OPF	Guo, 2010 ¹³⁹	yes (rabbit osteochondral defect)	no (rabbit osteochondral defect)	Rabbit BMSC
Electrospun PEUU	Stella, 2008 ¹⁴⁰	no	yes	Rat vascular SMCs

Adapted from J Biomed Mater Res B Appl Biomater 83(1):16-43.¹¹⁶ TEHV=tissue engineered heart valve; VICs=valvular interstitial cells; HA=hyaluronan; PV=pulmonic valve; PEG=poly(ethylene) glycol; -meth HA=methacrylated HA cross-linked into the PEG hydrogel; PVA=poly(vinyl alcohol); PHA=poly(hydroxyalkanoate); PGA=poly(glycolic acid); PLGA=polylactide-co-glycolide; OPF=oligo (PEG) fumarate; PEUU=poly(ester urethane) urea; BMSC=bone marrow stem cells; SMC=smooth muscle cells.

There is also complexity in the valve at the cellular level. Not only are there a number of cell types within the valve, but the predominant valve cell type, the VIC, is a heterogeneous population. Work is on going to elucidate the VIC subpopulations and their roles in valve health and disease. Undoubtedly it will be important to take into consideration this heterogeneity in the tissue engineering of a valve. Very few groups have included these important VICs in their tissue engineering design, which appears to be a major oversight¹¹ considering their role in producing and maintaining the extracellular matrix of the valve which is essential for proper valve function.⁶⁹ While effort is ongoing in developing a tissue engineered heart valve, the structure, mechanics, and pathology of the native valve must be better understood before an adequate tissue engineered heart valve can be made.

G. Summary

i. Synopsis of Previous Work

Undoubtedly much has been learned in the last several decades in terms of heart valve biology, mechanics, and the pathophysiology of various valve diseases. These studies have revealed that the valve is not simply a passive flap at the mercy of the changing pressures and flow patterns within the heart, but instead a complex structure that actively remodels in response to its environment. These previous studies have shown the intricate valve microstructure and how that impacts its mechanical properties, the importance of VICs within the leaflet, and the role of the extracellular matrix, among other key findings. While these previous studies have laid important groundwork, a

number of questions remain unanswered. These studies have primarily been carried out in adults, however, valve diseases affect patients of all ages and potentially tissue engineered heart valves could be utilized in a wide range of ages. If there are age-specific considerations, these remain to be explored more thoroughly. Additionally, these studies largely have not considered regional valve heterogeneity or heterogeneity within the VIC population. Furthermore, while considerable work has been performed in creating scaffolds and bioreactors for a tissue engineered heart valve, the effect of scaffold mechanical properties on the VICs themselves has not been considered. These are some of the unanswered questions to be addressed by this thesis.

ii. Thesis Motivation, Scope, and Structure

The overarching goal of this body of work was to gain a better understanding of heart valves in health and disease for the design of an age-specific tissue engineered heart valve. In accordance with this goal, the various studies which compose this body of work can be divided into three main categories, those which address 1) the characterization of normal valves, especially aspects related to aging and valve heterogeneity; 2) characterization of valves in disease states including congenital valve disease, myxomatous mitral valve disease, dilated cardiomyopathy and “functional” mitral regurgitation, iatrogenic valve wounds, and calcific aortic valve disease; and lastly, 3) preliminary attempts at tissue engineering such a valve using PEG hydrogels.

The motivation for this work largely stemmed from the need for a tissue engineered heart valve to replace the current inadequate treatments for pediatric valve disease. The literature lacked information required for the development of design criteria

for such a tissue engineered heart valve, including material properties and matrix composition of different aged heart valves, as well as compositional and cellular heterogeneity within valves that may need to be incorporated into a tissue engineered heart valve design. This led to Specific Aim 1 of this thesis' proposal, which was the characterization of porcine valve throughout development and aging using immunohistochemistry, fluorophore-assisted carbohydrate electrophoresis, and mechanical testing (Chapters 3, 4, 7). However, since the initial proposal, this original specific aim has been expanded to also include studies regarding valve compositional changes during the perinatal period (Chapter 5) and heterogeneity in AV regional composition in elderly valves (Chapter 6). The specific aim has also been further expanded to include studies related to heterogeneity in valve composition and motion (Chapters 8, 9) and cellular heterogeneity in the valve (Chapters 10, 11).

Therefore, in this expanded portion of the thesis addressing normal valve mechanobiology, the chapters are grouped into those assessing age-related changes in normal valves, those analyzing valve heterogeneity, and finally cell-matrix interactions in the normal valve. First among the studies analyzing valve aging are included compositional and structural analyses of fetal and postnatal aging (Chapters 3 and 4), perinatal changes (Chapter 5), regional compositional heterogeneity of elderly valves (Chapter 6), and postnatal aging with respect to material properties and relationship to composition and structure (Chapter 7). The studies of normal valve heterogeneity include analyses of composition and motion of the mitral annulus (Chapter 8) and mitral leaflets (Chapter 9) and studies related to heterogeneity in VICs, specifically the

development of a method to isolate the myofibroblast-like VIC subpopulation (Chapter 10) and functional characterization of that subpopulation (Chapter 11).

In the process of developing a tissue engineered heart valve, it is important to define both positive and negative design criteria. Furthermore, characterization of congenitally diseased valves may also lead to insight into pathogenesis and possible novel treatment strategies for this debilitating disease. Therefore, Specific Aim 3, as originally stated in this thesis' proposal, was to characterize altered matrix composition and hyaluronan metabolism in pediatric pathological valves. However, since that time, this portion of the thesis has been greatly expanded to include a number of valve diseases as well as encompass Specific Aim 4 from the original thesis proposal, which was to study valve remodeling in an ovine model of isolated mitral regurgitation. Therefore, this portion of the thesis now more broadly studies valve injury and disease and includes investigations of congenital valve disease (Chapter 14, as well as a review of congenital valve disease in Chapter 13), studies of the mitral valve in dilated cardiomyopathy and "functional" mitral regurgitation (Chapters 15-17), studies of valve wound healing (Chapter 18), studies of myxomatous mitral valve disease (Chapter 19, as well as Chapter 24 in the Appendix), and studies of calcific aortic valve disease (Chapters 20, 21).

The final portion of this thesis brings the knowledge learned in the above studies to bear upon a preliminary tissue engineered heart valve construct. Originally stated in the thesis proposal as Specific Aim 2 to determine the optimal stiffness of hydrogel scaffolds for different aged porcine valvular interstitial cells, this aim has been revised to study both age-related effects as well as aspects of valve heterogeneity. This study comprises Chapter 22.

Chapter 23 reviews the knowledge obtained from the main portion of this body of work, highlights its unique contributions to the literature, and discusses possible implications and future directions. The appendix includes a study of myxomatous mitral valve disease in which I was integrally involved, but was not central to my proposal (Chapter 24), as well as two papers on which I was co-first author regarding myocardial mechanics (Chapters 25, 26).

While the studies included in this thesis span a broad range of topics, they are unified by several themes including valve heterogeneity, the importance of the extracellular matrix, the role of the valvular interstitial cell, the interrelationship between structure and function, and the importance of the valve's mechanical environment. The knowledge obtained from this body of work can serve as design criteria for a tissue engineered heart valve. Furthermore, the studies of diseased valves give insight into the various diseases' pathogenesis, and therefore, may allow the development of novel or more refined treatment strategies.

REFERENCES

1. American Heart Association. *Heart Disease and Stroke Statistics--2005 Update*. Dallas, Texas: American Heart Association; 2005.
2. LeBlanc JG, Russell JL. Pediatric Cardiac Surgery in the 1990's. *Surg Clin North Amer*. 1998;78(5):729-747.
3. Ferencz C, Rubin JD, Loffredo CA, Magee CM. The epidemiology of congenital heart disease, the Baltimore-Washington Infant Study (1981-1989). *Perspectives in Pediatric Cardiology*. Mount Kisco, NY: Future Publishing Co., Inc.; 1993.
4. National Center for Health Statistics: National Heart, Lung, Blood Institute; 2005.
5. Hoffman J. Congenital heart disease and inheritance. *Pediatr Clin North Am*. 1990;37:25-43.
6. Davachi F, Moller J, Edwards J. Diseases of the mitral valve in infancy. An anatomic analysis of 55 cases. *Circulation*. 1971;43:565-579.
7. Bartram U, Bartelings M, Kramer H, Gittenberger-de Groot A. Congenital polyvalvular disease: a review. *Pediatr Cardiol*. 2001;22(2):93-101.
8. Vlad P. Mitral valve anomalies in children, editorial. *Circulation*. 1971;43:465-466.
9. Oechslin E, Harrison D, Harris L, Downar E, Webb G, Siu S, Williams W. Reoperation in adults with repair of tetralogy of fallot: indications and outcomes. *J Thorac Cardiovasc Surg*. 1999;118(2):245-251.
10. Booth C, Korossis SA, Wilcox HE, Watterson KG, Kearney JN, Fisher J, Ingham E. Tissue engineering of cardiac valve prostheses I: development and histological characterization of an acellular porcine scaffold. *J Heart Valve Dis*. 2002;11(4):457-462.
11. Vesely I. Tissue Engineering of Heart Valves. *Encyclopedia of Biomaterials and Biomedical Engineering*. Vol 4. 2nd ed. New York: Informa Health Care; 2008:2737-2750.
12. Dunn JM. Porcine valve durability in children. *Ann. Thorac. Surg*. 1981;32:357-368.
13. Lam J, Ranganathan N, Wigle E, Silver M. Morphology of the human mitral valve. I. Chordae tendineae: a new classification. *Circulation*. 1970;41(3):449-458.
14. Ranganathan N, Lam J, Wigle E, Silver M. Morphology of the human mitral valve. II. The valve leaflets. *Circulation*. 1970;41(3):449-458.
15. Bellhouse BJ, Bellhouse FH. Mechanism of closure of the aortic valve. *Nature*. 1968;217(5123):86-87.
16. Grande-Allen KJ, Calabro A, Gupta V, Wight TN, Hascall VC, Vesely I. Glycosaminoglycans and proteoglycans in normal mitral valve leaflets and chordae:

- association with regions of tensile and compressive loading. *Glycobiology*. 2004;14(7):621-633.
17. Kunzelman K, Cochran R, Murphree S, Ring W, Verrier E, Eberhart R. Differential collagen distribution in the mitral valve and its influence on biomechanical behaviour. *J Heart Valve Dis*. 1993;2(2):236-244.
 18. Gross L, Kugel M. Topographic anatomy and histology of the valves in the human heart. *Am. J. Pathol*. 1931;25(1):445-456.
 19. Mol A, Bouten C, Baaijens F, Zund G, Turina M, Hoerstrup S. Review article: Tissue engineering of semilunar heart valves: current status and future developments. *J Heart Valve Dis*. 2004;13(2):272-280.
 20. Cole WG, Chan D, Hickey AJ, Wilcken DE. Collagen composition of normal and myxomatous human mitral heart valves. *Biochem J*. 1984;219(2):451-460.
 21. Keller F, Leutert G. [Age dependence of collagen structures of the human heart]. *Z Gerontol*. 1994;27(3):186-193.
 22. Vesely I. The role of elastin in aortic valve mechanics. *J Biomech*. 1998;31(2):115-123.
 23. Sauren A, van Hout M, van Steenhoven A, Veldpaus F, Janssen J. The mechanical properties of porcine aortic valve tissues. *J Biomech*. 1983;16(5):327-337.
 24. Vesely I, Noseworthy R. Micromechanics of the fibrosa and the ventricularis in aortic valve leaflets. *Journal of biomechanics*. 1992;25(1):101-113.
 25. Arteaga-Solis E, Gayraud B, Ramirez F. Elastic and collagenous networks in vascular diseases. *Cell Struct Funct*. 2000 25(2):69-72.
 26. Ushiki T. Collagen fibers, reticular fibers and elastic fibers. A comprehensive understanding from a morphological viewpoint. *Arch Histol Cytol*. 2002;65(2):109-126.
 27. McDonald PC, Wilson JE, McNeill S, Gao M, Spinelli JJ, Rosenberg F, Wiebe H, McManus BM. The challenge of defining normality for human mitral and aortic valves: geometrical and compositional analysis. *Cardiovasc Pathol*. 2002;11(4):193-209.
 28. Carew E, Garg A, Barber J, Vesely I. Stress relaxation preconditioning of porcine aortic valves. *Ann Biomed Eng*. 2004;32(4):563-572.
 29. Kielty CM, Sherratt MJ, Shuttleworth CA. Elastic fibres. *J Cell Sci*. 2002;115(Pt 14):2817-2828.
 30. Lis Y, Burleigh MC, Parker DJ, Child AH, Hogg J, Davies MJ. Biochemical characterization of individual normal, floppy and rheumatic human mitral valves. *Biochem J*. 1987;244(3):597-603.
 31. Grande-Allen KJ, Griffin BP, Ratliff NB, Cosgrove DM, Vesely I. Glycosaminoglycan Profiles of Myxomatous Mitral Leaflets and Chordae Parallel the Severity of Mechanical Alterations. *J Am Coll Cardiol*. 2003;42(2):271-277.

32. Rothenburger M, Volker W, Vischer P, Glasmacher B, Scheld HH, Deiwick M. Ultrastructure of proteoglycans in tissue-engineered cardiovascular structures. *Tissue Eng.* 2002;8(6):1049-1056.
33. Lander AD. Proteoglycans. In: Kreis T, Vale R, eds. *Guidebook to the Extracellular Matrix, Anchor, and Adhesion Proteins*. 2nd ed. Oxford: Oxford University Press; 1999:351-356.
34. Kinsella MG, Bressler SL, Wight TN. The regulated synthesis of versican, decorin, and biglycan: extracellular matrix proteoglycans that influence cellular phenotype. *Crit Rev Eukaryot Gene Expr.* 2004;14(3):203-234.
35. Rothenburger M VW, Vischer P, Glasmacher B, Scheld HH, Deiwick M. Ultrastructure of proteoglycans in tissue-engineered cardiovascular structures. *Tissue Eng.* 2002;8(6):1049-1056.
36. Yeo TK, Yeo KT, Wight TN. Differential transport kinetics of CS/DS. *Arch Biochem Biophys.* 1992;294:9-16.
37. Isogai Z, Aspberg A, Keene DR, Ono RN, Reinhardt DP, Sakai LY. Versican interacts with fibrillin-1 and links extracellular microfibrils to other connective tissue networks. *J Biol Chem.* 2002;277(6):4565-4572.
38. Olin AI, Morgelin M, Sasaki T, Timpl R, Heinegard D, Aspberg A. The proteoglycans aggrecan and Versican form networks with fibulin-2 through their lectin domain binding. *J Biol Chem.* 2001;276(2):1253-1261.
39. Scott JE, Orford CR. Dermatan sulphate-rich proteoglycan associates with rat tail-tendon collagen at the d band in the gap region. *Biochem J.* 1981;197(1):213-216.
40. Toole BP, Lowther DA. Dermatan sulfate-protein: isolation from and interaction with collagen. *Arch Biochem Biophys.* 1968;128(3):567-578.
41. Danielson KG, Baribault H, Holmes DF, Graham H, Kadler KE, Iozzo RV. Targeted disruption of decorin leads to abnormal collagen fibril morphology and skin fragility. *J Cell Biol.* 1997;136(3):729-743.
42. Hildebrand A, Romaris M, Rasmussen LM, Heinegard D, Twardzik DR, Border WA, Ruoslahti E. Interaction of the small interstitial proteoglycans biglycan, decorin and fibromodulin with transforming growth factor beta. *Biochem J.* 1994;302 (Pt 2):527-534.
43. Demoor-Fossard M RF, Boittin M, Pujol JP. Expression of decorin and biglycan by rabbit articular chondrocytes. Effects of cytokines and phenotypic modulation. *Biochim Biophys Acta.* 1998;1398(2):179-191.
44. Schonherr E, Jarvelainen HT, Kinsella MG, Sandell LJ, Wight TN. Platelet-derived growth factor and transforming growth factor-beta 1 differentially affect the synthesis of biglycan and decorin by monkey arterial smooth muscle cells. *Arterioscler Thromb.* 1993;13(7):1026-1036.

45. Bassols A, Massague J. Transforming growth factor beta regulates the expression and structure of extracellular matrix chondroitin/dermatan sulfate proteoglycans. *J Biol Chem.* 1988;263(6):3039-3045.
46. Kahari VM, Hakkinen L, Westermarck J, Larjava H. Differential regulation of decorin and biglycan gene expression by dexamethasone and retinoic acid in cultured human skin fibroblasts. *J Invest Dermatol.* 1995;104(4):503-508.
47. Kaji T, Yamada A, Miyajima S, Yamamoto C, Fujiwara Y, Wight TN, Kinsella MG. Cell density-dependent regulation of proteoglycan synthesis by transforming growth factor-beta(1) in cultured bovine aortic endothelial cells. *J Biol Chem.* 2000;275(2):1463-1470.
48. Romaris M, Heredia A, Molist A, Bassols A. Differential effect of transforming growth factor beta on proteoglycan synthesis in human embryonic lung fibroblasts. *Biochim Biophys Acta.* 1991;1093(2-3):229-233.
49. Westergren-Thorsson G, Antonsson P, Malmstrom A, Heinegard D, Oldberg A. The synthesis of a family of structurally related proteoglycans in fibroblasts is differently regulated by TFG-beta. *Matrix.* 1991;11(3):177-183.
50. Laurent TC. Biochemistry of hyaluronan. *Acta Otolaryngol Suppl.* 1987;442:7-24.
51. Itano N, Atsumi F, Sawai T, Yamada Y, Miyaishi O, Senga T, Hamaguchi M, Kimata K. Abnormal accumulation of hyaluronan matrix diminishes contact inhibition of cell growth and promotes cell migration. *Proc. Natl. Acad. Sci.* 2002;99(6):3609-3614.
52. Trochon V, Mabilat C, Bertrand P, Legrand Y, Smadja-Joffe F, Soria C, Delpech B, Lu H. Evidence of involvement of CD44 in endothelial cell proliferation, migration and angiogenesis in vitro. *Int J Cancer.* 1996;66(5):664-668.
53. Pienimaki JP, Rilla K, Fulop C, Sironen RK, Karvinen S, Pasonen S, Lammi MJ, Tammi R, Hascall VC, Tammi MI. Epidermal growth factor activates hyaluronan synthase 2 in epidermal keratinocytes and increases pericellular and intracellular hyaluronan. *J Biol Chem.* 2001;276(23):35111-35122.
54. Foschi D, Castoldi L, Radaelli E, Abelli P, Calderini G, Rastrelli A, Mariscotti C, Marazzi M, Trabucchi E. Hyaluronic acid prevents oxygen free-radical damage to granulation tissue: a study in rats. *Int J Tissue React.* 1990;12(6):333-339.
55. Baier Leach J, Bivens KA, Patrick CW, Jr, Schmidt CE. Photocrosslinked hyaluronic acid hydrogels: natural, biodegradable tissue engineering scaffolds. *Biotechnol Bioeng.* 2003;82(5):578-589.
56. West DC, Hampson IN, Arnold F, Kumar S. Angiogenesis induced by degradation products of hyaluronic acid. *Science.* 1985;228(4705):1324-1326.
57. Toole BP, Hascall VC. Hyaluronan and tumor growth. *Am J Pathol.* 2002;161(3):745-747.

58. Ishida O, Tanaka Y, Morimoto I, Takigawa M, Eto S. Chondrocytes are regulated by cellular adhesion through CD44 and hyaluronic acid pathway. *J Bone Miner Res.* 1997;12(10):1657-1663.
59. Lesley J, Hascall VC, Tammi M, Hyman R. Hyaluronan binding by cell surface CD44. *J Biol Chem.* 2000;275(35):26967-26975.
60. McKee CM, Penno MB, Cowman M, Burdick MD, Strieter RM, Bao C, Noble PW. Hyaluronan (HA) fragments induce chemokine gene expression in alveolar macrophages. *J Clin Invest.* 1996;98(10):2403-2413.
61. Schmits R, Filmus J, Gerwin N, Senaldi G, Kiefer F, Kundig T, Wakeham A, Shahinian A, Catzavelos C, Rak J, Furlonger C, Zakarian A, Simard JJ, Ohashi PS, Paige CJ, Gutierrez-Ramos JC, Mak TW. CD44 regulates hematopoietic progenitor distribution, granuloma formation, and tumorigenicity. *Blood.* 1997;90(6):2217-2233.
62. Travis JA, Hughes MG, Wong JM, Wagner WD, Geary RL. Hyaluronan enhances contraction of collagen by smooth muscle cells and adventitial fibroblasts: Role of CD44 and implications for constrictive remodeling. *Circ Res.* 2001;88(1):77-83.
63. Allison DD, Grande-Allen KJ. Review. Hyaluronan: A powerful tissue engineering tool. *Tissue Eng.* 2006;12(8):2131-2140.
64. Falkowski M, Schledzewski K, Hansen B, Goerdts S. Expression of stabilin-2, a novel fasciclin-like hyaluronan receptor protein, in murine sinusoidal endothelia, avascular tissues, and at solid/liquid interfaces. *Histochem Cell Biol.* 2003;120(5):361-369.
65. Polyakova V, Hein S, Kostin S, Ziegelhoeffer T, Schaper J. Matrix metalloproteinases and their tissue inhibitors in pressure-overloaded human myocardium during heart failure progression. *J Am Coll Cardiol.* 2004;44(8):1609-1618.
66. Kaden JJ, Vocke DC, Fischer CS, Grobholz R, Brueckmann M, Vahl CF, Hagl S, Haase KK, Dempfle CE, Borggreffe M. Expression and activity of matrix metalloproteinase-2 in calcific aortic stenosis. *Z Kardiol.* 2004;93(2):124-130.
67. Fondard O, Detaint D, Iung B, Choqueux C, Adle-Biassette H, Jarraya M, Hvass U, Couetil JP, Henin D, Michel JB, Vahanian A, Jacob MP. Extracellular matrix remodelling in human aortic valve disease: the role of matrix metalloproteinases and their tissue inhibitors. *Eur Heart J.* 2005;26(13):1333-1341.
68. Steffensen B, Häkkinen L, Larjava H. Proteolytic events of wound-healing--coordinated interactions among matrix metalloproteinases (MMPs), integrins, and extracellular matrix molecules. *Crit Rev Oral Biol Med.* 2001;12(5):373-398.
69. Taylor PM, Batten P, Brand NJ, Thomas PS, Yacoub MH. The cardiac valve interstitial cell. *IJBCB.* 2003;35:113-118.
70. Messier RH, Jr, Bass BL, Aly HM, Jones JL, Domkowski PW, Wallace RB, Hopkins RA. Dual structural and functional phenotypes of the porcine aortic valve interstitial population: characteristics of the leaflet myofibroblast. *J Surg Res.* 1994;57(1):1-21.

71. Latif N, Sarathchandra P, Taylor PM, Antoniow J, Yacoub MH. Localization and pattern of expression of extracellular matrix components in human heart valves. *J Heart Valve Dis.* 2005;14(2):218-227.
72. Latif N, Sarathchandra P, Thomas PS, Antoniow J, Batten P, Chester AH, Taylor PM, Yacoub MH. Characterization of structural and signaling molecules by human valve interstitial cells and comparison to human mesenchymal stem cells. *J Heart Valve Dis.* 2007;16(1):56-66.
73. Rabkin E, Aikawa M, Stone JR, Fukumoto Y, Libby P, Schoen FJ. Activated interstitial myofibroblasts express catabolic enzymes and mediate matrix remodeling in myxomatous heart valves. *Circulation.* 2001;104(21):2525-2532.
74. Dreger SA, Taylor PM, Allen SP, Yacoub MH. Profile and localization of matrix metalloproteinases (MMPs) and their tissue inhibitors (TIMPs) in human heart valves. *J Heart Valve Dis.* 2002;11(6):875-880.
75. Della Rocca F, Sartore S, Guidolin D, Bertiplaglia B, Gerosa G, Casarotto D, Pualetto P. Cell composition of the human pulmonary valve: a comparative study with the aortic valve--the VESALIO Project. *Vitalitate Exornatum Succedaneum Aorticum labore Ingegnoso Obtinebitur. Ann Thorac Surg.* 2000;70(5):1594-1600.
76. Taylor PM, Allen SP, Dreger SA, Yacoub MH. Human cardiac valve interstitial cells in collagen sponge: a biological three-dimensional matrix for tissue engineering. *J Heart Valve Dis.* 2002;11(3):298-306.
77. Vesely I. Reconstruction of loads in the fibrosa and ventricularis of porcine aortic valves. *ASAIO J.* 1996;42(5):M739-M746.
78. Christie GW, Gross JF, Eberhardt CE. Mechanical properties of porcine pulmonary valve leaflets: how do they differ from aortic leaflets? *Ann Thorac Surg.* 1995;60(2 Suppl):S195-199.
79. Stradins P, Lacis R, Ozolanta I, Purina B, Ose V, Feldmane L, Kasyanov V. Comparison of biomechanical and structural properties between human aortic and pulmonary valve. *Eur J Cardiothorac Surg.* 2004;26(3):634-639.
80. Nagy ZL, Fisher J, Walker PG, Watterson KG. The in vitro hydrodynamic characteristics of the porcine pulmonary valve and root with regard to the ross procedure. *J Thorac Cardiovasc Surg.* 2000;120:284-289.
81. Ikhumetse JD, Konduri S, Warnock JN, Xing Y, Yoganathand AP. Cyclic aortic pressure affects the biological properties of porcine pulmonary valve leaflets. *J Heart Valve Dis.* 2006;15(2):295-302.
82. Kunzelman KS, Cochran RP. Stress/strain characteristics of porcine mitral valve tissue: parallel versus perpendicular collagen orientation. *J Card Surg.* 1992;7(1):71-78.
83. Cochran RP, Kunzelman KS, Chuong CJ, Sacks MS, Eberhart RC. Nondestructive analysis of mitral valve collagen fiber orientation. *ASAIO Trans.* 1991;37(3):M447-448.

84. Millington-Sanders C, Meir A, Lawrence L, Stolinski C. Structure of chordae tendineae in the left ventricle of the human heart. *J Anat.* 1998;192(Pt 4):573-581.
85. Timek TA, Dagum P, Lai DT, Liang D, Daughters GT, Ingels NB, Miller DC. Pathogenesis of mitral regurgitation in tachycardia-induced cardiomyopathy. *Circulation.* 2001;104(12 Suppl 1):I47-53.
86. Grande-Allen KJ, Borowski AG, Troughton RW, Houghtaling PL, Dipaola NR, Moravec CS, Vesely I, Griffin BP. Apparently normal mitral valves in patients with heart failure demonstrate biochemical and structural derangements: an extracellular matrix and echocardiographic study. *J Am Coll Cardiol.* 2005;45(1):54-61.
87. Kunzelman KS, Quick DW, Cochran RP. Altered collagen concentration in mitral valve leaflets: biochemical and finite element analysis. *Ann Thorac Surg.* 1998;66(6 Suppl):S198-205.
88. Tamura K, Jones M, Yamada I, Ferrans VJ. Wound healing in the mitral valve. *J Heart Valve Dis.* 2000;9(1):53-63.
89. Tamura K, Murakami M, Washizu M. Healing of wound sutures on the mitral valve: an experimental study. *Gen Thorac Cardiovasc Surg.* 2007;55(3):98-104.
90. Durbin AD, Gotlieb AI. Advances towards understanding heart valve response to injury. *Cardiovasc Pathol.* 2002;11(2):69-77.
91. Durbin A, Nadir N, Rosenthal A, Gotlieb AI. Nitric oxide promotes in vitro interstitial cell heart valve repair. *Cardiovasc Pathol.* 2005;14(1):12-18.
92. Lester W, Damji A, Gedeon I, Tanaka M. Interstitial cells from the atrial and ventricular sides of the bovine mitral valve respond differently to denuding endocardial injury. *In Vitro Cell Dev Biol.* 1993;29A(1):41-50.
93. Mohler E, Gannon F, Reynolds C, Zimmerman R, Keane M, Kaplan F. Bone formation and inflammation in cardiac valves. *Circulation.* 2001;103(11):524-525.
94. Kaden JJ, Dempfle CE, Grobholz R, Fischer CS, Vocke DC, Kilic R, Sarikoc A, Pinol R, Hagl S, Lang S, Brueckmann M, Borggreffe M. Inflammatory regulation of extracellular matrix remodeling in calcific aortic valve stenosis. *Cardiovasc Pathol.* 2005;14(2):80-87.
95. Hakuno D, Kimura N, Yoshioka M, Fukuda K. Molecular mechanisms underlying the onset of degenerative aortic valve disease. *J Mol Med.* 2009;87(1):17-24.
96. Aikawa E, Whittaker P, Farber M, Mendelson K, Padera RF, Aikawa M, Schoen FJ. Human semilunar cardiac valve remodeling by activated cells from fetus to adult: implications for postnatal adaptation, pathology, and tissue engineering. *Circulation.* 2006;113(10):1344-1352.
97. Kruithof BP, Krawitz SA, Gaussin V. Atrioventricular valve development during late embryonic and postnatal stages involves condensation and extracellular matrix remodeling. *Dev Bio.* 2006;302(1):208-217.

98. Camenisch T, Spicer A, Brehm-Gibson T, Biesterfeldt J, Augustine M, Calabro A, Kubalak S, Klewer S, McDonald J. Disruption of hyaluronan synthase-2 abrogates normal cardiac morphogenesis and hyaluronan-mediated transformation of epithelium to mesenchyme. *J Clin Invest.* 2000;106(3):349-360.
99. Henderson DJ, Copp AJ. Versican expression is associated with chamber specification, septation, and valvulogenesis in the developing mouse heart. *Circ Res.* 1998;83(5):523-532.
100. Hinton RB, Jr, Lincoln J, Deutsch GH, Osinska H, Manning PB, Benson DW, Yutzey KE. Extracellular matrix remodeling and organization in developing and diseased aortic valves. *Circ Res.* 2006;98(11):1431-1438.
101. Bashey RI, Torii S, Angrist A. Age-related collagen and elastin content of human heart valves. *J Gerontology.* 1967;9(19):203-208.
102. Angrist A. Aging heart valves and a unitary pathological hypothesis for sclerosis. *J Gerontol.* 1964;19:135-143.
103. Sell S, Scully RE. Aging Changes in the Aortic and Mitral Valves. Histologic and Histochemical Studies, with Observations on the Pathogenesis of Calcific Aortic Stenosis and Calcification of the Mitral Annulus. *Am J Pathol.* 1965;46:345-365.
104. Christie GW, Barratt-Boyes BG. Age-dependent changes in the radial stretch of human aortic valve leaflets determined by biaxial testing. *Ann Thorac Surg.* 1995;60(2 Suppl):S156-159.
105. Schoen FJ, Levy RJ. Tissue Heart Valves: Current Challenges and Future Research Perspectives. *J Biomed Mater Res.* 1999;47:439-465.
106. Elkins RC, Dawson PE, Goldstein S, Walsh SP, Black KS. Decellularized human valve allografts. *Ann Thorac Surg.* 2001;71(5 Suppl):S428-432.
107. Bin F, Yinglong L, Nin X, Kai F, Laifeng S, Xiaodong Z. Construction of tissue-engineered homograft bioprosthetic heart valves in vitro. *ASAIO J.* 2006;52(3):303-309.
108. Johnston DE, Boughner DR, Cimini M, Rogers KA. Radial artery as an autologous cell source for valvular tissue engineering efforts. *J Biomed Mater Res A.* 2006;78(2):383-393.
109. Hoerstrup SP, Kadner A, Melnitchouk S, Trojan A, Eid K, Tracy J, Sodian R, Visjager JF, Kolb SA, Grunfelder J, Zund G, Turina MI. Tissue Engineering of functional trileaflet heart valves from human marrow stromal cells. *Circulation.* 2002;106(II43).
110. Maish MS, Hoffman-Kim D, Krueger PM, Souza JM, Harper JJ, 3rd, Hopkins RA. Tricuspid valve biopsy: a potential source of cardiac myofibroblast cells for tissue-engineered cardiac valves. *J Heart Valve Dis.* 2003;12(2):264-269.
111. Schmidt D, Mol A, Breymann C, Achermann J, Odermatt B, Gossi M, Neuenschwander S, Pretre R, Genoni M, Zund G, Hoerstrup SP. Living autologous heart valves engineered from human prenatally harvested progenitors. *Circulation.* 2006;114(1 Suppl):I125-131.

112. Shinoka T, Shum-Tim D, Ma PX, Tanel RE, Langer R, Vacanti JP, Mayer JE, Jr. Tissue-engineered heart valve leaflets: does cell origin affect outcome? *Circulation*. 1997;96(9 Suppl):II102-107.
113. Hoerstrup SP, Kadner A, Breymann C, Maurus CF, Guenter CI, Sodian R, Visjager JF, Zund G, Turina MI. Living, autologous pulmonary artery conduits tissue engineered from human umbilical cord cells. *Ann Thorac Surg*. 2002;74(1):46-52.
114. Sonnenblick E, Napolitano L, Daggett W, Cooper T. An intrinsic neuromuscular basis for mitral valve motion in the dog. *Circ Res*. 1967;21(1):9-15.
115. Rothenburger M, Volker W, Vischer JP, Berendes E, Glasmacher B, Scheld HH, Deiwick M. Tissue engineering of heart valves: formation of a three-dimensional tissue using porcine heart valve cells. *ASAIO J*. 2002;48(6):586-591.
116. Brody S, Pandit A. Approaches to heart valve tissue engineering scaffold design. *J Biomed Mater Res B Appl Biomater*. 2007;83(1):16-43.
117. Murphy WL, Mooney DJ. Controlled delivery of inductive proteins, plasmid DNA and cells from tissue engineering matrices. *J Periodontal Res*. 1999;34(7):413-419.
118. Breuer CK, Shinoka T, Tanei RE, Zund G, Mooney J, Ma PX, Miura T, Colan S, Langer R, Mayer JE, P VJ. Tissue Engineering Lamb Heart Valve Leaflets. *Biotechnol Bioeng*. 1996;50:562-567.
119. Sarraf CE, Harris AB, McCulloch AD, Eastwood M. Tissue engineering of biological cardiovascular system surrogates. *Heart Lung Circ*. 2002;11(3):142-150.
120. Manothaya C, Vattanapat S, Somabutr C. New technique for construction of tissue heart valves. *Thorax*. 1980;35(8):611-614.
121. Cimini M, Boughner DR, Ronald JA, Johnston DE, Rogers KA. Dermal fibroblasts cultured on small intestinal submucosa: Conditions for the formation of a neotissue. *J Biomed Mater Res A*. 2005;75(4):895-906.
122. Masters KS, Shah DN, Leinwand LA, Anseth KS. Crosslinked hyaluronan scaffolds as a biologically active carrier for valvular interstitial cells. *Biomaterials*. 2005;26(15):2517-2525.
123. Robinson PS, Johnson SL, Evans MC, Barocas VH, Tranquillo RT. Functional tissue-engineered valves from cell-remodeled fibrin with commissural alignment of cell-produced collagen. *Tissue Eng Part A*. 2008;14(1):83-95.
124. Butcher JT, Nerem RM. Porcine aortic valve interstitial cells in three-dimensional culture: comparison of phenotype with aortic smooth muscle cells. *J Heart Valve Dis*. 2004;13(3):478-485; discussion 485-476.
125. Gombotz W, Wang G, Horbett T, Hoffman A. Protein adsorption to poly(ethylene oxide) surfaces. *J Biomed Mater Res*. 1991;25(12):1547-1562.

126. Zheng S, Liu Y, Palumbom F, Luo Y, Prestwich G. In situ crosslinkable hyaluronan hydrogels for tissue engineering. *Biomaterials*. 2004;25(7-8):1339-1348.
127. Lee S, Miller J, Moon J, West J. Proteolytically degradable hydrogels with a fluorogenic substrate for studies of cellular proteolytic activity and migration. *Biotechnol Prog*. 2005;21(6):1736-1741.
128. Mann B, Gobin A, Tsai A, Schmedlen R, West J. Smooth muscle cell growth in photopolymerized hydrogels with cell adhesive and proteolytically degradable domains: synthetic ECM analogs for tissue engineering. *Biomaterials*. 2001;22(22):3045-3051.
129. Hill-West J, Chowdhury S, Sawhney A, Pathak C, Dunn R, Hubbell J. Prevention of postoperative adhesions in the rat by in situ photopolymerization of bioresorbable hydrogel barriers. *Obstet Gynecol*. 1994;83(1):59-64.
130. Cushing M, Jaeggli M, Masters K, Leinwand L, Anseth K. Serum deprivation improves seeding and repopulation of acellular matrices with valvular interstitial cells. *J Biomed Mater Res A*. 2005;75(1):232-241.
131. Barron V, Lyons E, Stenson-Cox C, McHugh PE, Pandit A. Bioreactors for cardiovascular cell and tissue growth: a review. *Ann Biomed Eng*. 2003;31(9):1017-1030.
132. Hahn MS, Teply BA, Stevens MM, Zeitels SM, Langer R. Collagen composite hydrogels for vocal fold lamina propria restoration. *Biomaterials*. 2006;27(7):1104-1109.
133. Steinhoff G, Stock U, Karim N, Mertsching H, Timke A, Meliss RR, Pethig K, Haverich A, Bader A. Tissue engineering of pulmonary heart valves on allogenic acellular matrix conduits: in vivo restoration of valve tissue. *Circulation*. 2000;102(19 Suppl 3):III50-55.
134. Cushing MC, Liao J, Jaeggli MP, Anseth KS. Material-based regulation of the myofibroblast phenotype *Biomaterials*. 2007;28:3378-3387.
135. Martens PJ, Bryant SJ, Anseth KS. Tailoring the degradation of hydrogels formed from multivinyl poly(ethylene glycol) and poly(vinyl alcohol) macromers for cartilage tissue engineering. *Biomacromolecules*. 2003;4(2):283-292.
136. Sodian R, Sperling JS, Martin DP, Egozy A, Stock U, Mayer JE, Jr., Vacanti JP. Fabrication of a trileaflet heart valve scaffold from a polyhydroxyalkanoate biopolyester for use in tissue engineering. *Tissue Eng*. 2000;6(2):183-188.
137. Hoerstrup SP, Sodian R, Daebritz S, Wang J, Bacha EA, Martin DP, Moran AM, Guleserian KJ, Sperling JS, Kaushal S, Vacanti JP, Schoen FJ, Mayer JE, Jr. Functional living trileaflet heart valves grown in vitro. *Circulation*. 2000;102(19 Suppl 3):III44-49.
138. Sutherland FW, Perry TE, Yu Y, Sherwood MC, Rabkin E, Masuda Y, Garcia GA, McLellan DL, Engelmayr GC, Jr., Sacks MS, Schoen FJ, Mayer JE, Jr. From stem cells to viable autologous semilunar heart valve. *Circulation*. 2005;111(21):2783-2791.
139. Guo X, Park H, Young S, Kretlow JD, van den Beucken JJ, Baggett LS, Tabata Y, Kasper FK, Mikos AG, Jansen JA. Repair of osteochondral defects with biodegradable

hydrogel composites encapsulating marrow mesenchymal stem cells in a rabbit model. *Acta Biomater.* 2010;6(1):39-47.

- 140.** Stella JA, Liao J, Hong Y, David Merryman W, Wagner WR, Sacks MS. Tissue-to-cellular level deformation coupling in cell micro-integrated elastomeric scaffolds. *Biomaterials.* 2008;29(22):3228-3236.

Chapter 2: The Use of Collagenase III for the Isolation of Porcine Aortic Valvular Interstitial Cells: Rationale and Optimization

In this chapter a collagenase III-based method for isolating valvular interstitial cells (VICs) was optimized. While this study does not directly address questions related to valve mechanobiology, this method of enzymatic isolation of VICs was used throughout the thesis work. Therefore, the optimization of this method was important to performing many other studies contained in this thesis work, as well as provides an optimized protocol that can be used by other researchers.

ABSTRACT

Background: Substantial heart valve research relies on the isolation of valvular interstitial cells (VICs). While a wide variety of conditions have been reported for VIC isolation, the effectiveness of these methods has rarely been compared. It is also likely that the age of the valve donor will influence these valvular tissue dissociation conditions. The aim of this study was to increase the efficiency and cost-effectiveness of VIC isolation, while taking into account possible differences due to the age of the valve donor.

Methods: Aortic valves were obtained from 6-month-old (n=24) and 6-week-old pigs (n=45) within 24 hrs of death. After removal of endothelial cells, the tissues were minced and subjected to various enzymatic digestions for variable lengths of time.

Results: The optimal concentration of collagenase III was determined to be 1 mg/ml for 6-week-old pigs and 2 mg/ml for 6-month-old pigs. The optimal duration of digestion was 4 hours for both ages. Addition of neutral protease (2 mg/ml) further increased yield, while additional DNase and hyaluronidase had no effect. Yield was not influenced by the volume of enzyme solution or the use of previously frozen enzyme solution.

Conclusions: These findings provide age-specific conditions for improving the yield of VIC isolation, which should have utility in experimental evaluations of valvular cell biology and tissue engineering investigations.

The work contained in this chapter was published as:

Stephens EH, Carroll JL, Grande-Allen KJ. **The Use of Collagenase III for the Isolation of Porcine Aortic Valvular Interstitial Cells: Rationale and Optimization.** *Journal of Heart Valve Disease.* 2007;16(2):175-183.

INTRODUCTION

Given the severity and prominence of heart valve disease and problems with artificial and bioprosthetic valves, production of tissue engineered heart valves for the treatment of heart valve disease is of high importance,¹ particularly for the treatment of pediatric valve disease.² Not only do artificial replacement valves have higher complication rates in children, but pediatric patients must undergo multiple open heart surgeries before adulthood alone to replace artificial valves the child has outgrown.² While an autologous tissue engineered heart valve is the ultimate goal because of immune and coagulation issues, recent research has focused on the basic science of valves in order to determine biological design criteria.^{3, 4} This research often relies on valvular interstitial cell isolation from valves of a widely investigated animal model, the pig.

Techniques for the isolation of primary cells generally fall into one of three categories: enzymatic, mechanical, and primary explant.⁵ Primary explant, while avoiding exposing tissue to harsh enzymes, selects for a mobile cell phenotype and therefore is only recommended for use when tissue is extremely limited or fragile.⁵ Enzymatic and mechanical disaggregation results in a more representative cell population in a shorter amount of time.⁵ In enzymatic disaggregation, a balance is sought between sufficient enzymatic degradation to allow for the release of cells and minimizing the damaging effects of the enzymes on the viability of cells. Of the variety of enzymes used, the collagenases and neutral protease (a.k.a dispase) are considered gentle enzymes but provide incomplete disaggregation.⁵ Trypsin and pronase, on the other hand, are harsher enzymes that produce the most complete dissociation, but are more damaging.

The most common enzyme used is trypsin, referring to a mixture of pancreatic enzymes (also called pancreatin).^{6, 7} Trypsin is effective and generally well tolerated by a large variety of cell types, and has the benefit that any residual activity is neutralized by culture media serum.⁵ However, trypsin is ineffective in fibrous tissues, such as the collagen-rich heart valves, in which collagenase is preferred.⁵ There are several classes of collagenases; collagenases I and II have high clostripain tryptic activity, collagenase III has lower tryptic activity and thus is less harsh, and collagenase IV is recommended for specific use in isolation of pancreatic islet cells.⁷ Additional enzymes are often added to the enzymatic solution, such as DNase, which degrades the DNA from ruptured cells since DNA can inhibit proteolysis and cause cellular aggregation.⁵ Hyaluronidase is particularly useful in digesting the glycosaminoglycan (GAG) hyaluronan, which can be prevalent in the extracellular matrix surrounding the cells.

Table 2-1. Reported Enzymatic VIC Isolation Techniques.

Enzyme	Conc.	Time	Ref.
Collagenase (W)	600 U/ml	Overnight	²⁰
Collagenase II (S)	1000 U/ml	30 min	²¹
Collagenase (G)	0.08%=100 U/ml	24 hr	²²
Collagenase II (B)	1000 U/ml	Step 1: 5 min	⁴
		Step 2: 30 min	
Collagenase I (W) and Elastase III (S)	165 U/ml 15 U/ml	Overnight	²³
Collagenase (B)	0.6 mg/ml	Step 1: 30 min	²⁴
		Step 2: 60 min	
Collagenase (S)	0.16%*	2 hr	¹²

*the unit concentration could not be determined;
W=Worthington, S=Sigma, G=Gibco, B=Boehringer.

For the study of heart valves, reported conditions for cell isolation vary dramatically from time durations of 30 minutes⁴ to 24 hours,⁸ and include a variety of enzymes at different concentrations (Table 2-1); it should be noted that units of enzyme activity vary between manufacturers, although these units are less frequently reported by investigators. Enzymes used in heart valve digestion tend to be various mixtures of collagenases, although no optimization of enzymes and digestion conditions has been published. Furthermore, consideration has not been given to how methods should be modified for cell isolation from different aged valve donors. Such modification is likely necessary and in fact has been reported previously by Angrist et al., who found that valve tissues showed reduced susceptibility to collagenase digestion with advancing age (geriatric).⁹ Furthermore, recent research has shown significant changes in valve composition with age, including quantity of proteoglycans and glycosaminoglycans (GAGs), changes in collagen content and crosslinking,¹⁰ and the density of cells.¹¹ Given these differences, it is likely that enzymatic degradation of the extracellular matrix of aortic valves from different aged donors will require different dissociation conditions, whether these donors are human surgical subjects or animal models.

Although optimization studies have rarely been published for valvular cell isolation,¹² such experiments have been performed in other tissues. For example, optimization experiments with osteoblasts found that enzymatic isolation, rather than the primary explant technique, gave the osteogenic differentiation desired.¹³ In contrast, in the optimization of human gingival cells isolation better results were found with the direct explant technique rather than enzymatic isolation.¹⁴ The effectiveness of different enzymatic mixtures has also been compared in other tissues.¹⁵ From these works it is

clear that the optimum dissociation conditions and enzymes used for cell isolation depends on the tissue matrix content and desired cell phenotype.

Our hypotheses were that valve tissues from different aged donors, given their distinct compositions, would require different digestion conditions for optimal yield. We also hypothesized that there would be a range of conditions that improves not only yield but also cost effectiveness. Therefore, we examined various combinations of enzymatic digestion mixtures (with collagenase III as the base enzyme for reasons stated above) and incubation conditions to determine the optimal cocktail for the isolation of cells from porcine aortic valves. Valves from both 6-week-old and 6-month-old pigs were used to determine the need to tailor dissociation conditions to valve donor age.

METHODS

General Procedure

Porcine aortic heart valves were obtained from an abattoir (Fisher Ham and Meat, Spring, TX, USA) within 24 hours of death. These valves were dissected and rinsed with PBS. For 6-month-old valves (n=24), each aortic valve leaflet was further cut in half, each half acting as a sample (total 137 samples), while for the 6-week-old valves (n=45) a whole aortic valve leaflet constituted a sample (total 134 samples). In both cases the wet weight of the sample was recorded. Next, to remove the endothelial cells, the tissue was incubated for 30 minutes in collagenase II (2 mg/ml of 246 U/mg, Worthington Scientific, Lakewood, NJ, USA) and 2.5% antibiotic/antimycotic (ABAM, from stock concentration of 10,000 IU penicillin, 10,000 ug/ml streptomycin, 25 ug/ml amphotericin B, Mediatech, Herndon, VA, USA) in DMEM (Mediatech) in a shaking incubator (160

rpm, 37° C). The loosened endothelial cells were then removed by gently brushing the leaflet surfaces with a sterile cotton swab; our laboratory has previously shown that this treatment removes endothelial cells (the final cell population does not stain for CD31).¹⁶

Table 2-2. Experimental Conditions.

Duration (hours)	Concentrations of Enzymes				Other Factors	
	Coll III	Hyase*	DNase	NP	Volume (ml)	Freezing
6-month-old						
2,4,o/n	1,2,5,10					
4,6	1,2,4,7					
4	2					Fresh, Frozen
4	2	0.1,0.2,0.5	0.1			
4	2	0.2	0,0.1,0.2,0.33			
4	2			0.5,2,5		
4	2					
6-week-old						
2,4,o/n	1,2,5,10					
4,6	1,2,4,7					
3,4,5	1					
4	1				8, 20	
4	1					Fresh, Frozen
4	1	0.1,0.2,0.5	0.1			
4	1	0.2	0,0.1,0.2,0.5			
4	1	0.2		0.5,2,5		

*concentrations are on top of baseline (0.1 mg/ml HA); Coll = collagenase, NP = neutral protease, o/n=overnight.

The tissue was finely minced and placed into the enzymatic mixture being tested (Table 2-2). The tissue in solution was placed in a shaking incubator (160 rpm, 37° C) for a variable number of hours (Table 2-2). After that time the mixture was filtered through a 70 micron cell strainer (BD Falcon, Bedford, MA, USA). The cells were pelleted via centrifugation (1500xg, 5 min) and resuspended in 1 ml DMEM:F12 with 10% Bovine Growth Serum (Hyclone, Logan, UT, USA), with 1% ABAM and 5.6 ml/500 ml HEPES buffer (Mediatech).

Assessment of Cell Number: MTT Assay and Trypan Blue Exclusion

To determine cell yield, either an MTT assay or a hemocytometer (trypan blue exclusion) was used immediately after cell isolation, as well as 48 hours later to determine if the harvested cells maintained cell viability. Trypan blue exclusion was only used in the initial experiment; all subsequent experiments used the MTT assay that offered more precision and efficiency. Manual counting of cells using the trypan blue exclusion method was performed using a hemocytometer according to standard techniques. For each MTT test, 130 μ l aliquots of the resuspended cell mixture were seeded in duplicate in sterile 24 well plates; based on initial counts this volume contained approximately 100,000 cells. The MTT assay consisted of adding MTT reagent (5 mg/ml sterile 3-(4,5-dimethylthiazol-2-yl)-2,5-diphenyl tetrazolium bromide (Sigma-Aldrich, St. Louis, MO, USA) in PBS), gently mixing by rocking the plate back and forth, and then storing in the incubator for 3 hours. Afterwards 1 ml of MTT solvent (1N HCl in isopropyl alcohol) was added and each well triturated thoroughly. Triplicates of the assay solution from each well were measured in a 96 well plate. Plates were read by a spectrophotometer (SpectraMax M2, Molecular Devices, Sunnyvale, CA, USA) at two different wavelengths (A570-A690). The difference of the two wavelengths for each well was taken as directly proportional to cell number. Both methods were normalized first to tissue weight to obtain cell density. To compare data between different experiments, the cell densities resulting from the different collagenase III concentrations and digestion durations were normalized to the 1 mg/ml (6-week-old) or 2 mg/ml (6-month-old)/ 4 hour results from that same experimental group.

Experimental Conditions

The baseline enzymatic cocktail consisted of 2.5% ABAM, 2.5% HEPES buffer, and 10 mg/100 ml hyaluronidase (499 USP/NF U/mg, Worthington Scientific) in DMEM, as well as collagenase III (149 U/mg, Worthington Scientific) at varying concentrations. To test the effect of digestion duration, the minced valve tissues were incubated for 2, 3, 4, or 6 hours as well as overnight (Table 2-2). To test the effect of collagenase III concentration, 1, 2, 4, 5, 7, and 10 mg/ml solutions were evaluated. Under the rationale that increased volume may allow more opportunity for enzyme-tissue interaction, the effect of the volume of solution added to the minced tissue was tested by using a digestion mixture of 20 ml (instead of our standard 8 ml) in one experiment. To test the effect of freezing the enzyme mixture prior to use, one digestion mixture was frozen for several days and then thawed before use in an experiment where it was compared to a freshly prepared mixture of identical composition. Additionally, various concentrations of additional enzymes were tested to determine if they would improve cell yield (Table 2-2). These supplemental enzymes included hyaluronidase (an additional 0.1, 0.2, and 0.5 mg/ml on top of the baseline 0.1 mg/ml), DNase (0.1, 0.2, and 0.5 mg/ml), and neutral protease (NP, 0.5, 2, and 5 mg/ml; 0.28 U/mg, Worthington Scientific).

Statistical and Cost Benefit Analyses

Multifactorial analysis of variance tests were performed using SigmaStat (SPSS, Chicago, IL, USA) to determine if concentration and duration effects were significant

($p < 0.05$). Post-hoc Tukey tests were performed as needed to compare subgroups. Calculations of cost were based on 2006 Worthington Scientific prices for enzymes and assumed equivalent volumes of enzymatic mixtures per sample.

RESULTS

Valvular Interstitial Cell Isolation from 6-Month-Old Pig

Initial studies showed that at low concentrations of collagenase III (1-2 mg/ml) the overnight digest gave the most cells compared to the 2 and 4 hour digests, up to tenfold higher for 1 mg/ml overnight compared to 2 hour. Cell yield greatly increased (average of ~4X) with higher concentrations of collagenase III (5-10 mg/ml). However at the high concentrations the overnight digest yielded lower cell densities (~75%) than 2 or 4 hours. Based on this initial study, the overnight digestion was omitted and only shorter digestion times used. This same experiment also showed that most collagenase III concentrations on average yielded a higher (1-2X) cell density at 4 hours than after 2 hours. For that reason, subsequent experiments compared the effectiveness of four hour and six hour digestions.

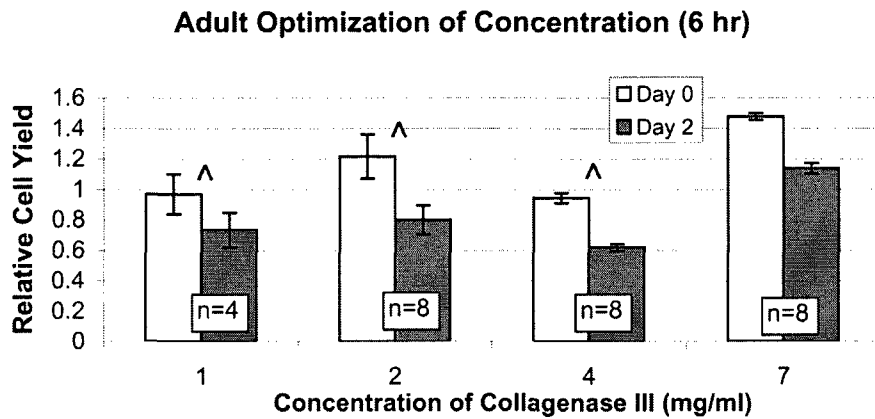
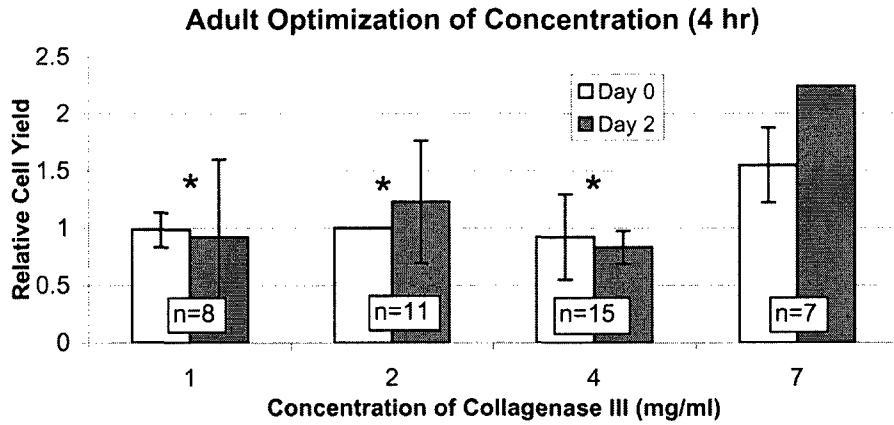


Fig. 2-1: Optimization of collagenase III concentration for 6-month-old (“adult”) valves. Above: 4 hour digestion duration, showing MTT cell yield on day 0 and day 2: $p < 0.001$; $* = p < 0.01$ vs. 7 mg/ml. Below: cell yields resulting from 6 hour digestion duration: $p < 0.001$; $\wedge = p < 0.005$ vs. 7 mg/ml. Relative cell yield = yield for each combination of enzyme concentration and digestion duration normalized to the MTT result from the 2 mg/ml and 4 hour data.

Given that the day 2 analysis of cell viability indicated that the 4 hour digestion culture consistently contained a higher number of cells than the 6 hour digestion culture, 4 hours was determined to be the optimum digestion duration ($p < 0.001$, Fig. 2-1). While the greatest yield was obtained with the highest concentration of collagenase III (for 4 hour digestion $p < 0.001$; $p < 0.01$ for 7 vs. each of 1, 2, and 4 mg/ml), taking into account

the cost (Fig. 2-2), 2 mg/ml was determined to be the optimal collagenase III concentration for the 6-month-old valve.

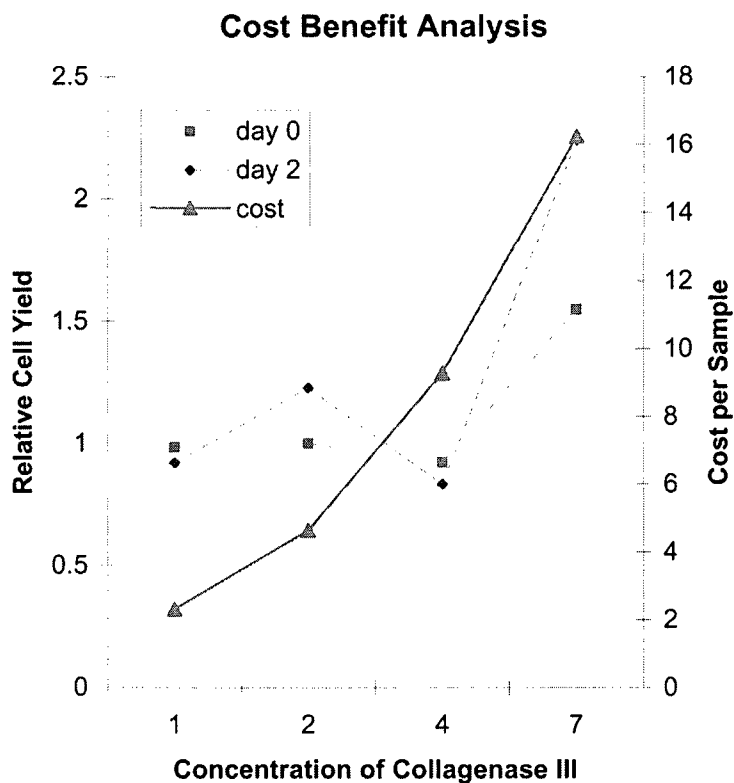


Fig. 2-2: Cost benefit analysis showing that the cell yield and cost per sample curves cross at approximately 3 mg/ml. Because 4 mg/ml gave poorer yields than 2 mg/ml, the lower concentration of collagenases III was selected as optimal.

Additional hyaluronidase by itself or in combination with DNase did not increase yield above that of the baseline cocktail (Fig. 2-3). Similarly, the addition of DNase did not result in higher yield compared to baseline at any concentration, but neutral protease at a concentration of 2 mg/ml resulted in a significant increase in the number of day 2 viable cells ($p < 0.001$).

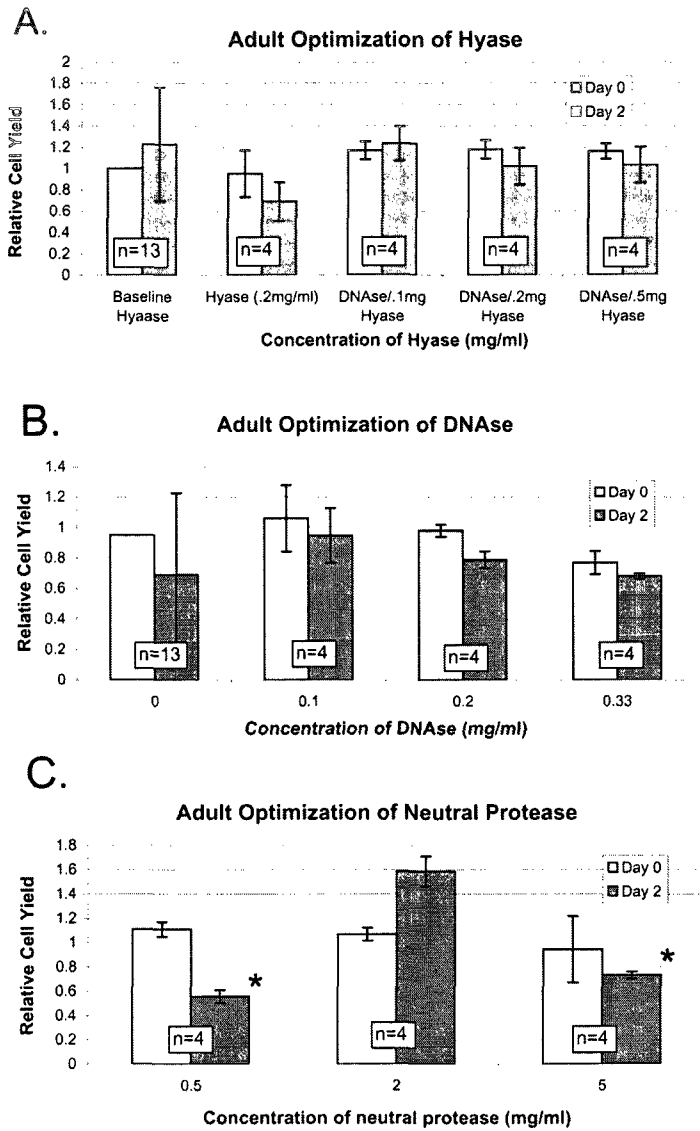
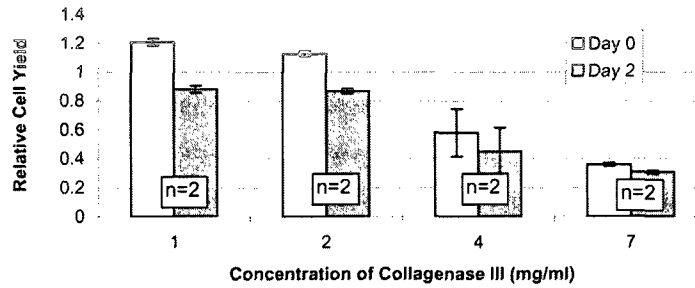


Fig. 2-3: Optimization of additional enzymes for 6-month-old ("adult") valves. A) Optimization of hyaluronidase. B) Optimization of DNase. C) Optimization of neutral protease, for day 2: $p < 0.001$; *= $p < 0.001$ vs. 2 mg/ml. For all experiments each sample (n) consisted of one half of an aortic valve leaflet. Hyase=hyaluronidase.

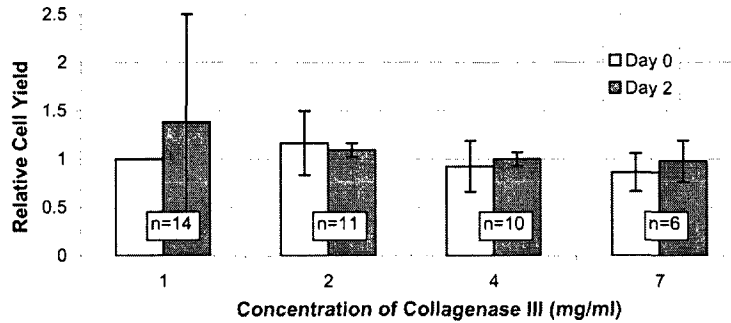
Valvular Interstitial Cell Isolation from 6-Week-Old Pig

Initial studies in 6-week-old valves showed that the yield for the overnight digest was an average of approximately 50% less than the 4 hours digest for all concentrations. These studies also showed that for most concentrations the yield for the 4 hour digest was higher (~1.2-5X)

A. Suckling Optimization of Concentration (6 hr)



B. Suckling Optimization of Concentration (4 hr)



C. Suckling Optimization of Digestion Time

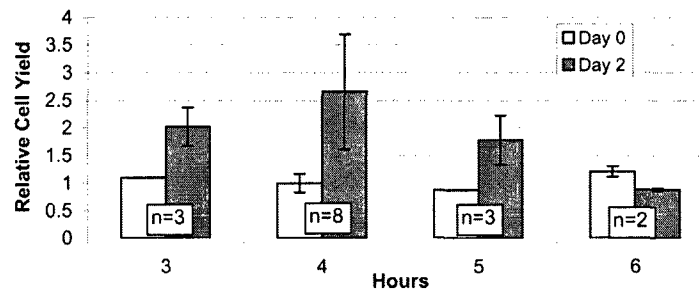


Fig. 2-4: Optimization of digestion duration and collagenase III concentration for 6-week-old ("suckling") valves. A) Optimal collagenase III concentration for 6 hour digestion duration was 1 mg/ml, $p=0.038$. B) Optimization of collagenase III concentrations in 4 hour digestion duration. C) Optimization of digestion time. For all parts of figure each sample (n) consisted of one whole aortic valve leaflet. Relative cell yield = yield for each combination of enzyme concentration and digestion duration normalized to the MTT result from the 1 mg/ml and 4 hour data.

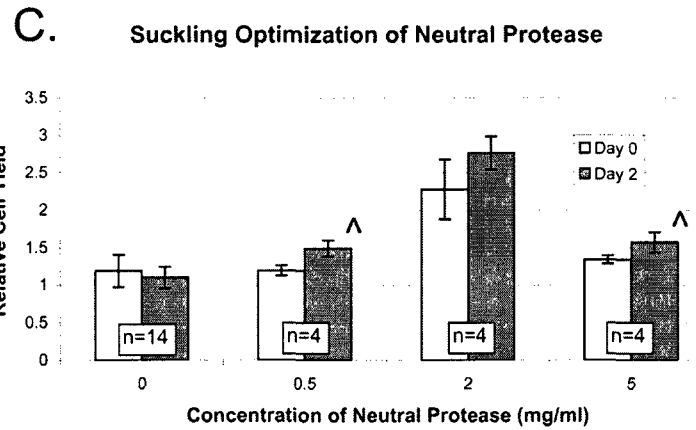
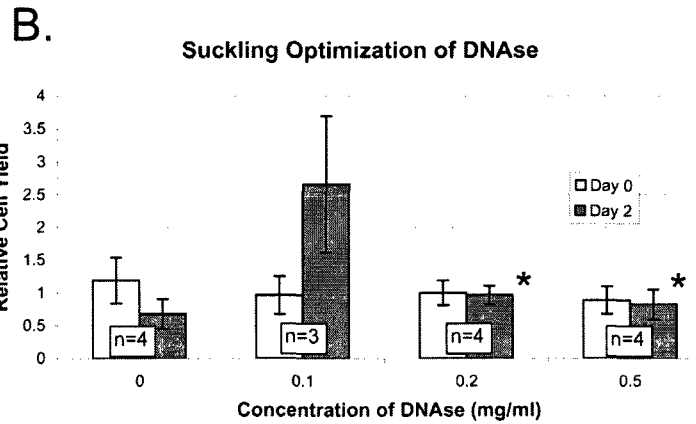
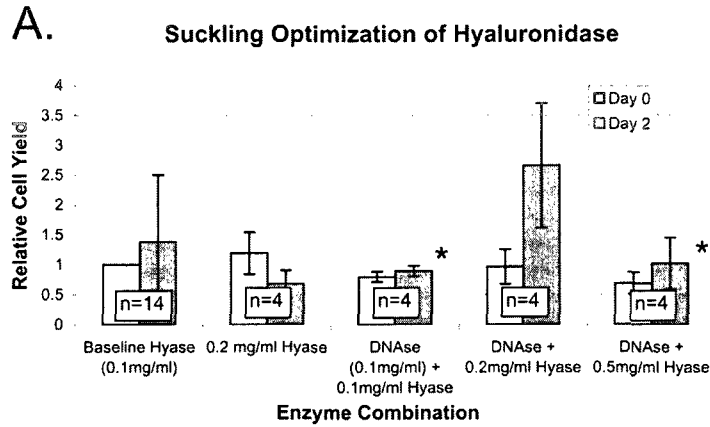


Fig. 2-5: Optimization of additional enzymes for 6 week-old (“suckling”) valves. A) Optimization of hyaluronidase concentration, for day 2: $p < 0.001$; $* = p < 0.001$ vs. DNase + 0.2 mg/ml hyaluronidase. B) Optimization of DNase, for day 2: $p < 0.001$; $* = p < 0.001$ vs. 0.1 mg/ml DNase. DNase was in addition to 0.2mg/ml hyaluronidase. C) Optimization of neutral protease, for day 2: $p < 0.001$; $\wedge = p < 0.005$ vs. 2 mg/ml neutral protease. Neutral Protease was in addition to 0.2mg/ml hyaluronidase. For all parts of figure each sample (n) consisted of one whole aortic valve leaflet.

than the 2 hour digest. Subsequent experiments, therefore, included 3, 4, 5, and 6 hour digests. The optimum duration for digestion for 6-week-old valves was found to be 4 hours because this gave the greatest number of viable cells on day 2 (Fig. 2-4). In 6-week-old valves the optimal concentration appeared to be, by a small margin, 1 mg/ml ($p=0.08$). Given this result and considering the cost of the enzyme, 1 mg/ml collagenase III was determined to be the optimal concentration. Of the additional enzymes used to supplement the digestion mixture (hyaluronidase, DNase, and neutral protease), the optimal hyaluronidase concentration was 0.2 mg/ml (for a total of 0.3 mg/ml) ($p=0.024$; $p<0.001$ for 0.2 vs. 0.1 mg/ml). The optimum DNase concentration was 0.1 mg/ml DNase, which substantially increased yield ($p<0.001$; $p<0.005$ for 0.1 vs. both 0.2 and 0.5 mg/ml, Fig. 2-5). Neutral protease increased yield at a concentration of 2 mg/ml and improved day 2 viability at all concentrations ($p<0.001$).

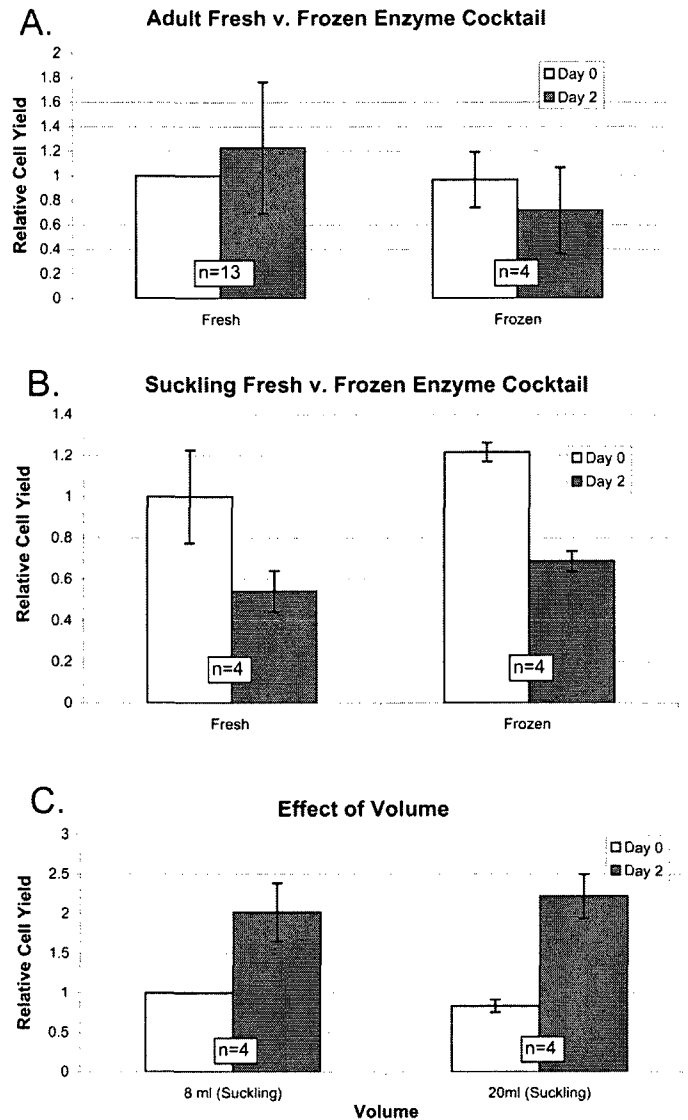


Fig. 2-6: A,B) Fresh versus frozen enzymatic cocktail. C) Effect of volume (performed in 6-week-old “suckling” valves only). Samples in 6-month-old (“adult”) valve experiments consisted of one half of one aortic valve leaflet. Samples in 6-week-old valve experiments consisted of one whole aortic valve leaflet.

In both age groups, freezing the enzymatic preparation ahead of time did not diminish cell yield (Fig. 2-6). Increased volume (tested in 6-week-old valves) also did not affect yield (Fig. 2-6). Table 2-3 summarizes the optimal disaggregation conditions that were determined for each age group.

Table 2-3. Optimized Enzymatic Digestion Mixtures for 6-Week-Old and 6-Month-Old Porcine Heart Valves.

Step 2*: Solution Components	6-week-old	6-month-old
Collagenase III	1 mg/ml	2 mg/ml
Hyaluronidase	0.3 mg/ml	0.1 mg/ml
DNAse	0.1 mg/ml	----
Neutral Protease	2 mg/ml	2 mg/ml

*Step 1 for both age groups loosens the endothelial cells and the mixture contains collagenase II (2 mg/ml of 246 U/mg) and 2.5% antibiotic/antimycotic (from stock concentration of 10,000 IU penicillin, 10,000 ug/ml streptomycin, 25 ug/ml amphotericin B) in DMEM.

DISCUSSION

A wide range of collagenase III concentrations was found to be effective in the isolation of VICs from porcine aortic valves, although with different resulting cell yield. This result confirms the notion that in enzymatic disaggregation a balance is sought between sufficient enzymatic degradation of the tissue to allow for the release of cells and minimizing the damaging effects of the enzymes on the viability of cells.

Collagenase III was found to be very effective as the main enzyme in valvular disaggregation, as expected given that collagenase is reported to be particularly appropriate for either delicate tissues or fibrous tissues.⁵ The collagenases are a family of enzymes that are composed of differing proportions of clostridopeptidase A (which specifically cleaves Pro-X-Gly-Pro) with other proteases, polysaccharidases, and lipases.⁷ In general, crude enzymatic preparations (used in this study) are often more successful in cell isolation; since they are less pure, they contain contaminating nonspecific proteases that aid in digestion.⁵ However, higher purity preparations of enzymes are advantageous for being less toxic to cells and more specific to distinct types of ECM.⁵ At different

points in the enzymatic digestion process, different preparations of collagenase are more appropriate. Within the collagenase family, collagenase II is harsher and has more tryptic clostripain activity than collagenase III.⁷ Therefore, collagenase II can be used briefly to loosen the endothelial cells but is likely too harsh for a sustained digestion duration.

Although DNase is known to improve yield by degrading DNA from cells that have ruptured, since DNA both inhibits proteolysis and causes cellular aggregation⁵, this enzyme only increased day 2 viability, not yield. While the addition of hyaluronidase did not improve 6-month-old valve dissociation, it did improve 6-week-old valve dissociation, consistent with increased GAG content in human infant valves compared to human adult valves.¹¹ Neutral protease, which is a gentler, less tryptic enzyme (similar to the collagenases⁷), was found to increase yield and 2 day viability for both age groups. Based on developmental milestones and growth studies, a 6-week-old pig is approximately equivalent to approximately an 8-year-old human; whereas a 6-month-old pig is approximately equivalent to a 17-19 year-old human¹⁷⁻¹⁹ (Table 2-4).

Table 2-4. Human and Porcine Age Equivalencies.

Porcine Age	Corresponding Human Age
5 days	infant ¹⁸
4 weeks	toddler ¹⁸
5 weeks	4-5 years-old ¹⁷
6 weeks	~8 years [^]
4 months	adolescent ¹⁸
5 months	13.7 years-old ¹⁹
6 months	17 year-old female, 19 year-old male [^]
6 year-old sow	old [^]
<u>life span: 10-15 years, but for sows considerably shorter (esp. if reproducing)[^]</u>	

[^]=personal communication with Dr. Gil Costas, DVM, Texas Heart Institute.

Valves from the different age groups were shown to require different concentrations of collagenases. The need for a higher concentration of collagenase III in the older group was not surprising considering numerous researchers have used the digestion time of valve tissue as an indication of crosslinking (with an increase in digestion time indicating more crosslinking), and reported differences between age groups.⁹ The cell yield from 6-month-old valves also increased with the concentration of collagenase, while 6-week-old valve disaggregation was improved with lower concentrations and optimal at 1 mg/ml, implying that higher concentrations may be too harsh for younger cells. Similarly, the finding that 0.1 mg/ml DNase improved the 6-week-old valve disaggregation suggests that these cells are more prone to rupture and therefore the DNase was able to prevent the released DNA from forming sticky cell aggregates.

Cost effectiveness was a major factor in determining the optimal enzymatic mixture. In 2006, a bottle of 100 mg of collagenase III cost \$29 from Worthington Biochemical. Per sample, 1 mg/ml of collagenase III cost \$2.32, while 4 mg/ml cost \$4.64, and 7 mg/ml cost \$16.24. The specialized enzymes were also costly; optimizing their effectiveness should offer substantial savings.

Limitations in this study were shown by the day 2 tests, which often showed that a small percentage of cells died after seeding; this experimental design also could not indicate long-term viability. However, since many valvular cell studies need to expand these cells in culture, the MTT test on day 2 indicated which technique produces the greatest number of viable, proliferating cells in the short term. Another limitation is that we only used collagenase products from the Worthington Biochemical and results may

not translate to enzymes from all other manufacturers. To enable comparison between manufacturers, the caseinase, clostripain, collagenase, and tryptic assay numbers for a given product should be examined. The unit activities of the collagenases that we used are given in Table 2-5; these data indicate the tight range of activity present between the two different lots of collagenase III that were used in this study.

Table 2-5. Activities of Enzymes in Crude Collagenase III Preparation.

Specific Enzyme	Activity
Collagenase	130-150 u/mg dw
Caseinase	148 u/mg dw
Clostripain	1.85-1.97 u/mg dw
Trypsin	0.24-0.28 u/mg dw

dw = dry weight

CONCLUSIONS

The optimum enzymatic digest mixtures were determined to be 1 mg/ml of collagenase III for 6-week-old pigs, along with 0.3 mg/ml hyaluronidase, 0.1 mg/ml DNase, and 2 mg/ml neutral protease dissolved in DMEM containing 2.5% antibiotic/antimycotic solution and 2.5% HEPES buffer. The optimum mixture for 6-month-old pigs was 2 mg/ml collagenase III and 2 mg/ml neutral protease, dissolved in the same DMEM/ABAM/HEPES. The optimized duration of digestion was 4 hours for each age of aortic valve. These findings provide age-specific and cost-effective conditions for improving the yield of VIC isolation, which should have utility in experimental evaluations of valvular cell biology and tissue engineering investigations.

In this chapter enzymatic valvular interstitial cell (VIC) isolation was optimized. This optimization was foundational to the thesis, as it was used in many other studies throughout this thesis work. In the next chapter, the first of the studies directly examining valve mechanobiology, some of the questions related to how normal valves change with age are addressed. Specifically, in the next study changes in aortic and mitral valve collagen content and turnover in fetal and postnatal aging are analyzed.

REFERENCES

1. LeBlanc JG, Russell JL. Pediatric cardiac surgery in the 1990s. *Surg Clin North Am.* 1998;78(5):729-747.
2. Vesely I. Tissue Engineering of Heart Valves. *Encyclopedia of Biomaterials and Biomedical Engineering.* New York, NY: Marcel Dekker, Inc; 2004.
3. Kershaw JD, Misfield M, Sievers HH, M.H. Y, Chester AH. Specific regional and directional contractile responses of aortic cusp tissue. *J Heart Valve Dis.* 2004;13(5):798-803.
4. Taylor PM, Allen SP, Dreger SA, Yacoub MH. Human cardiac valve interstitial cells in collagen sponge: a biological three-dimensional matrix for tissue engineering. *J Heart Valve Dis.* 2002;11(3):298-306.
5. Freshney RI. *Culture of animal cells.* 4th Edition ed. New York, NY: Wiley-Liss; 2000.
6. Waymouth C. To disaggregate or not to disaggregate injury and cell disaggregation, transient or permanent? *In Vitro.* 1974;10:97-111.
7. Worthington V, ed. *Enzymes related biochemicals manual.* Lakewood, NJ: Worthington Biochemical Corporation; 1993.
8. Messier RH, Jr, Bass BL, Aly HM, Jones JL, Domkowski PW, Wallace RB, Hopkins RA. Dual structural and functional phenotypes of the porcine aortic valve interstitial population: characteristics of the leaflet myofibroblast. *J Surg Res.* 1994;57(1):1-21.
9. Angrist A. Aging heart valves and a unitary pathological hypothesis for sclerosis. *J Gerontol.* 1964;19:135-143.
10. Bashey RI, Torii S, Angrist A. Age-related collagen and elastin content of human heart valves. *J Gerontology.* 1967;9(19):203-208.
11. Aikawa E, Whittaker P, Farber M, Mendelson K, Padera RF, Aikawa M, F.J. S. Human semilunar cardiac valve remodeling by activated cells from fetus to adult: implications for postnatal adaptation, pathology, and tissue engineering. *Circulation.* 2006;113(10):1344-1352.
12. Hoffman-Kim D, Maish MS, Krueger PM, Lukoff H, Bert A, Hong T, Hopkins RA. Comparison of three myofibroblast cell sources for the tissue engineering of cardiac valves. *Tissue Eng.* 2005;11(1-2):288-301.
13. Declercq H, Van den Vreken N, De Maeyer E, Verbeeck R, Schacht E, De Ridder L, Cornelissen M. Isolation, proliferation and differentiation of osteoblastic cells to study cell/biomaterial interactions: comparison of different isolation techniques and source. *Biomaterials.* 2004;25(5):757-768.
14. Kedjarune U, Pongprerachok S, Arpornmaeklong P, Ungkusonmongkhon K. Culturing primary human gingival epithelial cells: comparison of two isolation techniques. *J Craniomaxillofac Surg.* 2001;29(4):224-231.

15. Sharefkin JB, Van Wart HE, Cruess DF, Albus RA, Levine EM. Adult human endothelial cell enzymatic harvesting. Estimates of efficiency and comparison of crude and partially purified bacterial collagenase preparations by replicate microwell culture and fibronectin degradation measured by enzyme-linked immunosorbent assay. *J Vasc Surg.* 1986;4(6):567-577.
16. Blevins TL, Carroll JL, Raza AM, Grande-Allen KJ. Phenotypic characterization of isolated valvular interstitial cell subpopulations. *J Heart Valve Dis.* 2006;15(6):815-822.
17. Brody S, Ragsdale AC. The equivalence of age in animals. *Journal of General Physiology.* 1922;5(2):205-213.
18. Durham SR, Raghupathi R, Helfaer MA, Marwaha S, Duhaime A-C. Age-related differences in acute physiologic responses to focal traumatic brain injury in piglets. *Pediatr Neurosurg.* 2000;33:76-82.
19. Mumford FB, Hogan AG, Bernard PM. Growth curves of swine. *Missouri Agr Exp Sta Research Bulletin.* 1923;62:36-39.
20. Butcher JT, Nerem RM. Porcine aortic valve interstitial cells in three-dimensional culture: comparison of phenotype with aortic smooth muscle cells. *J Heart Valve Dis.* 2004;13(3):478-485.
21. Roy A BN, Yacoub MH. Molecular characterization of interstitial cells isolated from human heart valves. *J Heart Valve Dis.* 2000;9(3):459-464.
22. Messier RH Jr BB, Aly HM, Jones JL, Domkowski PW, Wallace RB, Hopkins RA. Dual structural and functional phenotypes of the porcine aortic valve interstitial population: characteristics of the leaflet myofibroblast. *J Surg Res.* 1994;57(1):1-21.
23. Wiester LM, Giachelli CM. Expression and function of the integrin alpha9beta1 in bovine aortic valve interstitial cells. *J Heart Valve Dis.* 2003;12(5):605-616.
24. Johnson CM, Hanson MN, Helgeson SC. Porcine cardiac valvular subendothelial cells in culture: cell isolation and growth characteristics. *J Mol Cell Cardiol.* 1987;19(12):1185-1193.

Chapter 3: Age-Related Changes in Collagen Synthesis and Turnover in Porcine Heart Valves

This chapter is the first of four chapters (Chapters 3-6) examining age-related changes in matrix composition and structure in normal aortic and mitral valves. In this chapter changes in collagen content and turnover in fetal and postnatal aging are analyzed.

ABSTRACT

Background: The 6-month-old pig is commonly used to study human heart valve biology and several age-specific valve diseases. However, correlation of porcine valve biology and development with that of humans has not been thoroughly assessed. Given the matrix's important role in valve function, we characterized porcine valve matrix structure and collagen turnover during development and aging.

Methods: Porcine aortic (AV) and mitral valves (MV) throughout fetal development and at 6-weeks, 6-months, and 6-years, were examined using Movat pentachrome stain and immunohistochemistry for collagen III, markers of collagen synthesis [molecular chaperone HSP47, hydroxylating enzyme prolyl 4-hydroxylase (P4H), crosslinking enzyme lysyl oxidase (LOX)] and collagen degradation (matrix metalloproteinase (MMP)-13), and a marker of an "activated" cellular phenotype, smooth muscle alpha-actin (SMaA). Analysis of variance was used to compare staining intensities.

Results: Cell density measurements showed layer differentiation in the 1st trimester ($p < 0.003$) and decreased ten-fold from 2nd trimester to 6-year-old ($p < 0.025$). Matrix turnover was identified by co-localization of P4H, HSP47, and MMP13 and correlated to an “activated” cellular phenotype. SMaA expression was noted on the inflow surface of both valves. P4H and LOX were maximally expressed around mature collagen ($p < 0.001$). P4H increased during fetal development ($p < 0.01$) and in the 6-year-old AV fibrosa ($p < 0.05$). Collagen-related markers were consistently higher in the AV than MV (HSP47 in fetal; P4H, Col III, and LOX in 6-year-old).

Conclusions: Substantial changes occur in porcine valve matrix throughout life. These changes should be considered when comparing clinical studies with the porcine model for studying age-specific diseases.

The work contained in this chapter was published as:

Stephens EH, Grande-Allen KJ, **Age-related Changes in Collagen Synthesis and Turnover in Porcine Heart Valves.** *Journal of Heart Valve Disease.* 2007;16(6):672-682.

INTRODUCTION

Because of anatomic and structural similarities¹⁻³ and convenient availability, the 6-month-old pig is a widely used animal model for investigating human heart valve biology and disease, including age-specific diseases such as calcific aortic stenosis and myxomatous mitral valve disease.⁴ Additionally, much of the work towards developing a tissue engineered valve has focused upon thoroughly characterizing valves using the tissues and cells from 6-month-old pigs. However, the biology of the porcine valve has not been assessed in depth for concurrence with human biology nor has its valve development been related to human valve development. A critical component of the heart valve is the extracellular matrix (ECM), whose synthesis and degradation enables both valve development and maintenance of the mature valve. Once merely thought to act as a scaffold, it is now known that the ECM is intimately involved in morphogenesis, cell migration, growth factor and other cell regulation, material behavior,⁵ and mechanosensing.⁶ Although previous studies of the ECM in porcine valve aging have been performed, these have largely evaluated histological changes,⁴ such as those evident in Movat pentachrome stained samples, or collagen crosslinking.^{7,8} In this investigation, we characterized porcine valve matrix composition, structure, and turnover during development and aging. Our particular focus was on collagen, since it is the primary load bearing component of the valvular ECM.⁸ By utilizing immunohistochemistry to stain for various enzymes regulating collagen synthesis and degradation, we were able to localize sites of active turnover within the intricate structure of the valve, as well as observe the co-localization of these markers.

METHODS

General Procedure

Porcine hearts were obtained from an abattoir within 24 hours of death (Fisher Ham and Meat, Spring, TX for 6-week-old pigs and 6-month-old pigs, Animal Technologies, Tyler, TX for fetal and 6-year-old pigs). The sample set consisted of porcine mitral (MV) and aortic valves (AV) aged first fetal trimester, second trimester, third trimester, 6-week-old, 6-month-old, and 6-year-old (Table 3-1). One leaflet per AV

Table 3-1. Sample Size.

Age	MV	AV
Fetal 1 st trimester	5	4
Fetal 2 nd trimester	3	4
Fetal 3 rd trimester	3	4
6-week-old	5	4
6-month-old	3	3
6-year-old	4	5

*Each sample represents a heart valve from a different animal.

Multiple sections of each sample were stained.

(chosen randomly from the non-coronary, right coronary, and left coronary leaflets) was used; for the MV only the anterior leaflet was used. Tissues were fixed overnight in 10% formalin and 5 mm wide cross sections of the leaflet were cut from the annulus to the free edge. For the aortic valve, cross sections were taken slightly off center thereby avoiding the nodule of Arantius. These cross sections were embedded in paraffin, sectioned to a thickness of five microns and mounted on slides according to standard procedures. A schematic of the sections analyzed for each valve is shown in Fig. 3-1.

Histology and Immunohistochemistry

Table 3-2. Collection of Antibodies Used in Immunohistochemistry.

Antibody	Abbreviation	Function	Dilution
Collagen III ^a	Col III	type of collagen	1:100
Prolyl-4 Hydroxylase ^b	P4H	collagen synthesis	1:200
Heat Shock Protein 47 ^a	HSP47	collagen synthesis	1:200
Matrix Metalloproteinase-13 ^b	MMP13	collagen degradation	1:200
Matrix Metalloproteinase-1 ^c	MMP1	collagen degradation	1:200
Matrix Metalloproteinase-2 ^c	MMP2	collagen degradation	1:100
Matrix Metalloproteinase-9 ^c	MMP9	collagen degradation	1:100
Tissue Inhibitor of MMP-1 ^c	TIMP1	inhibition of collagen degradation	1:100
Lysyl Oxidase ^d	LOX	collagen and elastin crosslinking	1:250
Smooth Muscle Alpha-Actin ^e	SMAA	activated phenotype	1:1000

^aAbcam (Cambridge, MA); ^bChemicon (Temecula, CA); ^cAssay Designs (Ann Arbor, MI);

^dImgenex (San Diego, CA); ^eDakocytomation (Denmark).

Each sample was stained histologically with Movat pentachrome and immunohistochemically (IHC) for markers involved in the synthesis and turnover of collagen (Table 3-2), including collagen III (col III), lysyl oxidase (LOX), prolyl 4-hydroxylase (P4H), matrix metalloproteinase 13 (MMP13), and heat shock protein 47 (HSP47). P4H is an enzyme located in the rough endoplasmic reticulum that is required for the critical step of proline hydroxylation in collagen synthesis.⁹ MMP13 is a major enzyme responsible for collagen degradation and HSP47 is a molecular chaperone that is specific to procollagen biosynthesis.¹⁰ In contrast to P4H and HSP47, LOX has two major roles in matrix metabolism, namely the initiation and regulation of crosslinking in elastic fibers and collagen.¹¹

In addition to these collagen-related markers, sections were stained for smooth muscle alpha-actin (SMAA) to serve as an indicator of an activated cellular phenotype. Recognizing that P4H, MMP13, and HSP47 have common roles in collagen metabolism and that these markers were frequently co-localized, we summed their intensities to

create a new marker denoted “total P4H, MMP13, HSP47” (tPMH). In addition, several representative slides for each age group were stained for MMP1, MMP2, MMP9, and Tissue Inhibitor of Matrix Metalloproteinase (TIMP)-1. Negative controls were stained with either secondary antibody only or the appropriate isotype control (mouse or rabbit IgG) with their corresponding secondary antibody.

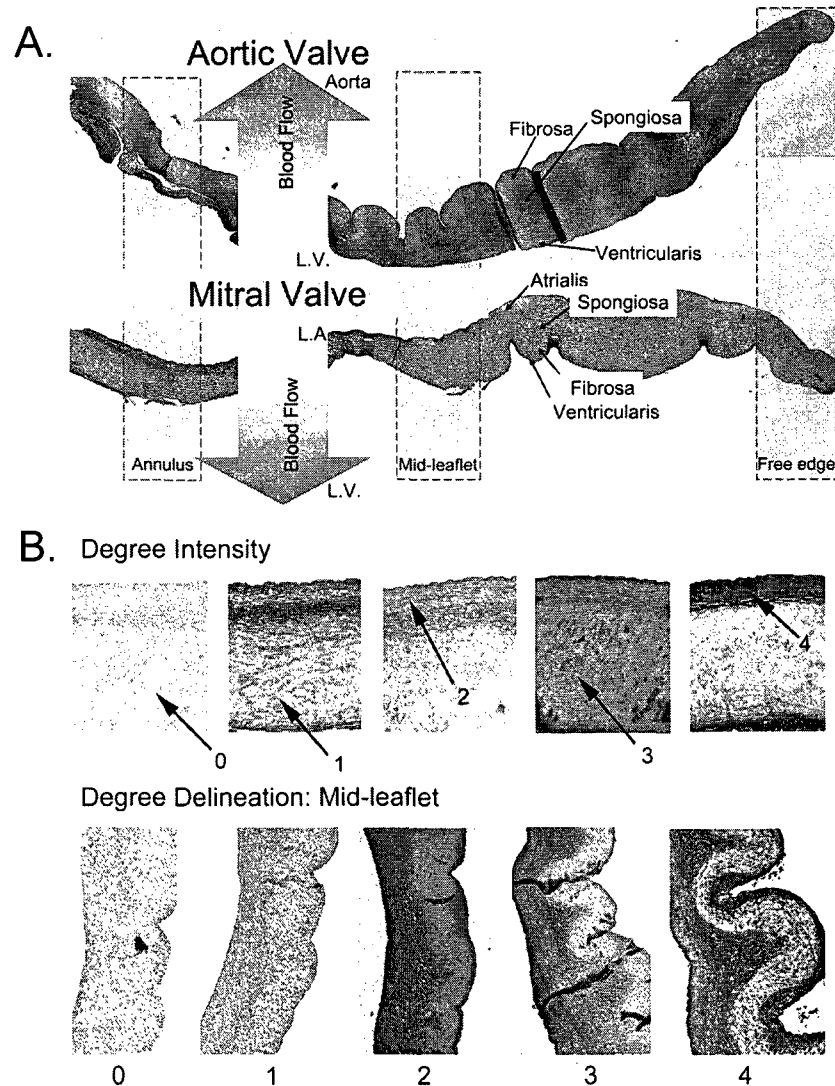


Fig. 3-1: A) Diagrams of histological layers of MV and AV. Shaded dashed-line boxes indicate approximate portions used in grading. B) Example of grading rubrics. Top: rubric for quantification of staining intensity illustrating the range in intensities using several histological layers. Intensity was quantified for each histological layer and leaflet portion using this rubric. Pictured examples are from the annulus of the MV. Bottom: rubric used for quantification of degree delineation in the mid-leaflet. Lower grades indicate less differentiation between histological layers. Both contrast in intensity between layers and clarity of the boundary between the layers were considered in the quantification. Pictured examples are from the AV.

IHC samples were graded on a scale of 0-4 for each characteristic in the different portions of the leaflet (annulus, mid-leaflet, and free edge) and in each histological layer (ventricularis, atrialis (mitral only), spongiosa, and fibrosa), except for the free edge, which was considered one layer. The term “inflow layer” was defined to be the atrialis of the MV and ventricularis of the AV. A corresponding “outflow layer” was not compared between AV and MV because of their inherent differences in composition. Characteristics evaluated included marker intensity, delineation (marker’s contrast between valve layers), and “fibrosa correlation” (degree of marker co-localization with the Movat saffron stained collagen). Quantification was based on a grading rubric for each characteristic (Fig. 3-1). Between 1 to 3 sections of a given valve sample were stained with a given antibody. Replicates, whether within the same IHC batch or in different IHC batches, were averaged. The quantification was performed twice, once by an unblinded observer and once by a trained blinded observer. Intra- and inter-observer variabilities as well as intra- and inter-IHC batch variabilities were all calculated to be less than 15% based on replicated sections.

Overall collagen content and alignment was analyzed using picrosirius red staining. Sections were stained in picrosirius red (0.1% w/v) for 1 hour followed by a water wash and dehydration. Sections were visualized using a Nikon Eclipse E600 microscope and polarization filter (Melville, NY), and Image Pro software (Media Cybernetics, Bethesda, MD). Collagen type was inferred based on hue (red=collagen I, yellow/green=reticular collagen).¹²

Cell Density Assessment

Cell density was assessed by counting nuclei within specific layers of the annulus and mid-leaflet regions of either Movat or IHC slides counterstained with hematoxylin. All evaluations were done by a trained individual blinded to the valve identity.

Statistical Analysis

Multifactorial analysis of variance was performed using SigmaStat (SPSS, Chicago, IL). When the data for a given characteristic (marker intensity, delineation, and fibrosa correlation) was normally distributed (as determined by the software), the program continued with a three factor ANOVA for age (factor 1: 6-week-old, 6-month-old, and 6-year-old), histological layer (factor 2: ventricularis, atrialis, spongiosa, and fibrosa), and valve region (factor 3: annulus, mid-leaflet, and free edge). When the data set was not normally distributed, a comparison on ranks was used. In both cases the level of significance was set at 0.05. The Holm-Sidak all-pairwise multi-comparison method was used for post-hoc testing.

RESULTS

Cellular Density

The valvular cell density decreased throughout fetal development and aging ($p < 0.001$, Fig. 3-2). First and second trimester fetal valves were approximately 50 and 10 times more cellular, respectively, than that of the 6-year-old (unless otherwise indicated, results refer to both MV and AV and include all layers). This magnitude reduction in cell density corroborates research in human¹³ and chick valves.¹⁴

Differentiation of cell density between layers was previously reported in chick valves, but only for the late gestation stage at which point rudimentary layers are apparent by Movat.¹⁴ Here, we found that as early as the 1st trimester the spongiosa layer had 65-67% lower cell density than the other layers (data not shown, $p < 0.003$).

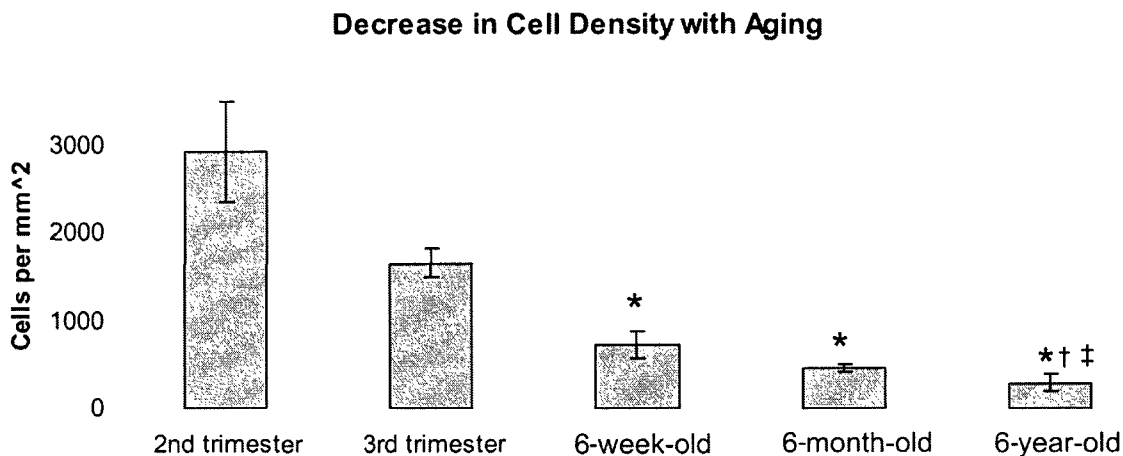


Fig. 3-2: Decrease in cell density with aging. Error bars indicate standard deviation. †= $p \leq 0.001$ vs. 1st trimester, *= $p < 0.025$ vs. 2nd trimester fetal, $\delta = p < 0.05$ vs. 3rd trimester fetal. $\gamma = p < 0.05$ vs. 6-week-old.

Movat Tissue Organization

Early fetal valves appeared as a largely amorphous collection of GAGs that became more delineated with trimester, confirming reports in other species.¹³⁻¹⁵ This delineation by Movat staining was accompanied by differential protein expression demonstrated immunohistochemically (Fig. 3-3). These findings are consistent with

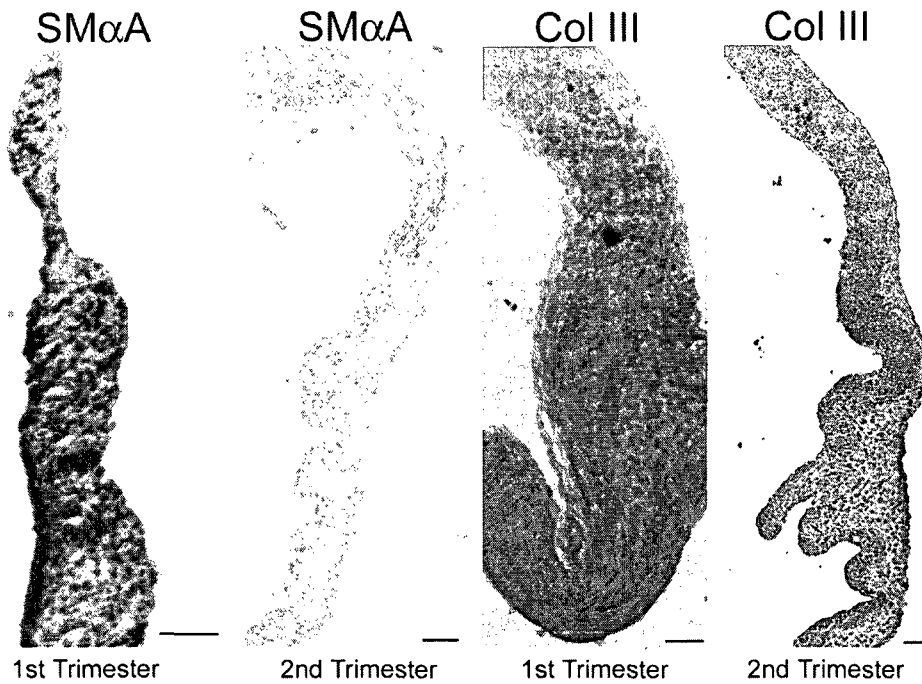


Fig. 3-3: Differential protein expression evident in 2nd trimester MV as compared to 1st trimester MV. Left hand side: SMAαA staining; right hand side: collagen III staining. Scale bars are 50 μm.

reports describing fetal human valves as consisting primarily of proteoglycans with minor disorganized collagen in the second trimester, a bilaminar structure at 20 weeks, and a trilaminar structure at 36 weeks.¹³

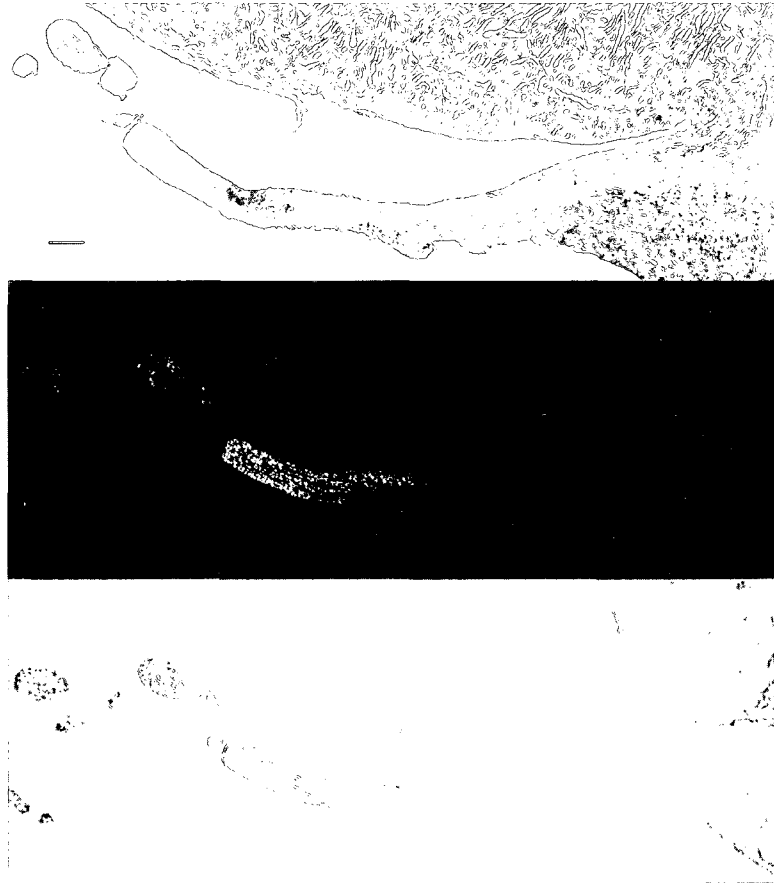


Fig. 3-4: Visualization of picosirius red stained 3rd trimester MV under polarized light (middle panel) demonstrates a rudimentary collagen I fibrosa. Bottom panel shows the same section visualized without polarization and top panel shows the corresponding Movat stain. Scale bar is 100 μ m.

Visualization of picosirius red stained fetal valve sections demonstrated that aligned type I collagen was evident at points of chordal development, and was even evident as a rudimentary fibrosa in third trimester mitral valves (Fig. 3-4). The third trimester valve was still profoundly less differentiated than the 6-week-old valve and the 6-month-old valve was significantly more delineated than the 6-week-old valve (Fig. 3-5), implying substantial postnatal valve development as reported by others^{13, 14} and as recently documented in mice.¹⁵ Paralleling this increase in organization was an increase in collagen content demonstrated by Movat. However, even in the 3rd

trimester valve the yellow stained Movat collagen was weakly evident and intermixed with GAGs, whereas in the fibrosa of the 6-week-old the Movat collagen formed a continuous band, which then appeared more densely collagenous in the 6-month-old.

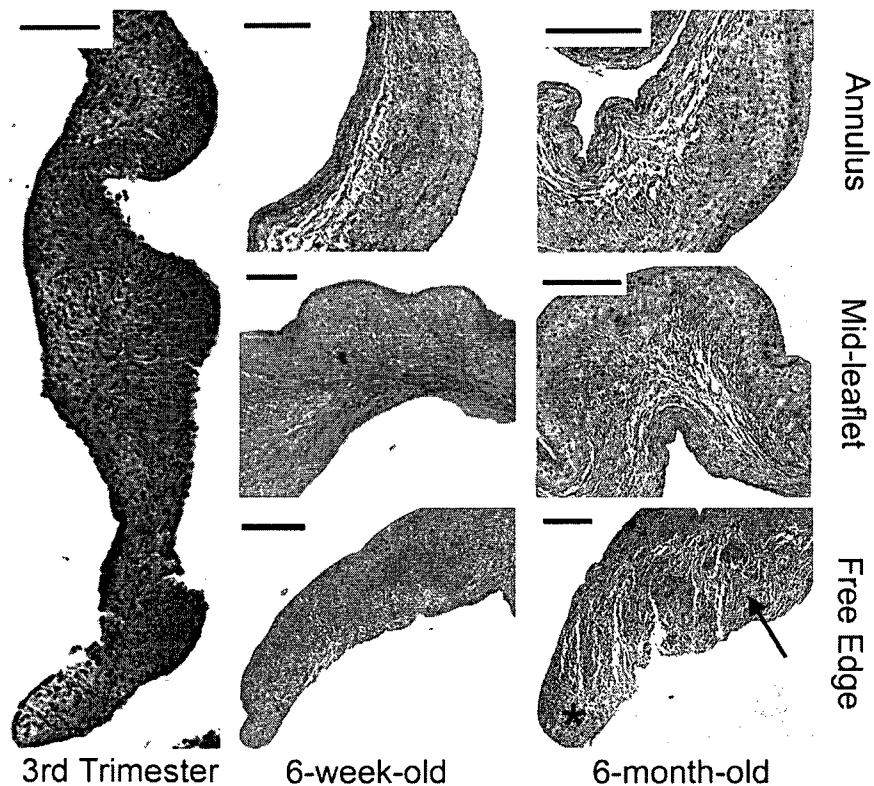


Fig. 3-5: Right two panels contain comparison of 6-month-old and 6-week-old AV at each region of the leaflet illustrates greater tissue organization in 6-month-old compared to 6-week-old. Asterisk marks collagen capping the free edge tip. Arrow points to presence of collagen in the spongiosa. Scale bars on the right two panels are 200 μm . Left panel shows Movat of 3rd trimester AV, which is less differentiated than the 6-week-old AV. Scale bar on fetal picture is 100 μm . Movat pentachrome stains glycosaminoglycans blue, collagen yellow, and elastic fibers black.

In the 6-month-old, some collagen was present within the spongiosa and towards the free edge, sometimes even encasing the tip of the free edge (Fig. 3-5). This increase in tissue organization from the fetal stage to adulthood was found despite a significant age-related reduction in cell density (Fig. 3-2), and confirms other reports of an

increase in collagen content and orientation during this age period.¹³ With advanced aging, collagen fiber organization has been documented to decrease⁴ consistent with the decrease in organized collagen III staining found here ($p < 0.01$).

Fetal Valve Immunohistochemistry

The abundance of the collagen synthesis enzyme P4H increased with increasing fetal age, corresponding to increased Movat collagen ($p < 0.01$). The collagen degrading enzyme MMP13 also tended to increase over the trimesters, whereas MMP1 decreased during fetal development ($p < 0.05$), and collagen III remained stable. While increased MMP13 expression is consistent with findings in humans, the decrease in MMP1 is not.¹³ This contradiction could simply be a result of different antibody specificity, or may be a true species difference. Fetal valves also stained positively for MMP2 and MMP9, with TIMP1 staining on the leaflet edge.

Matrix Turnover and the “Activated” Cell Phenotype

The markers P4H, MMP13, and HSP47 were frequently found to co-localize in all age groups (Fig. 3-6). Considering the specificity of P4H and HSP47 for collagen synthesis, and MMP13 for matrix degradation, such areas of co-localization were identified as possible regions of active collagen turnover, i.e., areas of ongoing collagen synthesis and degradation. Wherever all three proteins were expressed, SMaA staining was distinctly apparent. These results build upon previous immunoblotting studies showing a correlation between HSP47 and SMaA⁶ by demonstrating specific spatial correspondence between areas of collagen synthesis and the “activated” cell phenotype.

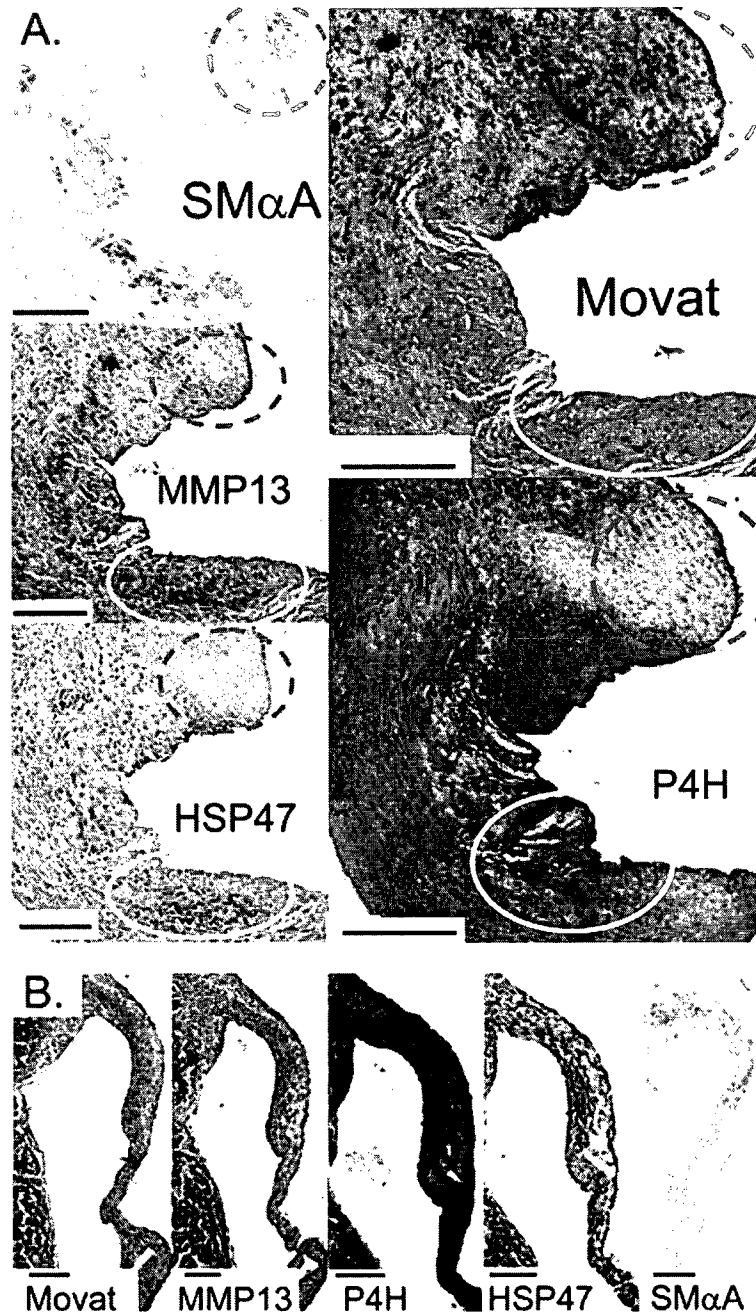


Fig. 3-6: Co-localization of P4H, MMP13, HSP47, and SMαA indicate areas of collagen turnover and an activated cell phenotype. A) 6-month-old AV free edge: dashed red circles indicate areas of degradation without new synthesis. White circles indicate areas of degradation and new synthesis. SMαA co-localizes with both. Scale bars are 200 μm. B) Third trimester fetal MV shows similar co-localization. Scale bars are 100 μm.

Valvular interstitial cells are thought to transition from a quiescent, fibroblast-like state to this “activated” myofibroblast-like state in the context of remodeling,¹⁶ pathological

states such as myxomatous mitral valve disease,¹⁷ and immature tissue engineered constructs.¹⁸ In valves, this “activated” cell phenotype is also characterized by positive staining for non-muscle myosin (produced by activated mesenchymal cells) and negative staining for myosin.^{17, 18} In this study, P4H, MMP13, and HSP47 were frequently, but not always, co-localized suggesting that different stages of active collagen synthesis occur throughout the valve. In several fetal valves, localized expression of SMαA was especially dramatic, particularly in locations that would later become rich in highly aligned collagen, such as the chordae and fibrosa (Fig. 3-7). The activated nature of those cells in those regions, and the observation that those regions later demonstrated low staining for the collagen synthesis and crosslinking enzymes, may indicate that collagen in the fibrosa and chordae matures very early.

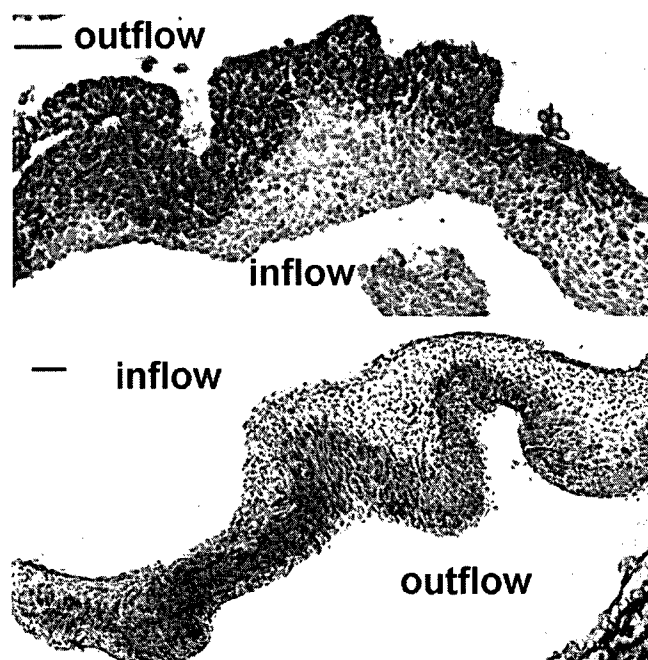


Fig. 3-7: SMαA expression in fetal valves. Upper: 1st trimester MV; lower: 3rd trimester AV. Scale bars are 50 μm.

Common Findings between Aortic and Mitral Valves

In both valves, staining for P4H and LOX was strongest surrounding the well-defined fibrosa of the mid-leaflet (Fig. 3-8); across all age groups, the fibrosa had the

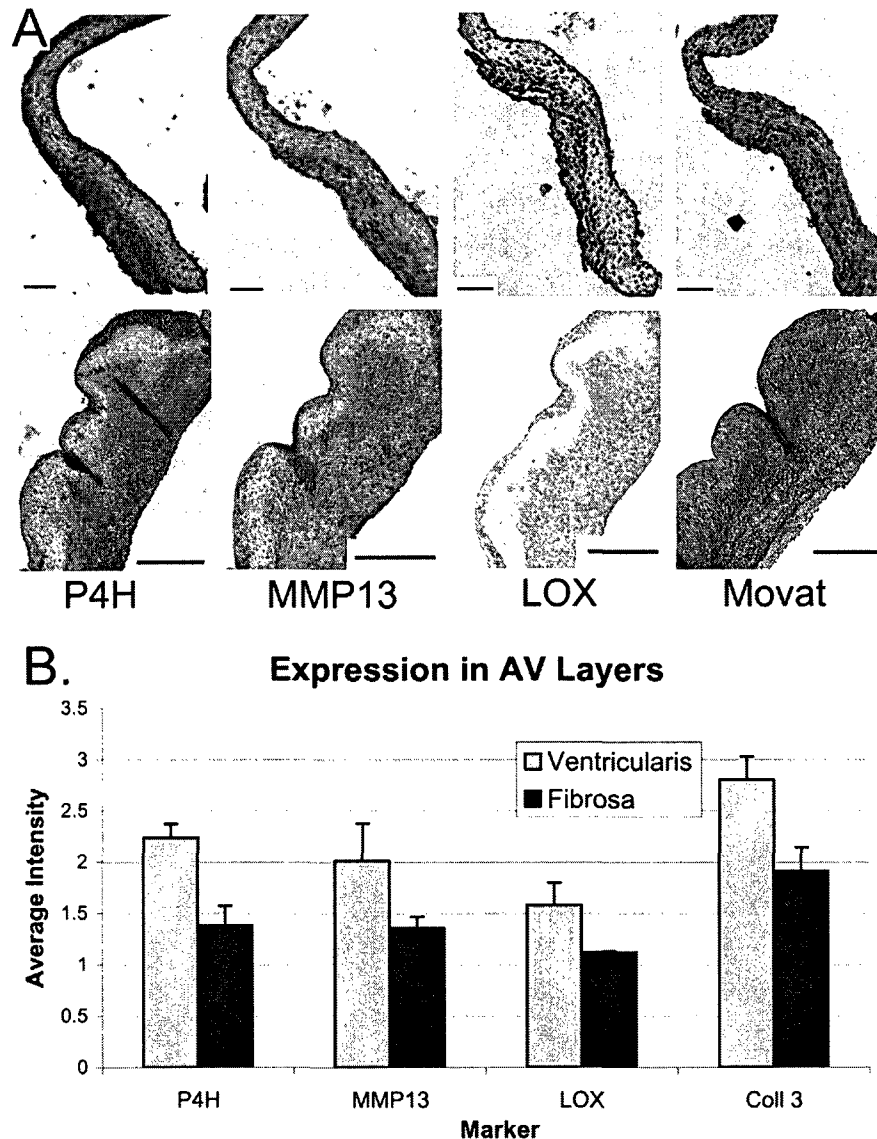


Fig. 3-8: A) Co-localization of LOX with P4H and MMP13. Note that LOX, P4H, and MMP13 do not stain where the well-defined, mid-leaflet fibrosa appears in Movat. Top: 2nd trimester MV with 50 μm scale bars; bottom: 6-year-old AV with 200 μm scale bars. B) Graph illustrating significantly lower collagen-related marker expression in the fibrosa as opposed to the ventricularis. Data is taken from mid-leaflet portion of all ages of AV (data was not significantly different across age groups, $p=0.12$). Error bars are standard errors of the mean.

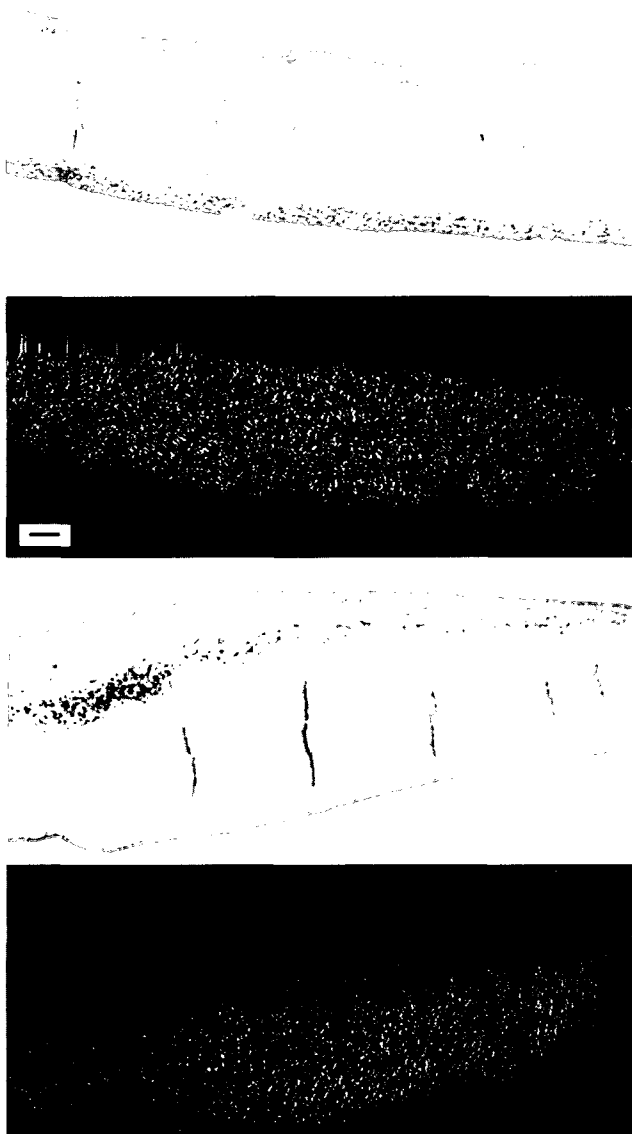


Fig. 3-9: Visualization of picrosirius red stained 6-month-old MV under polarized light shows aligned collagen type I corresponding to the Movat yellow stained tissue. The upper two images show the annulus and the lower two images show the mid-leaflet. For each pair of images, the top image is the Movat stained section and the bottom image is the picrosirius red stained section viewed under polarized light. Scale bar is 100 μ m.

least staining for these two markers ($p < 0.001$; no statistical effect of age). This pattern suggests that active collagen synthesis occurs surrounding, but not within, the yellow Movat staining collagen of the fibrosa, which could be considered “mature.” In fact, other markers, including collagen III, MMP13, and the combination tPMH, all stained the least in the fibrosa of both valves ($p < 0.001$). While visualization of picrosirius red stained sections under polarized light confirmed previous reports that the fibrosa mainly consists of load bearing type I collagen (Fig. 3-9),¹⁹ localization of the network-forming type III collagen^{20, 21} to areas outside of the fibrosa likely demonstrates the need for flexibility and even stress transfer within these regions. The

networking of collagen III could include interaction with elastic fibers,²¹ which may be

responsible for high LOX expression in the atrialis of the MV and the ventricularis of both valves (Table 3-3).

Table 3-3. Differential Protein Expression Between Layers.

Markers	Mitral Valve	Aortic Valve
tPMH	at > v > sp > f*	sp > v >> f*
P4H	at > sp = v > f*	sp > v > f*
MMP13	at = v > sp > f*	v > sp > f*
HSP47	v = at = sp > f*	--
Col III	at > sp = v = f*	v > sp > f*
LOX	at > v > sp > f*	v > sp > f*

v=ventricularis, sp=spongiosa, f=fibrosa, fe=free edge, at=atrialis,

*p≤0.05, "--" indicates no significant difference.

Differences between Aortic and Mitral Valves

Overall, the AV demonstrated greater expression of collagen-related markers, particularly collagen III, than found in the MV (Table 3-4). The AV spongiosa exhibited

Table 3-4. Comparison of Protein Expression between Mitral Valve and Aortic Valve.

Markers	All Layers	Fibrosa, Spongiosa, Free edge	Tissue Structure
tPMH	--	sp AV > MV‡	--
P4H	--	sp and f AV > MV*	fc AoV > MV‡, d AV > MV*
MMP13	--	fe AV > MV‡	--
HSP47	--	f AV > MV‡	--
Col III	AV > MV*	sp AV > MV‡, fe AV > MV†	--
LOX	--	--	--

v=ventricularis, sp=spongiosa, f=fibrosa, fe=free edge, at=atrialis; fc=fibrosa correlation, d=delineation; *p≤0.001, †p≤0.01, ‡p≤0.05, "--" indicates no significant difference.

greater expression of P4H, collagen III, and the combined “turnover” marker tPMH (all p<0.05). Similarly, the fibrosa of the AV had more P4H and HSP47 expression, and the free edge of the AV had more collagen III and LOX expression. Interestingly, HSP47

expression was significantly higher in the fetal AV than in the fetal MV ($p < 0.035$); given that these fetal valves do not experience major differences in their mechanical environments, this pattern may reflect the inherent differences between the valves' embryonic origins.²² Taken together, these patterns may reflect inherent structural and load bearing differences, or the differential effects of aging,⁴ between valves.

The relative intensities between histological layers also differed between MV and AV. In the MV, the marker combination tPMH showed highest expression in the inflow elastic layer (atrialis) and decreased progressively in the ventricularis and then spongiosa ($p < 0.001$). In the AV, however, tPMH staining was strongest in the spongiosa, and lower in the inflow elastic layer (ventricularis, $p < 0.001$). In the MV, P4H was more abundant in the inflow (atrialis) and less in the spongiosa and ventricularis, while in the AV, P4H was higher in the spongiosa and lower in the inflow (ventricularis, $p < 0.001$). This different pattern could be interpreted as the spongiosa playing more of a role in load-bearing in the AV than in the MV. Furthermore, the AV contained a gradient of P4H expression from the annulus (low) to the free edge (high); the P4H staining was also more organized (as measured by delineation and fibrosa correlation, $p < 0.035$) in the AV compared to the MV. The correlation of this marker with the valve anatomy and layers suggests that P4H expression may be related to the valve mechanical behavior, since the layered nature of the valve and the interaction between the layers contributes to the material properties.²³

Postnatal Aging Changes in Aortic and Mitral Valves

While the most marked changes with aging were evident during fetal development, the expression of several markers changed significantly with postnatal aging. For instance, the metalloproteinases MMP2 and MMP9 and their inhibitor TIMP1 were only expressed in the 6-year-old valves and even that was very slight. This finding is interesting given findings in pigs and humans showing expression of these markers in age-related valvular heart disease.^{24, 25} In contrast, slight staining of MMP1 was evident in the 6-month-old and 6-year-old porcine valves. Another change noted in both valves was a decrease in the delineation of the combination marker tPMH in the 6-year-old ($p < 0.015$) that may reflect the presence of collagen in all leaflet layers. Surprisingly, we observed MMP13 expression in all age groups in contradiction to previous reports noting that either the MV contains MMP1 but not MMP13,²⁶ or that MMP13 was present in interstitial cells from younger valves but not adult.¹⁸ Such discrepancies could be due to differences in antibody, or may be a true species difference that would need to be taken into consideration when using the pig as an animal model.

Changes with aging were also seen in the individual valve types. The AV showed significantly greater expression of P4H, LOX, and collagen III in the 6-year-old (all $p < 0.05$). In the AV fibrosa both P4H and tPMH were strongest in the 6-year-old (both $p < 0.05$), corroborating studies showing increased collagen content and crosslinking in aged heart valves.⁸ This result may also be explained by aging-related decreases in aortic compliance, which results in greater force applied to the AV fibrosa, the main load-

bearing element.⁴ Interestingly, the abundance of collagen III in the AV was higher in the 6-week-old and 6-year-old than in the 6-month-old ($p < 0.024$, Fig. 3-10A). A similar

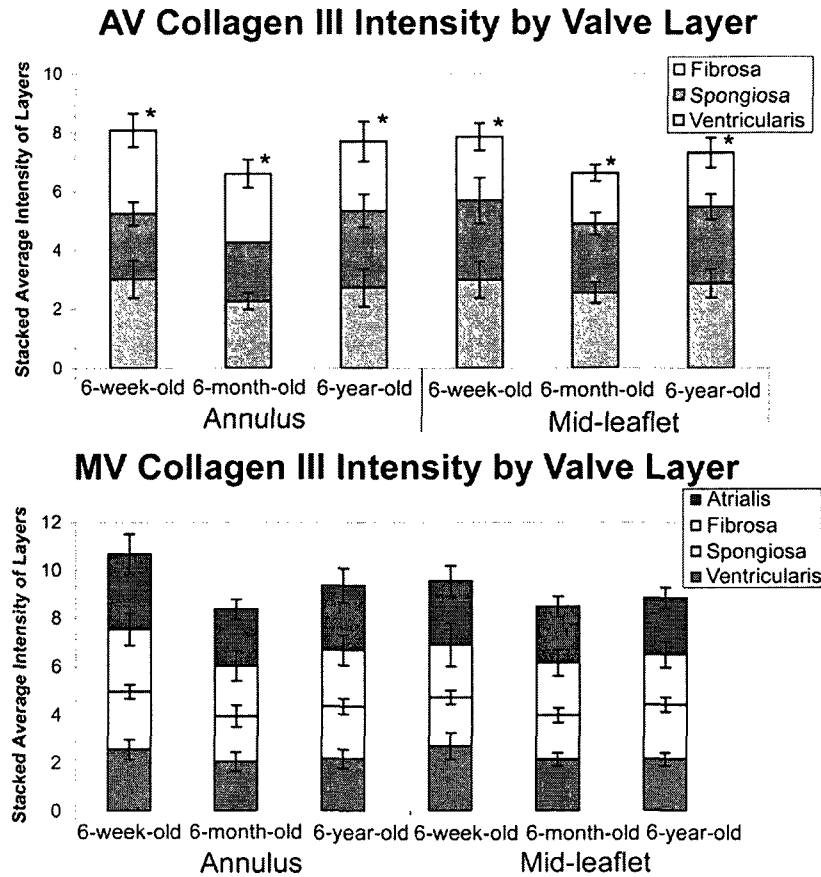


Fig. 3-10: A) Graph of collagen III intensity in layers of AV (each layer graded on a scale of 0-4, so maximum intensity is 12), displayed in a stacked format for visual demonstration. *total collagen III different between ages, $p < 0.024$. B) Graph of collagen III intensity in layers of MV (each layer graded on a scale of 0-4, so maximum intensity is 16), displayed in a stacked format for visual demonstration.

trend was seen in the MV (Fig. 3-10B). We speculate that the increased collagen III in the 6-week-old results from the AV adjusting to the higher pressures of the postnatal circulatory system²⁷ along with increased demands of growth. In the 6-year-old valve the increase in collagen III staining intensity, which was accompanied by less delineation

($p < 0.02$) suggests that the age-related AV fibrosis involves type III collagen becoming diffusely abundant throughout the valve.

Both the 6-week-old and 6-year-old (but not the 6-month-old) AV demonstrated more MMP13 staining towards the leaflet free edge ($p < 0.05$), again emphasizing the unique mechanical demands of these age valves. An age-related increase in MMP13 expression at the AV free edge suggests that this location may experience sustained remodeling. Slightly different age effects were found in the MV. Collagen III expression in the fibrosa was greatest at 6 weeks ($p < 0.025$), which may be due to the MV adjusting to higher postnatal pressures.²⁷ In the ventricularis (elastic outflow layer), collagen III expression was greatest at 6 years and may aid in withstanding the increased pressures resulting from an overall decrease in aortic compliance.

Novel Finding of SMaA Expression

SMaA, the marker indicating cell activation, was found in a subendothelial line both along the inflow and outflow surfaces of both valve types as well as deeper approaching the fibrosa (Fig. 3-11). This pattern was evident in all age groups. These findings confirm previously reported expression of SMaA as present in the subendothelial outflow layer as well as deeper within the valve interior;¹³ we have additionally noted a second, previously unreported anatomical distribution on the inflow surface, and have localized the interior expression to the fibrosa. When SMaA was not in these anatomical distributions, it was co-localized with tPMH. This data suggests that SMaA expression is both constitutive (with a particular anatomic distribution) as well as inducibly linked to collagen turnover and the “activated” cell phenotype.

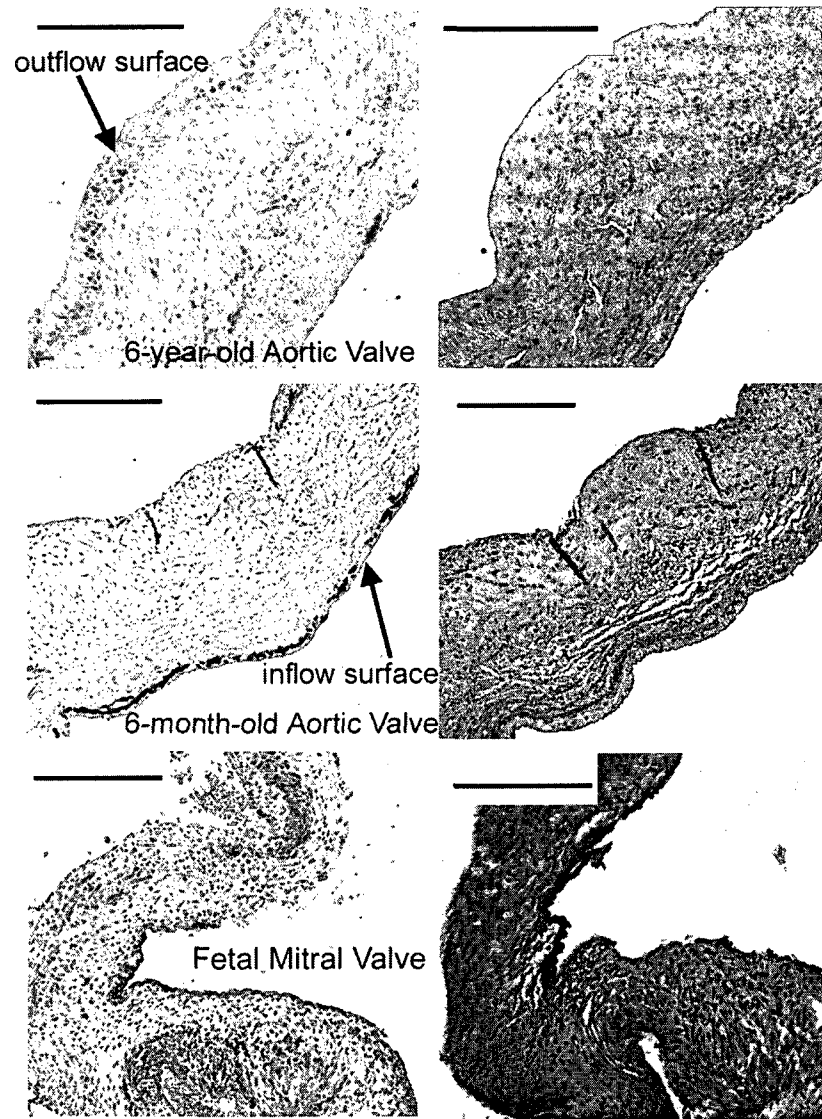


Fig. 3-11: Two anatomical distributions of SMAA (inflow and outflow). Top: 6-year-old AV, middle: 6-month-old AV, bottom: 3rd trimester MV. Left: SMAA staining, right: Movat pentachrome stain. Scale bars are 200 μ m.

DISCUSSION

In this study we characterized changes in matrix composition and turnover in porcine MV and AV with age, concentrating on collagen, the primary component of the valve ECM. Our studies both confirm previous studies into changes in collagen

crosslinking and stability with age;^{4, 7, 8} as well as expand upon those results by addressing active collagen synthesis and degradation. These findings are applicable to porcine models for basic and translational studies of heart valve disease relevant to different human age groups, and give further insight into the role of matrix turnover of the MV and AV during the development and aging processes.

Significant differences between various ages of human valves have recently been described¹³ – these same differences should be present in the optimal animal model for human valves. In the study of valve biology, age is an important consideration because valves of different ages likely respond to mechanical or biological stimuli in fundamentally different ways. Age-related changes are similarly an important consideration in the study of valve pathology and pathogenesis given that a number of valve diseases are age-related (i.e., calcific aortic stenosis or congenital defects). Furthermore, knowledge of age-related changes in valve composition and turnover is essential for attempts to tissue engineer a valve for different aged patients.

These findings regarding collagen turnover and organization both complement and build on previous reports of valvular collagen concentration, degree of crosslinking, and fiber morphology. In those investigations, biochemical, enzymatic, microscopic, and advanced optical approaches were used to demonstrate an age-related increase in collagen concentration,⁸ crosslinking,⁷ alignment,¹³ and fragmentation,⁴ although the AV demonstrates greater collagen crosslink stability with age compared to the MV.²⁸

Relevance to Human Valves

The observed differences in matrix organization and turnover between heart valves of different aged pigs suggest that specific ages of pigs may be age-appropriate models for various human heart valve diseases and for use in engineering a heart valve for different age groups. As far as the correlation of these findings to human disease, based on developmental milestones and growth studies, a 6-week-old pig is approximately equivalent to an 8-year-old human, whereas a 6-month-old pig is approximately equivalent to a 17-19 year-old human (see Chapter 2, Table 2-4).²⁹⁻³¹ However, several caveats should be noted about the pig as an animal model. It appears that the MMP profile of porcine valves differs from humans, especially for MMP13 and MMP1. If these are true species differences, this altered MMP profile could affect studies of calcific aortic stenosis and myxomatous mitral valves. Furthermore, given the age correlation for the 6-month-old pig discussed above, the 6-month-old pig may not be the appropriately aged pig in which to study aging-related human valve diseases.

Limitations

Study limitations included the use of a semi-quantitative grading system and two observers; however, we quantified the between-observer, within-observer, and between-batch variability as 14%, 11%, and 14% respectively, and inter-batch variability as 14%. While IHC staining using a collagen I antibody would have been a more specific method for demonstrating the location of collagen I, numerous antibodies and pretreatment methods were unable to demonstrate the presence of collagen type I within the yellow Movat stained fibrosa, likely due to the abundance of mature crosslinks blocking

antigenic binding sites. Therefore, picrosirius red allowed us to look at collagen types as well as fiber alignment. Also, we analyzed consistent leaflet sections but did not assess the variability in leaflet makeup around the entire circumference of the valve. Despite these limitations, numerous significant patterns were found between leaflet regions, layers, valves, and age groups. Another possible limitation could be that MMP13 is not specific for collagen degradation and requires activation,³² and therefore MMP13 expression may not directly translate to collagen degradation. That noted, MMP13 is considered a major regulator of collagen turnover.³² Furthermore, the other major MMPs involved in the degradation of matrix that were assessed, including MMP1, MMP2, and MMP9, as well as the main inhibitor, TIMP1, were negative in all ages of valves except the 6-year-old pig. While we recognize that more quantitative methods for assessing matrix turnover are available, the use of immunohistochemistry has enabled us to localize expression of these synthesis and degradation markers within the heterogeneous leaflet microstructure.

CONCLUSIONS

In summary, in this novel study of markers of collagen synthesis and degradation we have presented data that suggests matrix turnover tends to occur at the edge of “mature” collagen, an observation that was evident at all ages tested. Furthermore, we have shown that this turnover is associated with an “activated” cell phenotype. The difference in MMP profiles between the pig and that reported in humans may need to be taken into account when using the pig as an animal model, in particular for studies in diseases involving the MMPs. Furthermore, considering that a 6-month-old pig is

equivalent to a human young adult, this age pig may not be an appropriate animal model for age-related pathologies like calcific aortic stenosis and myxomatous mitral valve disease. Future studies into other extracellular matrix components need to be performed in order to give a more complete picture of development and aging of the heart valve.

This chapter, which analyzed changes in collagen content and turnover in fetal and postnatal aging, was the first of four chapters (Chapters 3-6) examining age-related changes in matrix composition and structure in normal aortic and mitral valves. In the next chapter in this series of studies, age-related changes in aortic and mitral valve proteoglycan and glycosaminoglycan content will be addressed.

REFERENCES

1. Crick S, Sheppard M, Ho S, Gebstein L, Anderson R. Anatomy of the pig heart: comparisons with normal human cardiac structure. *J Anat.* 1998;193:105-119.
2. Sands MP, Rittenhouse EA, Mohri H, Merendino KA. An anatomical comparison of human pig, calf, and sheep aortic valves. *Ann Thorac Surg.* 1969;8(5):407-414.
3. Sim EK, Muskawad S, Lim CS, Yeo JH, Lim KH, Grignani RT, Durrani A, Lau G, Duran C. Comparison of human and porcine aortic valves. *Clin Anat.* 2003;16(3):193-196.
4. Sell S, Scully RE. Aging Changes in the Aortic and Mitral Valves. Histologic and Histochemical Studies, with Observations on the Pathogenesis of Calcific Aortic Stenosis and Calcification of the Mitral Annulus. *Am J Pathol.* 1965;46:345-365.
5. Engler A, Sen S, Sweeney H, Discher D. Matrix elasticity directs stem cell lineage specification. *Cell.* 2006;126(4):677-689.
6. Merryman WD, Youn I, Lukoff HD, Krueger PM, Guilak F, Hopkins RA, Sacks MS. Correlation between heart valve interstitial cell stiffness and transvalvular pressure: implications for collagen biosynthesis. *Am J Physiol Heart Circ Physiol.* 2006;290(1):H224-231.
7. Angrist A. Aging heart valves and a unitary pathological hypothesis for sclerosis. *J Gerontology.* 1964;19:135-143.
8. Bashey RI, Torii S, Angrist A. Age-related collagen and elastin content of human heart valves. *J Gerontology.* 1967;9(19):203-208.
9. Kivirikko K, Myllyla R. Post-translational processing of procollagens. *Ann N Y Acad Sci.* 1985;460:187-201.
10. Masuda H, Hosokawa T, Nagata K. Expression and localization of collagen-binding stress protein Hsp47 in mouse embryo development: comparison with types I and II collagen. *Cell Stress & Chaperones.* 1998;3(4):256-264.
11. Rucker B, Murray J. Cross-linking amino acids in collagen and elastin. *Am J Clin Nutr.* 1978;31(7):1221-1236.
12. Zhang H, Sun L, Wang W, Ma X. Quantitative analysis of fibrosis formation on the microcapsule surface with the use of picro-sirius red staining, polarized light microscopy, and digital image analysis. *J Biomed Mater Res.* 2006;76A:120-125.
13. Aikawa E, Whittaker P, Farber M, Mendelson K, Padera RF, Aikawa M, Schoen FJ. Human semilunar cardiac valve remodeling by activated cells from fetus to adult: implications for postnatal adaptation, pathology, and tissue engineering. *Circulation.* 2006;113(10):1344-1352.

14. Hinton RB, Jr, Lincoln J, Deutsch GH, Osinska H, Manning PB, Benson DW, Yutzey KE. Extracellular matrix remodeling and organization in developing and diseased aortic valves. *Circ Res.* 2006;98(11):1431-1438.
15. Kruithof BP, Krawitz SA, Gaussin V. Atrioventricular valve development during late embryonic and postnatal stages involves condensation and extracellular matrix remodeling. *Dev Bio.* 2006;302(1):208-217.
16. Rabkin-Aikawa E, Farber M, Aikawa M, Schoen FJ. Dynamic and reversible changes of interstitial cell phenotype during remodeling of cardiac valves. *J Heart Valve Dis.* 2002;13(5):841-847.
17. Rabkin E, Aikawa M, Stone J, Fukumoto Y, Libby P, Schoen F. Activated interstitial myofibroblasts express catabolic enzymes and mediate matrix remodeling in myxomatous heart valves. *Circulation.* 2001;104(21):2525-2532.
18. Rabkin E, Hoerstrup SP, Aikawa M, Mayer JE, Schoen FJ. Evolution of Cell Phenotype and Extracellular Matrix in Tissue-Engineered Heart Valves during In-Vitro Maturation and In-Vivo Remodeling. *J Heart Valve Dis.* 2001;11:308-314.
19. Keller F, Leutert G. [Age dependence of collagen structures of the human heart]. *Z Gerontol.* 1994;27(3):186-193.
20. Arteaga-Solis E, Gayraud B, Ramirez F. Elastic and collagenous networks in vascular diseases. *Cell Struct Funct.* 2000 25(2):69-72.
21. Ushiki T. Collagen fibers, reticular fibers and elastic fibers. A comprehensive understanding from a morphological viewpoint. *Arch Histol Cytol.* 2002;65(2):109-126.
22. Larsen WJ. *Human Embryology.* 3rd ed. New York: Churchill Livingstone; 2001.
23. Vesely I. Reconstruction of loads in the fibrosa and ventricularis of porcine aortic valves. *ASAIO J.* 1996;42(5):M739-M746.
24. Polyakova V, Hein S, Kostin S, Ziegelhoeffer T, Schaper J. Matrix metalloproteinases and their tissue inhibitors in pressure-overloaded human myocardium during heart failure progression. *J Am Coll Cardiol.* 2004;44(8):1609-1618.
25. Kaden JJ DC, Grobholz R, Fischer CS, Vocke DC, Kilic R, Sarikoc A, Pinol R, Hagl S, Lang S, Brueckmann M, Borggreffe M. Inflammatory regulation of extracellular matrix remodeling in calcific aortic valve stenosis. *Cardiovasc Pathol.* 2005;14(2):80-87.
26. Dreger SA, Taylor PM, Allen SP, Yacoub MH. Profile and localization of matrix metalloproteinases (MMPs) and their tissue inhibitors (TIMPs) in human heart valves. *J Heart Valve Dis.* 2002;11(6):875-880.
27. Anderson PAW. The heart and development. *Sem Perinatol.* 1996;20(6):482-509.
28. Aldous IG, Lee JM. Collagen structure reveals differing strategies for resisting fatigue loading in heart valves. Paper presented at: 2005 Annual Fall Meeting of the Biomedical Engineering Society 2005; Baltimore, MD.

29. Durham SR, Raghupathi R, Helfaer MA, Marwaha S, Duhaime A-C. Age-related differences in acute physiologic responses to focal traumatic brain injury in piglets. *Pediatr Neurosurg.* 2000;33:76-82.
30. Brody S, Pandit A. Microarchitectural characterization of the aortic heart valve. *Adv Exp Med Biol.* 2004;553:167-186.
31. Mumford F, Hogan A, Bernard P. Growth curves of swine. *Missouri Agr Exp Sta Research Bulletin.* 1923;62:36-39.
32. Knauper V, Lopez-Otin C, Smith B, Knight G, Murphy G. Biochemical Characterization of Human Collagenase-3. *J Biol Chem.* 1996;271(3):1544-1550.

Chapter 4: Valve Proteoglycan Content and Glycosaminoglycan Fine Structure are Unique to Microstructure, Mechanical Load, and Age: Relevance to an Age-Specific Tissue Engineered Heart Valve

This chapter is the second of four chapters (Chapters 3-6) examining age-related changes in matrix composition and structure in normal aortic and mitral valves. In this chapter changes in proteoglycan and glycosaminoglycan in fetal and postnatal aging are analyzed.

ABSTRACT

Background: This study characterized valve proteoglycan and glycosaminoglycan composition during development and aging. This knowledge is important for the development of age-specific tissue engineered heart valves as well as treatments for age-specific valvulopathies.

Methods: Aortic valves and mitral valves from 1st-3rd trimester, 6-week, 6-month, and 6-year-old pigs were examined using immunohistochemistry for versican, biglycan, decorin, and hyaluronan, as well as elastin and fibrillin. The fine structure of glycosaminoglycans was examined by fluorophore-assisted carbohydrate electrophoresis.

Results: Decorin expression was strongest in the 6-year-old valves, particularly in the aortic valve spongiosa. The quantity of iduronate was also highest in the 6-year-old. The central tensile-loading region of the anterior mitral leaflet demonstrated reduced glycosaminoglycan content, chain length, and hydration and a larger fraction of 4-sulfated iduronate and lower fraction of 6-sulfation. With age, the anterior leaflet center showed a further increase in 4-sulfated iduronate and decrease in 6-sulfation. In contrast, the anterior leaflet free edge showed decreased iduronate and 4-sulfated glucuronate content with age. The young aortic valve was similar to the mitral valve free edge with a higher concentration of glycosaminoglycans and 6 rather than 4-sulfation, but aged to resemble the mitral anterior leaflet center, with an increase in 4-sulfated iduronate content and a decrease in the 6-sulfation fraction. Elastin and fibrillin often co-localized with the proteoglycans studied, but elastin co-localized most specifically with versican.

Conclusions: Composition and fine structure changes in valve proteoglycans and glycosaminoglycans with age are complex and distinct within valve type, histological layers, and regions of different mechanical loading.

The work contained in this chapter was published as:

Stephens EH, Chu C-K, Grande-Allen KJ. **Valve Proteoglycan Content and Glycosaminoglycan Fine Structure are Unique to Microstructure, Mechanical Load and Age: Relevance to an Age-Specific Tissue-Engineered Heart Valve.** *Acta Biomaterialia*. 2008;4(5):1148-1160.

INTRODUCTION

Proteoglycans (PGs) and glycosaminoglycans (GAGs) are critical to the function of numerous soft connective tissues, including heart valves, providing material properties such as viscoelasticity and resistance to compression and tension.^{1,2} PGs and GAGs also play crucial roles in tissue differentiation, growth factor regulation, and various pathologies.² During fetal development, PGs and GAGs are the predominant components of the nascent heart valves.³ In the mature mitral valve (MV), the composition of PGs and GAGs has been shown to vary regionally based on the type of mechanical loading experienced by these tissues.⁴ Altered proportions of selected PG and GAGs are found in myxomatous MV disease,⁵ are likely responsible for the altered material properties of these swollen tissues,⁶ and are possibly involved in the disease pathogenesis. The loss of the GAG and PG-rich spongiosa layer, which normally provides shear between the outer valve layers and thus enables complex valve leaflet movement,⁷ from porcine bioprosthetic aortic valves (AVs) is thought to be instrumental in the failure of these devices.⁸ Overall, knowledge of the composition and distribution of the various GAGs and PGs within heart valves appears to be essential information for understanding and recapitulating the complex mechanics of the heart valve leaflets. It is unknown, however, how the composition and distribution of these PGs and GAGs change throughout development and aging, when the heart valves experience significant changes in mechanical loading and tissue differentiation. Because these PG and GAG changes are likely important to valve function, characterizing them would contribute to the understanding of age-specific valve pathologies as well as the design of an age-specific tissue engineered heart valve (TEHV).

While a limited number of reports have described the GAGs found in valves,⁹⁻¹³ these largely have not considered the complex valvular microstructure, the effect of subject age, and GAG fine structure, i.e., the abundance of variously sulfated disaccharides. Sulfation patterns on GAG chains are thought to be critical to GAG function and cellular signaling.¹⁴⁻¹⁶ Although a previous study on GAGs in human MV considered age,⁴ the age-range was limited to the adult years. Moreover, characterizations of PGs and GAGs during heart and heart valve development have been limited to specific PGs and signaling pathways.^{17, 18} Reports characterizing GAGs in the AV are even fewer and largely assess bioprosthetic valves and TEHVs.¹⁹⁻²⁴

Therefore, it was the aim of this study to characterize the composition and fine structure of GAGs and PGs during development and aging of porcine AVs and MVs. As described above, this work represents the first such analysis of the AV, and changes in GAG composition during development have not been studied in either the AV or MV. In this study, a novel combination of two approaches, immunohistochemistry (IHC) and fluorophore-assisted carbohydrate electrophoresis (FACE) was used to provide detailed information regarding layer and region-specific PG and GAG distribution as well as the quantity and fine structure of various GAGs in different regions of the valve. IHC was also used to co-localize the specific PGs and GAGs with other matrix components with which they are known to interact, such as fibrillin, elastin, and transforming growth factor beta (TGF β). Porcine valves, which commonly serve as an animal model for human heart valve biology and pathology,²⁵ were used because they were available in large numbers at a wide range of ages. Considering the substantial regional differences in

mechanical loading of the MV, the MV leaflets were separated into regions experiencing compression (leaflet free edge, MVF) or tension (anterior leaflet center, MVAC).

METHODS

General Procedure

Porcine hearts were obtained within 24 hours of death (Fisher Ham and Meat, Spring, TX for 6-week- and 6-month-old pigs, Animal Technologies, Tyler, TX for fetal and 6-year-old pigs). Hearts were maintained on ice until processing. The sample set consisted of MVs and AVs from first fetal trimester, second trimester, third trimester, 6-week-, 6-month-, and 6-year-old pigs. Three to five valves from each age group were used for IHC, whereas 10-14 valves from each postnatal age group were used for FACE. One leaflet per AV was used, chosen randomly from the non-coronary, right coronary, and left coronary leaflets; for the MV only the anterior leaflet was used. Tissues used in IHC were fixed overnight in 10% formalin before cross sections of the leaflet were cut from the annulus to the free edge, embedded in paraffin, and sectioned to 5 μ m thickness. For the AV, cross sections were taken slightly off center to avoid the nodule of Arantius.

Histology and Histochemistry

Each sample was stained histologically with Movat pentachrome to demonstrate the overall distribution of collagen (saffron yellow), elastin (hematoxylin black), and PGs/GAGs (alcian blue) within the valves. This staining enabled the identification of the different leaflet layers.²⁶ Histochemistry was performed to demonstrate the PGs versican (clone 2B1, Associates of Cape Cod, Falmouth, MA), decorin (LF-122, gift from Dr.

Larry Fisher, NIH), and biglycan (LF-104, gift from Dr. Larry Fisher), since these are the predominant extracellular PGs found in valves,⁴ as well as the GAG hyaluronan (HA) using the biotinylated HA binding protein (Associates of Cape Cod). Sections were also stained using antibodies against the extracellular matrix components elastin and fibrillin (both from Abcam, Cambridge, MA) as well as the growth factor TGF β (Biovision, Mountain View, CA) since those proteins are known to interact with versican, decorin, and biglycan.^{1, 27-29} Because the PG antibodies' binding site is on the core protein obscured by GAG chains, an enzymatic digestion of the GAG chains was used (200mU/ml chondroitinase ABC (Associates of Cape Cod, Falmouth, MA) 1 hour, 37 degrees) before placement of the primary antibody. A citrate-buffer based antigen retrieval (30 min, 80 degrees) was used in the staining of elastin, fibrillin, and TGF β . IHC samples were graded on a scale of 0-4 to evaluate marker intensity and delineation (marker's contrast between valve layers) in each histological layer (ventricularis, atrialis (MV only), spongiosa, and fibrosa). Further details on grading, as well as an example of a grading rubric, can be found in Chapter 3. Overall PG intensity was assessed using the combination marker "tPG," which was the sum of versican, decorin, and biglycan staining for a given region/layer. The term "inflow layer" was defined to be the atrialis of the MV and ventricularis of the AV. A corresponding "outflow layer" was not compared between AV and MV because of their inherent differences in composition.

Fluorophore-Assisted Carbohydrate Electrophoresis (FACE)

Fluorophore-assisted carbohydrate electrophoresis (FACE) was used to analyze the quantity and fine structure of the different GAG classes, HA and the

chondroitin/dermatan sulfates (CS/DS).^{4, 30} Note on nomenclature: CS is defined as only containing glucuronate while DS is defined as containing some quantity of iduronate. First, the AV (random leaflet) and MV (anterior leaflet) were dissected from the different postnatal aged porcine hearts within 24 hours of death. The mass of tissue obtained from fetal valves was insufficient for FACE analysis; therefore FACE was performed on the different postnatal valves only. The MV anterior leaflet was trimmed of chordae then divided into the “tensile loading” center region (MVAC) and the “compressive loading” free edge (MVF). Each sample was weighed before and after lyophilization; hydration was calculated as (wet weight - lyophilized weight)/wet weight. The GAGs in the lyophilized samples were then analyzed by FACE.^{4, 5} In brief, the lyophilized samples were rehydrated with 100 μ L of 100 mM ammonium acetate, minced, and digested with 100 μ l of 10 mg/ml proteinase K (EMD Pharmaceutical, Durham, NC) at 60°C, 16-48 hrs. After boiling 5 min to inactivate the Proteinase K, aliquot volumes containing approximately 5 μ g of uronic acid were digested with either chondroitinase ABC and chondroitinase ACII (3 μ l each, Associates of Cape Cod, Falmouth, MA) or ACII alone, 3 hrs, 37°C. The samples were then vacuum dried and the GAGs fluorescently tagged using 2-aminoacridone HCl (Molecular Probes, Eugene, OR). Samples were resolved on 20% acrylamide gels. Fluorescently labeled known quantities of maltotriose were mixed with the samples and run on the gel to generate a standard curve relating concentration to fluorescence intensity. The gels were imaged and the bands analyzed using Gel-Pro (Media Cybernetics, Silver Spring, MD). Specific GAGs were identified by correspondence to bands in a disaccharide standard lane and quantified using the

integrated optical density of the band(s) and the fluorescence standard curve as previously described.⁴

The resulting GAG profiles were used to calculate several factors specific to particular PGs. The ratios of 6-sulfation to 4-sulfation and glucuronate to iduronate containing disaccharides were calculated.⁴ The average CS/DS chain length was estimated by calculating on a lane-by-lane basis the total amount of the CS/DS Δ disaccharides and dividing it by the total amount of saccharides at the nonreducing termini of the chains. The measured GAG class contents from each sample were normalized to the tissue dry weight to estimate the tissue concentrations and proportions of the different classes were calculated relative to the total GAG quantity as measured by FACE.

Statistical Analysis

Multifactorial analysis of variance was performed using SigmaStat (SPSS, Chicago, IL). When the data for a given characteristic was normally distributed (as determined by the software), the program continued with an ANOVA. When the data set was not normally distributed, a comparison on ranks was used. In both cases the level of significance was set at 0.05. In a few, select cases the p-value for a non-normally distributed data set was >0.05 after rank transformation, while the original ANOVA had a p-value <0.05 ; in these instances the p-value from the original ANOVA is listed followed by an "R." In all other cases of non-normalized data sets, the p-value from the rank transformed ANOVA is shown. The Holm-Sidak all-pairwise multi-comparison method was used for post-hoc testing.

RESULTS

Proteoglycan Distribution

During the first fetal trimester, valve leaflets were largely an amorphous mass of PG and GAGs, demonstrated by Movat staining as a deep alcian blue present throughout

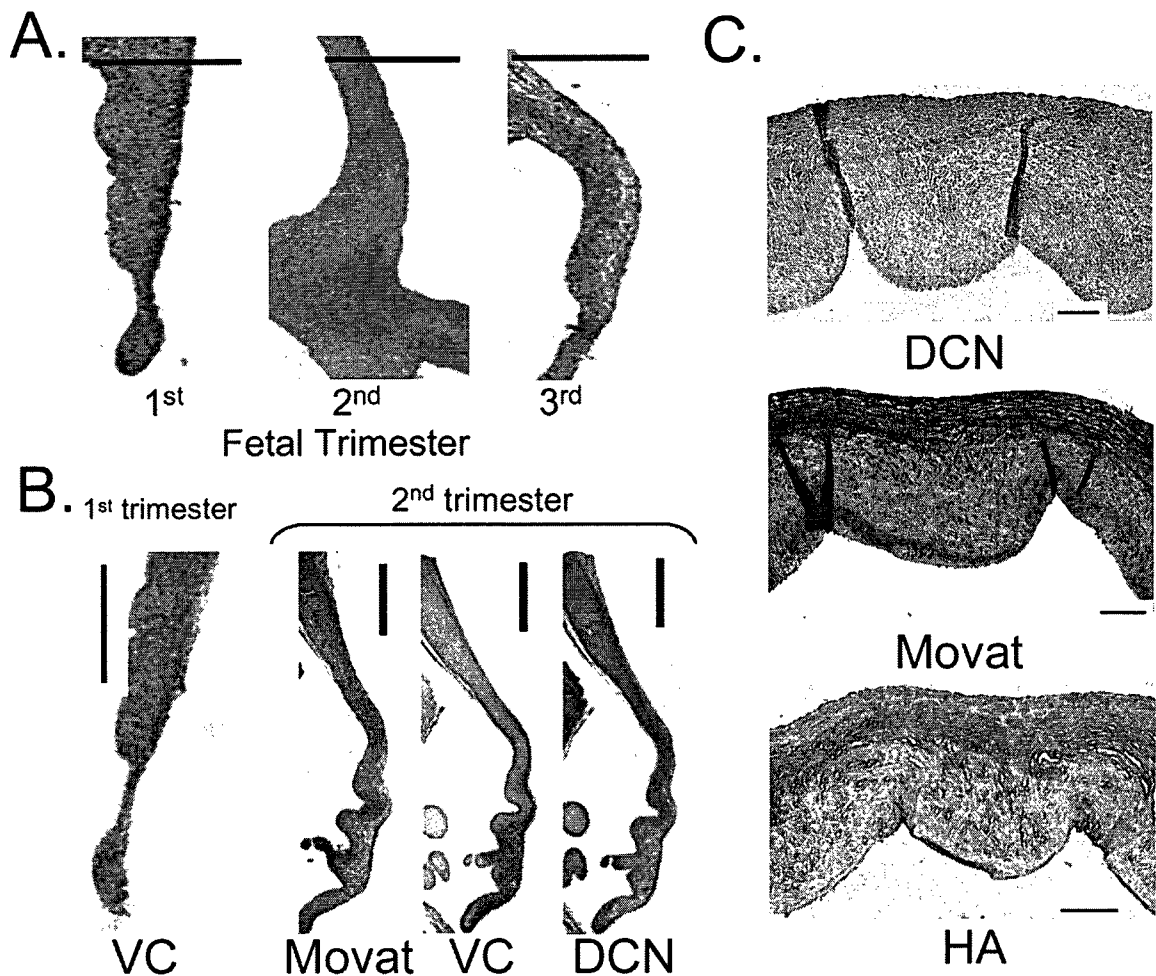


Fig. 4-1: A) 1st trimester valves largely consisted of an amorphous mass of proteoglycans (PGs) and glycosaminoglycans (GAGs). Over the course of fetal development rudimentary layers became apparent. B) In 1st trimester valves, the PG expression was largely ubiquitous. Expression became more localized over the course of fetal development. Scale bars indicate 100 μ m. C) Movat stain showed maximum PGs and GAGs in the spongiosa, but staining for DCN (and VC and BGN) was often stronger in other layers. In contrast, staining for hyaluronan (HA) was often strongest in the spongiosa. Sections are from the aortic valve and are oriented so that the ventricularis is at the top and fibrosa is at the bottom. Scale bars indicate 100 μ m.

the leaflet (Fig. 4-1A). As the trimesters progressed, rudimentary leaflet layers became apparent and PG staining became more localized (Fig. 4-1B). Postnatally, there tended to be a decrease in alcian blue-staining PG and GAGs intermixed in the annular fibrosa. This presence of intermixed PG and GAGs within the fibrosa also tended to be more prevalent in the AV compared to the MV, but neither of these trends was statistically significant. In the 6-month old valves, however, there was significantly stronger staining with alcian blue throughout the AV compared to the MV (p=0.042), a result that was predominantly due to the increased abundance of PG and GAGs in the annulus of the AV.

Table 4-1A. IHC Differential Protein Expression Between Layers of Postnatal Valves.

Marker	Mitral	Aortic
tPG [^]	v > sp,f > at*	v > sp > f*
DCN	--	v > sp,f [‡]
BGN	--	v >> sp > f [§]
VC	v > sp,f > at*	sp > v > f*
HA	at,v > sp > f*	sp > v > f*
Elastin	at > v,sp > f*	v > sp > f*
Fibrillin	at > sp,v > f [‡]	sp > v > f*

v=ventricularis, sp=spongiosa, f=fibrosa, at=atrialis, [^]tPG=sum of intensities of decorin (DCN), versican (VC), and biglycan (BGN). HA=hyaluronan.*=p≤0.001; [‡]=p≤0.01; [§]=p≤0.05. "--" indicates that there was no statistically significant difference.

The combination marker “tPG” (the sum of versican, decorin, and biglycan staining) showed significantly different staining intensity between layers as well as between the AV and MV. In the MV, tPG was strongest in the ventricularis, less abundant in the spongiosa and fibrosa, and least abundant in the atrialis (p<0.001, Table

4-1A). In contrast, in the AV, tPG staining was strongest in the ventricularis and lowest in the fibrosa (p<0.001). In both valves, tPG intensity increased with age, particularly in the spongiosa (p<0.01, Table 4-1B). Overall, tPG expression was higher in the AV than

Table 4-1B. IHC Changes in Protein Expression in Postnatal Valves with Aging.

Markers	Mitral		Aortic	
	All Layers	Individual Layers	All Layers	Individual Layers
tPG [^]	↑ w age*	sp ↑ w age*	max in 6yo [‡]	sp ↑ in 6yo [‡]
DCN	↑ in 6yo*	--	max in 6yo [§]	sp ↑ esp in 6yo [§]
BGN	↑ w age*	sp ↑ w age [§]	↑ in 6yo [§]	sp ↑ in 6yo [§]
VC	--	--	--	--
HA	--	--	--	--
Elastin	↓ in 6yo [‡]	fe ↓↓ in 6yo [§]	↓ w age*	v ↓ w age, esp 6yo [§]
Fibrillin	--	at ↓ w age [§]	↓ w age, [↑] [§]	sp ↓ w age

v=ventricularis, sp=spongiosa, f=fibrosa, at=atrialis, fe=free edge. [^]tPG=sum of intensities of decorin (DCN), versican (VC), and biglycan (BGN). HA=hyaluronan. *=p≤0.001; [‡]=p≤0.01; [§]=p≤0.05. 6yo=6-year-old; 6wk=6-week-old; 6mo=6-month-old. [↑]=increasing gradient from annulus to free edge. "--" indicates that there was no statistically significant difference.

in the MV; this difference was again most notable in the spongiosa (p<0.02, Table 4-1C).

When comparing the elastin-rich inflow layers of the 2 valves, tPG expression was also higher in the AV than in the MV (p<0.001).

Table 4-1C. IHC Differences in Protein Expression Between Postnatal MV and AV.

Markers	All Layers	Layer/Region
tPG [^]	AV > MV [‡]	sp AV > MV [§]
DCN	AV > MV [§]	--
BGN	AV > MV*	sp AV > MV [‡]
VC	--	--
HA	MV > AV [§]	--
Elastin	AV > MV [‡]	--
Fibrillin	--	--

sp=spongiosa. AV=aortic valve, MV=mitral valve. [^]tPG=sum of intensities of of decorin (DCN), versican (VC), and biglycan (BGN). HA=hyaluronan. *=p≤0.001; [‡]=p≤0.01; [§]=p≤0.05. "--" indicates that there was no statistically significant difference.

In the AV, decorin was more abundant in the ventricularis than in the spongiosa and fibrosa ($p < 0.005$, Table 4-1A); no such distinction in decorin staining between layers was detected in the MV. In both valves (and particularly in the AV spongiosa), decorin was most abundant in the 6-year-old leaflets ($p < 0.005$, Table 4-1B). Decorin was evident in fetal valves but showed no significant pattern of localization or age. Although decorin expression was not strongest in the fibrosa layer, it was the PG that was most often found within the collagen-rich fibrosa.

Biglycan expression was more ubiquitous than the other PGs, confirming other reports.³¹ No difference in biglycan was detected between MV layers, but in the AV the expression of biglycan was strongest in the ventricularis, less in the spongiosa, and lowest in the fibrosa ($p < 0.025$, Table 4-1A). Fetal valves showed moderate biglycan staining without detectable changes throughout trimesters. With age, biglycan staining in the AV both increased and became more diffuse ($p < 0.035$, Table 4-1B). Similar to decorin, the expression of biglycan was higher in the AV than in the MV, particularly in the spongiosa ($p < 0.003$, Table 4-1C).

Compared to the other PGs, versican expression in postnatal valves was unusual in that its abundance across layers did not increase with age; in fact, versican expression on the AV inflow surface decreased from the ages of 6-weeks to 6-months ($p < 0.009$). In the MV, versican expression was highest in the ventricularis, lower in the spongiosa and fibrosa, and lowest in the atrialis (Table 4-1A). However, in the AV, versican abundance was highest in the spongiosa, with progressively lower amounts in the ventricularis and then the fibrosa ($p < 0.001$). Versican was weakly abundant throughout the fetal valves

with stronger staining specifically co-localized with elastin. A change in versican expression over the trimesters was not detected.

Hyaluronan Distribution

The GAG HA was often abundant in the spongiosa, particularly in the AV ($p < 0.001$). Compared to the AV, HA appeared to be more abundant in the MVF; this finding may be explained by noting that the MV free edge consists almost exclusively of spongiosa, in contrast to the free edge of the AV, which has a more layered structure. Interestingly, HA was also abundant in the atrialis and ventricularis of the MV, which are rich in elastin (Table 4-1A). When all layers were considered together, the abundance of HA was greater in the MV than in the AV ($p < 0.05$, Table 4-1C), and did not change significantly with age. With respect to the fetal valves, the MV showed greater HA expression than AV ($p < 0.001$) and in both fetal MV and AV, the expression of HA increased over the trimesters ($p = 0.004$).

Distribution of Other Matrix Components and Co-localization with PGs

Prenatally, elastin was present in the first trimester as a heavy outline on the ventricularis that moved interiorly over the trimesters, even though elastic fibers were not demonstrated by Movat staining during the early trimesters. Indeed, 1st trimester MV sections showed marked differentiation of elastin expression, with elastin distinctly located in both the atrialis and ventricularis (Fig. 4-2). Elastin expression decreased

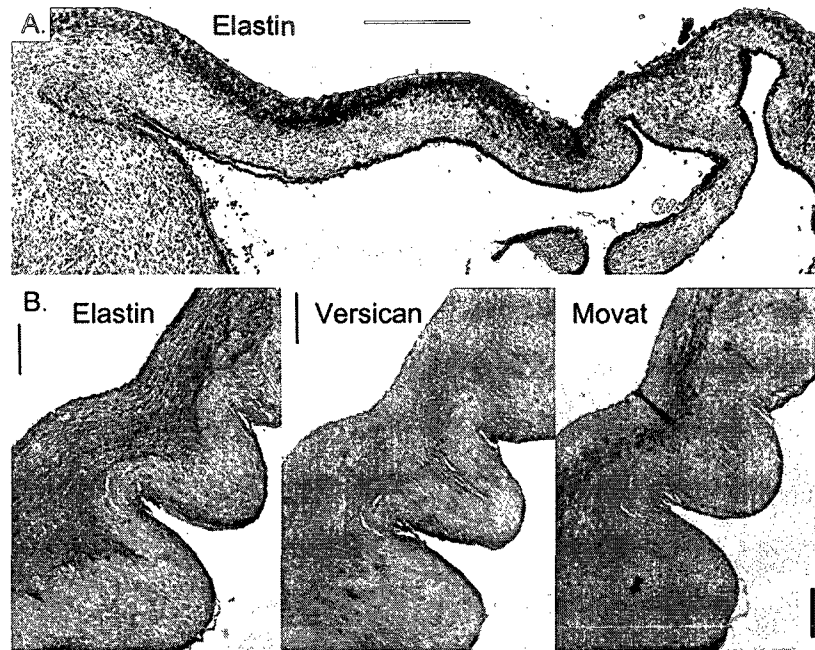


Fig. 4-2: A) Strong expression of elastin within both atrialis and ventricularis layers of 1st trimester mitral valve. Scale bar indicates 200 μ m. B) Out of the three proteoglycans (PGs) examined, versican (VC) co-localized most closely with elastin, shown here in an aortic valve. In this figure the ventricularis is on the left and the fibrosa is on the right. Scale bars indicate 200 μ m.

postnatally and was least abundant in the AV ventricularis of 6-year-olds and in the MVF ($p < 0.039$, Table 4-1B). Similarly, the amount of elastic fibers detected by Movat decreased with age in both valves (both $p < 0.010$). Within the layers of the MV, elastin was most abundant in the atrialis, less so in the spongiosa and ventricularis, and least abundant in the fibrosa ($p < 0.001$, Table 4-1A). The AV showed a comparable pattern, with elastin intensity highest in the ventricularis, lower in the spongiosa, and lowest in the fibrosa ($p < 0.001$). Compared to the MV, elastin in the AV was more abundant both across the whole leaflet (Table 4-1C) and in the fibrosa layer, but was less abundant on the outflow surface ($p < 0.01$).

Unlike elastin, fibrillin staining remained diffuse and weak in the prenatal valves. Postnatally, fibrillin abundance within the MV was highest in the atrialis, lower in the spongiosa and ventricularis, and negligible in the fibrosa ($p < 0.01$, Table 4-1A). In the AV, fibrillin was strongest in the spongiosa, lower in the ventricularis, and lowest in the fibrosa ($p < 0.001$). Fibrillin expression on the AV inflow surface was high in 6-week old pigs but decreased progressively with age ($p < 0.025$, Table 4-1B). Fibrillin was often inversely localized with the collagenous fibrosa and was also found independent of elastin in locations, such as the free edge, that never develop elastic fibers; the abundance of fibrillin was lowest at the annulus, gradually increasing to its greatest abundance at the free edge ($p = 0.008$). TGF β staining closely followed fibrillin and elastin, but also co-localized with the regions of “lone” fibrillin expression (without corresponding elastin).

PGs were frequently co-localized with elastin and fibrillin, particularly in the mid-leaflet. In 6-week-old and 6-year-old valves, versican was frequently present when elastin and fibrillin were found in the same area, e.g., likely present as mature elastic fibers (Fig. 4-2). In 2nd and 3rd trimester fetal valves, all of the PGs co-localized with the concomitant expression of elastin and fibrillin, with versican expression most closely matching elastin expression. TGF β was most closely co-localized with decorin out of all the PGs examined.

Hydration

The MVAC had significantly lower hydration than the MVF and AV (each $p < 0.015$, Fig. 4-3A). With increasing age, all regions showed a decrease in hydration (each $p \leq 0.006$).

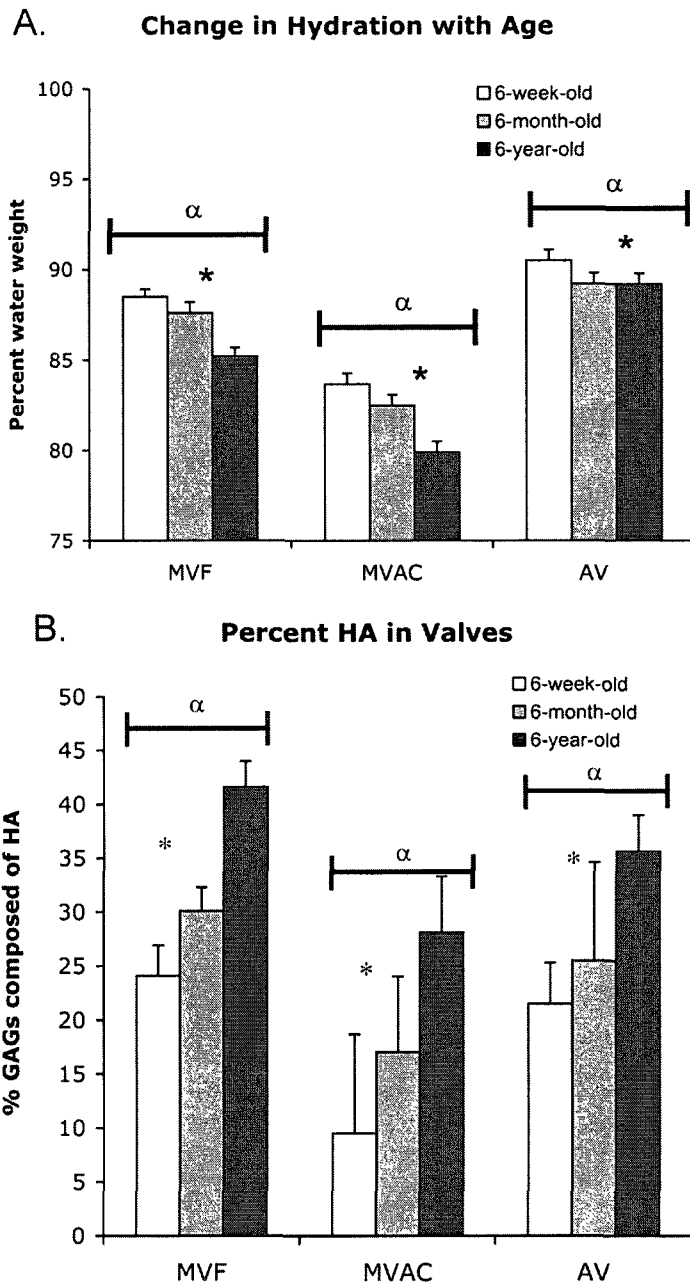


Fig. 4-3: A) Percent hydration examined by valve and age. $*=p<0.001$ between different valves. $\alpha=p\leq 0.003$ between different ages. Error bars are standard error of the mean. B) Percent of total glycosaminoglycan (GAG) composed of hyaluronan (HA) (as measured by FACE) examined by valve and age. $*=p<0.001$ MVF > AV > MVAC. $\alpha=p<0.001$ between different age groups. MVF= mitral valve (MV) free edge; MVAC=MV anterior center; AV=aortic valve. Error bars are standard error of the mean.

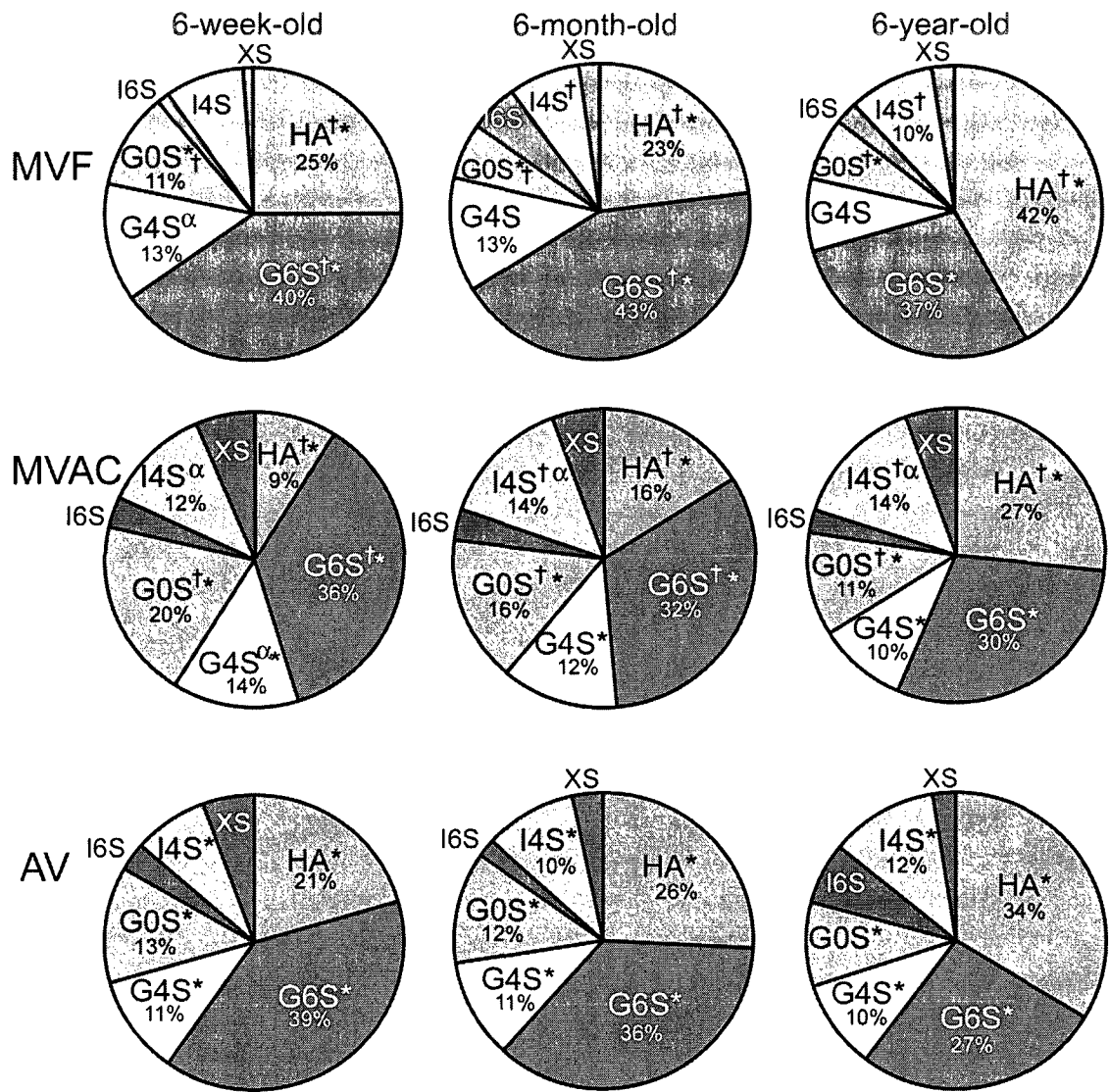


Fig. 4-4: Proportion of glycosaminoglycans (GAGs) in valves of different ages, as calculated from FACE data. Statistical differences are marked between different ages of a given valve and between the MVAC and MVF regions of the same age. (Differences between AV and the MVF regions for a given age have not been marked. Differences between MVAC and MVF in fractions when considering all ages have not been marked, but are discussed in the text.). †=MVAC significantly different than MVF for the 6-week-old, 6-month-old, or 6-year-old. *=significant change in a given GAG across ages in a given valve region (MVF, MVAC, and AV). All marked differences are $p \leq 0.05$ except $\alpha = p < 0.03R$. MVF= mitral valve (MV) free edge; MVAC=MV anterior center; AV=aortic valve. G0S=unsulfated glucuronate, G4S=4-sulfated glucuronate, G6S=6-sulfated glucuronate, I4S=4-sulfated iduronate, I6S=6-sulfated iduronate, and XS=di- and tri-sulfated glucuronate/iduronate. Only percentages >10% are labeled.

GAG Compositional Analysis

The general effects of aging evident across all valve regions included an increase in HA ($p < 0.013$ for each valve region, Fig. 4-3B), a decrease in unsulfated glucuronate (G0S, $p < 0.001$, Fig. 4-4) and 6-sulfated glucuronate (G6S, $p < 0.003$), and a decrease in the ratio of CS to DS ($p < 0.004$, Table 4-2).

Table 4-2. Ratio of GAG Components.

Valve	Age	CS:DS	D4S:D6S	CS/DS-6:CS/DS-4
MVF	6-week-old	7.79 ± 0.39*	4.45 ± 0.44	2.31 ± 0.05 [^]
	6-month-old	6.65 ± 0.50 [^]	3.41 ± 0.28	2.27 ± 0.05 [^]
	6-year-old	4.20 ± 0.19 [^]	3.51 ± 0.32	2.15 ± 0.06 [^]
MVAC	6-week-old	6.85 ± 0.53*	7.81 ± 0.84 [†]	1.78 ± 0.05 [^]
	6-month-old	3.93 ± 0.19 [^]	8.74 ± 1.19 [†]	1.51 ± 0.06 [^]
	6-year-old	4.09 ± 0.30 [^]	159.00 ± 41.56 [†]	1.59 ± 0.06 [^]
AV	6-week-old	24.24 ± 3.70 ^{*†}	3.32 ± 0.31	2.85 ± 0.07*
	6-month-old	8.29 ± 0.95 ^{*†}	3.25 ± 0.19	2.08 ± 0.07*
	6-year-old	4.97 ± 0.31 ^{*†}	10.87 ± 1.28	1.85 ± 0.07*
Comparison across all ages		AV>MVF>MVAC	MVAC>AV,MVF ^α	AV,MVF>MVAC

Data are mean ± the standard error; [^]MVF>MVAC for a given age, differences between AV and MVF or MVAC have not been marked; ^α= $p=0.009R$; [†]6-week-old significantly higher than 6-month-old and 6-year-old; [‡]6-year-old significantly higher than 6-week-old and 6-month-old ($p=0.013R$). *=overall decrease with age. All marked differences have p -values ≤ 0.05 , except otherwise noted. MVF= mitral valve (MV) free edge; MVAC=MV anterior center; AV=aortic valve. CS=chondroitin sulfate, defined as only containing glucuronate. DS= dermatan sulfate, defined as containing some quantity of iduronate. D4S=dermatan 4-sulfate, C4S=chondroitin 4-sulfate. CS/DS-6=6-sulfated glucuronate or iduronate. CS/DS-4=4-sulfated glucuronate or iduronate. See methods for complete explanation of statistical methods.

The MVAC, which experiences tension, contained a lower concentration of total GAGs than the MVF ($p < 0.001$), due to reduced concentrations of G0S ($p < 0.04$), 4-sulfated glucuronate (G4S, $p < 0.04$), G6S, ($p < 0.04R$) and HA ($p < 0.001$). Compared to MVF, MVAC had more 4-sulfated GAGs ($p < 0.001$, Fig. 4-4, Table 4-3), which were predominantly 4-sulfated iduronate (I4S) and less 6-sulfated GAGs ($p < 0.001$). Even though the overall concentration of GAGs was greatly reduced in the MVAC compared

Table 4-3. Patterns of GAG composition expressed as fraction of total GAG in valve regions measured by FACE.

Component	Comparison
glucuronate	AV,MVF > MVAC
G0S	MVAC > AV > MVF
G4S	--
G6S	AV,MVF > MVAC
iduronate	MVAC > AV,MVF
I4S	MVAC > AV,MVF
I6S	--
HA	MVF > AV > MVAC
4 sulfation	MVAC > AV,MVF
6 sulfation	AV,MVF > MVAC

All $p < 0.05$. "--" indicates no statistically significant difference detected. "4 sulfation" includes both G4S and I4S; "6 sulfation" includes both G6S and I6S. MVF= mitral valve (MV) free edge; MVAC=MV anterior center; AV=aortic valve. G0S, G4S, G6S, I4S, and I6S are all defined in the legend for Fig. 4-4.

to the MVF, the MVAC contained a greater concentration of hypersulfated GAGs (XS, $p < 0.001$). With increasing age, the MVAC demonstrated a further reduction in 6-sulfated GAGs ($p = 0.002$, Fig. 4-5) and a further increase in I4S ($p \leq 0.026R$).

Conversely, the MVF had greater fractions of HA ($p < 0.001$), G6S, 6-sulfated GAGs, and lower fractions of XS and iduronate, particularly I4S (p -values given above). With aging, the MVF showed a decrease in 4-sulfated GAGs ($p = 0.015$) and an increase in 6-sulfated GAGs ($p = 0.014$) that was mainly evident between 6-weeks and 6-months.

The AV showed characteristics that largely resembled the MVF (Table 4-3). Like the MVF, the AV contained high concentrations of total GAGs, glucuronate, and HA (each $p < 0.001$) and a high ratio of 6 to 4-sulfation ($p < 0.025$, Table 4-2). However, the AV also showed a number of traits that were similar to the MVAC, such as low amounts of HA and 6-sulfated GAGs (both $p < 0.001$). With aging, the AV appeared to become

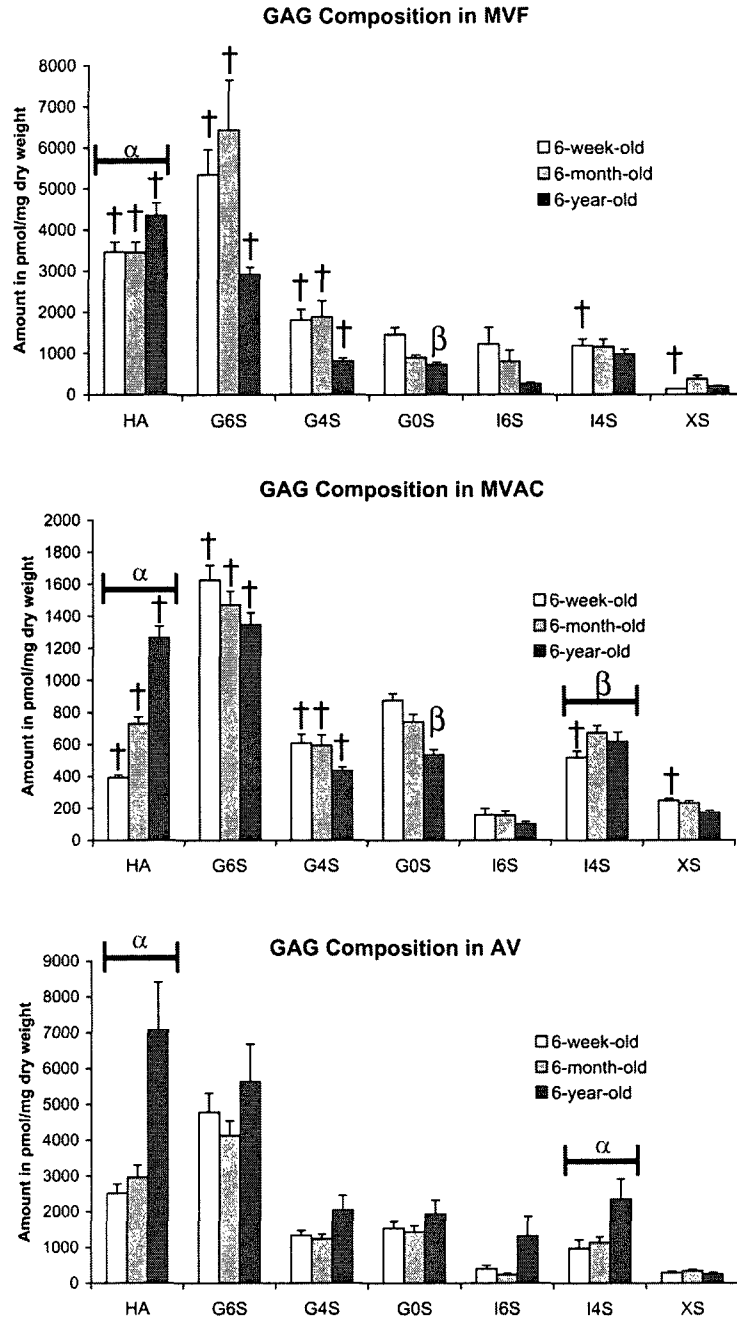


Fig. 4-5: Glycosaminoglycan (GAG) composition for each valve and each age group, as calculated from the FACE analysis. Note that the middle graph has a different scale on the y-axis. Statistically significant differences ($p \leq 0.05$) are marked between different ages of a given valve and between the MVAC and MVF regions of the same age. (Differences between AV and MVF as well as AV and MVAC for a given age have not been marked. Differences between MVAC and MVF in concentrations when considering all ages have not been marked, but are discussed in the text.). Error bars are standard error of the mean. α =significant change in a given GAG in a given valve across ages, $\beta=p < 0.03R$. \dagger = significant difference between MVAC and MVF in the 6-week-old, 6-month-old, or 6-year-old. MVF= mitral valve (MV) free edge; MVAC=MV anterior center; AV=aortic valve. G0S, G4S, G6S, I4S, I6S, and XS are all defined in the legend for Fig. 5-4.

more like the MVAC in composition, with a decrease in 6-sulfated GAGs ($p < 0.001$), an increase in 4-sulfated GAGs ($p = 0.038$), and an increase in I4S ($p = 0.005$).

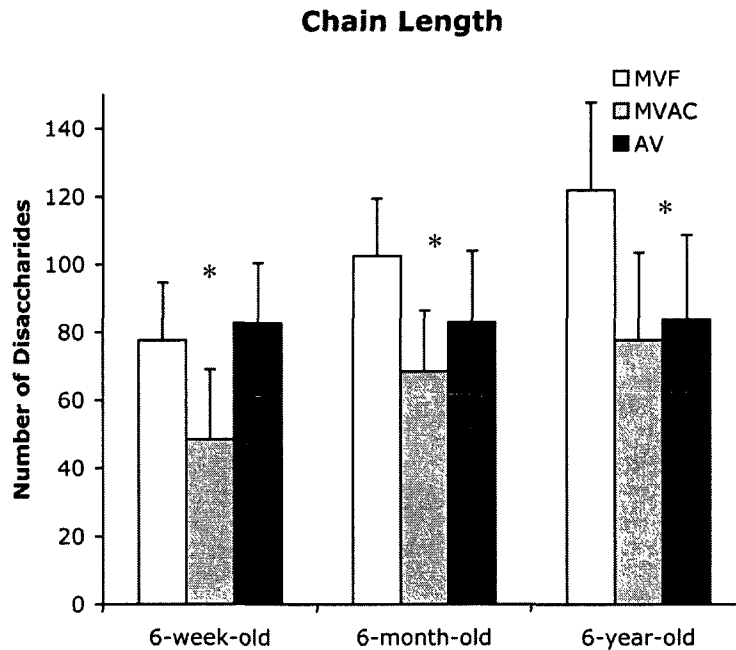


Fig. 4-6: Chain length of valve regions by age, as calculated from FACE data. Overall $p = 0.059$ by ANOVA. MVF = mitral valve (MV) free edge; MVAC = MV anterior center; AV = aortic valve. Error bars are standard error of the mean.

Chain Length

Overall, the average lengths of the CS/DS chains in the MVAC tissues were shorter than those found in the MVF tissues ($p < 0.002$, Fig. 4-6). There was no significant change in chain length with age.

DISCUSSION

This study showed that the distribution of PGs and GAGs within porcine AV and MV is complex, region and layer-specific, associated with different mechanical environments, and strongly age-dependent. The MVF, which experiences compression, contains an abundance of water and GAGs, particularly G6S and HA, while the MVAC, which experiences tension, contains relatively fewer GAGs but higher proportions of I4S and XS. General aging trends included an increase in HA and in iduronate-containing GAGs, and a decrease in hydration. This study was also the first to examine the GAG profile of porcine AVs, which are important in the production of bioprosthetic replacement valves. The younger AVs largely resembled the MVF, but aged to become more like the MVAC. In the IHC analysis, it was shown that decorin, important in collagen fibrillogenesis, was the PG most often found within the collagen-rich fibrosa layer, and the expression of the small leucine-rich PGs decorin and biglycan increased with age. In contrast, the GAG HA was strongly expressed in the more loosely organized spongiosa layer of the valves. Overall, the expression of PGs in the AV was stronger than in the MV. Many regions of distinct PG expression also demonstrated rich expression of elastin and fibrillin.

PGs and GAGs Vary in Distribution Between Layers and Loading Regions

These results indicate that each PG has a unique distribution within heart valves that is likely related to its unique functions. Decorin was the PG most often co-localized with collagen, which would support the critical role of decorin in collagen fibrillogenesis.³² In the AV, HA and versican expression was strongest in the spongiosa,

consistent with their contribution to compressive resistance. Decorin and biglycan expression was strong in the ventricularis layer of the AV, which experiences cyclic tension³³ and is primarily comprised of elastic fibers, likely reflecting the roles of these PGs in tension^{4, 34} and in elastogenesis.³⁵ Interestingly, although the Movat alcian blue dye stained most strongly in the spongiosa, IHC did not always demonstrate maximal expression of PGs in this layer. This discrepancy could be due to the presence of HA in the spongiosa; HA reportedly comprises 60% of all GAGs.³¹

The results in this study largely corroborate the previously reported distribution of PGs within human valves, which considered all four valves as a group.³¹ This previous study reported PGs, especially decorin, to be abundant on the valve inflow surfaces, which agreed with the PG expression in the ventricular layer of the porcine AV, but conflicted with the atrialis layer of the porcine MV. In human valves, biglycan and versican were ubiquitously distributed. In porcine valves, biglycan expression was generally ubiquitous, but the AV demonstrated differential expression of all PGs between layers, and the MV showed layer-specific versican expression.

The characterization of GAGs in the porcine MV largely agrees with our previous study of the human MV.⁴ In both studies, the MVAC had less water, total GAGs, and HA, and more iduronate and 4-sulfated GAGs compared to the MVF which contained more glucuronate and 6-sulfated GAGs. Both studies found age-associated decreases in hydration and the fractions of G6S in the MVAC, decreases in the fractions of G4S and G6S in the MVF, and a decrease in CS and increase in DS in the MV as a whole.¹¹ Unlike in human valves, however, the porcine MVAC did not demonstrate age-associated decreases in total GAGs, HA, or I4S, and in fact actually showed increases in both HA

and I4S with age. In addition, the porcine MVF showed no significant decrease in average GAG chain length with age, as found in human valves. Differences between the findings of these two studies may be due in part to inter-species differences in valve composition, differences in gender makeup (gender of the 6-week and 6-month old pigs was unknown), and the distribution of sample ages.

Valve PG and GAG Composition Reflects Mechanical Requirements

Given evidence that valvular interstitial cells respond to their mechanical environment through altering extracellular matrix synthesis,³⁶ mechanical loading can explain several of the observed layer-specific and age-related patterns of PGs and GAGs. The ventricular inflow surface of the AV experiences high shear, laminar flow, and tensile forces,³⁷ which would necessitate abundant decorin and biglycan to mediate collagen fibrillogenesis.³⁸ Differences in loading patterns, as well as geometry, may also explain the differences in composition between the AV and MV. The overall increase in valve PG expression with age is consistent with reports of increased GAGs with aging.^{26,}
³⁹ Given the general role of PGs and GAGs in providing compressive strength, the increase in PGs in the AV may be in response to increased transvalvular pressures, since diastolic function and aortic compliance both decrease with age.^{40, 41} Correspondingly, the increase in overall PGs in the MV may be a response to increased left atrial pressure.⁴² The FACE data indicated that with aging, the compressive regions showed a decrease in the fraction of 4-sulfated GAGs (associated with tension) and an increase in the fraction of 6-sulfated GAGs (associated with compression), whereas the tensile regions showed the opposite pattern. Cartilage tissues, which bear compressive loading,

also demonstrate an increase in the 6S:4S ratio with aging⁴³ suggesting that the inherent differences in mechanical loading experienced by the MVAC and MVF are associated with these age-related changes. Other studies have shown increased GAG sulfation with age⁴⁴ and with mechanical loading.⁴⁵ However, as shown here in valves, not all types of sulfation increased uniformly, and changes in glucuronate sulfation with age were distinctly different between valve regions.

Aging Transforms AV Composition from Compressive to Tensile

The GAG composition of the 6-week-old AV was largely similar to that of the MVF, containing an abundance of total GAGs, high fractions of G6S and HA, and low fractions of I4S and XS, consistent with previous findings.⁴⁶ With age, however, the AV GAG composition changed to become more like that of the MVAC. For example, both the MVAC and the AV had an aging-related increase in the fraction of I4S and demonstrated more 4-sulfation and less 6-sulfation. Whereas for the MVAC these aging-related changes accentuated the tensile tissue phenotype, these changes reversed the compressive tissue phenotype observed in the younger AV. These tensile phenotypic changes in the AV may reflect increased tensile loading on the AV leaflet tissues that would accompany an age-related decrease in aortic compliance.

Interplay of PGs with Elastin and Fibrillin

PGs were frequently co-localized with elastin and fibrillin, particularly in the mid-leaflet region. These patterns are consistent with previous reports that versican, biglycan, and decorin co-localize with fibrillin^{29, 47} and that both versican and decorin are involved

in elastogenesis.^{48, 49} TGF β , which was most often co-localized with decorin, also interacts with various PGs and is reported to upregulate biglycan and versican expression but downregulate decorin expression.²⁷ TGF β has also been shown to increase the expression of elastin.⁵⁰ The presence of TGF β within these valves is also intriguing because this growth factor can induce the “activated” phenotype of valvular interstitial cells.⁵¹

The strong expression of elastin in the nascent ventricularis layer of the fetal valves may reflect the need for tissue extensibility as early as the 1st trimester as blood flows through the fetal heart. With increasing postnatal age, there was a decrease in the valvular elastin content, although other studies have found an increase in mature elastic fibers with age,^{26, 52} particularly between the 2nd and 5th decades of human life⁵³ and in pathological valves.⁵⁴ Given that elastic fibers, at least of the lung parenchyma, are thought to last the lifetime of the animal,⁵⁵ it may be that the elastin antibodies have reduced binding to the more mature elastic fibers in older animals.

It is intriguing that fibrillin was often found in these heart valves unaccompanied by elastin. While fibrillin is primarily found as part of elastic fibers, fibrillin on its own is known to demonstrate elastomeric material behavior⁵⁶ and regulates growth factors, such as by binding to TGF β .⁵⁷

Implications for Valve Disease and Tissue Engineered Heart Valves

Altered PG and GAG composition have been shown to play an important role in many heart valve diseases. For example, in myxomatous MV disease the valve has increased hydration and concentration of GAGs, especially G6S and HA.⁵⁸ As opposed

to the changes associated with myxomatous valves, it was shown here that normally aging valves are less hydrated and contain more iduronate, which supports the premise that myxomatous MV disease is not caused by aging. Furthermore, studies of bioprosthetic valves have implicated loss of PG and GAG content with bioprosthetic valve failure.⁸ Recent evidence also suggests that PG and GAG may act as a key component in the development of calcific AV disease.⁵⁹

These results also demonstrate the incredible regional and layer-specific complexity in the matrix composition of the native valve, which has important implications for heart valve tissue engineering. Although some of these compositional differences may appear quite subtle, such as the presence and location of sulfation on GAG chains, these fine structural distinctions may have important biological roles such as serving as binding sites for other matrix components or for signaling cell differentiation.¹⁴⁻¹⁶ Future studies will need to examine how these components contribute to proper valve function and how to recapitulate this complex composition within a tissue engineered construct, for example through mechanical stimulation. Lastly, these results show that a tissue engineered heart valve should optimally contain age-specific components and should take into account the substantial changes that occur throughout development and aging.

Limitations

In this study, two different techniques (IHC and FACE) were employed in an effort to circumvent the inherent limitations of each separate approach. The use of IHC permits very specific localization of markers of interest within the different valve layers

and anatomic regions. Previous studies using IHC have largely limited the assessment of this localization to qualitative observations and if a grading system was used it largely discounted such localization. However, in this study we have employed a systematic valve layer and region-specific semi-quantitative grading system that allows assessment of this localization. The quantitative analysis of region-specific tissue by FACE nicely complements the IHC data of this study. FACE allows for specific and truly quantifiable measurements of GAG fine structural features, including the presence and location of sulfation and epimerization. Although FACE was applied to samples from distinct anatomic regions of the MV, those regions were not able to be subdivided into the different leaflet layers. In addition, due to the miniscule size of fetal valves, FACE could not be performed on tissue from the various trimesters. Another limitation is that, while there is evidence that certain PGs tend to contain certain GAG types,⁴ we have not directly correlated GAG composition to particular PGs. In the future, it will be of great interest to examine the quantitative differences in GAG fine structure between developmental, postnatal, and aged valves and the different valve layers, to confirm the presence of different PGs using Western blotting, and to correlate matrix composition, age, and material behavior via mechanical testing and selective degradation of matrix components. Lastly, this study has found distinct patterns between matrix composition and mechanical environment, but showing causality between mechanical stimulation and matrix production will require more in vitro experimentation.³⁴

CONCLUSIONS

In this novel study of MV and AV composition during development and aging, FACE and IHC were used to localize PGs and GAGs within the individual layers of heart valves, to examine the association between mechanical environment and the GAG composition and fine structure, and to determine how these characteristics change with age. The resulting data revealed that the valvular PGs and GAGs are complex in their distributions and age-related changes, but that some patterns are apparent. Regions experiencing tension contain fewer GAG overall, with lower fractions of HA, glucuronate, 6-sulfation, and water, compared to regions experiencing compression. The composition of PGs and GAGs was also different between layers, such as the abundance of versican in the spongiosa of the AV. Age-related changes were also frequently unique to specific histological layers as well as associated with differences in mechanical loading. For example, the increase in decorin that was observed in the aging AV largely occurred in the spongiosa layer. Overall, the GAG and PG composition of the AV demonstrated a compressive tissue phenotype, but aged to exhibit more of a tensile tissue phenotype. In the MV, the differences between the MVAC (tensile) and MVF (compressive) became more pronounced with age. Clearly, the inherent complexity within valve tissues, due to the histological layers, mechanical forces, matrix composition, and effects of aging, impact the function of normal valves and will impose challenges on the development of a TEHV.

This chapter, which analyzed changes in proteoglycan and glycosaminoglycan content in fetal and postnatal aging, was the second of four chapters (Chapters 3-6) examining age-related changes in matrix composition and structure in normal aortic and mitral valves. In the next chapter in this series of studies, changes in aortic and mitral valve matrix composition and structure during the perinatal period are analyzed.

REFERENCES

1. Kinsella MG, Bressler SL, Wight TN. The regulated synthesis of versican, decorin, and biglycan: extracellular matrix proteoglycans that influence cellular phenotype. *Crit Rev Eukaryot Gene Expr.* 2004;14(3):203-234.
2. Rothenburger M, Volker W, Vischer P, Glasmacher B, Scheld HH, Deiwick M. Ultrastructure of proteoglycans in tissue-engineered cardiovascular structures. *Tissue Eng.* 2002;8(6):1049-1056.
3. Aikawa E, Whittaker P, Farber M, Mendelson K, Padera RF, Aikawa M, Schoen FJ. Human semilunar cardiac valve remodeling by activated cells from fetus to adult: implications for postnatal adaptation, pathology, and tissue engineering. *Circulation.* 2006;113(10):1344-1352.
4. Grande-Allen KJ, Calabro A, Gupta V, Wight TN, Hascall VC, Vesely I. Glycosaminoglycans and proteoglycans in normal mitral valve leaflets and chordae: association with regions of tensile and compressive loading. *Glycobiology.* 2004;14(7):621-633.
5. Grande-Allen KJ, Griffin BP, Ratliff NB, Cosgrove DM, Vesely I. Glycosaminoglycan profiles of myxomatous mitral leaflets and chordae parallel the severity of mechanical alterations. *J Am Coll Cardiol.* 2003;42(2):271-277.
6. Barber J, Kasper F, Ratliff N, Cosgrove D, Griffin B, Vesely I. Mechanical properties of myxomatous mitral valves. *J Thorac Cardiovasc Surg.* 2001;122(5):955-962.
7. Vesely I. Tissue Engineering of Heart Valves. *Encyclopedia of Biomaterials and Bioengineering.* New York: Marcel Dekker; 2004:1545-1558.
8. Vyavahare N, Ogle M, Schoen FJ, Zand R, Gloeckner DC, Sacks M, Levy RJ. Mechanisms of bioprosthetic heart valve failure: fatigue causes collagen denaturation and glycosaminoglycan loss. *J Biomed Mater Res* 1999;46(1):44-50.
9. Castagnaro M, Amedeo S, Bertolotto A, Manzardo E, Riccio A, Guarda F. Morphological and biochemical investigations of mitral valve endocardiosis in pigs. *Res Vet Sci.* 1997;62(2):121-125.
10. Deiss WP, Leon AS. Mucopolysaccharides of Heart Valve Mucoprotein. *J Biol Chem.* 1954;215(2):685-689.
11. Moretti A, Whitehouse MW. Changes in the mucopolysaccharide composition of bovine heart valves with age. *Biochem J.* 1963;87:396-402.
12. Bostrom H, Moretti A, Whitehouse M. Studies on the biochemistry of heart valves. I. On the biosynthesis of mucopolysaccharides in bovine heart valves. *Biochim Biophys Acta.* 1963;74:213-221.
13. Torii S, Bashey RI, Nakao K. Acid mucopolysaccharide composition of human heart valve. *Biochim Biophys Acta.* 1965;101:285-291.

14. Kuschert G, Coulin F, Power C, Proudfoot A, Hubbard R, Hoogewerf A, Wells T. Glycosaminoglycans interact selectively with chemokines and modulate receptor binding and cellular responses. *Biochemistry*. 1999;38(39):12959-12968.
15. Linhardt R, Toida T. Role of Glycosaminoglycans in Cellular Communication. *Acc Chem Res*. 2004;37(7):431-438.
16. Wille I, Rek A, Krenn E, Kungl A. Biophysical investigation of human heparan sulfate D-glucosaminyl 3-O-sulfotransferase-3A: a mutual effect of enzyme oligomerisation and glycosaminoglycan ligand binding. *Biochim Biophys Acta*. 2007;1774(11):1470-1476.
17. Wagner M, Siddiqui MA. Signal transduction in early heart development (II): ventricular chamber specification, trabeculation, and heart valve formation. *Exp Biol Med (Maywood)*. 2007;232(7):866-880.
18. Henderson DJ, Copp AJ. Versican expression is associated with chamber specification, septation, and valvulogenesis in the developing mouse heart. *Circ Res*. 1998;83(5):523-532.
19. Dainese L, Barili F, Topkara VK, Cheema FH, Formato M, Aljaber E, Fusari M, Micheli B, Guarino A, Biglioli P, Polvani G. Effect of cryopreservation techniques on aortic valve glycosaminoglycans. *Artif Organs*. 2006;30(4):259-264.
20. Mercuri JJ, Lovekamp JJ, Simionescu DT, Vyavahare NR. Signal transduction in early heart development (II): ventricular chamber specification, trabeculation, and heart valve formation. *Biomaterials*. 2007;28(3):496-503.
21. Lovekamp JJ, Simionescu DT, Mercuri JJ, Zubiato B, Sacks MS, Vyavahare NR. Stability and function of glycosaminoglycans in porcine bioprosthetic heart valves. *Biomaterials*. 2006;27(8):1507-1518.
22. Simionescu DT, Lovekamp JJ, Vyavahare NR. Degeneration of bioprosthetic heart valve cusp and wall tissues is initiated during tissue preparation: an ultrastructural study. *J Heart Valve Dis*. 2003;12(2):226-234.
23. Butcher JT, Nerem RM. Porcine aortic valve interstitial cells in three-dimensional culture: comparison of phenotype with aortic smooth muscle cells. *J Heart Valve Dis*. 2004;13(3):478-485; discussion 485-476.
24. Bhatia A, Vesely I. The effect of glycosaminoglycans and hydration on the viscoelastic properties of aortic valve cusps. *Conf Proc IEEE Eng Med Biol Soc*. 2005;3:2979-2980.
25. Gallegos RP, Nockel PJ, Rivard AL, Bianco RW. The current state of in-vivo pre-clinical animal models for heart valve evaluation. *J Heart Valve Dis*. 2005;14(3):423-432.
26. McDonald PC, Wilson JE, McNeill S, Gao M, Spinelli JJ, Rosenberg F, Wiebe H, McManus BM. The challenge of defining normality for human mitral and aortic valves: geometrical and compositional analysis. *Cardiovasc Pathol*. 2002;11(4):193-209.
27. Kahari VM, Larjava H, Uitto J. Differential regulation of extracellular matrix proteoglycan (PG) gene expression. Transforming growth factor-beta 1 up-regulates

- biglycan (PGI), and versican (large fibroblast PG) but down-regulates decorin (PGII) mRNA levels in human fibroblasts in culture. *J Biol Chem.* 1991;266(16):10608-10615.
28. Hinek A, Smith AC, Cutiongco EM, Callahan JW, Gripp KW, Weksberg R. Decreased elastin deposition and high proliferation of fibroblasts from Costello syndrome are related to functional deficiency in the 67-kD elastin-binding protein. *Am J Hum Genet.* 2000;66(3):859-872.
 29. Kiely CM, Whittaker SP, Shuttleworth CA. Fibrillin: evidence that chondroitin sulphate proteoglycans are components of microfibrils and associate with newly synthesised monomers. *FEBS Lett.* 1996;386(2-3):169-173.
 30. Calabro A, Benavides M, Tammi M, Hascall VC, Midura RJ. Microanalysis of enzyme digests of hyaluronan and chondroitin/dermatan sulfate by fluorophore-assisted carbohydrate electrophoresis (FACE). *Glycobiology.* 2000;10(3):273-281.
 31. Latif N, Sarathchandra P, Taylor PM, Antoniow J, Yacoub MH. Localization and Pattern of Expression of Extracellular Matrix Components in Human Heart Valves. *J Heart Valve Dis.* 2005;14:218-227.
 32. Reed CC, Iozzo RV. The role of decorin in collagen fibrillogenesis and skin homeostasis. *Glycoconjug J.* 2002;19(4-5):249-255.
 33. Vesely I. The role of elastin in aortic valve mechanics. *J Biomech.* 1998;31(2):115-123.
 34. Gupta V, Werdenburg JA, Blevins TL, Grande-Allen KJ. Synthesis of glycosaminoglycans in differently loaded regions of collagen gels seeded with valvular interstitial cells. *Tissue Eng.* 2007;13(1):41-49.
 35. Reinboth B, Hanssen E, Cleary E, Gibson M. Molecular interactions of biglycan and decorin with elastic fiber components: biglycan forms a ternary complex with tropoelastin and microfibril-associated glycoprotein 1. *J Biol Chem.* 2001;277(6):3950-3957.
 36. Merryman WD, Youn I, Lukoff HD, Krueger PM, Guilak F, Hopkins RA, Sacks MS. Correlation between heart valve interstitial cell stiffness and transvalvular pressure: implications for collagen biosynthesis. *Am J Physiol Heart Circ Physiol.* 2006;290(1):H224-231.
 37. Schoen FJ. Aortic valve structure-function correlations: role of elastic fibers no longer a stretch of the imagination. *J Heart Valve Dis.* 1997;6(1):1-6.
 38. Stephens E, Grande-Allen K. Age-related changes in collagen synthesis and turnover in porcine heart valves. *J Heart Valve Dis.* 2007;16(6):672-682.
 39. Barzilla JE, Blevins TL, Grande-Allen J. Age-related structural changes in cardiac valves: implications for tissue-engineered repairs. *Am J Geriatr Cardiol.* 2006;15(5):311-315.
 40. Cheitlin M. Cardiovascular physiology-changes with aging. *Am J Geriatr Cardiol.* 2003;12(1):9-13.

41. O'Rourke M, Nichols W. Aortic diameter, aortic stiffness, and wave reflection increase with age and isolated systolic hypertension. *Hypertension*. 2005;45(4):652-658.
42. Anderson PA. The heart and development. *Semin Perinatol*. 1996;20(6):482-509.
43. Hickery M, Bayliss M, Dudhia J, Lewthwaite J, Edwards J, Pitsillides A. Age-related changes in the response of human articular cartilage to IL-1alpha and transforming growth factor-beta (TGF-beta): chondrocytes exhibit a diminished sensitivity to TGF-beta. *J Biol Chem*. 2003;278(52):53063-53071.
44. Grzesik W, Frazier C, Shapiro J, Sponseller P, Robey P, Fedarko N. Age-related changes in human bone proteoglycan structure. Impact of osteogenesis imperfecta. *J Biol Chem*. 2002;277(46):43638-43647.
45. Sauerland K, Raiss R, Steinmeyer J. Proteoglycan metabolism and viability of articular cartilage explants as modulated by the frequency of intermittent loading. *Osteoarthritis Cartilage*. 2003;11(5):343-350.
46. Grande-Allen KJ, Mako WJ, Calabro A, Shi Y, Ratliff NB, Vesely I. Loss of chondroitin 6-sulfate and hyaluronan from failed porcine bioprosthetic valves. *J Biomed Mater Res A*. 2003;65(2):251-259.
47. Isogai Z, Aspberg A, Keene DR, Ono RN, Reinhardt DP, Sakai LY. Versican interacts with fibrillin-1 and links extracellular microfibrils to other connective tissue networks. *J Biol Chem*. 2002;277(6):4565-4572.
48. Hinek A, Braun KR, Liu K, Wang Y, Wight TN. Retrovirally mediated overexpression of versican V3 reverses impaired elastogenesis and heightened proliferation exhibited by fibroblasts from costello syndrome and hurler disease patients. *Am J Pathol*. 2004;164:119-131.
49. Neame P, Kay C, McQuillan D, Beales M, Hassell J. Independent modulation of collagen fibrillogenesis by decorin and lumican. *Cell Mol Life Sci*. 2000;57(5):859-863.
50. Debelle L, Tamburro A. Elastin: molecular description and function. *Int J Biochem Cell Biol*. 1999;31(2):261-272.
51. Walker GA, Masters KS, Shah DN, Anseth KS, Leinwand LA. Valvular myofibroblast activation by transforming growth factor-beta: implications for pathological extracellular matrix remodeling in heart valve disease. *Circ Res*. 2004;95(3):253-260.
52. Bashey RI, Torii S, Angrist A. Age-related collagen and elastin content of human heart valves. *J Gerontology*. 1967;9(19):203-208.
53. Sell S, Scully RE. Aging changes in the aortic and mitral valves. Histologic and histochemical studies, with observations on the pathogenesis of calcific aortic stenosis and calcification of the mitral annulus. *Am J Pathol*. 1965;46:345-365.

54. Imayama S, Braverman I. A hypothetical explanation for the aging of skin. Chronologic alteration of the three-dimensional arrangement of collagen and elastic fibers in connective tissue. *Am J Pathol.* 1989;134(5):1019-1025.
55. Shapiro S, Endicott S, Province M, Pierce J, Campbell E. Marked longevity of human lung parenchymal elastic fibers deduced from prevalence of D-aspartate and nuclear weapons-related radiocarbon. *J Clin Invest.* 1991;87(5):1828-1834.
56. Kielty C, Wess T, Haston L, Ashworth J, Sherratt M, Shuttleworth C. Fibrillin-rich microfibrils: elastic biopolymers of the extracellular matrix. *J Muscle Res Cell Motil.* 2002;23(5-6):581-596.
57. Kaartinen V, Warburton D. Fibrillin controls TGF-beta activation. *Nat Genet.* 2003;33(3):331-332.
58. Grande-Allen K, Griffin B, Ratliff N, Cosgrove D, Vesely I. Glycosaminoglycan profiles of myxomatous mitral leaflets and chordae parallel the severity of mechanical alterations. *J Am Coll Cardiol.* 2003;42(2):271-277.
59. Grande-Allen KJ, Osman N, Ballinger ML, Dadlani H, Marasco S, Little PJ. Glycosaminoglycan synthesis and structure as targets for the prevention of calcific aortic valve disease. *Cardiovasc. Res.* 2007;76:19-28.

Chapter 5: Perinatal Changes in Mitral and Aortic Valve

Structure and Composition

This chapter is the third of four chapters (Chapters 3-6) examining age-related changes in matrix composition and structure in normal aortic and mitral valves. In this chapter changes in matrix composition and structure during the perinatal period are analyzed.

ABSTRACT

Background: At birth, the mechanical environment of valves changes radically as fetal shunts close and pulmonary and systemic vascular resistances change. Given that valves are reported to be mechanosensitive, we investigated remodeling induced by perinatal changes by examining compositional and structural differences of aortic and mitral valves (AV, MV) between 2-day old and 3rd fetal trimester porcine valves using immunohistochemistry and Movat pentachrome staining.

Methods: 2-day old and 3rd trimester fetal porcine valves were stained with Movat pentachrome to examine leaflet structure, as well as immunohistochemically stained for markers of collagen synthesis and turnover pro-collagen I, pro-collagen III, prolyl 4-hydroxylase, matrix metalloproteinase 13, and periostin. Samples were also stained for elastin, hyaluronan, hyaluronan receptor for endocytosis (HARE), and the proteoglycans biglycan, versican, and decorin. Staining intensity was quantified using ImageJ software.

Results: AV composition changed more with birth than the MV, consistent with a greater change in AV hemodynamics. At 2 days, AV demonstrated a trend of greater versican and elastin ($p=0.055$) as well as greater hyaluronan turnover (HARE, $p=0.049$) compared to the 3rd trimester samples. AV also demonstrated decreases in proteins related to collagen synthesis and fibrillogenesis with birth including pro-collagen I, prolyl 4-hydroxylase, biglycan (all $p\leq 0.005$), and decorin ($p=0.059$, trend). Both AV and MV demonstrated greater delineation between the leaflet layers in 2-day old compared to 3rd trimester samples, and AV demonstrated greater saffron-staining collagen intensity suggesting more mature collagen in 2-day old compared to 3rd trimester samples (each $p<0.05$). The proportion of saffron-staining collagen also increased in AV with birth ($p<0.05$).

Conclusions: The compositional and structural changes that occur with birth, as noted in this study, likely are important to proper neonatal valve function. Furthermore, normal perinatal changes in hemodynamics often do not occur in congenital valve disease; the corresponding perinatal matrix maturation may also be lacking and could contribute to poor function of congenitally malformed valves.

The work contained in this chapter was published as:

Stephens EH, Post AD, Laucirica DR, Grande-Allen KJ. **Perinatal Changes in Composition of Mitral and Aortic Valves.** *Pediatric and Developmental Pathology*, in press.

INTRODUCTION

At birth, the body undergoes a number of profound changes, one of which includes a dramatic restructuring of the circulation. No longer able to rely on the placenta for oxygenation, circulation in the neonate is redirected: fetal shunts such as the ductus venosus, foramen ovale, and ductus arteriosus begin to close and blood flow to the nascent lungs greatly increases.¹ The systemic vascular resistance also significantly increases, along with the pressures of the left side of the heart.^{1,2} While the right side of the heart dominates during fetal life, with greater cardiac output in comparison to the left side of the heart,³ with birth the left side of the heart becomes predominant, since it is responsible for the blood flow to the rest of the body. Such a substantial and abrupt change in hemodynamics undoubtedly affects the heart valves, which are essential components of the heart and are responsible for the propagation of blood flow, but this topic has not been widely studied.

Heart valves are essential to proper heart function. Once thought to be passive flaps, heart valves are now known to be complex structures, complete with their own vasculature⁴ and nerves,⁵ that actively participate in heart function and cardiac pathologies.^{6, 7} Additionally, heart valves dynamically respond to their mechanical environment. Studies have shown that extracellular matrix production and valve cell phenotype in adult valves changes in response to altered mechanical stimulation.⁸⁻¹⁰ Although investigation of valve composition and valve cell phenotype in developing valves has been limited, it has been demonstrated that valve composition changes during fetal development^{11, 12} and continues to mature after birth.^{13, 14} Fetal valves also demonstrate altered composition that correlates with changes in their mechanical

environment.¹⁵ However, how this dramatic change in hemodynamics that occurs with birth affects valve structure and composition has not been studied in detail. Given the mechanosensitive nature of valves that has been extensively studied in adult valves,¹⁶⁻¹⁹ as well as evidence that valve composition changes during fetal and postnatal development, we hypothesized that these perinatal events drive changes in mitral and aortic valve composition and valve cell phenotype.

Further understanding of normal valve changes around birth would not only add to fundamental knowledge of developmental cardiac physiology, but would also contribute to the field of congenital heart disease. Heart valves are malformed in the majority of congenital heart disease cases,²⁰ posing a considerable burden for pediatric patients. With current valve replacements and repair options inadequate for many patients,^{21, 22} research is underway to develop tissue engineered heart valves. Given that pediatric heart valves have unique, age-specific tissue and cell phenotypes compared to older valves,^{13, 14} tissue engineering heart valves for neonates will require knowledge of valve compositional changes surrounding the birth event. Additionally, understanding the normal perinatal development of valves could lead to other types of interventions for this vulnerable population.

To this end, aortic and mitral valves from 3rd trimester pigs and 2-day old pigs were analyzed to assess differences in leaflet structure and extracellular matrix composition, namely elastin, collagen types I and III, regulatory proteins related to collagen synthesis and turnover, proteoglycans, and glycosaminoglycans.

METHODS

Tissue Procurement and Sample Preparation

Hearts from third trimester pigs and 2-day old pigs were obtained within 24 hours of death (3rd trimester obtained from Animal Technologies (Tyler, TX) and 2-day old obtained from Baylor College of Medicine); all were conventional cross-bred pigs. The animal sample set included aortic valves (AV) from four 3rd trimester pigs and mitral valves (MV) from three 3rd trimester pigs, and AV and MV from four 2-day old pigs. The specific time point within the 3rd trimester from which those valves were taken is unknown. Multiple tissue strips were taken from the valve of each animal. The study protocol was approved by the Animal Care and Use Committee of Baylor College of Medicine and was conducted in accordance with the NIH guidelines. The AV leaflets and the anterior leaflet of the MV, along with accompanying myocardium, were dissected from the hearts (Fig. 5-1A). Tissues were fixed overnight in 10% formalin, embedded in paraffin, sectioned to a thickness of five μm , and mounted on slides according to standard procedures. Samples of human congenitally diseased valves were also obtained at time of surgery and similarly prepared. The research use of these tissues was approved by the Institutional Review Boards at Rice University and Texas Children's Hospital.

Histology and Immunohistochemistry

Each sample was stained histologically with Movat pentachrome to demonstrate the relative distribution of collagen, glycosaminoglycans and proteoglycans (PGs), and elastic fibers. Each sample was also stained immunohistochemically (IHC) for markers involved in the synthesis and turnover of collagen, including pro-collagen I (Col I)²³ and

pro-collagen III (Col III)²³ (antibodies LF-41 and LF-69, gifts of Dr. Larry Fisher, NIH), prolyl 4-hydroxylase (P4H, MAB2701, Chemicon, Temecula, CA), matrix metalloproteinase 13 (MMP13, MAB3321, Chemicon), and periostin (MAB3548, R&D Systems, Minneapolis, MN). Collagen I is the predominant collagen found in adult valves²⁴ and is responsible for the valve's tensile strength, while collagen III is a reticular collagen. P4H is an enzyme located in the rough endoplasmic reticulum that is required for the critical step of proline hydroxylation in collagen fiber synthesis.²⁵ MMP13 is a major enzyme responsible for collagen degradation. The quantity of elastin, the major component of elastic fibers that are necessary for valve recoil, was also assessed via IHC (ab9519, Abcam, Cambridge, MA). Periostin is an adhesion molecule of the fasciclin family²⁶ that appears to modulate collagen fibrillogenesis²⁷ and has been shown to play a role in valve development,²⁶ as well as cardiac remodeling.^{28,29} IHC was also performed for the PGs decorin (DCN) and biglycan (BGN) (antibodies LF-122 and LF-104, gifts of Dr. Larry Fisher, NIH), both involved in collagen fibrillogenesis.³⁰ IHC was performed for the large PG versican (VC, antibody 2-B-1, Associates of Cape Cod, Falmouth, MA)), which is involved in elastic fiber formation³¹ and is also necessary for several early events in valvulogenesis.³² The abundance of the glycosaminoglycan hyaluronan (HA), which like VC is necessary for valvulogenesis,³³ was assessed using hyaluronan binding protein³⁴ (400763-1, Associates of Cape Cod). HA turnover was assessed by IHC for HA receptor for endocytosis (HARE)³⁵ (antibody mab159, gift of Dr. Paul Weigel, University Oklahoma Health Science Center, Oklahoma City, OK). Representative sections were also stained for CD44 (F10-44-2, Abcam), a cell surface receptor for HA, lysyl oxidase (LOX, IMX-5121, Imgenex, San Diego, CA), which is involved in both elastic and

collagen fiber crosslinking, and transforming growth factor-beta (TGF β , 5559-100, Biovision, Mountain View, CA), a growth factor involved in valve cell activation.

IHC staining intensity was quantified within each histological layer (ventricularis, atrialis (MV only), spongiosa, and fibrosa) and leaflet region (annulus and mid-leaflet (spongiosa evaluated in mid-leaflet only)) using ImageJ software (NIH, Bethesda, MD). Semi-quantitative grading (on a scale from 0 to 4, in which 0 was minimum) was also performed on blinded Movat-stained sections to evaluate delineation between leaflet layers and intensity of saffron-staining collagen. The fraction of leaflet composed of saffron-staining collagen was also estimated from blinded Movat-stained sections. Percent change in protein intensity was calculated as the difference in intensities between the two groups relative to 3rd trimester intensities. For purposes of comparisons between AV and MV, the ventricularis of the AV was considered analogous to the elastin-rich atrialis of the MV.

Statistical Analysis

Multifactorial analysis of variance was performed using SigmaStat (SPSS, Chicago, IL), as described in Chapter 4. Correlations between staining intensities of different proteins within individual leaflet layers, regions, and segments (to assess protein co-localization) were calculated using a Pearson rank order test if the data was normally distributed and Spearman rank order correlation test if data was not normally distributed. For correlations between intensities of different proteins, the level of significance was reduced to account for the large number of proteins being considered, and thus $p \leq 0.015$ was considered a trend and $p \leq 0.0056$ considered statistically significant.

RESULTS

Perinatal Changes in Valve Structure

Movat-stained sections demonstrated, to varying degrees, the layered structure of the valve leaflets, namely the collagen-rich fibrosa layer, the GAG-rich spongiosa in the middle, and a layer rich in elastic fibers on the leaflets' inflow surface. These sections also revealed substantial changes in valve structure with birth (Fig. 5-1B), including increases in leaflet layer delineation, the intensity of saffron-staining collagen, and the proportion of the valve leaflet thickness comprised of saffron-staining collagen (Fig. 5-2). In the AV these structural changes with birth were all statistically significantly different (delineation $p < 0.001$ (221% increase), saffron-collagen intensity $p = 0.029$ (106% increase), fraction saffron-staining collagen $p = 0.019$ (57% increase)). In the MV, however, only the increase in leaflet layer delineation was statistically significant ($p = 0.027$, 127% increase).

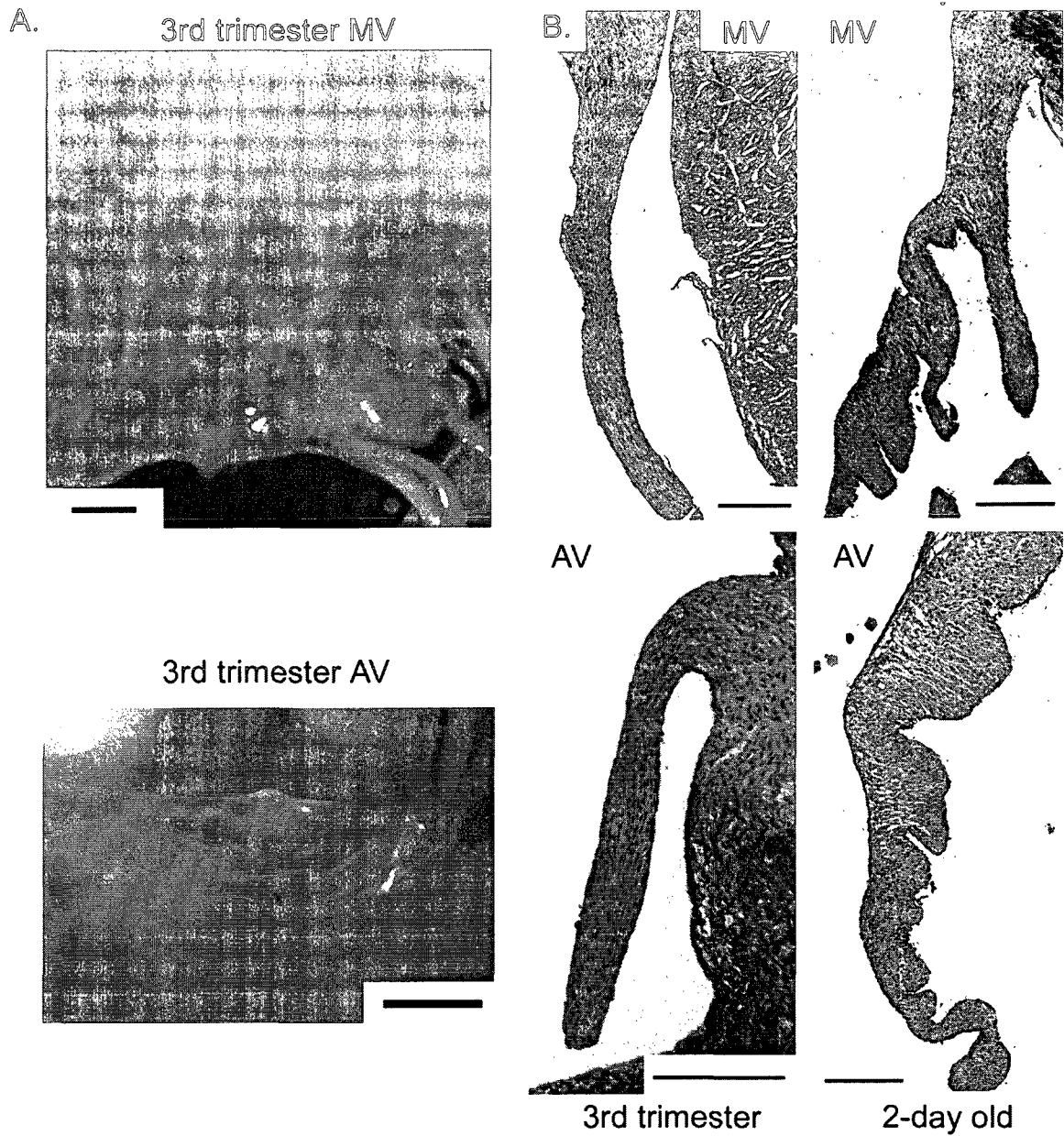


Fig. 5-1: A) Photographs of 3rd trimester MV anterior leaflet (top) and AV (bottom). Scale bar indicates 1 mm. B) Representative Movat-stained 3rd trimester fetal and 2-day old AV and MV. Scale bar indicates 200 μ m.

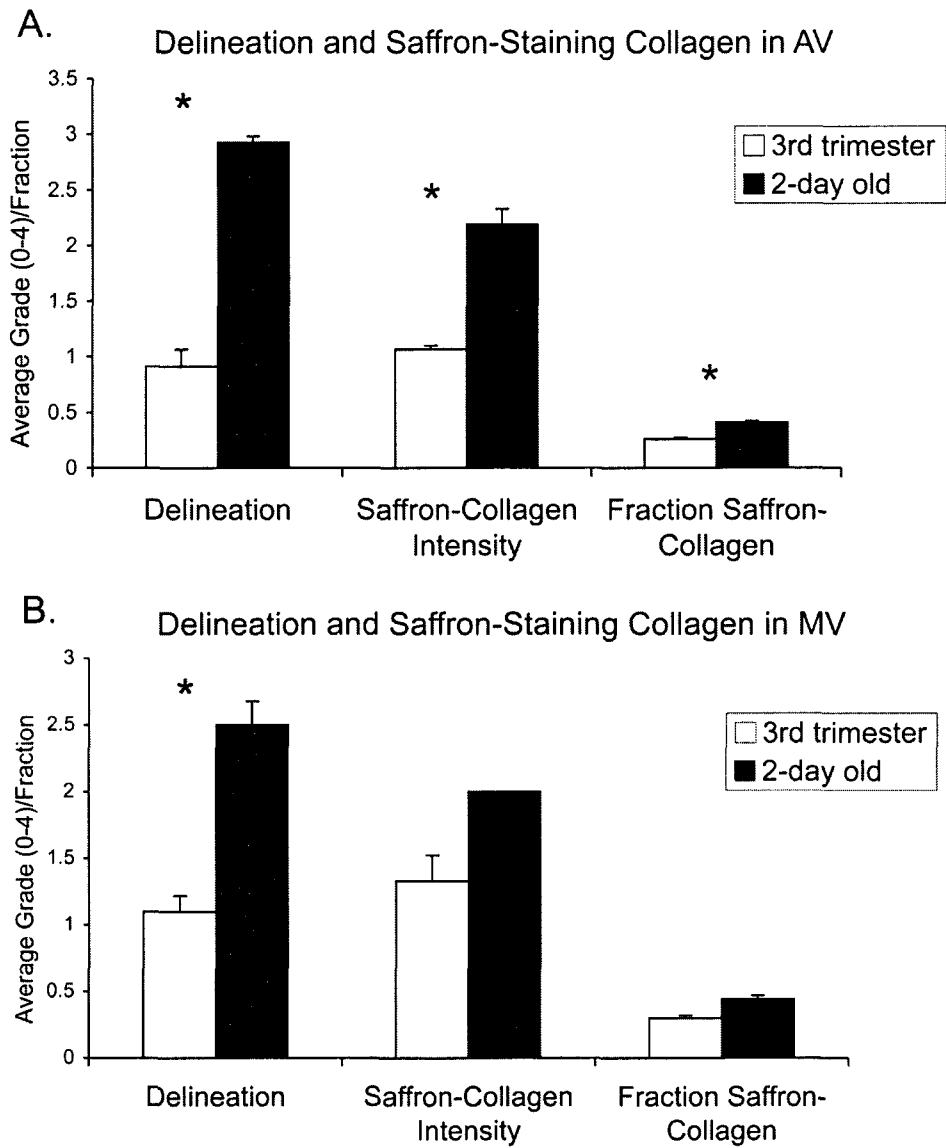


Fig. 5-2: Delineation and saffron-staining collagen in AV (A) and MV (B), * $p < 0.05$. Error bars indicate standard error of the mean.

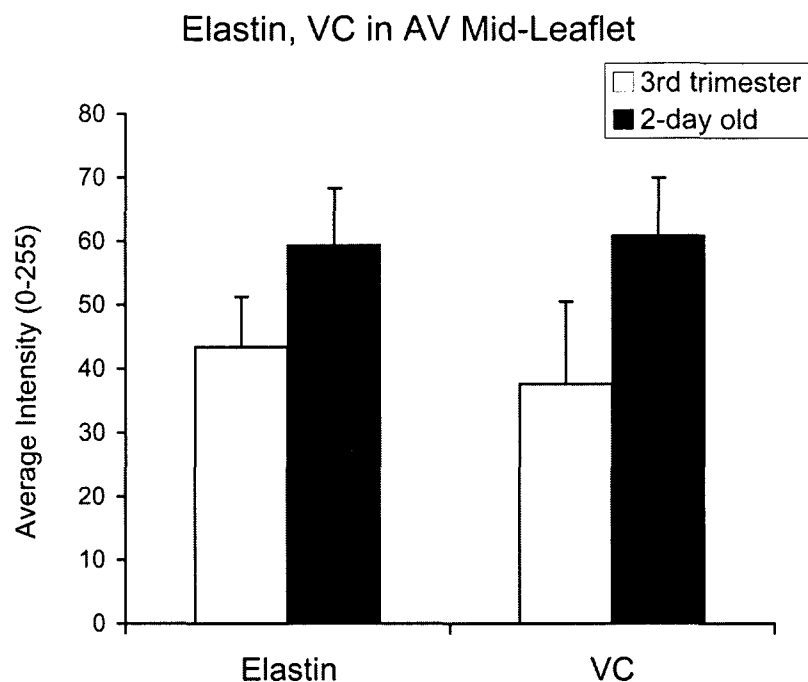


Fig. 5-3: Elastin and VC in AV mid-leaflet, overall $p=0.055$. Error bars indicate standard error of the mean.

Perinatal Changes in Valve Composition

Elastin and VC in the AV mid-leaflet tended to be greater in the 2-day old age group compared to the 3rd trimester age group (36% and 61% increases, respectively, overall $p=0.055$, Fig. 5-3). There was no significant change in the annular region. HARE, involved in HA turnover, was greater in the AV annulus and mid-leaflet of the 3rd trimester group compared to that of the 2-day old group (47% decrease, $p=0.049$, Fig. 5-4), although no significant difference between age groups was noted for HA. The mid-leaflet of the AV in the 3rd trimester group demonstrated greater expression of the

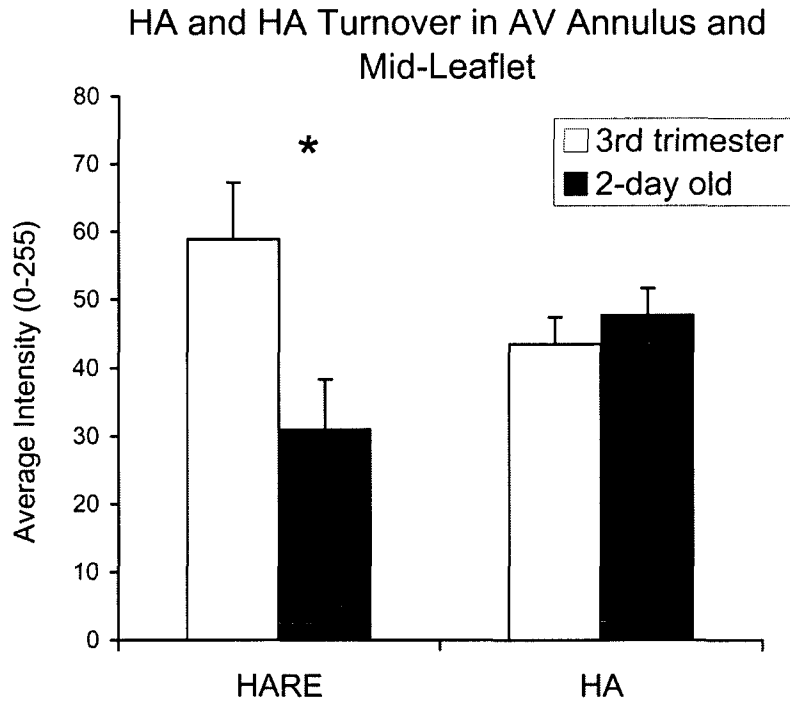


Fig. 5-4: HA and HARE in AV annulus and mid-leaflet, * $p < 0.05$. Error bars indicate standard error of the mean.

collagen-related markers Col I (52% decrease, $p < 0.001$, Fig. 5-5), P4H (33% decrease, $p = 0.005$), and the proteoglycans BGN (43% decrease, $p < 0.001$) and DCN (36% decrease, $p = 0.059$, trend), which are involved in collagen fibrillogenesis among other biological and mechanical roles.³⁰ The ratio of Col III to Col I was also found to increase with birth for both the mid-leaflet and annular regions of the AV ($p = 0.037$ and $p = 0.002$); however, no significant change was found in the MV. However, MMP13 in the mid-leaflet and annulus of 2-day old MV was greater than 3rd trimester MV (27% increase, $p = 0.023$). Col III displayed no significant difference between age groups for either MV or AV. While periostin appeared to increase with birth in both MV and AV, the change was not statistically significant. Unlike in the AV, which demonstrated significant perinatal

changes in a number of matrix components, in the MV only MMP13 showed evidence of significant perinatal change in expression.

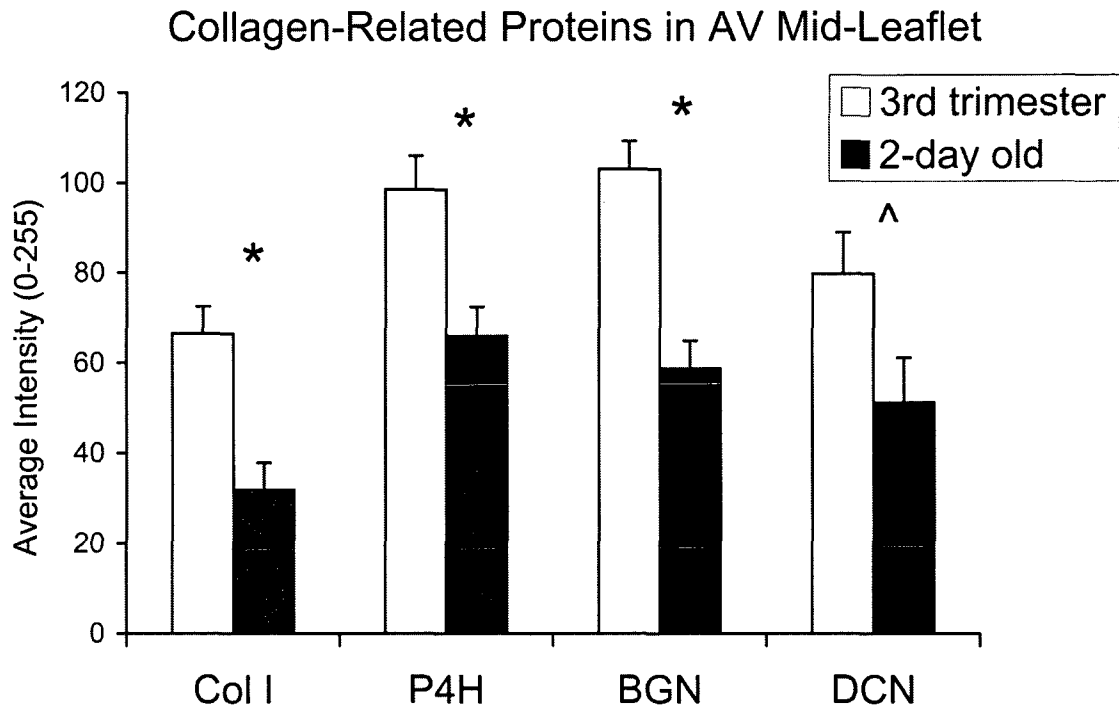


Fig. 5-5: Collagen-related proteins in AV mid-leaflet, * $p < 0.05$, ^ $p = 0.059$. Error bars indicate standard error of the mean.

Perinatal Changes in Relative Composition of AV and MV

The degree of expression of multiple matrix components, such as BGN, HARE, and elastin, was similar between AV and MV within the 3rd trimester group, but then became different within the 2-day old group (Fig. 5-6). Similarly, while the expression of VC in AV and MV were different within the 3rd trimester age group, the difference between VC expression in AV and MV became greater within the 2-day old age group.

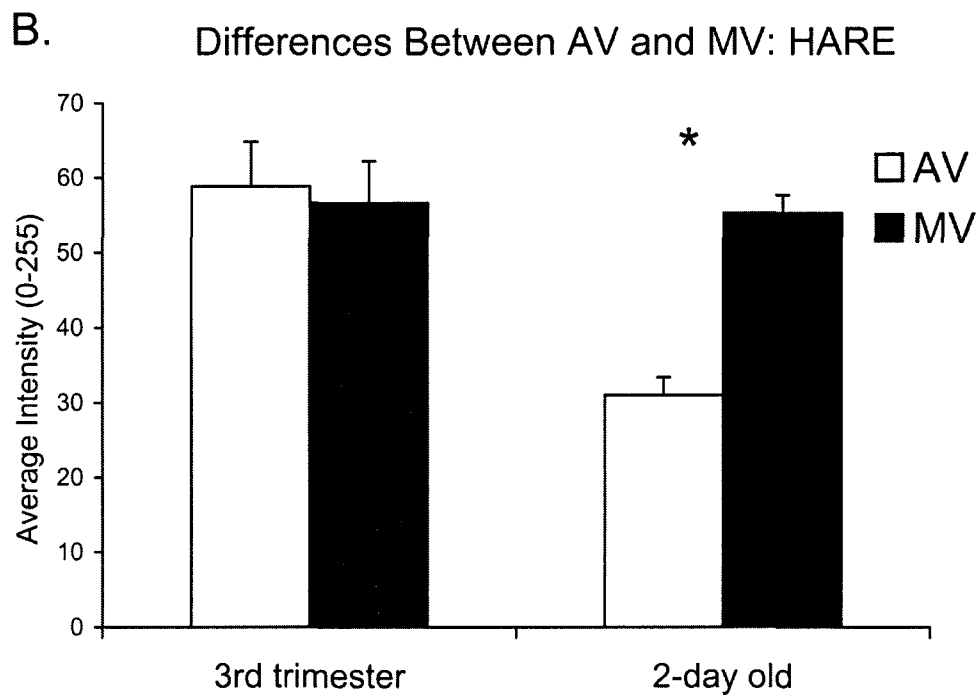
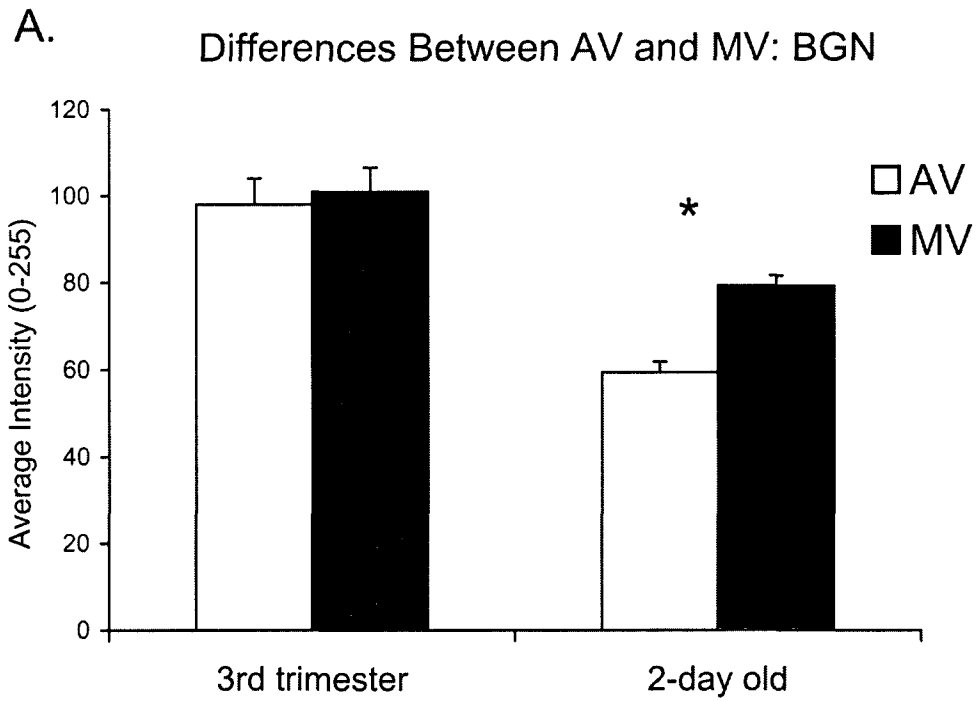


Fig. 5-6: Differences between AV and MV in the 3rd trimester and 2-day old age groups for BGN (A) and HARE (B), * $p < 0.05$. Error bars indicate standard error of the mean.

Location and Co-localization of Matrix Components

As expected from adult heart valves, the PGs BGN and DCN demonstrated similar localization, predominantly to the fibrosa, although BGN staining was generally more diffuse. The PG VC was generally enhanced in the spongiosa layer, as well as the elastin rich layers (ventricularis and atrialis of MV and ventricularis of AV). Elastin showed very distinct, often nearly linear localization to the ventricularis of the AV and atrialis of the MV, along with a much thinner line of distribution along the ventricularis of the MV and subendothelial outflow (aortic side) of the AV. Elastin distribution was spread throughout more of the thickness of the leaflet in the mid-leaflet and free edge. Col III demonstrated a similar distribution as Col I, although Col III staining was more diffuse. P4H was generally more diffuse than both Col I and Col III. HARE was often localized to the fibrosa in both MV and AV (Fig. 5-7A). Periostin, which appeared to co-localize with Col I, was also concentrated in the fibrosa in both MV and AV (Fig. 5-7A). MMP13 expression was also co-localized with Col I (Fig. 5-7B). Although before birth HARE tended to be more diffusely expressed throughout the layers of the leaflet, after birth HARE expression appeared to be localized to the fibrosa (Fig. 5-8). This increased localization of staining with birth was commonly seen with a number of matrix components. LOX, which is involved in crosslinking of collagen and elastic fibers, demonstrated relatively diffuse staining in both valves and age groups (Fig. 5-7B). In both valves and age groups TGF β and CD44 demonstrated diffuse staining, without notable layer or region-specific localization (Fig. 5-9).

Statistical correlations between the intensities of different matrix components within certain layers and regions of the MV and AV gave further insight into the

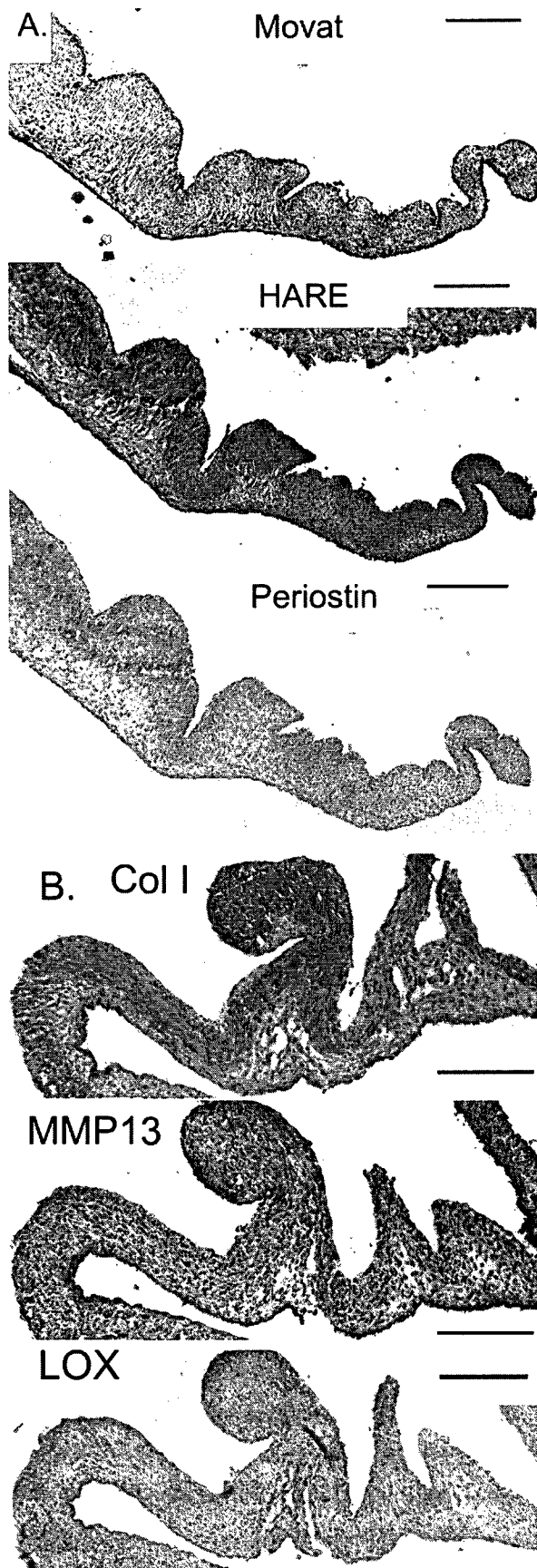


Fig. 5-7:
A) Localization of both periostin and HARE to the fibrosa; shown here in a 2-day old AV sample. Scale bar indicates 200 μ m.
B) Co-localization of MMP13 with Col I in the fibrosa, while LOX staining was diffuse; shown here in a 2-day old MV sample. Scale bar indicates 200 μ m.

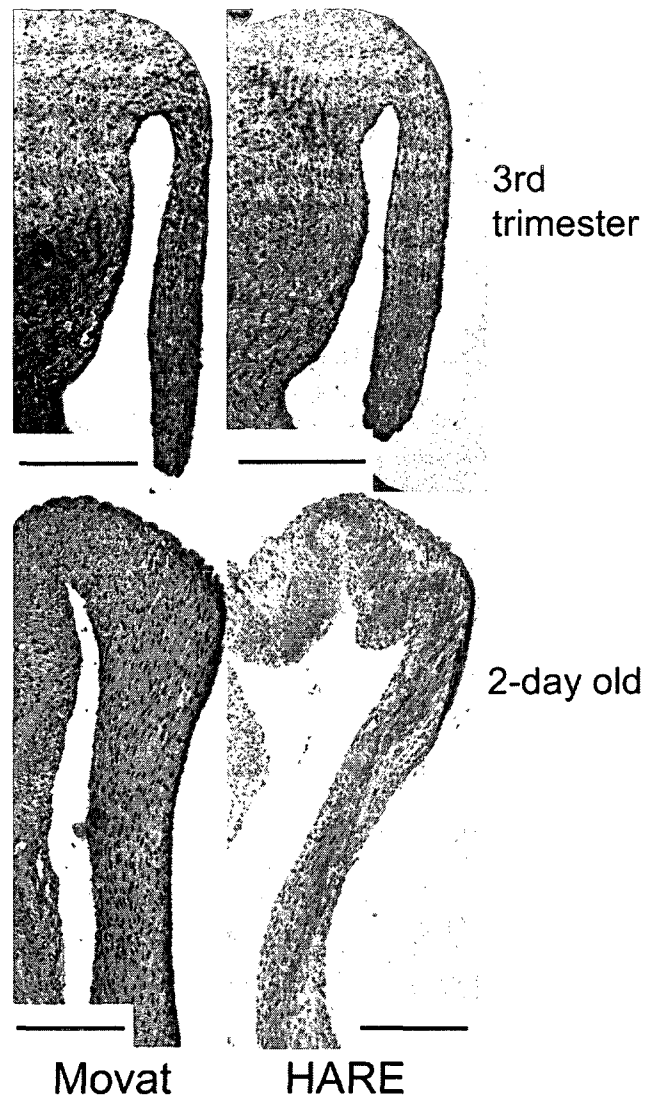


Fig. 5-8: HARE showed more diffuse expression in 3rd trimester valves compared to 2-day old valves, as illustrated here with AV samples. Scale bar indicates 200 μ m.

interrelated roles of these components in perinatal valves. For instance, consistent with the common functions of BGN and DCN, in the fibrosa of the AV BGN was correlated with DCN (annulus: $r=0.864$, $p=0.0057$; mid-leaflet: $r=0.794$, $p=0.0038$). Similarly, consistent with the common roles of BGN and P4H in collagen fibrillogenesis, BGN was

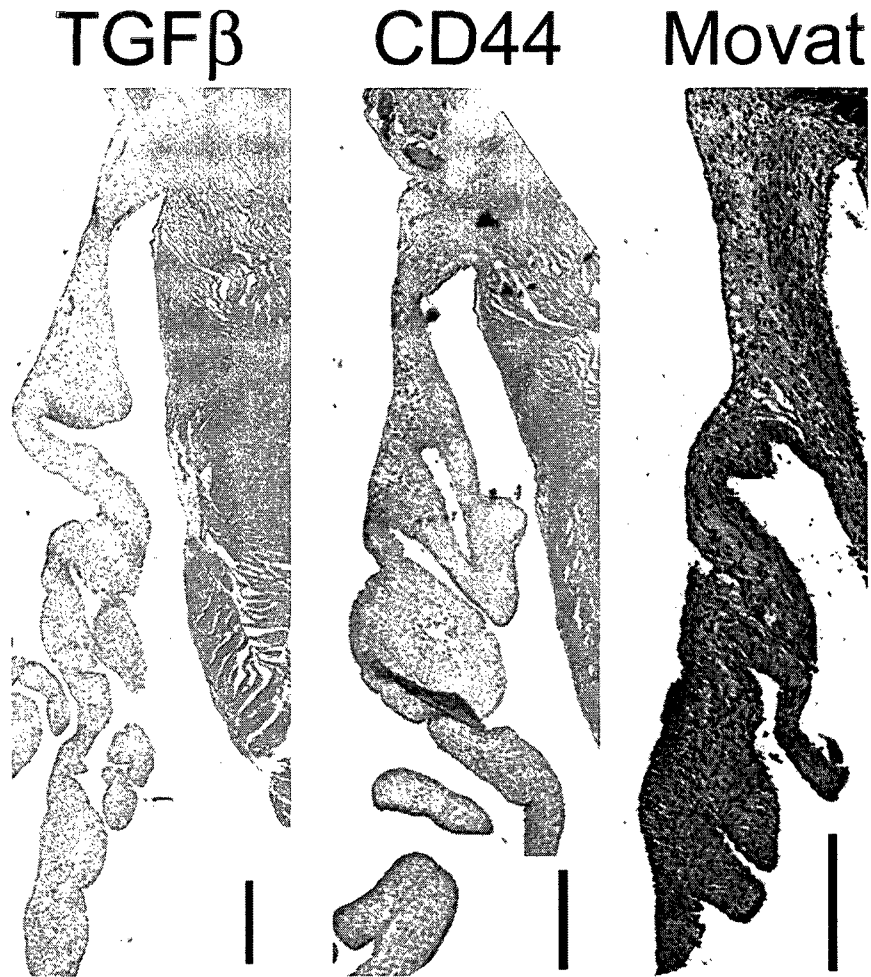


Fig. 5-9: CD44 and TGFβ demonstrated diffuse staining in both MV and AV of both age groups that did not localize to individual layers or regions. Shown here is a 2-day old MV sample. Magnification: 5x objective, scale bar indicates 200 μm.

correlated with P4H in the mid-leaflet fibrosa of the AV ($r=0.794$, $p=0.0038$). In the ventricularis layer of the AV, Col I was correlated with HARE in the annular region ($r=0.907$, $p=0.0019$) and with P4H in the mid-leaflet region ($r=0.83$, $p=0.0056$). In the annular fibrosa of the MV, elastin was correlated with Col III ($r=0.894$, $p=0.0066$).

DISCUSSION

This histological and immunohistochemical study showed that the composition and structure of the aortic and mitral valves change with birth, although these changes were more evident in the AV than in the MV. In general, perinatal changes in valve structure included increased delineation of leaflet layers and abundance of saffron-stained collagen. Perinatal changes in valve composition, found solely in the AV, included increases in proteins related to turnover of elastic fibers and decreases in proteins and receptors related to collagen and HA turnover. These changes could have important functional consequences as well as clinical implications.

Perinatal Changes in AV and MV Structure and Composition

The AV and MV appeared relatively similar before birth and became more distinct with birth. While the AV demonstrated numerous structural and compositional changes perinatally, including an increase in leaflet layer delineation, an increase in intensity of saffron-staining collagen, and an increase in the proportion of leaflet thickness comprised of saffron-staining collagen, all were evident in the AV, only an increase in delineation with birth was evident in the MV. Additionally, compositional changes with birth were almost exclusively only evident in the AV, not the MV. This greater change in AV composition and structure with birth compared to the MV could relate to greater change in the hemodynamic environment of the AV as opposed to the MV with birth. The hemodynamic environments (i.e., blood flow velocities, afterload pressures) of the two valves are relatively similar in the fetal circulation.^{1, 36} At birth,

however, the diastolic pressure borne by the AV increases by 51%, whereas the MV must bear a 23% greater diastolic pressure.² Thus, the mechanosensitive valves may be demonstrating levels of remodeling that are consistent with their changing mechanical environments.

Indeed, a large body of research in adult valves has examined the roles of specific mechanical factors in valve biology and remodeling. The role of pressure in AV composition has been studied in the *ex vivo* setting, where it was demonstrated that elevated static pressure caused an increase in collagen synthesis¹⁸ whereas cyclic pressure evoked a magnitude and frequency dependent response in valve composition.¹⁷ The effect of pressure on valve cells has also been implicated in modulation of cell phenotype and matrix synthesis based on differences in transvalvular pressures across the AV and pulmonic valve. AV valvular interstitial cells (VICs) were found to be stiffer and contain more smooth muscle alpha-actin and heat shock protein 47 (a marker of collagen synthesis) than VICs from the pulmonic valve.⁸ In addition, Platt et al.¹⁹ found that the application of shear stress to intact AV leaflets decreased the expression of cathepsins but increased the expression of MMPs. The effect of strain on adult AV leaflets and VICs has been extensively studied and found to affect collagen, MMP, and GAG production in a magnitude and frequency dependent manner.^{16, 37-41}

Although collagen synthesis (as shown by P4H expression) and pro-collagen I content decreased in the AV mid-leaflet with birth, it is interesting to note that the collagen in the fibrosa of 2-day old valves appeared more aligned and mature, as evidenced by greater intensity and proportion of Movat saffron-staining collagen. Additionally, the collagen remodeling enzyme MMP13 increased with birth in the MV,

and was localized to the fibrosa layer. Taken together, these results suggest that while less collagen is being produced immediately after birth, the collagen undergoes significant remodeling with birth as it becomes more mature and aligned. *Ex vivo* studies in which the AV was subjected to mechanical stimulation have demonstrated greater MMP expression with cyclic strain,³⁹ as well as thicker, more aligned collagen fibers.⁹ Alterations in the ratio of Col III to Col I have also been noted in cardiac remodeling, such as dilated cardiomyopathy,⁴²⁻⁴⁴ although a consensus has not been reached as to the exact nature of these changes and their implications.

Regional Heterogeneity in Perinatal Changes in Valve Composition

Perinatal changes in valve composition were predominantly found in the mid-leaflet as opposed to in the annular region of the valve. This regional heterogeneity could be attributed to the greater impact of the perinatal hemodynamic changes on the mid-leaflet region. More specifically, the myocardial anchorage of the annular region of the leaflet may partly shield that region from hemodynamic changes. In addition, the annular region can transduce forces to the myocardium, whereas the mid-leaflet does not have this anchorage. Greater compositional changes in the mid-leaflet as opposed to the annular region of the leaflet have also been observed in other animal models of altered hemodynamics.⁷

Localization of Matrix Components within AV and MV

The hyaluronan receptor for endocytosis (HARE), also known as stabilin-2, was localized to the fibrosa of the 2-day old valves. Although HARE has been previously

demonstrated in adult mouse valves^{45,46} and human adult normal and myxomatous mitral valves,⁴⁷ its function in valves remains enigmatic. In one relevant study in mice, HARE was reported to be absent during development but present in the postnatal murine heart; in these murine valves, HARE was found limited to the valvular endothelium.⁴⁶ Another study, however, demonstrated HARE throughout the valve thickness in adult mice.⁴⁵ In general, the predominant role of HARE is considered to be HA metabolism, i.e., the removal of HA from the bloodstream or extracellular space. Given the involvement of HA in valvulogenesis,³³ and the observed decrease in HA during atrioventricular endocardial cushion development in chicks,¹⁵ it is not surprising that HA metabolism would change during valve development and that the abundance of HARE would decrease with birth. However, the localization of HARE to the fibrosa layer and its colocalization with collagen in postnatal valves may be more related to other binding sites within the HARE molecule; HARE is known to bind to pro-collagen,⁴⁸ although the purpose of this binding in the context of valves is unclear. HARE can also mediate both heterophilic⁴⁹ and homophilic cell-cell interactions,⁵⁰ and HA binding to HARE triggers intracellular extracellular signal-regulated kinase (ERK) activation;⁵¹ these results suggest that HARE enables cells to sense matrix turnover. Furthermore, considering the many binding sites for diverse molecules along its length,⁵² HARE could potentially act as a scaffolding protein providing structure for and promoting interaction between these molecules. Clearly, the roles of HARE are diverse, meaning broader than HA metabolism alone, and many of these roles have yet to be elucidated, especially in the context of heart valves. Although CD44, one of the cellular receptors for HA, did not demonstrate a change in abundance with birth, the receptor activity of CD44 could have

changed while expression levels remained relatively constant. There are also a number of other cell surface receptors for HA and other proteins involved in HA metabolism that could be changing during this time period.

The co-localization of periostin with collagen in the fibrosa seen in this study is consistent with studies demonstrating that periostin directly binds collagen I and is involved in collagen fibrillogenesis.²⁷ Several other studies have also demonstrated the location of periostin in the AV and MV, both during development and in mature valves. In a report of murine embryological development, periostin showed widespread expression in the AV, but greater expression in the atrial aspect (elastic layer) of the MV.⁵³ In adult mice, however, two studies have demonstrated periostin expression localized within the collagenous fibrosa layer of the AV and MV.^{53, 54} During chick embryological development, periostin was found in the ventricular aspect of the MV (the fibrosa), but the AV showed lower expression relative to the MV.⁵⁵ In general, an increase in periostin with birth would be consistent with the role of periostin in cardiac remodeling in response to increased mechanical stimulation.²⁹

The localization of collagens and proteoglycans corroborate previous studies of different aged human and porcine MV and AV. Col III, a reticular collagen,⁵⁶ demonstrated more diffuse staining than Col I, as previously reported in human MV and AV.⁵⁷ The finding that P4H, a marker of collagen synthesis, was more diffusely present either collagen, and was even found outside the fibrosa layer, is consistent with previous evidence that collagen turnover is not limited to the fibrosa layer in porcine AV and MV.¹³ The enhanced staining of the proteoglycans BGN and DCN in the fibrosa is also consistent with previous studies¹⁴ and supports the role of these proteoglycans in collagen

integrity.^{58,59} The change in DCN expression could have affected collagen fiber diameter, given the known role that DCN plays in regulating collagen fiber diameter during collagen fibrillogenesis.^{58, 60} The localization of VC in the spongiosa and elastin-rich regions also corroborates previous reports in porcine valves,¹⁴ and supports a role for VC in elastic fiber homeostasis.³¹ LOX staining, which was relatively diffuse in the valves, suggested ongoing maturation of nascent matrix throughout the leaflet in both age groups.

Proposed Functional Consequences of Valve Structural and Compositional Changes

These observed valve compositional and structural changes likely affected the leaflet tissue and overall function. The increase in leaflet layer delineation, which is consistent with previous studies,¹³ would reduce flexural stress.⁶¹ The increase in elastin would aid in valve flexion and elastic recoil, as well as maintaining proper collagen fiber configuration.⁶² The increase in collagen maturation would result in greater tensile strength, allowing the valve to withstand the perinatal increase in pressures. A recent study by Balguid et al.⁶³ elegantly demonstrated a positive correlation between collagen crosslinking and tensile elastic modulus in the adult AV. Additionally, our lab has recently demonstrated that an increase in AV and MV tensile strength with postnatal age was associated with an increase in the amount of Movat saffron-staining collagen.⁶⁴ The role of decreased HA turnover with birth, as suggested by HARE expression, is less clear. HA has numerous roles, both biological and mechanical,^{65, 66} and the derangement of its regulation has been implicated in several pathologies in a variety of tissues including valves.⁴⁷ Therefore, alterations in HA metabolism observed with birth could have

important biological and mechanical consequences, although the exact nature of those remain to be determined. Similarly, perinatal changes in abundance and localization of proteoglycans could affect tissue mechanics, collagen homeostasis, cell signaling, growth factor regulation, and cell phenotype regulation. For example, DCN sequesters transforming growth factor-beta (TGF β),³⁰ a growth factor that modulates valve cell phenotype,⁶⁷ and is implicated in a number of valve diseases including myxomatous mitral valve disease.⁶⁸ Indeed, previous studies have demonstrated the co-localization of DCN with TGF β in porcine valves,¹⁴ although in this set of valves TGF β staining was found to be relatively diffuse. The proteoglycan VC is commonly found to be up-regulated in disease states as well as development,³⁰ and given its role in elastic fibrillogenesis the perinatal increase in VC could directly relate to the increase in elastin content with birth found in this study.³¹ Greater elastin could result in functional changes in leaflet bending properties as the leaflet adapts to the altered hemodynamics. Clearly, further study is required to better understand the functional consequences of these perinatal compositional and structural changes.

Implications

These data regarding the perinatal development of heart valves have several implications. First, as work continues to develop tissue engineered heart valves, a broad characterization of valve composition will be necessary to provide design criteria for valves for neonates. This age group is of particular interest given the large number of congenital heart disease (CHD) patients, who often undergo neonatal surgical repair procedures. Additionally, if the perinatal hemodynamic changes do not occur normally,

such as is the case in CHD, valve composition may be affected, which could in turn impact valvular cell phenotype and subsequent valvular maturation. Therefore, the results of this study suggest a potential mechanism for causing or contributing to the compositional and structural abnormalities observed in congenital valve disease. As illustrated by a representative example in Fig. 5-10, these congenitally diseased valves typically lack a layered leaflet structure and a mature collagenous fibrosa layer, and tend to be enriched in GAGs. Further characterization of these compositional abnormalities in

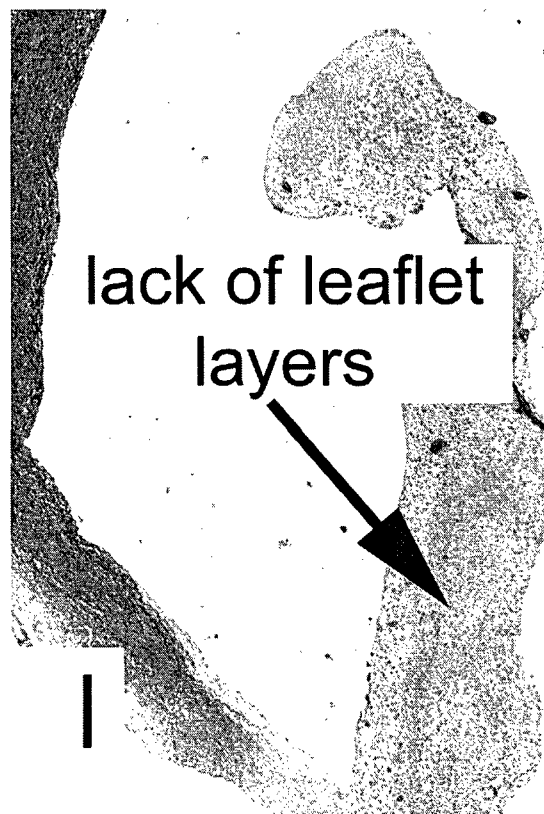


Fig. 5-10: Congenitally diseased AV from a 3 month-old female demonstrating lack of layered leaflet structure and enriched GAG composition. Scale bar indicates 200 μm .

congenitally diseased valves is currently underway in this laboratory. Lastly, these results could also have implications for the timing of surgical intervention in this patient population, in that early restoration of normal neonatal hemodynamics may promote normal development of valve composition and function.

Limitations

Although there were numerous statistically significant findings within this work, certain limitations must be mentioned. Samples were analyzed using immunohistochemistry, a powerful and appropriate method for examining both the abundance and localization of valve matrix components. However, this method is limited by some inherent variability in the staining technique, which in our hands has been quantified to be approximately 14%.⁷ To diminish the effect of this variability on our results, multiple samples were taken from each valve, and multiple sections cut from each sample were stained; the results were averaged. In addition, there are numerous other aspects of extracellular matrix maturation that should be addressed in future studies, such as collagen crosslinking and fiber diameter, that will further elucidate the nature of remodeling within the perinatal period. Furthermore, it will also be important to translate experimental mechanobiology studies, examining the effect of specific mechanical factors on the observed valve remodeling, from the time frame of adult valves to the perinatal and pediatric periods. This study also used an animal model; however, porcine valves are considered to be anatomically excellent animal models for human valves,⁶⁹ and indeed are commonly used as animal models for human valve biology and mechanics.⁷⁰ Lastly, some of the observed perinatal changes in the tissues may have

been due to changes in the biological milieu, such as circulating growth factors, cytokines, and even inflammatory mediators. Further study is warranted to understand the contribution of these other factors on valve remodeling with birth. In the future, it will also be important to elucidate the functional consequences of this perinatal valve remodeling and investigate how altered hemodynamics may relate to the altered valve structure and composition observed in congenital valve disease.

CONCLUSIONS

This study demonstrated that the AV and MV undergo significant remodeling with birth, including increased leaflet layer delineation and alignment of collagen, as well as changes in the amount of collagen turnover, hyaluronan metabolism, elastin, and proteoglycans. These perinatal changes were more pronounced in the AV than in the MV, consistent with greater hemodynamic changes experienced by the AV. These results contribute to a growing body of evidence that the valve dynamically adapts to its mechanical environment. Future study is warranted to examine the functional consequences of these changes, especially for patients with congenital valve disease.

This chapter, which analyzed changes in matrix composition and structure during the perinatal period, was the third of four chapters (Chapters 3-6) examining age-related changes in matrix composition and structure in normal aortic and mitral valves. In the next chapter in this series of studies, preliminary data is

presented analyzing regional heterogeneity in glycosaminoglycan composition in the aged aortic valve.

REFERENCES

1. Friedman AH, Fahey JT. The transition from fetal to neonatal circulation: normal responses and implications for infants with heart disease. *Semin Perinatol*. 1993;17(2):106-121.
2. Anderson PA, Glick KL, Manring A, Crenshaw C, Jr. Developmental changes in cardiac contractility in fetal and postnatal sheep: in vitro and in vivo. *Am J Physiol*. 1984;247(3 Pt 2):H371-379.
3. Sansoucie DA, Cavaliere TA. Transition from fetal to extrauterine circulation. *Neonatal Netw*. 1997;16(2):5-12.
4. Cooper T, Napolitano LM, Fitzgerald MJ, Moore KE, Daggett WM, Willman VL, Sonnenblick EH, Hanlon CR. Structural basis of cardiac valvar function. *Arch Surg*. 1966;93(5):767-771.
5. Borin C, Vanhercke D, Weyns A. Innervation of the atrioventricular and semi-lunar heart valves: a review. *Acta Cardiol*. 2006;61(4):463-469.
6. Grande-Allen KJ, Borowski AG, Troughton RW, Houghtaling PL, Dipaola NR, Moravec CS, Vesely I, Griffin BP. Apparently normal mitral valves in patients with heart failure demonstrate biochemical and structural derangements: an extracellular matrix and echocardiographic study. *J Am Coll Cardiol*. 2005;45(1):54-61.
7. Stephens EH, Timek TA, Daughters GT, Kuo JJ, Patton AM, Baggett LS, Ingels NB, Miller DC, Grande-Allen KJ. Significant changes in mitral valve leaflet matrix composition and turnover with tachycardia-induced cardiomyopathy. *Circulation*. 2009;120(11 Suppl):S112-119.
8. Merryman WD, Youn I, Lukoff HD, Krueger PM, Guilak F, Hopkins RA, Sacks MS. Correlation between heart valve interstitial cell stiffness and transvalvular pressure: implications for collagen biosynthesis. *Am J Physiol Heart Circ Physiol*. 2006;290(1):H224-231.
9. Balachandran K, Konduri S, Sucusky P, Jo H, Yoganathan A. An ex vivo study of the biological properties of porcine aortic valves in response to circumferential cyclic stretch. *Ann Biomed Eng*. 2006;34(11):1655-1665.
10. Gupta V, Werdenberg JA, Mendez JS, Jane Grande-Allen K. Influence of strain on proteoglycan synthesis by valvular interstitial cells in three-dimensional culture. *Acta Biomater*. 2008;4(1):88-96.
11. Aikawa E, Whittaker P, Farber M, Mendelson K, Padera RF, Aikawa M, Schoen FJ. Human semilunar cardiac valve remodeling by activated cells from fetus to adult: implications for postnatal adaptation, pathology, and tissue engineering. *Circulation*. 2006;113(10):1344-1352.
12. Hinton RB, Jr, Lincoln J, Deutsch GH, Osinska H, Manning PB, Benson DW, Yutzey KE. Extracellular matrix remodeling and organization in developing and diseased aortic valves. *Circ Res*. 2006;98(11):1431-1438.

13. Stephens EH, Grande-Allen KJ. Age-related changes in collagen synthesis and turnover in porcine heart valves. *J Heart Valve Dis.* 2007;16(6):672-682.
14. Stephens EH, Chu CK, Grande-Allen KJ. Valve proteoglycan content and glycosaminoglycan fine structure are unique to microstructure, mechanical load and age: Relevance to an age-specific tissue-engineered heart valve. *Acta Biomater.* 2008;4(5):1148-1160.
15. Butcher J, McQuinn T, Sedmera D, Turner D, Markwald R. Transitions in early embryonic atrioventricular valvular function correspond with changes in cushion biomechanics that are predictable by tissue composition. *Circ Res.* 2007;100(10):1503-1511.
16. Ku CH, Johnson PH, Batten P, Sarathchandra P, Chambers RC, Taylor PM, Yacoub MH, Chester AH. Collagen synthesis by mesenchymal stem cells and aortic valve interstitial cells in response to mechanical stretch. *Cardiovasc Res.* 2006;71(3):548-556.
17. Xing Y, Warnock JN, He Z, Hilbert SL, Yoganathan AP. Cyclic pressure affects the biological properties of porcine aortic valve leaflets in a magnitude and frequency dependent manner. *Ann Biomed Eng.* 2004;32(11):1461-1470.
18. Xing Y, He Z, Warnock JN, Hilbert SL, Yoganathan AP. Effects of constant static pressure on the biological properties of porcine aortic valve leaflets. *Ann Biomed Eng.* 2004;32(4):555-562.
19. Platt MO, Xing Y, Jo H, Yoganathan AP. Cyclic pressure and shear stress regulate matrix metalloproteinases and cathepsin activity in porcine aortic valves. *J Heart Valve Dis.* 2006;15(5):622-629.
20. Hoffman J, Kaplan S. The incidence of congenital heart disease. *J Am Coll Cardiol.* 2002;39(12):1890-1900.
21. Dunn JM. Porcine valve durability in children. *Ann Thorac Surg.* 1981;32(4):357-368.
22. Solymar L, Rao PS, Mardini MK, Fawzy ME, Guinn G. Prosthetic valves in children and adolescents. *Am Heart J.* 1991;121(2 Pt 1):557-568.
23. Fisher LW, Stubbs JT, 3rd, Young MF. Antisera and cDNA probes to human and certain animal model bone matrix noncollagenous proteins. *Acta Orthop Scand Suppl.* 1995;266:61-65.
24. Cole WG, Chan D, Hickey AJ, Wilcken DE. Collagen composition of normal and myxomatous human mitral heart valves. *Biochem J.* 1984;219(2):451-460.
25. Kivirikko K, Myllyla R. Post-translational processing of procollagens. *Ann N Y Acad Sci.* 1985;460:187-201.
26. Butcher JT, Norris RA, Hoffman S, Mjaatvedt CH, Markwald RR. Periostin promotes atrioventricular mesenchyme matrix invasion and remodeling mediated by integrin signaling through Rho/PI 3-kinase. *Dev Biol.* 2007;302(1):256-266.

27. Norris RA, Damon B, Mironov V, Kasyanov V, Ramamurthi A, Moreno-Rodriguez R, Trusk T, Potts JD, Goodwin RL, Davis J, Hoffman S, Wen X, Sugi Y, Kern CB, Mjaatvedt CH, Turner DK, Oka T, Conway SJ, Molkentin JD, Forgacs G, Markwald RR. Periostin regulates collagen fibrillogenesis and the biomechanical properties of connective tissues. *J Cell Biochem.* 2007;101(3):695-711.
28. Oka T, Xu J, Kaiser RA, Melendez J, Hambleton M, Sargent MA, Lorts A, Brunskill EW, Dorn GW, 2nd, Conway SJ, Aronow BJ, Robbins J, Molkentin JD. Genetic manipulation of periostin expression reveals a role in cardiac hypertrophy and ventricular remodeling. *Circ Res.* 2007;101(3):313-321.
29. Borg TK, Markwald R. Periostin: more than just an adhesion molecule. *Circ Res.* 2007;101(3):230-231.
30. Kinsella MG, Bressler SL, Wight TN. The regulated synthesis of versican, decorin, and biglycan: extracellular matrix proteoglycans that influence cellular phenotype. *Crit Rev Eukaryot Gene Expr.* 2004;14(3):203-234.
31. Merrilees MJ, Lemire JM, Fischer JW, Kinsella MG, Braun KR, Clowes AW, Wight TN. Retrovirally mediated overexpression of versican v3 by arterial smooth muscle cells induces tropoelastin synthesis and elastic fiber formation in vitro and in neointima after vascular injury. *Circ Res.* 2002;90(4):481-487.
32. Henderson DJ, Copp AJ. Versican expression is associated with chamber specification, septation, and valvulogenesis in the developing mouse heart. *Circ Res.* 1998;83(5):523-532.
33. Wagner M, Siddiqui MA. Signal transduction in early heart development (II): ventricular chamber specification, trabeculation, and heart valve formation. *Exp Biol Med (Maywood).* 2007;232(7):866-880.
34. Lara S, Evanko S, Wight T. Morphological evaluation of proteoglycans in cells and tissues. *Methods Mol Biol.* 2001;171:271-290.
35. Harris EN, Weigel JA, Weigel PH. Endocytic function, glycosaminoglycan specificity, and antibody sensitivity of the recombinant human 190-kDa hyaluronan receptor for endocytosis (HARE). *J Biol Chem.* 2004;279(35):36201-36209.
36. Allan LD, Chita SK, Al-Ghazali W, Crawford DC, Tynan M. Doppler echocardiographic evaluation of the normal human fetal heart. *Br Heart J.* 1987;57(6):528-533.
37. Gupta V, Tseng H, Lawrence BD, Jane Grande-Allen K. Effect of cyclic mechanical strain on glycosaminoglycan and proteoglycan synthesis by heart valve cells. *Acta Biomater.* 2009;5(2):531-540.
38. Gupta V, Werdenburg JA, Blevins TL, Grande-Allen KJ. Synthesis of glycosaminoglycans in differently loaded regions of collagen gels seeded with valvular interstitial cells. *Tissue Eng.* 2007;13(1):41-49.

39. Balachandran K, Sucosky P, Jo H, Yoganathan AP. Elevated cyclic stretch alters matrix remodeling in aortic valve cusps: implications for degenerative aortic valve disease. *Am J Physiol Heart Circ Physiol*. 2009;296(3):H756-764.
40. Balachandran K, Konduri S, Sucosky P, Jo H, Yoganathan AP. An ex vivo study of the biological properties of porcine aortic valves in response to circumferential cyclic stretch. *Ann Biomed Eng*. 2006;34(11):1655-1665.
41. Merryman WD, Lukoff HD, Long RA, Engelmayr GC, Jr., Hopkins RA, Sacks MS. Synergistic effects of cyclic tension and transforming growth factor-beta1 on the aortic valve myofibroblast. *Cardiovasc Pathol*. 2007;16(5):268-276.
42. Pauschinger M, Doerner A, Remppis A, Tannhauser R, Kuhl U, Schultheiss HP. Differential myocardial abundance of collagen type I and type III mRNA in dilated cardiomyopathy: effects of myocardial inflammation. *Cardiovasc Res*. 1998;37(1):123-129.
43. Marijianowski MM, Teeling P, Mann J, Becker AE. Dilated cardiomyopathy is associated with an increase in the type I/type III collagen ratio: a quantitative assessment. *J Am Coll Cardiol*. 1995;25(6):1263-1272.
44. Sivakumar P, Gupta S, Sarkar S, Sen S. Upregulation of lysyl oxidase and MMPs during cardiac remodeling in human dilated cardiomyopathy. *Mol Cell Biochem*. 2008;307(1-2):159-167.
45. Falkowski M, Schledzewski K, Hansen B, Goerd S. Expression of stabilin-2, a novel fasciclin-like hyaluronan receptor protein, in murine sinusoidal endothelia, avascular tissues, and at solid/liquid interfaces. *Histochem Cell Biol*. 2003;120(5):361-369.
46. Lindsley A, Li W, Wang J, Maeda N, Rogers R, Conway SJ. Comparison of the four mouse fasciclin-containing genes expression patterns during valvuloseptal morphogenesis. *Gene Expr Patterns*. 2005;5(5):593-600.
47. Gupta V, Barzilla JE, Mendez JS, Stephens EH, Lee EL, Collard CD, Laucirica R, Weigel PH, Grande-Allen KJ. Abundance and location of proteoglycans and hyaluronan within normal and myxomatous mitral valves. *Cardiovasc Pathol*. 2009;18(4):191-197.
48. Hansen B, Longati P, Elvevold K, Nedredal GI, Schledzewski K, Olsen R, Falkowski M, Kzhyshkowska J, Carlsson F, Johansson S, Smedsrod B, Goerd S, McCourt P. Stabilin-1 and stabilin-2 are both directed into the early endocytic pathway in hepatic sinusoidal endothelium via interactions with clathrin/AP-2, independent of ligand binding. *Exp Cell Res*. 2005;303(1):160-173.
49. Jung MY, Park SY, Kim IS. Stabilin-2 is involved in lymphocyte adhesion to the hepatic sinusoidal endothelium via the interaction with alphaMbeta2 integrin. *J Leukoc Biol*. 2007;82(5):1156-1165.
50. Park SY, Jung MY, Kim IS. Stabilin-2 mediates homophilic cell-cell interactions via its FAS1 domains. *FEBS Lett*. 2009;583(8):1375-1380.

51. Kyosseva SV, Harris EN, Weigel PH. The hyaluronan receptor for endocytosis mediates hyaluronan-dependent signal transduction via extracellular signal-regulated kinases. *J Biol Chem.* 2008;283(22):15047-15055.
52. Harris EN, Weigel PH. The ligand-binding profile of HARE: hyaluronan and chondroitin sulfates A, C, and D bind to overlapping sites distinct from the sites for heparin, acetylated low-density lipoprotein, dermatan sulfate, and CS-E. *Glycobiology.* 2008;18(8):638-648.
53. Norris RA, Moreno-Rodriguez RA, Sugi Y, Hoffman S, Amos J, Hart MM, Potts JD, Goodwin RL, Markwald RR. Periostin regulates atrioventricular valve maturation. *Dev Biol.* 2008;316(2):200-213.
54. Snider P, Hinton RB, Moreno-Rodriguez RA, Wang J, Rogers R, Lindsley A, Li F, Ingram DA, Menick D, Field L, Firulli AB, Molkentin JD, Markwald R, Conway SJ. Periostin is required for maturation and extracellular matrix stabilization of noncardiomyocyte lineages of the heart. *Circ Res.* 2008;102(7):752-760.
55. Kern CB, Hoffman S, Moreno R, Damon BJ, Norris RA, Krug EL, Markwald RR, Mjaatvedt CH. Immunolocalization of chick periostin protein in the developing heart. *Anat Rec A Discov Mol Cell Evol Biol.* 2005;284(1):415-423.
56. Ushiki T. Collagen fibers, reticular fibers and elastic fibers. A comprehensive understanding from a morphological viewpoint. *Arch Histol Cytol.* 2002;65(2):109-126.
57. McDonald PC, Wilson JE, McNeill S, Gao M, Spinelli JJ, Rosenberg F, Wiebe H, McManus BM. The challenge of defining normality for human mitral and aortic valves: geometrical and compositional analysis. *Cardiovasc Pathol.* 2002;11(4):193-209.
58. Danielson KG, Baribault H, Holmes DF, Graham H, Kadler KE, Iozzo RV. Targeted disruption of decorin leads to abnormal collagen fibril morphology and skin fragility. *J Cell Biol.* 1997;136(3):729-743.
59. Reed CC, Iozzo RV. The role of decorin in collagen fibrillogenesis and skin homeostasis. *Glycoconj J.* 2002;19(4-5):249-255.
60. Derwin K, Soslowsky L, Kimura J, Plaas A. Proteoglycans and glycosaminoglycan fine structure in the mouse tail tendon fascicle. *J Orthop Res.* 2001;19(2):269-277.
61. Kunzelman KS, Cochran RP, Murphree SS, Ring WS, Verrier ED, Eberhart RC. Differential collagen distribution in the mitral valve and its influence on biomechanical behaviour. *J Heart Valve Dis.* 1993;2(2):236-244.
62. Vesely I. The role of elastin in aortic valve mechanics. *J Biomech.* 1998;31(2):115-123.
63. Balguid A, Rubbens M, Mol A, Bank R, Bogers A, van Kats J, de Mol B, Baaijens F, Bouten C. The role of collagen cross-links in biomechanical behavior of human aortic heart valve leaflets--relevance for tissue engineering. *Tissue Eng.* 2007;13(7):1501-1511.

64. Stephens EH, de Jonge N, McNeill MP, Durst CA, Grande-Allen KJ. Age-related changes in material behavior of porcine mitral and aortic valves and correlation to matrix composition. *Tissue Eng.* 2010;16(3):867-878.
65. Toole BP. Hyaluronan in morphogenesis. *Semin Cell Dev Biol.* 2001;12(2):79-87.
66. Toole BP. Hyaluronan: from extracellular glue to pericellular cue. *Nat Rev Cancer.* 2004;4(7):528-539.
67. Walker GA, Masters KS, Shah DN, Anseth KS, Leinwand LA. Valvular myofibroblast activation by transforming growth factor-beta: implications for pathological extracellular matrix remodeling in heart valve disease. *Circ Res.* 2004;95(3):253-260.
68. Disatian S, Orton EC. Autocrine serotonin and transforming growth factor beta 1 signaling mediates spontaneous myxomatous mitral valve disease. *J Heart Valve Dis.* 2009;18(1):44-51.
69. Sim EK, Muskawad S, Lim CS, Yeo JH, Lim KH, Grignani RT, Durrani A, Lau G, Duran C. Comparison of human and porcine aortic valves. *Clin Anat.* 2003;16(3):193-196.
70. Vesely I. Reconstruction of loads in the fibrosa and ventricularis of porcine aortic valves. *ASAIO J.* 1996;42(5):M739-M746.

Chapter 6: Regional Heterogeneity in Aortic Valve GAG

Composition

This chapter is the fourth of four chapters (Chapters 3-6) examining age-related changes in matrix composition and structure in normal aortic and mitral valves. The work contained in this chapter follows upon a question that arose in the analysis of glycosaminoglycan fine structure composition in Chapter 4, namely whether the aortic valve displayed regional heterogeneity in glycosaminoglycan fine structure, regions that may age distinctly, similar to that observed within the mitral valve. The first step to address this question was to see if regional heterogeneity in glycosaminoglycan fine structure in the aortic valve existed. Aged aortic valves were chosen for the preliminary studies in this chapter with the rationale that older valves would have been exposed to heterogeneous loading longer, allowing more time for regional compositional heterogeneity to develop; therefore, if there were such heterogeneity, it was most likely to be evident in these valves. Given that the work contained in this chapter represents a preliminary study, it has been included at the end of the series on age-related changes in matrix composition and structure.

ABSTRACT

Background: While the need for a tissue engineered heart valve (TEHV) is well established, there has been only limited characterization of valvular extracellular matrix composition, such as glycosaminoglycans (GAGs), that will need to be recapitulated

within the TEHV. GAGs are known to be critical to tissue differentiation, structure, and mechanics. Furthermore, GAG fine structure, meaning GAG chain length and sulfation pattern, is thought to be important to biological function. While recent studies have shown differences in GAG fine structure between regions of the mitral valve that experience different mechanical loading, and even that the GAG compositions of these regions demonstrate distinct changes with age, such patterns of regional complexity and correlation with mechanical loading have not been examined in the aortic valve (AV).

Methods: Fluorophore-assisted carbohydrate electrophoresis (FACE) was used to analyze GAG composition in different regions of the 6-year-old porcine AV (coaptation, attachment, nodule, and belly) and interpreted this data in light of known patterns of mechanical loading.

Results: The relative abundances of hyaluronan (HA), chondroitin 6-sulfate (C6S), and 4-sulfated N-acetylgalactosamine (galNAc4) were significantly different between regions (each $p < 0.05$), with the nodule region containing the most HA, C6S, and galNAc4 per dry weight. Overall GAG content was also significantly different between regions ($p < 0.001$) with the nodule region containing the greatest amount, followed by the attachment region, belly region, and then coaptation region. Percent hydration was not significantly different among the regions analyzed.

Conclusions: This study provides promising preliminary information regarding regional heterogeneity of GAG distribution within the AV. Further study in this area should yield

insight into the role of mechanical loading in AV tissue composition as well as inform the design of TEHVs for the aortic position. Assessment of the regional GAG composition of different aged AVs will be important to determine whether these regions undergo distinct aging processes in terms of GAG content, similar to that observed in MV regions; this AV aging data could then be applied to age-specific tissue engineered AV design.

The work contained in this chapter was preliminary data and will not be submitted for publication.

INTRODUCTION

Glycosaminoglycans (GAGs) play key roles in valve structure and function that vary from the cellular level, such as their involvement in the sequestration of growth factors and cell signaling,¹ to the microstructural level, such as regulating collagen fibrillogenesis,² to the tissue as a whole, such as providing lubrication between layers and resistance against compression.³ GAGs also play a role in valvulopathies, such as in myxomatous mitral valve disease⁴ and likely in calcific aortic valve disease.⁵ A recent study of GAG composition of different aged mitral and aortic valves (MV, AV) demonstrated significant differences in hydration, GAG types and sulfation patterns, and GAG chain length between the center and free edge regions of the MV anterior leaflet, which undergo distinct loading patterns.⁶ However, it is unknown whether this manner of regional heterogeneity in GAG content and hydration also exists within the AV. Evidence suggests that regions of the AV, like the MV, experience significantly different mechanical environments. Finite element modeling of human AV and aortic roots suggested that the peak stresses within the AV leaflet were in the belly region, with relatively low stresses in the coaptation and attachment regions.⁷ In another computational model of the AV leaflet, regional heterogeneity in stresses and strains were also observed.⁸ In this model, the annular attachment region experienced low stress, whereas maximum stresses were found at the commissures and slightly lower stresses were present in the belly region.⁸ A recent study utilizing porcine AVs in a physiologic left-heart simulator found that radial strain was greatest near the tip of the leaflet, while circumferential strain was greatest at the base of the leaflet.⁹ Within this left-heart simulator, the basal portion of the leaflet was also found to be substantially stiffer than

the tip of the leaflet.⁹ A number of studies have similarly shown regional heterogeneity in terms of collagen composition and structure within the AV.^{8, 10, 11} Given evidence that the differently loaded regions of the MV demonstrate altered GAG content,^{6, 12} as well as additional evidence that valve cells in the *in vitro* setting respond to mechanical stimulation by altered GAG synthesis,¹³ it was the hypothesis of this study that GAG composition would vary among the different regions of the AV that experience different mechanical environments. Characterization of such regional heterogeneity in GAG composition would not only allow better understanding of the interaction of AV structure and its mechanical environment, and how that might be similar to or distinct from that of the MV, but also provide design criteria for a tissue engineered AV.

Therefore, the experiments contained in this chapter were designed as a pilot study to provide an initial overview of GAG content within different regions of the AV. The abundance of specific GAG classes (using fluorophore-assisted carbohydrate electrophoresis (FACE)) and percent hydration were examined within the attachment, coaptation, belly, and nodule regions of the AV (Fig. 6-1). It was hypothesized that if regional differences in GAG content within the AV existed, they would be most pronounced in an elderly animal, such as the 6-year-old pig, given that those leaflets hypothetically had been exposed to regional differences in mechanical environment for the longest amount of time. Therefore, these studies were undertaken using 6-year-old pig valves.

METHODS

General Procedure

Hearts from 6-year-old pigs were obtained within 24 hours of death (n=3, Animal Technologies, Tyler, TX). Hearts were maintained on ice until processing. One leaflet per AV was used, chosen randomly from the non-coronary, right coronary, and left coronary leaflets. The attachment, coaptation, nodule, and belly regions were dissected from the leaflets (Fig. 6-1), and hydration and GAG content was analyzed as described below.

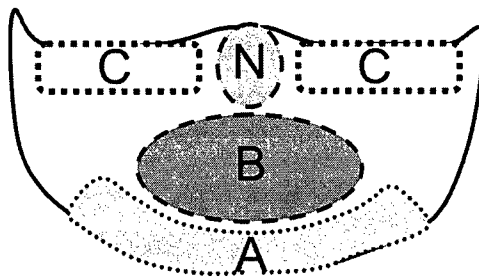


Fig. 6-1: Diagram illustrating regions analyzed. A=attachment, B=belly, C=coaptation, N=nodule.

Fluorophore-Assisted Carbohydrate Electrophoresis (FACE)

Fluorophore-assisted carbohydrate electrophoresis (FACE) was used to analyze the quantity and fine structure of the different GAG classes, HA and the chondroitin/dermatan sulfates (CS/DS).^{12, 14} Note on nomenclature: CS is defined as only containing glucuronate while DS is defined as containing some quantity of iduronate. First, the AV was dissected from porcine hearts within 24 hours of death. Each sample was weighed before and after lyophilization; hydration was calculated as (wet weight -

lyophilized weight)/wet weight. The GAGs in the lyophilized samples were then analyzed by FACE,^{12, 15} as described in detail in Chapter 4. Each sample was run and analyzed at least 2 times and the results were averaged.

Statistical Analysis

Multifactorial analysis of variance was performed using SigmaStat (SPSS, Chicago, IL), as described in Chapter 4.

RESULTS

The results for the wet and drive weights for samples from the different regions are listed in Table 6-1.

Table 6-1. Wet and Dry Weights for Samples.

	<u>Dry Weight</u>	<u>Wet Weight</u>
A	14.7±1.9	82.2±10.6
B	7.7±0.5	46.5±5.3
C	3.3±1.1	19.0±2.5
N	4.0±0.4	33.2±5.3

Average weight (mg) ± standard error of the mean;
A=attachment, B=belly, C=coaptation, N=nodule.

The amounts of hyaluronan (HA), chondroitin 6-sulfate (C6S), and 4-sulfated N-acetylgalactosamine (galNAc4) were significantly different between regions (Fig. 6-2). Among these regions, the nodule region had the highest HA, C6S, and galNAc4 per dry

GAG Composition in AV Regions

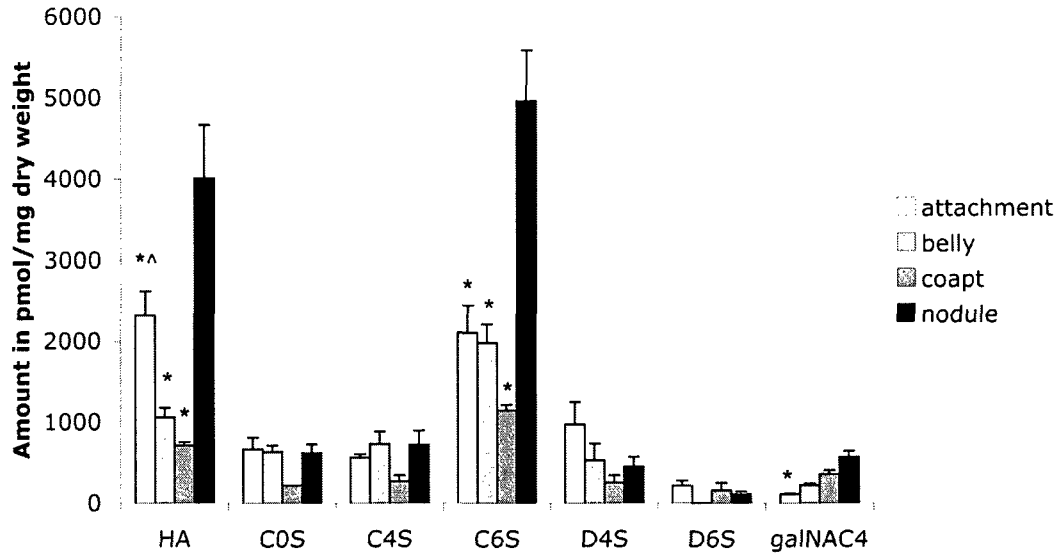


Fig. 6-2: Amount of various GAGs, normalized to mg of dry tissue weight, in different regions of the AV leaflet as determined by FACE. *= $p < 0.05$ vs. nodule for a given GAG; ^= $p < 0.05$ vs. attachment for a given GAG. Error bars indicate standard error of the mean.

weight. The attachment region had lower HA content than the nodule region, but higher content than the coaptation regions (each $p \leq 0.007$ R). Dermatan 4-sulfate (D4S) was higher in the attachment region relative to the coaptation region, although there was no statistically significant difference between regions for D4S and a substantially larger number of samples would need to be analyzed to verify that such a difference exists. Overall within this pilot study, chondroitin 0-sulfate (C0S) and chondroitin 4-sulfate (C4S) appeared relatively constant across regions. In terms of the relative amounts of the different GAG classes, HA and C6S content were significantly higher than each of the other GAG classes (each $p < 0.001$).

Average GAG Composition in AV Regions

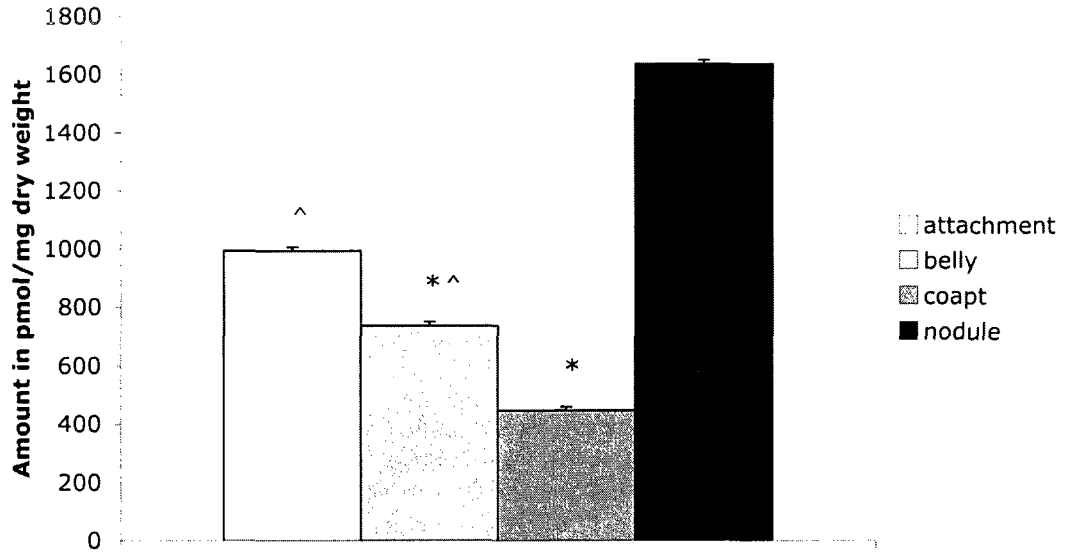


Fig. 6-3: GAG composition, normalized to mg of dry tissue weight, in different regions of the AV leaflet as determined by FACE. Overall regions were significantly different ($p < 0.001$). $*$ = $p < 0.001$ vs. nodule region; \wedge = $p < 0.003$ vs. coaptation region. Error bars indicate standard error of the mean.

The average GAG content was also significantly different between regions (Fig. 6-3, $p < 0.001$), with the content of the nodule region the highest, followed by the attachment region, belly region, and then coaptation region.

Proportional GAG Content in AV Regions

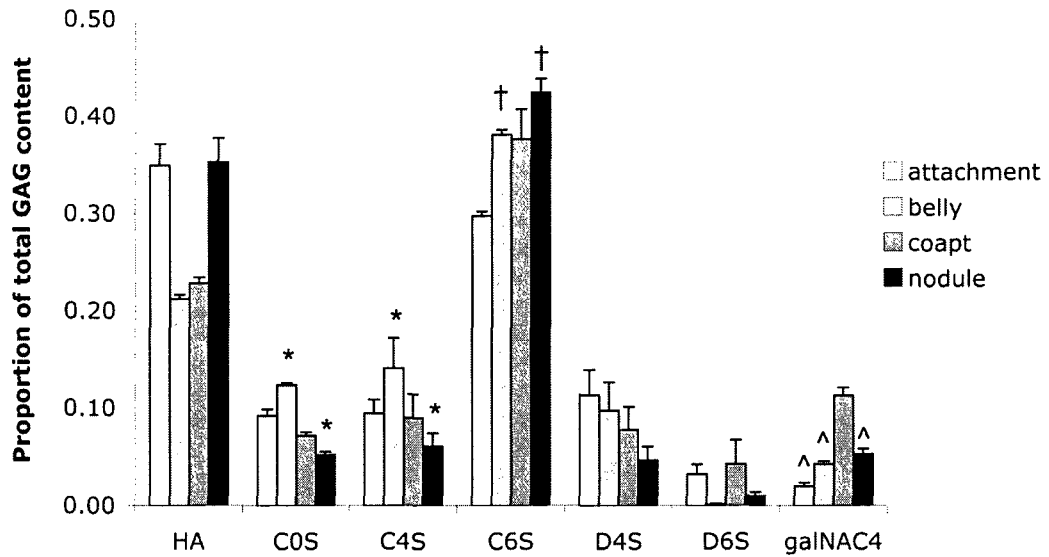


Fig. 6-4: Proportion of various GAGs relative to total GAG content in different regions of the AV leaflet as determined by FACE. *= $p < 0.05$ regions significantly different for a given GAG; ^= $p < 0.05$ vs. coaptation region for that GAG; †= $p < 0.05$ vs. attachment region for that GAG. Error bars indicate standard error of the mean.

Analysis of proportional GAG content (i.e., amount of a given GAG relative to total GAG content in that region) revealed that the proportional C0S content of the belly region was greater than the coaptation region ($p=0.002$, Fig. 6-4), proportional galNAC4 content of the coaptation region was greater than the other regions (each $p \leq 0.005$), proportional C4S content of the belly region was greater than the nodule region ($p=0.006$), and proportional C6S content of the belly and nodule regions were greater than the attachment region (each $p \leq 0.009$).

Overall, across regions the proportional content of C6S was substantially higher than each of the other GAG classes except HA (each $p < 0.001$) and HA content was greater than D4S and D6S (each $p < 0.004$).

Hydration in AV Regions

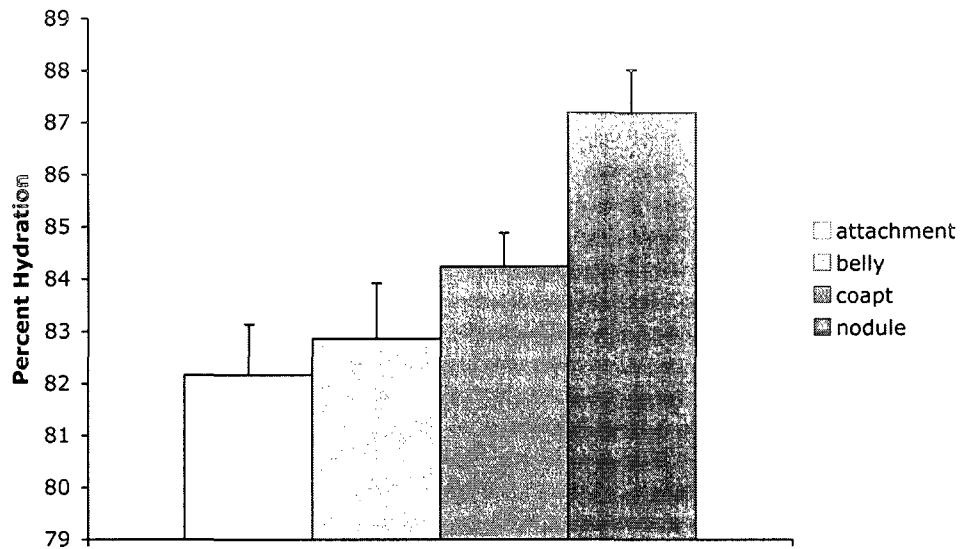


Fig. 6-5: Percent hydration in different regions of the AV leaflet. Percent hydration was not statistically significant different between regions. Error bars indicate standard error of the mean.

Percent hydration was not significantly different between the regions analyzed (Fig. 6-5).

DISCUSSION

Although these experiments were designed as a pilot study with a small number of samples, and clearly a much larger number of samples would need to be analyzed to verify and further demonstrate potential differences between the regions, the results of this study provide insight regarding differences in overall GAG content and in specific GAG types between regions of the AV. Given that significant differences were observed, this pilot study also provides motivation for further study in this area, both in terms of a larger number of samples, as well as different aged AV given evidence for age-related changes in AV regional stresses.¹⁶

Regional Heterogeneity in AV Composition

The results of this pilot study indicate that regional differences in GAG composition exist in the AV. While further work needs to be done in this regard, from these initial findings the nodule region stood out as being distinct from the other regions both in terms of individual GAG classes, especially HA and C6S, as well as overall GAG content. The regional GAG composition heterogeneity evident in this study builds upon other studies that have demonstrated regional AV heterogeneity in collagen content and structure.^{8, 10, 11} Of particular note, Balguid et al.⁸ found that collagen fiber bundle diameters were highest in the commissural regions, somewhat smaller in the belly, and smallest in the annular attachment region. Decorin and biglycan, two proteoglycans rich in dermatan sulfate,^{12, 17} are integrally associated with collagen fibrillogenesis as well as collagen fiber bundle formation.^{17, 18} Decorin has been shown *in vitro* and in knock-out animal models to decrease collagen fiber diameter by preventing lateral fusion of collagen fibers.¹⁷⁻¹⁹ It is worth noting that the attachment region in this study did appear to have increased dermatan 4-sulfate, which would correlate to the region of low fiber bundle diameter in the study by Balguid et al. It would be interesting in future studies to investigate the relative distributions of dermatan sulfate and these two proteoglycans with respect to this reported regional heterogeneity in collagen fiber bundles, as has been done in other connective tissues.²

Potential Relationship between Regional Heterogeneity in AV Mechanics and GAG Composition

Studies examining heterogeneity in GAG composition among differently loaded regions of the MV demonstrated that regions that undergo tension contain more dermatan and 4-sulfated GAG, less hydration, less chondroitin sulfate, and less 6-sulfation compared to regions undergoing compression.^{6, 12} In this study the nodular region, which would undergo compression, demonstrated greater HA and C6S compared to the other regions. Hydration also was higher in this region, although that difference was not statistically significant. Theoretically, this greater HA and C6S (the C6S is likely associated with the proteoglycan versican¹²) would aid in the compressive strength of this thickened valve region, and thus serve to prevent regurgitation. Dermatan 4-sulfate (D4S) was higher in the attachment region relative to the other regions. This increased D4S content may relate to the observed greater stiffness in this region,⁹ and would be consistent with similar correlations between D4S and stiffness in the MV.^{6, 12, 20} In terms of correlations to the loading pattern experienced by that region, some computational studies have suggested high stresses in that region,¹⁶ although other computational models disagree.^{7, 8}

While the relationship between regional GAG compositional heterogeneity and function within the AV is still being elucidated, previous studies demonstrating AV regional heterogeneity in collagen structure have correlated these compositional differences to functional roles. For instance, Balguid et al. found that the regions of higher stress within their computational model correlated to regions with larger diameter collagen fiber bundles.⁸ Sacks et al. demonstrated that the different regions of the AV

with varying degrees of collagen fiber alignment responded uniquely to increasing trans-valvular pressure.¹¹ In fact, given the role of decorin and biglycan in binding and organizing collagen fibers, these proteoglycans and their GAG chains may play an important part in the ability of different regions of the AV to reorganize their collagen fibers observed in the study by Sacks et al. Clearly more is to be learned regarding the particular role played by regional heterogeneity in GAG composition plays in AV function, but these roles are likely to be important based on these previous studies of GAG composition and correlations to function in the MV and studies of collagen regional heterogeneity and their relation to function in the AV.

Nodule of Arantius: Structure and Function

The nodule of Arantius is a grossly apparent thickening in the center of the AV free edge. This nodule is so clearly distinct from the adjacent thin, transparent regions of coaptation that it has been described by anatomists for centuries. Despite the grossly apparent distinct nature of this region, other studies that have examined AV regional heterogeneity in terms of collagen content and structure have largely not addressed the nodule of Arantius.^{8, 10, 11} Only one of these studies comments on structural differences in this nodule region, which was found to have lower degrees of collagen fiber orientation compared to adjacent regions.¹¹

Examination of the potential functional role of the nodule of Arantius has been made in terms of its geometric effect on leaflet stress.²¹ It has been postulated that the localized thickening of the nodule divides the leaflet into two abutting curved segments each with its own radius of curvature.²¹ Based on the law of Laplace, this configuration

should reduce leaflet stress relative to a cusp without a nodule of Arantius.²¹ Bioprosthetic valves made from pericardium do not have a nodule of Arantius, which could lead to increased leaflet stress at the free edge of these valves relative to native valves, and potentially could relate to deterioration of this free edge known to occur in such bioprosthetic valves.²¹ One could hypothesize that these localized thickenings, shown in this study to be enriched in elements associated with compressive strength, could aid in preventing regurgitation.

Limitations and Future Studies

The major limitation to this study was the small number of samples, as it was designed to be a pilot study. However, given that despite such a small number of samples and their small dry weights, regional differences in GAG composition were found to be statistically significant, this study can act as motivation for further study in this area. Additionally, given previous studies demonstrating that different regions of the MV age differently in terms of GAG content,²⁰ as well as studies demonstrating that regional stresses in the AV vary with age,¹⁶ subsequent studies should examine GAG composition in various aged AVs. Future studies examining particular PGs in relation to regional AV GAG composition and mechanics would provide added insight into the role of GAGs and PGs in AV function. Furthermore, although FACE allows for quantification of GAG fine structure, the role of the AV layered structure and layer-specific composition was not addressed using this technique. In the future, manual dissection of the layers followed by FACE analysis or immunohistochemistry on tissue cross-sections could allow examination of the role of the layered structure of the valve in regional compositional

heterogeneity. Mechanical testing of distinct leaflet regions should also be performed to relate regional compositional heterogeneity to material properties. Additionally, it would be very informative if future experiments (perhaps *in vitro*) are able to demonstrate a direct, as opposed to associative, relationship between composition and loading patterns.

CONCLUSIONS

This study provides a preliminary characterization of the regional heterogeneity in GAG composition within the AV. The significant heterogeneity in GAG content that was evident from the results provides motivation for further study in this area. Understanding such heterogeneity in relation to the different loading of the various regions of the AV will yield insight into the relationship between structure and function within the AV, as well as inform the design of TEHV for the aortic position. Subsequent studies assessing whether these regions undergo distinct aging processes in terms of GAG content will be important to age-specific tissue engineered AV design.

This chapter, which analyzed regional heterogeneity in glycosaminoglycan fine structure in the aged aortic valve, was the fourth of four chapters (Chapters 3-6) examining age-related changes in matrix composition and structure in normal aortic and mitral valves. As stated in the preface to this chapter, this work follows upon the work in Chapter 4 that demonstrated regions in the mitral valve contained distinct glycosaminoglycan fine structure profiles that aged differently. In the present chapter preliminary work suggested that distinct regions may also exist in

the aortic valve, although it remains to be determined if these regions also age differently.

The next chapter continues within the broad category of studies examining normal aging, but moves from the topic of age-related changes in matrix composition and structure addressed in Chapter 3-6, to the topic of age-related changes in material properties. Specifically, in the next chapter changes in aortic and mitral valve material properties during postnatal aging, and the relationship of those changes to alterations in matrix compositional and structural changes, will be addressed.

REFERENCES

1. Kinsella MG, Bressler SL, Wight TN. The regulated synthesis of versican, decorin, and biglycan: extracellular matrix proteoglycans that influence cellular phenotype. *Crit Rev Eukaryot Gene Expr.* 2004;14(3):203-234.
2. Watanabe T, Hosaka Y, Yamamoto E, Ueda H, Sugawara K, Takahashi H, Takehana K. Control of the collagen fibril diameter in the equine superficial digital flexor tendon in horses by decorin. *J Vet Med Sci.* 2005;67(9):855-860.
3. Simionescu DT, Lovekamp JJ, Vyavahare NR. Degeneration of bioprosthetic heart valve cusp and wall tissues is initiated during tissue preparation: an ultrastructural study. *J Heart Valve Dis.* 2003;12(2):226-234.
4. Grande-Allen K, Griffin B, Ratliff N, Cosgrove D, Vesely I. Glycosaminoglycan profiles of myxomatous mitral leaflets and chordae parallel the severity of mechanical alterations. *J Am Coll Cardiol.* 2003;42(2):271-277.
5. Grande-Allen KJ, Osman N, Ballinger ML, Dadlani H, Marasco S, Little PJ. Glycosaminoglycan synthesis and structure as targets for the prevention of calcific aortic valve disease. *Cardiovasc. Res.* 2007;76:19-28.
6. Stephens EH, Chu CK, Grande-Allen KJ. Valve proteoglycan content and glycosaminoglycan fine structure are unique to microstructure, mechanical load and age: Relevance to an age-specific tissue-engineered heart valve. *Acta Biomater.* 2008;4(5):1148-1160.
7. Grande KJ, Cochran RP, Reinhall PG, Kunzelman KS. Stress variations in the human aortic root and valve: the role of anatomic asymmetry. *Ann Biomed Eng.* 1998;26(4):534-545.
8. Balguid A, Driessen NJ, Mol A, Schmitz JP, Verheyen F, Bouten CV, Baaijens FP. Stress related collagen ultrastructure in human aortic valves--implications for tissue engineering. *J Biomech.* 2008;41(12):2612-2617.
9. Weiler MJ, Balachandran K, Padala M, Yap CH, Yoganathan AP. Spatial analysis of aortic valve leaflet deformation characteristics. Paper presented at: Biomedical Engineering Society; October 10, 2009; Pittsburgh, PA.
10. Doehring T, Kahelin M, Vesely I. Mesostructures of the aortic valve. *J Heart Valve Dis.* 2005;14(5):679-686.
11. Sacks MS, Smith DB, Hiester ED. The aortic valve microstructure: effects of transvalvular pressure. *J Biomed Mater Res.* 1998;41(1):131-141.
12. Grande-Allen KJ, Calabro A, Gupta V, Wight TN, Hascall VC, Vesely I. Glycosaminoglycans and proteoglycans in normal mitral valve leaflets and chordae: association with regions of tensile and compressive loading. *Glycobiology.* 2004;14(7):621-633.

13. Gupta V, Werdenburg JA, Blevins TL, Grande-Allen KJ. Synthesis of glycosaminoglycans in differently loaded regions of collagen gels seeded with valvular interstitial cells. *Tissue Eng.* 2007;13(1):41-49.
14. Calabro A, Benavides M, Tammi M, Hascall VC, Midura RJ. Microanalysis of enzyme digests of hyaluronan and chondroitin/dermatan sulfate by fluorophore-assisted carbohydrate electrophoresis (FACE). *Glycobiology.* 2000;10(3):273-281.
15. Grande-Allen KJ, Griffin BP, Ratliff NB, Cosgrove DM, Vesely I. Glycosaminoglycan profiles of myxomatous mitral leaflets and chordae parallel the severity of mechanical alterations. *J Am Coll Cardiol.* 2003;42(2):271-277.
16. Singh R, Strom JA, Ondrovic L, Joseph B, VanAuker MD. Age-related changes in the aortic valve affect leaflet stress distributions: implications for aortic valve degeneration. *J Heart Valve Dis.* 2008;17(3):290-298; discussion 299.
17. Derwin KA, Soslowsky LJ, Kimura JH, Plaas AH. Proteoglycans and glycosaminoglycan fine structure in the mouse tail tendon fascicle. *J Orthop Res.* 2001;19(2):269-277.
18. Danielson KG, Baribault H, Holmes DF, Graham H, Kadler KE, Iozzo RV. Targeted disruption of decorin leads to abnormal collagen fibril morphology and skin fragility. *J Cell Biol.* 1997;136(3):729-743.
19. Nakamura N, Hart DA, Boorman RS, Kaneda Y, Shrive NG, Marchuk LL, Shino K, Ochi T, Frank CB. Decorin antisense gene therapy improves functional healing of early rabbit ligament scar with enhanced collagen fibrillogenesis in vivo. *J Orthop Res.* 2000;18(4):517-523.
20. Stephens EH, de Jonge N, McNeill MP, Durst CA, Grande-Allen KJ. Age-related changes in material behavior of porcine mitral and aortic valves and correlation to matrix composition. *Tissue Eng Part A.* 2010;16(3):867-878.
21. Aazami MH, Salehi M. The Arantius nodule: a 'stress-decreasing effect'. *J Heart Valve Dis.* 2005;14(4):565-566.

Chapter 7: Age-Related Changes in Material Behavior of Porcine Mitral and Aortic Valves and Correlation to Matrix Composition

This chapter continues within the broad category of studies examining normal aging, but moves from the topic of age-related changes in matrix composition and structure addressed in Chapter 3-6, to the topic of age-related changes in material properties. Specifically in this chapter changes in aortic and mitral valve material properties during postnatal aging, and the relationship of those changes to alterations in matrix compositional and structural changes, are addressed.

ABSTRACT

Background: Recent studies showing significant changes in valvular matrix composition with age offer design criteria for age-specific tissue engineered heart valves (TEHV). However, knowledge regarding aging-related changes in valvular material properties is limited.

Methods: 6-week, 6-month, and 6-year-old porcine aortic (AV) and mitral valves (MV) were subjected to uniaxial tensile testing. In addition to standard material parameters, the radius of transition curvature (RTC) was measured to assess the acuteness of the transition region of the tension-strain curve.

Results: Radially, the MV had greater stiffness and a smaller RTC compared to the AV. Circumferentially, the center of the MV anterior leaflet (MVAC) had the highest stiffness (MVAC>AV>MV free edge (MVF)), greater stress relaxation (MVAC>MVF/AV), lowest extensibility (MVAC<AV<MVF), and smaller RTC compared to MVF (AV<MVAC<MVF). AV and MV radial strips had a larger RTC compared to circumferential strips. Aging elevated stiffness for MV and AV radial and circumferential strips, elevated stress relaxation in AV and MVF circumferential strips, and increased RTC for MV radial and MVF circumferential strips.

Conclusions: There are significant age-related differences in the material properties of heart valves, which parallel differences in tissue composition and structure, likely impact valve function, and highlight the need for age-specific design goals for TEHVs.

The work contained in this chapter was published as:

Stephens EH, De Jonge N, McNeill MP, Durst CA, Grande-Allen KJ. **Age-Related Changes in Material Behavior of Porcine Mitral and Aortic Valves and Correlation to Matrix Composition.** *Tissue Engineering*, 2010;16(3):867-78.

INTRODUCTION

Although heart valve composition and microstructure are known to change with aging,¹⁻⁶ and a number of valve diseases show increase incidence with aging,^{7, 8} the effects of aging on valvular material properties remain largely unknown, with the exception of one study of radial failure strain of aortic valves (AV).⁹ It is likely that valve material behavior varies with age given age-related changes in valve composition, including increased collagen content^{1, 2} and crosslinking,^{2, 4} as well as changes in the abundance and turnover of specific extracellular matrix (ECM) components.^{3, 10, 11} Potential age-related changes in the material behavior of valves likely contribute to proper physiologic function as cardiac hemodynamics change during the normal aging process.¹² Ultimately, a properly designed tissue engineered heart valve would similarly need specific material properties allowing it to withstand these different hemodynamics depending on the patient age.

Valves are considered to be quasi-viscoelastic,^{13, 14} highly anisotropic tissues,¹⁵⁻²⁰ that demonstrate stress relaxation^{14, 17, 20-24} but low hysteresis^{13, 14} and no creep.^{13, 14} Tensile testing of valves results in a characteristic load-elongation curve with a low slope pre-transition region in which the collagen fibers are crimped and the elastic fibers are bearing load, followed by a transition region during which loading is transferred to the collagen fibers, and then a post-transition region whose high slope reflects load-bearing by the collagen fibers.^{21, 22, 25} Valve anisotropy, in which valves are stiffer and less extensible in the circumferential direction compared to the radial direction,¹⁵⁻²⁰ is attributed to collagen fiber alignment in the circumferential direction.^{15, 26} Stiffness also

varies regionally within the mitral valve (i.e., between the anterior center (MVAC) and the free edge (MVF)),¹⁵ as does ECM composition in these regions.²⁷

Therefore, the primary objective of this study was to assess age-related differences in the material properties of porcine mitral valve (MV) and AV and to consider these differences in the context of valve microstructure and ECM composition. In addition to standard material parameters, we developed a novel parameter termed “radius of transition curvature” (RTC) to quantify the acuteness of the transition from the pre-transition to post-transition region of the tension-strain curve.

METHODS

Tissue Sample Procurement

Based on comparable anatomy between porcine and human valves,²⁸⁻³⁰ valves from 6-week, 6-month, and 6-year-old pigs were used (corresponding to child, young adult, and older adult ages in humans¹¹). Porcine hearts were obtained from abattoirs

Table 7-1. Sample Set.

	Circumferential Strips						Radial Strips				
	MV MVAC	MV MVF	AV NC	AV LC	AV RC	total	MV	AV NC	AV LC	AV RC	total
6 wk	6	5	7	7	6	25	7	8	7	6	28
6 mo	5	5	4	5	4	18	6	5	4	3	18
6 yr	9	11	6	6	8	31	6	8	9	9	32

MV=mitral valve, AV=aortic valve, MVAC=MV anterior center, MVF=MV free edge, NC=AV non-coronary leaflet, RC=AV right coronary leaflet, LC=AV left coronary leaflet.

(Fisher Ham and Meat, Spring, TX, for 6-week-old and 6-month-old pigs; Animal Technologies, Tyler, TX, for 6-year-old pigs) and measured to normalize leaflet thickness

to heart size (maximum circumference and longitudinal length from the origin of the pulmonary artery to heart apex). MVs and AVs were dissected from the hearts, chordae were removed from the MV, and circumferential and radial strips of 5 mm diameter were cut from both MV and AV (Table 7-1). Given known differences between the material properties of the MVAC (defined as the central region without chordal attachments) and MVF,¹⁵ circumferential strips were taken from both of these regions (Fig. 7-1A). MV radial strips spanned the entire leaflet height from annulus to free edge. Tissues were stored in phosphate buffered saline (PBS) at 4 degrees until testing and tissues were tested within 4 days of harvesting (based on studies showing material properties of valves do not change in that time period^{31,32}).

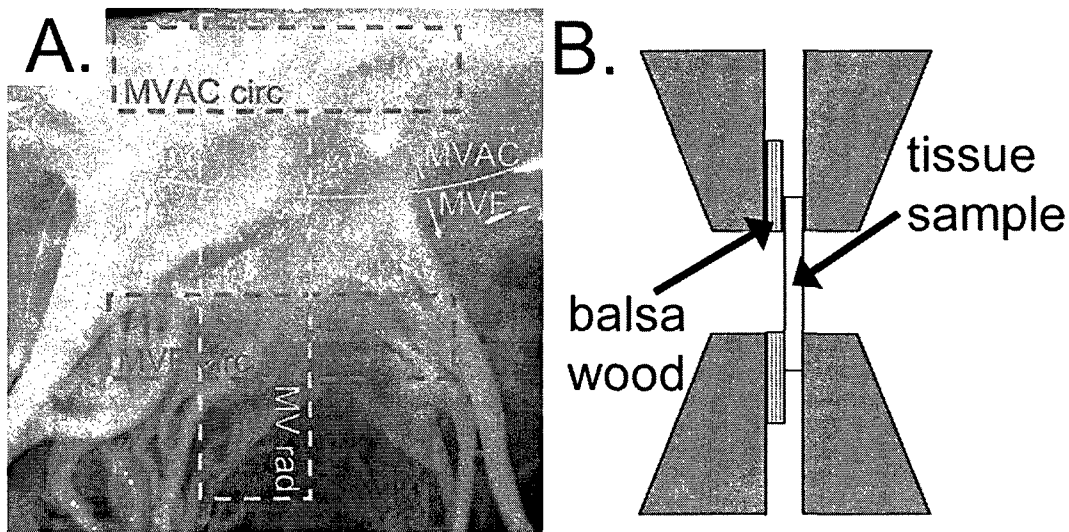


Fig. 7-1: A) Orientation of tissue strips cut from the MV (indicated by dashed boxes). Curved solid line indicates the border between the center (MVAC) and free edge (MVF) of the anterior leaflet. Rad=radial, circ=circumferential. B) Diagram illustrating the placement of glued balsa/valve tissue sample construct within grips of materials testing system.

Mechanical Testing

The thickness of the tissue was measured at 4 locations using a displacement gauge (Mitutoyo, Japan). Tissue samples were glued to balsa wood with cyanoacrylate and clamped within an EnduraTec ELF 3200 (Bose, Minnetonka, MN) such that the edge of the balsa wood aligned with the end of the grips (Fig. 7-1B). The balsa wood improved traction of the tissue within the grips, thereby preventing slippage during testing. Mechanical testing was performed within a 37°C PBS bath as described previously.³³ Briefly, mechanical testing began with the tissue in an unloaded state and consisted of 25 cycles of pre-conditioning at 1 Hz followed by one load-elongation cycle (0.5 Hz). The tissue was then allowed to rest for 15 seconds before another 3 cycles of pre-conditioning and a stress relaxation test (duration 100 seconds).

Data Analysis

Gauge length, defined as the length at which the tissue first starts bearing load, was calculated by fitting a cubic function to the pre-transition region of the load-elongation curve and then determining the tissue length corresponding to the local minimum, similar to the method used by Carew and Vesely.³⁴ Recorded displacement values were then divided by gauge length to calculate strains and load converted to tension by dividing by tissue width. The slope of the post-transition portion of the tension-strain curve (post-transition “stiffness”) was calculated by first fitting a straight line to the maximum load and the preceding four points. Additional preceding points were added and the slope of the linear least squares fit line was re-calculated until its value changed by more than 1%. The pre-transition stiffness was determined as the slope

of the linear least squares fit between zero strain to one half of “end-transition” strain (where the “end-transition” point was the closest point to the origin that was used in the post-transition slope calculation). Extensibility was defined as the intersection of the linear least-squares fit of the post-transition region with the x-axis (strain). The stress relaxation data was fit to the following two-phase decay equation:

$$y = y_0 + A_0 e^{-K_{fast} X} + A_1 e^{-K_{slow} X}$$

The K_{fast} and K_{slow} values were calculated iteratively using Graphpad Prism (GraphPad Software, La Jolla, CA). The percentage relaxation (%SR) was calculated as the difference between the initial load and the load remaining at 100 seconds as a percent of the initial load. The y_0 value refers to the plateau stress in the tissue (where t is approaching 100 seconds). A_0 and A_1 are best-fit values from a nonlinear regression referring to the span of the fast and slow portions of the curve. The radius of transition curvature (RTC) was calculated by first dividing the y-axis of the tension-strain curve by 100 N/m to make both axes dimensionless, and then rotating the tension-strain curve clockwise so that pre-transition and post-transition lines were at equal angles from the vertical (which converted the vertex of the transition region to a global minimum). A hyperbola was then fit to the points in the transition region (from 0 to 1.5* end-transition strain) and the RTC was calculated as the inverse of the second derivative of this global minimum.

Histology and Immunohistochemistry

To evaluate the valvular material behavior in context of the ECM composition, representative tissue strips equivalent to those used for mechanical testing were fixed in 10% formalin overnight, dehydrated, paraffin embedded, and sectioned for histological examination. Movat pentachrome was used to visualize the different ECM components and leaflet layers. Immunohistochemistry was also performed as previously described^{11, 35} to identify and localize the PGs decorin, biglycan, and versican (decorin (LF122) and biglycan (LF104) from Larry Fisher, NIH, Bethesda, MD; ³⁶ versican (2B1) from Associates of Cape Cod, East Falmouth, MA), the GAG hyaluronan (HA, using hyaluronan binding protein, Associates of Cape Cod), and collagen type III (Col III, which has been shown to change with age,¹¹ LF69, from Larry Fisher³⁷). Based on studies showing that valve cell contractility can affect valvular material behavior,³⁸ staining was also performed for the myofibroblast marker non-muscle myosin heavy chain-IIB (NMM, Covance, Berkeley, CA) as previously described.³⁹ Briefly, immunohistochemical staining consisted of antigen retrieval (citrate buffer, Biocare Medical, Concord, CA), except for PGs in which chondroitinase ABC was used³⁶ (Associates of Cape Cod)), followed by quenching of endogenous peroxidases. Non-specific staining was blocked using goat serum buffer, followed by application of primary antibody. Rinses in PBS were performed before application of the appropriate species-specific secondary antibody. Positive staining was visualized using Vectastain Elite ABC and diaminobenzidine kits (Vector laboratories, Burlingame, CA), followed by hematoxylin counterstaining. Radially oriented strips of the MV and AV, which were

previously stained in this same manner as described in a previous publication,^{10, 11} were also used to provide context.

Statistical Analysis

Multifactorial analysis of variance was performed using SigmaStat (SPSS, Chicago, IL), as described in Chapter 4.

RESULTS

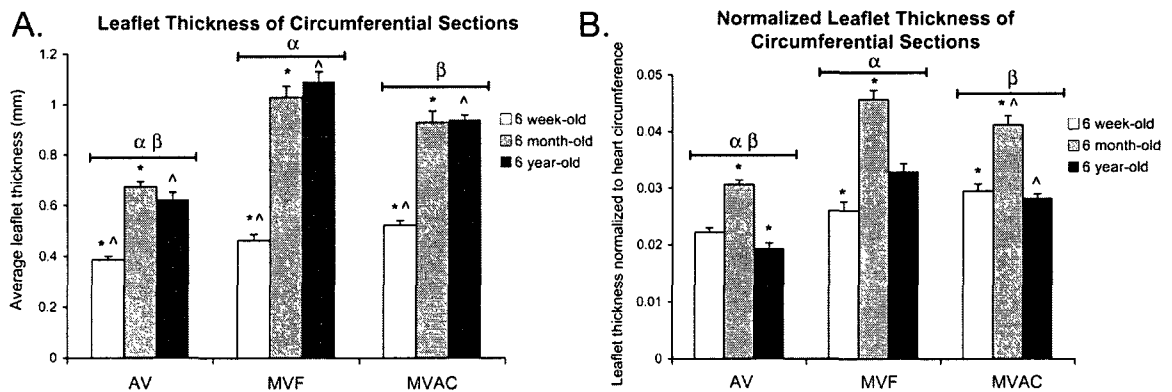


Fig. 7-2: A) Thickness of circumferential valve strips with age. Results for radial strips were comparable (data not shown). B) Thickness of circumferential valve strips with age normalized to heart size (maximum circumference of heart). *, ^ = significantly different between ages within a given valve region. α, β = valve regions significantly different for a given direction (radial or circumferential).

Thickness

All test strips cut from the MV were thicker than in the AV ($p < 0.001$), whether in the circumferential direction (Fig. 7-2) or radial direction. For all valve strips, thickness increased with age (each $p < 0.001$), as reported previously for human valves.⁴⁰ The normalized thickness of circumferential and radial strips (whether normalized to the

circumferential or longitudinal dimension of the heart) of 6-month-olds was greater than for other age groups ($p \leq 0.035$ for each valve or leaflet region; thickness normalized to circumference).

Post-Transition and Pre-Transition Stiffnesses

In the post-transition region of the tension-strain curves, MV and AV radial stiffness was less than circumferential ($p < 0.001$), consistent with previously published studies.¹⁵⁻²⁰ The radial stiffness of MV was greater than for AV ($p < 0.001$, Fig. 7-3).

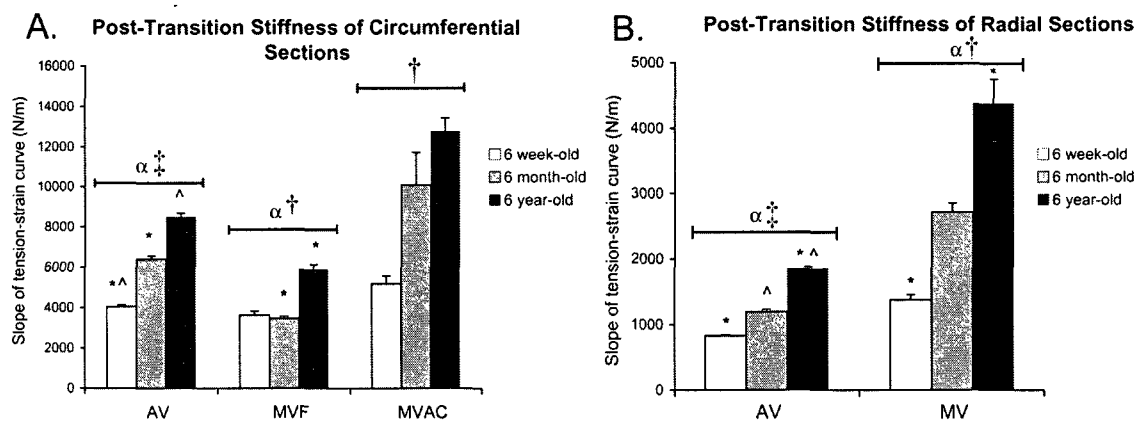


Fig. 7-3: Slope of post-transition region of tension-strain curves for A) Circumferential strips and B) Radial strips. *, ^=significantly different between ages within a given valve region by post-hoc of ANOVA comparing all ages. α =AV, MV significantly different for a given direction (radial or circumferential). †=AV radial significantly different from AV circumferential; ‡=MVAC circumferential, MVF circumferential, and MV radial strips each significantly different from one another.

Among circumferential strips, the stiffness of MVAC was greatest, followed by AV, and then MVF ($p=0.005$). With increasing age, MV and AV radial stiffness increased (each $p \leq 0.003$), as did MV and AV circumferential stiffness (each $p \leq 0.010$).

In the pre-transition region of the curves, there were no significant differences between circumferential and radial stiffnesses in either the AV or MV. Amongst MV and AV circumferential samples, MVF pre-transition stiffness was greater than MVAC, followed by AV (Fig. 7-4, $p < 0.001$). With increasing age, the pre-transition stiffness of MV samples (both circumferential and radial) and AV radial samples increased (each $p < 0.001$).

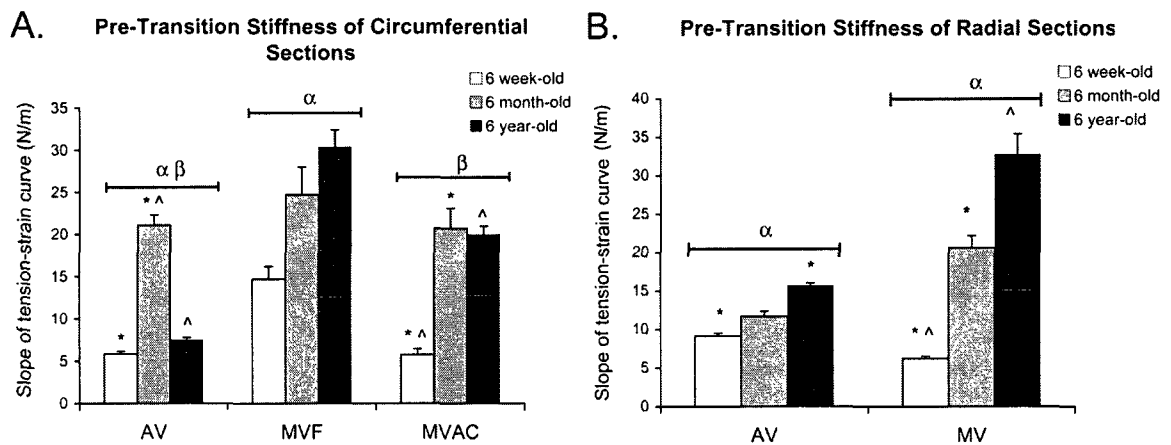


Fig. 7-4: Slope of the pre-transition region of tension-strain curves for A) Circumferential strips and B) Radial strips. *, ^ = significantly different between ages within a given valve region by post-hoc of ANOVA comparing all ages. α, β = AV, MV significantly different for a given direction (radial or circumferential).

Stress Relaxation

In the AV, radial sections showed a higher K_{fast} but a lower K_{slow} than circumferential strips (Table 7-2, each $p < 0.001$). In the MV, however, the K_{fast} and K_{slow} of MVAC circumferential strips were higher than for MV radial (each $p < 0.005$). Among radially oriented sections, the AV K_{fast} and K_{slow} were both greater than for the MV (each $p \leq 0.002$). Among circumferential sections, K_{fast} of MVAC was greater than AV,

followed by MVF ($p < 0.001$), but K_{slow} was greatest in AV ($AV > MVAC > MVF$, $p < 0.001$). With increasing age, AV circumferential K_{fast} was reduced ($p = 0.006$), as was MVF circumferential K_{slow} ($p = 0.046$). With respect to the relative magnitudes of relaxation, %SR was greater for AV circumferential than for AV radial (Fig. 7-5,

Table 7-2. Stress Relaxation Time Constants.

Valve		Direction	Age	K_{fast}	K_{slow}	
Valve	region					
AV	total	rad ^{1,2}	6 wk	0.545±0.025	0.0295±0.0010	
			6 mo	0.596±0.030	0.0321±0.0013	
			6 yr	0.543±0.023	0.0312±0.0010	
	MVF	circ ^{2,5,6}	6 wk	0.548±0.023*	0.0361±0.0010	
			6 mo	0.445±0.030*	0.0329±0.0013	
			6 yr	0.485±0.023	0.0352±0.0010	
		total	rad ^{1,3}	6 wk	0.493±0.046	0.0270±0.0013
				6 mo	0.477±0.056	0.0264±0.0015
				6 yr	0.463±0.056	0.0240±0.0015
MVAC	circ ^{3,4,5}	6 wk	0.545±0.052	0.0299±0.0014		
		6 mo	0.566±0.069	0.0330±0.0019		
		6 yr	0.707±0.046	0.0285±0.0013		

Units for K_{fast} and K_{slow} are N/sec. Data represents mean ± SEM.

*=significant difference between indicated ages within a given valve region/direction. Samples with the same numeric superscripts indicate significant differences between K_{fast} as well as K_{slow} values for those samples across ages, except 4 in which K_{fast} was only significantly different between samples and 6 in which only K_{slow} was significantly different between samples. All differences marked represent $p < 0.05$.

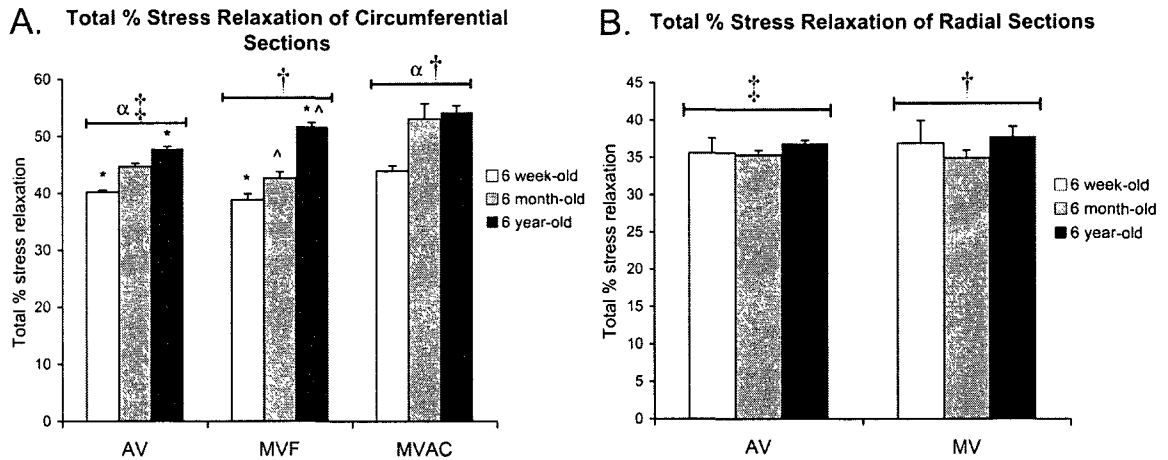


Fig. 7-5: Total percent SR for A) Circumferential strips and B) Radial strips. *, ^=significantly different between ages within a given valve region by post-hoc of ANOVA comparing all ages. α =valve regions significantly different for a given direction (radial or circumferential). †= MVAC circumferential, MVF circumferential, and MV radial strips each significantly different from one another.

$p < 0.001$) and greater for MVAC circumferential, followed by MVF circumferential, then MV radial ($p < 0.001$). Among circumferential strips, %SR of MVAC was greater than for either AV or MVF ($p = 0.014$). With increasing age, %SR was increased in AV circumferential strips ($p = 0.009$) and in MVF circumferential sections ($p = 0.005$).

Extensibility

In both the AV and MV, circumferential strips were less extensible than radial strips (Fig. 7-6, $p < 0.001$). There were no differences between extensibilities of AV and MV strips. In both MV and AV radial strips, as well as in MVAC circumferential strips, extensibility was reduced with age (each $p \leq 0.010$). There was no effect of age on the extensibility of MVF circumferential strips. Among AV circumferential strips, the 6-month-old samples were the least extensible ($p < 0.001$).

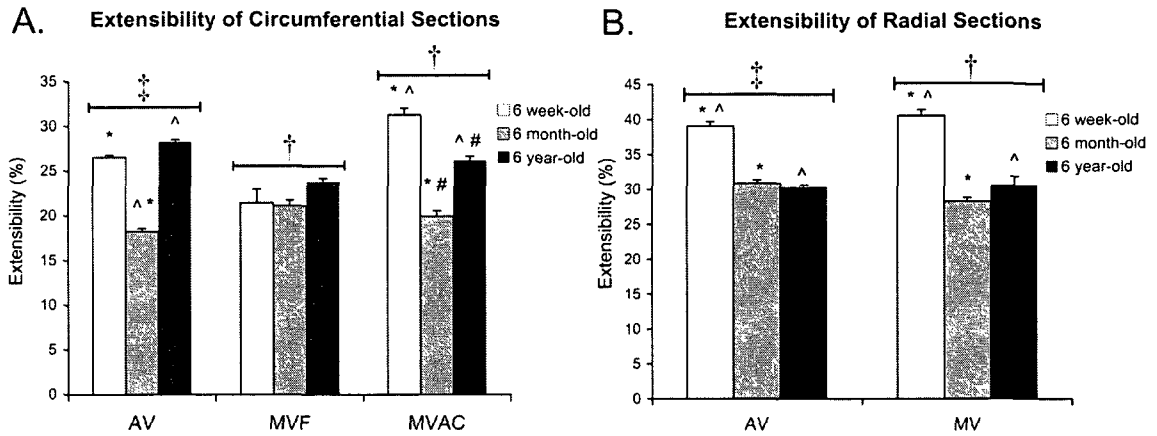


Fig. 7-6: Extensibility for A) Circumferential strips and B) Radial strips. *, ^, # = significantly different between ages within a given valve region by post-hoc of ANOVA comparing all ages. ‡ = AV radial significantly different from AV circumferential; † = MV radial strips are significantly different from both MVAC and MVF circumferential strips.

Radius of Transition Curvature (RTC)

AV circumferential RTC was less than AV radial RTC (Fig. 7-7, $p < 0.001$). MVAC circumferential RTC was less than MVF circumferential RTC, and then MV radial RTC ($p < 0.001$). Among circumferential strips, AV RTC was less than MVAC RTC, which was less than MVF RTC ($p < 0.001$). With age MVF circumferential and MV radial RTC increased ($p = 0.003$ and $p = 0.033$), but no age-associated changes were evident in AV strips.

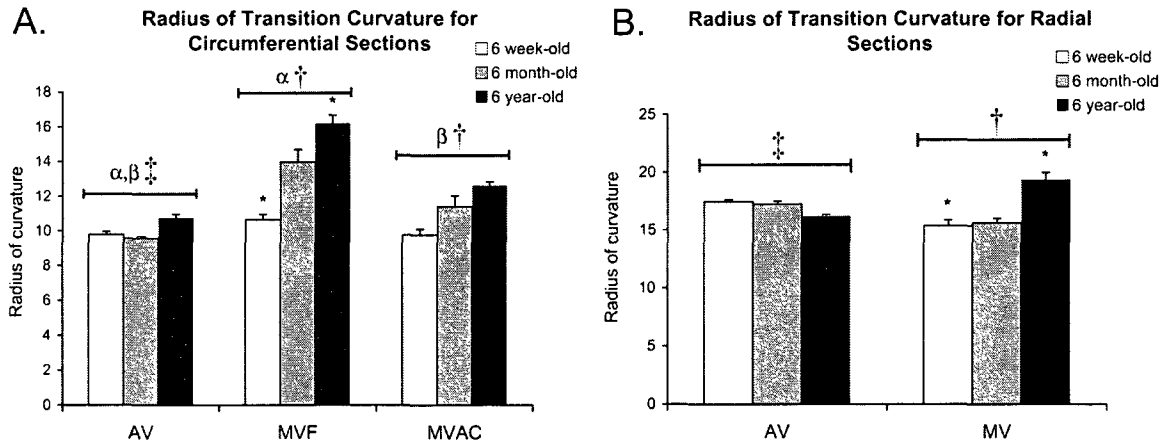


Fig. 7-7: Radius of transition curvature. A) Circumferential strips and B) Radial strips. * = significantly different between ages within a given valve region by post-hoc of ANOVA comparing all ages. α, β = AV, MV significantly different for a given direction (radial or circumferential). \dagger = AV radial significantly different from AV circumferential; \ddagger = MVAC circumferential, MVF circumferential, and MV radial strips each significantly different from one another.

Differences between AV Leaflets

In 6-year-old AVs, the non-coronary leaflet was thicker than the left or right coronary leaflets ($p=0.007$), as previously reported for human valves.^{40, 41} However, there was no significant difference in thickness between AV leaflets in the other age groups. For both radially and circumferentially oriented strips, K_{fast} of the non-coronary leaflet was greater than for the other two leaflets (each $p \leq 0.037$). However, the circumferential %SR for the non-coronary leaflet was less than for the other two leaflets ($p=0.039$). RTC of AV non-coronary leaflets was less than the coronary leaflets ($p=0.031$).

Differences in Valve Matrix Composition

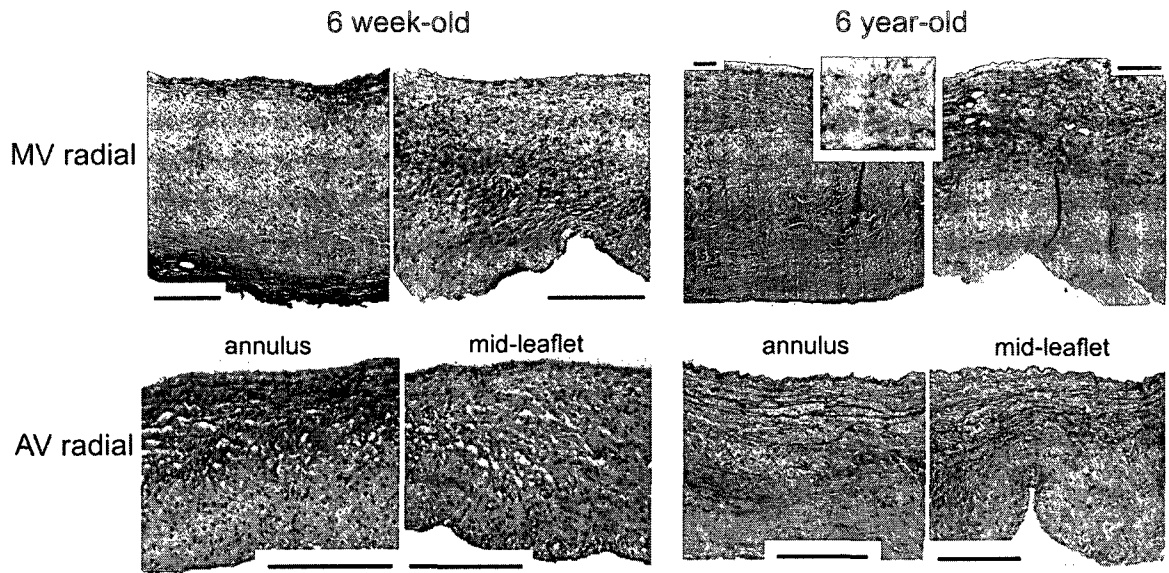


Fig. 7-8: Representative Movat stained tissue sample sections for 6-week-old and 6-year-old radial strips. In Movat pentachrome stained tissue yellow=aligned collagen, black=elastic fibers, and green/blue=PGs/GAGs. To facilitate comparison between AV and MV, valves are all oriented with the fibrosa at the bottom of the image and sized to show the complete leaflet thickness allowing visualization of all leaflet layers. Because of differences in leaflet thickness (see Fig. 7-2), magnifications differ between images. Scale bars indicate 200 μm . Note that the MV radial annulus is almost exclusively fibrosa (corresponding to the MVAC), while AV radial annulus shows a considerably smaller proportion of the leaflet thickness composed of fibrosa. Also of note is the marbling of PG/GAG with collagen in the fibrosa of 6-year-old MV radial annular strips (see inset close-up) and MVAC circumferential strips compared to 6-week-old strips. This marbling may, in part, account for the increase in SR seen with age (see Discussion).

By Movat staining, it was evident that the annulus portion of MV radial strips (corresponding to the MVAC) contained a higher proportion of the collagen-rich fibrosa layer compared to AV radial strips (Fig. 7-8). MVAC circumferential strips contained a much thicker fibrosa than found in MVF (Fig. 7-9). With age, the fibrosa thickened and collagen content increased throughout the valve layers, but this increase was particularly evident in the fibrosa layer and in the ventricularis layer, where collagen surrounded elastic fibers. Interestingly, there also was a marbling of PG/GAGs (see inset in Fig. 7-8)

in the fibrosa of the 6-year-old MV radial annulus and MVAC circumferential section, which was not evident in the younger ages. Immunohistochemistry revealed that the PGs versican, biglycan, and decorin, as well as the GAG hyaluronan, were present within this marbling. Circumferential strips also contained more Col III with age (Fig. 7-10), as

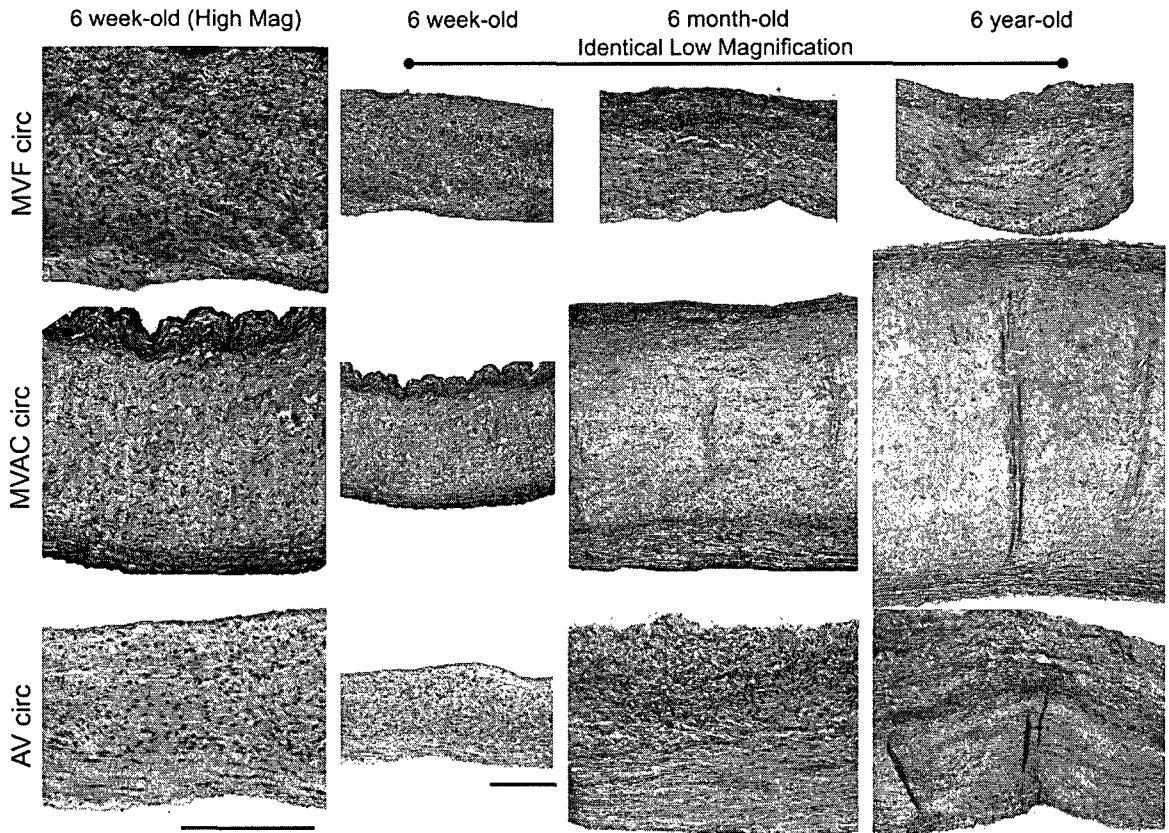


Fig. 7-9: Representative Movat stained tissue sample sections for 6-week-old, 6-month-old, and 6-year-old circumferential. In Movat pentachrome stained tissue yellow=aligned collagen, black=elastic fibers, and green/blue=PGs/GAGs. To facilitate comparison between AV and MV, valves are all oriented with the fibrosa at the bottom of the image. Images in column 1 show high magnification of 6-week-old valves (all images in column 1 are the same magnification). Images in columns 2-4 are lower magnification to demonstrate the differences in leaflet thickness (all images in columns 2-4 are the same magnification). Scale bars indicate 200 μ m. Compared to MVF, MVAC circumferential sections contain much higher proportion of fibrosa. For all valve regions an increase in collagen is noted throughout the valve layers with age, but most particularly in the fibrosa and ventricularis.

found previously for radial strips.¹¹ The myofibroblast marker NMM was more strongly expressed in 6-year-old strips of MVAC than in younger valves.

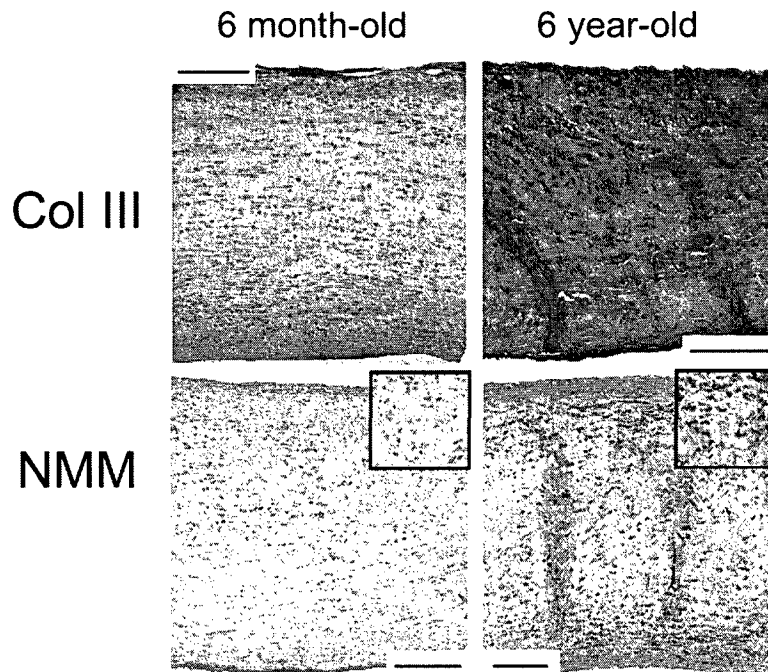


Fig. 7-10: MVAC circumferential sections showing increased Col III and NMM in 6-year-old sections compared to 6-month-old sections. Similar differences were noted for the staining of Col III for other valve regions between the 6-year-old aged sections and the younger ages. Scale bar indicates 200 μm . Insets in NMM images are 1.5x higher magnification for improved visualization of cells.

DISCUSSION

This study showed, for the first time, that there are significant age-related differences in numerous material properties of mitral and aortic valves. At each age, the valves were more extensible and less stiff radially than circumferentially, as is well known.¹⁵⁻²⁰ All valves, however, demonstrated age-associated increases in post-transition stiffness and most also showed increased pre-transition stiffness. In general, extensibility

was reduced with age, especially radially. Stress relaxation parameters also varied with age, particularly circumferentially. The overall shape of the tension-strain curves also changed with age, as demonstrated by the novel parameter RTC, which generally increased with age in the MV and was larger radially than circumferentially. These age-related changes in material properties paralleled an increase in collagen content, particularly in the fibrosa and ventricularis (which is normally rich in elastic fibers), and a marbling appearance of the fibrosa, in which PG/GAGs were interspersed throughout the collagen. Because this study tested mitral and aortic valves from the same hearts, it was also possible to demonstrate differences in material properties between mitral and aortic valves.

With increasing age, the leaflets showed greater post-transition stiffness both radially and circumferentially. This finding is consistent with age-related stiffening of other connective tissues such as cartilage⁴² and tendon,⁴³ which are mainly attributed to increased collagen crosslinking.⁴³ Leaflet composition explains much of the differences in stiffness among sample groups. For example, the preponderance of the collagenous fibrosa layer within the MV annulus likely contributes to the greater radial stiffness of MV compared to AV and the greater circumferential stiffness of MVAC compared to MVF. Age-related increases in fibrosa thickness and collagen content shown here for numerous valve regions, as well as previously reported increases in collagen^{1, 2} and in crosslinking^{2, 4} in aging valves, could explain the increased stiffness with age. A greater proportion of cells in the 6-year-old MVAC expressed the activated myofibroblast phenotype, which has been linked with increased leaflet stiffness.³⁸ In addition, collagen crosslinking has been directly correlated with the stiffness of circumferential strips of

human AV, although no such correlation was found for radial strips.²⁶ Combined with evidence suggesting that the ventricularis is a key contributor to valvular material behavior in the radial direction,^{22, 44} the age-related increase in radial stiffness could be due to increased collagen in the ventricularis, as observed in the Movat-stained sections.

Interestingly, the pre-transition stiffness was also significantly increased with age. This parameter may be due in part to the stiffness of the elastic fibers,⁴⁵ but is not often reported^{15, 16, 18, 46} and has never previously been studied with respect to age. The increase in pre-transition stiffness with age could reflect the stiffening of aging elastic fibers,⁴³ as well as increased collagenous reinforcement of the elastic fibers, which was observed in Movat-stained sections. It was also noteworthy that the age-related increases in the thickness of the valve leaflets⁴⁰ were not proportional to the increase in heart size, possibly due to the ventricular hypertrophy found in older animals.^{47, 48}

Accompanying the age-related increase in the post-transition stiffness was a pronounced reduction in radial extensibility of older valves. Extensibility assesses the amount of tissue can stretch before the collagen fibers are fully uncrimped and able to bear load;²¹ its magnitude reflects both collagen fiber crimp and alignment. The finding that extensibility is greater radially than circumferentially confirms previous reports;^{16-18, 20} this anisotropy permits the leaflets to stretch radially during valve closure. These findings are also consistent with a previous report on an age-related reduction in maximal radial stretch of human cryopreserved valves.⁹ A reduction in extensibility with age could be attributed to factors that impact collagen uncrimping, such as increased collagen crosslinking^{2, 4} or elastic fiber fragmentation,⁴³ which can lead to gradual permanent tissue stretch and less crimped collagen fibers. Indeed, in tendon collagen, crimp

amplitude decreases and crimp wavelength increases with age;⁴⁹ these extensibility changes motivate future study of collagen crimp in aging heart valves. Similarly, heart valves subjected to glutaraldehyde fixation (crosslinking) under pressure demonstrated reduced collagen crimp and extensibility.⁵⁰

The novel finding of an increase in the percentage of circumferential stress relaxation (in AV and MVF) with age could be due to many factors. First, there is more hyaluronan with age¹⁰ as well as marbling of PGs/GAGs in the collagenous fibrosa, which would allow more sliding of collagen bundles relative to one another.⁵¹ Alternatively, the greater numbers of PGs decorin and biglycan,¹⁰ which bind to the surface of collagen fibrils,⁵² could be transferring more load from collagen to other matrix components, resulting in greater %SR. Indeed, age-related changes in %SR were most evident in the circumferential direction, the predominant collagen fiber direction.⁵³ Reductions in the functionality⁴³ and content¹⁰ of elastic fibers could also increase stress relaxation, according to studies in pericardium.⁵⁴ Lastly, the greater abundance of Col III, which dissipates more energy than does Col I,⁵⁵ could have contributed to the greater %SR with age. There is some disagreement in the heart valve literature regarding anisotropy in stress relaxation.^{14, 17, 20, 23, 24} Our finding of greater %SR in circumferential strips compared to radial strips corroborates work by Lee et al., who measured the %SR of fresh leaflets over 1000 seconds using uniaxial testing.²⁰

The viscoelasticity of valve tissues has been examined using a wide variety of constitutive models,^{17, 19, 33, 56-59} but the effects of age have not been previously investigated. In particular, the QLV model developed by Fung et al.⁶⁰ has been applied to fresh and fixed valve tissues,^{19, 33, 56} analysis using this technique, however, is

computationally intense. In this study, a Maxwell-Weichert model with 3 elements was used to examine biphasic decay behavior of the stress relaxation curve.^{61, 62} The age-related decreases in K_{fast} of AV circumferential samples and in K_{slow} of MVF samples both indicate more viscous behavior, which could relate to the increased abundance of PGs and GAGs.¹⁰ The K_{fast} and K_{slow} values reported in this study also serve as baseline parameters for evaluating mechanical properties of tissue engineered heart valves. While current tissue engineered heart valve studies have focused primarily on linear material properties, understanding viscoelastic properties will continue to be of significant value, especially as more advanced materials are developed.

The novel parameter RTC, which quantifies the acuteness of the transition region of the tension-strain curve, can be compared across samples for any soft tissues that display bi-linear tension-strain or stress-strain curves. Collagen fibers that are highly aligned and uniformly crimped will have a very acute transfer of load-bearing from elastic fibers to the straightened collagen fibers, and hence a very small RTC. If collagen fibers are not uniformly crimped, their transition to load-bearing would be more gradual, resulting in a greater RTC. A larger RTC would also result from a random fiber alignment, in which some fibers would be initially aligned with the applied load and begin bearing load at low strains, but the remaining collagen bundles would require varying amounts of additional strain and/or rotational realignment before bearing load.²¹ Indeed, the angular distribution of collagen fibers significantly changes within this transition region.²¹ The smaller RTC of MVAC circumferential strips compared to MVF likely indicates greater alignment⁵³ and homogeneity of collagen fiber crimping in MVAC compared to the other valve regions. In the valve, collagen bundles are

predominantly oriented circumferentially,⁵³ therefore RTC would be lower circumferentially than radially, as found here. The age-related increase in RTC of MVF and MV radial strips could be due to greater collagen crosslinking^{2, 4} and a greater abundance of network-forming collagen type III. In the future, it will be important to relate this parameter to changes in the soft tissue microstructure during this transition region of loading.

This study is also the first to show differences in material properties between non-coronary (NC) and coronary AV leaflets, such as lower %SR and RTC in the NC leaflet. These differences may be due to the lack of coronary blood flow within the NC sinus; simulations of human AVs have shown that NC experiences higher stress⁶³ and greater diastolic pressure loading than the other leaflets.⁶⁴ The NC leaflet also contains smaller diameter collagen fiber bundles,⁶⁵ which may permit easier rotation of collagen fibers as they align in the direction of loading, and hence contribute to a lower RTC. An additional subset of valves was frozen at -20°C for 2 months before testing; as previously demonstrated by Clark,¹⁸ significant differences were found between fresh AV and previously frozen AV (data not shown).

CONCLUSIONS

In this study, aortic and mitral valves from the same porcine hearts were subjected to tensile testing. In the analysis of the tensile testing data, we developed a novel parameter, radius of transition curvature, which may be useful in quantifying the dynamic stress-strain behavior of biological tissues. Overall, our results showed that between aortic and mitral valves, and within each valve, there are profound heterogeneities and

age-related changes that reflect the ECM and microstructural composition. In addition, the effects of age on the heart valve tissues differ between valves, valve regions, and material testing orientations. Given the documented similarities between porcine and human valves, these results provide further justification (as well as baseline data) for the development of age-specific tissue engineered heart valves. These age-related changes in valve material properties likely contribute to proper physiologic function of valves at different ages. For instance, the age-related increase in leaflet stiffness likely allows the aortic and mitral valves to withstand the increase in cardiac pressures and concomitant decrease in aortic compliance with age.¹² Clearly, considerable work remains in understanding the structural and mechanical complexity of heart valves, their extracellular matrix and cell composition, and the contributions of these characteristics to valve function.

This chapter concludes the studies addressing the topic of normal aortic and mitral valve aging; this topic included studies analyzing age-related changes in matrix composition and structure (Chapter 3-6), as well as analysis of changes in material properties contained in this chapter. The next series of chapters, which open Volume 2 of this thesis, addresses heterogeneity in the normal valve. These chapters are subdivided into those related to heterogeneity in mitral valve composition and motion (Chapters 8 and 9) and those related to heterogeneity in the valvular interstitial cell population (Chapters 10 and 11). Specifically in the next

chapter, analysis of regional mitral valve leaflet composition in relationship to *in vivo* leaflet length changes is presented.

REFERENCES

1. Keller F, Leutert G. [Age dependence of collagen structures of the human heart]. *Z Gerontol.* 1994;27(3):186-193.
2. Angrist A. Aging heart valves and a unitary pathological hypothesis for sclerosis. *J Gerontol.* 1964;19:135-143.
3. Aikawa E, Whittaker P, Farber M, Mendelson K, Padera RF, Aikawa M, Schoen FJ. Human semilunar cardiac valve remodeling by activated cells from fetus to adult: implications for postnatal adaptation, pathology, and tissue engineering. *Circulation.* 2006;113(10):1344-1352.
4. Bashey RI, Torii S, Angrist A. Age-related collagen and elastin content of human heart valves. *J Gerontology.* 1967;9(19):203-208.
5. Sell S, Scully RE. Aging changes in the aortic and mitral valves. Histologic and histochemical studies, with observations on the pathogenesis of calcific aortic stenosis and calcification of the mitral annulus. *Am J Pathol.* 1965;46:345-365.
6. McDonald PC, Wilson JE, McNeill S, Gao M, Spinelli JJ, Rosenberg F, Wiebe H, McManus BM. The challenge of defining normality for human mitral and aortic valves: geometrical and compositional analysis. *Cardiovasc Pathol.* 2002;11(4):193-209.
7. Goldberg SH, Elmariah S, Miller MA, Fuster V. Insights into degenerative aortic valve disease. *J Am Coll Cardiol.* 2007;50(13):1205-1213.
8. Aronow WS. Heart disease and aging. *Med Clin North Am.* 2006;90(5):849-862.
9. Christie GW, Barratt-Boyes BG. Age-dependent changes in the radial stretch of human aortic valve leaflets determined by biaxial testing. *Ann Thorac Surg.* 1995;60(2 Suppl):S156-159.
10. Stephens EH, Chu C-K, Grande-Allen KJ. Valve proteoglycan content and glycosaminoglycan fine structure are unique to microstructure, mechanical load and age: Relevance to an age-specific tissue-engineered heart valve. *Acta Biomaterialia.* 2008;4(5):1148-1160.
11. Stephens EH, Grande-Allen K. Age-related changes in collagen synthesis and turnover in porcine heart valves. *J Heart Valve Dis.* 2007;16(6):672-682.
12. VanAuker MD. Age-related changes in hemodynamics affecting valve performance. *Am J Geriatr Cardiol.* 2006;15(5):277-283; quiz 284-275.
13. Grashow J, Yoganathan AP, Sacks MS. Biaxial stress-stretch behavior of the mitral valve anterior leaflet at physiologic strain rates. *Ann Biomed Eng.* 2006;34(2):315-325.
14. Stella J, Liao J, Sacks MS. Time-dependent biaxial mechanical behavior of the aortic heart valve leaflet. *J Biomech.* 2007;40(14):3169-3177.

15. Kunzelman KS, Cochran RP. Stress/strain characteristics of porcine mitral valve tissue: parallel versus perpendicular collagen orientation. *J Card Surg.* 1992;7(1):71-78.
16. May-Newman K, Yin F. Biaxial mechanical behavior of excised porcine mitral valve leaflets. *Am J Physiol.* 1995;269(4 Pt 2):H1319-1327.
17. Leeson-Dietrich J, Boughner D, Vesely I. Porcine pulmonary and aortic valves: a comparison of their tensile viscoelastic properties at physiological strain rates. *J Heart Valve Dis.* 1995;4(1):88-94.
18. Clark R. Stress-strain characteristics of fresh and frozen human aortic and mitral leaflets and chordae tendineae. Implications for clinical use. *J Thorac Cardiovasc Surg.* 1973;66(2):202-208.
19. Sauren A, van Hout M, van Steenhoven A, Veldpaus F, Janssen J. The mechanical properties of porcine aortic valve tissues. *J Biomech.* 1983;16(5):327-337.
20. Lee J, Courtman DW, Boughner D. The glutaraldehyde-stabilized porcine aortic valve xenograft. I. Tensile viscoelastic properties of the fresh leaflet material. *J Biomed Mater Res.* 1984;18(1):61-77.
21. Liao J, Yang L, Grashow J, Sacks MS. The relation between collagen fibril kinematics and mechanical properties in the mitral valve anterior leaflet. *J Biomech Eng.* 2007;129(1):78-87.
22. Vesely I, Noseworthy R. Micromechanics of the fibrosa and the ventricularis in aortic valve leaflets. *J Biomech.* 1992;25(1):101-113.
23. Grashow J, Sacks MS, Liao J, Yoganathan AP. Planar biaxial creep and stress relaxation of the mitral valve anterior leaflet. *Ann Biomed Eng.* 2006;34(10):1509-1518.
24. Vesely I, Boughner D, Leeson-Dietrich J. Bioprosthetic valve tissue viscoelasticity: implications on accelerated pulse duplicator testing. *Ann Thorac Surg.* 1995;60(2 Suppl):S379-382.
25. Merryman WD, Engelmayr GC, Jr., Liao J, Sacks MS. Defining biomechanical endpoints for tissue engineered heart valve leaflets from native leaflet properties. *Prog Pediatr Cardiol.* 2006;21:153-160.
26. Balguid A, Rubbens M, Mol A, Bank R, Bogers A, van Kats J, de Mol B, Baaijens F, Bouten C. The role of collagen cross-links in biomechanical behavior of human aortic heart valve leaflets--relevance for tissue engineering. *Tissue Eng.* 2007;13(7):1501-1511.
27. Grande-Allen KJ, Calabro A, Gupta V, Wight TN, Hascall VC, Vesely I. Glycosaminoglycans and proteoglycans in normal mitral valve leaflets and chordae: association with regions of tensile and compressive loading. *Glycobiology.* 2004;14(7):621-633.
28. Crick S, Sheppard M, Ho S, Gebstein L, Anderson R. Anatomy of the pig heart: comparisons with normal human cardiac structure. *J Anat.* 1998;193:105-119.

29. Sands MP, Rittenhouse EA, Mohri H, Merendino KA. An anatomical comparison of human pig, calf, and sheep aortic valves. *Ann Thorac Surg.* 1969;8(5):407-414.
30. Sim EK, Muskawad S, Lim CS, Yeo JH, Lim KH, Grignani RT, Durrani A, Lau G, Duran C. Comparison of human and porcine aortic valves. *Clin Anat.* 2003;16(3):193-196.
31. Patel J. *Effect of absolute specimen size on the tensile properties of porcine aortic valve tissues, Masters Thesis.* Cleveland, Case Western Reserve; 2003.
32. Grande-Allen K, Barber J, Klatka K, Houghtaling P, Vesely I, Moravec C, McCarthy P. Mitral valve stiffening in end-stage heart failure: evidence of an organic contribution to functional mitral regurgitation. *J Thorac Cardiovasc Surg.* 2005;130(3):783-790.
33. Carew E, Barber J, Vesely I. Role of preconditioning and recovery time in repeated testing of aortic valve tissues: validation through quasilinear viscoelastic theory. *Ann Biomed Eng.* 2000;28:1093-1100.
34. Carew E, Vesely I. A new method of estimating gauge length for porcine aortic valve test specimens. *J Biomech.* 2003;36(7):1039-1042.
35. Gupta V, Barzilla JE, Mendez JS, Stephens EH, Lee EL, Collard CD, Laucirica R, Weigel PH, Grande-Allen KJ. Abundance and location of proteoglycans and hyaluronan within normal and myxomatous mitral valves. *Cardiovasc Pathol.* 2008.
36. Fisher LW, Stubbs JT, 3rd, Young MF. Antisera and cDNA probes to human and certain animal model bone matrix noncollagenous proteins. *Acta Orthop Scand Suppl.* 1995;266:61-65.
37. Bernstein EF, Chen YQ, Kopp JB, Fisher L, Brown DB, Hahn PJ, Robey FA, Lakkakorpi J, Uitto J. Long-term sun exposure alters the collagen of the papillary dermis. Comparison of sun-protected and photoaged skin by northern analysis, immunohistochemical staining, and confocal laser scanning microscopy. *J Am Acad Dermatol.* 1996;34(2 Pt 1):209-218.
38. Merryman W, Huang H, Schoen F, Sacks M. The effects of cellular contraction on aortic valve leaflet flexural stiffness. *J Biomech.* 2006;39(1):88-96.
39. Stephens EH, Nguyen TC, Itoh A, Ingels NB, Jr., Miller DC, Grande-Allen KJ. The effects of mitral regurgitation alone are sufficient for leaflet remodeling. *Circulation.* 2008;118(14 Suppl):S243-249.
40. Sahasakul Y, Edwards WD, Naessens J, Tajik A. Age-related changes in aortic and mitral valve thickness: implications for two-dimensional echocardiography based on an autopsy study of 200 normal human hearts. *Am J Cardiol.* 1988;62:424-430.
41. Silver M, Roberts WC. Detailed anatomy of the normally functioning aortic valve in hearts of normal and increased weight. *Am J Cardiol.* 1985;55(4):454-461.

42. Charlebois M, McKee MD, Buschmann MD. Nonlinear tensile properties of bovine articular cartilage and their variation with age and depth. *J Biomech Eng.* 2004;126(2):129-137.
43. Bailey AJ. Molecular mechanisms of ageing in connective tissues. *Mech Ageing Dev.* 2001;122(7):735-755.
44. Stella J, Sacks MS. On the biaxial mechanical properties of the layers of the aortic valve leaflet. *J Biomech Eng.* 2007;129(5):757-766.
45. Vesely I. The role of elastin in aortic valve mechanics. *J Biomech.* 1998;31(2):115-123.
46. Ghista DN, Rao AP. Mitral-valve mechanics--stress-strain characteristics of excised leaflets, analysis of its functional mechanics and its medical application. *Med Biol Eng.* 1973;11(6):691-702.
47. Safar M. Ageing and its effects on the cardiovascular system. *Drugs.* 1990;39(Suppl 1):1-8.
48. Gardin J, Savage D, Ware J, Henry W. Effect of age, sex, and body surface area on echocardiographic left ventricular wall mass in normal subjects. *Hypertension.* 1987;9(2 Pt 2):II36-39.
49. Diamant J, Keller A, Baer E, Litt M, Arridge RG. Collagen; ultrastructure and its relation to mechanical properties as a function of ageing. *Proc R Soc Lond B Biol Sci.* 1972;180(60):293-315.
50. Broom ND, Thomson FJ. Influence of fixation conditions on the performance of glutaraldehyde-treated porcine aortic valves: towards a more scientific basis. *Thorax.* 1979;34(2):166-176.
51. Scott J. Elasticity in extracellular matrix 'shape modules' of tendon, cartilage, etc. A sliding proteoglycan-filament model. *J Physiol.* 2003;553(Pt 2):335-343.
52. Kinsella MG, Bressler SL, Wight TN. The regulated synthesis of versican, decorin, and biglycan: extracellular matrix proteoglycans that influence cellular phenotype. *Crit Rev Eukaryot Gene Expr.* 2004;14(3):203-234.
53. Cochran RP, Kunzelman KS, Chuong CJ, Sacks MS, Eberhart RC. Nondestructive analysis of mitral valve collagen fiber orientation. *ASAIO Trans.* 1991;37(3):M447-448.
54. Rabkin S, Berghause DG, Bauer HF. Mechanical properties of the isolated canine pericardium. *J Appl Physiol.* 1974;36(1):69-73.
55. Silver F, Horvath I, Foran D. Mechanical implications of the domain structure of fiber-forming collagens: comparison of the molecular and fibrillar flexibilities of the alpha1-chains found in types I-III collagen. *J Theor Biol.* 2002;216(2):243-254.
56. Carew EO, Talman EA, Boughner DR, Vesely I. Quasi-Linear Viscoelastic theory applied to internal shearing of porcine aortic valve leaflets. *J Biomech Eng.* 1999;121(4):386-392.

57. Carew E, Garg A, Barber J, Vesely I. Stress relaxation preconditioning of porcine aortic valves. *Ann Biomed Eng.* 2004;32(4):563-572.
58. Duncan AC, Boughner D, Vesely I. Dynamic glutaraldehyde fixation of a porcine aortic valve xenograft. I. Effect of fixation conditions on the final tissue viscoelastic properties. *Biomaterials.* 1996;17(19):1849-1856.
59. Duncan AC, Boughner D, Vesely I. Viscoelasticity of dynamically fixed bioprosthetic valves. II. Effect of glutaraldehyde concentration. *J Thorac Cardiovasc Surg.* 1997;113(2):302-310.
60. Fung YC. *Biomechanics : mechanical properties of living tissues.* 2nd ed. New York: Springer-Verlag; 1993.
61. Peleg M, Normand M. Comparison of 2 Methods for Stress-Relaxation Data Presentation of Solid Foods. *Rheologica Acta.* 1983;22(1):108-113.
62. Mayne AS, Christie GW, Smaill BH, Hunter PJ, Barratt-Boyes BG. An assessment of the mechanical properties of leaflets from four second-generation porcine bioprostheses with biaxial testing techniques. *J Thorac Cardiovasc Surg.* 1989;98(2):170-180.
63. Grande KJ, Cochran RP, Reinhall PG, Kunzelman KS. Stress variations in the human aortic root and valve: the role of anatomic asymmetry. *Ann Biomed Eng.* 1998;26(4):534-545.
64. Lin S, Liu C, Young S, Lin M, Chiou C. Age-related changes in aortic valve with emphasis on the relation between pressure loading and thickened leaflets of the aortic valves. *Int J Cardiol.* 2005;103(3):272-279.
65. Doehring T, Kahelin M, Vesely I. Mesostructures of the aortic valve. *J Heart Valve Dis.* 2005;14(5):679-686.

RICE UNIVERSITY

**Composition, Turnover, and Mechanics of Extracellular
Matrix in Developing, Aging, and Pathological Valves**

for application in the design of age-specific tissue engineered heart valves

by
Elizabeth Humes Stephens

May 2010

VOLUME II

Chapter 8: Cellular and Extracellular Matrix Basis for Heterogeneity in Mitral Annular Contraction

Having addressed normal valve aging in the preceding chapters (Chapters 3-7) contained in Volume 1 of this thesis, the next series of chapters that opens Volume 2 of this thesis addresses heterogeneity in the normal valve. These chapters are subdivided into those related to heterogeneity in mitral valve composition and motion (Chapters 8 and 9) and those related to heterogeneity in the valvular interstitial cell population (Chapters 10 and 11). Specifically in this chapter, analysis of regional mitral valve leaflet composition in relationship to *in vivo* leaflet length changes is presented.

ABSTRACT

Background: Regional heterogeneity of mitral annular contraction, generally ascribed to the fibrous vs. muscular annular composition, has been well described in the mammalian mitral valve. It is unknown, however, whether the cells in the annulus, and the extracellular matrix that they produce, contribute to this heterogeneity. We set out to investigate the relationship between ultrastructure and regional geometry of the normal ovine mitral annulus.

Methods: Fourteen sheep underwent implantation of 8 radiopaque markers around the mitral annulus defining four segments: septal (SEPT), lateral (LAT), and anterior (ANT-

C) and posterior (POST-C) commissures. Maximum and minimum annular segmental lengths during the cardiac cycle were calculated using biplane videofluoroscopy. Immunohistochemistry of annular cross sections assessed regional matrix content, matrix turnover, and cell phenotype, as well as degree of fibrosa insertion.

Results: Regional annular contraction was inversely related to the degree of fibrosa insertion into annular muscle. Whereas SEPT contained more collagen I and III ($p < 0.001$), LAT demonstrated more collagen and elastin turnover as shown by greater decorin, lysyl oxidase, and matrix metalloprotease (MMP)-13 ($p \leq 0.033$) and smooth muscle alpha-actin (SMaA, indicating myofibroblastic valve cell activation, $p < 0.001$). This greater matrix turnover was consistent with greater annular contraction in LAT compared to SEPT ($18.1 \pm 4.4\%$ vs. $3.9 \pm 2.6\%$, $p < 0.001$). Similarly, POST-C had more SMaA and MMP13 than ANT-C ($p < 0.02$), consistent with greater annular contraction in POST-C ($15.4 \pm 5.7\%$ vs. $9.9 \pm 3.5\%$, $p < 0.001$). Correlations between intensities of matrix turnover-related proteins and proteins indicating the activation of valvular interstitial cells (VICs) strengthen the presumed role of myofibroblasts in the observed compositional heterogeneity.

Conclusions: These data illustrate that matrix turnover and expression of activated VICs correlate with regional annular length change, and could be therapeutic targets when annular motion is impaired. Conversely, alterations in this heterogeneous annular contraction, whether through disease or secondary to ring annuloplasty, could disrupt this

normal pattern of cell-mediated matrix remodeling and further adversely impact mitral valve function.

The work contained in this chapter is in preparation for submission to *Journal of Heart Valve Disease*.

INTRODUCTION

The mitral valve (MV) annulus demonstrates heterogeneity in both structure and motion. Structurally, the MV annulus is an asymmetric, hyperbolic paraboloid or saddle-shaped oval ring.¹ Annular deformation during the cardiac cycle is complex and diverse, involving tilting around multiple axes,^{2, 3} translation,² and contraction,⁴⁻⁶ each occurring to varying degrees throughout the different regions of the annulus. In general, lateral annular contraction is substantially greater than that of the septal annulus during the cardiac cycle.⁴⁻⁶ Elimination of this dynamic movement of the MV annulus *in vivo* may be deleterious to cardiac function.⁷⁻⁹ This heterogeneity has been primarily attributed to the fibrous *vs.* muscular composition of the septal and lateral annulus, respectively,^{4-6, 10} but the role of the MV annular cells and the extracellular matrix that they produce in the observed heterogeneous annular contraction has not been previously investigated.

Cells from a wide range of tissues,¹¹ including valves,^{12, 13} both respond to and influence their mechanical environment via phenotypic modulation and synthesis of extracellular matrix. The relationship between the highly dynamic *in vivo* mechanics and composition of the valve annulus, however, remains unknown. Establishing such a link between annular geometry and composition would have important implications regarding the ultrastructural mechanisms of annular dilation in valve diseases, the potential for preventative treatments, and the design of better annular repair strategies and annuloplasty rings. Therefore, the aim of this study was to correlate the regional heterogeneity of normal MV annular length change during the cardiac cycle with regional

extracellular matrix composition and valve cell activation using immunohistochemistry (IHC). IHC was performed for a number of proteins related to cell activation as well as the abundance, synthesis, and degradation of extracellular matrix.

METHODS

All animals received humane care in accordance with the guidelines of the US Department of Health and Human Services (NIH Publ. 85-23, Revised 1985). The use of animals in this study was approved by the Stanford Medical Center Laboratory Research Animal Review Committee.

Animal Protocol

Eight (8) radiopaque markers were implanted into 14 sheep to delineate four annular segments (Fig. 8-1): septal (SEPT, the distance of segments between markers 2 and 4) and lateral (LAT, markers 6-8) annulus, and anterior (ANT-C, markers 4-6) and posterior (POST-C, the distance of segments between markers 1 and 2 and markers 2 and 8) commissures. Procedures for marker implantation and biplane video fluoroscopy have been described previously.¹⁴ Annular segment contraction was calculated as the percentage change from maximum to minimum segment length during the cardiac cycle both at baseline and during inotropic augmentation with calcium infusion⁵ in open-chest animals. The hearts were then harvested and stored in formalin.

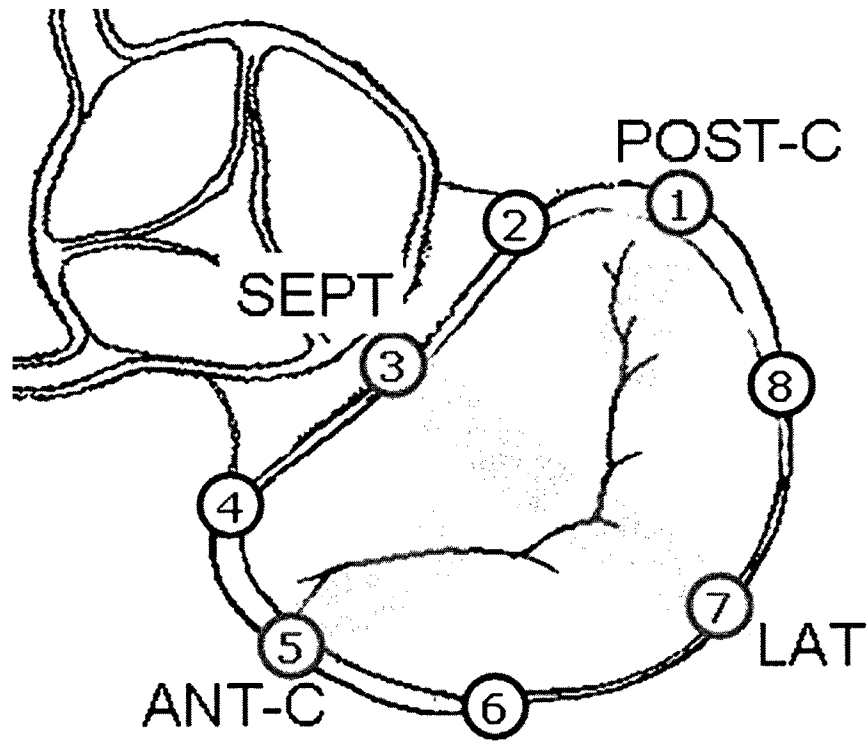


Fig. 8-1: Location of the different annular segments from which tissue sections were taken. In the case of septal segment (SEPT) and lateral segment (LAT) 2 tissue sections were analyzed, in the case of the anterior and posterior commissures (ANT-C, POST-C), one tissue section was taken from either side of the tantalum marker based on quality of the leaflet on each side. For calculation of annular contraction, the distance between the segments between markers 2 and 4 was defined as SEPT, markers 6-8 as LAT, markers 4-6 as ANT-C, and the distance of segments between markers 1 and 2 and markers 2 and 8 as POST-C.

Histology and Immunohistochemistry

For each segment of the MV annulus a 3-5 mm wide strip was cut from the myocardium to the leaflet free edge (Fig. 8-1, locations #1, 3, 5, 7). Cross sections were embedded in paraffin and sectioned to a thickness of five microns. Each sample was stained with Movat pentachrome as well as IHC to demonstrate specific extracellular

Table 8-1. Panel of Antibodies Used in IHC.

Protein	Function
<u>Collagens and Collagen-Turnover Proteins</u>	
Collagen I (Col I) ^a	Predominant collagen in valve, provides tensile strength
Collagen III (Col III) ^a	Reticular collagen
Matrix Metalloproteinase (MMP)-13 ^b	Collagen degradation
<u>Elastic Fiber-Related Proteins</u>	
Matrix Metalloproteinase (MMP)-9 ^c	Elastin degradation
Lysyl oxidase (LOX) ^d	Involved in collagen and elastin crosslinking
Elastin ^e	Predominant component of elastic fibers
<u>Proteoglycans (PG) and Glycosaminoglycans (GAG)</u>	
Hyaluronan (HA) ^f	GAG providing compressibility
Decorin (DCN) ^a	PG involved in collagen fibrillogenesis
<u>Valve Cell Activation</u>	
Smooth muscle alpha-actin (SM α A) ^g	Indicates an "activated" myofibroblast-like phenotype
Non-muscle Myosin Heavy Chain (NMM) ^h	Indicates an "activated" myofibroblast-like phenotype

^a gift of Dr. Larry Fisher, NIH (Bethesda, MD); ^b Chemicon (Temecula, CA); ^c Assay Designs (Ann Arbor, MI); ^d Imgenex (San Diego, CA); ^e Abcam (Cambridge, MA); ^f Associates of Cape Cod (Falmouth, MA); ^g Dakocytomation (Denmark); ^h Covance (Berkeley, CA).

matrix components, enzymes involved in matrix turnover, and cell phenotype (Table 8-1). Staining intensity in each layer (fibrosa, atrialis, and muscle, Fig. 8-2A) of the four MV annulus segments of blinded samples was quantified using ImageJ software (NIH, Bethesda, MD). Semiquantitative grading of blinded samples was also performed to evaluate the degree of fibrosa insertion into annular muscle using a pre-determined rubric (Fig. 8-2B, see legend for specific criteria for each grade).

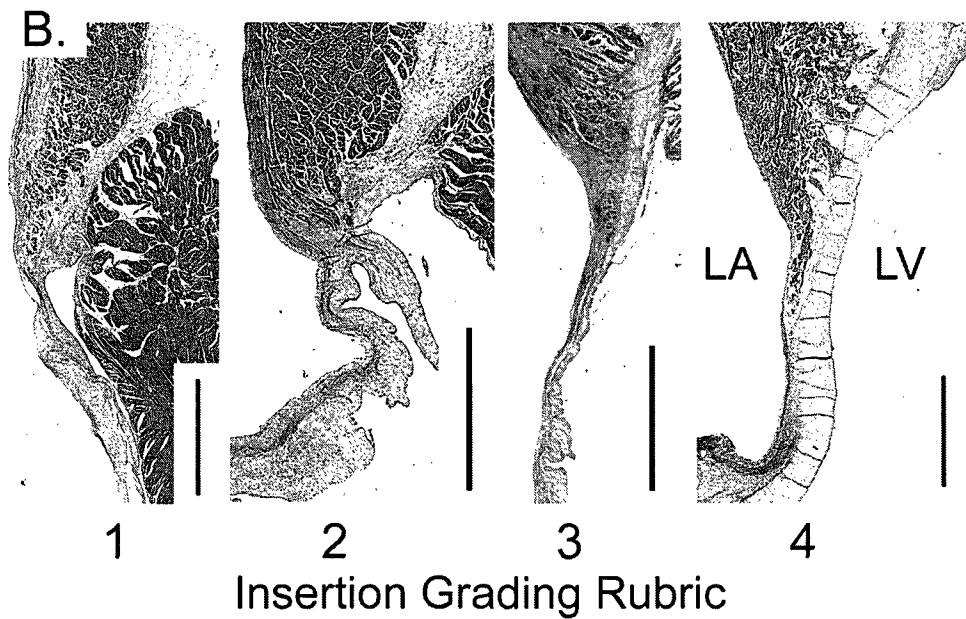
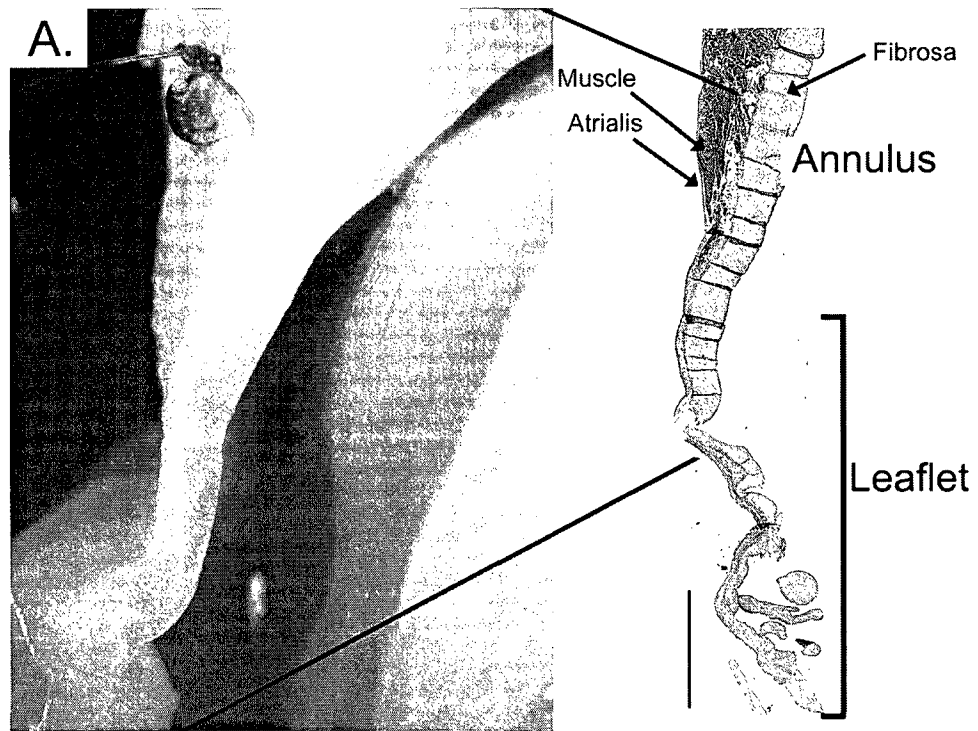


Fig. 8-2: A) Right image shows location of layer of annulus analyzed in tissue section relative to leaflet below and annular fluoroscopy marker seen in left photograph of gross specimen. Arrows point to layers of the MV annulus (atrialis, fibrosa, and muscle). Scale bar represents 2 mm. B) Semi-quantitative grading scale for degree of insertion: 1=insertion either appears spongy, does not contain collagen, or insertion fibrosa remains superficial (does not penetrate muscle); 2=insertion is either not collagen, or poorly aligned collagen, or is a combination of collagen and spongy material; 3=mostly collagen, but thinner or does not insert as far into the muscle. 4=collagen-rich, substantial (thick) fibrosa that continues well into muscle. LA=left atrium, LV=left ventricle.

Statistical Analysis

Multifactorial analysis of variance (ANOVA) was performed using SigmaStat (SPSS, Chicago, IL), as described in Chapter 4. Because of the multiple segments and layers analyzed, data is reported as mean \pm standard error of the mean, unless otherwise indicated. Paired t-tests were used to compare annular contraction with and without calcium infusion. Correlations between staining intensities of different proteins within individual annular layers and segments were used to assess protein co-localization related to matrix turnover and cell phenotype. Correlations between protein intensities and annular contraction were analyzed to investigate the mechanobiology of compositional differences. These correlations were calculated using Pearson and Spearman tests, as described in Chapter 5. For correlations between intensities of different proteins $p \leq 0.02$ was considered a trend and $p \leq 0.00625$ considered significant (since 8 proteins were being compared); for correlations between intensities of proteins and annular contraction each protein was considered individually, therefore $p \leq 0.05$ was considered significant, but only the most significant of these correlations with $p < 0.03$ are listed.

RESULTS

Heterogeneity of Annular Segment Contraction

Without calcium infusion, annular contraction was greatest in LAT, followed by POST-C, ANT-C, and lastly SEPT (Table 8-2, $p < 0.001$). With calcium infusion, annular contraction was greatest in LAT and POST-C, followed by ANT-C, and lastly SEPT (Table 8-2, $p < 0.001$). The contraction of each annular segment except SEPT increased with calcium infusion compared to baseline (each $p < 0.036$).

Table 8-2. Percent Contraction of Annular Segments at Baseline and During Calcium Infusion.

	Baseline	With Calcium
SEPT	3.9±2.6	4.7±2.7
LAT	18.1±4.4††	20.9±4.4††*
ANT-C	9.9±3.5†	12.3±3.5†*
POST-C	15.4±5.7††	20.3±6.0††*

*p<0.05 v. Baseline; †p<0.05 v. SEPT; ††p<0.05 v. ANT-C; data presented as mean ± standard deviation.

Differences in Leaflet Insertion Structure

The degree to which the fibrosa inserted into the musculature was greatest in SEPT followed by ANT-C, POST-C, and lastly LAT (mean grades of 4.0, 2.3, 2.0, and 1.75 respectively, overall ANOVA comparing all segments p<0.001). These grades were inversely correlated with the relative percent contraction in the annular segments (Table 8-2). The degree of insertion grades indicate that the fibrosa in SEPT continued deep into the musculature as a substantial, collagen-rich band, whereas in LAT the fibrosa remained more superficial to the annular musculature. Additionally, in LAT the leaflet appeared to be a continuation of the muscular tissue (Fig. 8-3), as opposed to an independent structure into which the muscle inserted. In contrast, in both ANT-C and POST-C the leaflet was more structurally distinct from the adjacent musculature.

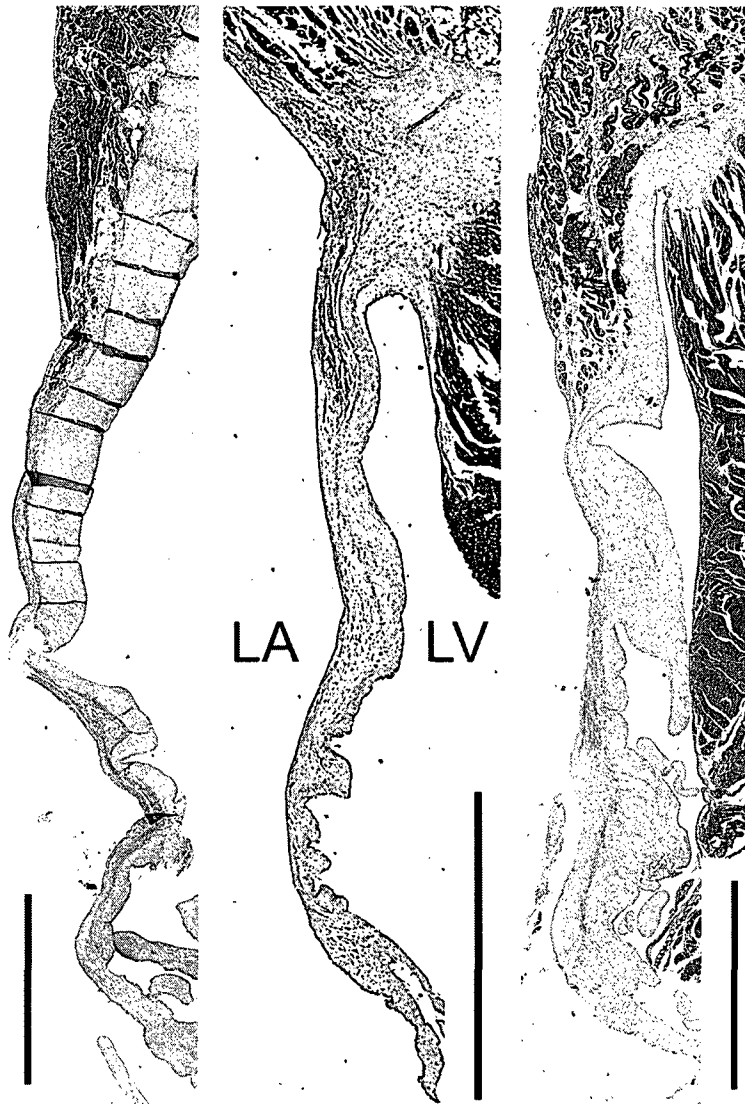


Fig. 8-3: Examples of differences in insertion structure in different MV annular segments. In the left panel is an image representing the typical insertion of the LAT leaflet with the large base, middle panel represents the commissural segments, and right panel represents the SEPT leaflet. Scale bars represent 2 mm. LA=left atrium, LV=left ventricle.

Compositional Heterogeneity between Septal and Lateral Segments and between Commissures

Compared to the LAT annulus, the SEPT annulus contained more Col I and III both across layers (Fig. 8-4, each $p < 0.001$) and in the muscle layer individually (each

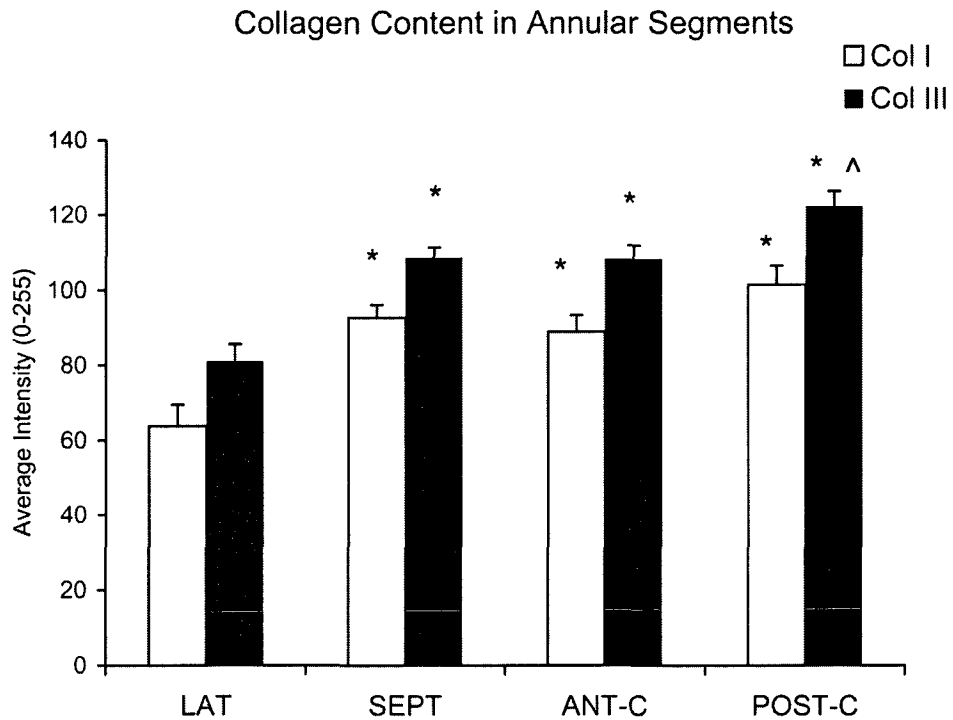


Fig. 8-4: Relative amounts of Col I and III across the different annular segments. Overall ANOVA comparison between segments for Col I and Col III each $p < 0.001$. * $p < 0.001$ vs. LAT for a given protein (Col I or Col III). ^ $p < 0.01$ vs. SEPT for a given protein (Col I or Col III). For all graphs, error bars indicate standard error of the mean.

$p < 0.001$). In contrast, LAT showed greater expression of proteins related to collagen and elastic fiber turnover including the collagen-degrading enzyme MMP13 (Fig. 8-5, $p < 0.001$); the proteoglycan DCN, which is involved in collagen fibrillogenesis (LAT 152.6 ± 2.7 , SEPT 144.8 ± 2.7 , $p = 0.033$); LOX, an enzyme involved in both elastin and collagen crosslinking (LAT 130.8 ± 5.2 , SEPT 117.9 ± 3.9 , $p = 0.006$); and elastin (Fig. 8-6, $p < 0.005$). LAT also demonstrated greater expression of two indicators of cell activation, SMaA (Fig. 8-5, $p < 0.001$) and NMM (LAT 69.0 ± 2.6 , SEPT 64.7 ± 2.4 , $p = 0.012$). Interestingly, LAT also displayed greater expression of the glycosaminoglycan HA (LAT

Collagen Turnover and Cell Activation in Annular Segments

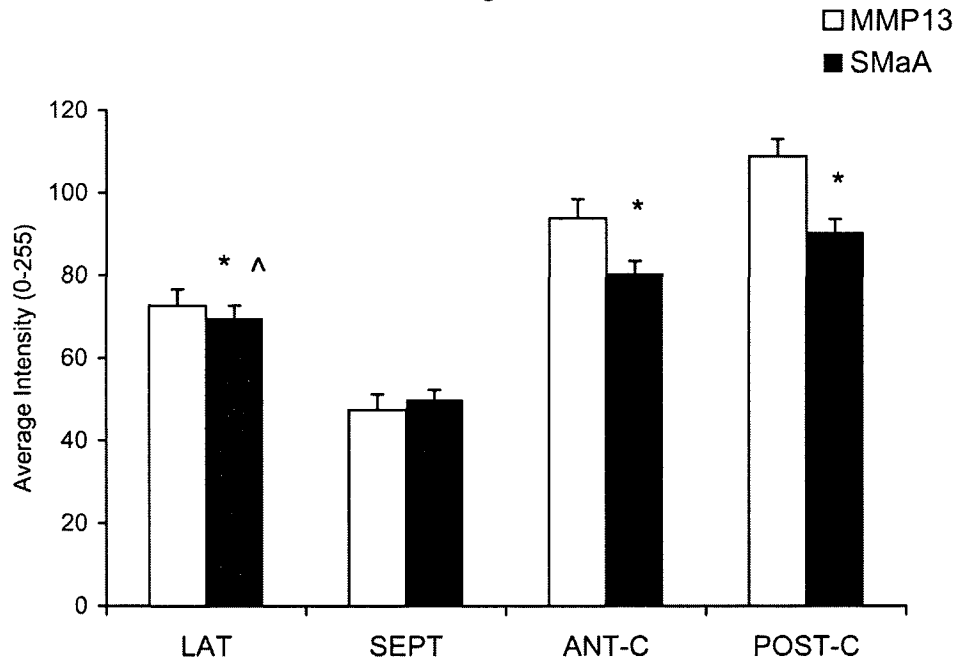


Fig. 8-5: Relative amounts of MMP13 and SMaA across the different annular segments. Overall ANOVA comparison between segments for MMP13 and SMaA each $p < 0.001$. All comparisons between annular segments were significant for MMP13, therefore those are not indicated on the graph. * $p < 0.001$ vs. SEPT for SMaA. ^ $p < 0.001$ vs. POST-C for SMaA.

105.3±4.4 vs. SEPT 94.2±3.0, $p < 0.006$) compared to SEPT. These results of greater collagen and elastic fiber turnover in LAT compared to SEPT parallel the contractile patterns of these regions (baseline contraction: LAT 18.1±4.4% vs. SEPT 3.9±2.6%, $p < 0.001$, Table 8-2). In addition, MMP13 expression in the LAT fibrosa and muscle layers was correlated with the magnitude of annular contraction at baseline ($r = 0.780-0.823$, $p < 0.023$). Compared to ANT-C, the POST-C annulus contained significantly more Col III ($p < 0.015$), as well as MMP13 ($p < 0.02$) and SMaA ($p = 0.006$), which may be consistent with the greater annular contraction in the POST-C annular segment (baseline contraction: POST-C 15.4±5.7% vs. ANT-C 9.9±3.5%, $p < 0.001$, Table 8-2).

Elastin in Annular Segments

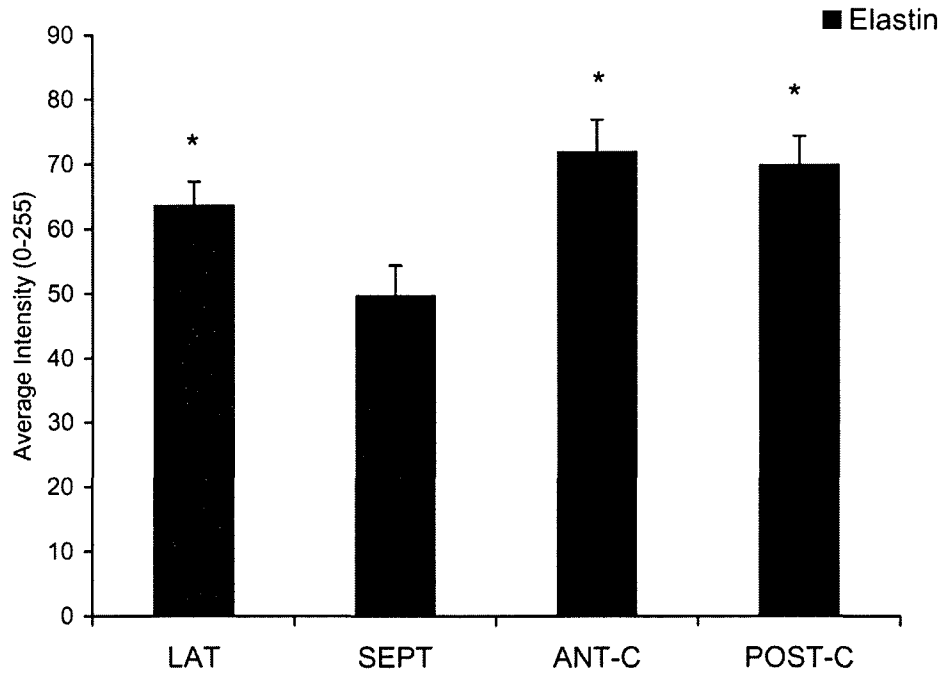


Fig. 8-6: Relative amounts of elastin across the different annular segments. Overall ANOVA comparison between segments $p < 0.001$. * $p < 0.005$ vs. SEPT.

Compositional Heterogeneity among Septal, Lateral, and Commissural Segments

In the comparison of all the different annular segments, POST-C showed the greatest Col I and III of all the segments (Fig. 8-4, both overall $p < 0.001$). Col I and III in ANT-C were both greater than LAT (both $p < 0.001$). Both commissures also had greater expression of MMP13 (Fig. 8-5, $p < 0.001$), LOX (POST-C 139.7 ± 5.5 , ANT-C 136.5 ± 5.0 , LAT 130.8 ± 5.2 , SEPT 117.9 ± 3.9 , $p = 0.005$), and elastin (Fig. 8-6, $p < 0.001$). Consistent with the greater expression of matrix turnover proteins, ANT-C and POST-C showed the greatest expression of SMaA (Fig. 8-5, $p < 0.001$). Lastly, ANT-C and POST-C showed

the greatest expression of the glycosaminoglycan HA among the segments (POST-C 114.0±5.7, ANT-C 110.4±7.3, LAT 105.3±4.4, SEPT 94.2±3.0, overall p=0.001).

Across annular segments, several strong correlations were noted between proteins indicating either cell activation or matrix turnover with magnitudes of annular contraction. In the muscle and fibrosa layers, SMaA was strongly correlated with annular contraction with and without calcium infusion (muscle: 0.687-0.718, each p<0.00001; fibrosa: 0.587-0.611, each p<0.00035), as was MMP13 expression (muscle: 0.622-0.626, each p<0.0012; fibrosa: 0.675-0.732, each p<0.0002).

Correlations between Expressions of Different Proteins

The presence of the myofibroblast cell phenotype was suggested by several correlations between the two proteins indicating cell activation, NMM and SMaA, and collagen or MMPs. These correlations included NMM and Col III in the SEPT fibrosa (r=0.88, p<0.001), NMM and MMP9 in the POST-C atrialis (r=0.89, p=0.018), and SMaA and MMP13 in the fibrosa and muscle layers of ANT-C and POST-C (r=0.764, p=0.006). Across all annular segments, strong correlations were evident between MMP13 and SMaA throughout the layers (atrialis 0.875, p<0.00001, fibrosa 0.687, p<0.00008, muscle 0.88, p<0.000001), and MMP9 with NMM in the fibrosa (0.556, p=0.0013). MMP9 also correlated with elastin (0.590, p=0.0025), which further suggests elastic fiber turnover.

DISCUSSION

This study provides evidence documenting a novel relationship between the *in vivo* length change of various segments of the mitral annulus and the matrix composition, layered structure, and valvular cell phenotype within that segment. Annular contraction was inversely related to the degree of fibrous insertion into the muscle, but was directly related to matrix turnover and cell activation. The LAT portion of the annulus demonstrated greater collagen and elastic fiber turnover, as well as cell activation, compared to the SEPT annulus, paralleling greater contraction in LAT compared to SEPT. Similarly, collagen turnover and cell activation was high in the POST-C annulus, paralleling greater annular contraction in POST-C compared to ANT-C. Overall, the commissural annular segments had the highest collagen content as well as most pronounced collagen and elastic fiber turnover. Strong correlations between the expression of matrix synthesis and turnover-related proteins and myofibroblast proteins within individual layers of the different annular segments suggest the involvement of myofibroblasts in annular compositional and contractile heterogeneity.

Functional Implication of Heterogeneous Valve Insertion Structure

Differences in the insertion of the heavily collagenous fibrosa within the annular musculature relate to the mechanical behavior of the different portions of the mitral annulus. Although this contractile nature of the mitral annulus has been widely investigated,⁴⁻⁶ the microstructural aspects of the mitral leaflets' anchorage within the annulus, and how these vary across annular segments, have been largely overlooked.

Across the different segments of the MV annulus, the degree of fibrosa insertion was inversely related to the magnitude of contraction. Regarding the insertion of the SEPT leaflet, the substantial bands of collagen demonstrated here could greatly reduce contraction of the SEPT annular segment relative to remainder of the annulus, as observed in this and other studies.^{4, 5, 15, 16} Differences in insertion structure between the annular segments could potentially affect the flexibility of this leaflet region. The thick annular insertion base anchoring the LAT and commissural leaflets would reduce flexibility compared to the thin, narrow base anchoring the SEPT leaflet. Indeed, compared to LAT, the SEPT leaflet displays greater excursion³ and closure rate.⁶

Annular Compositional Heterogeneity and Relation to Contraction

The overall abundance of collagen within the various annular segments was consistent with the data patterns regarding degree of insertion. For example, the greater collagen content in SEPT vs. LAT reflected the collagen-rich fibrosa inserting into the muscle of SEPT. However, collagen was not limited to the fibrosa layer; the muscle layer of SEPT also contained more collagen than did LAT. This finding suggests that the frequently described “fibrous” nature of the SEPT annulus is characterized by collagen that is highly organized within the fibrosa layer and diffusely abundant throughout the muscular layer.

Both within the LAT and SEPT annular and the commissural annular comparisons, the relative magnitudes of annular contraction paralleled those of matrix turnover and cell activation proteins. These results, combined with strong statistical correlations between these same variables within individual annular segments, suggest a

relationship between annular contraction and matrix turnover/cell activation. Correlations were predominantly found between annular contraction and proteins of matrix turnover and cell activation in the muscle and fibrosa layers, which is consistent with the structural and functional roles of these layers. Interestingly, when all four annular segments were compared, the commissures demonstrated not only the greatest collagen content but also the greatest collagen turnover and level of cell activation. The commissures as a group, however, did not undergo significantly greater annular contraction compared to LAT, which would have been expected given their greater collagen turnover and cell activation (although this contraction-turnover relationship was demonstrated in the POST-C/ANT-C comparison). Reasons for this inconsistency might include the density of collagen within the fibrosa layer (very high in commissures but admixed with PGs and GAGs in LAT) or the influence of other mechanical stimuli, in addition to contraction, that could affect the annulus in a heterogeneous manner.

Potential Functional Contributions of Myofibroblasts

Given the known roles of myofibroblasts in matrix remodeling,^{17, 18} correlations in the fibrosa layer between proteins associated with myofibroblasts and those indicating matrix degradation imply that myofibroblasts contribute to the annular compositional heterogeneity. Moreover, myofibroblasts respond to their mechanical environment.¹⁹ Therefore, we speculate that these cells provide an important link between annular cell/matrix composition and function by sensing annular contraction and responding by synthesizing extracellular matrix. Consequently, the altered matrix composition would affect the material behavior of the annular tissue and in turn influence the capacity for

contraction. In addition, myofibroblasts also demonstrate contractile properties,²⁰ which have been shown to alter valve stiffness,²¹ and thus may also affect annular contraction, even though the muscular layer is certainly the major effector of contraction. Taken together, these results suggest a link between myofibroblasts and annular length change. As such, the myofibroblast may be a therapeutic target for diseases in which annular composition and contraction is altered.

Implications

The link between annular contraction and composition evident in this study implies that altered annular contraction, such as occurs with annuloplasty ring placement,^{22, 23} as well as in disease processes such as ischemic and functional mitral regurgitation,^{14, 24} may lead to alterations in valve cell phenotype and mitral annular composition, which could lead to further deterioration in MV function. Therefore, this study provides further motivation for the ongoing refinement of annuloplasty ring designs to maintain physiologic, heterogeneous annular contraction. In addition, the heterogeneity of the insertions of the mitral valve leaflets into the annulus, which are essential mechanical linkages connecting the leaflets to the mitral annular/left ventricular complex, will need to be carefully replicated in the design of a tissue engineered mitral valve to ensure proper function. In the future, it will be important to understand and account for the numerous forces acting on the mitral annulus and how those forces interplay with annular composition to provide a more complete picture of the complex structure-function relationship in the mitral annulus.

Limitations

One of the limitations in this study is the inherent variability of IHC, which was quantified to be 13.7% within batches and 16.5% between batches. In order to limit this variability, duplicate sections were cut from the SEPT and LAT annular segments, and the staining results were averaged. Furthermore, all samples from a given annular segment were stained for a given protein in one batch. Despite any remaining variability, we have found significant results. Additionally, there are some anatomic differences between the annuli of ovine and humans.²⁵ Therefore, significant caution should be practiced before applying the results of this study to human patients.

CONCLUSIONS

This study reveals heterogeneity in MV annular composition in terms of individual matrix components, matrix turnover, presence of myofibroblasts, and structure of leaflet insertion. Furthermore, this study provides the first evidence of a direct correlation between the heterogeneity in mitral valve annular matrix composition and heterogeneity of annular contraction. Such a link could prove instrumental both in clinical strategies to treat valves with altered matrix composition as well as in strategies for designing a heterogeneous tissue engineered heart valve.

This chapter, in which regional mitral valve leaflet composition was analyzed in relationship to *in vivo* leaflet length changes, opens the series of four chapters addressing normal valve heterogeneity. This series of chapters is subdivided into those related to heterogeneity in mitral valve composition and motion (Chapters 8

and 9) and those related to heterogeneity in the valvular interstitial cell population (Chapters 10 and 11). In the next chapter, analysis of the composition of the mitral annular leaflet attachment region in relationship to *in vivo* changes in annular segment length will be presented.

REFERENCES

1. Levine R, Hung J, Otsuji Y, Messas E, Liel-Cohen N, Nathan N, Handschumacher M, Guerrero J, He S, Yoganathan A, Vlahakes G. Mechanistic insights into functional mitral regurgitation. *Curr Cardiol Rep.* 2002;4(2):125-129.
2. Komoda T, Hetzer R, Oellinger J, Sinlawski H, Hofmeister J, Hubler M, Felix R, Uyama C, Maeta H. Mitral annular flexibility. *J Card Surg.* 1997;12(2):102-109.
3. Karlsson M, Glasson J, Bolger A, Daughters G, Komeda M, Foppiano L, Miller D, Ingels N, Jr. Mitral valve opening in the ovine heart. *Am J Physiol.* 1998;274(2 Pt 2):H552-563.
4. Glasson J, Komeda M, Daughters G, Niczyporuk M, Bolger A, Ingels N, Miller D. Three-dimensional regional dynamics of the normal mitral annulus during left ventricular ejection. *J Thorac Cardiovasc Surg.* 1996;111(3):574-585.
5. Timek TA, Green GR, Tibayan FA, Lai DT, Rodriguez F, Liang D, Daughters GT, Ingels NB, Jr., Miller DC. Aorto-mitral annular dynamics. *Ann Thorac Surg.* 2003;76(6):1944-1950.
6. Tsakiris A, Von Bernuth G, Rastelli G, Bourgeois M, Titus J, Wood E. Size and motion of the mitral valve annulus in anesthetized intact dogs. *J Appl Physiol.* 1971;30(5):611-618.
7. Okada Y, Shomura T, Yamaura Y, Yoshikawa J. Comparison of the Carpentier and Duran prosthetic rings used in mitral reconstruction. *Ann Thorac Surg.* 1995;59(3):658-662; discussion 662-653.
8. David TE, Komeda M, Pollick C, Burns RJ. Mitral valve annuloplasty: the effect of the type on left ventricular function. *Ann Thorac Surg.* 1989;47(4):524-527; discussion 527-528.
9. van Rijk-Zwicker G, Delemarre B, Huysmans HA. Mitral valve anatomy and morphology: Relevance to Mitral Valve Replacement and Valve Reconstruction. *J Card Surg.* 1994;9[Suppl]:255-261.
10. Anderson R, Wilcox B. The anatomy of the mitral valve. In: Shapiro L, ed. *Mitral Valve Disease.* Oxford: Butterworth-Heinemann; 1996:4.
11. Peyton SR, Ghajar CM, Khatiwala CB, Putnam AJ. The emergence of ECM mechanics and cytoskeletal tension as important regulators of cell function. *Cell Biochem Biophys.* 2007;47(2):300-320.
12. Merryman WD, Youn I, Lukoff HD, Krueger PM, Guilak F, Hopkins RA, Sacks MS. Correlation between heart valve interstitial cell stiffness and transvalvular pressure: implications for collagen biosynthesis. *Am J Physiol Heart Circ Physiol.* 2006;290(1):H224-231.

13. Balachandran K, Konduri S, Sucusky P, Jo H, Yoganathan A. An ex vivo study of the biological properties of porcine aortic valves in response to circumferential cyclic stretch. *Annals of biomedical engineering*. 2006;34(11):1655-1665.
14. Timek TA, Dagum P, Lai DT, Liang D, Daughters GT, Tibayan F, Ingels NB, Jr, Miller DC. Tachycardia-induced cardiomyopathy in the ovine heart: Mitral annular dynamic three-dimensional geometry. *J Thorac Cardiovasc Surg*. 2003;125(2):315-324.
15. Lansac E, Lim K, Shomura Y, Goetz W, Lim H, Rice N, Saber H, Duran C. Dynamic balance of the aortomitral junction. *J Thorac Cardiovasc Surg*. 2002;123(5):911-918.
16. Parish L, Jackson B, Enomoto Y, Gorman R, Gorman J, 3rd. The dynamic anterior mitral annulus. *Ann Thorac Surg*. 2004;78(4):1248-1255.
17. Rabkin-Aikawa E, Farber M, Aikawa M, Schoen FJ. Dynamic and reversible changes of interstitial cell phenotype during remodeling of cardiac valves. *J Heart Valve Dis*. 2004;13(5):841-847.
18. Tomasek JJ, Gabbiani G, Hinz B, Chaponnier C, Brown RA. Myofibroblasts and mechano-regulation of connective tissue remodelling. *Nat Rev Mol Cell Biol*. 2002;3(5):349-363.
19. Wang J, Chen H, Seth A, McCulloch CA. Mechanical force regulation of myofibroblast differentiation in cardiac fibroblasts. *Am J Physiol Heart Circ Physiol*. 2003;285(5):H1871-1881.
20. Messier RH, Jr., Bass BL, Aly HM, Jones JL, Domkowski PW, Wallace RB, Hopkins RA. Dual structural and functional phenotypes of the porcine aortic valve interstitial population: characteristics of the leaflet myofibroblast. *J Surg Res*. 1994;57(1):1-21.
21. Merryman W, Huang H, Schoen F, Sacks M. The effects of cellular contraction on aortic valve leaflet flexural stiffness. *J Biomech*. 2006;39(1):88-96.
22. Glasson JR, Green GR, Nistal JF, Dagum P, Komeda M, Daughters GT, Bolger AF, Foppiano LE, Ingels NB, Jr., Miller DC. Mitral annular size and shape in sheep with annuloplasty rings. *J Thorac Cardiovasc Surg*. 1999;117(2):302-309.
23. Green GR, Dagum P, Glasson JR, Nistal JF, Daughters GT, 2nd, Ingels NB, Jr., Miller DC. Restricted posterior leaflet motion after mitral ring annuloplasty. *Ann Thorac Surg*. 1999;68(6):2100-2106.
24. Kaplan SR, Bashein G, Sheehan FH, Legget ME, Munt B, Li XN, Sivarajan M, Bolson EL, Zeppa M, Arch MZ, Martin RW. Three-dimensional echocardiographic assessment of annular shape changes in the normal and regurgitant mitral valve. *Am Heart J*. 2000;139(3):378-387.
25. Walmsley R. Anatomy of human mitral valve in adult cadaver and comparative anatomy of the valve. *Br Heart J*. 1978;40(4):351-366.

Chapter 9: Relationship of Mitral Leaflet Compositional Heterogeneity to Leaflet Deformation

The work contained in this chapter continues the topic of normal valve heterogeneity, and specifically the topic of mitral valve composition in relationship to *in vivo* strains addressed in the previous chapter. In this chapter analysis of mitral annular composition in relationship to *in vivo* changes in annular segment length is presented.

ABSTRACT

Background: Mitral valve (MV) leaflets must undergo regionally heterogeneous dynamics to ensure proper valve closure. The compositional and cellular basis for this regional heterogeneity, however, is incompletely understood. We studied regional leaflet matrix composition, matrix turnover, and cell phenotype as it relates to regional deformation.

Methods: Matrix composition and cell phenotypes were immunohistochemically evaluated in three regions (basal leaflet (BL), mid-leaflet (ML), and free edge) within the septal (SEPT), lateral (LAT), and anterior and posterior commissural leaflets (ANT-C, POST-C) of 14 sheep. Videofluoroscopy imaging of radiopaque markers implanted in the septal and lateral leaflet of the same sheep was used to calculate maximum radial and circumferential lengths during the cardiac cycle, and related to regional composition.

Results: Collagens I and III in SEPT were greater than in LAT ($p < 0.025$ for ML, BL). LAT, however, showed greater collagen turnover (matrix metalloprotease (MMP)-13 $p < 0.005$ in each region, lysyl oxidase $p < 0.008$ in ML) and cell activation (smooth muscle alpha-actin, SMaA, $p < 0.001$ in each region and non-muscle myosin (NMM) $p < 0.001$ in ML, BL). SMaA and MMP13 in POST-C ML were greater than ANT-C (each $p < 0.008$). Correlations between MMP13, MMP9, NMM, and SMaA suggested the role of myofibroblasts in this compositional heterogeneity. MMP13, NMM, and SMaA were strongly correlated with length changes in both SEPT and LAT.

Conclusions: This work demonstrates significant heterogeneity in MV leaflet composition and suggests a link between MV deformation and matrix turnover. Additionally, these results suggest that myofibroblasts, given their contractility and synthetic capability, contribute to the heterogeneity in both leaflet composition and deformation. This information should guide new approaches to MV repair techniques and ring design to preserve this normal coupling between leaflet composition and motion.

The work contained in this chapter is in preparation for submission to *Journal of Heart Valve Disease*.

INTRODUCTION

Mitral valve (MV) competence is critical to cardiac function. Indeed, mitral regurgitation portends a significantly higher morbidity and mortality to patients with myocardial infarction independent of left ventricular function.¹ MV competence relies on adequate, timely coaptation between the leaflets. For this to be accomplished, the different segments of the MV undergo complex, heterogeneous motion^{2, 3} culminating in the distal leaflet regions of the various segments forcefully joining in a precise alignment to prevent blood backflow. Recent studies have shown that the degree of coaptation is critical to mitral regurgitation in diseases such as dilated cardiomyopathy.⁴ Numerous studies have characterized leaflet motion and found it to be heterogeneous, with the anterior or septal leaflet motion being substantially further² and its closure rate more rapid than for the posterior or lateral leaflet.⁵ Strains were even found to be heterogeneous within the septal leaflet.⁶ The underlying basis for this heterogeneity, however, remains unknown.

Although relationships between *in vivo* leaflet strain and composition have not been previously reported, differences in material behavior between regions of the septal leaflet and between the septal and lateral leaflets^{7, 8} have been generally attributed to differential thickness of the collagen-rich fibrosa layer across the leaflet anatomy.^{7, 9} However, these previous studies performed materials testing on strips of excised leaflets, and did not address *in vivo* strains and hemodynamics, the valve environment, or the commissural leaflets. In addition, these explanations omit the possible contributions of heart valve cells to tissue mechanics, even though valve cells are known to be contractile¹⁰ and to produce extracellular matrix in response to mechanical stimulation.¹¹⁻

¹³ It was the hypothesis of this study that valvular cell-mediated differences in extracellular matrix composition and turnover underlie the observed heterogeneity in leaflet deformation. Therefore, immunohistochemistry (IHC) was performed to characterize valve cell phenotype, matrix composition, and matrix turnover within the different segments of the mitral leaflets, and in the septal and lateral leaflets related to *in vivo* regional leaflet length changes.

METHODS

All animals received humane care in accordance with the guidelines of the US Department of Health and Human Services (NIH Publ. 85-23, Revised 1985). The use of animals in this study was approved by the Stanford Medical Center Laboratory Research Animal Review Committee.

Animal Protocol

Radiopaque markers were implanted into fourteen sheep delineating the septal (SEPT) and lateral (LAT) MV leaflets (Fig. 9-1). Procedures for marker implantation and biplane video fluoroscopy have been described previously.¹⁴ Leaflet segment length change, defined as the percent change from minimum to maximum dimensions throughout the cardiac cycle, was calculated. It was not possible to calculate radial or circumferential leaflet length change for ANT-C and POST-C due to limitations on marker positioning. The hearts were then harvested and stored in formalin.

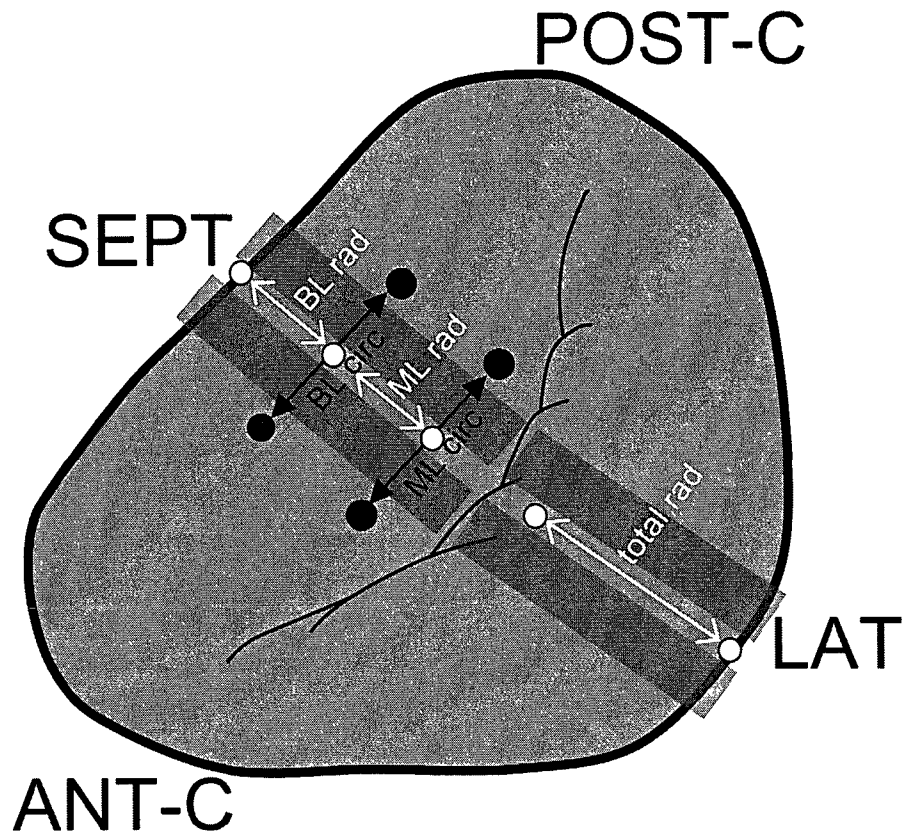


Fig. 9-1: Circles indicate the location of the implanted radiopaque markers. Dark gray rectangles indicate tissue section location (sections did not include markers or their sutures). Two tissue sections were analyzed and the results averaged for the septal (SEPT) and lateral (LAT) segments, respectively; one tissue section was used for each of the commissures (ANT-C, POST-C). BL=basal leaflet, ML=mid-leaflet. Double-headed arrows indicate leaflet segment length measurements; rad=radial, circ=circumferential. For SEPT, BL rad + ML rad=total rad.

Histology and Immunohistochemistry

For each MV segment a 3-5 mm wide strip was cut from insertion region to free edge (Fig. 9-1), embedded in paraffin, and sectioned to a thickness of five microns. Each sample was stained with Movat pentachrome as well as IHC to demonstrate the myofibroblast valve cell phenotype, extracellular matrix components, and matrix turnover. Components stained for included collagen I (Col I), collagen III (Col III), matrix metalloproteinase (MMP)-13, MMP9, lysyl oxidase (LOX), elastin, hyaluronan

(HA), decorin (DCN), smooth muscle alpha-actin (SMaA), and non-muscle myosin (NMM) (for list of matrix components, their roles, and antibodies used, see Chapter 8, Table 8-1). Staining intensity was quantified on blinded IHC sections using ImageJ software (NIH, Bethesda, MD) for three regions of the valve, (BL, ML, and free edge (Fig. 9-2)) and for each histological layer (fibrosa, atrialis, and spongiosa (spongiosa was only quantified in the ML)). Analysis of blinded Movat-stained sections included measurement of the distance of muscle insertion relative to total leaflet length using Image Pro software (Media Cybernetics, Bethesda, MD). Semi-quantitative grading was performed to evaluate delineation between leaflet layers using a pre-determined grading rubric ranging from 0 (minimum) to 4 (maximum) as previously described.¹⁵

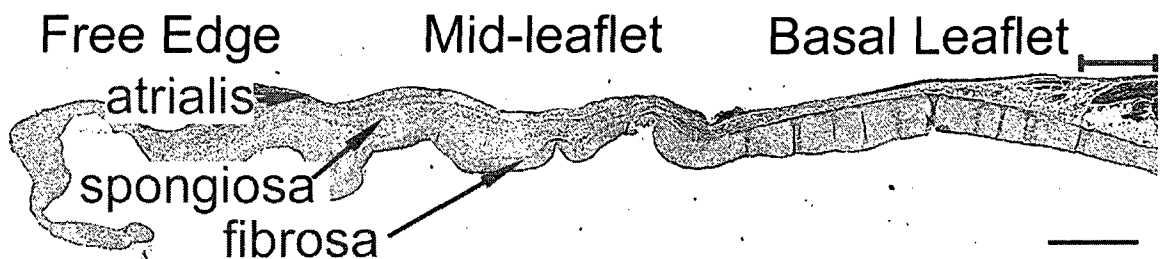


Fig. 9-2: Locations of leaflet regions and histological layers. Bracket in upper right corner indicates measurement for calculating proportion of muscle insertion into leaflet. Scale bar represents 2 mm.

Statistical Analysis

Multifactorial analysis of variance was performed using SigmaStat (SPSS, Chicago, IL), as described in Chapter 4. Because of the multiple segments, regions, and layers analyzed, data is reported as mean \pm standard error of the mean, unless otherwise indicated. Paired t-tests were used to compare leaflet length changes between segments.

Correlations between staining intensities of different proteins within individual leaflet layers of specific regions and segments were used to assess protein co-localization and correlations between protein intensities and leaflet length change were analyzed to assess further relationships between deformation and composition. These correlations were calculated using Pearson and Spearman tests, as described in Chapter 5. For correlations between intensities of different proteins, $p \leq 0.02$ was considered a trend and $p \leq 0.00625$ was considered significant since 8 proteins were compared. For correlations between intensities of proteins and regional leaflet length changes, each protein was considered individually, therefore $p \leq 0.05$ was considered significant, but only highly significant correlations with $p < 0.03$ are reported.

RESULTS

Differences in Leaflet Length Changes across Annular Segments

Over the cardiac cycle, the change in the radial length of LAT was greater than in SEPT ($p=0.004$, Table 9-2). Within SEPT, the radial and circumferential leaflet length changes in ML were greater than in BL ($p=0.001$).

Table 9-1. Minimum and Maximum Leaflet Segment Lengths.

(cm)	Min	Max
SEPT		
ML circ	1.60±0.41	2.00±0.47
BL circ	1.21±0.37	1.34±0.36
ML rad	0.86±0.17	1.09±0.21
BL rad	0.90±0.19	0.98±0.17
tot rad	1.79±0.24	2.14±0.20
LAT		
tot rad	0.92±0.11	1.27±0.12

Data presented as mean ± standard deviation.

Differences in Leaflet Structure across Annular Segments

Delineation between leaflet layers was greatest in SEPT, then in ANT-C/POST-C, and lastly in LAT (Fig. 9-3, $p=0.011$). The length of the muscle insertion into the leaflet region relative to total leaflet length was highest in ANT-C (0.32), much less in LAT (0.13) and POST-C (0.10), and minimal in SEPT (0.02, $p<0.001$). Analysis of Movat-stained sections revealed further structural differences between the leaflets. In the ML region of LAT where the chordae tendineae insert, the leaflet fibrosa contained collagen, PGs, and other matrix components, and the chordae tendineae insertions were apparent as branches coming off of fibrosa. In contrast, in the commissural leaflets the collagen-rich chordae tendineae often appeared as continuous with the fibrosa. Therefore, the leaflet fibrosa of the commissures contained proportionately more collagen than LAT (Fig 9-4).

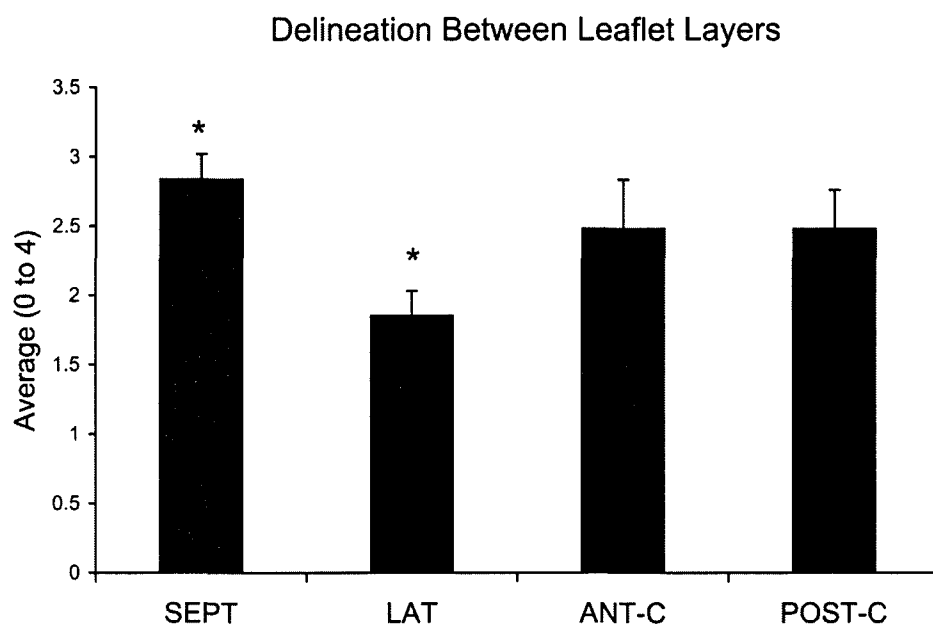


Fig. 9-3: A) Degree of delineation between layers. $*=p<0.001$. For all bar graphs error bars indicate the standard error of the mean.

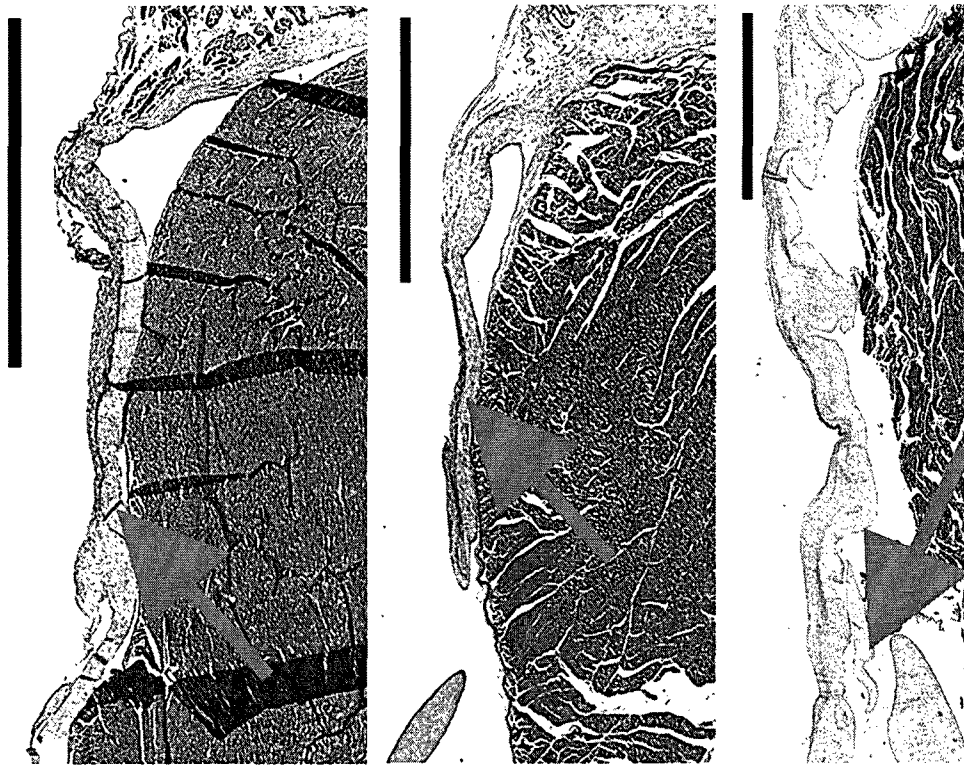


Fig. 9-4: The two left sections represent examples of commissure sections in which the collagen core of the chordae tendinae is continuous with the fibrosa of the leaflet resulting in a particularly collagen-rich fibrosa in this section of the leaflet. That pattern contrasts with the chordal origins in LAT (far right), in which chordae has branched off of the existing fibrosa. Arrows in left two images point to chordae continuous with leaflet fibrosa; arrow in right image points to chordae branching off fibrosa. Scale bars represent 2 mm.

Compositional Heterogeneity between Septal and Lateral Segments and between Commissures

The expression of Col I in SEPT was greater than in LAT across all leaflet regions (Fig. 9-5; SEPT BL: 95.1 ± 4.0 vs. LAT BL: 76.3 ± 6.8 ; BL, ML each $p < 0.025$; SEPT free edge: 89.6 ± 7.7 vs. LAT free edge: 61.1 ± 7.9 , free edge $p = 0.06$ (trend)), as was Col III (Fig. 9-5; SEPT BL: 109.2 ± 4.1 vs. LAT BL: 85.8 ± 6.6 ; SEPT free edge: 122.5 ± 3.6 vs. LAT free edge: 72.8 ± 11.0 , BL, ML, free edge each $p < 0.005$). In contrast, the

expression of collagen-degrading enzyme MMP13 was greater in LAT than in SEPT (Fig. 9-6; LAT BL: 71.1 ± 5.0 vs. SEPT BL: 50.5 ± 4.8 ; BL, ML each $p < 0.005$). LOX, an enzyme involved in collagen and elastin crosslinking, was similarly greater in LAT ML compared to SEPT ML (LAT 114.0 ± 5.5 vs. SEPT 94.8 ± 4.4 , $p < 0.008$). The proteoglycan DCN, which mediates collagen fibrillogenesis, was greater in LAT BL than in SEPT BL (LAT 160.5 ± 3.5 vs. SEPT 146.2 ± 3.5 , $p < 0.007$). Two indicators of valve cell activation, SMaA and NMM, were greater in LAT (both BL and ML) than in SEPT (SMaA: Fig. 9-6; LAT BL: 73.3 ± 3.9 vs. SEPT BL 50.9 ± 3.8 ; BL, ML each $p < 0.0002$; NMM: LAT BL 77.6 ± 2.9 vs. SEPT BL 64.9 ± 2.5 , LAT ML 71.6 ± 2.5 vs. SEPT ML 64.6 ± 2.5 ; BL, ML $p < 0.0001$).

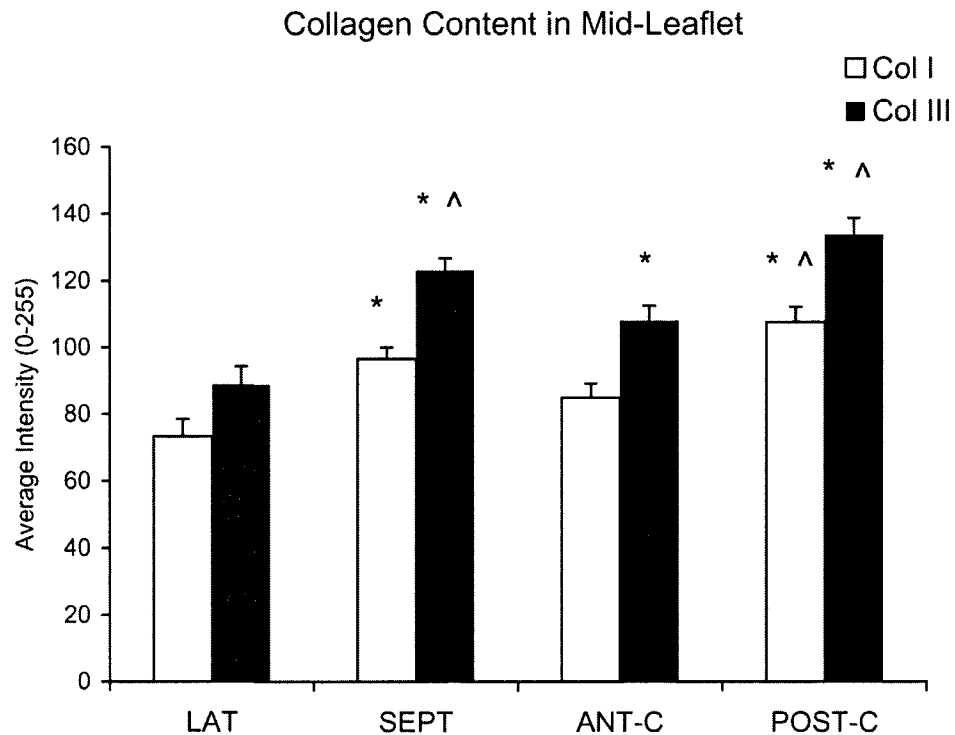


Fig. 9-5: Relative amounts of Col I and III in the mid-leaflet. Overall Col I and Col III each $p < 0.001$. * $p < 0.008$ vs. LAT and ^ $p < 0.011$ vs. ANT-C for a given protein (Col I or Col III).

These patterns of collagen turnover and cell activation paralleled those of radial and circumferential segmental leaflet length changes. For example, MMP13 abundance correlated with the change in radial change in SEPT BL ($r=0.99$, $p=0.001$). SMaA expression correlated with circumferential length change in the atrialis layer of SEPT BL (0.935 , $p<0.001$) and with radial length change in SEPT ML ($r=0.700$, $p=0.03$). In LAT ML, NMM correlated with changes in radial lengths ($r=0.857$, $p=0.006$). Furthermore, consistent with greater leaflet length change in SEPT ML compared to BL, the abundance

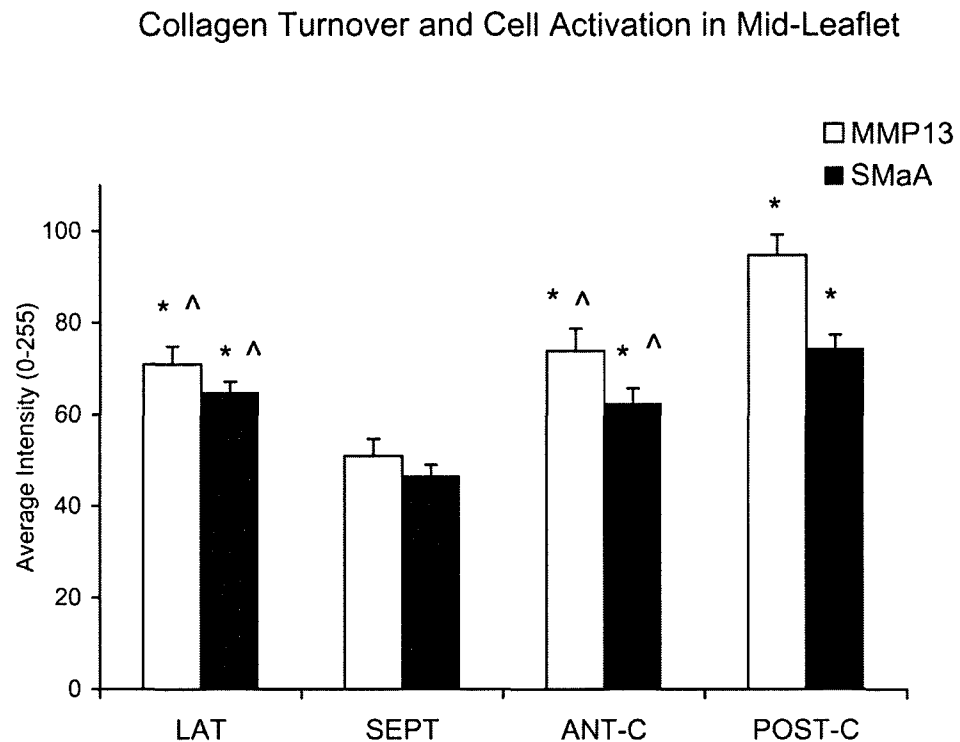


Fig. 9-6: Relative amounts of MMP13 and SMaA in the mid-leaflet. Overall MMP13 and SMaA each $p<0.001$. * $p<0.001$ vs. SEPT and ^ $p<0.015$ vs. POST-C for a given protein (MMP13 or SMaA).

of NMM, SMaA, and MMP13 was greater in the SEPT ML fibrosa than in the BL fibrosa (p=0.037).

Compared to ANT-C, POST-C demonstrated greater expression of Col I and Col III in BL and ML (Fig. 9-5; Col I: POST-C BL 120.6 ± 5.0 vs. ANT-C BL 87.4 ± 5.0 , Col III: POST-C BL 145.4 ± 5.2 vs. ANT-C BL 111.7 ± 4.9 , each $p < 0.0005$), SMaA in ML (Fig. 9-6, $p < 0.008$), and MMP13 in ML (Fig. 9-6, $p < 0.003$).

Compositional Heterogeneity across MV Segments

When comparing all segments, Col I and Col III in both ML and BL were greatest in POST-C, followed by SEPT, then ANT-C, and lastly LAT (overall $p < 0.001$ for each of

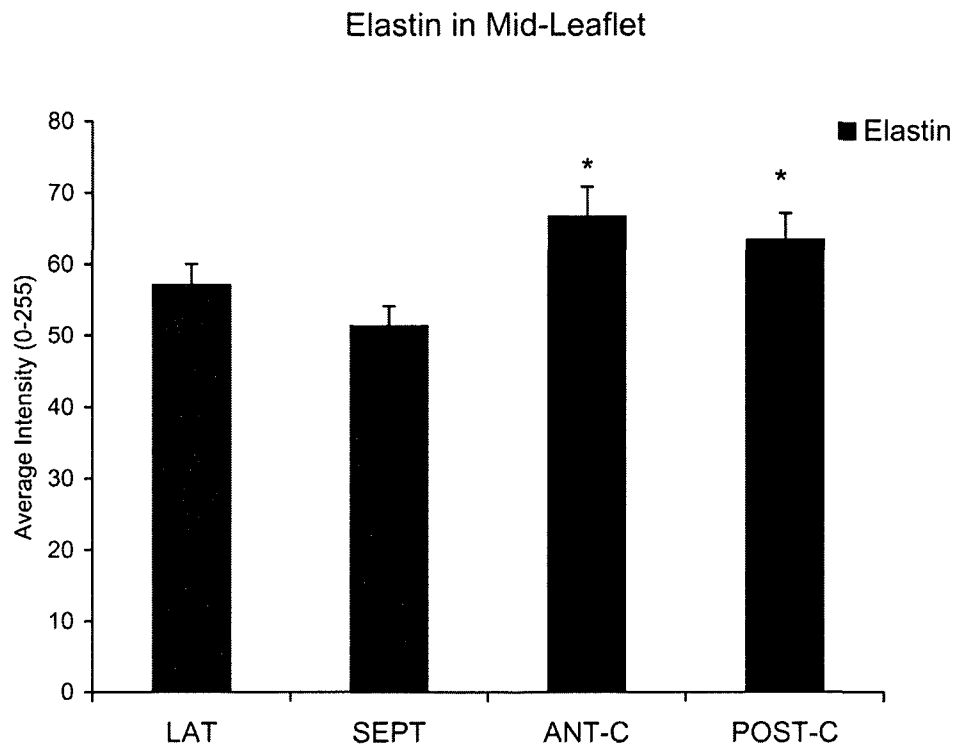


Fig. 9-7: Relative amounts of elastin in the mid-leaflet. Overall $p < 0.001$. * $p < 0.001$ vs. SEPT.

ML and BL). MMP13 was greatest in POST-C, followed by ANT-C, then LAT, and lastly SEPT (each region overall $p < 0.007$). In BL, LOX was greatest in ANT-C/POST-C and LAT, followed by SEPT (ANT-C: 132.2 ± 5.5 , LAT: 130.7 ± 6.2 , POST-C: 128.6 ± 5.5 , SEPT: 112.6 ± 4.5 , overall $p = 0.022$), whereas in ML, LOX was greatest in ANT-C/POST-C, followed by LAT, and then SEPT (POST-C: 120.2 ± 5.6 , ANT-C: 120.1 ± 5.1 , LAT: 114.0 ± 5.5 , SEPT: 94.8 ± 4.4 , overall $p < 0.001$). In BL, DCN was greatest in LAT, followed by ANT-C/POST-C, and then SEPT (LAT: 160.5 ± 3.5 , ANT-C: 162.5 ± 4.6 , POST-C: 158.8 ± 4.7 , SEPT: 146.2 ± 3.5 , overall $p = 0.019$).

With regards to cell activation, SMaA in BL and ML was greatest in POST-C, followed by ANT-C and LAT, and then SEPT (Fig. 9-6; POST-C BL: 85.9 ± 4.9 , ANT-C BL: 77.6 ± 5.7 , LAT BL: 73.3 ± 3.9 , SEPT BL: 50.9 ± 3.8 ; BL and ML each overall $p < 0.001$ for each of BL and ML). In BL, NMM was greatest in LAT, followed by POST-C/ANT-C, and then SEPT (LAT: 77.6 ± 2.9 , POST-C: 71.9 ± 3.4 , ANT-C: 68.2 ± 4.1 , SEPT: 64.9 ± 2.5 , overall $p = 0.016$).

For proteins related to elastic fibers, elastin in ML was greatest in ANT-C/POST-C, followed by SEPT and LAT (Fig. 9-7, overall $p < 0.001$) and MMP9 in ML was greatest in ANT-C/POST-C, followed by SEPT and LAT (ANT-C: 65.9 ± 3.4 , POST-C: 64.6 ± 3.2 , SEPT: 56.5 ± 2.6 , LAT: 55.9 ± 2.5 , overall $p = 0.032$). The glycosaminoglycan HA was greatest in POST-C ML, followed by ANT-C and LAT, and then SEPT (POST-C: 135.5 ± 5.5 , ANT-C: 125.4 ± 5.5 , LAT: 121.9 ± 4.3 , SEPT: 111.3 ± 3.9 , $p = 0.005$).

Correlations between Proteins within Leaflet Regions

Within specific leaflet regions and layers, strong correlations between proteins associated with cell activation and proteins involved in matrix synthesis and degradation suggested the presence of myofibroblasts. These correlations were between MMP13 and SMaA in the ML across all layers (0.764, $p < 0.00001$), as well as in the BL fibrosa (0.810, $p < 0.00001$) and free edge (0.656, $p = 0.003$); MMP9 and each of SMaA and NMM in the BL fibrosa (0.576, $p < 0.0022$ and 0.578, $p < 0.0014$, respectively); and SMaA and Col III in the BL fibrosa (0.578, $p < 0.0008$).

DISCUSSION

This study demonstrates significant compositional and cellular heterogeneity across the segments of the MV. While collagen content in SEPT was greater than LAT, collagen turnover was greater in LAT, consistent with greater leaflet length changes in that leaflet. The presence of myofibroblast-like valve cells paralleled this greater deformation and collagen turnover in LAT. Comparison between regions of the valve revealed that the commissures had the highest collagen content, as well as the highest collagen and elastic fiber turnover and valve cell activation. Strong correlations between cell activation and matrix turnover markers suggest the role of myofibroblasts in the observed compositional heterogeneity. Additionally, leaflet length changes in SEPT and LAT paralleled compositional differences, suggesting a relationship between leaflet deformation and composition for the first time in the *in vivo* MV.

Characterization of Commissural Leaflets

This work also provided novel information regarding the structure and dynamic matrix composition of the commissural leaflets. The composition of these leaflets has been largely overlooked for decades, with one exception describing their collagen fiber alignment.¹⁶ In an extensive study of MV histology from 1956, it was noted that the “junctional” tissues of the normal MV are “anatomically and histologically not different from the rest of the valvular tissue.”¹⁷ In contrast, this study demonstrated that the commissures have significantly different structure and composition compared to the other MV segments. As a result, ANT-C and POST-C defy easy classification as resembling either SEPT or LAT, or even as resembling each other. In terms of collagen content, delineation of leaflet layers, and extent of muscle insertion, ANT-C resembled LAT and POST-C resembled SEPT. In terms of collagen turnover and cell activation, however, ANT-C more closely resembled SEPT (lower MMP13 and SMaA), and POST-C more resembled LAT. Significant differences in protein expression between ANT-C and POST-C (Col I, Col III, SMaA, and MMP13) suggest inherent differences between the two commissures. It is also noteworthy that MMP13, LOX, elastin, and SMaA were all greater in the commissures than in SEPT/LAT, which suggests that the commissural leaflets undergo some of the highest rates of remodeling across the entire MV. This finding could reflect differences between ANT-C/POST-C and SEPT/LAT in leaflet deformation; in the future, it will be important to attach markers to the valve in a manner that permits direct comparison of percent leaflet length change between ANT-C/POST-C and SEPT/LAT.

Differences in Leaflet Structure

Significant heterogeneity in composition between the different MV leaflets reflects their differences in structure as well as function. For instance, the SEPT leaflet showed greater abundance of Col I and III compared to LAT throughout the layers, but less collagen remodeling than in LAT. The amount of cardiac muscle present atop the proximal leaflet has not been previously reported, even though the general nature of the muscular and fibrous portions of the mitral annulus has been widely observed. Compared to SEPT, muscle was found to extend much further into the leaflets of LAT, ANT-C, and POST-C. This muscle tissue would likely impart significant contractility to these regions, and is consistent with greater changes in leaflet lengths across the cardiac cycle in LAT compared to SEPT. It is interesting to note that SEPT had significantly greater delineation of leaflet layers compared to LAT. Since a layered leaflet structure decreases the resistance to bending,⁹ this greater delineation of SEPT may functionally allow the SEPT leaflet to bend further compared to LAT, as previously reported.² Bending of SEPT is also likely aided by the thinness of the BL within the center “clear zone” of the anterior leaflet.

Relation between Leaflet Composition, Leaflet Deformation, and the Role of the Myofibroblast

While future work is required to further verify the relationship between leaflet deformation and composition, overall, these results suggest that there is a relationship between leaflet deformation during the cardiac cycle, levels of matrix turnover proteins, and valve cell activation towards the myofibroblast phenotype, as demonstrated by

comparisons between MV segments and regions, as well as direct statistical correlations. The finding of greater deformation in the mid-leaflet compared to the basal leaflet of SEPT is consistent with more rigorous modeling of *in vivo* marker data from similar such experiments,¹⁸ and was found to correlate to composition of these regions across animals. This work provides an important, initial *in vivo* validation for previous *ex vivo* aortic valve studies showing that leaflet strain leads to altered leaflet composition, such as increased collagen content and SMaA expression¹⁹ and altered MMP expression,²⁰ as well as multiple *in vitro* studies that have demonstrated altered matrix synthesis¹¹⁻¹³ and increased SMaA¹¹ by valve cells exposed to different strains or residing in valves experiencing different transvalvular pressures. The myofibroblast cell phenotype may contribute to the observed heterogeneity in composition. Myofibroblasts can sense and respond to their mechanical environment.²¹ These cells are also synthetic in nature, express abundant MMPs,²² and are contractile.¹⁰ Although this contractility does not occur at the time scale of the valve opening and closing, it does affect leaflet stiffness *in vitro*,²³ and could affect deformation. Therefore, this cell type may, at least in part, act as the link between the deformation experienced by a leaflet region and the composition of that region, as evident in this study. Taken together, these results suggest that the normal MV continually undergoes matrix remodeling in response to its mechanical environment, and that these processes may be mediated in part by cells demonstrating the myofibroblast phenotype.

Implications

The potential relationships between leaflet deformation and composition, while only partially characterized in this study, emphasize the need to restore normal leaflet deformation in valve repair procedures, such as through judicious design of annuloplasty rings. Restoring normal leaflet deformation could be important not only for preventing mitral regurgitation by proper leaflet coaptation, but also for maintaining normal leaflet composition, which in turn effects both leaflet material properties and could be important to the progression of various valve diseases. Indeed, the results from this study suggests that the myofibroblast could be key to this link between deformation and composition, and the myofibroblast is thought to be critical to the progression of myxomatous mitral valve disease.²² Furthermore, these results provide a more complete picture of the complexity of MV composition and structure. In particular there is growing interest in the commissural leaflets,^{24, 25} which have been far less characterized, yet may be relevant to the design of a tissue engineered mitral valve and in commissural repair procedures. Future studies are warranted to determine causative mechanisms of the relationship between *in vivo* deformation, cell phenotype, and matrix composition. It will also be important to investigate other aspects of the *in vivo* mechanical activity of the valve, such as flexure, shear, and coaptation, on regional leaflet composition and structure.

Limitations

While IHC is a powerful tool in determining localization and abundance of specific proteins, one of its limitations is the inherent variability of the technique, which was quantified to be 13.7% within batches and 16.5% between batches. Averaging of

duplicate sections and batch staining methods were performed to limit this variability. Similarly, while radiopaque markers allow precise determination of *in vivo* leaflet motion, limitations in the number and locations of marker placement did not allow measurement of commissural leaflet length changes or fully account for leaflet curvature. However, these leaflet length measurements did allow assessment of relative length changes necessary to examine the relationship between deformation and composition. While further work remains to better characterize this relationship between composition and deformation in the *in vivo* setting, this study represents an important step forward in that regard. Additionally, slight anatomic differences between the ovine and human MV²⁶ could affect translation of these data to human patients.

CONCLUSIONS

This study demonstrates significant compositional and cellular heterogeneity across the MV, and suggests a relationship between *in vivo* valve deformation, collagen turnover, and cell activation. Myofibroblast-like valve cells, which demonstrate contractile and synthetic capabilities, may contribute to both the observed compositional heterogeneity as well as the heterogeneity in leaflet deformation important for proper leaflet coaptation. In the future, the myofibroblast may be an important therapeutic target for diseases in which leaflet motion and composition are altered. Furthermore, it will be important for valve repair techniques and annuloplasty ring design to preserve this heterogeneity in leaflet strain and thereby attempt to prevent any further deterioration in leaflet composition that accompanies these disease processes.

This chapter, in which mitral annular composition was analyzed in relationship to *in vivo* changes in annular segment length, concludes the portion of normal valve heterogeneity studies addressing the relationship between normal valve composition and *in vivo* strains. The next two chapters (Chapters 10 and 11) address heterogeneity in the valvular interstitial cell (VIC) population. Specifically, in the next chapter a method for isolating the myofibroblast VIC subpopulation will be presented.

REFERENCES

1. Grigioni F, Enriquez-Sarano M, Zehr KJ, Bailey KR, Tajik AJ. Ischemic mitral regurgitation: long-term outcome and prognostic implications with quantitative Doppler assessment. *Circulation*. 2001;103(13):1759-1764.
2. Karlsson MO, Glasson JR, Bolger AF, Daughters GT, Komeda M, Foppiano LE, Miller DC, Ingels NB, Jr. Mitral valve opening in the ovine heart. *Am J Physiol*. 1998;274(2 Pt 2):H552-563.
3. Tsakiris A, Von Bernuth G, Rastelli G, Bourgeois M, Titus J, Wood E. Size and motion of the mitral valve annulus in anesthetized intact dogs. *J Appl Physiol*. 1971;30(5):611-618.
4. Chaput M, Handschumacher MD, Tournoux F, Hua L, Guerrero JL, Vlahakes GJ, Levine RA. Mitral leaflet adaptation to ventricular remodeling: occurrence and adequacy in patients with functional mitral regurgitation. *Circulation*. 2008;118(8):845-852.
5. Tsakiris AG, Gordon DA, Mathieu Y, Irving L. Motion of both mitral valve leaflets: a cinerentgenographic study in intact dogs. *J Appl Physiol*. 1975;39(3):359-366.
6. Sacks MS, Enomoto Y, Graybill JR, Merryman WD, Zeeshan A, Yoganathan AP, Levy RJ, Gorman RC, Gorman JH, 3rd. In-vivo dynamic deformation of the mitral valve anterior leaflet. *Ann Thorac Surg*. 2006;82(4):1369-1377.
7. Stephens EH, de Jonge N, McNeill MP, Durst CA, Grande-Allen KJ. Age-related changes in material behavior of porcine mitral and aortic valves and correlation to matrix composition. *Tissue Eng*. 2010;16(3):867-878.
8. Kunzelman KS, Cochran RP. Stress/strain characteristics of porcine mitral valve tissue: parallel versus perpendicular collagen orientation. *J Card Surg*. 1992;7(1):71-78.
9. Kunzelman KS, Cochran RP, Murphree S, Ring W, Verrier E, Eberhart R. Differential collagen distribution in the mitral valve and its influence on biomechanical behaviour. *J Heart Valve Dis*. 1993;2:236-244.
10. Messier RH, Jr., Bass BL, Aly HM, Jones JL, Domkowski PW, Wallace RB, Hopkins RA. Dual structural and functional phenotypes of the porcine aortic valve interstitial population: characteristics of the leaflet myofibroblast. *J Surg Res*. 1994;57(1):1-21.
11. Merryman WD, Youn I, Lukoff HD, Krueger PM, Guilak F, Hopkins RA, Sacks MS. Correlation between heart valve interstitial cell stiffness and transvalvular pressure: implications for collagen biosynthesis. *Am J Physiol Heart Circ Physiol*. 2006;290(1):H224-231.
12. Gupta V, Werdenberg JA, Mendez JS, Jane Grande-Allen K. Influence of strain on proteoglycan synthesis by valvular interstitial cells in three-dimensional culture. *Acta Biomater*. 2008;4(1):88-96.

13. Ku CH, Johnson PH, Batten P, Sarathchandra P, Chambers RC, Taylor PM, Yacoub MH, Chester AH. Collagen synthesis by mesenchymal stem cells and aortic valve interstitial cells in response to mechanical stretch. *Cardiovasc Res.* 2006;71(3):548-556.
14. Timek TA, Dagum P, Lai DT, Liang D, Daughters GT, Tibayan F, Ingels NB, Jr., Miller DC. Tachycardia-induced cardiomyopathy in the ovine heart: mitral annular dynamic three-dimensional geometry. *J Thorac Cardiovasc Surg.* 2003;125(2):315-324.
15. Stephens EH, Nguyen TC, Itoh A, Ingels NB, Jr., Miller DC, Grande-Allen KJ. The effects of mitral regurgitation alone are sufficient for leaflet remodeling. *Circulation.* 2008;118(14 Suppl):S243-249.
16. Cochran RP, Kunzelman KS, Chuong CJ, Sacks MS, Eberhart RC. Nondestructive analysis of mitral valve collagen fiber orientation. *ASAIO Trans.* 1991;37(3):M447-448.
17. Chiechi M, Lees W, Thompson R. Functional anatomy of the normal mitral valve. *J Thoracic Surg.* 1956;32(3):378-398.
18. Krishnamurthy G, Itoh A, Bothe W, Swanson JC, Kuhl E, Karlsson M, Craig Miller D, Ingels NB, Jr. Stress-strain behavior of mitral valve leaflets in the beating ovine heart. *J Biomech.* 2009.
19. Balachandran K, Konduri S, Sucusky P, Jo H, Yoganathan A. An ex vivo study of the biological properties of porcine aortic valves in response to circumferential cyclic stretch. *Ann Biomed Eng.* 2006;34(11):1655-1665.
20. Balachandran K, Sucusky P, Jo H, Yoganathan AP. Elevated cyclic stretch alters matrix remodeling in aortic valve cusps: implications for degenerative aortic valve disease. *Am J Physiol Heart Circ Physiol.* 2009;296(3):H756-764.
21. Wang J, Chen H, Seth A, McCulloch CA. Mechanical force regulation of myofibroblast differentiation in cardiac fibroblasts. *Am J Physiol Heart Circ Physiol.* 2003;285(5):H1871-1881.
22. Rabkin E, Aikawa M, Stone JR, Fukumoto Y, Libby P, Schoen FJ. Activated interstitial myofibroblasts express catabolic enzymes and mediate matrix remodeling in myxomatous heart valves. *Circulation.* 2001;104(21):2525-2532.
23. Merryman W, Huang H, Schoen F, Sacks M. The effects of cellular contraction on aortic valve leaflet flexural stiffness. *J Biomech.* 2006;39(1):88-96.
24. Quill JL, Hill AJ, Laske TG, Alfieri O, Iaizzo PA. Mitral leaflet anatomy revisited. *J Thorac Cardiovasc Surg.* 2009;137(5):1077-1081.
25. Aubert S, Barreda T, Acar C, Leprince P, Bonnet N, Ecochard R, Pavie A, Gandjbakhch I. Mitral valve repair for commissural prolapse: surgical techniques and long term results. *Eur J Cardiothorac Surg.* 2005;28(3):443-447.
26. Walmsley R. Anatomy of human mitral valve in adult cadaver and comparative anatomy of the valve. *Br Heart J.* 1978;40(4):351-366.

Chapter 10: Fibronectin-Based Isolation of Valvular

Interstitial Cell Subpopulations: Relevance to Valve Disease

The work contained in this chapter continues the topic of normal valve heterogeneity and specifically addresses heterogeneity in the valvular interstitial cell (VIC) population. In this chapter a method for separating the myofibroblast VIC subpopulation is presented.

ABSTRACT

Background: Myxomatous mitral valves (MVs) contain elevated proportions of unique cell populations such as myofibroblasts. Without a reliable technique to isolate such cell populations, however, it has been difficult to study the role of these cells. The goal of this study was to use fibronectin (FN) to isolate distinct cell subpopulations from normal porcine MVs.

Methods: Cells from porcine posterior MV leaflets were separated based on time-dependent adhesion to either tissue culture plastic (TCP) flasks or FN-coated flasks. The resultant “FAST” and “SLOW” adhering subpopulations from each technique were phenotyped using flow cytometry and immunocytochemistry to detect expression of myofibroblast markers, enzymes for collagen synthesis, and mitogen-activated protein kinases.

Results: Compared to FN SLOW, FN FAST showed significantly higher expression of prolyl 4-hydroxylase, heat shock protein-47 (HSP47), smooth muscle alpha-actin (SMaA), non-muscle myosin (Smem), extracellular-related signaling kinase (ERK) 1, ERK2, and phosphorylated-ERK. In contrast, TCP FAST showed higher expression of only HSP47, SMaA, and Smem compared to TCP SLOW.

Conclusions: Differential adhesion to FN successfully separated a myofibroblast-like subpopulation from the posterior leaflet of the MV. This subpopulation may be useful in studying myxomatous MV disease, although additional studies remain to verify that this myofibroblast-like population resembles that observed in myxomatous MV disease.

The work contained in this chapter was published as:

Stephens EH, Huynh TN, Cieluch JD, Grande-Allen KJ. **Fibronectin-Based Isolation of Valve Interstitial Cell Subpopulations: Relevance to Valve Disease.** *Journal of Biomedical Materials Research A.* 2010;92(1):340-9.

INTRODUCTION

While myofibroblasts are known to be involved in disease processes in multiple tissues including the kidney,^{1,2} lung,³ pancreas,⁴ and heart valves,⁵ it has been difficult to isolate these cell subpopulations from valves to allow their systematic study. In order to develop novel medical treatments for these diseases, it will be important to understand the phenotypic regulation of the cells involved and how these cells contribute to disease progression. The myofibroblast-like valve cell phenotype in particular is common to a number of valve diseases and thought to be influential in the development and progression of diseases such as myxomatous degeneration.^{5, 6} Numerous publications have described the valvular interstitial cells as a heterogeneous population with some fibroblastic-like cells and others that appear more myofibroblastic-like.⁷⁻⁹ The myofibroblast-like valve cell, when characterized in situ or induced via treatment with transforming growth factor- β , is marked by greater production of matrix, expression of matrix metalloproteases, expression of muscle related markers, and contractility.^{5, 6, 10} Furthermore, many of the valve diseases that are characterized by altered proportions of distinct cell phenotypes also contain altered composition of valvular extracellular matrix.^{5, 11} It was therefore hypothesized that matrix components could be used to isolate specific valvular interstitial cell (VIC) subpopulations, which are critical for further studies regarding the etiology and treatment of valve diseases. It was the general goal of this study to develop a matrix-based technique for the isolation of this myofibroblast-like cell phenotype.

Previous studies from our laboratory explored the utility of two related methods to isolate the myofibroblast subpopulation from aortic valve cells:¹² differential detachment

(trypsinization) from tissue culture plastic (TCP) and differential adhesion to TCP. Although it was observed that these two methods yielded similar cell subpopulations,¹² it was speculated that the detachment method could cause the loss of the very proteins that make this adhesive population unique. It was further speculated that differences in adhesiveness could be the basis for phenotypic differences among VICs;¹² therefore, this study was developed to investigate the nature of differentially adherent cells. In addition, our previous study used only one phenotypic marker, smooth muscle alpha-actin (SMaA), whereas this study involved a much more comprehensive assessment of cell phenotypes. Furthermore, the present study utilized VICs harvested from the posterior leaflet of the mitral valve, since these cells will be more relevant to future studies of the mechanisms of myxomatous mitral valve disease (which primarily affects the posterior leaflet).

Most importantly, this study investigated the phenotypes of cell subpopulations resulting from differential adhesion to fibronectin, a protein that is relevant to both normal and diseased cell-matrix interactions and is present in both normal and myxomatous valves.^{10, 13, 14} Fibronectin was evaluated for this matrix-based technique to isolate myofibroblasts for several reasons. Myofibroblasts are known to exert force on their adhesive substrates through fibronectin-linked, enlarged focal adhesions (also known as the fibronexus).^{15, 16} It was thus hypothesized that the myofibroblast subpopulation within a mixture of primary cultured VICs would adhere to fibronectin more strongly than other VIC phenotypes. Fibronectin is also more abundant in injured and regenerating tissues.¹⁷⁻²² In renal fibroblasts, for example, differentiation to the myofibroblast phenotype results in extracellular fibronectin accumulation.²³ In heart

valves, it has been shown that activated VICs remodel the orientation of fibronectin fibers in the matrix.⁶ Furthermore, fibronectin has been associated with valve cell “injury” in that VICs that migrate into a region devoid of cells (using a scrape wounding *in vitro* model) then secrete fibronectin.²⁴ For these reasons, fibronectin may be an appropriate matrix component to serve as the basis for isolating myofibroblastic VICs associated with valve injury.

Therefore, the purpose of this investigation was to compare the utility of fibronectin-coated vs. uncoated tissue culture plastic for differential adhesion-based isolation of the myofibroblast-like subpopulation of VICs. Following cell separation on these two substrates, flow cytometry and immunocytochemistry were used to assess a number of phenotypic characteristics relevant to myofibroblasts.

METHODS

Isolation of Valvular Interstitial Cells

This investigation utilized cultured VICs, which have been previously reported to demonstrate phenotypes largely representative of valve cells *in vivo*⁸ and to maintain aspects of this phenotype over multiple passages.²⁵⁻²⁷ These VICs were cultured from porcine valves, a widely used, anatomically comparable model for human heart valves.^{10, 28-31} Porcine hearts from healthy 6-month-old pigs were purchased from Fisher Ham and Meats, Spring Cypress, TX, USA; valves from several hearts were pooled together (between 3–10 hearts per cell harvest) were harvested for primary culture according to standard methods.³²⁻³⁴ Valve tissues were pooled to limit potential effects of inherent variability between animals. The isolation of primary cells from pooled valve tissues was

performed on at least six different occasions. The posterior leaflets of the mitral valves were dissected from the hearts, trimmed of attached chordae, placed in 2 mg/mL collagenase II (Worthington Biochemical Corp., Worthington, VA) in serum-free Dulbecco's modified Eagle's medium (Mediatech, Herndon, VA) containing 1% antibiotic/antimycotic/antifungal solution (Mediatech), and incubated in a shaker for 20 min (37°C, 140 rpm).³⁴ Afterwards, the loosened endothelial cells were removed by wiping the leaflet surfaces with sterile cotton swabs. The tissues were then finely minced and dissociated in a solution of collagenase II and hyaluronidase (1 mg/ml and 0.1 mg/mL, respectively in serum-free medium) in an incubated shaker for 4 hours. The resulting VICs were counted, seeded in tissue culture flasks at a density of 10,000 cells/cm², and maintained at 37°C, 95% humidity, and 5% CO₂. Cells were grown in medium containing 10% bovine growth serum (BGS, HyClone, Logan, UT) and 1% antibiotic/antimycotic/antifungal solution and passaged after reaching 90% confluence. Experiments were performed on cells between their first and third passages.

Isolation of Subpopulations

VICs were separated into subpopulations based on adhesion time to either uncoated or fibronectin-coated tissue culture plastic (TCP). Primary cultures of VICs were removed from culture plates using trypsin, pelleted, and resuspended in 10 ml of media. These VICs were then seeded into an uncoated TCP T-75 flask (Fig. 10-1, flask #1) and incubated. After 30 minutes approximately 20% of the cells had adhered to the flask. The media and unattached cells were then removed from flask #1 and placed into a new T-75 flask (flask #2) while fresh media was added to flask #1. After 2 more hours,

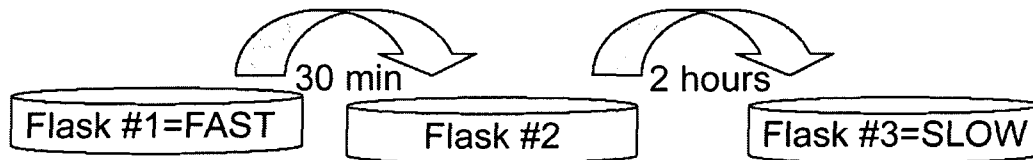


Fig. 10-1: Schematic illustrating the process of isolating subpopulations from plastic flasks. The same method was used for subpopulations isolated from fibronectin-coated flasks, except with different time increments.

the unattached cells and media from flask #2 were removed and seeded into a new T-75 flask (flask #3). The subpopulation that adhered within 30 min (in flask #1) was called TCP FAST, while the population that had not adhered after 2.5 hours (grown in flask #3) was called TCP SLOW. While the TCP SLOW population may have been exposed to an increased number of dead cells, previous studies of viability and phenotype of valve cells after various durations of ischemia suggest that it would be unlikely for the presence of non-viable cells to alter the phenotype and viability of the surviving cells.³⁵ The same procedure was repeated with VICs on fibronectin (FN)-coated TCP flasks (Becton Dickinson, Franklin, NJ) but the time intervals were shortened because VICs adhered to FN-coated flasks faster than to normal TCP flasks. Therefore, in the case of FN-coated flasks the subpopulation that adhered within the first 15 minutes was called FN FAST and the subpopulation that adhered after 1.5 hours was called FN SLOW. To demonstrate repeatability, this adhesion-based separation process was performed on six separate groups of primary cell cultures. Cells attached to the #2 flasks were considered to have an intermediate rate of adhesion and a mixed phenotype (neither distinctly FAST nor SLOW), and were discarded.

Adhesion of Subpopulations to TCP

Each of the separated VIC subpopulations (FN FAST, FN SLOW, TCP FAST, TCP SLOW) was seeded within quadruplicate wells of a TCP 6-well plate at a density of 4.0×10^4 cells/cm². Control cells, which were primary cells (harvested as described above from the pooled valve tissues) that had not been subjected to the separation process, were seeded in identical conditions. After 30 min, 90 min, 150 min, and 24 hours, the medium containing the unadhered cells were removed and the adherent cells were trypsinized and counted using trypan blue staining and a hemocytometer.

Flow Cytometry

The various adhesive VIC subpopulations (FN FAST, FN SLOW, TCP FAST, TCP SLOW) were evaluated using flow cytometry to assess their expression of several phenotypic characteristics. These markers included prolyl 4-hydroxylase (P4H, Chemicon, Temecula, CA) and heat shock protein-47 (HSP47, Abcam, Cambridge, MA), both markers of active collagen synthesis; smooth muscle alpha-actin (SMaA, Dakocytomation, Denmark), non-muscle myosin heavy chain (Smem, GeneTex, San Antonio, TX and Covance, Berkeley, CA), which are markers of VIC activation and the myofibroblast phenotype; smooth muscle myosin (SMM, Sigma, St. Louis, MO), which differentiates myofibroblasts from smooth muscle cells; and extracellular signal-regulated kinase (ERK)-1, ERK2, and p-MAP kinase1/2 (pERK, Chemicon). ERK1, ERK2, and pERK are all signaling proteins in the mitogen-activated protein (MAP) kinase pathway that are involved in fibroblast activation to myofibroblast in a number of tissues,^{23, 36-38} and have been shown to be responsive to tension such as that the cell experiences during

adhesion.^{39, 40} These proteins are also related to the production of matrix metalloproteases, which are abundant in myxomatous mitral valves.⁴¹

In preparation for flow cytometry, after 2-4 days, the separated VIC subpopulations were trypsinized, counted, washed twice with 10 ml of PBS, and placed in fixative (1% paraformaldehyde in PBS) at 2.00×10^6 cells/ml. After 1 hour, the fixed cells were incubated in permeability buffer (0.1% Triton-X 100 in PBS; 1 ml per 1×10^6 cells) for 10 minutes. Separate tubes containing 1×10^6 cells were prepared for each antibody and for a negative isotype control (to be treated with IgG and secondary antibody only). An additional tube of cells, which would remain untreated, was prepared for a “blank” control and used for gating purposes. The cells were mixed with 1 mL of flow cytometry (FC) buffer (PBS containing 0.5% BSA, 0.05% sodium azide), then pelleted by centrifuging for 1 minute at 13,200 rpm. The cells were then incubated in 100 μ L of primary antibody (or IgG for controls) for 1 hour on ice, then mixed with 1 mL of FC buffer and pelleted by centrifuging for 1 minute at 13,200 rpm. Next, the cells were mixed with 100 μ L of FITC-conjugated secondary antibody and stored in the dark. After 1 hour, 500 μ L of FC buffer was added, samples were spun for 1 minute at 13,200 rpm, and the supernatant was decanted. The pellet was resuspended in 250 μ L of FC buffer and transferred to 5 ml tubes.

A FACScan flow cytometer with Cell Quest Pro software (Becton Dickinson) was used for data acquisition and analysis. Data was gated based on size (forward scatter), complexity (side scatter), and non-specific fluorescence following calibration with the isotype control samples and unstained samples. The fluorescence-based gate was set such that less than 1% of the non-specific fluorescence fell within the gate. Data reported

includes only that located within the above gates. Each sample was analyzed at least twice to confirm the mean fluorescence values, which has been shown to be proportional to the number of proteins on the cells.⁴² Flow cytometry measurements were performed three times on VIC subpopulations from 3 different adhesion-based separations. Data was reported as an average of all 3 measurements.

Immunocytochemistry

Cells from the 4 different adhesive subpopulations were seeded at a density of 5,000 cells/cm² on glass microscope slides and maintained in medium/10% serum/1% antibiotic solution in an incubator. After 2 days, the cells were rinsed with PBS and fixed in 100% acetone at room temperature. The slides were incubated in a solution containing 5% goat serum in PBS for 1 hour to block non-specific binding. The slides were then incubated in primary antibodies that were diluted in PBS containing 1% bovine serum albumin and 0.1% TritonX-100 (Roche Diagnostics, Mannheim, Germany). Antibodies used were the same as those in the flow cytometry assessment as well as vimentin (Dako). All primary antibodies were diluted 1:100 except for vimentin (1:200). After washing three times in PBS, the slides were incubated in appropriate secondary antibodies for 1 hour (goat anti-mouse and anti-rabbit IgG FITC, Jackson ImmunoResearch, West Grove, PA, 1:100 dilution). Negative controls were prepared without primary antibodies but with secondary antibodies. The slides were washed three times with PBS, drained, mounted with Vectashield with DAPI (Vector Laboratories, Burlingame, CA), coverslipped, and sealed. This staining procedures and the imaging described below were repeated three times on three different batches of subpopulations.

The stained slides used for quantification of fluorescence were imaged using the 10X and 20X objectives of an Axioplan fluorescent microscope (Zeiss, Thornwood, NY) and Metamorph software (Molecular Devices, Sunnyvale, CA). Three 20X images were taken from non-overlapping, randomly chosen regions of each slide. The total number of cells in each image was manually and automatically counted using the DAPI nucleic acid marker. The results of manual and automatic counting were comparable (data not shown), therefore, the automatic count was applied to all samples. All images for the same marker were obtained using identical acquisition parameters in one imaging session. Cells staining positive were evaluated to obtain the fluorescence intensity per pixel (from 0 to 4025, where 4025 was the highest fluorescence.) The background intensity, due to non-specific binding, was eliminated by establishing a threshold of 700-800. Once the threshold had been applied, the integrated intensity of an area was divided by the number of nuclei in that same area to give the average intensity per cell.

Preliminary Analysis of Human Myxomatous Valves and VICs

In a preliminary translation of these methods to human valve studies, these FN and TCP-based subpopulation isolation techniques were also performed on VICs isolated from 4 human myxomatous mitral valves. Myxomatous mitral valve specimens were obtained from 4 patients after surgery to correct severe mitral regurgitation due to a prolapsing valve. These four patients (3 females aged 50, 61, and 69 years old and one 59 year-old male) underwent quadrilateral resection of the posterior leaflet and implantation of an annuloplasty ring. These tissues were obtained from the Cooperative Human Tissue Network and their use was authorized by the Institutional Review Board.

Following the adhesive separation process on passage 4-5 cells, the 4 human VIC subpopulations were subjected to flow cytometry analysis for SMAA, Smem, pERK, and ERK2.

We also performed immunohistochemistry to confirm the presence of fibronectin in human normal and myxomatous mitral valve leaflets. Posterior leaflets from four myxomatous mitral valves (mean patient age 65.0 ± 10.5) removed during valve repair surgery and three normal valves (no history of cardiac disease, mean subject age 64.7 ± 14.5) removed at autopsy were formalin-fixed, paraffin-embedded, and sectioned to a thickness of 5 μm . Slides were stained using an antibody to fibronectin (Chemicon, Temecula, CA) after citrate-based antigen retrieval, visualized using Vectastain Elite ABC and diaminobenzidine kits (Vector Laboratories, Burlingame, CA), and counterstained with hemotoxylin (Richard-Allan Scientific, Kalamazoo, MI). The use of these valve tissues for research was approved by the Institutional Review Board.

Statistical Analysis

Multifactorial analysis of variance was performed using SigmaStat software (SPSS, Chicago, IL), as described in Chapter 4. The Holm-Sidak all-pairwise multi-comparison method was used for post-hoc testing. Statistical comparisons of immunocytochemical data, as well as the myxomatous cell flow cytometry data because of the limited nature of that data set, were performed using a student's paired t-test and the same level of significance (0.05).

RESULTS

Confirmation of FAST and SLOW Subpopulations Adhesion Rate

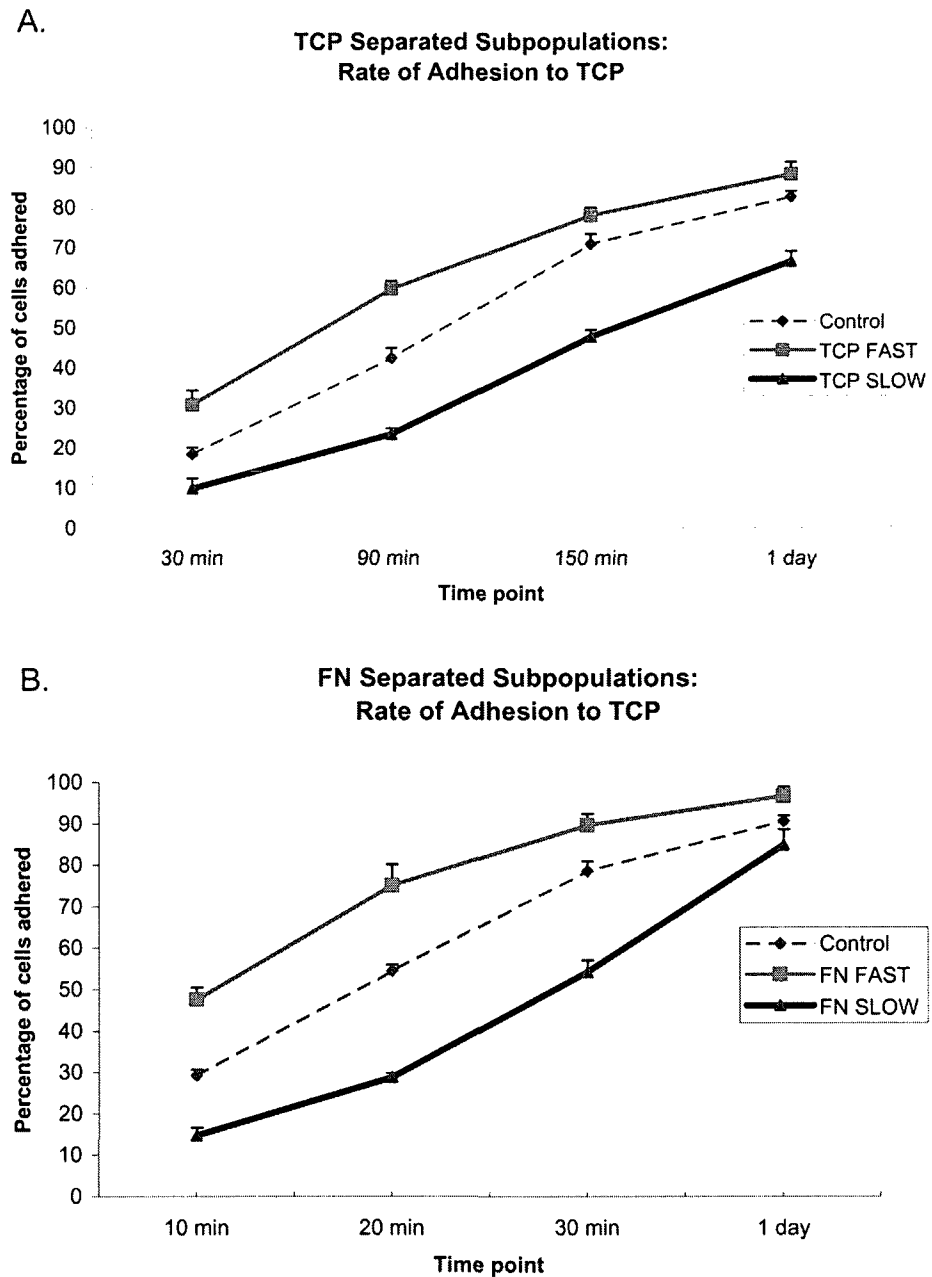


Fig. 10-2: A) Adhesion to TCP over time using subpopulations previously separated using TCP. B) Adhesion to TCP over time using subpopulations previously separated using FN-coated flasks. Our laboratory has previously reported that such VIC subpopulations retain their adhesive properties over multiple passages.¹²

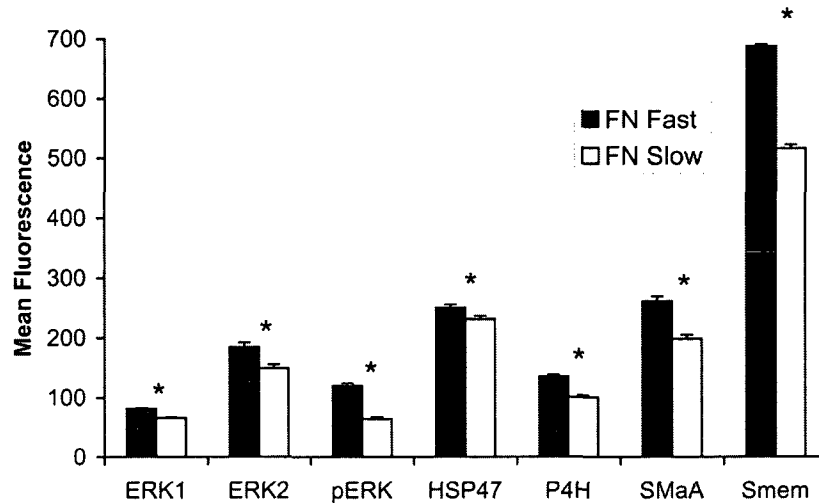
After the TCP and FN separation techniques were performed, the resulting subpopulations' adhesion rates to TCP were evaluated to confirm that distinctly adherent FAST and SLOW subpopulations had been generated (Fig. 10-2A, B). For both the FN and TCP separation techniques, the FAST cells adhered more rapidly than did the SLOW cells, and both were different from the control (unseparated cells). Furthermore, the final percentage of cells adhered in the FAST subpopulations was higher than the SLOW subpopulation for both surfaces. Lastly, the final percentage of adhered cells for FN FAST was higher than TCP FAST and similarly the final percentage of adhered cells for FN SLOW was higher than TCP SLOW.

Flow Cytometry – Porcine VICs

Compared with the cells that adhered slowly to fibronectin (FN SLOW), the cells that adhered quickly to fibronectin (FN FAST) showed significantly higher expression of the markers of collagen synthesis P4H ($p < 0.001$) and HSP47 ($p = 0.043$), markers of the myofibroblast phenotype SMaA ($p < 0.001$) and Smem ($p = 0.002$), and proteins in the MAP kinase pathway ERK1 ($p = 0.005$), ERK2 ($p = 0.011$), and pERK ($p < 0.001$) (Fig. 10-3A). In contrast, following differential adhesion to tissue culture plastic, only ERK1 was significantly different between the fast and SLOW subpopulations ($p < 0.001$), and in fact was lower in the TCP FAST group (Fig. 10-3B). There were also trends of increased ERK2 and pERK expression in the TCP FAST cells compared to the TCP SLOW cells ($p = 0.074$ and $p = 0.064$ respectively). SMM expression was negligible in all groups, confirming that these isolated cells were not smooth muscle cells.^{5, 43, 44} These same

expression patterns were found in all replicate flow cytometry measurements, regardless of whether the cells had been cultured for 2 or 4 days following the subpopulation separation procedure.

A. FC Marker Fluorescence for FN Differential Adhesion Subpopulations



B. FC Marker Fluorescence for TCP Differential Adhesion Subpopulations

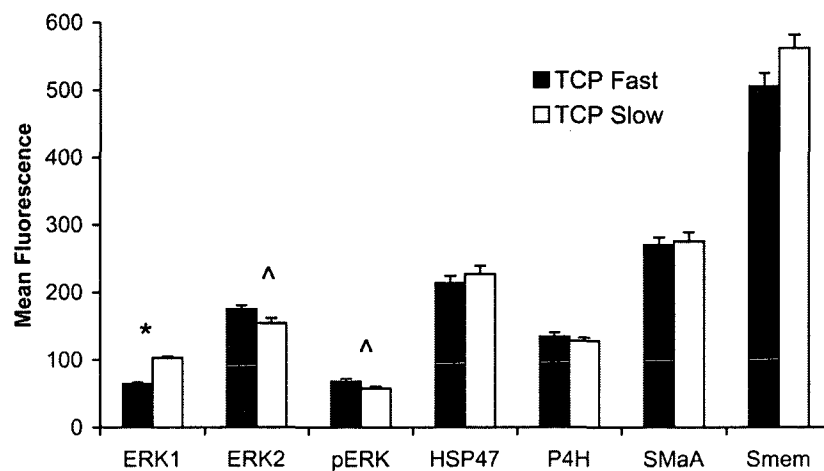


Fig. 10-3: A) Flow cytometry marker fluorescence of TCP differential adhesion subpopulations. Error bars indicate standard error of the mean, as the graph includes data from 3 independent experiments. $*=p<0.05$. B) Flow cytometry marker fluorescence of FN differential adhesion subpopulations. Error bars indicate standard error of the mean, as the graph includes data from 3 independent experiments. $*=p<0.05$, $\wedge=p<0.075$.

When comparing the FN FAST group to the TCP FAST, both of which were the ~20% most adhesive VICs isolated from the posterior leaflet, the FN FAST cells showed higher expression of two markers, ERK1 ($p=0.0002$) and Smem ($p=0.0001$). In contrast, when comparing the two least adherent VIC subpopulations, those separated using fibronectin had lower expression of ERK1, pERK, and SMAA than the TCP SLOW ($p\leq 0.002$).

Flow Cytometry and Immunohistochemistry – Human Myxomatous Valves

In the small group of human VIC subpopulations, FN FAST tended to show greater expression of the markers SMAA, NMM, pERK, and ERK2 compared to FN

A. Differential Marker Expression in Human Myxomatous Valve Cell Subpopulations

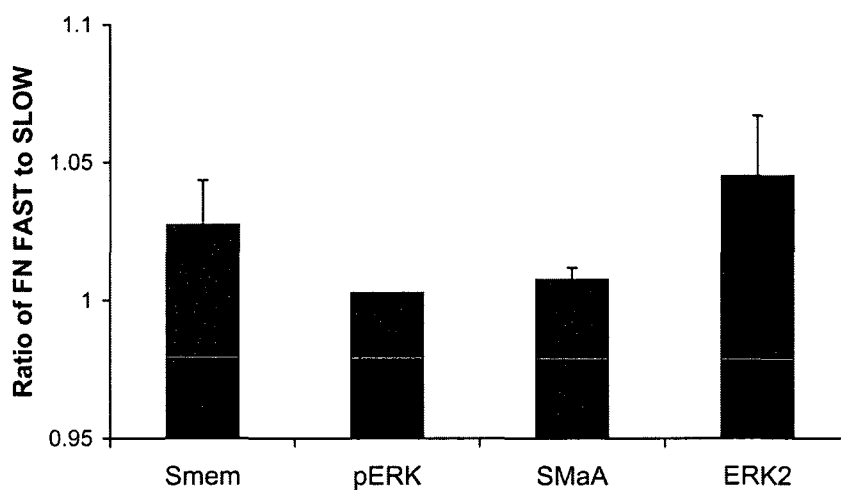


Fig. 10-4A: Ratio of FN FAST to FN SLOW flow cytometry marker mean fluorescence for human myxomatous VIC subpopulations. Error bars indicate standard error of the mean.

B.

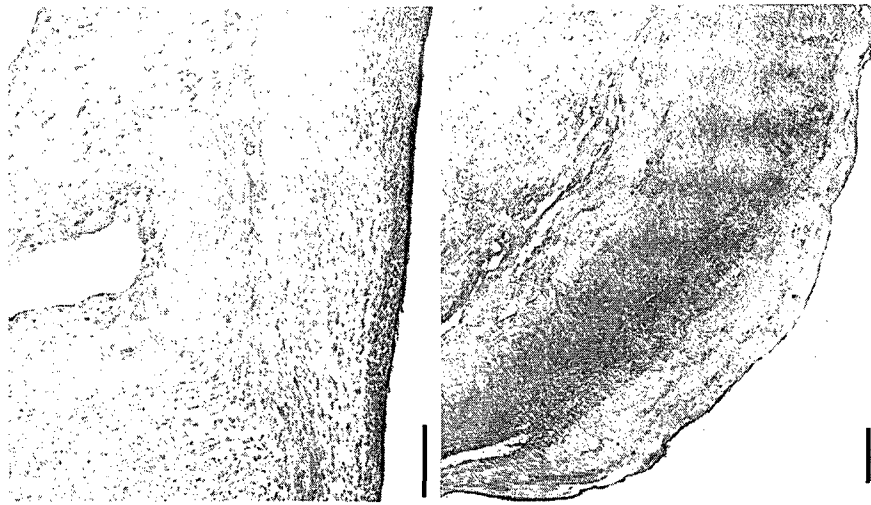


Fig. 10-4B: Immunohistochemical staining illustrates the presence of fibronectin in both normal (left, 79 year-old male) and myxomatous heart valves (right, 70 year-old male). Scale bar represents 200 μ m.

SLOW (Fig. 10-4A, $p=0.064$ by paired t-test). However, no difference was detected between TCP FAST and TCP SLOW ($p=0.452$). Immunohistochemical staining of a representative set of myxomatous and normal posterior mitral valve leaflets demonstrated positive staining for FN in all samples (Fig. 10-4B).

Immunocytochemistry

Immunocytochemical results were similar to the flow cytometry results. In immunocytochemistry FN FAST showed higher expression of ERK2 ($p<0.001$), pERK ($p<0.001$), HSP47 ($p<0.006$), SMaA ($p<0.01$), and Smem ($p<0.001$) compared to FN SLOW (Fig. 10-5A), while the TCP subpopulations were not as markedly different with

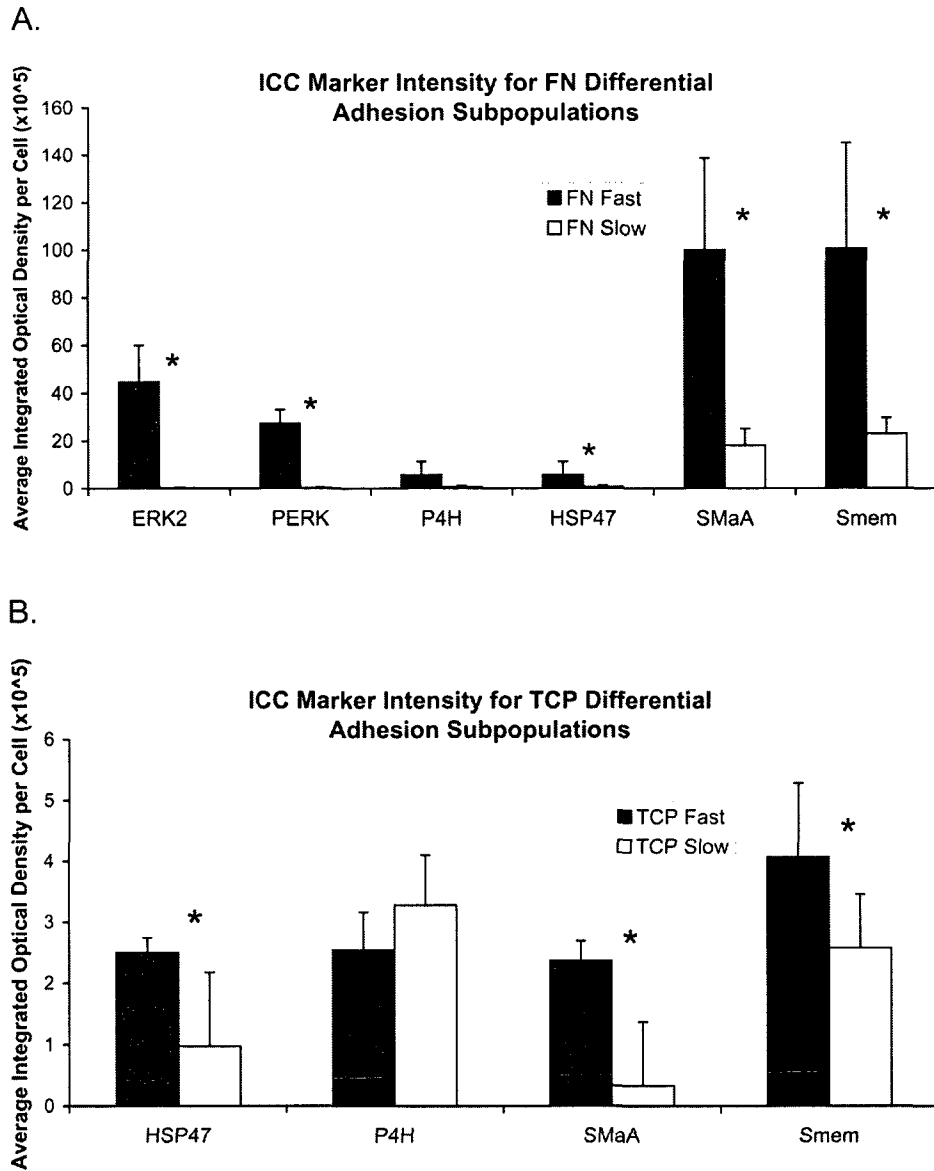


Fig. 10-5: A) Immunocytochemistry marker integrated optical density per cell of TCP differential adhesion subpopulations. Error bars indicate standard deviation, as the graph includes data from one representative experiment. Data between experiments showed the same differences between cell subpopulations, but varied in integrated optical density. $*=p<0.05$. B) Immunocytochemistry marker integrated optical density per cell of FN differential adhesion subpopulations. Error bars indicate standard deviation, as the graph includes data from one representative experiment. Data between experiments showed the same differences between cell subpopulations, but varied in integrated optical density. $*=p<0.05$.

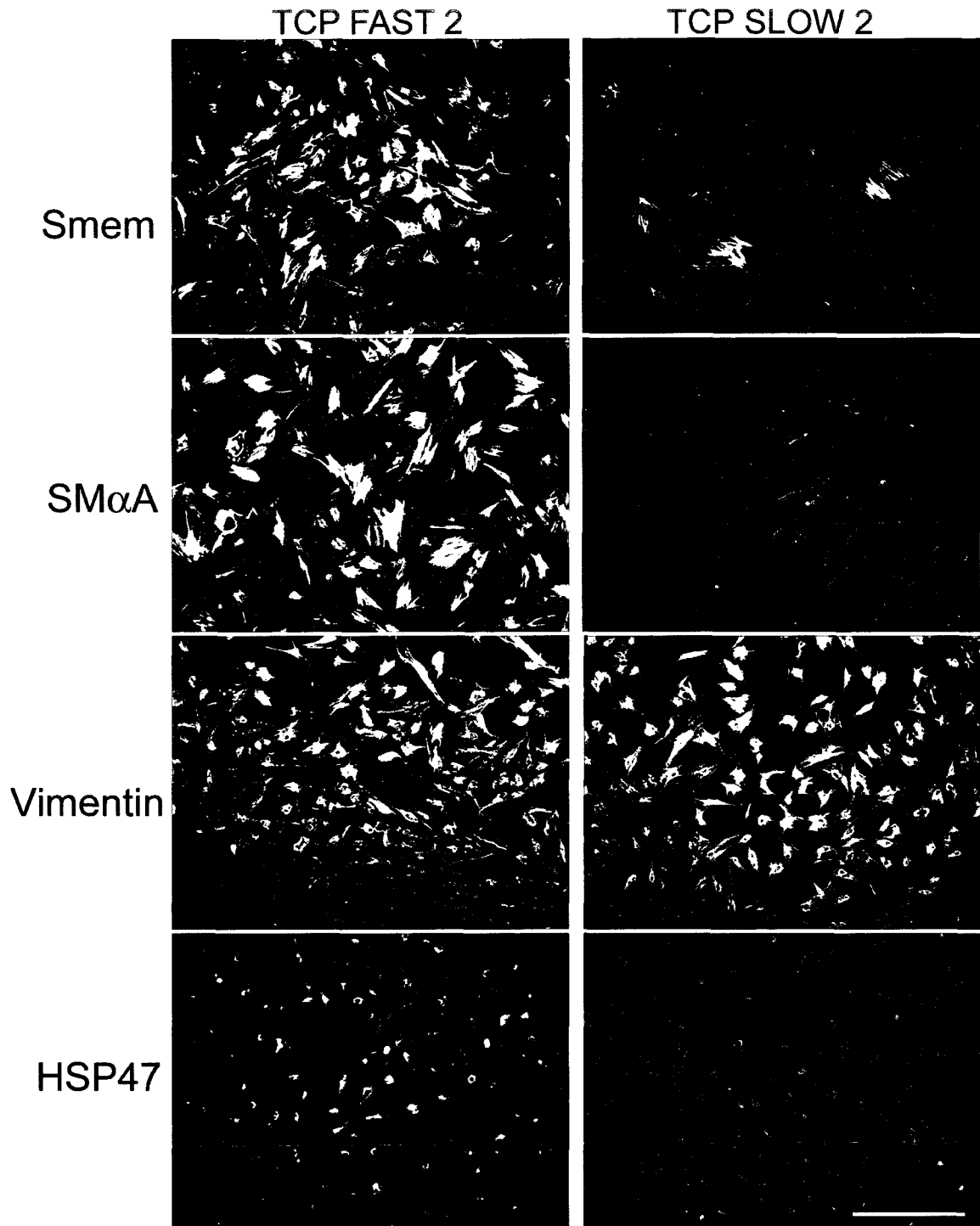


Fig. 10-6: Representative images of immunocytochemistry for given markers on TCP differential adhesion subpopulations. Images were captured using 10X objective. Scale bar represents 100 μ m and applies to all images.

TCP FAST only having higher expression of HSP47 ($p=0.021$), SMaA ($p<0.001$), and Smem ($p<0.001$) in TCP FAST compared to TCP SLOW (Figs. 10-5B and 10-6). Although the immunocytochemical data from different cell labeling preparations and different cell subpopulation separations could not be averaged because of possible variations in staining and imaging parameters, the statistically significant differences between subpopulations were consistent across experiments.

DISCUSSION

Differential adhesion to fibronectin was successful in isolating VICs with an activated, myofibroblast-like phenotype as evidenced by greater expression of myofibroblast-related markers by the FN FAST subpopulation compared to FN SLOW. Although the phenotyping presented in this paper was performed on freshly isolated subpopulations, our previous studies have shown that subpopulations retain their adhesive and phenotypic properties over multiple passages.¹² Therefore, this method may be an effective means of isolating the myofibroblast-like valve cell population for further study. Overall, these results confirmed and extended the results of our previous subculturing study.¹² These cells that adhered the most rapidly to fibronectin demonstrated stronger expression of Smem as well as other proteins associated with the myofibroblast phenotype including markers of collagen synthesis^{10, 45} and the MAP kinase pathway.⁴⁶⁻⁴⁸ While the mechanism behind the differential adhesive properties these VIC subpopulations is still under investigation, myofibroblasts expressing SMaA have been shown to exert stronger forces than their SMaA-negative counterparts,^{49, 50} a feature that is attributed to more abundant cell-matrix contacts,⁵¹ isoform-specific

terminal peptide adhesions,⁵² and specialized, enlarged focal adhesions incorporating unique proteins such as tensin.¹⁵

The findings that the VICs that were more adhesive to fibronectin showed the greatest expression of the myofibroblast markers, compared to tissue culture plastic, suggests that the fibronectin aids in promoting the myofibroblast phenotype. Fibronectin was utilized in this study because it is present throughout mitral valve leaflets (Fig. 10-4) and chordae¹⁴ and because it is involved in myofibroblast adhesion.^{15, 16} Others have shown that adhesion to fibronectin causes fibroblasts to differentiate towards the myofibroblast phenotype²¹ and that VICs cultured on fibronectin-coated plates had significantly higher SMaA expression compared to VICs cultured on TCP.⁵³ Therefore, it is possible that the fibronectin coating both enables the separation of cell subpopulations and manipulates the cell phenotype of the cells that adhere. Given that the FN SLOW cells did not become myofibroblast-like, we speculate that the ability of fibronectin to potentiate activation of the myofibroblast phenotype is specific to certain cell types. The slow to adhere cells may represent a more true fibroblastic phenotype.

Our demonstration that the abundance of unphosphorylated and phosphorylated ERK was more abundant in the FN FAST cells is promising given that the activation of valve cells to myofibroblasts is thought to occur via the MAP kinase pathway. Correspondingly, it was recently shown that the use of heparin to prevent the activation of the FGF2 receptor complex, which inhibits MAP kinase, resulted in an increase in the myofibroblast phenotype of VICs.⁵⁴ The link between MAP kinase pathway activation and SMaA has been shown in VICs⁴⁶⁻⁴⁸ as well as cardiac fibroblasts,³⁶ and the role of the MAP kinase pathway in fibroblast activation to myofibroblasts has been shown in

cells derived from a number of tissues including vascular adventitia,³⁸ liver,³⁷ and kidney²³ among others.

Both immunocytochemistry and flow cytometry showed that differential adhesion to fibronectin (*vs.* TCP) resulted in a more definitive isolation of the myofibroblast phenotype. However, there were some differences between the results of these two assessment methods. The difference in SMAA expression between TCP FAST and TCP SLOW was detected by immunocytochemistry, but not by flow cytometry. On the other hand, the greater expression of ERK1, ERK2, and pERK by the TCP FAST cells (*vs.* TCP SLOW) was only detected by flow cytometry, as was the greater ERK1 expression in FN FAST compared to FN SLOW. Some differences are to be expected between the results of these two methods given that in each technique the cells are in different adhesive states. In immunocytochemistry the cells are actively attached to a surface, while in flow cytometry the cells have been removed from their surface. The process of the cells removal and the cells' adhesive state may affect the states of signaling. It should also be noted that in immunocytochemistry, the tested cells had been cultured on glass for several days, rather than TCP or FN-coated flasks as in the case of the cells tested by flow cytometry. This difference in cell substrate could have also contributed between differences in results between flow cytometry and immunocytochemistry, as substrate stiffness has been shown to alter fibroblast⁵⁵ and valve cell phenotype,²⁷ and given that glass is significantly stiffer than TCP.⁵⁶ Interestingly, in the present study the TCP FAST cells did not show significantly higher expression of SMAA by flow cytometry as was found in the previous study. This discrepancy may be because mean fluorescence after gating was used to assess marker expression in flow cytometry rather than the median

fluorescence as was done in the last study. For both immunocytochemistry and flow cytometry, it would be beneficial to use a multi-labeling/imaging technique to determine which markers are expressed together on a given cell.

Fibronectin often serves as a substrate in a number of cell-matrix adhesions including focal adhesions and fibrillar adhesions. These two types of adhesions are quite different structurally. Focal adhesions are large rod-shaped complexes and contain a number of cytoplasmic plaque proteins.^{57, 58} In contrast, fibrillar adhesions are smaller consisting mainly of $\alpha_5\beta_1$ integrins and tensin, lacking the cytoplasmic plaque proteins found in focal adhesions.^{57, 58} Based on these structural differences it is likely that these two types of adhesions have significant differences in function. Fayet et al. have recently shown that VICs growing in monolayers form fibrillar adhesions at the edges of a scrape wound “injury.”²⁴ Future studies into this FN-based separation technique could involve using antibodies unique to fibrillar adhesions to determine if this differential adhesion method is separating the cell population principally based on focal adhesions or fibrillar adhesions, or both. Characterizing the specific method of isolation in relation to these two types of adhesions could have important implications for normal and diseased VIC-matrix interactions. Indeed, given that fibrillar adhesions form in response to VIC injury,²⁴ investigating proteins specific to fibrillar adhesions, such as tensin, may be useful in characterizing this myofibroblastic, injury-related VIC population. Clearly, much research remains to be done in this area.

While this paper has provided a means for separating the myofibroblast-like VIC phenotype from the mitral posterior leaflet, and preliminary results suggest that the method is also effective for human myxomatous valve cells, it will be important to

substantiate the utility of this method in the study of myxomatous mitral valve disease with a larger sample number of diseased valves. While myxomatous valves contain greater numbers of myofibroblasts,⁵ myxomatous valve cells may secrete excess GAGs and PGs into their pericellular matrix, which may make them less adhesive, but this remains to be shown. Elucidating the basis, mechanism, and optimal substrate for differential adherence of these cells will be essential in isolating the myofibroblast-like cells from a pool of myxomatous mitral valve cells. It is possible that further study will show that the myofibroblast-like population from myxomatous valves shares expression of many of the same markers as the myofibroblast-like cells isolated in this study.

CONCLUSIONS

This study demonstrated the successful separation of VIC subpopulations using differential adhesion. Differential adhesion to fibronectin produced a larger difference between subpopulations and moreover the FN FAST subpopulation demonstrated the phenotype associated with the VIC myofibroblast. This study demonstrated that an extracellular matrix component, fibronectin, which is abundant in tissues undergoing remodeling, can be used to isolate a unique cell population that is also commonly found in remodeling and diseased valves. Developing and validating such techniques for isolating specific cell subpopulations will be crucial in enabling the study of these subpopulations in diseased heart valves.

This chapter, in which a method for separating the myofibroblast valvular interstitial cell (VIC) population was presented, continued the theme of heterogeneity in the normal valve. In the next chapter this series of chapters related to valve heterogeneity (Chapters 8-11) is concluded with a study characterizing this fibronectin-separated myofibroblast VIC subpopulation.

REFERENCES

1. Hewitson T, Martic M, Darby I, Kelynack K, Bisucci T, Tait M, Becker G. Intracellular cyclic nucleotide analogues inhibit in vitro mitogenesis and activation of fibroblasts derived from obstructed rat kidneys. *Nephron Exp Nephrol*. 2004;96(2):e59-66.
2. Florquin S, Rouschop K. Reciprocal functions of hepatocyte growth factor and transforming growth factor-beta1 in the progression of renal diseases: a role for CD44? *Kidney Int Suppl*. 2003;86:S15-20.
3. Wynes M, Frankel S, Riches D. IL-4-induced macrophage-derived IGF-I protects myofibroblasts from apoptosis following growth factor withdrawal. *J Leukoc Biol*. 2004;76(5):1019-1027.
4. Gómez J, Molero X, Vaquero E, Alonso A, Salas A, Malagelada J. Vitamin E attenuates biochemical and morphological features associated with development of chronic pancreatitis. *Am J Physiol Gastrointest Liver Physiol*. 2004;287(1):G162-169.
5. Rabkin E, Aikawa M, Stone JR, Fukumoto Y, Libby P, Schoen FJ. Activated interstitial myofibroblasts express catabolic enzymes and mediate matrix remodeling in myxomatous heart valves. *Circulation*. 2001;104(21):2525-2532.
6. Walker GA, Masters KS, Shah DN, Anseth KS, Leinwand LA. Valvular myofibroblast activation by transforming growth factor-beta: implications for pathological extracellular matrix remodeling in heart valve disease. *Circ Res*. 2004;95(3):253-260.
7. Taylor P, Allen S, Yacoub M. Phenotypic and functional characterization of interstitial cells from human heart valves, pericardium and skin. *J Heart Valve Dis*. 2000;9(1):150-158.
8. Taylor PM, Batten P, Brand NJ, Thomas PS, Yacoub MH. The cardiac valve interstitial cell. *Int J Biochem Cell Biol*. 2003;35(2):113-118.
9. Chester AH, Taylor P. Molecular and functional characteristics of heart-valve interstitial cells. *Philos Trans R Soc Lond B Biol Sci*. 2007;362(1484):1437-1443.
10. Messier RH, Jr., Bass BL, Aly HM, Jones JL, Domkowski PW, Wallace RB, Hopkins RA. Dual structural and functional phenotypes of the porcine aortic valve interstitial population: characteristics of the leaflet myofibroblast. *J Surg Res*. 1994;57(1):1-21.
11. Grande-Allen K, Griffin B, Ratliff N, Cosgrove D, Vesely I. Glycosaminoglycan profiles of myxomatous mitral leaflets and chordae parallel the severity of mechanical alterations. *J Am Coll Cardiol*. 2003;42(2):271-277.
12. Blevins TL, Carroll JL, Raza AM, Grande-Allen KJ. Phenotypic characterization of isolated valvular interstitial cell subpopulations. *J Heart Valve Dis*. 2006;15(6):815-822.
13. Latif N, Sarathchandra P, Thomas PS, Antoniow J, Batten P, Chester AH, Taylor PM, Yacoub MH. Characterization of structural and signaling molecules by human valve interstitial cells and comparison to human mesenchymal stem cells. *J Heart Valve Dis*. 2007;16(1):56-66.

14. Akhtar S, Meek KM, James V. Ultrastructure abnormalities in proteoglycans, collagen fibrils, and elastic fibers in normal and myxomatous mitral valve chordae tendineae. *Cardiovasc Pathol.* 1999;8(4):191-201.
15. Hinz B. Masters and servants of the force: The role of matrix adhesions in myofibroblast force perception and transmission. *Eur J Cell Biol.* 2006;85:175-181.
16. Critchley D. Focal adhesions - the cytoskeletal connection. *Curr Opin Cell Biol.* 2000;12(1):133-139.
17. Bauters C, Marotte F, Hamon M, Oliviero P, Farhadian F, Robert V, Samuel J, Rappaport L. Accumulation of fetal fibronectin mRNAs after balloon denudation of rabbit arteries. *Circulation.* 1995;92(4):904-911.
18. Colombi M, Zoppi N, De Petro G, Marchina E, Gardella R, Taviani D, Ferraboli S, Barlati S. Matrix assembly induction and cell migration and invasion inhibition by a 13-amino acid fibronectin peptide. *J Biol Chem.* 2003;278(16):14346-14355.
19. Farhadian F, Contard F, Sabri A, Samuel J, Rappaport L. Fibronectin and basement membrane in cardiovascular organogenesis and disease pathogenesis. *Cardiovasc Res.* 1996;32(3):433-442.
20. French-Constant C, Van de Water L, Dvorak H, Hynes R. Reappearance of an embryonic pattern of fibronectin splicing during wound healing in the adult rat. *J Cell Biol.* 1989;109(2):391-402.
21. Magnusson M, Mosher D. Fibronectin: structure, assembly, and cardiovascular implications. *Arterioscler Thromb Vasc Biol.* 1998;18(9):1363-1370.
22. Ulrich M, Janssen A, Daemen M, Rappaport L, Samuel J, Contard F, Smits J, Cleutjens J. Increased expression of fibronectin isoforms after myocardial infarction in rats. *J Mol Cell Cardiol.* 1997;29(9):2533-2543.
23. Yang M, Huang H, Li J, Li D, Wang H. Tyrosine phosphorylation of the LDL receptor-related protein (LRP) and activation of the ERK pathway are required for connective tissue growth factor to potentiate myofibroblast differentiation. *Faseb J.* 2004;18(15):1920-1921.
24. Fayet C, Bendeck M, Gotlieb A. Cardiac valve interstitial cells secrete fibronectin and form fibrillar adhesions in response to injury. *Cardiovasc Pathol.* 2007;16(4):203-211.
25. Lester W, Rosenthal A, Granton B, Gotlieb A. Porcine mitral valve interstitial cells in culture. *Lab Invest.* 1988;59(5):710-719.
26. Johnson CM, Fass DN. Porcine Cardiac Valvular Endothelial Cells in Culture. *Lab Invest.* 1983;49(5):589-598.
27. Pho M, Lee W, Watt D, Laschinger C, Simmons C, McCulloch C. Cofilin is a marker of myofibroblast differentiation in cells from porcine aortic cardiac valves. *Am J Physiol Heart Circ Physiol.* 2008;294(4):H1767-1778.

28. Kunzelman KS, Cochran RP. Stress/strain characteristics of porcine mitral valve tissue: parallel versus perpendicular collagen orientation. *J Card Surg.* 1992;7(1):71-78.
29. Vesely I. Reconstruction of loads in the fibrosa and ventricularis of porcine aortic valves. *ASAIO J.* 1996;42(5):M739-M746.
30. Sim EK, Muskawad S, Lim CS, Yeo JH, Lim KH, Grignani RT, Durrani A, Lau G, Duran C. Comparison of human and porcine aortic valves. *Clin Anat.* 2003;16(3):193-196.
31. Sands MP, Rittenhouse EA, Mohri H, Merendino KA. An anatomical comparison of human pig, calf, and sheep aortic valves. *Ann Thorac Surg.* 1969;8(5):407-414.
32. Taylor PM, Allen SP, Dreger SA, Yacoub MH. Human cardiac valve interstitial cells in collagen sponge: a biological three-dimensional matrix for tissue engineering. *J Heart Valve Dis.* 2002;11(3):298-306.
33. Johnson CM, Hanson MN, Helgeson SC. Porcine cardiac valvular subendothelial cells in culture: cell isolation and growth characteristics. *J Mol Cell Cardiol.* 1987;19(12):1185-1193.
34. Stephens EH, Carroll JL, Grande-Allen KJ. The use of collagenase III for the isolation of porcine aortic valvular interstitial cells: rationale and optimization. *J Heart Valve Dis.* 2007;16(2):175-183.
35. Cimini M, Rogers K, Boughner D. Aortic valve interstitial cells: an evaluation of cell viability and cell phenotype over time. *J Heart Valve Dis.* 2002;11(6):881-887.
36. Wang J, Chen H, Seth A, McCulloch CA. Mechanical force regulation of myofibroblast differentiation in cardiac fibroblasts. *Am J Physiol Heart Circ Physiol.* 2003;285(5):H1871-1881.
37. Furukawa F, Matsuzaki K, Mori S, Tahashi Y, Yoshida K, Sugano Y, Yamagata H, Matsushita M, Seki T, Inagaki Y, Nishizawa M, Fujisawa J, Inoue K. p38 MAPK mediates fibrogenic signal through Smad3 phosphorylation in rat myofibroblasts. *Hepatology.* 2003;38(4):879-889.
38. Liu P, Zhang C, Feng J, Zhao Y, Wang X, Yang J, Zhang M, Wang X, Zhang Y. Cross-Talk Among Smad, MAPK, and Integrin Signaling Pathways Enhances Adventitial Fibroblast Functions Activated by Transforming Growth Factor {beta} 1 and Inhibited by Gax. *Arterioscler Thromb Vasc Biol.* 2008(Epub Jan 10).
39. MacKenna DA, Dolfi F, Vuori K, Ruoslahti E. Extracellular signal-regulated kinase and c-Jun NH2-terminal kinase activation by mechanical stretch is integrin-dependent and matrix-specific in rat cardiac fibroblasts. *J Clin Invest.* 1998;101(2):301-310.
40. Atance J, Yost MJ, Carver W. Influence of the extracellular matrix on the regulation of cardiac fibroblast behavior by mechanical stretch. *J Cell Physiol.* 2004;200(3):377-386.

41. Pillinger M, Marjanovic N, Kim S, Scher J, Izmirly P, Tolani S, Dinsell V, Lee Y, Blaser M, Abramson S. Matrix metalloproteinase secretion by gastric epithelial cells is regulated by E prostaglandins and MAPKs. *J Biol Chem.* 2005;280(11):9973-9979.
42. Antal-Szalmas P, Strijp J, Weersink A, Verhoef J, Van Kessel K. Quantitation of surface CD14 on human monocytes and neutrophils. *J Leukoc Biol.* 1997;61(6):721-728.
43. Aikawa M, Rabkin E, Voglic S, Shing H, Nagai R, Schoen F, Libby P. Lipid lowering promotes accumulation of mature smooth muscle cells expressing smooth muscle myosin heavy chain isoforms in rabbit atheroma. *Circ Res.* 1998;83(10):1015-1026.
44. Aikawa M, Sivam P, Kuro-o M, Kimura K, Nakahara K, Takewaki S, Ueda M, Yamaguchi H, Yazaki Y, Periasamy M. Human smooth muscle myosin heavy chain isoforms as molecular markers for vascular development and atherosclerosis. *Circ Res.* 1993;73(6):1000-1012.
45. Merryman WD, Youn I, Lukoff HD, Krueger PM, Guilak F, Hopkins RA, Sacks MS. Correlation between heart valve interstitial cell stiffness and transvalvular pressure: implications for collagen biosynthesis. *Am J Physiol Heart Circ Physiol.* 2006;290(1):H224-231.
46. Cushing MC, Mariner PD, Liao JT, Sims EA, Anseth KS. Fibroblast growth factor represses Smad-mediated myofibroblast activation in aortic valvular interstitial cells. *Faseb J.* 2008;22(6):1769-1777.
47. Setola V, Hufeisen SJ, Grande-Allen KJ, Vesely I, Glennon RA, Blough B, Rothman RB, Roth BL. 3,4-methylenedioxymethamphetamine (MDMA, "Ecstasy") induces fenfluramine-like proliferative actions on human cardiac valvular interstitial cells in vitro. *Mol Pharmacol.* 2003;63(6):1223-1229.
48. Xu J, Jian B, Chu R, Lu Z, Li Q, Dunlop J, Rosenweig-Lipson S, McGonigle P, Levy RJ, Liang B. Serotonin mechanisms in heart valve disease II: the 5-HT₂ receptor and its signaling pathway in aortic valve interstitial cells. *Am J Pathol.* 2002;161(6):2209-2218.
49. Hinz B, Mastrangelo D, Iseline C, Chaponnier C, Gabbiani G. Mechanical tension controls granulation tissue contractile activity and myofibroblast differentiation. *Am J Pathol.* 2001;159(3):1009-1020.
50. Hinz B, Celetta G, Tomasek J, Gabbiani G, Chaponnier C. Alpha-smooth muscle actin expression upregulates fibroblast contractile activity. *Mol Biol Cell.* 2001;12(9):2730-2741.
51. Singer I, Kawka D, Kazazis D, Clark R. In vivo co-distribution of fibronectin and actin fibers in granulation tissue: immunofluorescence and electron microscope studies of the fibronexus at the myofibroblast surface. *J Cell Biol.* 1984;98(6):2091-2106.
52. Hinz B, Gabbiani G, Chaponnier C. The NH₂-terminal peptide of alpha-smooth muscle actin inhibits force generation by the myofibroblast in vitro and in vivo. *J Cell Biol.* 2002;157(4):657-663.

53. Cushing MC, Liao JT, Anseth KS. Activation of valvular interstitial cells is mediated by transforming growth factor-beta1 interactions with matrix molecules. *Matrix Biol.* 2005;24(6):428-437.
54. Cushing MC, Liao J, Jaeggli MP, Anseth KS. Material-based regulation of the myofibroblast phenotype *Biomaterials.* 2007;28:3378-3387.
55. Arora P, Narani N, McCulloch C. The compliance of collagen gels regulates transforming growth factor-beta induction of alpha-smooth muscle actin in fibroblasts. *Am J Pathol.* 1999;154(3):871-882.
56. Féréol S, Fodil R, Labat B, Galiacy S, Laurent V, Louis B, Isabey D, Planus E. Sensitivity of alveolar macrophages to substrate mechanical and adhesive properties. *Cell Motil Cytoskeleton.* 2006;63(6):321-340.
57. Zamir E, Katz B, Aota S, Yamada K, Geiger B, Kam Z. Molecular diversity of cell-matrix adhesions. *J Cell Sci.* 1999;112:1655-1669.
58. Katz B, Zamir E, Bershadsky A, Kam Z, Yamada KM, Geiger B. Physical state of the extracellular matrix regulates the structure and molecular composition of cell-matrix adhesions. *Mol Biol Cell.* 2000;11:1047-1060.

Chapter 11: Functional Characterization of Fibronectin-Separated Valvular Interstitial Cell Subpopulations: Application to Study of Valve Disease

This chapter concludes the series of chapters addressing normal valve heterogeneity, and specifically heterogeneity in the valvular interstitial cell (VIC) population, with a study characterizing the myofibroblast VIC subpopulation isolated using the method detailed in the previous chapter.

ABSTRACT

Background: Myxomatous mitral valves (MVs) contain elevated proportions of myofibroblasts, a valvular interstitial cell (VIC) subpopulation likely important in disease pathogenesis. We recently developed a novel technique for the isolation of VIC myofibroblasts using time dependent adhesion to fibronectin (FN). Cells that quickly adhere to FN (“FAST”) demonstrate myofibroblast cell phenotype markers, in contrast to cells that fail to adhere after a longer time (“SLOW”). The aim of this study was to characterize the functionality of these subpopulations using 3D collagen constructs.

Methods: VICs were harvested from porcine mitral valve posterior leaflets. FAST and SLOW subpopulations, as well as unseparated VIC populations grown on FN and TCP (UNSEP TCP, UNSEP FN) were seeded within 3D collagen gels and cultured for 3 weeks. Collagen gel contraction was assessed throughout the culture duration and

mechanical properties of the resulting collagen constructs were assessed using uniaxial tensile testing.

Results: FAST cells demonstrated greater contraction of collagen gels compared with SLOW cells, particularly after 10 days ($p < 0.05$). Interestingly, the collagen gel contraction by both FN-separated VIC subpopulations (FAST and SLOW) was greater than for gels seeded with UNSEP TCP VICs ($p < 0.05$). Further, the contraction of UNSEP FN gels was greater than UNSEP TCP throughout culture duration ($p \leq 0.002$), suggesting that the subculture of VICs on FN potentiated these phenotypic changes. Finally, the collagen constructs seeded with FAST cells were stiffer than those seeded with SLOW, followed by UNSEP TCP ($p < 0.001$). The same pattern was found for failure stress ($p = 0.006$).

Conclusions: Time dependent adhesion to FN produced a VIC subpopulation (FAST) whose function in 3D culture was consistent with that of myofibroblasts; FN exposure alone also caused VICs to function more like myofibroblasts. This novel isolation method may prove valuable in future studies of myofibroblasts in valve disease.

The work contained in this chapter was published as:

Stephens EH, Carroll JL, Post AD, Kuo JJ, Grande-Allen KJ. **Functional Characterization of Fibronectin-Separated Valve Interstitial Cell Subpopulations: Application to Study of Valve Disease.** *Journal of Heart Valve Disease*, in press.

INTRODUCTION

Myxomatous mitral valves (MVs) contain elevated proportions of myofibroblasts,¹ a valvular interstitial cell (VIC) subpopulation proposed to play an important role in disease pathogenesis. However, study of this cell type and its potential role in valve disease pathogenesis has been limited by difficulties in isolating this cell type. Recently we developed a novel isolation technique utilizing fibronectin (FN),² an extracellular matrix component known to be involved in myofibroblast adhesion.^{3, 4} In this isolation technique VICs are seeded onto FN-coated tissue culture flasks and sorted into “FAST” to adhere and “SLOW” to adhere subpopulations.² Previously, we used immunocytochemistry and flow cytometry to show that the FAST subpopulation of VICs demonstrate a more myofibroblast-like cell phenotype relative to the SLOW population.² While these results were promising, suggesting that this technique may be an effective method for the isolation of the VIC myofibroblast subpopulation, that study was limited to expression of phenotypic markers. To assess whether this FAST subpopulation also behaved functionally like myofibroblasts, this study was performed to characterize the behavior of the FAST and SLOW VIC populations using 3D collagen gel constructs.

While much can be learned by study of cell behavior and function in the 2D *in vitro* culture environment, cells *in vivo* function in a 3D environment. Indeed numerous studies have shown that cell morphology and basic behaviors such as cell migration⁵ and the composition of cellular adhesions⁶ are different when cells are cultured in a 3D environment. Cell-seeded collagen gels, first developed by Bell,⁷ are widely used for the study of cells in a controlled, *ex vivo* 3D environment. Among the several types of collagen contraction models (free floating, constrained, and attached and delayed

release⁸), in this study we chose to use a constrained collagen gel model, which was considered to be more representative of the *in vivo* mechanical environment that VICs experience. Thus, FAST and SLOW VIC subpopulations, along with primary unseparated VICs cultured on FN-coated and uncoated tissue culture plastic (TCP), were seeded into collagen gel constructs. Functionality of the cells was evaluated as their ability to contract the collagen gel over a 3 week period, as well as the mechanical behavior of the resulting collagen construct.

METHODS

VIC Isolation

The specific approaches employed for the isolation of VICs and the separation of VIC subpopulations using differential adhesion to fibronectin (FN) have been described in detail previously,² and are summarized here. Mitral valves were dissected from fresh 6-month-old pig hearts obtained from an abattoir (Fisher Ham and Meat, Spring, TX). VICs were isolated from the posterior leaflet using a two-stage collagenase digestion as previously described.⁹ Cells were cultured on tissue culture plastic (TCP) in DMEM containing 10% bovine growth serum (HyClone, Logan, UT) and 2% antibiotic/antimycotic (Mediatech, Herndon, VA) with changes of medium every 48 hours. Cells were passaged after reaching 80-90% confluence. Experiments were performed on VICs between their second and fourth passages.

Isolation of VIC Subpopulations

VIC subpopulations (FN FAST, FN SLOW) were generated utilizing differential adhesion to FN, as described in Chapter 10. The resultant FN FAST and FN SLOW subpopulations were grown in their respective FN-coated TCP flasks for 4 days until being seeded into the collagen constructs, described below. An additional population of unseparated VICs was grown on FN-coated TCP for 4 days (UNSEP FN). To serve as controls, unseparated VICs were grown only on TCP (UNSEP TCP).

Collagen Constructs

The methods for the formation and culture of cell-seeded collagen constructs have been described in detail previously.¹⁰ Briefly, 6-8 collagen constructs of each of the four groups of VICs (FN FAST, FN SLOW, UNSEP FN, and UNSEP TCP) were grown to approximately 80% confluence, trypsinized, and then added to a solution containing rat tail collagen type I (BD Biosciences, Franklin Lakes, NJ) and DMEM (Mediatech) to obtain a final collagen concentration of 2.0 mg/ml and final VIC concentration of 1.0×10^6 cells/ml. The collagen-VIC solution for each of the four VIC populations was pipetted into dog-bone shaped wells within a custom-made silicone rubber Petri dish insert (60 mm x 5 mm x 5 mm). The rounded ends of each well were equipped with a stainless steel wire post covered in porous polyurethane (Sawbones, Inc., Vashon, WA) in order to anchor the gels in static tension as the VICs contracted the collagen during the culture duration. Collagen gels were incubated for 3 weeks at 37 °C and 5% CO₂ and media was changed every 48 hours.

Images of the collagen gels were collected throughout the culture period and analyzed using ImagePro Software (Fig. 11-1, Media Cybernetics, Silver Spring, MD). Gel contraction was calculated as 100% minus the percent of well width occupied by the collagen construct. Measurements of gel contraction were made at 5 points along the

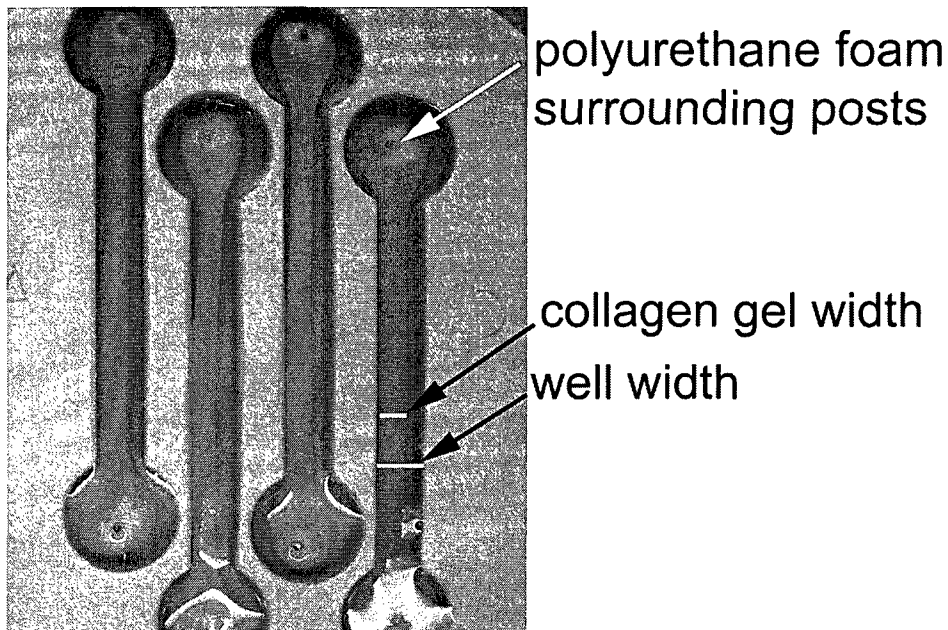


Fig. 11-1: Collagen constructs shown within silicone rubber wells. Stainless steel posts surrounded by porous polyurethane foam provided anchors for the constructs to develop uniaxial tension during the culture period. Contraction was calculated as the width of the collagen construct relative to the silicone rubber well width measured at five locations along the construct length.

length of the collagen construct, and the percentages averaged. Percentage gel contraction for all VIC populations was normalized to the average percentage contraction of UNSEP TCP at the first time point.

Mechanical Testing

At the end of the culture duration, each construct was dissected away from the wire posts, and divided in half yielding two constructs of approximately equal length. Each half was mechanically tested in uniaxial tension using an EnduraTec ELF 3200 (Bose, Framingham, MA). The construct was inserted into the grips for a final grip-to-grip distance of 10 mm. Before tension was applied, the grip-to-grip distance was decreased by 1 mm to ensure no pre-tension was applied to the construct before the application of strain. Based on previous studies showing the potential for creep during pre-conditioning,¹¹ samples were not pre-conditioned prior to testing. Constructs were then stretched at a rate of 3 mm/sec until failure. Data collected was plotted as a load-displacement curve and used to determine the gauge length, the length of the stretched construct at which load rose above 0. By normalizing displacement and load, respectively, by the gauge length and the cross-sectional area of the construct, the data was converted to a stress-strain curve (strain was defined as (gauge length-displacement)/gauge length). The modulus was defined as the slope of the best least-squares mean fit to the linear portion of the stress-strain curve. The failure stress was defined as the stress at which the collagen construct broke; failure strain was similarly defined. Failure stress and strain was only calculated for samples that broke in the middle of the construct.

Statistical Analysis

Multifactorial analysis of variance to compare differences between subpopulations was performed using SigmaStat (SPSS, Chicago, IL), as described in

Chapter 4. Post-hoc testing was performed using the Holm-Sidak method for all pairwise multiple comparisons.

RESULTS

Collagen Construct Contraction

Overall, collagen gels containing FAST cells and SLOW cells demonstrated comparable patterns of contraction throughout the culture duration. After 240 hours (10 days) the percentage of contraction of FAST was consistently greater than that of SLOW (Fig. 11-2A). This difference, however, was not apparent during the first 100 hours, and at several early time points the rate of contraction of SLOW was actually greater than FAST (Fig. 11-2B). Throughout the collagen gel culture period, gels seeded with FAST or SLOW cells both demonstrated significantly greater contraction compared to gels seeded with UNSEP TCP cells ($p < 0.05$ at each time point). Interestingly, the collagen gels containing unseparated cells exposed FN (FN UNSEP) contracted more at each time point than did the gels containing UNSEP TCP cells ($p \leq 0.002$). The gels containing the UNSEP FN cells also demonstrated rapid early contraction towards a relatively stable plateau, while collagen gels containing the other VIC populations (FAST, SLOW, and UNSEP TCP) all demonstrated more gradual increases in contraction over the culture duration.

A. Contraction of Collagen Constructs by VIC Subpopulations

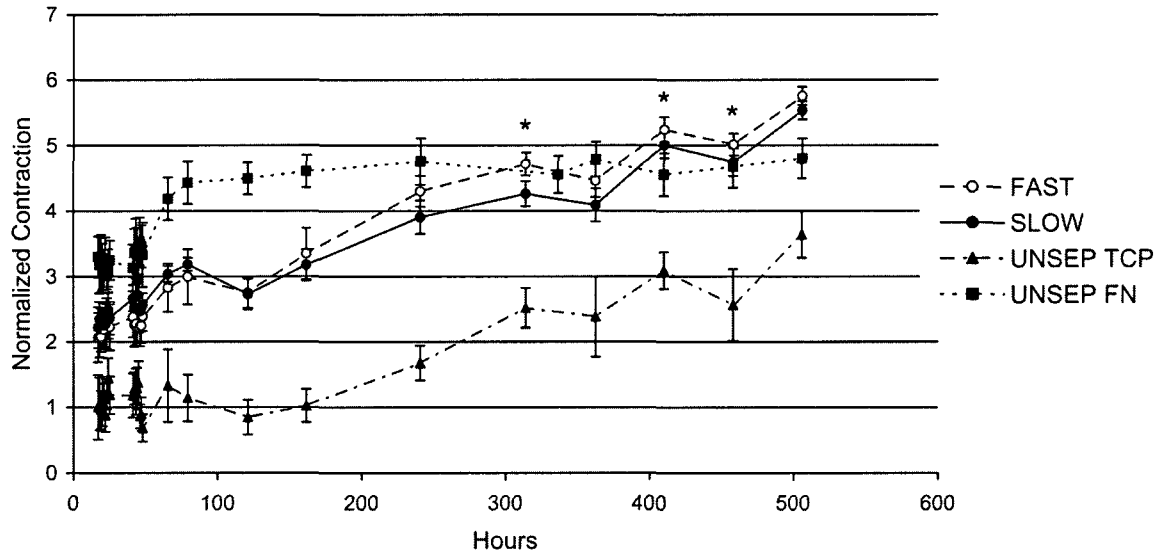


Fig. 11-2A: Normalized contraction of collagen constructs populated by the different VIC subpopulations. For all subpopulations, percentage contraction at each time point was normalized to the percentage contraction of the first time point of UNSEP TCP. * $p < 0.05$ FAST vs. SLOW for a given time point (only marked on the time points > 100 hours for this graph, for time points < 100 hours see part B). FAST and SLOW were each significantly different compared to UNSEP TCP at each time point ($p < 0.05$) and UNSEP FN was significantly different compared to UNSEP TCP at each time point ($p \leq 0.002$). Error bars indicate standard deviation.

B.

Early Contraction of Collagen Constructs by VIC Subpopulations

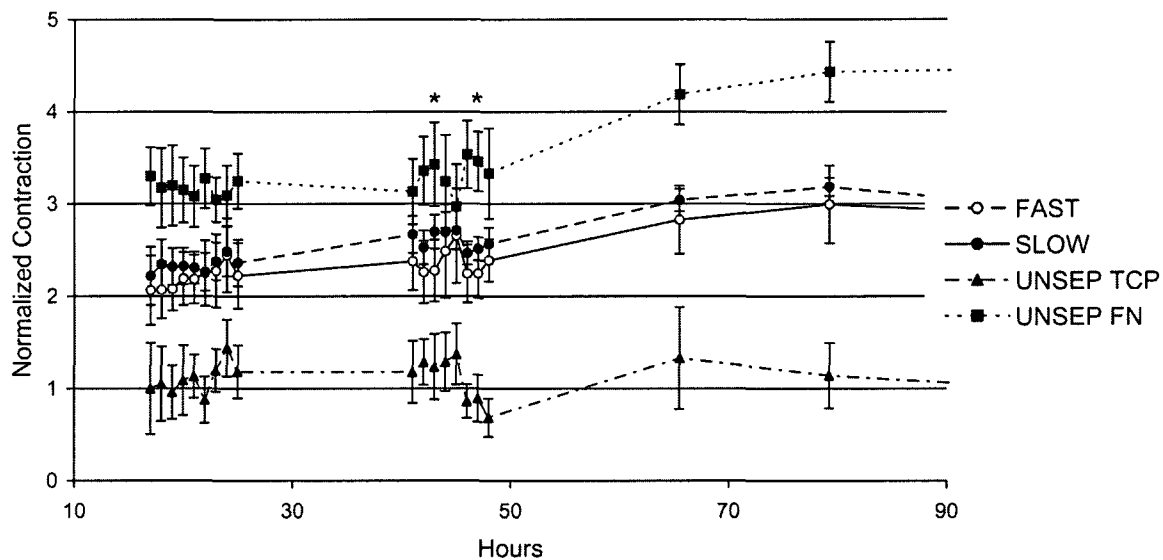


Fig. 11-2B: Contraction of collagen constructs populated by the different VIC subpopulations over the first 100 hours. * $p < 0.05$ FAST vs. SLOW for a given time point. FAST and SLOW were each significantly different compared to UNSEP TCP at each time point ($p < 0.05$) and UNSEP FN was significantly different compared to UNSEP TCP at each time point ($p \leq 0.002$). Error bars indicate standard deviation.

Material Properties of Collagen Constructs

The elastic moduli of the collagen gels were greatest for those seeded with FAST cells and lowest for those seeded with UNSEP TCP (Fig. 11-3, $p < 0.001$). Failure stress measurements showed the same pattern of differences between groups (Fig. 11-4, $p = 0.006$). Failure strain was not significantly different between groups.

Elastic Modulus

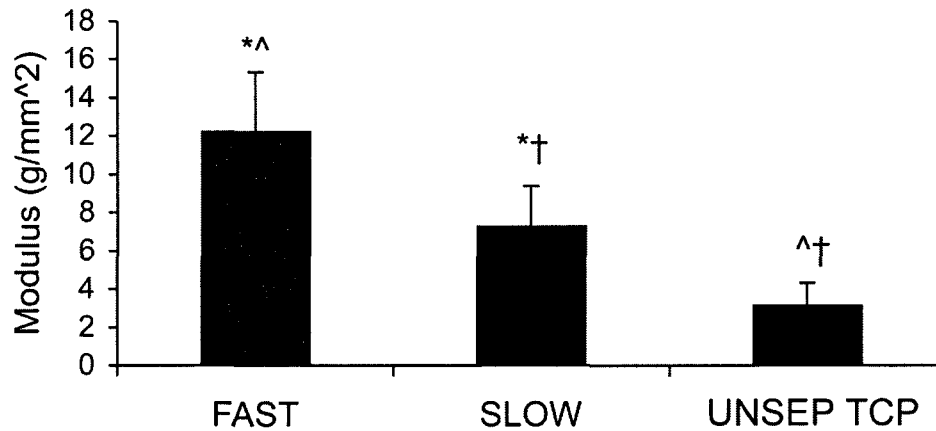


Fig. 11-3: Elastic modulus of collagen constructs populated by the different VIC subpopulations. Overall $p < 0.001$. *, ^, † indicate $p < 0.05$ between bars with shared symbol. Error bars indicate standard deviation.

Failure Stress

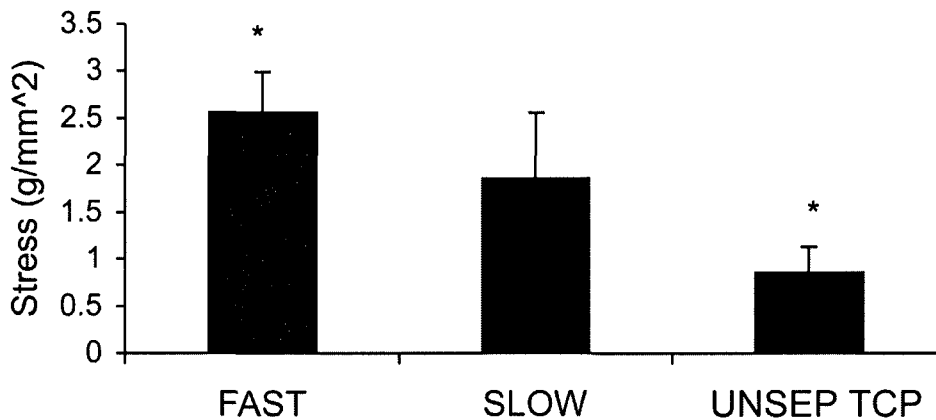


Fig. 11-4: Failure stress of collagen constructs populated by the different VIC subpopulations. Overall $p = 0.006$. * $p < 0.05$ between FAST and UNSEP TCP. Error bars indicate standard deviation.

DISCUSSION

The first major finding of this study was that the myofibroblast-like VIC subpopulation that adhered quickly to FN demonstrated greater collagen gel contraction and remodeled the gels to produce stronger constructs, when compared to the less adhesive VIC subpopulation (SLOW). This finding is consistent with connective tissue and wound healing literature showing that myofibroblasts exert more force than fibroblasts¹²⁻¹⁴ and have been shown to contract collagen gels more than their fibroblast counterparts.^{13, 15} Therefore, this work extends our previous report that this FAST subpopulation of VICs expresses many myofibroblast phenotypic markers² by showing that they also function like myofibroblasts. Differential adhesion to FN was chosen as the means for isolating the VIC myofibroblast subpopulation based on the role of FN in myofibroblast adhesion^{3, 16} as well as its presence in normal and myxomatous valves and chordae tendinae.^{2, 17} FN has also been shown to be secreted by VICs exposed to injury-like conditions,¹⁸ during which time the myofibroblast phenotype might also be expressed.¹⁹ Additionally, the expression of FN was increased in the mitral valves of dogs with chronic valve disease similar to human myxomatous mitral valve disease.²⁰ Based on these studies documenting enriched FN content in conjunction with elevated numbers of myofibroblasts, it was hypothesized that the myofibroblast VIC subpopulation may display greater affinity for FN relative to other VIC subpopulations, and therefore FN could be a useful tool for isolating this subpopulation. The mechanism underlying the VIC myofibroblasts' faster adhesion to FN is still under investigation, but may be due in part to greater adhesive strength. Although the adhesive strength of VIC

myofibroblasts has not been assessed, studies of other cell populations have shown that myofibroblasts exert stronger forces than their fibroblast counterparts¹²⁻¹⁴ and are better at contracting collagen gels.^{13, 15} This enhanced adhesion has been attributed to more extensive cell-matrix contacts,²¹ isoform-specific terminal peptide adhesions,²² and differences in focal adhesion structure and composition.³ Indeed, our previous work on these cell populations revealed that compared to the SLOW subpopulation, the FAST subpopulation expressed greater amounts of smooth muscle alpha-actin, which has been shown to correlate to contraction strength of myofibroblasts in other connective tissues.¹³ It is interesting to note that both FAST and SLOW subpopulations show similar contraction early, perhaps due to the potentiation effect of FN (as discussed below), although at later time points the FAST subpopulation started to contract the gels significantly more than the SLOW subpopulation. This late difference could have been because the FAST subpopulation created more stress within the gel, which further enhanced the myofibroblast phenotype and led to further contraction. The mechanical environment of fibroblasts/myofibroblasts, especially the stress that these cells experience, has been well documented to drive myofibroblast differentiation and contraction in other connective tissues.¹⁶

The second major finding was that exposure of unseparated VICs to FN resulted in a greater ability to contract collagen gels, compared to unseparated VICs grown on TCP, which suggests a potentiation effect of FN adhesion. Unexpectedly, this effect was greater than the difference between FAST and SLOW. This effect was examined when it was noted that the FAST and SLOW cells, which were isolated by culture on FN, were both better able to contract collagen gels more than the UNSEP TCP cells, which were

never exposed to FN. After unseparated VICs were exposed to FN for an equivalent amount of time as the FAST and SLOW cells, their overall contraction of collagen gels was comparable to FAST and SLOW, and in fact was more rapid. These results suggest that adhesion to FN potentiates the myofibroblast phenotype in VICs, which is consistent with our previous finding that the VIC subpopulation that quickly adhered to FN demonstrated greater myofibroblast phenotypic marker expression than the VIC subpopulation that quickly adhered to TCP.² This interpretation that FN potentiates the myofibroblast phenotype in VICs is also supported by studies demonstrating increased SMAA expression of VICs plated on FN-coated 2D surfaces,²³ as well as studies of fibroblasts from a range of other tissues.²⁴

Although several reports have described the culture of VICs within collagen gels, the mechanisms of VIC-collagen interactions are less understood. Generally collagen gel contraction by fibroblasts/myofibroblasts is thought to occur by the contraction of cells seeded within collagen gels (principally seen with myofibroblasts), the tractional forces that develop as the cells translocate and bundle collagen fibers, and the elongation and spreading of the initially spherical cells when they are seeded within the collagen gel (during the first 4 hours of cell-collagen gel culture).⁸ The relative contributions of these various mechanisms depend on the specific types of cells seeded within the collagen gel as well as the boundary conditions imposed on the collagen gel (i.e., free-floating versus constrained). In cell-populated constrained collagen gels, the local applied forces of fibroblasts on collagen are transmitted to effect global changes.¹⁶ As the collagen is reorganized by the seeded fibroblasts, matrix stiffening occurs, and cells align in the direction of tension and develop stress fibers.¹⁶ In an elegant study embedded beads and

collagen fibers within cell-seeded collagen gels were visualized to demonstrate that as fibroblasts apply traction to adjacent collagen fibers, small, local translocations of these fibers were apparent within minutes, and the cells continued to reorganize the collagen fibers into bundles, which became visually apparent by 3 hours.²⁵ The interconnected mesh-like nature of the collagen gel allowed the simultaneous transmission of these localized processes to large-scale global construct contraction.²⁵ While the basic mechanisms by which VICs remodel collagen gels have only started to be characterized,²⁶ based on the similarities between VICs and fibroblasts/myofibroblasts, the process of collagen gel contraction by VICs likely involves a similar series of events.

Ongoing progress to characterize the phenotype and function of VIC myofibroblasts has implications for a number of valve diseases, including myxomatous mitral valve disease¹ and calcific aortic stenosis.²⁷ VICs demonstrating the myofibroblast phenotype have also been demonstrated in other instances of valve injury¹⁹ as well as in cardiac diseases²⁸ and *ex vivo* experiments in which valves experience increased stress.²⁹ Given the speculated roles of this cell type in clinical valve disease, novel approaches to isolate these cells offer promise for future investigations of these diseases, especially since there is no single marker that can definitively distinguish this cell type. Additionally, adhesion of VICs to FN may prove to be a useful tool for manipulating VIC phenotype,³⁰ which could aid in regulating the material properties and calcification potential of tissue engineered heart valves.

While collagen gel studies are a useful *ex vivo* tool for studying cell function, the method was limited in only measuring these cells' interaction with collagen (as opposed to other extracellular matrix components) over a relatively short time course. As with

many *ex vivo* experimental studies, this method also did not incorporate *in vivo* factors that undoubtedly affect VIC function, such as hemodynamics, growth factor and cytokine signals, and dynamic strain during each cardiac cycle. Another limitation was that porcine VICs were used. While porcine valves are commonly and appropriately used as models for human valves,^{31, 32} future studies will need to expand on the approach described in this work by utilizing human VICs from both healthy and diseased valves. Although, further investigation of this FAST VIC subpopulation is clearly needed, this study represents an important first step in functionally characterizing this subpopulation.

CONCLUSIONS

In summary, rapid adhesion to FN produces a VIC subpopulation that behaves in a manner consistent with myofibroblasts, and generates collagen gels constructs that are stronger and stiffer than collagen constructs grown from less adhesive or non-FN treated VICs. Additionally, treatment with FN appeared to potentiate myofibroblast behavior in unseparated VICs. These results, taken together with previous results demonstrating strong expression of myofibroblast phenotype markers in the FAST VIC subpopulation, emphasize the promise of this approach for the isolation and study of the VIC myofibroblast subpopulation in valve biology and disease pathogenesis.

This chapter, which characterized the myofibroblast valvular interstitial cell (VIC) subpopulation isolated using the method detailed in the previous chapter, concludes the series of chapters addressing normal valve heterogeneity, and

specifically heterogeneity in the VIC population. In the next chapter the topic of VIC-matrix coupling is addressed with a study demonstrating the functional interaction of VICs and collagen in the mitral leaflet.

REFERENCES

1. Rabkin E, Aikawa M, Stone JR, Fukumoto Y, Libby P, Schoen FJ. Activated interstitial myofibroblasts express catabolic enzymes and mediate matrix remodeling in myxomatous heart valves. *Circulation*. 2001;104(21):2525-2532.
2. Stephens EH, Huynh TN, Cieluch JD, Grande-Allen KJ. Fibronectin-based isolation of valve interstitial cell subpopulations: relevance to valve disease. *J Biomed Mater Res A*. 92(1):340-349.
3. Hinz B. Masters and servants of the force: The role of matrix adhesions in myofibroblast force perception and transmission. *Eur J Cell Biol*. 2006;85:175-181.
4. Critchley D. Focal adhesions - the cytoskeletal connection. *Curr Opin Cell Biol*. 2000;12(1):133-139.
5. Friedl P, Brocker EB. The biology of cell locomotion within three-dimensional extracellular matrix. *Cell Mol Life Sci*. 2000;57(1):41-64.
6. Cukierman E, Pankov R, Stevens DR, Yamada KM. Taking cell-matrix adhesions to the third dimension. *Science*. 2001;294(5547):1708-1712.
7. Bell E, Ivarsson B, Merrill C. Production of a tissue-like structure by contraction of collagen lattices by human fibroblasts of different proliferative potential in vitro. *Proc Natl Acad Sci U S A*. 1979;76(3):1274-1278.
8. Dallon J, Ehrlich H. A review of fibroblast-populated collagen lattices. *Wound Repair Regen*. 2008;16(4):472-479.
9. Stephens EH, Carroll JL, Grande-Allen KJ. The use of collagenase III for the isolation of porcine aortic valvular interstitial cells: rationale and optimization. *J Heart Valve Dis*. 2007;16(2):175-183.
10. Gupta V, Werdenburg JA, Blevins TL, Grande-Allen KJ. Synthesis of glycosaminoglycans in differently loaded regions of collagen gels seeded with valvular interstitial cells. *Tissue Eng*. 2007;13(1):41-49.
11. Wagenseil JE, Wakatsuki T, Okamoto RJ, Zahalak GI, Elson EL. One-dimensional viscoelastic behavior of fibroblast populated collagen matrices. *J Biomech Eng*. 2003;125(5):719-725.
12. Hinz B, Mastrangelo D, Iseline C, Chaponnier C, Gabbiani G. Mechanical tension controls granulation tissue contractile activity and myofibroblast differentiation. *Am J Pathol*. 2001;159(3):1009-1020.
13. Hinz B, Celetta G, Tomasek J, Gabbiani G, Chaponnier C. Alpha-smooth muscle actin expression upregulates fibroblast contractile activity. *Mol Biol Cell*. 2001;12(9):2730-2741.

14. Wrobel LK, Fray TR, Molloy JE, Adams JJ, Armitage MP, Sparrow JC. Contractility of single human dermal myofibroblasts and fibroblasts. *Cell Motil Cytoskeleton*. 2002;52(2):82-90.
15. Arora PD, Narani N, McCulloch CA. The compliance of collagen gels regulates transforming growth factor-beta induction of alpha-smooth muscle actin in fibroblasts. *Am J Pathol*. 1999;154(3):871-882.
16. Hinz B, Gabbiani G. Mechanisms of force generation and transmission by myofibroblasts. *Curr Opin Biotechnol*. 2003;14(5):538-546.
17. Akhtar S, Meek KM, James V. Immunolocalization of elastin, collagen type I and type III, fibronectin, and vitronectin in extracellular matrix components of normal and myxomatous mitral heart valve chordae tendineae. *Cardiovasc Pathol*. 1999;8(4):203-211.
18. Fayet C, Bendeck M, Gotlieb A. Cardiac valve interstitial cells secrete fibronectin and form fibrillar adhesions in response to injury. *Cardiovasc Pathol*. 2007;16(4):203-211.
19. Tamura K, Jones M, Yamada I, Ferrans VJ. Wound healing in the mitral valve. *J Heart Valve Dis*. 2000;9(1):53-63.
20. Aupperle H, Marz I, Thielebein J, Kiefer B, Kappe A, Schoon HA. Immunohistochemical characterization of the extracellular matrix in normal mitral valves and in chronic valve disease (endocardiosis) in dogs. *Res Vet Sci*. 2009;87(2):277-283.
21. Singer I, Kawka D, Kazazis D, Clark R. In vivo co-distribution of fibronectin and actin fibers in granulation tissue: immunofluorescence and electron microscope studies of the fibronexus at the myofibroblast surface. *J Cell Biol*. 1984;98(6):2091-2106.
22. Hinz B, Gabbiani G, Chaponnier C. The NH2-terminal peptide of alpha-smooth muscle actin inhibits force generation by the myofibroblast in vitro and in vivo. *J Cell Biol*. 2002;157(4):657-663.
23. Cushing MC, Liao JT, Anseth KS. Activation of valvular interstitial cells is mediated by transforming growth factor-beta1 interactions with matrix molecules. *Matrix Biol*. 2005;24(6):428-437.
24. MacKenna D, Dolfi F, Vuori K, Ruoslahti E. Extracellular signal-regulated kinase and c-Jun NH2-terminal kinase activation by mechanical stretch is integrin-dependent and matrix-specific in rat cardiac fibroblasts. *J Clin Invest*. 1998;101(2):301-310.
25. Sawhney RK, Howard J. Slow local movements of collagen fibers by fibroblasts drive the rapid global self-organization of collagen gels. *J Cell Biol*. 2002;157(6):1083-1091.
26. Smith S, Taylor PM, Chester AH, Allen SP, Dreger SA, Eastwood M, Yacoub MH. Force generation of different human cardiac valve interstitial cells: relevance to individual valve function and tissue engineering. *J Heart Valve Dis*. 2007;16(4):440-446.

27. Olsson M, Rosenqvist M, Nilsson J. Expression of HLA-DR antigen and smooth muscle cell differentiation markers by valvular fibroblasts in degenerative aortic stenosis. *J Am Coll Cardiol.* 1994;24(7):1664-1671.
28. Stephens EH, Timek TA, Daughters GT, Kuo JJ, Patton AM, Baggett LS, Ingels NB, Miller DC, Grande-Allen KJ. Significant changes in mitral valve leaflet matrix composition and turnover with tachycardia-induced cardiomyopathy. *Circulation.* 2009;120(11 Suppl):S112-119.
29. Balachandran K, Konduri S, Sucusky P, Jo H, Yoganathan AP. An ex vivo study of the biological properties of porcine aortic valves in response to circumferential cyclic stretch. *Ann Biomed Eng.* 2006;34(11):1655-1665.
30. Cushing MC, Liao J, Jaeggli MP, Anseth KS. Material-based regulation of the myofibroblast phenotype *Biomaterials.* 2007;28:3378-3387.
31. Sim EK, Muskawad S, Lim CS, Yeo JH, Lim KH, Grignani RT, Durrani A, Lau G, Duran C. Comparison of human and porcine aortic valves. *Clin Anat.* 2003;16(3):193-196.
32. Sands MP, Rittenhouse EA, Mohri H, Merendino KA. An anatomical comparison of human pig, calf, and sheep aortic valves. *Ann Thorac Surg.* 1969;8(5):407-414.

Chapter 12: Functional Coupling of Valvular Interstitial Cells and Collagen in the Mitral Leaflet

This chapter continues the topic of understanding normal valve mechanobiology by addressing cell-matrix interactions in the normal mitral valve. Specifically the study in this chapter demonstrates the functional interaction of valvular interstitial cells (VICs) and collagen.

ABSTRACT

Background: Recent studies have demonstrated that the anterior mitral leaflet (AML) *in vivo* exhibits a much higher stiffness than observed *ex vivo*. Such studies have also demonstrated dynamic *in vivo* leaflet stiffness modulation that cannot be accounted for by synthetic collagen remodeling or the cardiac muscle that extends into the AML. While valvular interstitial cells (VICs) could contribute to such apparent discrepancies between *in vivo* and *ex vivo* stiffness, as well as dynamic stiffness modulation, the exact mechanisms for VICs in AML force generation are not understood. This study tested the hypothesis that actin-mediated VIC force generation coupled to collagen via $\alpha_2\beta_1$ integrins is necessary for force generation in the AML.

Methods: In order to test this hypothesis, the central bare area of the AML was dissected from fresh porcine hearts, obtained from a local abattoir, and stained to visualize the VIC cytoplasm, nucleus, actin, and $\alpha_2\beta_1$ integrins. Second harmonic generated signal

was used to visualize collagen within the leaflets. Small (~1 cm x 5 mm) strips, with long axis in the AML circumferential direction, were sutured into a custom-designed strain-load device attached to a Zeiss Leica 510 LSM confocal microscope stage. Potassium chloride (KCl, 95 mM) was added to control samples (n=10), as well as samples incubated with either alpha₂beta₁ monoclonal blocking antibody (n=5) or 25 μM cytochalasin (n=4), and the resultant isometric force recorded using custom designed software.

Results: Fluorescent imaging revealed that VIC cell bodies were highly aligned in parallel with collagen fibers and their cytoplasm and nuclei were elongated in line with the collagen axis. High magnification microscopy revealed VIC cytoplasm tightly conforming to collagen fibers, with actin within VIC filopodia appearing to attach to the collagen fibers. Alpha₂beta₁ integrins were demonstrated to co-localize with VIC cytoplasmic staining as well as on the edge of collagen fibers. Functional studies of isometric force development demonstrated that while control samples developed force in response to KCl, either blocking alpha₂beta₁ integrins or blocking actin polymerization via cytochalasin abolished KCl-induced force development (p<0.001).

Conclusions: The imaging results from this study combined with the functional blocking experiments strongly suggest that VIC-collagen coupling, mediated by alpha₂beta₁ integrins, is necessary for KCl-induced force generation in the AML. This functional coupling between collagen and VICs via alpha₂beta₁ integrins is a good candidate for leaflet stiffness modulation *in vivo*.

The work contained in this chapter is under review by the journal *Cellular and Molecular Bioengineering*:

Stephens EH, Durst CA, Swanson JC, Grande-Allen KJ, Ingels NB, Jr., Miller DC. **Functional Coupling of Valvular Interstitial Cells and Collagen in the Mitral Leaflet.** *Journal of Cellular and Molecular Bioengineering*, under review.

INTRODUCTION

Recent studies indicate that *in vivo* mitral leaflet stiffness substantially exceeds what has been observed *ex vivo*.¹ Further studies suggest that dynamic, beat-to-beat modulation of leaflet stiffness occurs within the living heart on time scales much shorter than can be accounted for by synthetic remodeling of collagen or other extracellular matrix components.² While contraction of cardiac muscle extending from the left atrium into the leaflet accounts for some of these dynamic leaflet stiffness changes, pharmacologic blocking of contraction of this cardiac muscle revealed that there must be additional contractile elements contributing to the observed beat-to-beat leaflet stiffness modulation.^{2, 3} This growing body of evidence continues to revise the traditional view that mitral leaflets were passive flaps, suggesting, instead, a paradigm involving multiple contractile systems within the leaflets.

The role of valvular interstitial cells (VICs) in this unfolding paradigm remains unclear. While it is well known that VICs are fundamental to leaflet extracellular matrix synthesis and remodeling on longer time scales in both healthy and disease states,⁴⁻⁷ their role in the dynamic modulation of leaflet stiffness remains largely unknown. VICs are contractile^{8, 9} and, based on similarities to fibroblasts and myofibroblasts,¹⁰ VIC contraction is thought to occur via actin polymerization. Furthermore, studies have shown that vasoactive agents that cause VIC contraction also cause increased force generation in *ex vivo* viable valve leaflets^{9, 11-17} and increased aortic cusp flexural stiffness,¹⁸ suggesting that VIC contraction may play a role in leaflet stiffness modulation. The mechanisms underlying this modulation, however, have yet to be elucidated.

Transmission electron micrographs show VICs closely associated with collagen fibers,^{9, 19} suggesting an interaction between VICs and collagen in the leaflet, perhaps even acting together as a functional unit. Given that integrins are the primary proteins attaching cells to the surrounding matrix,²⁰ a potential interaction between VICs and collagen likely occurs through one of the integrins. Of the known collagen binding integrins, only $\alpha_2\beta_1$ and $\alpha_{11}\beta_1$ show higher affinity for type I collagen (the predominant collagen in heart valves²¹) than type IV.²² Based on fibroblast-collagen gel contraction²³ and fibroblast collagen fiber transport²⁴ studies, we hypothesized that $\alpha_2\beta_1$ integrins may be a mechanism by which VICs attach to collagen within the mitral valve leaflet. While a variety of integrins have been shown to be present on enzymatically isolated VICs, including $\alpha_2\beta_1$,^{25, 26} the potential functional role of integrins in valves, however, has not been studied.

Based on the hypothesized roles of actin and $\alpha_2\beta_1$ integrins in this proposed VIC-collagen mechanotransduction within the mitral valve, the aim of this study was to test the specific hypothesis that actin-mediated VIC force generation coupled to collagen via $\alpha_2\beta_1$ integrins was necessary for force generation in mitral leaflets.

METHODS

Immunofluorescence

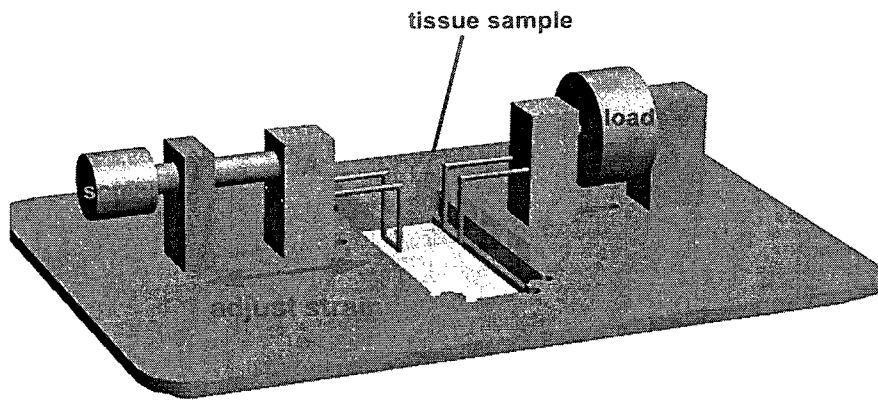
Porcine hearts (Yosemite Meat, Modesto, CA) were obtained within one hour of animal slaughter and transported in cold saline (0.9% sodium chloride, Hospira, Lake Forest, IL). The central bare area of each mitral anterior leaflet was dissected within 4

hours of animal slaughter and stained to visualize VIC cytoplasm, nucleus, actin, and/or $\alpha_2\beta_1$ integrins. VIC cytoplasm was stained using calcein AM (Invitrogen Molecular Probes, Eugene, OR), VIC nuclei were stained using Syto85 (Invitrogen Molecular Probes), and $\alpha_2\beta_1$ integrins were stained using a monoclonal antibody (MAB1998, Chemicon, Temecula, CA) conjugated to an AlexaFluor 684 fluorescent probe (Molecular Probes). Actin was stained using AlexaFluor 488 phalloidin (Invitrogen Molecular Probes) in tissues fixed in 10% formalin for 30 minutes and permeabilized with 0.5% Triton-X100 (Sigma-Aldrich, St. Louis, MO). Tissue was only fixed for actin staining; all other staining and force generation experiments utilized fresh tissues without fixation or permeabilization.

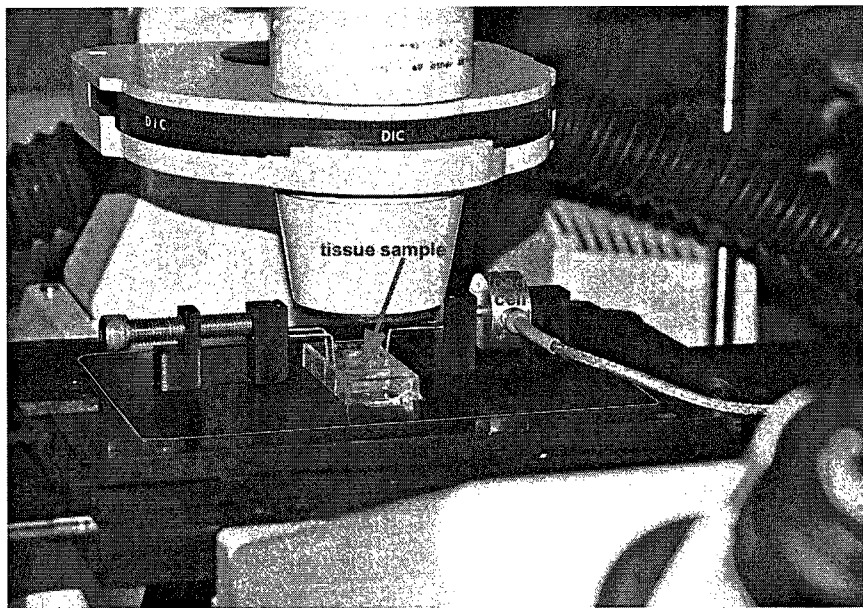
Confocal Microscopy

A Zeiss Leica 510 LSM confocal microscope (Zeiss, Oberkochen, Germany) with a Mira tunable Ti:Sa laser (Coherent, Santa Clara, CA) was used to visualize the fluorescent probes and the second-harmonic generated collagen signal (excitation at 820 nm, maximum emission at 410 nm). Specifically, calcein was visualized using a 488 nm Ar laser and 500-530 nm band pass (BP) filter, Syto85 was visualized using a 543 nm HeNe laser and 565-615 BP filter, AlexaFluor 684 conjugated $\alpha_2\beta_1$ integrins were visualized using a 633 nm HeNe laser and 650 low pass filter, and AlexaFluor 488 phalloidin was visualized using a 488 nm Ar laser and 500-530 nm BP filter. Second-harmonic generated collagen signal was obtained using an 820nm wavelength on the tunable Ti:Sa laser, and emission captured using a 390-465 nm BP filter. A key advantage of using second harmonic generation in these studies is that it allowed

A.



B.



C.

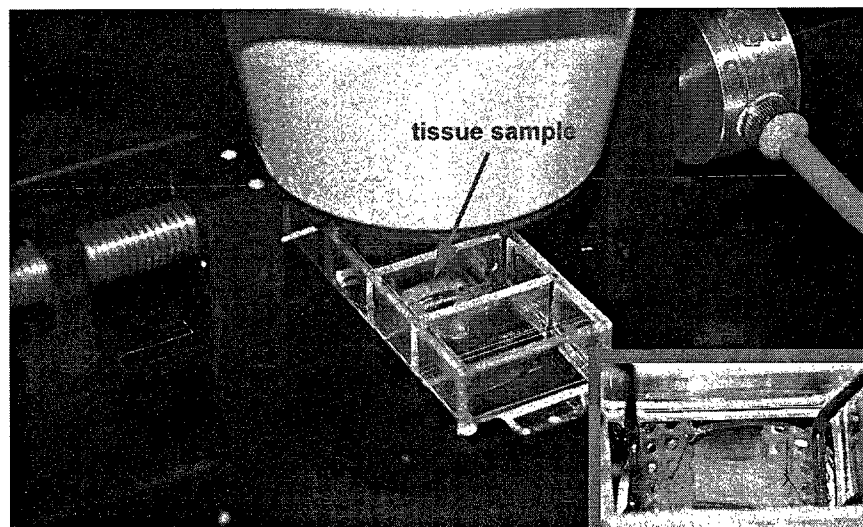


Fig. 12-1 (previous page): Custom-built strain-load device. A) Diagram illustrating strain-load device built to fit into a motorized confocal stage. Adjustable screw is shown at left; this screw, coupled with a block (labeled "A") that could freely slide in cut-out channel, allowed manipulation of strain on tissue as indicated by red arrow. Chamber glass, which held tissue sample in buffer, appears ghosted in on this diagram. The chamber glass was held above objective by virtue of a small metal lip. Placement of tissue sample within the set-up is indicated by the beige rectangle and load cell is labeled. B) Photo illustrating custom-built strain-load device diagrammed in (A) set in place on confocal stage. Edges of strain load device are outlined in red, tissue sample and load cell are labeled. Microscope objectives are located under the black stage (hidden from view) and microscope eye piece is evident in foreground of photo. Signal output from load cell is carried by silver cable to electronics not pictured. C) Close-up photo of in situ strain-load device. Note valve tissue sutured to plastic mesh between green wire struts. Microscope objective can be seen beneath cover glass. Tissue sample and load cell are labeled. Inset: view of tissue sample from above (microscope head piece removed) demonstrating tissue sutured in place within the chamber. Microscope objective can be seen below.

visualization of collagen without interfering with the potential VIC-collagen interaction, such as may have occurred with a fluorescent probe conjugated collagen antibody. Time-lapse images were taken with the 20x objective lens, while higher magnification images used 25x, 40x, 63x, and 100x oil immersion objective lenses. Images were processed using Zeiss LSM Image Browser software (Zeiss).

Custom-Built Strain-Load Device

Using computer assisted design software (SolidWorks, Dassault Systèmes, Lowell, MA), a strain-load device (Fig. 12-1) was built to fit, spring-loaded, into a motorized Zeiss Leica 510 LSM confocal microscope stage replacing the standard microscope slide holder. The device was fabricated from 6061 aluminum that was anodized for corrosion resistance. Tissue samples were placed in a 4-well cover glass chamber (LabTek II, Nalgene Nunc International, Naperville, IL) and sutured to plastic mesh attached to wire struts. These wire struts were secured with set screws in blocks on

either side of the wells. The blocks slid freely in one dimension in recessed channels. The 4-well cover glass chamber was suspended above the microscope objective using a small metal lip. An adjustable screw, coupled with the freely-sliding left block, allowed manipulation of strain on the tissue. A miniature tension load cell (Omega, Stamford, CT) was fit in-line with the sutured tissue. The load cell was powered using a 12 volt battery that delivered 10 volt DC to the load cell through the use of a voltage divider. Output from the load cell was captured by a USB data acquisition kit (USB 6008, National Instruments, Austin, TX), and recorded using a custom-designed virtual instrument (Lab View Signal Express, National Instruments).

Force Generation Studies

Small (~1 cm x 5 mm) circumferential strips of the central, bare area of the anterior mitral leaflet were sutured into the custom-designed strain-load device fit upon the microscope stage, as described above. After suturing the tissue in place, the tissue was allowed to equilibrate in Krebs's solution for at least 20 minutes (136.9 mM NaCl, 11.9 mM NaHCO₃, 2.7 mM KCl, 0.4 mM NaH₂PO₄, 2.5 mM MgCl₂, 2.5 mM CaCl₂, 11.1 mM glucose, 0.04 mM disodium EDTA, pH 7.4). Potassium chloride (95 mM) was added to control samples (n=10) and the load-cell output recorded using the custom-designed software described above. To investigate the roles of $\alpha_2\beta_1$ integrins and actin in VIC-mediated leaflet contraction, VIC cytoplasmic and nuclear staining was performed as described above, and tissues were incubated with either 10 μ g/ml $\alpha_2\beta_1$ monoclonal blocking antibody (n=5) (Chemicon) or 25 μ M cytochalasin (n=4) (Sigma Aldrich) before the addition of 95 mM KCl.

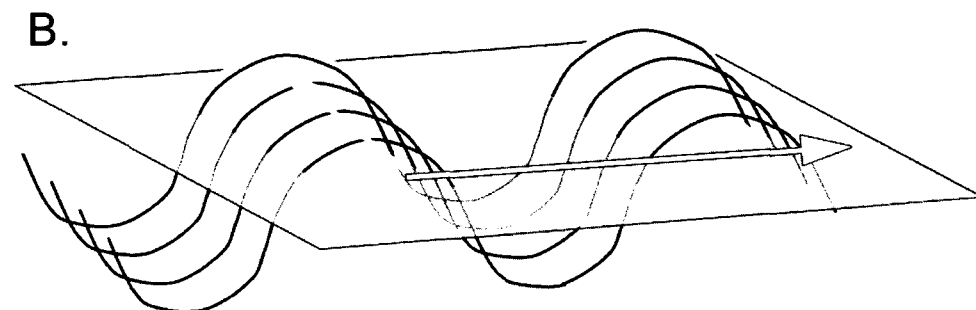
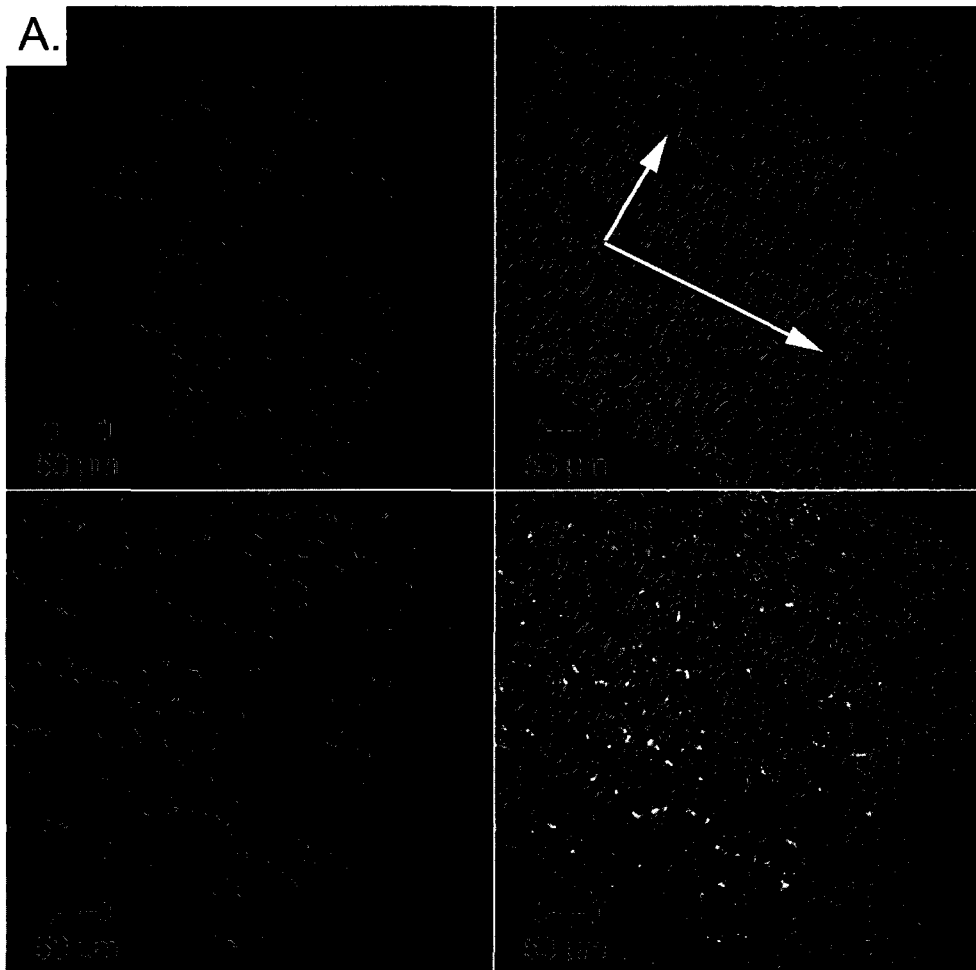


Fig. 12-2: A). Image demonstrating VIC alignment with respect to collagen fibers. Blue (upper left panel) indicates the VIC cytoplasm, green (upper right panel) indicates collagen fibers, red (lower left panel) indicates VIC nuclei, and lower right panel is the merged image of the 3 other panels. The yellow arrow in the upper right panel indicates the orientation of collagen ridges, and correlates to the yellow arrow in the schematic in part B. The white arrow in the upper right panel indicates the orientation of collagen fibers, and is analogous to the white arrow in the schematic of part B (note: in all remaining figures collagen fiber alignment is indicated by a white arrow). Scale bar indicates 50 μm . B). Schematic illustrating how undulating collagen fibers at this magnification appear as lines perpendicular to the direction of collagen fibers. White portions of undulating fibers above green plane represent portions of fibers in focus. The yellow arrow indicates the ridges visualized in the upper right panel of part A (and corresponds to the yellow arrow in part A), whereas the white arrow indicates the orientation of collagen fibers.

Statistical Analysis

Statistical comparisons between groups were made with one-way ANOVAs using SigmaStat software (SPSS, Chicago, IL), as described in Chapter 4. Post-hoc pair-wise comparisons were performed using Dunn's method. Data is presented as mean \pm standard error of the mean.

RESULTS

VICs Aligned and Integrated with Collagen Fibers

Fluorescent imaging of VICs revealed that VIC cell bodies were highly aligned in parallel with collagen fibers (Fig. 12-2). VIC cytoplasm and nuclei were elongated, with their long axis coinciding with that of the collagen fibers. High magnification images demonstrated the VIC cytoplasm tightly conforming to the undulating contour of the crimped collagen fibers (Fig. 12-3). Fluorescent imaging of VIC cytoskeletal actin revealed VIC actin similarly aligned with collagen fibers, and actin within VIC filopodia appeared to grasp collagen fibers (Fig. 12-4). Where collagen fibers were not highly aligned, VIC morphology and actin configuration were substantially different: VICs were less elongated and VIC filopodia extended in disparate directions, although still appearing to follow and potentially to attach to collagen fibers (Fig. 12-5).



Fig. 12-3: Image demonstrating VICs nestled into the curves of the collagen fibers. Green indicates collagen fibers, blue indicates VIC cytoplasm, and pink indicates VIC nuclei. White arrow indicates the direction of collagen fibers. Scale bar indicates 10 μ m.

VIC Alpha₂Beta₁ Integrins Localized to Collagen Fibers

VIC alpha₂beta₁ integrins, demonstrated on the edges of the VIC cytoplasm stain (Fig. 12-6), were found at high magnification to co-localize to the borders of collagen fibers (Fig. 12-7). VICs in alpha₂beta₁ integrin-blocked samples tended to show less alignment relative to collagen fibers compared to control samples taken from the same region of the same leaflet (Fig. 12-8).

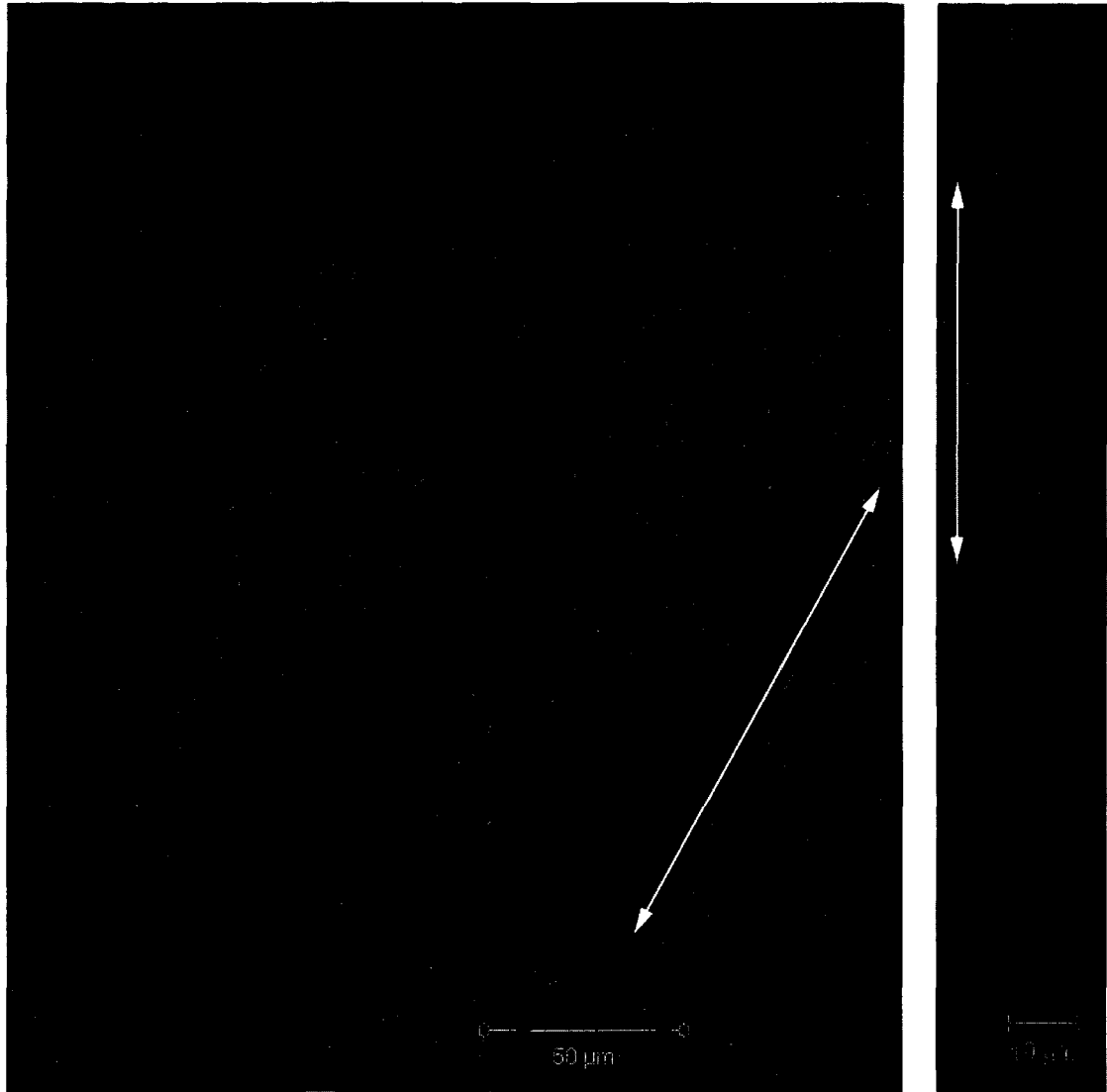


Fig. 12-4: Left panel demonstrates alignment of VIC actin with collagen fibers at lower magnification. Green indicates collagen fibers, blue indicates VIC actin, and pink indicates VIC nuclei. Scale bar indicates 50 μm . Right panel demonstrates VIC actin processes "grasping" collagen fibers at higher magnification. Scale bar indicates 10 μm . White arrow in both portions of the figure indicates orientation of collagen fibers.

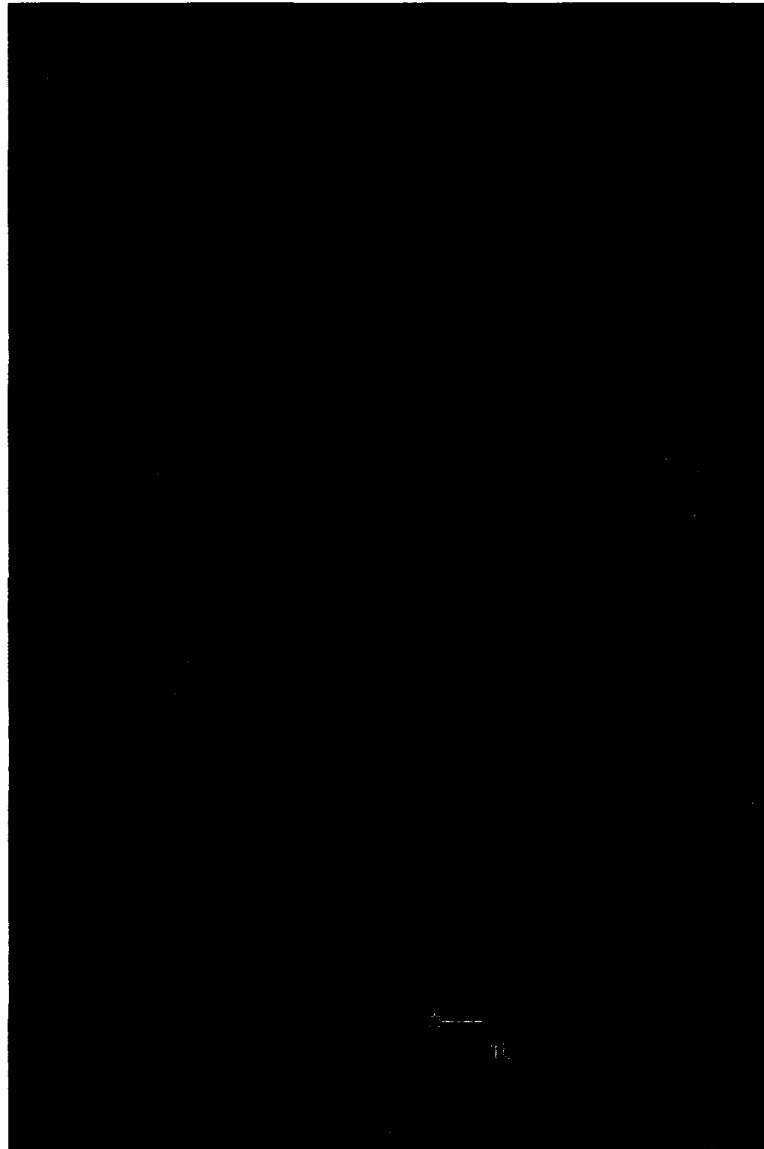


Fig. 12-5: VIC actin in a region in which collagen was not highly aligned. Note differences in actin configuration and VIC morphology. To facilitate visualization of actin, in this image green indicates VIC actin and blue indicates collagen fibers. Scale bar indicates 10 μm .

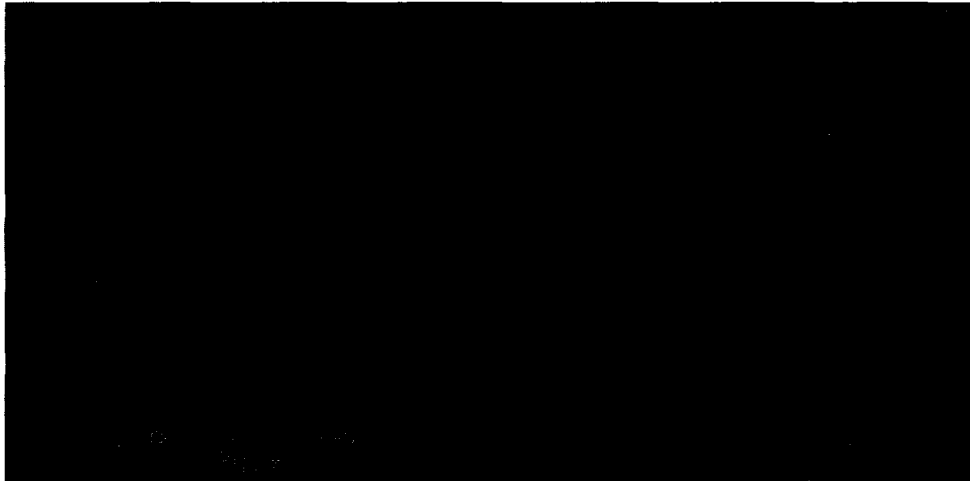


Fig. 12-6: *Alpha₂beta₁ integrins located on VIC cell membrane. Green indicates alpha₂beta₁ integrins, blue indicates VIC cytoplasm, and pink indicates VIC nuclei. Scale bar indicates 10 μ m.*



Fig. 12-7: *Alpha₂beta₁ integrins located on collagen fibers. Blue indicates collagen fibers, green indicates alpha₂beta₁ integrins, and red indicates VIC nuclei. Scale bar indicates 20 μ m. White arrow indicates direction of collagen fibers within the image.*

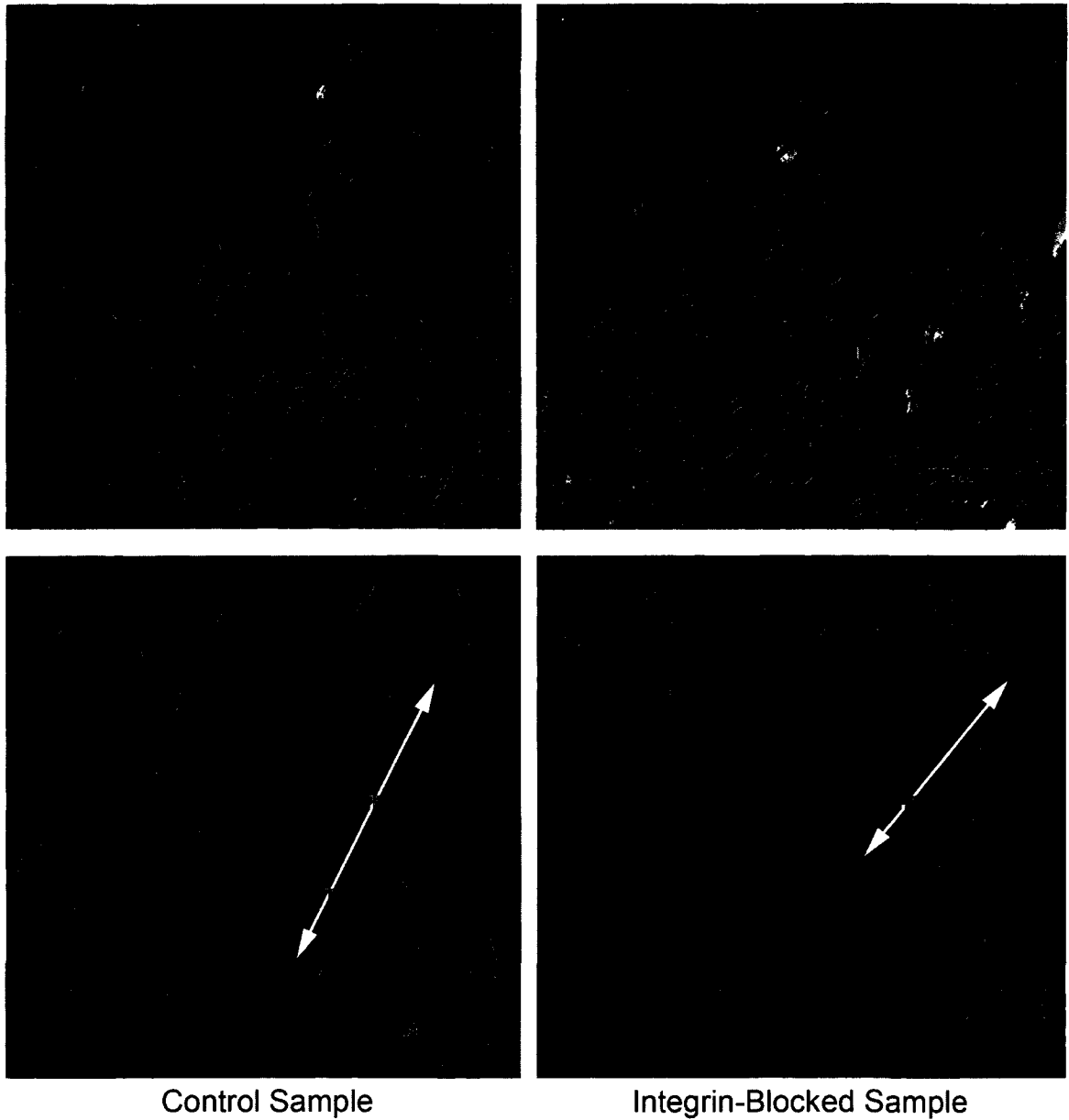


Fig. 12-8: VICs after blocking $\alpha_2\beta_1$ integrins tended to show less alignment with collagen fibers. Left panel demonstrates control sample, right panel demonstrates sample from adjacent region of the same leaflet in which $\alpha_2\beta_1$ integrins were blocked. The upper panels are merged images in which green indicates collagen fibers, blue indicates VIC cytoplasm, and pink indicates VIC nuclei. Lower images are identical to merged images above, but illustrate cytoplasm staining alone to better visualize VIC alignment relative to collagen fiber orientation (indicated by white arrows), demonstrating less alignment of VICs in $\alpha_2\beta_1$ integrin-blocked samples relative to collagen fibers. Scale bar indicates 20 μm .

Blocking Alpha₂Beta₁ Integrins or Actin Polymerization Prevented Force Generation

Consistent with previous studies,^{9, 11-17} the addition of 95 mM KCl resulted in force generation (Fig. 12-9) in the circumferential strip of mitral valve tissue. Blocking of either alpha₂beta₁ integrins or actin polymerization (via cytochalasin) was sufficient to prevent force generation in response to 95 mM KCl (control: 3.30±0.23 mN, integrin-blocked: 0.04±0.09 mN, cytochalasin 0.20±0.06 mN, p<0.001, p<0.001, Fig. 12-9).

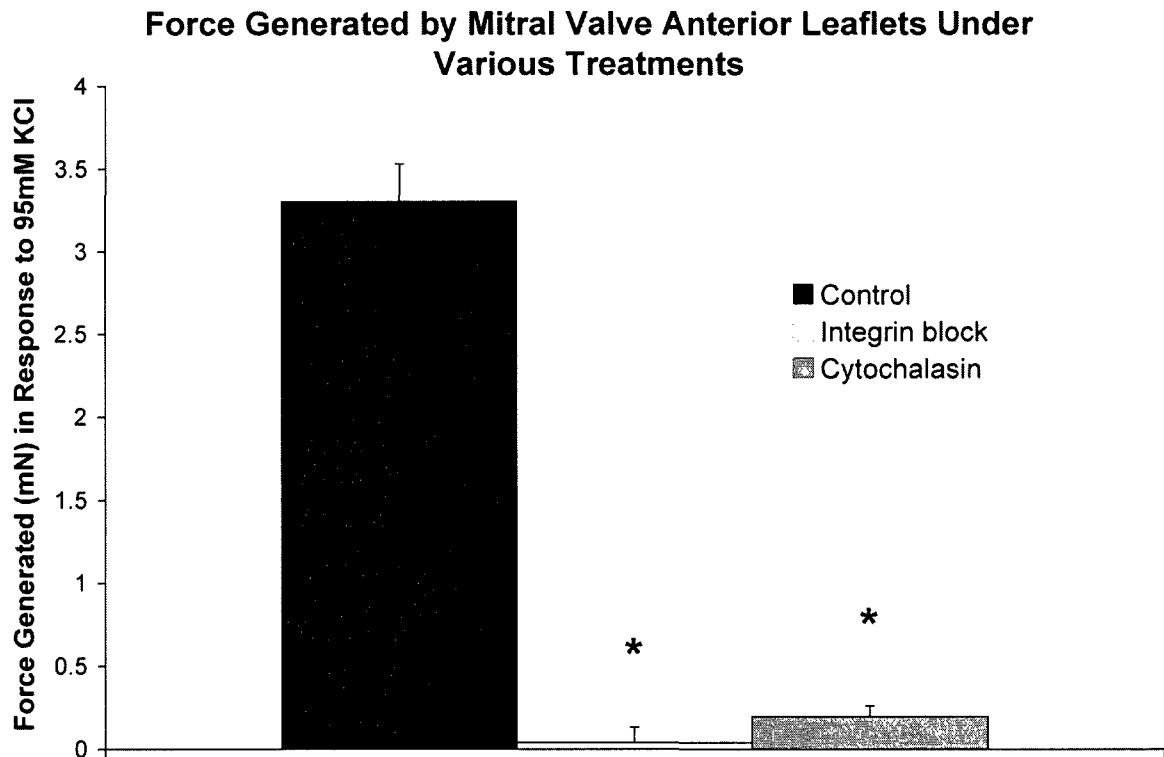


Fig. 12-9: Force generated by mitral valve anterior leaflets exposed to various treatments in response to 95 mM KCl after 10 minutes. Overall comparison between groups by one-way ANOVA: $p < 0.001$; pair-wise comparison (Dunn's method): * $p < 0.05$ vs. control. Error bars indicate standard error of the mean.

DISCUSSION

The imaging results of this study, taken together with the leaflet force data, support the hypothesis that VIC-collagen coupling, mediated by $\alpha_2\beta_1$ integrins, contributes to the leaflet stiffness modulation that has been observed in the *in vivo* leaflet.

Confocal microscopy imaging, used to investigate the structural relationship of VICs, collagen fibers, and $\alpha_2\beta_1$ integrins demonstrated VICs closely conformed to crimped collagen fibers and appeared to grasp collagen fibers with their filopodia. $\alpha_2\beta_1$ integrins localized to the VIC borders adjacent to collagen fibers. When these integrins were blocked, VICs appeared less aligned with the collagen fibers. These results provide a structural foundation for a proposed VIC/collagen functional unit.

Functional studies, utilizing KCl to elicit VIC contraction, built on this foundation, and demonstrated the necessary components of this functional unit for mitral valve force generation: VIC actin polymerization, collagen fibers, and $\alpha_2\beta_1$ integrins. Blocking either $\alpha_2\beta_1$ integrin (the hypothesized means by which VICs attach to collagen) or actin polymerization (the hypothesized means of VIC contraction) abolished leaflet force generation. These results suggest that contraction of VICs and their adherence to collagen are both necessary for force generation in the mitral leaflet.

Structural Interaction between VICs, Integrins, and Collagen Fibers

The second harmonic-generated collagen signal allowed visualization of the structural relationship between collagen fibers and viable VICs in freshly excised leaflets without altering their spatial arrangement with tissue fixation and processing, or

disrupting potential interactions between VICs and collagen fibers, as can occur with antibodies or other probes. This method of visualizing viable cells in freshly excised tissues is in contrast to the limited number of previous studies in which transmission electron microscopy demonstrated VICs abutting collagen fibers.^{9, 19} While these previous studies were important to our understanding of VICs within the valve matrix, such imaging modalities have significant limitations related to specimen preparation, which make interpretation of their results in the context of *in vivo* leaflets difficult. Our imaging modality enabled us to make inferences about functional implications of the structural interactions observed in the *in vivo* leaflet, and thereby relate the imaging results to the functional studies.

Of particular note was the parallel alignment of VICs relative to collagen fibers. While leaflet anisotropy has largely been attributed to collagen fiber alignment in the past,²⁷ the observed alignment of VICs in conjunction with the functional findings of this study and studies demonstrating that VIC contraction caused greater circumferential as opposed to radial force generation in aortic cusps,¹⁵ suggests that VIC alignment may contribute to the anisotropic material properties of valves.

VIC cytoplasm was not only observed to closely follow the contours of the crimped collagen fibers, in what could be considered a space-filling manner, but apparent direct attachments were observed between filopodia and collagen fibers, suggesting a structural link between VICs and collagen fibers. Furthermore, even in regions in which collagen fibers were not aligned, VIC filopodia appeared to reach out and grasp collagen fibers, further suggesting that VICs were directly interacting with the collagen as opposed

to simply possessing the same alignment as a result of space effects. These images could even suggest a role for VICs in aligning collagen fibers as the leaflet undergoes strain.

Confocal imaging demonstrated $\alpha_2\beta_1$ integrins on VICs within viable tissue strips, consistent with previously reported findings using enzymatically isolated VICs.^{25,}

²⁶ Imaging in this study, however, also suggested a potential functional role for these $\alpha_2\beta_1$ integrins: attaching VICs to adjacent collagen fibers. When $\alpha_2\beta_1$ integrins were blocked, VICs were less aligned with collagen fibers as compared with VICs in control samples taken from the same leaflet region.

VIC-Integrin-Collagen Functional Unit

This study demonstrated that blocking $\alpha_2\beta_1$ integrins abolished leaflet force development; this result suggests that VICs are functionally coupled with collagen via $\alpha_2\beta_1$ integrins allowing the force generated by VIC contraction to be transmitted to collagen, and thereby the mitral leaflet (Fig. 12-10). Similarly, when actin polymerization was blocked via cytochalasin,^{28, 29} leaflet force generation did not occur. This result suggests that leaflet force is developed by actin-dependent VIC contraction. Therefore, when either the actin portion of the functional unit or the integrin portion of the functional unit is blocked, force is not generated in the leaflet.

VIC-Integrin-Collagen in Stiffness Modulation

The proposed VIC-integrin-collagen functional unit and the force it can produce is likely dynamic, and may contribute to the leaflet stiffness modulation that has been

observed *in vivo*.^{2,3} Integrin binding is a dynamic process during which time the amount of force that is transduced also changes. Beginning with punctate integrin “focal

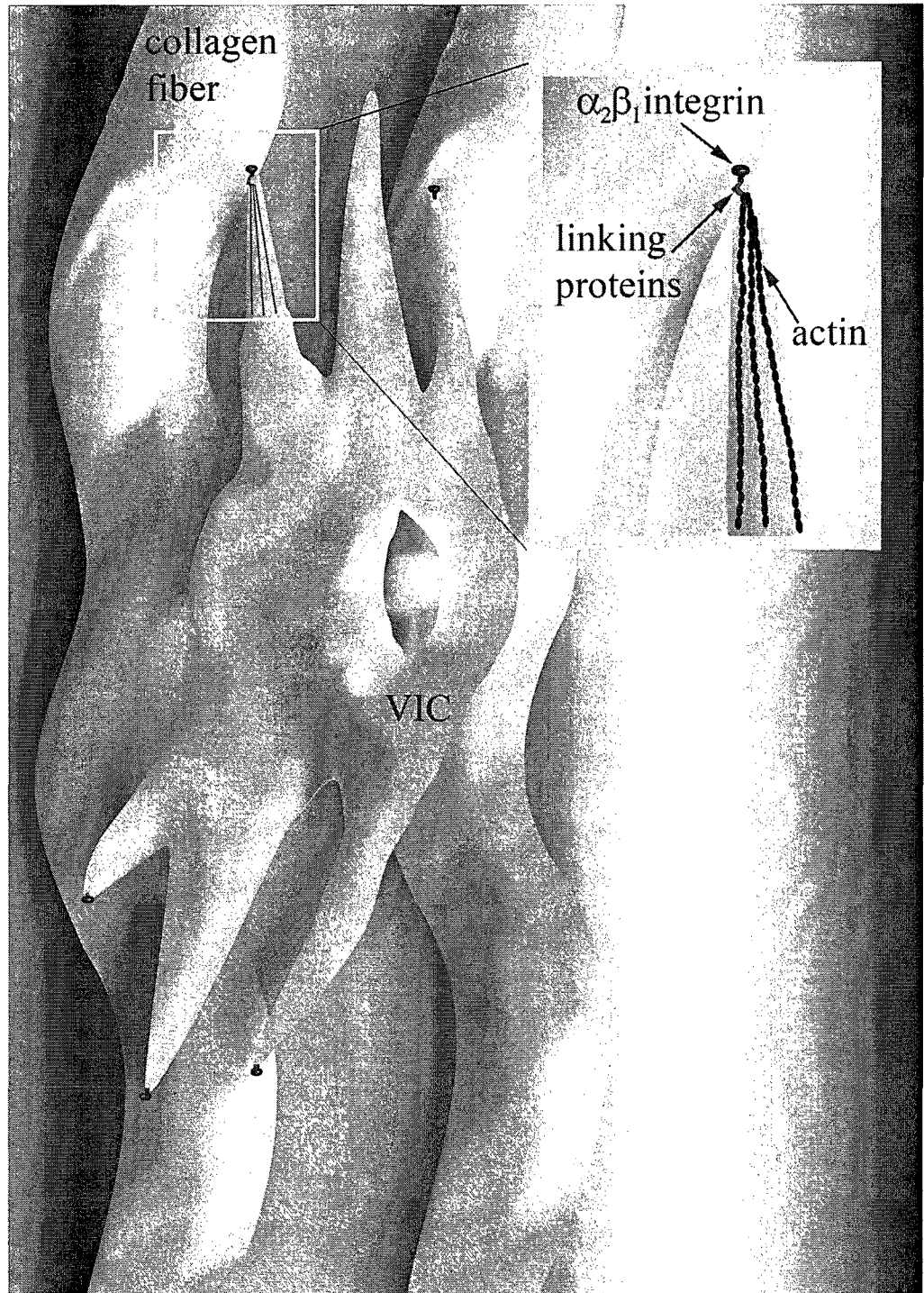


Fig. 12-10: Diagram illustrating the proposed VIC-integrin-collagen functional unit suggested by the results of this study. Inset on right displays an $\alpha_2\beta_1$ integrin with its external domain attaching to a collagen fiber and cytosolic domain attaching to the actin cytoskeleton via linking proteins.

complexes,”^{20, 30} integrin binding proceeds with the recruitment of additional proteins to form large supramolecular structures, “focal adhesions,” that enable greater force to be transmitted through the binding site.³¹ The actin microfilament portion of this contractile system, to which focal adhesions attach, also dynamically polymerize and depolymerize.³¹ These two constantly changing processes of integrin binding and actin microfilament polymerization affect each other in real time.³⁰ Even the strength of integrin binding is not static, but rather continually changing depending on a number of factors.³² The magnitude of the force that the integrin-actin complex exerts also changes depending upon the state of maturation of the integrin adhesion, as described above, as well as the number of binding sites and adhesive strength of the integrins. Similarly, the magnitude of actin force development is modulated by a number of factors, including signaling events such as those initiated by transforming growth factor beta, the ratio of polymerization to depolymerization, and expression of certain actin isoforms like smooth muscle alpha-actin.³³ Some of these changes, such as the transition from initial low affinity integrin binding to high affinity binding, occur on the order of 10 seconds.³² Taken together, this proposed VIC-integrin-collagen functional unit has the potential to dynamically alter the force it exerts, and therefore could contribute to leaflet stiffness modulation *in vivo*.

The supposition that VICs can modulate leaflet stiffness is supported by the work of Merryman et al., who showed an increase in aortic valve leaflet flexural stiffness with VIC contraction induced by KCl.¹⁸ Furthermore, treatment of valves tissues with

thapsigargin, which prevents VIC contraction via inhibiting ATPase, led to a dramatic decrease in leaflet flexural stiffness, suggesting that VICs are responsible for a basal level of valve tonus.

Valve Force Generation in an Isometric Setting

While force generation in valves is commonly reported in the context of uniaxial or biaxial tensile testing, in which case collagen strain is occurring, the force generation demonstrated in this study occurred within an isometric set-up without collagen strain. The mechanism, therefore, of force generation in this study must be an increase in stiffness. This is conceptualized in Figure 12-11. If the yellow stars represent hypothetical force measurements of a valve tissue (in the context of this experiment #1 represents the force measured before addition of KCl and #2 represents the force measured after addition of KCl), then the observed increased in force could be due to an increase in strain (as in a traditional uniaxial or biaxial mechanical testing set-up) in which the stiffness of the tissue remains constant (path “A”), or by a change in tissue stiffness (elastic modulus (E)) from E_1 to E_2 (path “B”). Examination of force development in an isometric setting has a number of advantages including isolating variables. While *in vivo* the leaflet clearly is not an isometric system (rather, collagen strain occurs as the valve is hemodynamically loaded), the VIC-collagen interactions demonstrated in this study are likely fundamental and therefore would occur in the setting of collagen strain as well. In fact, the VIC-collagen interaction may even have a greater role to play in the setting of collagen fiber strain, although that remains to be determined.

Conceptualizing Means of Force Generation in Valves

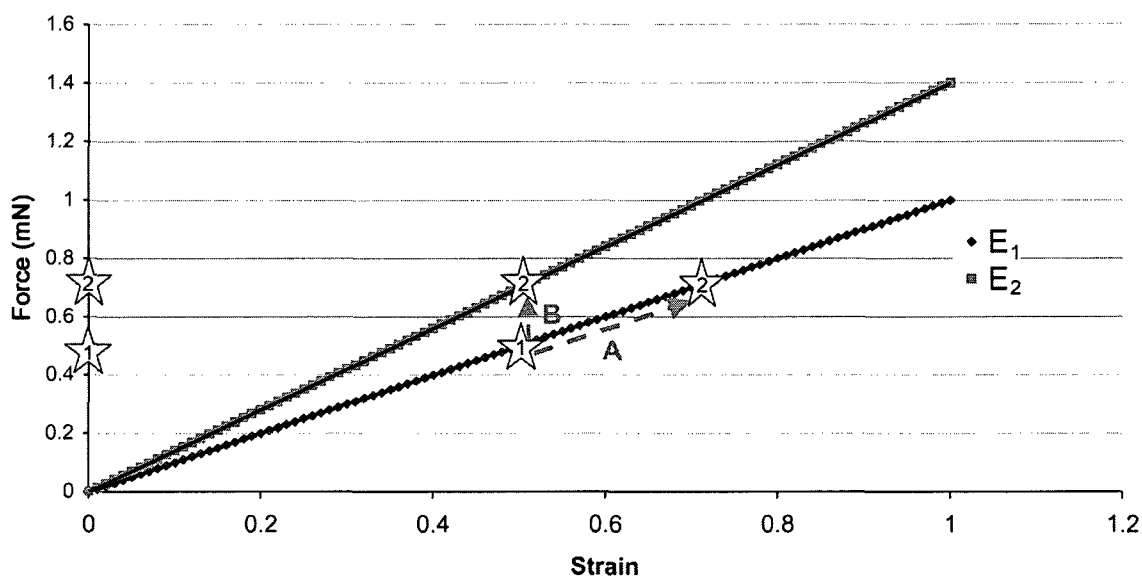


Fig. 12-11: Diagram conceptualizing different means by which force may be generated in valve leaflets. E =elastic modulus (tissue “stiffness”), E_1 =initial elastic modulus; E_2 =modified elastic modulus. The stars on the y-axis represent two hypothetical measurements of force of a valve tissue (i.e., in the context of these studies #1 would represent a measurement of force before addition of KCl and #2 after addition of KCl). This difference in force could be explained by either an increase in strain within the tissue (the path marked by the dashed line “A”) in which the elastic modulus does not change (therefore the path follows along the E_1 line), or by a change in elastic modulus of the valve tissue from E_1 to E_2 (the path marked by the dashed line “B”). In the case of path “B,” no change in tissue strain would occur.

Implications

The results from this study confirm and build upon a currently proposed working hypothesis of contractile systems within the MV. Itoh et al.² proposed a model of the MV that included 3 potential contractile elements including cardiac muscle, smooth muscle, and VICs to explain the dynamic stiffness changes that take place in the mitral valve in the beating heart. The results of this study confirm that VICs are a contractile element in the MV, and add to this proposed model by demonstrating how VICs generate force in concert with collagen via integrin coupling. The VIC-collagen coupling

demonstrated in this study was demonstrated isometrically, however it is likely that these are fundamental interactions that occur in the context of collagen strain in the *in vivo* valve as well.

A number of factors could affect the proposed VIC-integrin-collagen unit and potentially affect leaflet stiffness modulation as well as valve function in pathophysiological conditions. For example, changes in collagen fiber crosslinking and packing, as well as collagen turnover, could affect the ability of VICs to bind to collagen and transduce force. Circulating factors, including cytokines, inflammatory mediators, vasoactive agents, and pharmaceutical agents, could affect both the contractile and adhesive capabilities of VICs. Changes in VIC cell phenotype, as occur via alterations in the mechanoenvironment and chemical mediators, would also likely affect the ability of VICs to produce and transduce force. Lastly, sympathetic and parasympathetic innervation could affect this functional unit either directly or through paracrine mechanisms.

In fact, valve diseases demonstrate alterations in these factors. Changes in MV collagen content, collagen turnover, and matrix metalloproteinase expression have been documented in diseases such as dilated cardiomyopathy and functional mitral regurgitation.^{6, 7, 34} VICs in a number of valve diseases, such as myxomatous mitral valve disease, also demonstrate a more myofibroblastic cell phenotype including greater smooth muscle alpha-actin expression,⁴ which directly relates to force generation in myofibroblasts.³⁵ Changes in integrins expression and activation, has been demonstrated in the myocardium of a number of cardiac diseases,³⁶ and may be altered in valve

diseases as well. Therefore, the proposed functional unit may be impacted by, or even contribute to valve pathologies, although considerable work in this area is needed.

The results of this study may also have implications for the design of a tissue engineered heart valve (TEHV). Creating a TEHV complete with living VICs may be necessary not only for the TEHV to successfully adapt (via matrix remodeling) to changes in valve stresses, for example as the patient grows, or as cardiac pressures change with age, but living VICs within a TEHV will be important at a more fundamental level to provide these VIC-collagen functional units and their fundamental contributions to tonus, anisotropy, and dynamic modulation of stiffness. This study further demonstrates that an acellular elastomeric scaffold whose motion is determined by passive response to pressure gradients, would likely fall significantly short of the gold standard in TEHV: emulating the native valve.

Limitations and Future Studies

While this study represents an important step forward in examining the relationship between structure and function in the mitral leaflet, a number of limitations should be noted. Tighter control of temperature and carbon dioxide, such as with a closed chamber system more analogous to an organ bath set-up, would be ideal, however this was not feasible in the present set-up. More precise control of pre-load and of strain, perhaps using a micropositioner, would also enhance this set-up. Regardless, given the dramatic change in force generation with blocking agents, these limitations did not affect the ultimate interpretation of the study.

While the isometric set-up used in these experiments had a number of advantages, insight could also be gained by examining isotonic contraction, as well as utilizing other vasoconstrictive reagents. Exploring changes in mitral leaflet stiffness caused by different agents would also add to our understanding of VIC/leaflet contractility and how it relates to function. While much remains to be done in this area, including further characterization of VICs and collagen as a functional unit, this study is an important step in furthering our understanding of the roles played by VICs and collagen in mitral valve force generation.

CONCLUSIONS

This study demonstrated that VIC-collagen coupling via integrins contributes to force generation in mitral valves and supports the concept of multiple contractile systems in the mitral valve. Together with other studies demonstrating that the mitral valve possesses its own vasculature and innervation, and remodels in response to a variety of stimuli, this study adds to a growing body of evidence that the mitral valve is an active, dynamic entity as opposed to a passive flap. VICs, in concert with the extracellular matrix in which they are not only embedded, but also interact with and regulate the composition of, are a key component to this revised notion of the valve. As our concept of the valve continues to be refined, so too will our definition of valve diseases and therapeutic approaches to them.

This chapter, which demonstrated the functional interaction of valvular interstitial cells (VICs) and collagen in the mitral leaflet, concludes the series of chapters addressing normal valve mechanobiology (Chapters 3-12). In these chapters a variety of topics have been covered including age-related changes in matrix composition and structure (Chapters 3-6) and material properties (Chapter 7), as well as valve heterogeneity in terms of composition and motion (Chapters 8 and 9) and related to the VIC population (Chapters 10 and 11).

The next portion of the thesis (Chapters 13-21) address valves in the contexts of various diseased states including congenital valve disease (Chapters 13 and 14), dilated cardiomyopathy and “functional” mitral regurgitation (Chapters 15-17), valve wound healing (Chapter 18), myxomatous mitral valve disease (Chapter 19, as well as Chapter 24 in the Appendix), and calcific aortic valve disease (Chapters 20 and 21). This portion of the thesis addressing valves in diseased states opens with a review of congenital valve disease contained in the next chapter.

REFERENCES

1. Krishnamurthy G, Ennis DB, Itoh A, Bothe W, Swanson JC, Karlsson M, Kuhl E, Miller DC, Ingels NB, Jr. Material properties of the ovine mitral valve anterior leaflet in vivo from inverse finite element analysis. *Am J Physiol Heart Circ Physiol*. 2008;295(3):H1141-1149.
2. Itoh A, Krishnamurthy G, Swanson JC, Ennis DB, Bothe W, Kuhl E, Karlsson M, Davis LR, Miller DC, Ingels NB, Jr. Active stiffening of mitral valve leaflets in the beating heart. *Am J Physiol Heart Circ Physiol*. 2009;296(6):H1766-1773.
3. Krishnamurthy G, Itoh A, Swanson JC, Bothe W, Karlsson M, Kuhl E, Miller DC, Ingels NB, Jr. Regional stiffening of the mitral valve anterior leaflet in the beating ovine heart. *J Biomech*. 2009.
4. Rabkin E, Aikawa M, Stone JR, Fukumoto Y, Libby P, Schoen FJ. Activated interstitial myofibroblasts express catabolic enzymes and mediate matrix remodeling in myxomatous heart valves. *Circulation*. 2001;104(21):2525-2532.
5. Aikawa E, Whittaker P, Farber M, Mendelson K, Padera RF, Aikawa M, Schoen FJ. Human semilunar cardiac valve remodeling by activated cells from fetus to adult: implications for postnatal adaptation, pathology, and tissue engineering. *Circulation*. 2006;113(10):1344-1352.
6. Stephens EH, Nguyen TC, Itoh A, Ingels NB, Jr., Miller DC, Grande-Allen KJ. The effects of mitral regurgitation alone are sufficient for leaflet remodeling. *Circulation*. 2008;118(14 Suppl):S243-249.
7. Stephens EH, Timek TA, Daughters GT, Kuo JJ, Patton AM, Baggett LS, Ingels NB, Miller DC, Grande-Allen KJ. Significant changes in mitral valve leaflet matrix composition and turnover with tachycardia-induced cardiomyopathy. *Circulation*. 2009;120(11 Suppl):S112-119.
8. Messier RH, Jr., Bass BL, Aly HM, Jones JL, Domkowski PW, Wallace RB, Hopkins RA. Dual structural and functional phenotypes of the porcine aortic valve interstitial population: characteristics of the leaflet myofibroblast. *J Surg Res*. 1994;57(1):1-21.
9. Filip D, Radu A, Simionescu M. Interstitial cells of the heart valve possess characteristics similar to smooth muscle cells. *Circulation Research*. 1986;59(3):310-320.
10. Taylor PM, Batten P, Brand NJ, Thomas PS, Yacoub MH. The cardiac valve interstitial cell. *Int J Biochem Cell Biol*. 2003;35(2):113-118.
11. Pompilio G, Rossoni G, Sala A, Polvani GL, Berti F, Dainese L, Porqueddu M, Biglioli P. Endothelial-dependent dynamic and antithrombotic properties of porcine aortic and pulmonary valves. *Ann Thorac Surg*. 1998;65(4):986-992.
12. Wassenaar C, Bax WA, van Suylen RJ, Vuzevski VD, Bos E. Effects of cryopreservation on contractile properties of porcine isolated aortic valve leaflets and aortic wall. *J Thorac Cardiovasc Surg*. 1997;113(1):165-172.

13. Bowen I, Marr C, Chester A, Wheeler-Jones C, Elliott J. In-vitro contraction of the equine aortic valve. *J Heart Valve Dis.* 2004;13(4):593-599.
14. Chester A, Misfeld M, Yacoub M. Receptor-mediated contraction of aortic valve leaflets. *J Heart Valve Dis.* 2000;9(2):250-254.
15. Kershaw J, Misfeld M, Sievers H, Yacoub M, Chester A. Specific regional and directional contractile responses of aortic cusp tissue. *J Heart Valve Dis.* 2004;13(5):798-803.
16. Taylor P, Allen S, Yacoub M. Phenotypic and functional characterization of interstitial cells from human heart valves, pericardium and skin. *J Heart Valve Dis.* 2000;9(1):150-158.
17. Sonnenblick E, Napolitano L, Daggett W, Cooper T. An intrinsic neuromuscular basis for mitral valve motion in the dog. *Circ Res.* 1967;21(1):9-15.
18. Merryman W, Huang H, Schoen F, Sacks M. The effects of cellular contraction on aortic valve leaflet flexural stiffness. *J Biomech.* 2006;39(1):88-96.
19. Huang H, Liao J, Sacks M. In-situ deformation of the aortic valve interstitial cell nucleus under diastolic loading. *J Biomech Eng.* 2007;129(6):880-889.
20. Zamir E, Geiger B. Molecular complexity and dynamics of cell-matrix adhesions. *J Cell Sci.* 2001;114(Pt 20):3583-3590.
21. Cole WG, Chan D, Hickey AJ, Wilcken DE. Collagen composition of normal and myxomatous human mitral heart valves. *Biochem J.* 1984;219(2):451-460.
22. Barczyk M, Carracedo S, Gullberg D. Integrins. *Cell Tissue Res.* 2009.
23. Dallon J, Ehrlich H. A review of fibroblast-populated collagen lattices. *Wound Repair Regen.* 2008;16(4):472-479.
24. Meshel A, Wei Q, Adelstein R, Sheetz M. Basic mechanism of three-dimensional collagen fibre transport by fibroblasts. *Nat Cell Biol.* 2005;7(2):157-164.
25. Latif N, Sarathchandra P, Thomas PS, Antoniw J, Batten P, Chester AH, Taylor PM, Yacoub MH. Characterization of structural and signaling molecules by human valve interstitial cells and comparison to human mesenchymal stem cells. *J Heart Valve Dis.* 2007;16(1):56-66.
26. Wiester L, Giachelli C. Expression and function of the integrin $\alpha 9\beta 1$ in bovine aortic valve interstitial cells. *J Heart Valve Dis.* 2003;12(5):605-616.
27. Kunzelman KS, Cochran RP. Stress/strain characteristics of porcine mitral valve tissue: parallel versus perpendicular collagen orientation. *J Card Surg.* 1992;7(1):71-78.
28. Goddette DW, Frieden C. Actin polymerization. The mechanism of action of cytochalasin D. *J Biol Chem.* 1986;261(34):15974-15980.

29. Flanagan MD, Lin S. Cytochalasins block actin filament elongation by binding to high affinity sites associated with F-actin. *J Biol Chem*. 1980;255(3):835-838.
30. Geiger B, Spatz JP, Bershadsky AD. Environmental sensing through focal adhesions. *Nat Rev Mol Cell Biol*. 2009;10(1):21-33.
31. Vicente-Manzanares M, Choi CK, Horwitz AR. Integrins in cell migration--the actin connection. *J Cell Sci*. 2009;122(Pt 2):199-206.
32. Carman CV, Springer TA. Integrin avidity regulation: are changes in affinity and conformation underemphasized? *Curr Opin Cell Biol*. 2003;15(5):547-556.
33. Hinz B, Gabbiani G. Mechanisms of force generation and transmission by myofibroblasts. *Curr Opin Biotechnol*. 2003;14(5):538-546.
34. Grande-Allen KJ, Borowski AG, Troughton RW, Houghtaling PL, Dipaola NR, Moravec CS, Vesely I, Griffin BP. Apparently normal mitral valves in patients with heart failure demonstrate biochemical and structural derangements: an extracellular matrix and echocardiographic study. *J Am Coll Cardiol*. 2005;45(1):54-61.
35. Hinz B, Celetta G, Tomasek J, Gabbiani G, Chaponnier C. Alpha-smooth muscle actin expression upregulates fibroblast contractile activity. *Mol Biol Cell*. 2001;12(9):2730-2741.
36. Ross RS. The extracellular connections: the role of integrins in myocardial remodeling. *J Card Fail*. 2002;8(6 Suppl):S326-331.

Chapter 13: Insight into Histological and Pathological Abnormalities in Congenitally Diseased Valves Based on Advances in Understanding Normal Valve Microstructure and Extracellular Matrix

Having addressed normal valve mechanobiology, including the topics of valve aging and heterogeneity in Chapters 3-12, this next portion of the thesis (Chapters 13-21) addresses how valves are altered in various diseased states, including congenital valve disease (Chapters 13 and 14), dilated cardiomyopathy and “functional” mitral regurgitation (Chapters 15-17), valve wound healing (Chapter 18), myxomatous mitral valve disease (Chapter 19, as well as Chapter 24 in the Appendix), and calcific aortic valve disease (Chapters 20 and 21). This portion of the thesis opens with the topic of congenital valve disease, which is reviewed in this chapter.

ABSTRACT

Congenitally diseased valves are relatively frequent causes of significant morbidity and mortality. Pathology descriptions of such valves have primarily focused on gross structural features including the number of leaflets or commissures (bicuspid/bicommissural valve) and alterations in the contour, thickness and consistency of the leaflets (dysplastic valve). Functional correlates of these pathologic alterations are

valvar stenosis, insufficiency or both. Further characterization of the microstructural abnormalities seen in these malformed valves may not only provide insight into the correlation of distinct pathologies with their respective pathogenesis and clinical sequelae, but also may prove pivotal in uncovering new avenues for therapeutic interventions and prevention regimens. This review summarizes microstructural findings in congenital semilunar valve disease (CSVD) and discusses their relevance in light of recent advances in knowledge of normal valve microstructure, biology, and function. Specifically, the biological and mechanical roles of various matrix components and their interactions and the role of mechanical stimulation in valve health are discussed in the context of CSVD. Indeed, recent research in normal valves adds significant insight into CSVD, and raises many hypotheses that will need to be addressed by future studies.

The work contained in this chapter is in preparation for submission to *Cardiovascular Pathology*.

INTRODUCTION

Congenitally diseased valves are relatively frequent causes of morbidity and mortality,¹⁻³ including valvar stenosis and/or insufficiency, ventricular dysfunction, cardiac chamber and/or arterial dilation, substrates for infection and thrombus formation, arrhythmias, and sudden death. Pathology descriptions of such valves have primarily focused on gross structural features such as the number of leaflets or commissures (bicuspid/bicommissural valve) and alterations in the contour, thickness and consistency of the leaflets (dysplastic valve). The nature of these abnormalities at the microstructural level has received limited detailed study. Instead, published reports on malformed valves have focused on associations with other cardiac and systemic anomalies, clinical diagnosis and evaluation, potential genetic and developmental causes, and the risks, benefits, and long-term outcomes of various surgical repairs. However, more in depth characterization of congenitally diseased semilunar valves (CSVD) may aid in their classification into more distinct pathologies, correlating with their respective pathogenesis and clinical sequelae. Further characterization of the congenital abnormalities, as well as the superimposed acquired hemodynamic alterations that contribute to disease progression, may prove pivotal in uncovering new avenues for therapeutic intervention and prevention regimens. This review provides a brief background on normal valve macrostructure and microstructure pertinent to CSVD, describes what is known regarding CSVD macrostructure, microstructure, and matrix composition and discusses their relevance in light of recent advances in knowledge of normal valve microstructure, biology, and function. Specifically, the role of valvular interstitial cells, the biological and mechanical roles of various matrix components, the

interaction of these components with each other and bioactive molecules such as growth factors, and the role of mechanical stimulation in valve health will be discussed in the context of CSVD. Indeed, recent research in normal valve microstructure, developmental maturational changes and mechanisms of acquired hemodynamic effects on valve structure adds significant insight into CSVD, and raises many hypotheses that will need to be addressed by further studies.



Fig. 13-1: Atretic PV from 2 year-old demonstrating a domed valve and fused cusps.

SPECTRUM OF CONGENITAL SEMILUNAR VALVE DISEASE (CSVD)

CSVD can involve any of the valve's components, including the cusps, annulus, commissures and sinuses. Many diseases involve multiple structures either as a primary defect or secondary acquired hemodynamic abnormality. The two extremes of CSVD are

an atretic valve and absent valve. An atretic valve implies no luminal continuity from the ventricle to the great artery, often reflected by an outflow tract that ends blindly in a dimple with no valvular tissue, typical of aortic valve atresia (Fig. 13-1). Other forms of semilunar valve atresia include an imperforate small membrane or a dome-shaped, imperforate, unicuspid valve as seen in some cases of pulmonary valve atresia. Absent semilunar valve results in an unguarded valve orifice with either no valve tissue, a slight ridge, or very small nubbins of valve tissue at the annulus. A single semilunar valve is also seen with a persistent truncal valve in truncus arteriosus. In contrast to the absent or atretic valve where there are separate annuli for the aortic and pulmonary valves (albeit represented by a blind ending dimple), a persistent truncal valve indicates that there is a single, common valve annulus that never divided into aortic and pulmonary valves orifices. Truncal valves most often have 3 cusps; however bicuspid and quadricuspid valves are not uncommon.

The most common valve malformation is an abnormal number of cusps, usually a bicuspid valve. The two cusps may be of similar or unequal size, and one sinus will contain the abortive commissure or raphe. Unicuspid or quadricuspid valves may also occur. The unicuspid valve with its single commissure is inherently stenotic with a variably hypoplastic annulus and is usually part of a more complex constellation of lesions. Bicuspid or quadricuspid valves, with otherwise well formed cusps, are functionally normal at birth and may occur as isolated lesions. However long-term altered hemodynamics, particularly for the bicuspid aortic valve, often lead to acquired stenosis requiring surgical intervention in adulthood. The quadricuspid valve may remain asymptomatic or develop valvar regurgitation.⁴ Quantitative and qualitative

abnormalities can coexist, as in a bicuspid, dysplastic aortic valve. Position, alignment or connection of each component of a valve may be abnormal as in over-riding or straddling valves.

The valve abnormality most likely to require surgical intervention in childhood is a dysplastic semilunar valve. Valvar dysplasia is characterized by variably thickened cusps with altered contours resulting in valvar stenosis or, less commonly, regurgitation. The dysplastic aortic or pulmonary valve may occur as an isolated lesion, with multiple involved valves (polyvalvular dysplasia) or as part of a more complex constellation of cardiac lesions such as tetralogy of Fallot or Shone syndrome. It is not uncommon to have a combined dysplastic and bicuspid or unicuspid semilunar valve. The dysplastic quadricuspid valve is a feature of truncus arteriosus. A regurgitant, dysplastic valve is also more commonly seen with truncus arteriosus.

There are a number of differences between aortic and pulmonic congenital valvular disease. The most common form of isolated congenital pulmonary valvular stenosis is the domed deformity with fusion of the valve cusps around a central fixed orifice.⁵ In the aortic valve, the bicuspid, dysplastic valve is more common. Differences have also been noted between “absent” aortic valve and “absent” pulmonic valve. While in “absent” pulmonic valve there is usually a remnant of dysplastic valve-like tissue,^{6,7} in the syndrome of “absent” aortic valve there is usually only an endothelial ridge at the level of the valve annulus.⁷ Even within polyvalvular dysplasia, out of the four valves the aortic valve is the least involved.⁸

CSVD affecting multiple valves is often a manifestation of a syndrome (Marfan’s syndrome, polyvalvular dysplasia associated with Noonan syndrome or certain trisomies)

or a systemic metabolic storage disease (Mucopolysaccharidoses). This review largely focuses on cases of CSVD not associated with more extensive extracardiac disease, with particular attention to the most common CSVD requiring therapeutic interventions: dysplastic semilunar valves and the bicuspid aortic valve (BAV).



Fig. 13-2A: Normal AV from an 8 year-old viewed from the left ventricular outflow track.

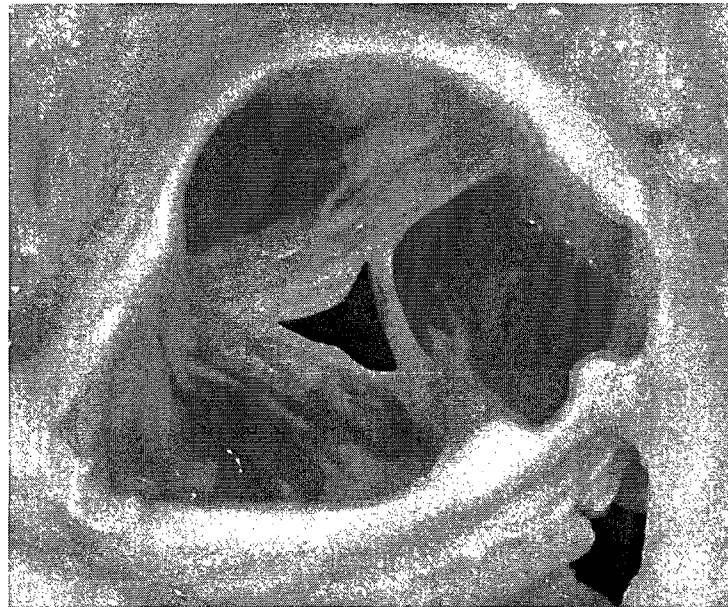


Fig. 13-2B: Aerial view of a normal AV from a 13 year-old demonstrating thin, delicate cusps.

NORMAL SEMILUNAR VALVE STRUCTURE

Valve Macrostructure

The major components of the semilunar valves include the three half-moon shaped cusps, three commissures, sinuses, the annulus, and surrounding supporting structures (Fig. 13-2A, B). Each cusp is anchored in place by an undulating ring of fibrous tissue (the valve annulus) that separates the ventricle below from the arterial wall above. The part of the annulus that separates two immediately adjacent cusps is the commissure. The annulus for each valve is continuous with, and supported by, the fibrous skeleton of the heart. The higher pressures generated on the left side of the heart require a more sturdy annulus for the aortic valve. This valve is centrally located at the base of heart and its' annulus shares fibrous continuity with the annuli of the other three cardiac valves. Accentuated areas of fibrous tissue connect the aortic valve with the mitral and tricuspid valves and are known as the left and right fibrous trigones respectively. The pulmonary valve has a more tenuous fibrous annulus and is connected to the aortic valve by a thin fibrous (conal) ligament. In addition to the essential role of the valve annuli and cardiac fibrous skeleton in anchoring the valve cusps during the billions of times the valve opens and closes over an individual's lifespan, the integrity of the adjacent ventricular and arterial wall support will impact valve function.

For each semilunar valve the sinuses of Valsalva are created by the pockets formed between the valve cusps and the adjacent arterial wall. Blood filling these sinuses during diastole of the cardiac cycle causes the cusps to centrally coapt against one another, closing the lumen. The cusps overlap one another for a distance extending several millimeters below the free edge, ensuring valve closure. The area of overlap, or

lunula, is demarcated at its lower margin by a ridge that becomes more accentuated with increasing age, and is more prominent on the aortic than pulmonary valve. The center of the lunula has a localized area of fibrous thickening forming a discrete nodule (nodule of Arantius) that further ensures a tight seal of the closed valve. With systolic opening of the valve, the cusps collapse against the wall of the valve sinus. The integral relationship between valve cusps, commissures, sinuses, annulus and supporting structures is essential for normal valve function. Abnormalities in the valves due to any of these components may cause valvular dysfunction and may impact cardiac physiology as a whole.

[For a description of normal valve tissue microstructure and valve cells, please see Chapter 1, Background]

Valve Changes with Age and Altered Hemodynamics

Recent studies have demonstrated that valve composition and accompanying mechanical properties normally change with age.⁹⁻¹¹ Not only does collagen content and crosslinking increase, as previously well established,¹²⁻¹⁴ but specific glycosaminoglycan (GAG) sulfation patterns change with age and these age-related changes appear to be valve and valve-region specific.¹¹ Mechanically, valves become stiffer and less extensible with age.¹⁰ These normal valve changes associated with the aging process complicates the study of congenital valve disease where normal aging is superimposed onto valves with structural and biological abnormalities. Additionally, altered hemodynamics and mechanical strains are known to stimulate certain compositional changes in normal valves, including increased collagen synthesis, matrix

metalloproteases (MMPs), and myofibroblast marker expression,¹⁵⁻¹⁷ but how a structurally and biologically abnormal valve responds to the altered hemodynamics and loading patterns commonly present in congenitally diseased valves remains largely unknown.

MACROSCOPIC CHARACTERIZATION OF CONGENITAL SEMILUNAR VALVE DISEASE (CSVD)

The bulk of the CSVD pathology literature focuses on constellations of anatomical formations examined at the macroscopic level. This review will address bicuspid aortic valves and dysplastic semilunar valves.

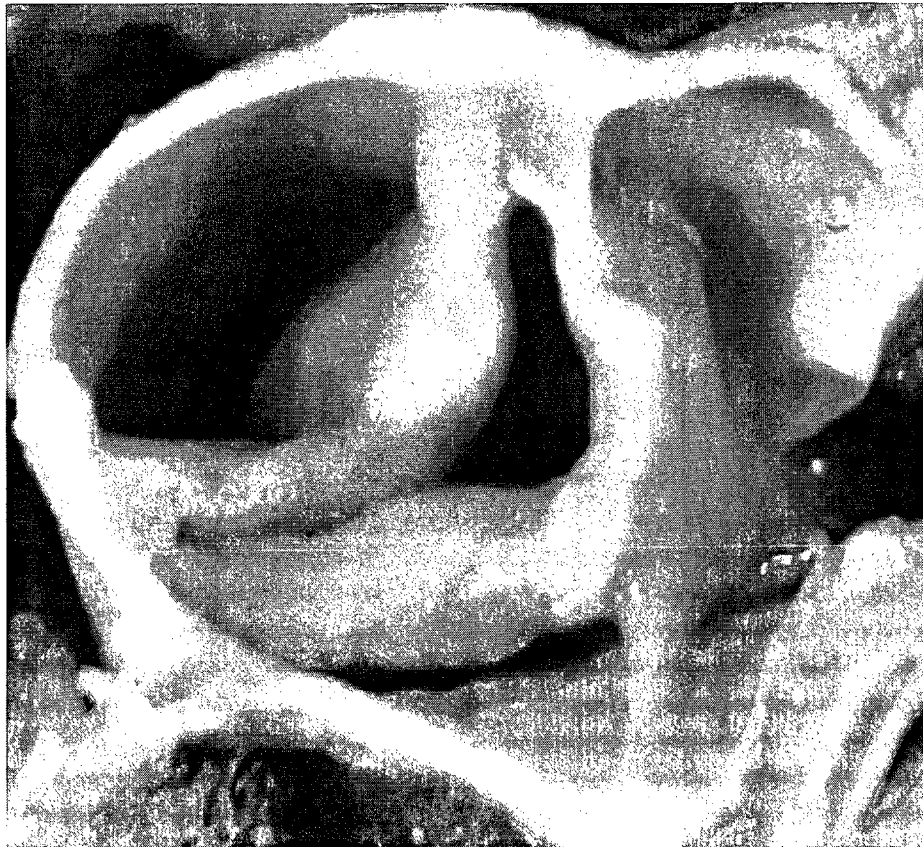


Fig. 13-3: Bicuspid stenotic AV from a 40 year-old demonstrating diffuse fibrosis.

Bicuspid Aortic Valve

The two cusps of the bicuspid valve are supported by two commissures; therefore the valve may be described as bicuspid/bicommissural (Fig. 13-3). A third abortive commissure or "raphe" is frequently present evidenced by a ridge within one sinus, either confined to the aortic wall or extending a variable distance onto the base of the cusp. The raphe should not be confused with a fused commissure between conjoined cusps in a tricuspid aortic valve. A raphe does not extend to the free margin of the cusp and its aortic attachment sits beneath the horizontal level of the cusp.⁸⁵ Although histologically the raphe often contains abundant elastic fibers similar to adjacent aortic wall, this is not a reliable distinguishing feature.⁸⁵ The two cusps of the bicuspid valve may be of similar or unequal size; however the raphe typically partitions the cusp into similarly sized components.⁸⁵

At birth, the valve cusps are most often thin and delicate, similar to the normal tricuspid valve and the valve is functionally asymptomatic. However, the altered physiology of a bicuspid valve results in progressive fibrous thickening, often apparent by the second decade of life, with increasing rigidity of the cusps.¹⁰³ Calcification is also common, within the cusp and forming nodular masses within the sinus, often involving the raphe.¹⁸ Calcification is a later manifestation of the dysfunctional bicuspid aortic valve, becoming increasing more apparent in the fourth and subsequent decades.¹⁰³ Bicuspid valves that become symptomatic earlier in childhood are often both bicuspid and dysplastic.¹⁹

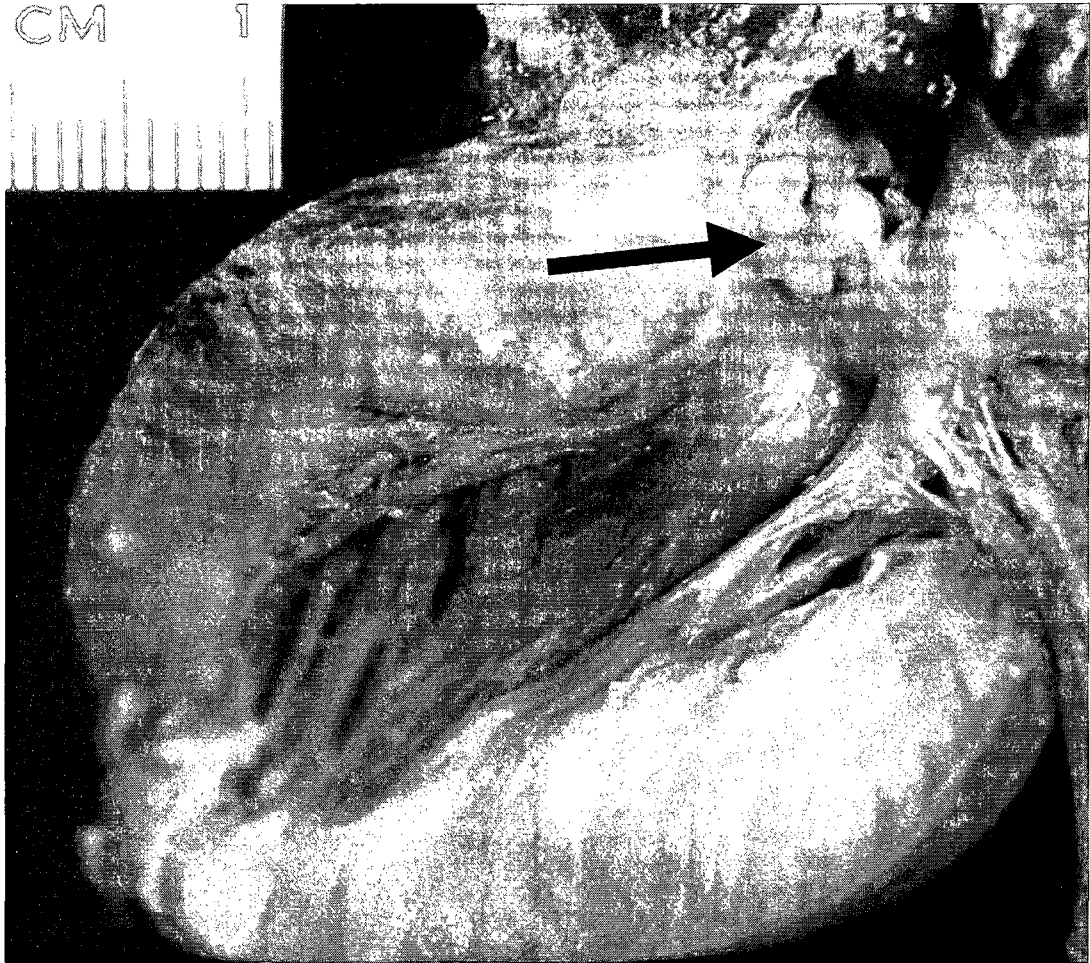


Fig. 13-4: Severely dysplastic AV (arrow) with associated left ventricular hypertrophy from a 2-3 month-old.

Dysplastic Semilunar Valves

Semilunar valve dysplasia implies congenital abnormalities in the valve morphology reflected by alterations in the size, thickness, contour and/or consistency of the cusps. In severe dysplasia the cusps appear as nodularly thickened, myxoid warty protrusions (Fig. 13-4). The spectrum of changes in milder forms of valve dysplasia includes more localized areas of myxoid nodularity (Fig. 13-5). Alternatively, the valve may be diffusely, uniformly thickened with redundancy at the free margins providing for

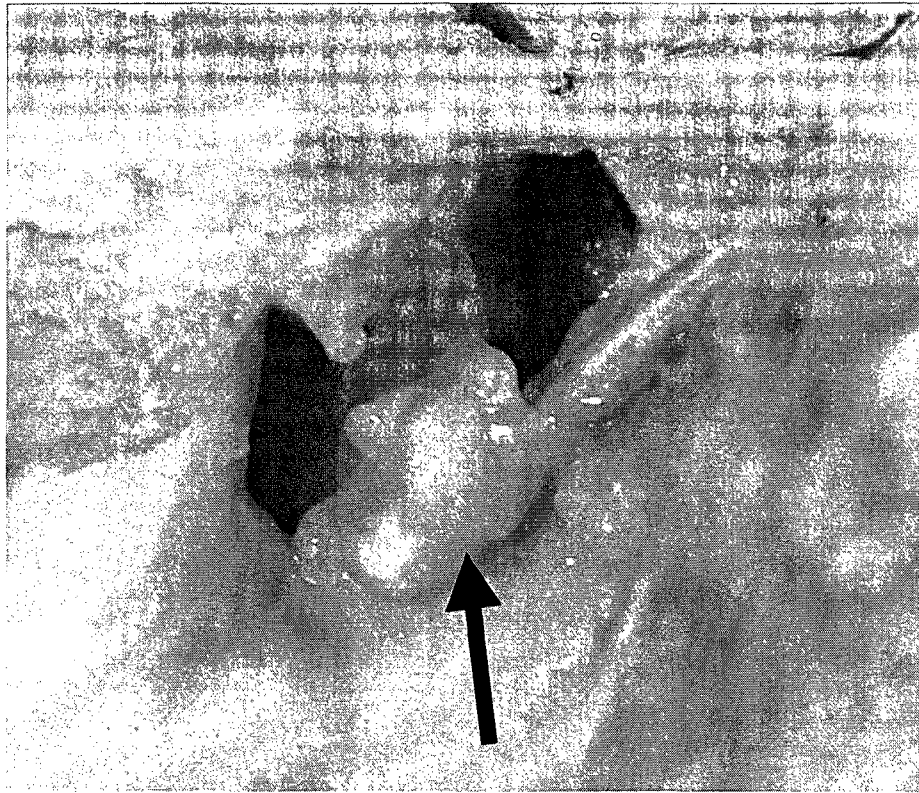


Fig. 13-5: Mildly dysplastic AV from an 8 month-old demonstrating localized areas of nodular thickening (arrow).

an irregular contour. The dysplastic valve may have 1, 2, 3 or 4 cusps and some degree of commissural thickening may be present.

While such macroscopic characterization is perfectly adequate for making the clinical diagnosis of dysplastic CSVD, with additional knowledge of matrix components and microstructure abnormalities, avenues for possible treatments and prevention may become evident.

Acquired Macroscopic Valve Changes

When assessing CSVD, particularly in older children and young adults, it may be difficult to distinguish some milder forms of underlying valve dysplasia from

superimposed pathological changes due to altered hemodynamics. These acquired alterations may include focal or diffuse thickening of the cusps in an environment of valvar stenosis and rolled, everted margins caused by the regurgitant stream on an insufficient valve. Other acquired changes to be considered include post-inflammatory effects of infective endocarditis and iatrogenic effects of interventional commissurotomies and balloon dilations.

MICROSCOPIC CHARACTERIZATION OF CONGENITAL SEMILUNAR VALVE DISEASE (CSVD)

CSVD Microstructure

Despite the variation in the macroscopic appearance of dysplastic semilunar valves, there is a unifying theme to the valve microstructure. The normal trilaminar valve structure is distorted by increased GAGs, reflected by an expanded spongiosa that is poorly demarcated from the fibrosa and associated with decreased to absent valvar elastic tissue (Fig. 13-6).^{8, 20, 21} Bharati and Lev also reported that compared to age-matched normal valves and normal valves exposed to altered hemodynamics, dysplastic valves showed an increase in the spongiosa layer with vacuolar and lacunar degeneration.^{8, 20, 21} Similarly, Hyams' study of a broad group of dysplastic valves, including both isolated and polyvalvular cases taken from fetuses to young adults, reported myxomatous nodules devoid of elastic tissue with pockets of collagenous tissue.²² Multiple other authors studying various types of congenitally diseased aortic and pulmonic valves report the same essential findings.^{5, 23, 24} More recently Hinton, in studying 6 explanted, bicuspid, stenotic aortic valves from infants and children aged 1 month to 14 years of age,

specifically reported finding loss of the trilaminar architecture with disorganized collagen and PGs in all layers and disorganized, decreased elastin. Thickening of the cusps was correlated with increased collagen, and PGs. VICs were also disorganized, focally forming clusters, although there was no increase in cell proliferation.²³

Ongoing studies demonstrate that VICs derived from CSVD valves, including isolated dysplastic valves, also demonstrate phenotypic differences compared to age-matched controls. These differences suggest that abnormal VIC function in dysplastic valves contribute to the altered extracellular matrix. It remains to be determined whether these VIC abnormalities are a primary or secondary phenomenon, and what *in utero* and/or postnatal factors modulate their effects on the valve architecture and composition.

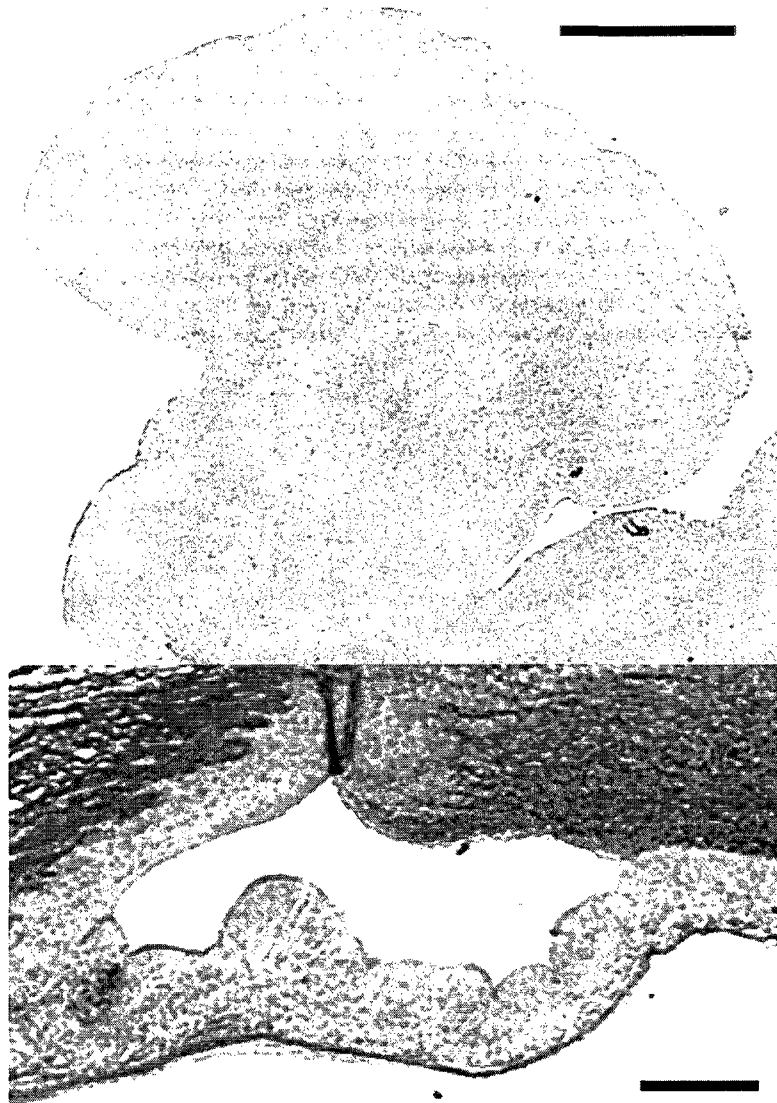


Fig. 13-6: *Movat pentachrome of a dysplastic PV from a 2 year-old (top) compared to a normal PV from a 2 year-old (bottom). Staining demonstrates loss of layered leaflet structure in dysplastic valve compared to control. Scale bar in upper panel indicates 1 mm; scale bar in lower panel indicates 500 μ m.*

Mechanical Implications of CSVD Microstructure

The observed microstructural changes seen in CSVD have important mechanical, and therefore functional implications. According to Bharati and Lev, the preponderance of the changes seen in CPVD was in the spongiosa layer,²¹ which based on the contribution the spongiosa makes to leaflet mechanics could effect leaflet bending

stress²⁵ and the ability of the leaflet to bear compression.²⁵ Computational modeling indicates that the layered nature of the valve decreases the stress of bending,²⁶ therefore the decreased leaflet layer delineation seen in many types of CSVD could decrease valve mobility, as well as increase stress on the leaflet. Furthermore, the complex interaction that exists between the layers of normal valves, which is important to valve mechanical properties,^{27,28} is lost. The increased valve thickness reported in a number of types of CSVD^{8,23} would also result in an increase in bending stress, according to computational analysis.²⁹ Increased collagen content, as reported in children with BAV,²³ would be expected to increase leaflet stiffness as well as leaflet and chordal stress.³⁰ However, the valve has a complex, heterogeneous distribution and alignment of collagen that contributes to anisotropic, region-specific valve material properties important to proper valve function.^{26,30,31} Therefore, the specific consequences of increased collagen would depend on the exact location and orientation of this additional collagen, but would in all likelihood also hinder valve function.

Other changes in CSVD have functional and mechanical implications. The nodularity common to many types of CSVD^{8,23} would change hemodynamics by disturbing fluid flow and altering shear stress on the valve endothelial cells. Valve endothelial cells are well known to respond to shear stress³² and endothelial cell injury may be a key step in calcification of the aortic valve.^{33,34} Elastic fibers, which are decreased in a variety of congenitally diseased valves,^{8,20,22,23} also have important mechanical consequences as the elastic fibers in the ventricularis layer provide recoil, returning the collagen in the fibrosa to its crimped configuration after each heart beat.³⁵ Based on studies in which functioning elastic fibers were removed from normal valves,

loss of elastic fibers in CSVD likely causes reduced extensibility and increased stiffness.³⁶

Insight into Possible Pathogenesis of CSVD

Observations on several congenital and acquired valvular disorders may provide insight into the pathogenesis of dysplastic valves. Infantile Marfan's syndrome, associated with mutations in the fibrillin-1 gene, is associated with macroscopic valvular changes similar to those seen in dysplastic valves.³⁷ Fibrillin is a major component of the extracellular matrix, essential to normal elastic tissue formation. Its functions include interaction with growth factors such as transforming growth factor-beta (TGF β) that then effect VICs.³⁸ The importance of fibrillin's interaction with TGF β in these valvulopathies is underscored by experiments demonstrating that in mouse models of Marfan's with fibrillin-1 mutations and mitral valve abnormalities, perinatal administration of neutralizing antibodies to TGF β rescued the normal mitral valve phenotype.³⁹ Other extracellular matrix abnormalities have also been noted in Marfan's syndrome. Skin fibroblasts from neonatal Marfan's patients produce markedly decreased decorin, a PG associated with elastogenesis⁴⁰ as well as collagen fibrillogenesis,⁴¹ both of which could affect tissue matrix integrity. The known interactions of fibrillin with the PG versican would also be expected to be impacted in Marfan's syndrome.⁴² The full spectrum of alterations in matrix composition and functional interactions in Marfan's syndrome, particularly in the cardiac valves, remain to be elucidated. However even these limited observations suggest an important role for the extracellular matrix in these valve pathologies.

Alterations in the interaction of VICs with the extracellular matrix may be operative in other forms of myxoid valvular heart disease. Mutations in filamins have been associated with familial mitral valve prolapse,³⁸ whose macrostructure and microstructure also resembles dysplastic valves. Filamin has also been postulated to interact with the TGF β pathway.³⁸ The effects of these varied genotypic matrix alterations leading to heart valves with similar microstructure, suggest that valvar dysplasia, as currently defined, may reflect a final common morphologic pathway resulting from alterations of components of the extracellular matrix. The potential central role of TGF β and its interaction with VICs and matrix components remain to be defined.

Others have noted that the microstructure of dysplastic valves, including increased GAG content, lack of differentiation between the valve layers, and decreased elastic tissue, are features of immature valves during normal development.^{20,61} Recent studies characterizing changes in specific valve matrix components and structure during fetal and postnatal valve development demonstrated that many of the matrix components in the first trimester were ubiquitous throughout the valve layers, but became localized to specific layers in later trimesters, with increasing elastic fiber content, paralleling delineation of layers evident in Movat.^{9,11,73} This has led some investigators to postulate that dysplastic valves represent an arrested step in development.⁴³ While there is evidence to support this, the pathogenesis of valvar dysplasia is likely more complex, resulting from a spectrum of genetic alterations in a matrix component, VICs, or one of the many factors operative in valve remodeling whose impact may first become apparent at a variety of time points during development. The *in utero* and postnatal effects of this genetic alteration would interfere with assembly of the normal valve architecture.

Further investigation of changes in valve composition during normal development may prove important representing a potential origin and pathogenesis for a specific valve dysplasia.

Role of Hemodynamics in CSVD

In the past it was hypothesized that generally congenitally diseased valves were secondary to other structural cardiac anomalies altering normal blood flow during development.⁴⁴ Studies show that indeed mechanical stimulation is a necessary part of valve development. For example, decreasing wall shear stress in zebrafish leads to the development of dysmorphic valves⁴⁵ and decreasing zebrafish heart contractility and blood flow before endocardial cushion development leads to failed valve development.⁴⁶ A study in mice found a correspondence between the hyaluronan and collagen composition of developing atrioventricular valve cushions, the cushions' biomechanics, and blood flow.⁴⁷ Although the mechanical environment contributes to normal valve development, there are other factors that contribute to valve dysplasia. Bharati and Lev specifically noted abnormalities in CPVD compared to both normal and hemodynamically altered aged-matched controls,⁸ suggesting altered hemodynamics alone cannot explain CPVD. The issue of mechanical stimulation becomes complex in the case of congenitally diseased valves because these valves often occur in the context of “structural” cardiac defects that alter the hemodynamics and forces that the valves experience. One could speculate that the effects from this mechanical environment then interact with altered biological processes within valves, such as dysfunctional collagen

turnover, to create the pathological microstructure that we see in congenitally diseased valves. The complexities of this process remain to be determined.

Not only are hemodynamics important in valve development and could contribute to congenital valve pathogenesis, but over the years altered hemodynamics construed by malformed valves and the frequently accompanying other congenital heart structural deformities, impose secondary changes on the valves, including greater collagen content and loss of the spongiosa layer (Fig. 13-7).²¹ Therefore, evaluation of congenital valves from older patients is complicated by secondary hemodynamic changes.

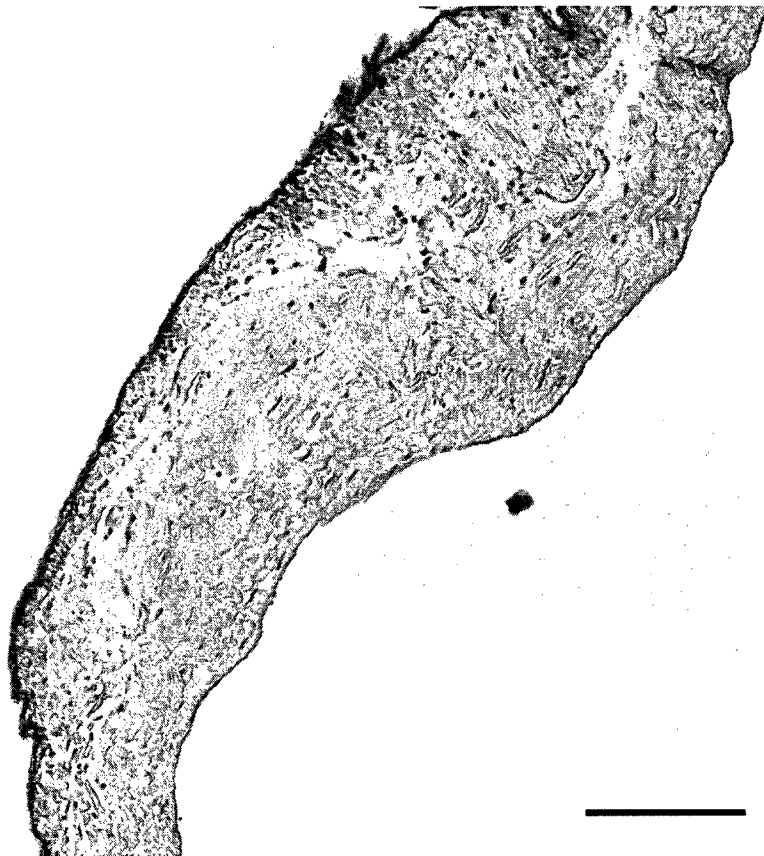


Fig. 13-7: *Movat pentachrome stained PV from a 14 year-old with insufficiency demonstrates increased collagen content and loss of spongiosa layer. Scale bar represents 200 μ m.*

A frequently related scenario encountered in congenital heart disease is the Ross procedure in which the normal PV is placed in the AV position to replace a malformed or otherwise deficient AV. Although in this case the PV is not malformed, it does expose the PV to increased pressures. A recent study has shown that these valves remodel in response to this altered mechanical environment,⁴⁸ with increased MMPs and VICs activation particularly early after the Ross procedure.

MICROSTRUCTURAL CHARACTERIZATION OF BICUSPID AORTIC VALVE (BAV) AND ITS IMPLICATIONS

Like many different types of CSVD, BAV can range from valves that appear normal microscopically, except for the macroscopic configuration of the cusps, to dysplastic leaflets complete with loss of the internal layered structure. Typically patients that present as symptomatic early in life have more dysplastic valves, while the valves from patients that present later in life demonstrate more normal microstructure with superimposed calcific changes.

Possible Pathogenesis of BAV

While some have argued that BAV is simply a fusion between two of the leaflets, recent evidence suggests that the pathogenesis may be more complex.⁴⁹⁻⁵² The “raphe,” or portion of the valve that appears fused, does not contain valve tissue, but instead elastic fibers that can become fibrotic.⁵³⁻⁵⁵ Some believe the increased incidence of valvular stenosis in BAV is purely due to the altered hemodynamics,⁵⁶ but as the following studies

show the BAV microstructure has alterations that could contribute to the development of stenosis in BAV.

Proteoglycans (PGs) and Glycosaminoglycans (GAGs) in BAV

Studies assessing specific matrix components and their structure in BAV are limited. Baig's 1979 study found less GAG content in BAV adults compared to age-matched controls.⁵⁷ In terms of particular GAGs, there was more dermatan sulfate in the 21-40 year-olds, and less hyaluronan and more chondroitin sulfate in the 41-60 year-olds in BAV compared to age-matched controls.⁵⁷ However, it is difficult to discern how much of these differences were secondary to years of altered hemodynamics created by the BAV. Nevertheless, altered GAG content has been implicated in the calcification of congenitally normal aortic valves⁵⁸ and could contribute to increased calcification seen in BAV. The altered chondroitin sulfate content reported by Baig in BAV likely mostly represents versican,⁵⁹ a PG critical to valvulogenesis⁶⁰ and therefore suspect to being altered in congenitally diseased valves. Versican is important to elastic fibrillogenesis,⁶¹ and alterations in versican could relate to abnormal elastic content²³ and fibrillar proteins⁶² observed in BAV. Baig's study also showed altered hyaluronan in BAV;⁵⁷ this could not only alter the tissue's mechanical properties, but affect other processes in which hyaluronan is involved, such as cell proliferation⁶³ and potentially valve calcification.⁵⁸ Baig also reports an alteration of dermatan sulfate in BAV,⁵⁷ which largely reflects decorin content.⁵⁹ Altered decorin content could affect collagen fibrillogenesis,⁴¹ regulation of TGF β ⁶⁴ and fibrillin-1,⁶⁵ and even wound healing in these valves.⁶⁶ In fact, abnormal collagen content and configuration has been reported in pediatric cases of

BAV.²³ In the future it will be important to examine growth factor expression, collagen fibril abnormalities, and expression of GAGs and PGs that may shed light on the role of altered matrix in BAV. Of course, it is difficult to tell whether the matrix abnormalities are the cause or the result of BAV, and most likely is a little of both.

Dysregulation of Fibrillar-Related Proteins in BAV

In terms of individual proteins, a more recent study in BAV from children revealed a deficiency in fibrillin-1.⁶² Interestingly, expression of fibulin and fibrillin correlate with the transition from immature mesenchymal tissue to mature valve, suggesting BAV could involve a suspension of development.⁴⁹ Furthermore, as mentioned earlier, fibrillin is integrally involved in TGF β regulation,⁶⁷ a growth factor essential to major signaling pathways including the endocardial-mesenchymal transition in atrioventricular valves development.⁶⁸ TGF β expression is associated with the pathogenesis of a number of valve diseases in adults without congenital diseases,^{69,70} and the myxomatous-like valve changes seen in Marfan's syndrome, as discussed earlier.³⁹ Potentially the deficiency of fibrillin-1 observed in BAV,⁶² could result in altered growth factor regulation and matrix abnormalities in BAV.

Another study showed that BAV, compared both to normal and diseased tricuspid aortic valves, showed increased MMP2 and MMP9 expression.⁷¹ MMP2 and 9 are both gelatinases that degrade elastic fibers; indeed, BAV from pediatric patients reported fragmented elastic fibers and a decrease in overall abundance.²³ As discussed earlier, this decrease in elastic fibers could have important implications for valvular mechanics. Increased MMP expression in BAV is particularly interesting in light of increased MMPs

evident in normal valves experiencing altered hemodynamics,^{72, 73} undergoing valve remodeling,^{48, 74} and demonstrating other valve pathologies.^{69, 75} In other words, increased MMP expression in valves may be a common pathway for various stresses, as others have postulated.⁷⁴

Associated Aortic Wall Abnormalities in BAV

The association of the BAV with a number of aortic wall abnormalities, including aortic aneurysm and dissection, led to speculation that matrix abnormalities in these patients are not limited to the aortic valve. Approximately 20-50% of patients with BAV have an associated cardiovascular complication,²² the most common being coarctation of the aorta, interrupted aortic arch, and aortic dissection.⁷⁶ In the past it was thought that these related pathologies of the aorta were secondary to the altered hemodynamics caused by BAV, (i.e. post-stenotic dilatation), however, multiple studies suggest there is an underlying structural defect in the aortas of BAV patients. A study showed BAV patients have significant dilation of the aorta even as children, independent of whether or not the valve was stenotic or regurgitant.⁷⁷ Furthermore, after valve replacement for aortic stenosis, patients with a tricuspid valve show a decrease in dilation of the aorta, while patients with bicuspid aortic stenosis show an increase in dilation of the aorta.⁵⁰ Microscopic analysis reveals elastic fiber fragmentation,⁷⁸ decreased number and wider spacing of elastic lamellae⁷⁹ in the aorta of BAV patients compared to controls. Indeed further analysis has shown that cystic media necrosis, an increase in MMPs, and smooth muscle cell apoptosis underlie these aortic wall pathologies.⁸⁰ An increase in MMPs is consistent with reports of decreased collagen I and III in the aortas of patients with

BAV.⁷⁸ Just as fibrillin-1 has been found to be decreased in the BAV, fibrillin-1 has also been reported to be decreased in the aortas of BAV adults compared to controls.⁴⁹ Some postulate that the BAV and aortic complications occur by a common mechanism of cellular apoptosis⁸¹ based on increased apoptosis of smooth muscle cells and higher expression of pro-apoptotic markers found in the aortas of BAV patients.⁸² Others suggest that dysregulation of MMPs lead to both BAV and its aortic complications.⁸³ Interestingly, the elastic content of the BAV raphe⁵³⁻⁵⁵ appears like the media of the aorta.⁵³ This accumulation of elastic fibers in the BAV raphe, increased MMP2 and MMP9 in BAV, and concomitant elastic degradation in the aortic wall suggest widespread elastic fiber dysregulation.

Insight BAV Provides into other Congenital Valve Diseases

Characterizations of matrix composition abnormalities in BAV certainly add considerable insight into BAV, but they also may provide insight into other types of congenital valve diseases. For instance, given that BAV matrix abnormalities are more widespread than just the valve, it could be hypothesized that for some congenital valve diseases there are matrix abnormalities in other portions of the heart and aorta. Indeed there is some evidence to support this hypothesis. For instance, a review of atrioventricular valve dysplasia reports concomitant myxomatous areas of the interatrial septum.⁸⁴ Another study reports both aortic and pulmonic valve atresia to be associated with myocardial disarray in the interventricular septum.⁸⁵ The preponderance of concomitant cardiac anomalies for congenital valve diseases could also be considered an argument for a broader, underlying pathological mechanism.

IMPORTANCE OF VALVES IN BROADER DISEASES' PATHOGENESIS AND PROGRESSION

Studies in diseases largely thought not to involve the heart valve have increasingly pointed to an important role played by the valves. For instance, a study has shown that in heart failure, a complex disease often thought not to organically involve the valve in its pathogenesis, apparently normal mitral valves were shown to have significant differences in composition including GAG content.⁸⁶ Similarly, in “functional” mitral regurgitation it has been assumed that the regurgitation was the result of structural changes in the annulus and left ventricle. While structural changes certainly contribute to the mitral regurgitation, recent studies have shown that the valve is intimately involved in the disease and may even be an independent factor contributing to the progression of regurgitation.⁷² In the future it will be important to look for the valves playing important roles in broader congenital heart diseases thought not to organically involve the valve.

CONCLUSIONS

This review has summarized the microstructural findings of CSVD, and in the light of recent advances in the knowledge of normal valve biology, microstructure, and mechanics, explored the implications of the aforementioned CSVD microstructure findings. This discussion not only yields further insight into CSVD, but presents important questions to be addressed in future CSVD research. Clearly, much work still remains in elucidating the pathogenesis of CSVD, and this review provides potential direction for doing so.

This chapter opens the portion of the thesis addressing valve alterations in diseased states (Chapters 13-21) with a review of congenital valve disease. In the following chapter, a study analyzing matrix remodeling and valvular interstitial cell (VIC) phenotypic changes in congenitally diseased semilunar valves is presented.

REFERENCES

1. LeBlanc JG, Russell JL. Pediatric cardiac surgery in the 1990s. *Surg Clin North Am.* 1998;78(5):729-747.
2. National Center for Health Statistics: National Heart, Lung, and Blood Institute; 2005.
3. Hoffman J, Kaplan S. The incidence of congenital heart disease. *J Am Coll Cardiol.* 2002;39(12):1890-1900.
4. Godefroid O, Colles P, Vercauteren S, Louagie Y, Marchandise B. Quadricuspid aortic valve: a rare etiology of aortic regurgitation. *Eur J Echocardiogr.* 2006;7(2):168-170.
5. Koretzky ED, Moller JH, Korns ME, Schwartz CJ, Edwards JE. Congenital pulmonary stenosis resulting from dysplasia of valve. *Circulation.* 1969;40(1):43-53.
6. Fischer D, Neches WH, Beerman L, Fricker F, Siewers R, Lenox C, Park S. Tetralogy of Fallot with absent pulmonic valve: analysis of 17 patients. *Am J Cardiol.* 1984;53(10):1433-1437.
7. Lin A, Chin A. Absent Aortic Valve: A Complex Anomaly. *Pediatr Cardiol.* 1990;11:195-198.
8. Bharati S, Lev M. *The Pathology of Congenital Heart Disease.* Armonk: Futura Publishing Company, Inc.; 1996.
9. Stephens EH, Grande-Allen KJ. Age-related changes in collagen synthesis and turnover in porcine heart valves. *J Heart Valve Dis.* 2007;16(6):672-682.
10. Stephens EH, de Jonge N, McNeill MP, Durst CA, Grande-Allen KJ. Age-related changes in material behavior of porcine mitral and aortic valves and correlation to matrix composition. *Tissue Eng.* 2010;16(3):867-878.
11. Stephens EH, Chu CK, Grande-Allen KJ. Valve proteoglycan content and glycosaminoglycan fine structure are unique to microstructure, mechanical load and age: Relevance to an age-specific tissue-engineered heart valve. *Acta Biomater.* 2008;4(5):1148-1160.
12. Bashey RI, Torii S, Angrist A. Age-related collagen and elastin content of human heart valves. *J Gerontology.* 1967;9(19):203-208.
13. Angrist A. Aging heart valves and a unitary pathological hypothesis for sclerosis. *J Gerontol.* 1964;19:135-143.
14. Keller F, Leutert G. [Age dependence of collagen structures of the human heart]. *Z Gerontol.* 1994;27(3):186-193.
15. Platt MO, Xing Y, Jo H, Yoganathan AP. Cyclic pressure and shear stress regulate matrix metalloproteinases and cathepsin activity in porcine aortic valves. *J Heart Valve Dis.* 2006;15(5):622-629.

16. Balachandran K, Sucosky P, Jo H, Yoganathan AP. Elevated cyclic stretch alters matrix remodeling in aortic valve cusps: implications for degenerative aortic valve disease. *Am J Physiol Heart Circ Physiol.* 2009;296(3):H756-764.
17. Balachandran K, Konduri S, Sucosky P, Jo H, Yoganathan AP. An ex vivo study of the biological properties of porcine aortic valves in response to circumferential cyclic stretch. *Ann Biomed Eng.* 2006;34(11):1655-1665.
18. Fenoglio JJ, Jr., McAllister HA, Jr., DeCastro CM, Davia JE, Cheitlin MD. Congenital bicuspid aortic valve after age 20. *Am J Cardiol.* 1977;39(2):164-169.
19. Cheitlin MD, Fenoglio JJ, Jr., McAllister HA, Jr., Davia JE, DeCastro CM. Congenital aortic stenosis secondary to dysplasia of congenital bicuspid aortic valves without commissural fusion. *Am J Cardiol.* 1978;42(1):102-107.
20. Bartram U, Bartelings M, Kramer H, Gittenberger-de Groot A. Congenital polyvalvular disease: a review. *Pediatr Cardiol.* 2001;22(2):93-101.
21. Bharati S, Lev M. Congenital polyvalvular disease. *Circulation.* 1973;47(3):575-586.
22. Hyams V, Manion W. Incomplete differentiation of the cardiac valves. *Am Heart J.* 1968;76:173-182.
23. Hinton RB, Jr, Lincoln J, Deutsch GH, Osinska H, Manning PB, Benson DW, Yutzey KE. Extracellular matrix remodeling and organization in developing and diseased aortic valves. *Circ Res.* 2006;98(11):1431-1438.
24. Gikonyo BM, Lucas RV, Edwards JE. Anatomic features of congenital pulmonary valvar stenosis. *Pediatr Cardiol.* 1987;8(2):109-116.
25. Lovekamp JJ, Simionescu DT, Mercuri JJ, Zubiate B, Sacks MS, Vyavahare NR. Stability and function of glycosaminoglycans in porcine bioprosthetic heart valves. *Biomaterials.* 2006;27(8):1507-1518.
26. Kunzelman KS, Cochran RP, Murphree SS, Ring WS, Verrier ED, Eberhart RC. Differential collagen distribution in the mitral valve and its influence on biomechanical behaviour. *J Heart Valve Dis.* 1993;2(2):236-244.
27. Vesely I, Noseworthy R. Micromechanics of the fibrosa and the ventricularis in aortic valve leaflets. *J Biomech.* 1992;25(1):101-113.
28. Vesely I. Reconstruction of loads in the fibrosa and ventricularis of porcine aortic valves. *ASAIO J.* 1996;42(5):M739-M746.
29. Kunzelman KS, Reimink M, Cochran RP. Annular dilatation increases stress in the mitral valve and delays coaptation: a finite element computer model. *Cardiovasc Surg.* 1997;5(4):427-434.
30. Kunzelman KS, Quick DW, Cochran RP. Altered collagen concentration in mitral valve leaflets: biochemical and finite element analysis. *Ann Thorac Surg.* 1998;66(6 Suppl):S198-205.

31. Kunzelman KS, Cochran RP. Stress/strain characteristics of porcine mitral valve tissue: parallel versus perpendicular collagen orientation. *J Card Surg*. 1992;7(1):71-78.
32. Butcher JT, Nerem RM. Valvular Endothelial Cells and the Mechanoregulation of Valvular Pathology. *Philosophical Transactions of the Royal Society*. 2007;362:1445-1457.
33. Mohler ER. Mechanisms of aortic valve calcification *Am J Cardiol*. 2004;94(11):1396-1402.
34. Mohler ER. Are atherosclerotic processes involved in aortic-valve calcification? *The Lancet*. 2000;356.
35. Vesely I. The role of elastin in aortic valve mechanics. *J Biomech*. 1998;31(2):115-123.
36. Lee T, Midura R, Hascall V, Vesely I. The effect of elastin damage on the mechanics of the aortic valve. *J Biomech*. 2001;34(2):203-210.
37. Lopes KR, Delezoide AL, Baumann C, Vuillard E, Luton D, Chitrit Y, Azancot A. Prenatal Marfan syndrome: report of one case and review of the literature. *Prenat Diagn*. 2006;26(8):696-699.
38. Levine RA, Slaughaupt SA. Molecular genetics of mitral valve prolapse. *Curr Opin Cardiol*. 2007;22(3):171-175.
39. Ng CM, Cheng A, Myers LA, Martinez-Murillo F, Jie C, Bedja D, Gabrielson KL, Hausladen JM, Mecham RP, Judge DP, Dietz HC. TGF-beta-dependent pathogenesis of mitral valve prolapse in a mouse model of Marfan syndrome. *J Clin Invest*. 2004;114(11):1586-1592.
40. Raghunath M, Superti-Furga A, Godfrey M, Steinmann B. Decreased extracellular deposition of fibrillin and decorin in neonatal Marfan syndrome fibroblasts. *Hum Genet*. 1993;90(5):511-515.
41. Danielson KG, Baribault H, Holmes DF, Graham H, Kadler KE, Iozzo RV. Targeted disruption of decorin leads to abnormal collagen fibril morphology and skin fragility. *J Cell Biol*. 1997;136(3):729-743.
42. Reinboth B, Hanssen E, Cleary EG, Gibson MA. Molecular interactions of biglycan and decorin with elastic fiber components: biglycan forms a ternary complex with tropoelastin and microfibril-associated glycoprotein 1. *J Biol Chem*. 2002;277(6):3950-3957.
43. Aikawa E, Whittaker P, Farber M, Mendelson K, Padera RF, Aikawa M, Schoen FJ. Human semilunar cardiac valve remodeling by activated cells from fetus to adult: implications for postnatal adaptation, pathology, and tissue engineering. *Circulation*. 2006;113(10):1344-1352.
44. Daliento L, Nava A, Fasoli G, Mazzucco A, Thiene G. Dysplasia of the atrioventricular valves associated with conduction system anomalies. *Br Heart J*. 1984;51:243-251.

45. Hove J, Koster R, Forouhar A, Acevedo-Bolton G, Fraser S, Gharib M. Intracardiac fluid forces are an essential epigenetic factor for embryonic cardiogenesis. *Nature*. 2003;421(6919):172-177.
46. Bartman T, Walsh E, Wen K, McKane M, Ren J, Alexander J, Rubenstein P, Stainier D. Early myocardial function affects endocardial cushion development in zebrafish. *PLoS Biol*. 2004;2(5):E129.
47. Butcher J, McQuinn T, Sedmera D, Turner D, Markwald R. Transitions in early embryonic atrioventricular valvular function correspond with changes in cushion biomechanics that are predictable by tissue composition. *Circ Res*. 2007;100(10):1503-1511.
48. Rabkin-Aikawa E, Aikawa M, Farber M, Kratz JR, Garcia-Cardena G, Kouchoukos NT, Mitchell MB, Jonas RA, Schoen FJ. Clinical pulmonary autograft valves: pathologic evidence of adaptive remodeling in the aortic site. *J Thorac Cardiovasc Surg*. 2004;128(4):552-561.
49. Fedak PW, de Sa MP, Verma S, Nili N, Kazemian P, Butany J, Strauss BH, Weisel RD, David TE. Vascular matrix remodeling in patients with bicuspid aortic valve malformations: implications for aortic dilatation. *J Thorac Cardiovasc Surg*. 2003;126(3):797-806.
50. Borger M, David TE. Management of the valve and ascending aorta in adults with bicuspid aortic valve disease. *Semin Thorac Cardiovasc Surg*. 2005;17(2):143-147.
51. Duran A, Frescura C, Sans-Coma V, Angelini A, Basso C, Thiene G. Bicuspid aortic valves in hearts with other congenital heart disease. *J Heart Valve Dis*. 1995;6:581-560.
52. Fedak P, David T, Borger M, Verma S, Butany J, Weisel R. Bicuspid aortic valve disease: recent insights in pathophysiology and treatment. *Expert Rev Cardiovasc Ther*. 2005;3(2):295-308.
53. Roberts WC. The congenitally bicuspid aortic valve: a study of 85 autopsy cases. *Am J Cardiol*. 1970;26:72-83.
54. Yener N, Oktar G, Erer D, Yardimci M, Yener A. Bicuspid aortic valve. *Ann Thorac Cardiovasc Surg*. 2002;8(5):264-267.
55. Pomerance A. Pathogenesis of aortic stenosis and its relation to age. *Br Heart J*. 1972;34:569-574.
56. Cohen L, Friedman W, Braunwald E. Natural history of mild congenital aortic stenosis elucidated by serial hemodynamic studies. *Am J Cardiol*. 1972;30(1):1-5.
57. Baig M. Acid mucopolysaccharides of congenitally defective, rheumatic, and normal human aortic valves. *Am J Pathol*. 1979;96(3):771-780.

58. Grande-Allen KJ, Osman N, Ballinger ML, Dadlani H, Marasco S, Little PJ. Glycosaminoglycan synthesis and structure as targets for the prevention of calcific aortic valve disease. *Cardiovasc. Res.* 2007;76:19-28.
59. Grande-Allen KJ, Calabro A, Gupta V, Wight TN, Hascall VC, Vesely I. Glycosaminoglycans and proteoglycans in normal mitral valve leaflets and chordae: association with regions of tensile and compressive loading. *Glycobiology.* 2004;14(7):621-633.
60. Henderson DJ, Copp AJ. Versican expression is associated with chamber specification, septation, and valvulogenesis in the developing mouse heart. *Circ Res.* 1998;83(5):523-532.
61. Hinek A, Braun KR, Liu K, Wang Y, Wight TN. Retrovirally mediated overexpression of versican V3 reverses impaired elastogenesis and heightened proliferation exhibited by fibroblasts from costello syndrome and hurler disease patients. *Am J Pathol.* 2004;164:119-131.
62. Huang P, Wang HW, Li YP, Cheng PX, Zhang ZL, Hu XF, Liu NB, Li XH, Zhu SH, Zheng N. [Expression of fibrillin-1 in congenital bicuspid aortic valves]. *Zhonghua Yi Xue Za Zhi.* 2007;87(22):1549-1552.
63. Chen WY, Abatangelo G. Functions of hyaluronan in wound repair. *Wound Repair Regen.* 1999;7(2):79-89.
64. Yamaguchi Y, Mann D, Ruoslahti E. Negative regulation of transforming growth factor-beta by the proteoglycan decorin. *Nature.* 1990;346(6281):281-284.
65. Schaefer L, Mihalik D, Babelova A, Kryzankova M, Grone H, Iozzo RV, Young MF, Seidler DG, Lin G, Reinhardt DP, Schaefer R. Regulation of fibrillin-1 by biglycan and decorin is important for tissue preservation in the kidney during pressure-induced injury. *Am J Pathol.* 2004;165(2):383-396.
66. Nakamura N, Hart D, Boorman R, Kaneda Y, Shrive N, Marchuk L, Shino K, Ochi T, Frank C. Decorin antisense gene therapy improves functional healing of early rabbit ligament scar with enhanced collagen fibrillogenesis in vivo. *J Orthop Res.* 2000;18(4):517-523.
67. Ramirez F, Rifkin DB. Extracellular microfibrils: contextual platforms for TGFbeta and BMP signaling. *Curr Opin Cell Biol.* 2009;21(5):616-622.
68. Nakajima Y, Yamagishi T, Hokari S, Nakamura H. Mechanisms involved in valvuloseptal endocardial cushion formation in early cardiogenesis: roles of transforming growth factor (TGF)-beta and bone morphogenetic protein (BMP). *Anat Rec.* 2000;258(2):119-127.
69. Rabkin E, Aikawa M, Stone JR, Fukumoto Y, Libby P, Schoen FJ. Activated interstitial myofibroblasts express catabolic enzymes and mediate matrix remodeling in myxomatous heart valves. *Circulation.* 2001;104(21):2525-2532.

70. Hakuno D, Kimura N, Yoshioka M, Fukuda K. Molecular mechanisms underlying the onset of degenerative aortic valve disease. *J Mol Med.* 2009;87(1):17-24.
71. Koullias GJ, Korkolis DP, Ravichandran P, Psyrris A, Hatzaras I, Elefteriades JA. Tissue microarray detection of matrix metalloproteinases, in diseased tricuspid and bicuspid aortic valves with or without pathology of the ascending aorta. *Eur J Cardiothorac Surg.* 2004;26(6):1098-1103.
72. Stephens EH, Nguyen TC, Itoh A, Ingels NB, Jr., Miller DC, Grande-Allen KJ. The effects of mitral regurgitation alone are sufficient for leaflet remodeling. *Circulation.* 2008;118(14 Suppl):S243-249.
73. Merryman WD, Youn I, Lukoff HD, Krueger PM, Guilak F, Hopkins RA, Sacks MS. Correlation between heart valve interstitial cell stiffness and transvalvular pressure: implications for collagen biosynthesis. *Am J Physiol Heart Circ Physiol.* 2006;290(1):H224-231.
74. Rabkin-Aikawa E, Farber M, Aikawa M, Schoen FJ. Dynamic and reversible changes of interstitial cell phenotype during remodeling of cardiac valves. *J Heart Valve Dis.* 2004;13(5):841-847.
75. Stephens EH, Timek TA, Daughters GT, Kuo JJ, Patton AM, Baggett LS, Ingels NB, Miller DC, Grande-Allen KJ. Significant changes in mitral valve leaflet matrix composition and turnover with tachycardia-induced cardiomyopathy. *Circulation.* 2009;120(11 Suppl):S112-119.
76. Ward C. Clinical significance of the bicuspid aortic valve. *Heart.* 2000;83(81-5).
77. Gurvitz M, Chang R, Drant S, Allada V. Frequency of aortic root dilation in children with a bicuspid aortic valve. *Am J Cardiol.* 2004;94(10):1337-1340.
78. Cotrufo M, Della Corte A, De Santo LS, Quarto C, De Feo M, Romano G, Amarelli C, Scardone M, Di Meglio F, Guerra G, Scarano M, Vitale S, Castaldo C, Montagnani S. Different patterns of extracellular matrix protein expression in the convexity and the concavity of the dilated aorta with bicuspid aortic valve: preliminary results. *J Thorac Cardiovasc Surg.* 2005;130(2):504-511.
79. Bauer M, Pasic M, Meyer R, Goetze N, Bauer U, Siniawski H, Hetzer R. Morphometric analysis of aortic media in patients with bicuspid and tricuspid aortic valve. *Ann Thorac Surg.* 2002;74(1):58-62.
80. Braverman A, Guven H, Beardslee M, Makan M, Kates A, Moon M. The Bicuspid Aortic Valve. *Curr Probl Cardiol.* 2005;30:470-522.
81. Bonderman D, Gharehbaghi-Schnell E, Wollenek G, Maurer G, Baumgartner H, Lang I. Mechanisms underlying aortic dilatation in congenital aortic valve malformation. *Circulation.* 1999;99(16):2138-2143.
82. Della Corte A, Quarto C, Bancone C, Castaldo C, Di Meglio F, Nurzynska D, De Santo L, De Feo M, Scardone M, Montagnani S, Cotrufo M. Spatiotemporal patterns of smooth

muscle cell changes in ascending aortic dilatation with bicuspid and tricuspid aortic valve stenosis: focus on cell-matrix signaling. *J Thorac Cardiovasc Surg.* 2008;135(1):8-18.

83. Friedman T, Mani A, Elefteriades J. Bicuspid aortic valve: clinical approach and scientific review of a common clinical entity. *Expert Rev Cardiovasc Ther.* 2008;6(2):235-248.
84. Bonnet D, Saygili A, Bonhoeffer P, Fermont L, Sidi D, Kachaner J. Atrio-ventricular valve dysplasia in 22 newborn infants. *Int J Cardiol.* 1997;59(2):113-118.
85. Bulkley BH, D'Amico B, Taylor AL. Extensive myocardial fiber disarray in aortic and pulmonary atresia. Relevance to hypertrophic cardiomyopathy. *Circulation.* 1983;67(1):191-198.
86. Grande-Allen KJ, Borowski AG, Troughton RW, Houghtaling PL, Dipaola NR, Moravec CS, Vesely I, Griffin BP. Apparently normal mitral valves in patients with heart failure demonstrate biochemical and structural derangements: an extracellular matrix and echocardiographic study. *J Am Coll Cardiol.* 2005;45(1):54-61.

Chapter 14: Extracellular Matrix Remodeling and Cell Phenotypic Changes in Dysplastic and Hemodynamically Altered Semilunar Heart Valves

Following upon the context provided by the congenital valve disease review presented in the previous chapter, in this chapter a study analyzing matrix remodeling and valvular interstitial cell (VIC) phenotypic changes in congenitally diseased semilunar valves is presented. The topic of congenital valve disease addressed in these two chapters is the first of a series of diseased states in which valve alterations are analyzed.

ABSTRACT

Background: While congenital cardiac valve disease is a common condition with substantial morbidity and mortality and suboptimal treatment options, little is known regarding the specific compositional changes in these valves. Characterization of the specific matrix and valve cell phenotypic abnormalities could lend insight into disease pathogenesis and potentially pave the way for novel therapies.

Methods: Aortic and pulmonic valves (AVs, PVs, n=35) were collected and categorized based on gross and microscopic assessment and clinical history into CTRL valves (n=21); dysplastic valves, valves (CTRL, n=21), dysplastic valves, all except one also displaying hemodynamic changes (HEMO/DYSP, n=6); and hemodynamic valves

(HEMO, n=8). Samples were subdivided by patient age into ≤ 2 years-old (n=13) and ≥ 9 years-old (n=21). Samples were immunohistochemically stained for matrix components, markers of matrix turnover, and markers of valve cell activation. Staining intensity was quantified in the mid-leaflet region, as well as in plaques and regions underlying plaques. Valvular interstitial cells (VICs) were also isolated from samples and analyzed for cell phenotypic markers and markers of hyaluronan and collagen metabolism using flow cytometry.

Results: CTRL AVs demonstrated decreased proteoglycans and hyaluronan with age, as well as decreased collagen turnover and valve cell activation. While both HEMO AVs and PVs ≥ 9 years-old demonstrated increased matrix metalloprotease (MMP)-13 and non-muscle myosin (NMM), and decreased fibrillin, prolyl 4-hydroxylase (P4H) and hyaluronan increased in HEMO AVs and decreased in HEMO PVs relative to CTRLs (HEMO v CTRL in AV and PV each $p < 0.001$, AV v PV $p < 0.001$). HEMO/DYSP AVs ≥ 9 years-old demonstrated distinct compositions compared to both HEMO AVs and CTRL AVs (each $p < 0.006$), including decreased collagen and elastic fiber synthesis and turnover. Plaques, and regions underlying plaques similarly displayed altered composition relative to CTRL valves (each $p < 0.001$), as well as distinctions between HEMO and HEMO/DYSP (each $p < 0.013$). Both HEMO and HEMO plaques and underlying regions displayed decreased P4H, LOX, Col 3, and hyaluronan in plaques and underlying regions, but MMP13 was increased in HEMO plaques and underlying regions, while MMP13 was decreased in HEMO/DYSP plaques. Flow cytometry of VICs from CTRL AVs and PVs revealed greater cell activation and collagen synthesis in AV VICs

than PV VICs ($p=0.02$). Both VICs from HEMO PVs and HEMO/DYSP PVs ≥ 9 years-old showed significantly different expression in the cell phenotype markers assayed compared to VICs from CTRL PVs (each $p<0.032$), especially increased NMM. Furthermore, VICs from HEMO PVs and from HEMO/DYSP AVs and PVs displayed greater size and complexity compared to VICs from CTRL valves (each $p<0.05$).

Conclusions: HEMO and HEMO/DYSP AVs and PVs demonstrated significant alterations in matrix composition and VIC phenotype compared to CTRL valves. Changes were distinct depending on valve and pathology. Furthermore, VICs isolated from these pathological valves displayed alterations in collagen synthesis, cell phenotype, and cell morphology. These results add to our understanding of dysplastic valves, namely that dysplastic valves are not simply valves with gross changes or a loss of layered leaflet structure microscopically, but these valves contain complex changes in matrix turnover, composition, and valve cell phenotype. Key processes, such as collagen and elastic fiber turnover, that appear to be dysregulated could be promising for novel therapeutics.

The work contained in this chapter is under review by the journal *Cardiovascular Pathology*:

Stephens EH, Shangkuan J, Kuo JJ, Carroll JL, Kearney DL, Carberry KA, Fraser CD, Grande-Allen KJ. **Extracellular Matrix Remodeling and Cell Phenotypic Changes in Dysplastic and Hemodynamically Altered Semilunar Cardiac Valves.** *Cardiovascular Pathology*, under review.

INTRODUCTION

Congenital valve disease imposes a heavy burden on our society, with a prevalence of approximately 1%¹ and high associated morbidity and mortality. In 2000 alone 213,000 life years were lost before age 65 because of congenital heart disease, nearly equal to the sum of leukemia, prostate cancer, and Alzheimer's disease.² The majority of congenital heart disease cases involve the valves and/or septa.³ Treatment options for patients with congenitally diseased valves are suboptimal at best. While mechanical valves and bioprosthetic valves perform relatively well in adults, they are wrought with complications in pediatrics. Bioprosthetic valves quickly calcify and mechanical valves require anti-coagulation, which is not compatible with a child's active lifestyle. Even if these issues could be solved, neither of these valve replacements grows with the child; therefore, these children must undergo multiple open-heart surgeries to replace valve replacements that the children have outgrown. In light of the heavy burden of congenital valve disease, there is a compelling need to better understand the pathology of this disease, as a foundation for the development of improved treatment options.

Prior research on congenital valve disease has largely focused on gross structural and epidemiological aspects. Pathological studies have examined the incidence of congenital valve disease, its association with other anatomic cardiac anomalies, and its gross anatomical features. While these valves are known to be histologically abnormal, the specific matrix changes that occur within these congenitally diseased valves remain largely unknown. The goal of this study was to characterize the matrix composition, matrix turnover, and valve cell phenotype in congenitally diseased semilunar cardiac valves.

METHODS

Sample Set

The research use of this tissue was approved by the institutional review boards at each institution. Patients were enrolled in the study after informed consent was obtained. A total of 32 surgically excised semilunar valves were collected from Texas Children's Hospital including 17 aortic valves (AVs) and 15 pulmonic valves (PVs). Three additional autopsy semilunar valves were obtained from Texas Children's Hospital (2 PVs) and Ben Taub General Hospital, Houston, TX (1 AV). Valves were surgically excised for valvar stenosis and/or regurgitation, or were received with cardiac explants.

Valves were grouped into 3 categories based on gross structural and histologic architecture. Valves with thin, delicate cusps and 3 clearly delineated, properly oriented histologic layers of normal thickness were designated controls (CTRL, n=21, 12 AVs, 9 PVs). Hemodynamically altered valves (HEMO, n=8, 3 AVs, 5 PVs) appeared thickened and fibrotic with 3 identifiable, but variably thickened layers, with or without fibrous plaques on the surface. Valves that were variably thickened and deformed and lacked delineated layers with increased myxoid matrix were defined as dysplastic. All except the youngest of these samples also displayed hemodynamic changes and were designated (HEMO/DYSP, n= 6, 3 AVs, 3 PVs). The one isolated dysplastic PV from 2 year-old was evaluated but not included in statistical analyses. Samples were subdivided into valves from patients ≤ 2 years-old (n=13) and ≥ 9 years-old (n=21); with one outlying HEMO/DYSP AV from a 5 year-old. Additionally a sub-group analysis was performed on valvular interstitial cells (VICs) from pulmonary autografts in the aortic position for >

3 years as part of the Ross procedure valves⁴ in which the PVs had been placed in the AV position for at least 3 years. The research use of this tissue was approved by the institutional review boards at each institution.

Histology and Immunohistochemistry

Samples were fixed in 10% formalin, paraffin embedded, and sectioned according

Table 14-1. Antibodies Used in Immunohistochemistry (IHC) and Flow Cytometry (FC).

Protein	IHC, FC Analysis	Function
<u>Collagen Turnover Proteins</u>		
Collagen III (Col III)	IHC	Reticular collagen
Matrix Metalloproteinase-13 (MMP13) [†]	IHC	Collagen degradation
Prolyl 4-Hydroxylase (P4H) [†]	IHC, FC	Marker of collagen synthesis
Heat Shock Protein-47 (HSP47)	IHC, FC	Marker of collagen synthesis
<u>Elastic Fiber-Related Proteins</u>		
Lysyl oxidase (LOX) [§]	IHC	Involved in collagen and elastin crosslinking
Fibrillin	IHC	Component of elastic fibers
Matrix Metalloproteinase-9 (MMP9) [‡]	IHC	Elastic fiber degradation
<u>Proteoglycans (PG), Glycosaminoglycans (GAG), and Glycoproteins</u>		
Hyaluronan (HA) [#]	IHC	GAG providing compressibility
Hyaluronan Receptor for Endocytosis (HARE) [^]	FC	Protein involved in HA turnover
CD44	FC	Cellular receptor for HA
Fibronectin [†]	FC	Extracellular glycoprotein
Decorin (DCN) [*]	IHC	PG involved in collagen fibrillogenesis
Biglycan (BGN) [*]	IHC	PG involved in collagen fibrillogenesis
Versican (VC) ^{##}	IHC	PG involved elastic fibrillogenesis and compressibility
<u>Valve Cell Activation/Cell Phenotype</u>		
Vimentin ^{**}	FC	Intermediate filament of mesenchymal cells
Non-muscle myosin (NMM) ^{^^}	IHC, FC	Marker of an "activated" myofibroblast-like phenotype
Smooth muscle alpha-actin (SMaA) ^{**}	IHC, FC	Marker of an "activated" myofibroblast-like phenotype

FC=flow cytometry, IHC=immunohistochemistry; ^{||}Abcam (Cambridge, MA); [†]Chemicon (Temecula, CA); [§]Imgenex (San Diego, CA); [‡]Assay Designs (Ann Arbor, MI); [#]detected using hyaluronan binding protein, Associates of Cape Cod (Falmouth, MA); ^{*}gift of Dr. Larry Fisher (NIH, Bethesda, MD); ^{##}Associates of Cape Cod; [^]gift of Dr. Paul Weigel (University of Oklahoma, Oklahoma City, OK); ^{**}Dakocytomation (Denmark); ^{^^}Covance (Berkeley, CA).

to standard procedures. Each sample was stained histologically with Movat pentachrome and immunohistochemically (IHC) for extracellular matrix components and valve cell phenotype (Table 14-1). IHC staining intensity of the mid-leaflet region of each section was quantified using ImageJ software (NIH, Bethesda, MD). Additionally IHC intensity in plaques and the underlying leaflet region was quantified.

Flow Cytometry

Valvular interstitial cells (VICs) were isolated from samples procured within 24 hours of surgery and cultured as previously described.⁵ VICs from a total of 26 surgical samples were analyzed using flow cytometry (13 AVs, 13 PVs). For each cell line, an unstained sample and a negative control (mouse or rabbit IgG) were run alongside specific antibody samples (Table 14-1). Cells were fixed and stained as described previously,⁶ with the exception of the following modifications: fixation time was > 1 hour, permeabilization time was 10 minutes, antibody incubation steps times 1 hour and the final resuspension volume was 250 μ L. Samples were run on a FACScan flow cytometer and data analyzed with Cellquest Pro software (both BD, Franklin Lakes, NJ). Each sample was run three times and the median fluorescence recorded. Using the isotype control sample, the cell population was identified and gated based on size (FSC) and complexity (SSC). This population was then further gated based on fluorescence such that less than 1% fluorescence fell within the gate. This gate was then used to compare changes in fluorescence between cells stained with different markers.

Statistical Analysis

Multifactorial analysis of variance (ANOVA) was performed using SigmaStat (SPSS, Chicago, IL), as described in Chapter 4. For comparisons between IHC intensity within plaques and the underlying leaflet, paired t-tests were performed. In all cases the level of significance was set at 0.05. Pearson and Spearman tests were used to calculate correlations between staining intensities, as described in Chapter 5. Significance was set at $p \leq 0.0042$ for correlations in IHC (12 proteins compared) and $p \leq 0.0071$ for flow cytometry (7 proteins compared).

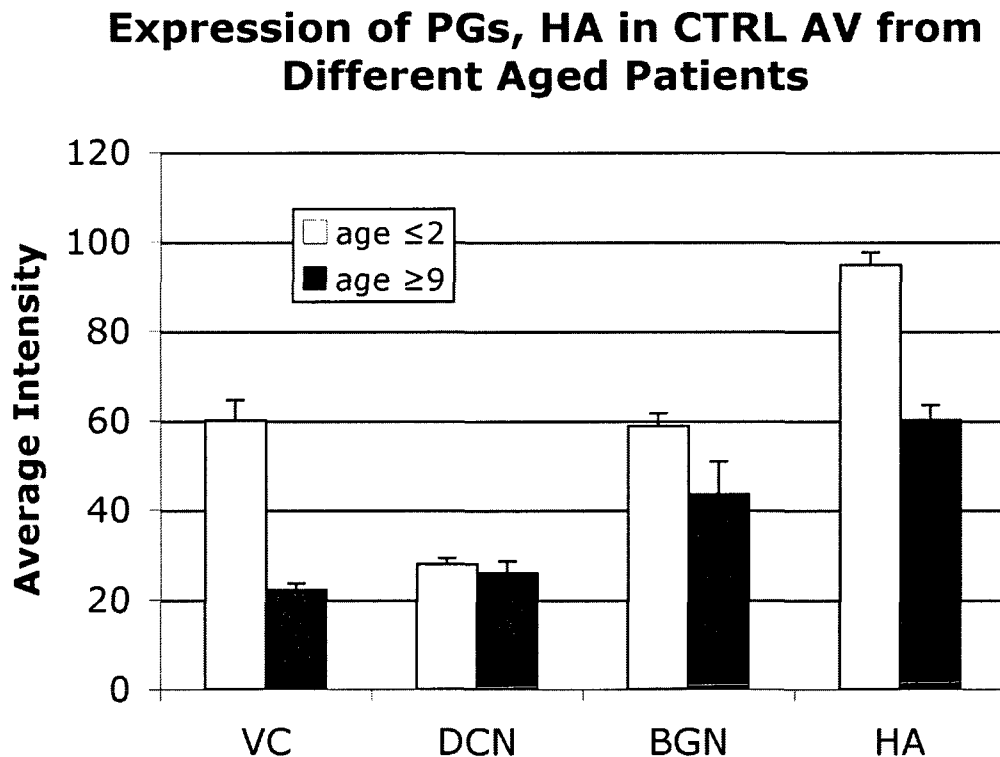


Fig. 14-1: Expression of PGs and HA in different aged CTRL AVs. Overall $p=0.002$. Error bars in all graphs indicate the standard error of the mean.

RESULTS

Age-Related Changes in Matrix Composition of Semilunar Valves

Analysis of CTRL AVs revealed decreased hyaluronan and proteoglycans versican and biglycan, but not decorin, with age (Fig. 14-1, $p=0.002$). Markers of collagen turnover (MMP13, P4H, HSP47), Col 3, and SMaA also decreased in CTRL AVs with age (Fig. 14-2, $p<0.001$). Analysis of CTRL PVs revealed similar age-related changes, with decreased markers of collagen turnover (MMP13, P4H, HSP47) and markers of VIC activation (NMM and SMaA) ($p=0.02$, data not shown). Expression of proteoglycans and hyaluronan in CTRL PVs of different ages showed similar tendencies as AVs, with decreased versican, biglycan, and hyaluronan and no change in decorin, but the age-related changes in versican and hyaluronan were smaller than in AVs.

Expression of Matrix Components in CTRL AV from Different Aged Patients

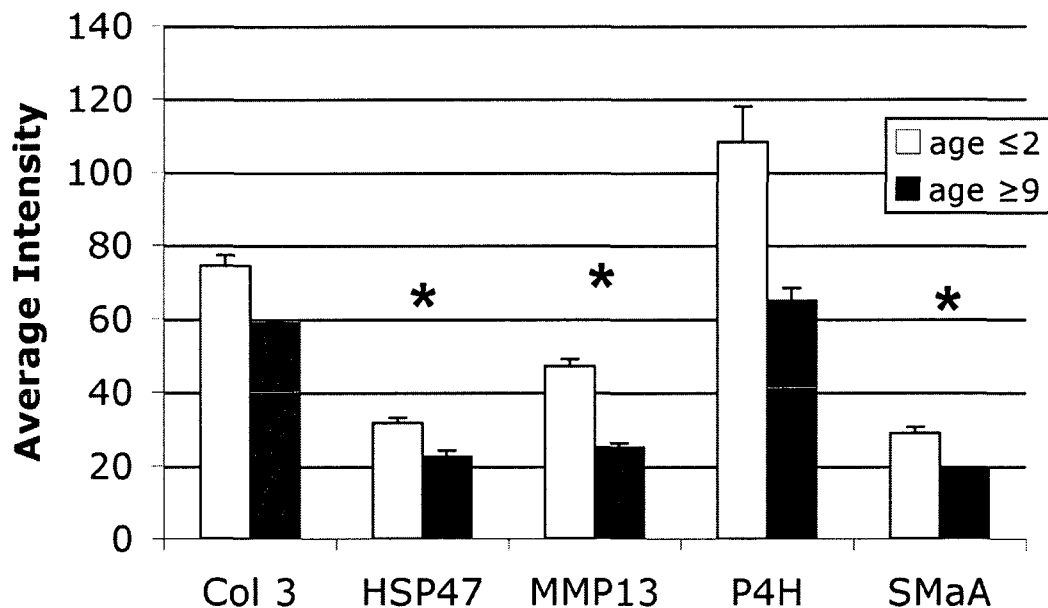


Fig. 14-2: Expression of markers of collagen turnover and activated VICs in different aged CTRL AVs. Overall $p<0.001$, $*p<0.05$ between age groups for a given marker.

Expression of Matrix in HEMO AV, HEMO PV vs CTRLs

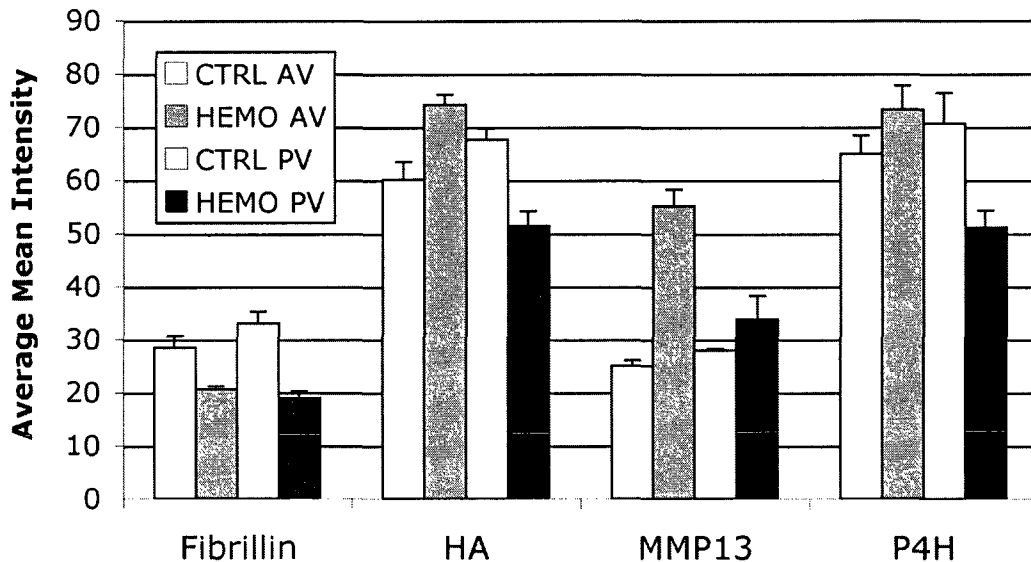


Fig. 14-3: Expression of matrix components in HEMO AVs and PVs from patients >9 years-old compared to CTRL AVs and PVs from patients ≥ 9 years-old. Overall $p < 0.001$ for HEMO vs. CTRL for each AV and PV; AV vs. PV within each HEMO and CTRL $p < 0.001$. HEMO vs. CTRL $p < 0.05$ for P4H and HA by Holm-Sidak post-hoc testing.

Matrix Changes in Pathological Semilunar Valves

HEMO AVs and PVs ≥ 9 years-old not only demonstrated altered matrix compared to CTRLs (Fig. 14-3, HEMO AV vs. CTRL, HEMO PV vs. CTRL each $p < 0.001$), but changes were distinct between AV and PV ($p < 0.001$). While both HEMO AVs and PVs demonstrated increased MMP13 and NMM, and decreased fibrillin, P4H and hyaluronan increased in HEMO AVs and decreased in HEMO PVs relative to CTRLs. HEMO/DYSP AVs ≥ 9 years-old demonstrated distinct compositions compared to both HEMO AVs and CTRL AVs (each $p < 0.006$, Fig. 14-4), including decreased

collagen and elastic fiber synthesis and turnover. The Ross valves within this HEMO PV group displayed changes consistent with HEMO PVs and distinct from HEMO AVs.

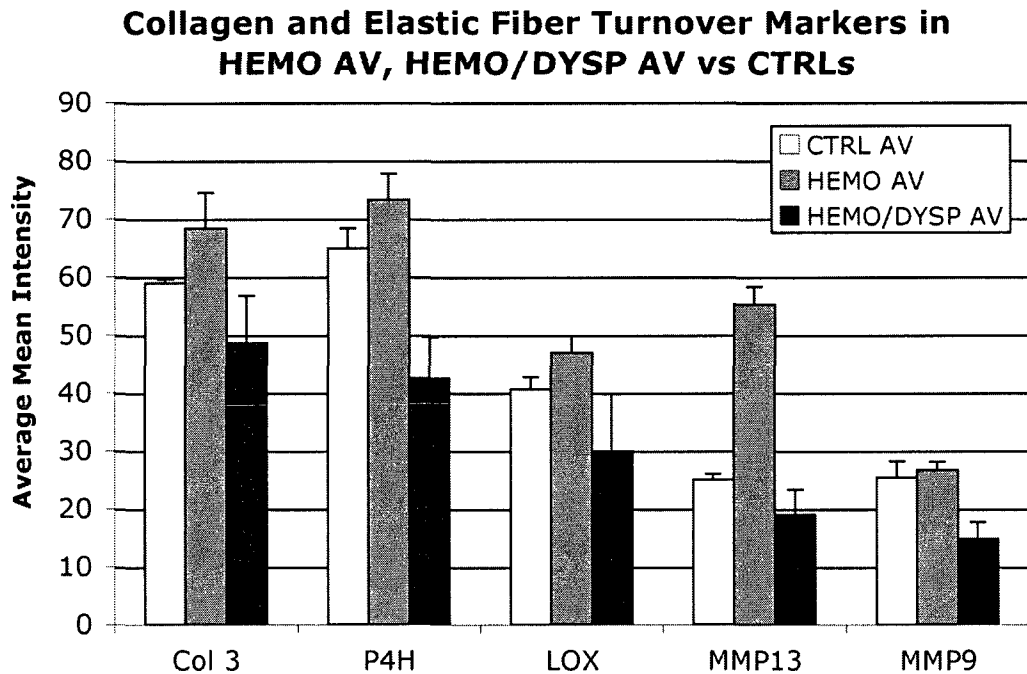


Fig. 14-4: Expression of matrix components in HEMO/DYSP AVs and HEMO AVs from patients ≥ 9 years-old compared to CTRL AVs from patients ≥ 9 years-old. Overall $p < 0.001$, HEMO, HEMO/DYSP, and CTRL each significantly different (each $p < 0.006$).

Plaques and underlying regions demonstrated altered matrix compositions relative to CTRL valves (Fig. 14-5, each $p < 0.001$), and these alterations were distinct between HEMO and HEMO/DYSP (Fig. 14-5, each $p < 0.013$). Both HEMO and HEMO/DYSP plaques and underlying regions displayed decreased P4H, LOX, Col 3, and hyaluronan in plaques and underlying regions, but MMP13 was increased in HEMO plaques and underlying regions, while MMP13 was decreased in HEMO/DYSP plaques. P4H was also greater in HEMO plaques relative to HEMO/DYSP and the decrease in hyaluronan

Matrix Expression in Plaques and Underlying Regions

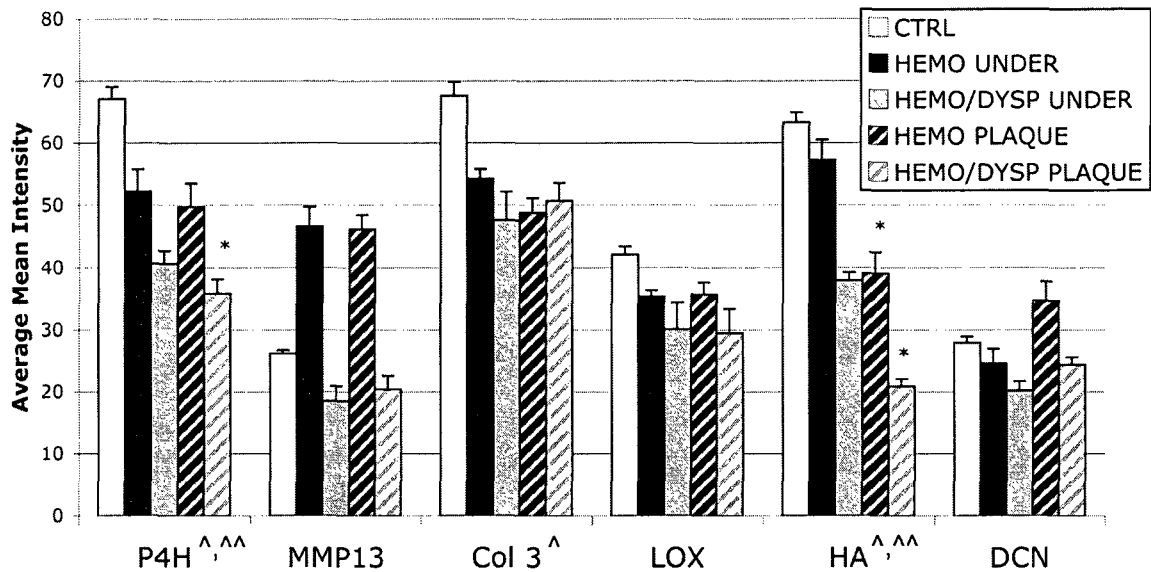


Fig. 14-5: A) Expression of matrix in HEMO and HEMO/DYSP plaques and the regions underlying plaques (UNDER) relative to CTRL valves. Overall plaque vs. CTRL $p < 0.001$, underlying regions vs. CTRL $p < 0.001$. Pathology (HEMO, HEMO/DYSP, CTRL) was significant for both plaques ($p < 0.001$) and underlying regions ($p = 0.001$), and HEMO was significantly different than HEMO/DYSP by post-hoc testing for both plaques ($p < 0.013$) and underlying regions ($p < 0.012$). * $p < 0.05$ vs. HEMO or HEMO/DYSP vs. CTRL for a given matrix component. [^] $p < 0.05$ CTRL vs. plaque and ^{^^} $p < 0.05$ CTRL vs. underlying plaques for a given matrix component.

was greater in HEMO/DYSP plaques and underlying regions compared to HEMO. Relative to their respective underlying leaflet regions, plaques in HEMO and HEMO/DYSP semilunar valves showed decreased hyaluronan (Fig. 14-6, $p < 0.001$) and MMP9 ($p < 0.05$), but increased decorin ($p < 0.002$). Plaques specifically found in HEMO semilunar valves demonstrated decreased HSP47 ($p = 0.013$) and decreased NMM ($p < 0.01$) relative to underlying leaflet regions.

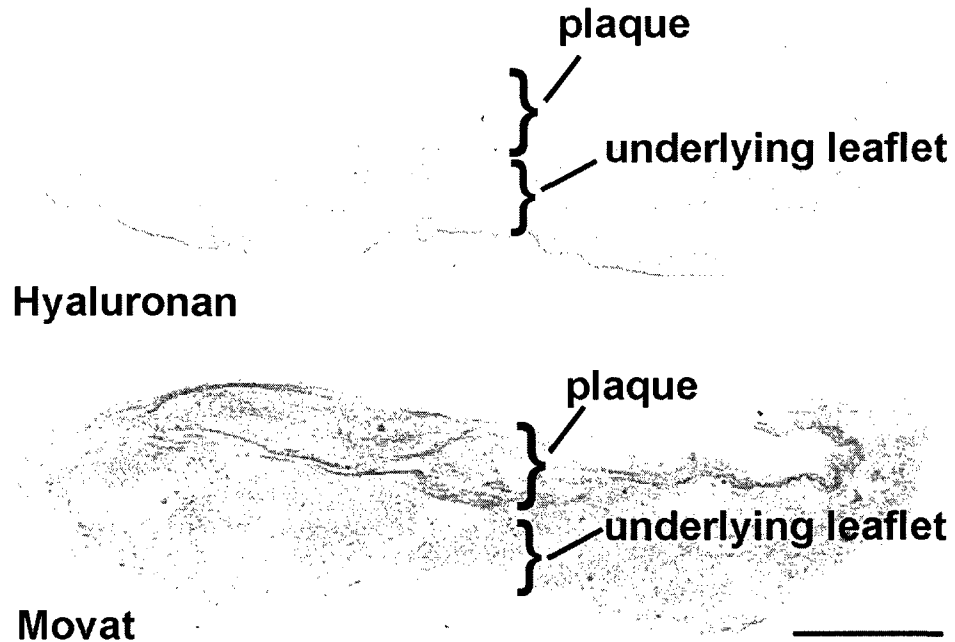


Fig. 14-6: Plaque in a HEMO/DYSP bicuspid AV from an 18 year-old patient demonstrating decreased HA expression in the plaque relative to the adjacent, underlying leaflet. Scale bar indicates 1 mm.

Remodeling of Leaflet Layers in Pathological Semilunar Valves

While CTRL valves demonstrated clearly delineated trilaminar leaflet structure with the Movat stain, accompanied by layer-predominant expression of different matrix components (Fig. 14-7), the architectural disruption in HEMO/DYSP valves was accompanied by altered localization of matrix components (Fig. 14-8). For instance, in CTRL valves hyaluronan was largely expressed in the spongiosa layer, with some

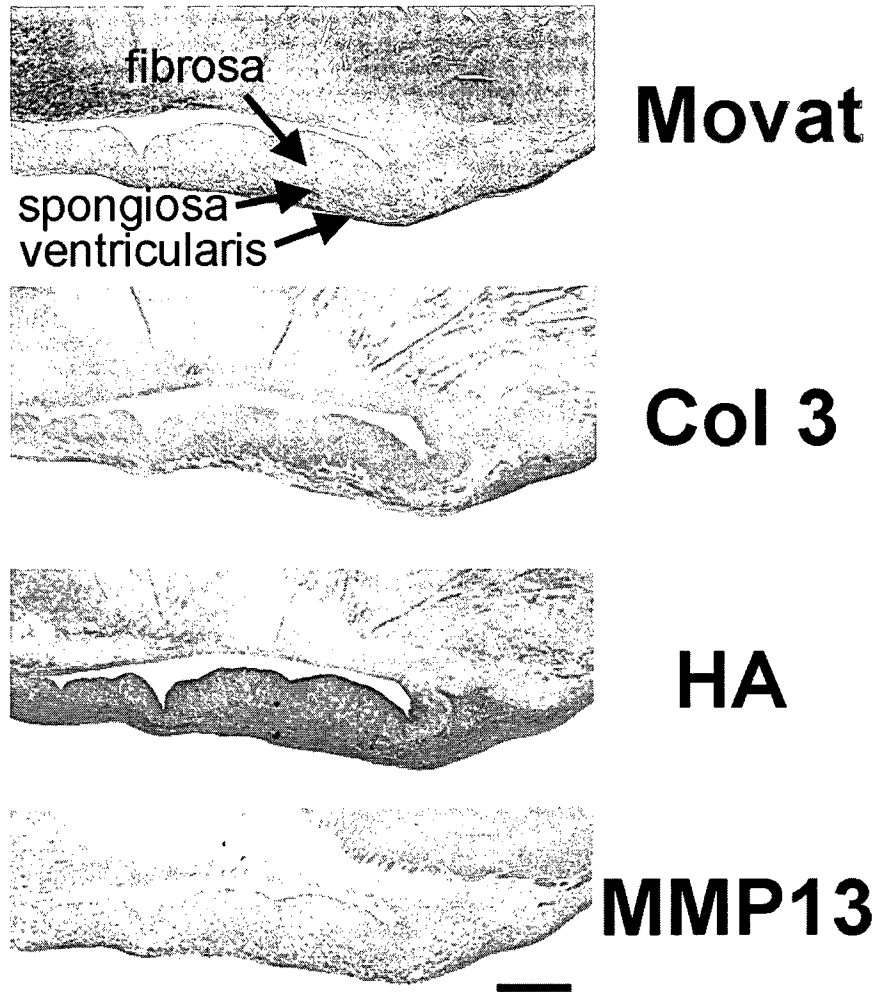


Fig. 14-7: CTRL AV from a 2 year-old demonstrating clearly delineated leaflet layers and layer-specific expression of matrix components characteristic of CTRL AVs and PVs. Scale bar indicates 500 μ m and applies to all panels of the figure.

expression in areas of elastic fibers, but in HEMO/DYSP valves hyaluronan was abnormally distributed throughout the valve; hyaluronan in the central region normally comprising the spongiosa appeared expanded and hyaluronan did not co-localize with elastic fibers (Fig. 14-8). Matrix components such as Col 3, MMP13, and hyaluronan also demonstrated marked marbling. Other HEMO/DYSP valves also

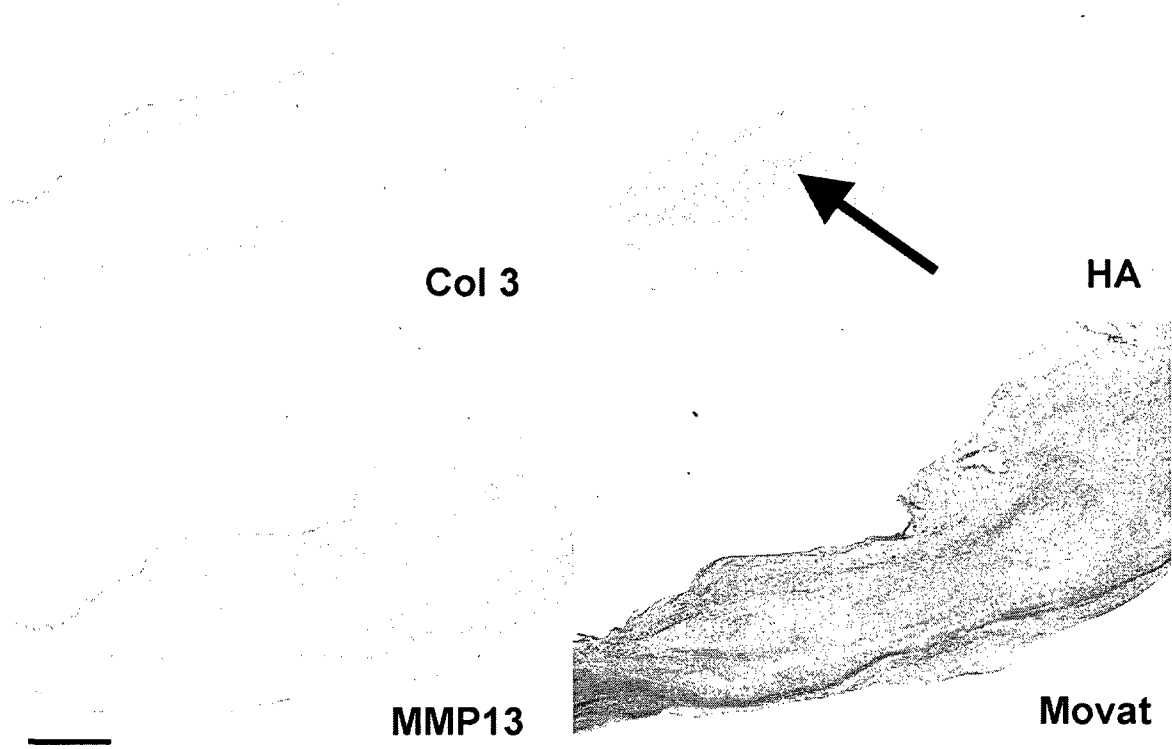


Fig. 14-8: HEMO/DYSP AV demonstrating a lack of clearly delineated leaflet layers, marbling of Col 3, HA, and MMP13. Arrow points to expansion of HA composition in the interior of the leaflet. Scale bar indicates 1 mm and applies to all panels of the figure.

showed profound abnormalities in marker expression within the central region normally comprising the spongiosa. For instance, in the HEMO/DYSP PV shown in Fig. 14-9, abnormally high levels of NMM, P4H, LOX, and fibrillin are evident. HEMO/DYSP valves also demonstrated variability in degree of loss of leaflet layer delineation throughout the length of the leaflet, as illustrated in Fig. 14-10. Also evident in this sample are pockets of collagen and elastic fiber remodeling in dysplastic regions. In several valves with plaques pockets of strong SMaA expression were noted both within

the plaque itself, and at the edge of the plaque (Fig. 14-11). These pockets of SMaA expression co-localized with high levels of MMP13 and biglycan (Fig. 14-11).

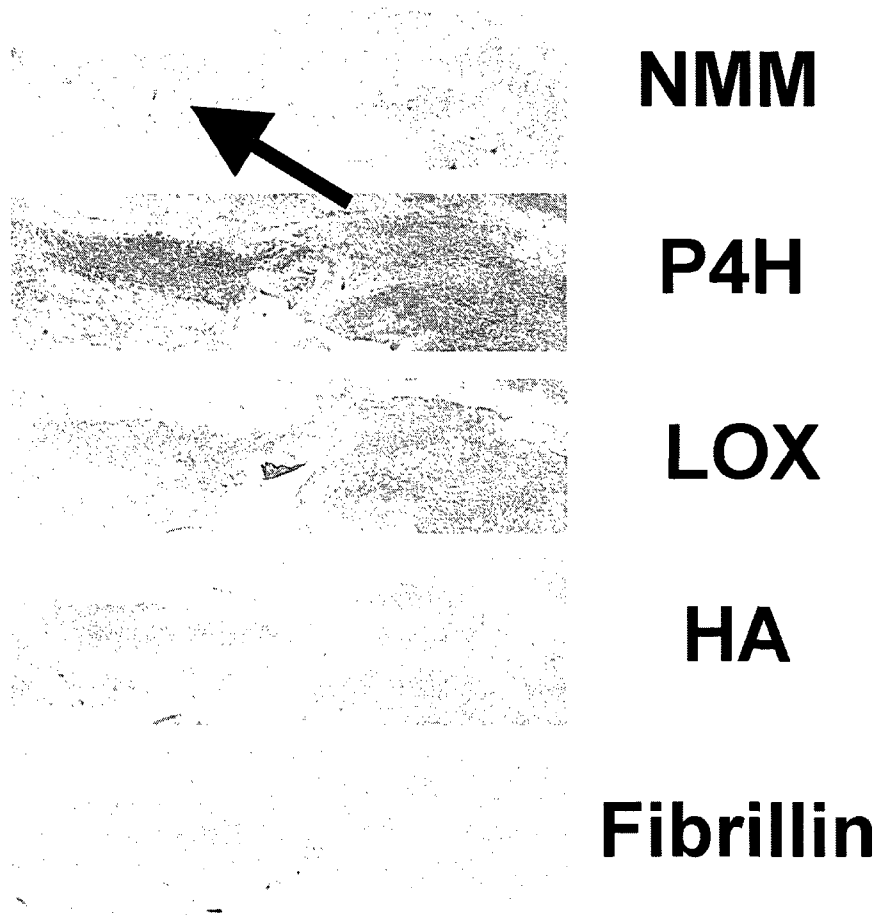


Fig. 14-9: HEMO/DYSP PV from a 12-year-old patient demonstrating strong expression of NMM, P4H, LOX, and fibrillin in the spongiosa (arrow). Note also the expansion of hyaluronan staining across the thickness of the leaflet. Scale bar indicates 500 μ m and applies to all panels of the figure.

Movat

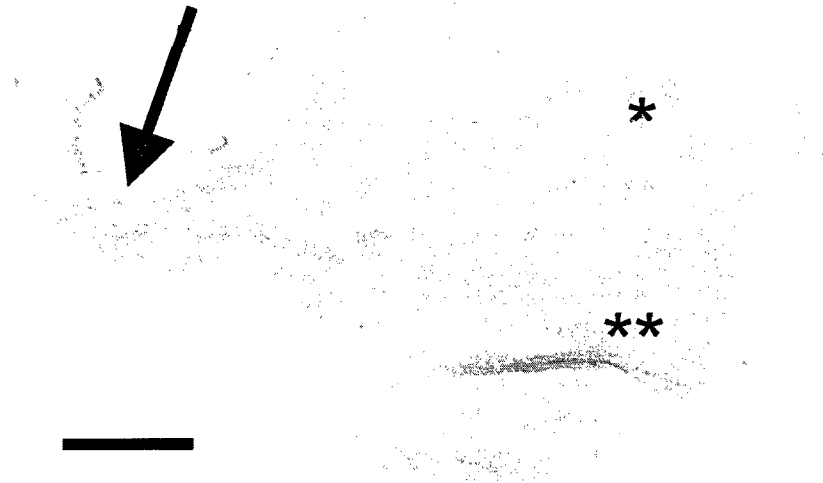


Fig. 14-10: HEMO/DYSP bicuspid AV from a 5 year-old patient demonstrating an annular region with relatively intact leaflet layers, indicated by the arrow, and nodular region with pockets of collagen (*) and elastic fiber remodeling (**). Scale bar indicates 1 mm.

Correlations between Matrix Components in Pathological Semilunar Valves

While HSP47 moderately correlated with P4H in CTRL AVs and PVs ($r=0.64$, $p<0.002$) as expected considering their common roles in collagen synthesis, in diseased valves HSP47 showed strong correlations with versican in regions underlying plaques ($r=0.91$, $p<0.001$). Furthermore, HEMO and HEMO/DYSP valves demonstrated distinct correlations related to collagen synthesis and turnover. While HSP47 correlated with decorin and versican in HEMO valves ($r=0.82$, $p=0.002$ and $r=0.80$, $p=0.003$, respectively), MMP13 correlated with decorin and versican in HEMO/DYSP valves ($r=0.91$, $p<0.001$ and $r=0.82$, $p<0.002$, respectively) and HSP47 correlated with MMP9 and fibrillin ($r=0.76$, $p=0.003$ and $r=0.76$, $p=0.002$, respectively).

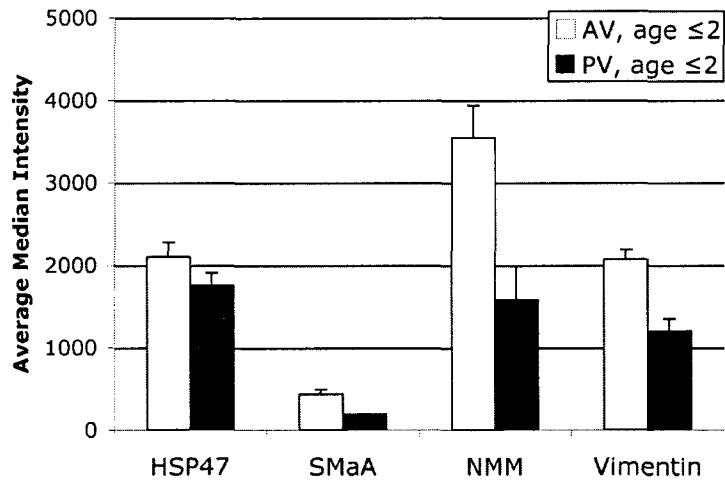


Fig 14-11: HEMO/DYSP bicuspid AV from an 18 year-old patient illustrating pockets of strong SMaA staining co-localizing with MMP13 and BGN expression (*). Brackets indicate location of plaques. Scale bar indicates 1 mm and applies to all panels of the figure.

Differences between AV and PV VICs

Flow cytometry analysis of VICs from CTRL AVs and PVs revealed greater cell activation and collagen synthesis in AV VICs than PV VICs (p=0.02, Fig. 14-12).

A. CTRL AV, PV VICs from Patients ≤ 2 yo



B. CTRL AV, PV VICs from Patients ≥ 9 yo

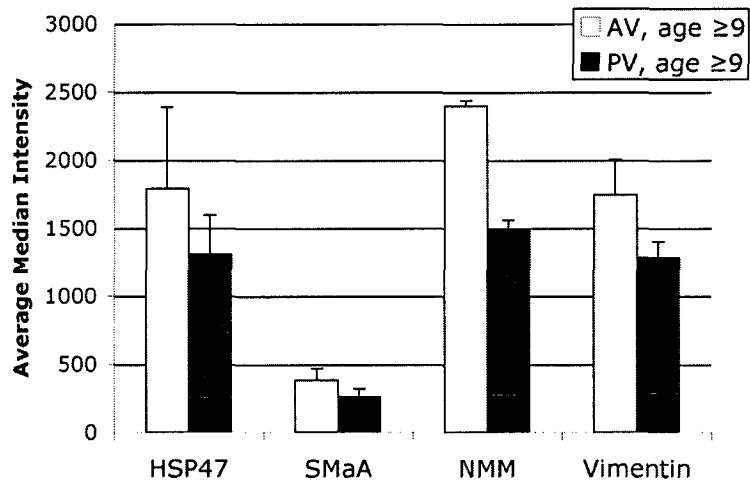
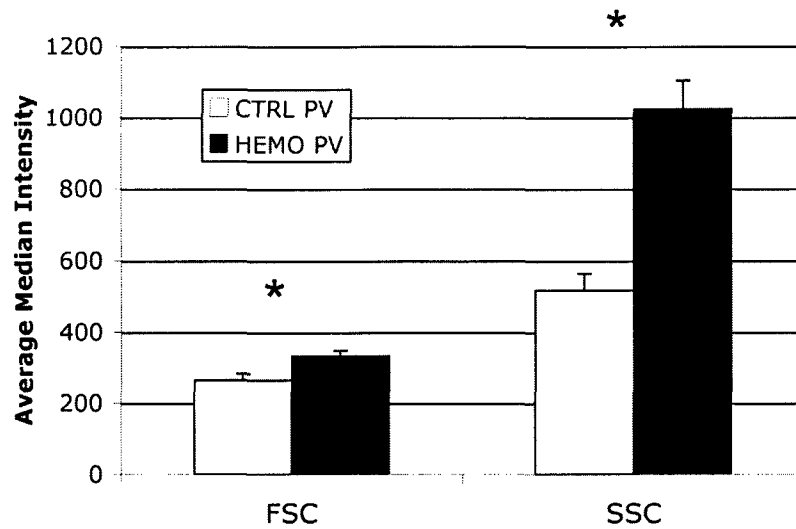


Fig. 14-12: Expression of cell phenotype markers in VICs from CTRL AV and PV from patients ≤ 2 years-old (A) and ≥ 9 years-old (B). Overall AV vs. PV $p=0.02$.

A. Cell Morphology of HEMO PV VICs from Patients ≥ 9 yo



B. Cell Morphology of HEMO/DYSP and CTRL AV, PV VICs from Patients ≥ 9 yo

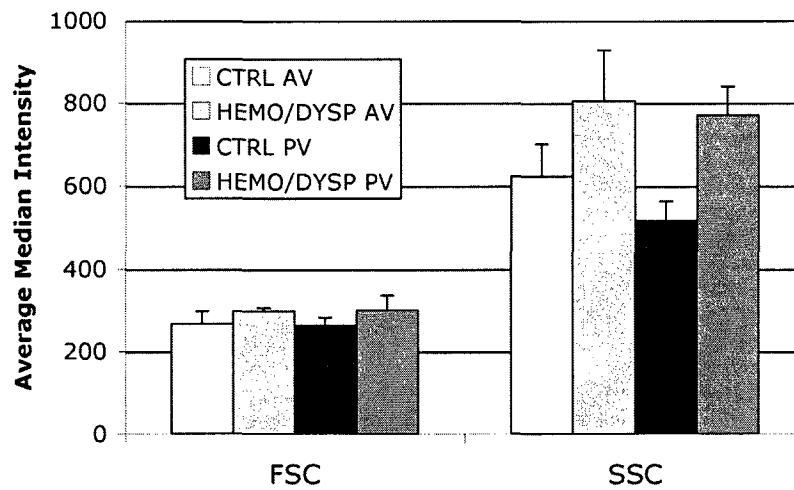


Fig. 14-13: A) Cell morphology of VICs from HEMO PV of patients ≥ 9 years-old compared to VICs from CTRL PV of patients ≥ 9 years-old. * $p < 0.001$ HEMO vs. CTRL for a given marker. B) Cell morphology of VICs from HEMO/DYSP AV and PV of patients ≥ 9 years-old compared to VICs from CTRL AV and PV of patients ≥ 9 years-old. HEMO/DYSP vs. CTRL for FSC $p = 0.041$, for SSC $p < 0.001$.

Changes in VICs from Pathological Semilunar Valves

Compared to VICs from CTRL PVs ≥ 9 years-old, VICs from both HEMO PVs and HEMO/DYSP PVs ≥ 9 years-old showed significantly different expression in the cell phenotype markers assessed ($p=0.022$ and $p=0.031$, respectively), especially increased NMM. Furthermore, VICs from HEMO PVs demonstrated slightly greater size (FSC, $p<0.001$) and dramatically greater complexity (SSC, $p<0.001$) than CTRL PV (Fig. 14-13A). VICs from HEMO/DYSP AV and PV ≥ 9 years-old similarly displayed greater size (FSC, $p=0.041$) and complexity (SSC, $p<0.001$) compared to VICs from CTRL AV and PV (Fig. 14-13B). Analysis of the subset of VICs from Ross valves (PV placed in

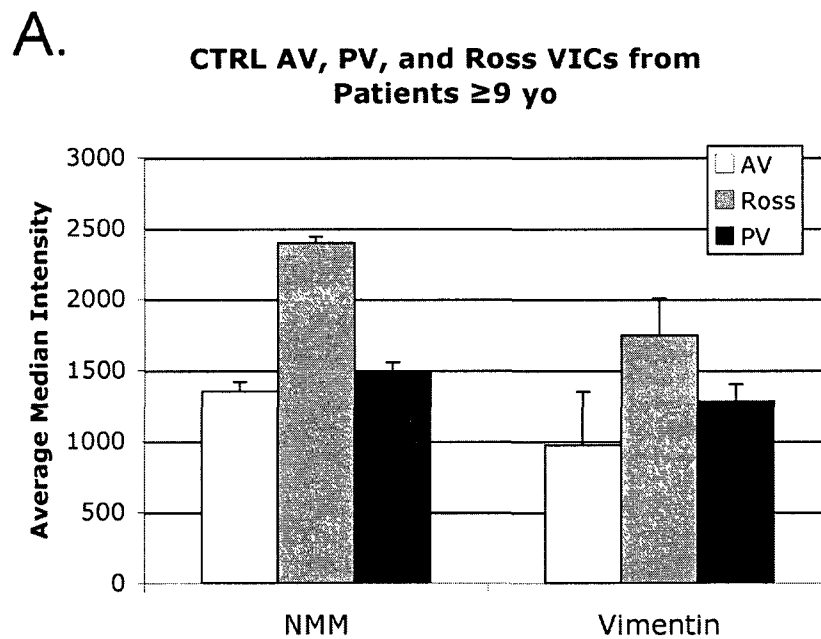


Fig. 14-14: A) Expression of cell phenotype markers in VICs from Ross valves (AV placed in the PV for > 3 years), CTRL AV, and CTRL PV from patients ≥ 9 years-old. Overall $p=0.016$.

B. Cell Morphology of CTRL AV, CTRL PV, and Ross VICs

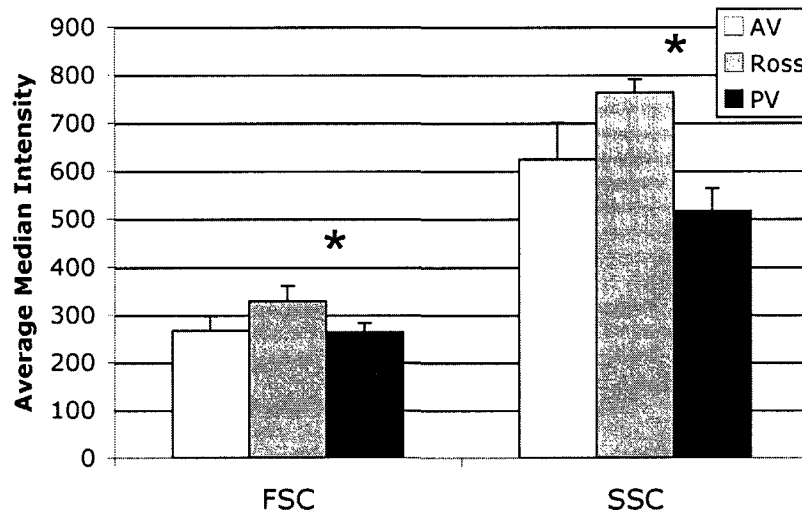


Fig. 14-14 (cont'd): B) Cell morphology of VICs from Ross valves, CTRL AV, and CTRL PV from patients ≥ 9 years-old. For FSC: Ross, AV, PV $p=0.013$, for SSC: Ross, AV, PV $p<0.001$. * $p<0.05$ Ross vs. PV for a given marker by Dunn's post-hoc testing.

the AV for at least 3 years) ≥ 9 years-old compared to VICs from CTRL AVs and PVs ≥ 9 years-old showed greater NMM and vimentin ($p=0.016$, Fig. 14-14A) and significantly greater size ($p=0.013$) and complexity ($p<0.001$, Fig. 14-14B).

DISCUSSION

Previous Studies of Matrix Composition in Congenitally Diseased Valves

While limited analyses of congenitally diseased valves in terms of general structure and composition using basic histological stains have been occasionally reported, analyses of specific matrix components are rare. In 1979 Baig reported more dermatan sulfate in the 21-40 year-olds BAV, and less hyaluronan and more chondroitin sulfate in the 41-60 year-old BAV compared to age-matched controls.⁷ A more recent study of

adult bicuspid AVs demonstrated increased MMP2 and 9,⁸ however, given the age of these patients in these studies, it is difficult to discern how much of these changes were a result of the years of altered hemodynamics.⁷ Given the patients' ages it also is likely that these valves were not highly dysplastic, unlike bicuspid AVs that present early in life.

In terms of basic histological analyses, Hinton reported disorganized collagen and elastin, proteoglycans in all layers, decreased elastin, and increased collagen in bicuspid AVs from six young patients (ranging from 1-184 months).⁹ Given the age of these patients, these valves may have been less affected by hemodynamic changes and potentially more dysplastic than those studied by Baig. In 1973 Bharati and Lev analyzed valves in congenital polyvalvular disease (CPVD, a specific congenital valve disease in which all four valves are affected) using basic histology.¹⁰ CPVD valves demonstrated an increase in the spongiosa layer with vacuolar and lacunar degeneration compared to age-matched normal valves and normal valves exposed to altered hemodynamics.¹⁰ These findings sharply contrast with those described in hemodynamically altered valves that have increased elastic fibers, and variably increased fibrous tissue with distinct, albeit altered trilaminar architecture.¹⁰ Koretzky in his study of PV dysplasia also reported changes principally in the spongiosa including expansion of that layer.¹¹ Hyams' study of a broad group of congenitally diseased valves, including both isolated and polyvalvular cases, reported myxomatous nodules devoid of elastic tissue with pockets of collagenous tissue.¹² However, rarely have alterations in specific proteins been studied in congenitally diseased valves and none reported for dysplastic

valves. Furthermore, none of the above studies assessed alterations in VIC cell phenotype.

Altered Matrix Composition and VIC Cell Phenotype in Pathological Valves

In the present study we found that HEMO and HEMO/DYSP valves demonstrated significant and distinct alterations in matrix composition compared to CTRL valves. In HEMO valves, increased VIC activation and collagen turnover (MMP13) were seen in both AVs and PVs, which are consistent with *ex vivo* studies in which porcine AVs were exposed to increased mechanical stress.^{13, 14} Fibrillin was also decreased in both HEMO AVs and PVs, suggesting elastic fiber degradation, as reported in hemodynamically altered valves.¹⁰ However, hyaluronan and P4H both decreased in HEMO PVs and increased in HEMO AVs, suggesting that the AV and PV may respond to altered hemodynamics differently. Within the HEMO PV group, Ross valves displayed changes consistent with HEMO PVs and distinct from HEMO AVs, suggesting that these Ross valves maintain inherent mechanobiological differences in their response to altered hemodynamics compared to AVs despite placement in the aortic position.

HEMO/DYSP AVs demonstrated distinct compositions relative to HEMO AVs, including decreased collagen and elastic fiber synthesis and turnover, as compared to increased collagen synthesis and turnover in HEMO AVs. Examination of leaflet layer remodeling in HEMO/DYSP valves revealed alterations in localization of matrix components, particularly in the region normally comprising the spongiosa layer, as well as pockets of collagen and elastic fiber remodeling, consistent with previous reports of dysplastic valves.¹⁰⁻¹² These findings are also consistent with collagen and elastic fiber

disarray previously reported in bicuspid (potentially dysplastic) AVs from young patients,⁹ and could suggest impaired ability of the valve to remodel in response to stress, which could have functional consequences. Distinct patterns of correlations between matrix components related to collagen turnover, elastic fiber turnover, and proteoglycans in HEMO valves relative to HEMO/DYSP valves suggest distinct interactions between matrix components within these different valves, which may contribute to the distinct pathological processes, although much remains to be learned in that regard.

The plaques and regions underlying plaques in HEMO and HEMO/DYSP valves demonstrated distinct matrix compositions relative to CTRL valves, with decreased markers of collagen synthesis and hyaluronan. Particularly notable were the differences between plaques on HEMO as compared to HEMO/DYSP valves, including increased MMP13 in HEMO but decreased MMP13 in HEMO/DYSP plaques relative to CTRLs, and a more substantial decrease in P4H and hyaluronan in HEMO/DYSP than HEMO plaques relative to CTRLs. Pockets of strong SMAA expression and increased expression of matrix components were also noted within and bordering plaques, suggesting involvement of VICs with a myofibroblast phenotype in plaque formation. Further work understanding the processes occurring in the leaflet regions underlying plaques, and how they may relate to plaque formation is warranted.

Not only did the congenitally diseased valves in this study display altered matrix composition, but the VICs contained in these valves displayed alterations in cell phenotype relative to VICs from CTRL valves. VICs from HEMO valves particularly demonstrated increased NMM, a marker of VIC activation, consistent with the IHC results. Both VICs from HEMO/DYSP valves and HEMO valves displayed altered cell

morphology, including increased size and complexity, relative to VICs from CTRL valves. Analysis of a subset of VICs from Ross valves suggests that these VICs display distinct cell phenotypes relative to VICs from CTRL valves. VICs from Ross valves also demonstrated increased VIC activation, consistent with the higher mechanical stress the PV must experience in the AV position, and consistent with previous analyses of tissues from Ross valves.¹⁵ As evident in VICs from HEMO and HEMO/DYSP valves, VICs from Ross valves also demonstrated increased cell size and complexity compared to CTRLs, suggesting these changes in cell morphology may be common to multiple forms of congenital valve disease. The differences in VICs from pathological valves relative to CTRL valves suggest that inherent abnormalities in the VICs could contribute to the documented matrix abnormalities and potentially plaque formation.

Age-related Changes and Differences between AV and PV among CTRL Samples

Analysis of CTRL AVs and PVs demonstrated decreased markers of collagen synthesis and turnover, VIC activation, proteoglycans (particularly in the AV), and hyaluronan with age. Decreased VIC activation and MMP13 is consistent with a previous study reporting decreases in these markers from fetal to ~6 year-old and then to ~50 year-old semilunar valves.¹⁶ Previous work examining age-related matrix changes in porcine valves and their relationship to changes in material properties¹⁷ among other studies, suggests that the changes in composition demonstrated in the present study could have important consequences for valve function.

Greater VIC activation and collagen synthesis in VICs from CTRL AVs compared to those from PVs is consistent with previous reports of cell activation and

collagen synthesis in VICs from ovine AVs and PVs¹⁸ and vimentin in VICs from human adult semilunar valves.¹⁹ These apparent inherent differences in cell phenotype between the valves could relate to differences in composition between the valves.²⁰

Implications

The results from this study have a number of implications both for our understanding of congenitally diseased valves and potential therapeutics, as well as for the design of a tissue engineered heart valve. In terms of the results from the analysis of CTRL AVs and PVs, the age-related changes in matrix composition demonstrated in AVs and PVs corroborate previous studies^{17, 21, 22} supporting the need for an age-specific tissue engineered heart valve. Previous studies demonstrating altered material properties of valves with age, and a correlation between these changes and age-related changes in the valve matrix,¹⁷ suggest that for ideal function a tissue engineered heart valve optimally should have distinct design requirements for different aged patients. Furthermore, the results from this study demonstrating inherent differences in cell phenotype between VICs from AVs and PVs should be considered in terms of potential cell sources for a tissue engineered heart valve.

With regard to the analysis of congenitally diseased valves contained in this study, the differences in VICs from pathological valves relative to CTRL valves suggest that inherent abnormalities in the VICs could contribute to the documented matrix abnormalities. As such, considerable caution would need to be exercised before utilizing autologous VICs in a tissue engineered heart valve for a patient with a congenitally diseased valve. The documented abnormalities in elastic and collagen fiber turnover in

these congenitally diseased valves provide a potential, novel therapeutic target for the treatment of these valves. If proper matrix composition and turnover could be encouraged pharmacologically, valve function may improve, which could prevent or delay the need for valve replacement. Clearly, however, considerable more work remains in this area.

Limitations and Future Studies

While this study provides important, foundational knowledge by detailing the specific the matrix composition and cell phenotypes within these diseased valves for the first time, there is still much research to be done in this nascent area, and a number of study limitations should be noted. First, the limited number of samples for each group made it difficult to obtain statistical significance for some of the group comparisons. Future collection of additional samples, including more age-matched autopsy samples, will allow narrower age groupings and more statistical power for group comparisons. Additionally, the complex conditions of these patients with congenitally diseased valves complicate these analyses. Future *in vitro* studies assessing signaling pathways that could potentially be involved in the observed matrix changes will greatly enhance our understanding of the disease and shed light on potential novel treatment strategies. Nevertheless, the results contained in this study lay necessary groundwork for future studies.

CONCLUSIONS

In sum, the results contained in this study provide a detailed characterization of the matrix changes of congenitally diseased semilunar valves. As such, the study adds to our understanding that dysplastic valves are not simply valves with gross changes or a loss of layered leaflet structure microscopically, but these valves contain complex changes in matrix turnover, composition, and valve cell phenotype.

This chapter, analyzing matrix remodeling and valvular interstitial cell (VIC) phenotype changes in congenitally diseased semilunar valves, combined with the review contained in the previous chapter, provides insight into congenital valve disease. In the following three chapters (Chapters 15-17), the topic of valve alterations in various diseased states is continued with a series of studies analyzing the mitral valve in the context of “functional” mitral regurgitation and dilated cardiomyopathy. In the next chapter, a study analyzing leaflet changes in response to mitral regurgitation is presented.

REFERENCES

1. LeBlanc JG, Russell JL. Pediatric Cardiac Surgery in the 1990's. *Surg Clin North Am.* 1998;78(5):729-747.
2. National Center for Health Statistics: National Heart, Lung, Blood Institute; 2005.
3. Hoffman J. Congenital heart disease and inheritance. *Pediatr Clin North Am.* 1990;37:25-43.
4. Ross DN. Replacement of aortic and mitral valves with a pulmonary autograft. *Lancet.* 1967;2(7523):956-958.
5. Stephens EH, Carroll JL, Grande-Allen KJ. The use of collagenase III for the isolation of porcine aortic valvular interstitial cells: rationale and optimization. *J Heart Valve Dis.* 2007;16(2):175-183.
6. Blevins TL, Carroll JL, Raza AM, Grande-Allen KJ. Phenotypic characterization of isolated valvular interstitial cell subpopulations. *J Heart Valve Dis.* 2006;15(6):815-822.
7. Baig M. Acid mucopolysaccharides of congenitally defective, rheumatic, and normal human aortic valves. *Am J Pathol.* 1979;96(3):771-780.
8. Koullias GJ, Korkolis DP, Ravichandran P, Psyrris A, Hatzaras I, Elefteriades JA. Tissue microarray detection of matrix metalloproteinases, in diseased tricuspid and bicuspid aortic valves with or without pathology of the ascending aorta. *Eur J Cardiothorac Surg.* 2004;26(6):1098-1103.
9. Hinton RB, Jr, Lincoln J, Deutsch GH, Osinska H, Manning PB, Benson DW, Yutzey KE. Extracellular matrix remodeling and organization in developing and diseased aortic valves. *Circ Res.* 2006;98(11):1431-1438.
10. Bharati S, Lev M. Congenital polyvalvular disease. *Circulation.* 1973;47(3):575-586.
11. Koretzky ED, Moller JH, Kornis ME, Schwartz CJ, Edwards JE. Congenital pulmonary stenosis resulting from dysplasia of valve. *Circulation.* 1969;40(1):43-53.
12. Hyams V, Manion W. Incomplete differentiation of the cardiac valves. *Am Heart J.* 1968;76:173-182.
13. Balachandran K, Konduri S, Sucusky P, Jo H, Yoganathan AP. An ex vivo study of the biological properties of porcine aortic valves in response to circumferential cyclic stretch. *Ann Biomed Eng.* 2006;34(11):1655-1665.
14. Balachandran K, Sucusky P, Jo H, Yoganathan AP. Elevated cyclic stretch alters matrix remodeling in aortic valve cusps: implications for degenerative aortic valve disease. *Am J Physiol Heart Circ Physiol.* 2009;296(3):H756-764.
15. Rabkin-Aikawa E, Aikawa M, Farber M, Kratz JR, Garcia-Cardena G, Kouchoukos NT, Mitchell MB, Jonas RA, Schoen FJ. Clinical pulmonary autograft valves: pathologic

evidence of adaptive remodeling in the aortic site. *J Thorac Cardiovasc Surg.* 2004;128(4):552-561.

16. Aikawa E, Whittaker P, Farber M, Mendelson K, Padera RF, Aikawa M, Schoen FJ. Human semilunar cardiac valve remodeling by activated cells from fetus to adult: implications for postnatal adaptation, pathology, and tissue engineering. *Circulation.* 2006;113(10):1344-1352.
17. Stephens EH, de Jonge N, McNeill MP, Durst CA, Grande-Allen KJ. Age-related changes in material behavior of porcine mitral and aortic valves and correlation to matrix composition. *Tissue Eng.* 2010;16(3):867-878.
18. Merryman WD, Liao J, Parekh A, Candiello JE, Lin H, Sacks MS. Differences in tissue-remodeling potential of aortic and pulmonary heart valve interstitial cells. *Tissue Eng.* 2007;13(9):2281-2289.
19. Della Rocca F, Sartore S, Guidolin D, Bertiplaglia B, Gerosa G, Casarotto D, Pauletto P. Cell composition of the human pulmonary valve: a comparative study with the aortic valve--the VESALIO Project. *Vitalitate Exornatum Succedaneum Aorticum labore Ingegnoso Obtinebitur. Ann Thorac Surg.* 2000;70(5):1594-1600.
20. Aldous IG, Veres SP, Jahangir A, Lee JM. Differences in collagen cross-linking between the four valves of the bovine heart: a possible role in adaptation to mechanical fatigue. *Am J Physiol Heart Circ Physiol.* 2009;296(6):H1898-1906.
21. Stephens EH, Chu CK, Grande-Allen KJ. Valve proteoglycan content and glycosaminoglycan fine structure are unique to microstructure, mechanical load and age: Relevance to an age-specific tissue-engineered heart valve. *Acta Biomater.* 2008;4(5):1148-1160.
22. Stephens EH, Grande-Allen KJ. Age-related changes in collagen synthesis and turnover in porcine heart valves. *J Heart Valve Dis.* 2007;16(6):672-682.

Chapter 15: The Effects of Mitral Regurgitation Alone are Sufficient for Leaflet Remodeling

This chapter continues the topic of valve alterations in various diseased states and is the first in a series of three chapters (Chapters 15-17) examining mitral valve alterations in the context of “functional” mitral regurgitation and dilated cardiomyopathy. Specifically in this chapter a study analyzing leaflet changes in response to mitral regurgitation is presented.

ABSTRACT

Background: Although chronic mitral regurgitation (MR) results in adverse left ventricular remodeling, its effect on the mitral valve leaflets *per se* is unknown. In a chronic ovine model, we tested whether isolated MR alone was sufficient to remodel the anterior mitral leaflet (AML).

Methods: Twenty-nine sheep were randomized to either control (CTRL, n=11) or experimental (HOLE, n=18) groups. In HOLE, a 2.8-4.8mm diameter hole was punched in the middle scallop of the posterior mitral leaflet to create “pure” MR. At 12 weeks, the AML was analyzed immunohistochemically to assess markers of collagen and elastin synthesis as well as matrix metalloproteinases and proteoglycans. A semi-quantitative grading scale for characteristics such as intensity and delineation of stain between layers

was used to quantify differences between HOLE and CTRL specimens across the heterogeneous leaflet structure.

Results: At 12 weeks, MR grade was greater in HOLE vs. CTRL (3.0 ± 0.8 vs. 0.4 ± 0.4 , $p<0.001$). In HOLE AML, saffron-staining collagen (Movat) decreased, consistent with an increase in matrix metalloprotease-13 throughout the leaflet. Type III collagen expression was increased in the mid-leaflet and free edge and expression of prolyl-4-hydroxylase (indicating collagen synthesis) was increased in the spongiosa layer. The proteoglycan decorin, also involved in collagen fibrillogenesis, was increased compared to CTRL (all $p\leq 0.05$).

Conclusions: In HOLE AML, the increased expression of proteins related to collagen synthesis and matrix degradation suggests active matrix turnover. These are the first observations showing that regurgitation alone can stimulate mitral leaflet remodeling. Such leaflet remodeling needs to be considered in reparative surgical techniques.

The work contained in this chapter was published as:

Stephens EH, Nguyen TC, Itoh A, Ingels NB, Miller CD, Grande-Allen KJ. **The Effects of Hemodynamics of Regurgitation Alone are Sufficient for Mitral Valve Leaflet Remodeling.** *Circulation*. 2008;118(11):S243-249.

INTRODUCTION

Mitral regurgitation (MR) is associated with a number of chronic heart diseases. The prevalence of at least mild severity MR is reported to be approximately 19%,¹ and MR in the context of dilated cardiomyopathy (DCM) portends a significantly worse prognosis.²⁻⁴ It has been hypothesized that the MR in DCM is “functional,” i.e., primarily due to left ventricular enlargement and annular dilatation resulting in impaired leaflet coaptation.⁵⁻⁷ Recent reports of altered leaflet matrix composition in patients with heart failure,⁸ however, suggests that the leaflet itself is involved in the changes associated with heart failure, perhaps contributing to MR. Indeed, the severity of MR in DCM often increases over time, a phenomenon referred to as “MR begets MR.”⁹ However, given that many factors contribute to MR in DCM, including ventricular and annular remodeling, ischemic damage, and low pressure volume overload,^{9, 10} it is unclear which variables drive the worsening regurgitation. The hypothesis of this study was that the altered hemodynamics of regurgitation alone could lead to adverse leaflet remodeling, thereby providing a possible mechanism for “MR begets MR.”⁹ The goal of this study was to investigate the effect of the isolated hemodynamic variable by creating “pure” primary MR (independent of left ventricular dysfunction) and examine the anterior leaflet for signs of adverse remodeling. The implications of this study would be that of the mitral valve during the course of chronic MR could contribute to worsening MR. Conversely, this causal relationship would also imply that improvements in valve hemodynamics following mitral valve repair surgery could reverse negative remodeling of the valvular extracellular matrix.

In order to test this hypothesis, an ovine animal model of “pure” regurgitation was created by punching a 2.8-4.8 mm hole in the center of the posterior leaflet of the mitral valve. MR was monitored for 12 weeks before the animals were sacrificed and the anterior mitral leaflet (AML) was analyzed to determine if adverse remodeling had occurred. Remodeling was assessed by histological analysis of extracellular matrix (ECM) constituents as well as markers of matrix turnover. ECM not only serves as a structural scaffold, but also plays an active role in critical processes such as tissue differentiation, cell migration, growth factor regulation, mechanical function and disease in various tissues including heart valves.^{11,12} In addition, given reports of cell activation and proliferation at the site of valve injury,¹³ these characteristics were examined as well.

METHODS

All animals received humane care in accordance with the guidelines of the US Department of Health and Human Services (NIH Publ. 85-23, Revised 1985). The use of animals in this study was approved by the Stanford Medical Center Laboratory Research Animal Review Committee.

Surgical Protocol

Twenty-nine sheep were randomized to either control (CTRL, n=11) or experimental (HOLE, n=18) groups. Epicardial echocardiography was used to qualitatively grade (0-4) mitral regurgitation (MR) at baseline based on color and width of the regurgitant jet.¹⁴ A left thoracotomy and atriotomy were employed to access the mitral valve, and after establishment of cardiopulmonary bypass a 2.8 mm to 4.8 mm

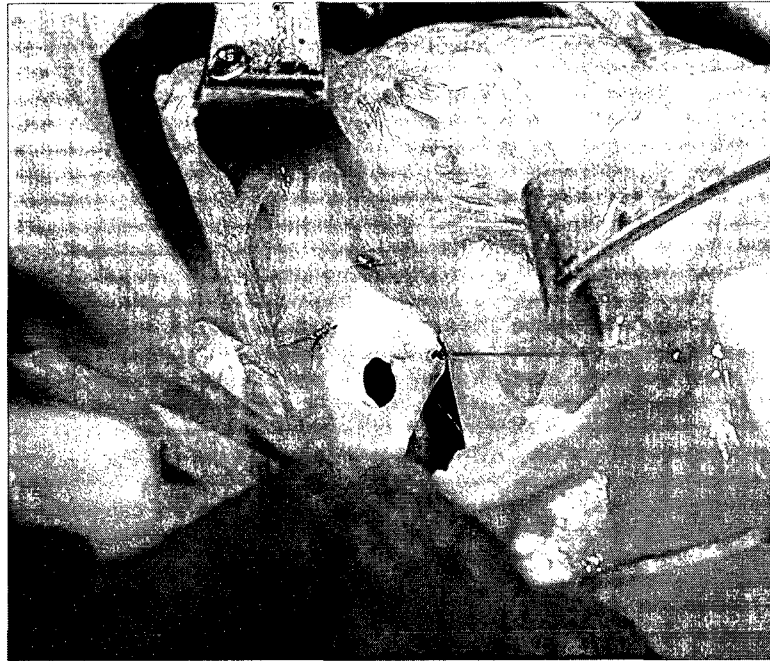


Fig. 15-1: Intraoperative picture of hole-punch made in posterior leaflet of mitral valve.

hole was created in the central scallop of the posterior mitral leaflet of HOLE animals with an aortic hole puncher (Fig. 15-1). CTRL animals underwent the exact same operation without the hole-punch. On a weekly basis, a blinded echocardiographer performed transthoracic echocardiography and graded the MR on the basis of color Doppler regurgitant jet extent and width. The MR grades taken at 6 and 12 weeks were combined to determine the “averaged final MR.” The end-diastolic volume index (EDVI) and end-systolic volume index (ESVI) were calculated based on the sum of 3D volumes enclosed by the mitral annular and left ventricular markers, indexed to the body surface area. The full explanation of these calculations and the description of additional measurements performed using this model has been published previously.¹⁵

Histology and Immunohistochemistry

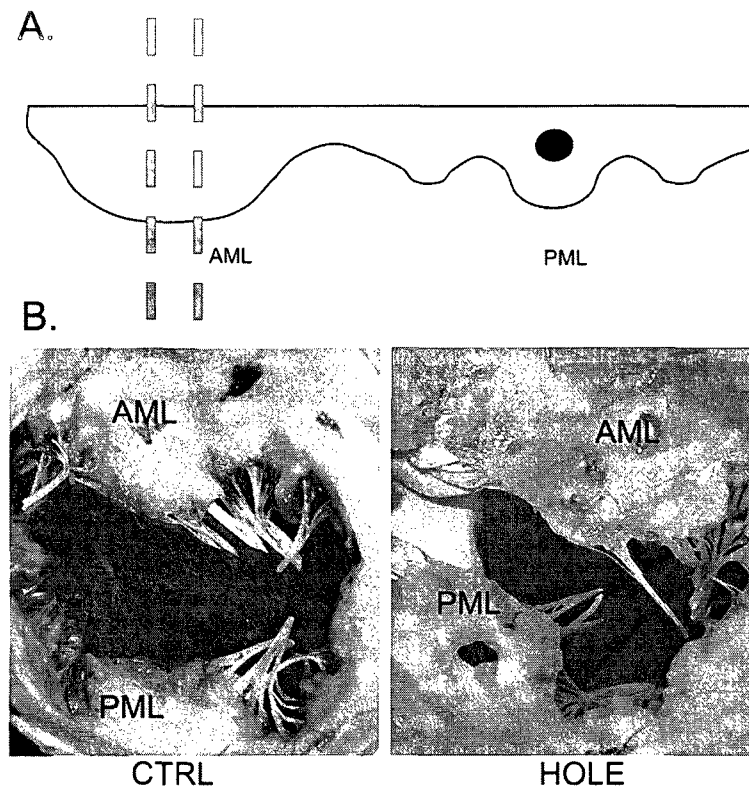


Fig. 15-2: A) Diagram showing location from which AML cross sections were taken. B) Photos of fixed CTRL and HOLE valves before sectioning.

The anterior leaflet (AML) was isolated and a 5 mm wide strip was cut from annulus to free edge (Fig. 15-2A). In order to control for heterogeneity in loading and microstructure among different regions of the AML, the strip was taken from the same region in all animals. These cross sections were embedded in paraffin and sectioned to a thickness of five microns. A cross section was also taken from each posterior leaflet (including the region with the hole-punch) and subjected to similar studies as those performed here for the AML. Those results are reported in Chapter 18. Each sample was stained histologically with Movat pentachrome to demonstrate the general collagen, elastic fiber, and proteoglycan/glycosaminoglycan content and to distinguish between the

different layers of the mitral valve. Picrosirius red staining was performed to examine the collagen content and alignment and infer type of collagen (red=collagen I, yellow/green=reticular collagen III¹⁶). Samples were also stained immunohistochemically to demonstrate specific ECM components and enzymes involved in matrix turnover (Table 15-1), including the proteoglycan decorin (DCN), involved in

Table 15-1. Antibodies Used in Immunohistochemistry.

Marker	Function
<u>Collagen-related Markers</u>	
Decorin (DCN)*	PG associated with tension and collagen fiber formation
Collagen III (Col III) [†]	Reticular type of collagen
Prolyl 4-Hydroxylase (P4H) [‡]	Hydroxylating enzyme in collagen synthesis
Heat shock protein 47 (HSP47) [†]	Molecular chaperone in collagen synthesis
Lysyl Oxidase (LOX) [§]	Crosslinking enzyme in collagen synthesis
<u>Elastic fiber-related</u>	
Elastin [†]	Primary component of elastic fibers
Fibrillin [†]	Elastic fiber component
Lysyl Oxidase (LOX) [§]	Crosslinking enzyme in elastic fiber formation
<u>Matrix Degradation</u>	
Matrix Metalloprotease (MMP)-1	Enzyme involved in matrix degradation
MMP2	Enzyme involved in matrix degradation
MMP9	Enzyme involved in matrix degradation
MMP13 [‡]	Enzyme involved in matrix degradation
<u>Cell Activation/Proliferation</u>	
Proliferating Cell Nuclear Antigen (PCNA) [†]	Marker of cell proliferation
Non-muscle Myosin (NMM) [#]	Marker of an "activated" cellular phenotype

*Gift from Dr. Larry Fisher, NIH; [†]Abcam, Cambridge, MA; [‡]Chemicon (Temecula, CA); [§]Imgenex (San Diego, CA); ^{||}Assay Designs (Ann Arbor, MI); [#]Covance (Berkeley, CA).
PG=proteoglycan.

collagen fibrillogenesis;¹⁷ type III collagen (Col III), which tends to be unregulated in remodeling tissues;¹⁸ the elastic fiber-related proteins elastin, fibrillin, and lysyl oxidase (LOX, involved in crosslinking both collagen and elastin); two markers of collagen synthesis, prolyl 4-hydroxylase (P4H) and heat shock protein-47 (HSP47); and markers of matrix degradation including the matrix metalloproteases (MMPs)-1, -2, -9, and -13.

To determine whether the regurgitation affected the phenotype of the cells within the valve, cell proliferation and valve cell activation were evaluated using antibodies against proliferating cell nuclear antigen (PCNA) and non-muscle myosin (NMM), respectively. In order to limit variability due to staining procedures all leaflets (both HOLE and CTRL) were stained for a given marker together in one batch. A semi-quantitative grading scale from 0 to 4 was used to assess the intensity of staining and the delineation of stain between layers, both throughout the leaflet and in the insertion, annulus, mid-leaflet, and free edge regions (Fig. 15-3). In addition, “background elastin staining” was defined as

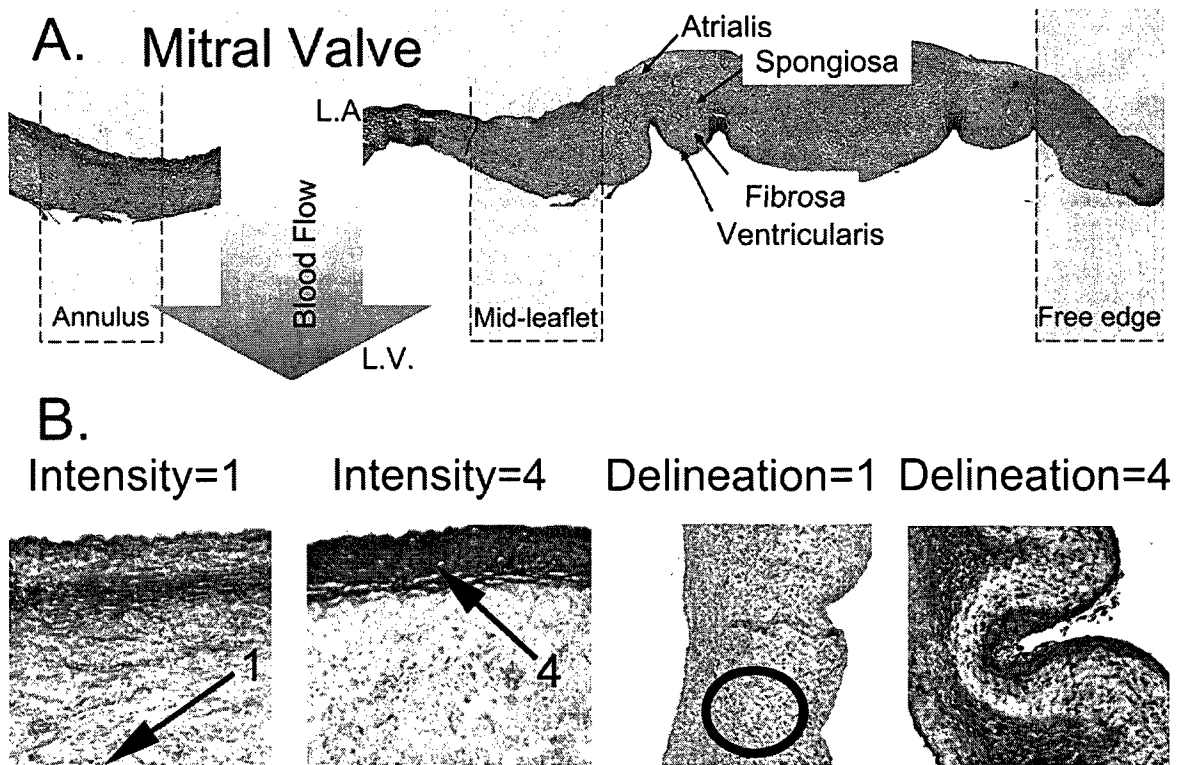


Fig. 15-3: A) Microstructure of a Movat pentachrome-stained mitral valve showing different regions and layers. Shaded arrow indicates direction of blood flow from left atrium (LA) to left ventricle (LV). Scale bar represents 2 mm. B) Examples of grading rubrics for the characteristics staining intensity and delineation. For the characteristic delineation, “1” indicates little differentiation in intensity between layers. “4” indicates maximum. The circle indicates the area graded for the characteristic “background elastin intensity.”

the intensity of staining in the fibrosa and spongiosa layers, i.e. between the strongly staining linear fibers found within the atrialis and ventricularis (see circled region in Fig. 15-3B). All evaluations were performed by a trained individual blinded to the identity of the leaflets.

Statistical Analysis

Data are presented as mean and standard deviation, unless otherwise noted. Multifactorial analysis of variance was performed using SigmaStat (SPSS, Chicago, IL), as described in Chapter 4. The Holm-Sidak all-pairwise multi-comparison method was used for post-hoc testing. Correlations between factors were calculated using Pearson and Spearman tests, as described in Chapter 5.

RESULTS

Throughout the study, the MR grade was greater in HOLE than in CTRL (Fig. 15-4A). At 12 weeks, the grades were 0.4 ± 0.4 vs. 3.0 ± 0.8 for CTRL vs. HOLE, respectively ($p < 0.001$). The regurgitant jet was largely centrally oriented (towards the atrium, Fig. 15-4B) and did not hit the AML directly. This MR was accompanied by a greater mitral

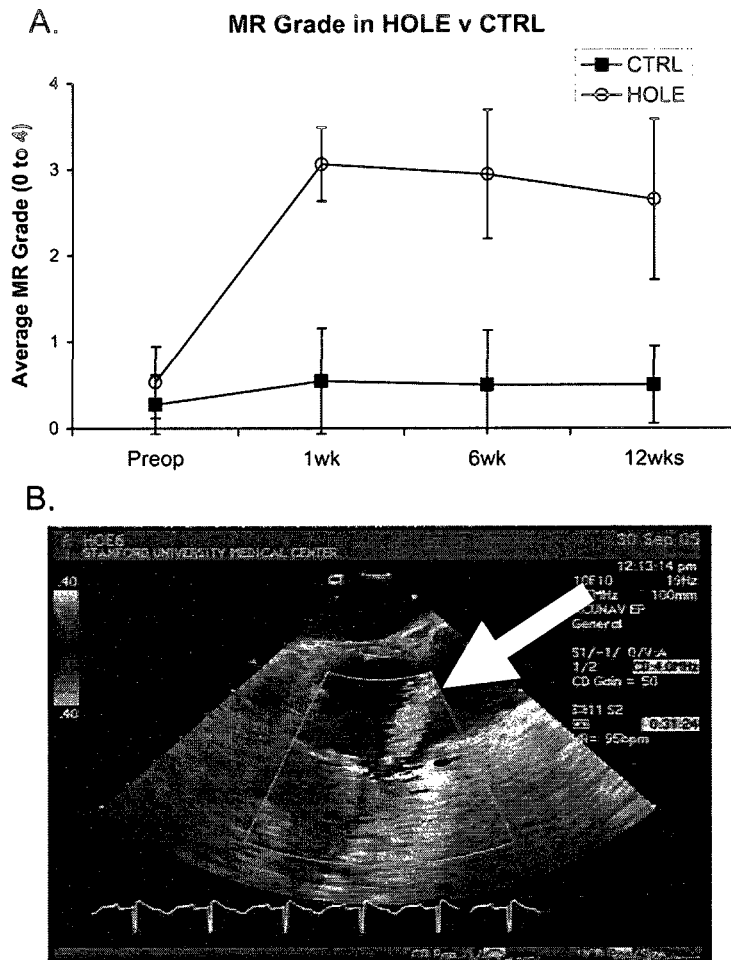


Fig 15-4: A) MR grade of HOLE versus CTRL. B) Sample echo image of regurgitant jet (white arrow) in a HOLE animal.

annulus area, primarily due to an increase in the commissure-to-commissure dimension, although there was no evidence of change in the 3D annular shape.¹⁵ EDVI and ESVI were both significantly greater in HOLE compared to CTRL at 12 weeks (EDVI: 109.1±30.0 ml/m² vs. 146.3±30.3 ml/m² for CTRL vs. HOLE, respectively; ESVI: 81.7±29.5 ml/m² vs. 106.3±18.7 ml/m² for CTRL vs. HOLE, respectively, p≤0.004 for both). Levels of circulating biochemical markers such as blood natriuretic peptide were not significantly different between groups. The full details of cardiac changes observed in the HOLE animals have been published previously.¹⁵

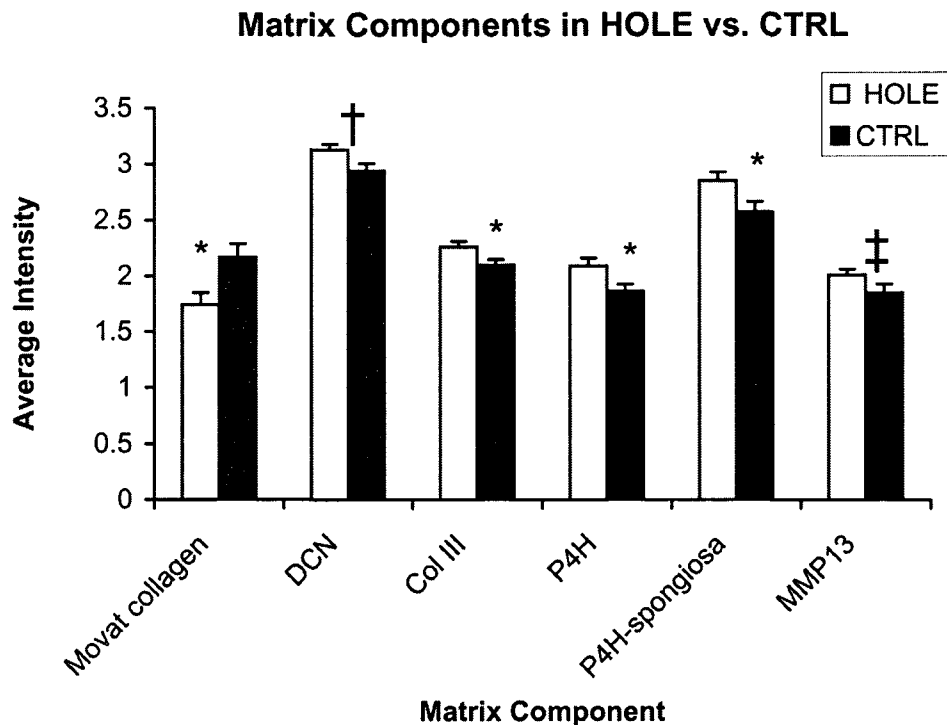
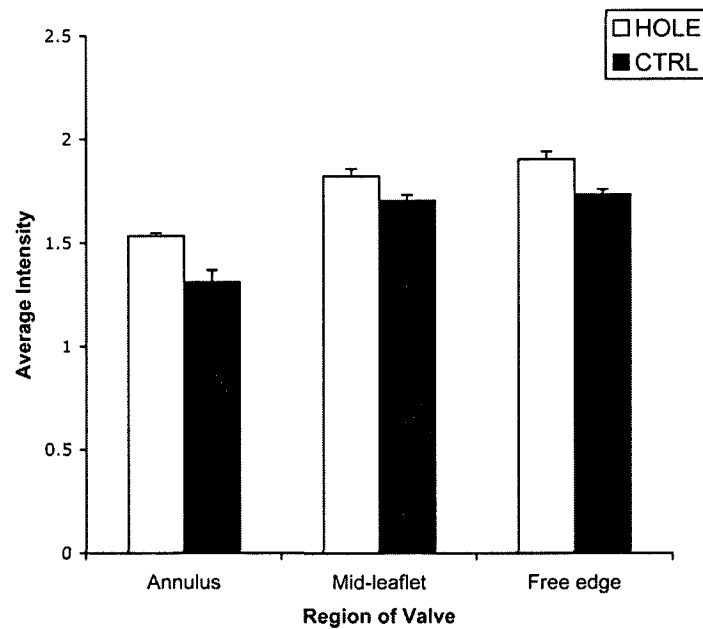


Fig. 15-5: Staining intensity of matrix components in HOLE and CTRL animals. $*=p<0.05$; $†=p=0.022$; $‡=p=0.081$. Error bars represent the standard error of the mean (SEM).

Numerous differences in the staining of several ECM markers within the AML were found between HOLE and CTRL animals. Cell proliferation, as detected by PCNA staining, tended to be greater in HOLE compared to CTRL ($p=0.089$), and NMM expression in the fibrosa positively correlated with the average final grade of MR ($r=0.225$, $p<0.027$). With respect to the overall amount of collagen, Movat-stained sections showed a significant reduction in saffron-staining collagen in HOLE ($p=0.041$, Fig. 15-5). Picrosirius red staining confirmed that Movat saffron-stained regions were composed predominantly of type I, rather than type III, collagen. (When viewed under polarized light the large, linear bundles of type I collagen fibers in picrosirius red-stained tissue appear red, while the small diameter, networked collagen type III fibers appear yellow/green¹⁶). HOLE AML showed greater Col III compared to CTRL ($p=0.024$, Fig.

A. MMP9 Expression in Regions of Leaflet



B. MMP1 Expression in the Fibrosa Layer

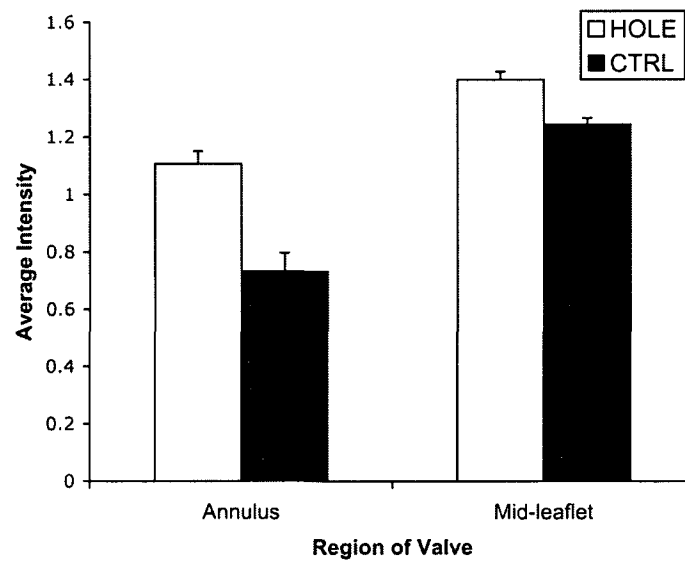


Fig. 15-6: A) MMP9 expression in various regions of valve, $p=0.021$. B) MMP1 staining in the fibrosa layer, $p=0.024$. Error bars represent SEM.

15-5), particularly in the mid-leaflet and free edge regions. HOLE AML also showed elevated P4H expression compared to CTRL ($p=0.024$), which was most notable in the

spongiosa layer ($p=0.024$). DCN expression was greater in HOLE ($p=0.022R$), which also showed a trend of higher MMP13 intensity compared to CTRL ($p=0.081R$). MMP9 staining across all regions of HOLE AML was greater than in CTRL AML ($p=0.021$, Fig. 15-6A) and MMP1 staining in the fibrosa of the annulus and mid-leaflet regions was greater for HOLE compared to CTRL ($p=0.024$, Fig. 15-6B). In these same two regions the background elastin staining (i.e., staining in the spongiosa and fibrosa) was significantly greater in the HOLE AML ($p=0.023$, Fig. 15-7). In the insertion region of AML, there was greater staining for Col III in HOLE compared to CTRL ($p=0.048$) due to an abundance of Col III in the fibrosa layer ($p=0.002$). The HOLE AML insertion region also showed a trend of greater MMP9 abundance ($p=0.070$) that was significant in the fibrosa layer ($p=0.022$).

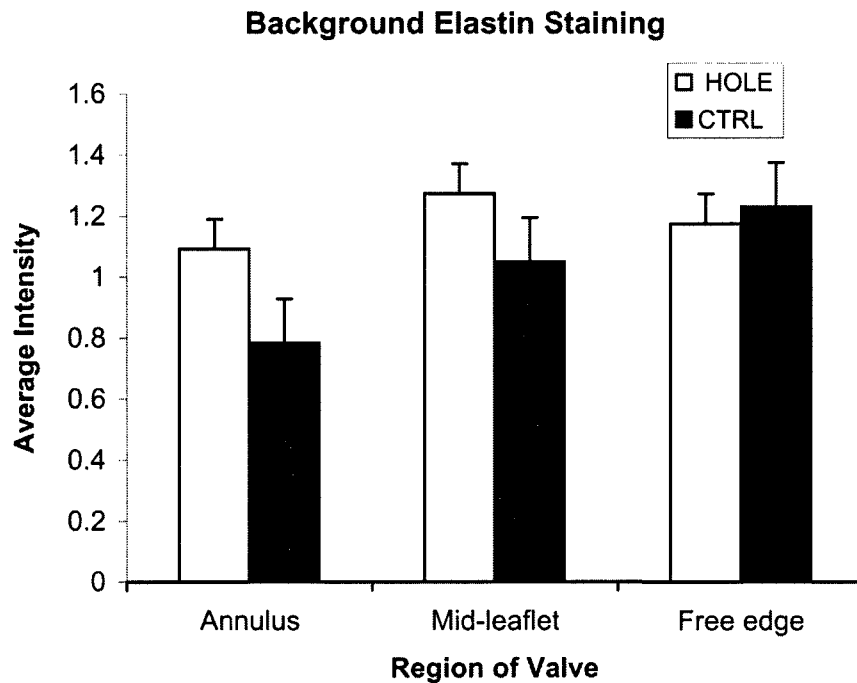


Fig. 15-7: Background elastin staining, overall $p=0.023$. Error bars represent SEM.

DISCUSSION

The principal findings of this study were that HOLE AML exhibited collagen remodeling, demonstrated by a reduction in collagen type I and elevated expression of type III collagen, P4H, DCN, and MMP1. Furthermore, HOLE AML showed evidence of elastic fiber remodeling, including greater MMP9 and elastin expression within the fibrosa and spongiosa layers. Consistent with valvular matrix remodeling, valve cell activation demonstrated by NMM expression was elevated in direct correlation with the average final grade of MR. These results suggest that isolated MR was sufficient to cause mitral valve leaflet remodeling.

Anterior Leaflet Remodeling and Functional Consequences

The finding of collagen remodeling in HOLE AML is demonstrated by the elevation in MMPs, reduction in type I collagen, and greater expression of reticular type III collagen. Additional evidence was provided by the greater abundance of P4H, which is involved in collagen synthesis, and of the proteoglycan DCN, which mediates collagen fibrillogenesis.¹⁷ These results are consistent with previous reports of DCN upregulation in human mitral valve prolapse¹⁹ and greater amounts of collagen III in rat mitral valves exposed to left ventricular pressure overload.²⁰ Because collagen type III does not have the tensile strength of collagen type I, a shift in the proportions of these collagens may result in decreased valve stiffness and perhaps an increased susceptibility to leaflet prolapse (at least at the 12 week time point).

The greater abundance of MMP9 along with the stronger background elastin staining demonstrated the remodeling of elastic fibers in HOLE AML. MMP9 can degrade elastin, but cannot degrade collagen I and III (the major collagen types in the valve, both substrates for MMP 1, 2, and 13).²¹ Furthermore, MMP9 expression has been found to co-localize with elastic fiber degradation in valves.²² The observations of cell activation and cell proliferation are also consistent with leaflet remodeling. MMP expression by mature valve cells is associated with valve remodeling and disease,^{23, 24} and cell proliferation is a well-documented (albeit non-specific) response to valve injury.¹³

The leaflet remodeling was heterogeneous, but in a manner reflecting the normal varied distribution of collagen and elastin and their distinct roles in leaflet function. For example, stronger background elastin staining was evident in the annulus and mid-leaflet, regions where elastin is normally most abundant, albeit in the atrialis and ventricularis as opposed to the fibrosa and spongiosa. Given that elastic fibers govern the elastic recoil of the tissue, this greater abundance of “background” elastin may indicate altered mechanical loading of the AML. With respect to collagen remodeling, the stronger MMP1 staining was specifically found in the fibrosa of the mid-leaflet and annulus, whereas the stronger type III collagen staining was predominantly found in the mid-leaflet and free edge. Type I collagen is normally most abundant in the fibrosa layer within the annulus and mid-leaflet regions, and is critical to the leaflet’s tensile strength. Given the specificity of MMP1 for collagen type I,²⁵ it is logical that MMP1 expression would be stronger in the fibrosa layer of these regions. It may be that the nature of the regurgitant jet and the altered coaptation patterns caused increased tension on the free

edge and mid-leaflet regions, which could explain the greater abundance of type III collagen in those regions. It is also interesting to note that the insertion region (annular ring) of HOLE AML showed greater abundance of Col III and MMP9.

We speculate that the MR resulting from the hole-punch led to altered stress on HOLE AML, which led to altered collagen turnover throughout the various leaflet regions. Functionally, in the mid-leaflet region this altered collagen content would reduce tensile strength, leading to leaflet prolapse that could worsen MR. Altered collagen turnover in the insertion region (part of the mitral fibrous annulus) would result in decreased tensile strength of this region and lead to annular dilation, as evident in HOLE. This annular dilation would also then worsen MR.⁵ Although less annular dilation occurs in the anterior as opposed to the posterior mitral annulus in DCM,²⁶ anterior annular dilation has been documented in both animal models²⁶ and human cases of DCM.²⁷

Potential Mechanism for Observed Changes

The proposed mechanism for the observed dysfunction in the HOLE animals involves interrelated changes at three hierarchical levels: cardiac, valve/hemodynamic, and leaflet ECM/microstructure. Cardiac changes include annular dilation caused by altered strain patterns in the left ventricle due to the HOLE-induced MR; this annular dilation would exacerbate MR.⁵ Considering the level of the valve, computer modeling has shown that during normal coaptation, the AML shares the burden of stress with the posterior leaflet.⁵ With regurgitation and annular dilation, however, coaptation is reduced, forcing the AML to bear greater stress.⁵ Indeed, leaflets under increased stress

production of new collagen (as suggested by the greater expression of P4H). Other findings, however, suggest that this remodeling is “pathological.” Elevated MMP9 expression has been associated with a number of valve pathologies, including non-rheumatic aortic stenosis.²⁹ Increases in other MMPs have also been reported in diseased valves including myxomatous mitral valves^{23, 30} and stenotic aortic valves.²² Myxomatous mitral valves also demonstrate a higher ratio of type III to type I collagen, as suggested by the results of this study.¹⁸

Potential Mechanism for “MR Begets MR”

This unique animal model created isolated regurgitation to investigate how the valve was affected by low pressure volume overload, and showed that regurgitation alone can initiate leaflet remodeling. Several animal models of chronic MR have been created previously, but these have all involved the confounding effects of ventricular ischemia and remodeling and/or created regurgitation using high pressure volume overload,³¹ which is significantly different than the hemodynamics seen in clinical MR.³² For instance, the severance of chordae has been shown to alter left ventricular geometry and strain patterns and cause global systolic dysfunction.³³ Many cases of chronic MR involve factors other than altered hemodynamics that contribute to increasing regurgitation. A paradigm often used to account for chronically increasing MR is that ventricular dilation, which frequently accompanies chronic MR, increases ventricular wall stress¹⁰ and impairs left ventricular ejection performance, which then augments regurgitation.¹⁰ Others see MR as principally due to annular dilatation that results in impaired leaflet coaptation.⁵⁻⁷ In these views the MR is “functional,” a result of changes

show increased collagen synthesis.²⁸ At the level of the ECM and individual valve layers, the collagen type I-rich fibrosa is responsible for the leaflet's tensile strength. Based on the greater staining for non-muscle myosin (a myofibroblastic phenotypic marker) in the fibrosa and the positive correlation between this staining and the average final MR, it appears that the fibrosa is experiencing increased stress related to MR. It also appears that collagen remodeling is occurring with type I collagen being replaced by flexible reticular type III collagen. Although this remodeling was likely initiated in reaction to the altered stresses, the altered collagen proportions could reduce the tensile strength of the AML and worsen MR.

Pathological versus Adaptive Leaflet Remodeling

While this study provides the first evidence to date that regurgitation alone is sufficient to cause leaflet remodeling, it is difficult to say whether or not these changes in the AML should be considered pathological (detrimental) or adaptive (advantageous). From a clinical and pathological perspective, these changes would seem to be detrimental. Certainly, a decrease in the amount of type I collagen would make the leaflet more prone to prolapse, but it is not clear whether other changes such as increased expression of P4H and similar markers should be considered detrimental. Increased DCN expression has been reported in prolapsed mitral valves,¹⁹ but it is not clear whether the changes in DCN expression were causing the prolapse or attempting to counteract prolapse. It is also important to note that in this study only a single time-point was examined. Therefore, the reduction in collagen may have been a transient event in a process of adaptive remodeling to restore leaflet integrity that would be followed by the

in left ventricular structure and function. However, the findings of the present study suggest that MR itself could be an independent factor contributing to chronically increasing MR via leaflet remodeling.

These results have implications for a number of clinical conditions. In this paper we have shown that a primarily hemodynamic insult results in secondary organic changes with functional consequences. Hemodynamics may similarly affect very different conditions, such as myxomatous mitral valves. Leaflets that have undergone organic changes (i.e., myxomatous degeneration) may be sensitive to changes in loading that could further deteriorate cardiac function. Likewise, myxomatous valves in which regurgitation has been surgically corrected would experience improved hemodynamics, and may undergo positive remodeling. Overall, changes in left ventricular and annular structure and function, organic changes in the mitral valve leaflets, and cardiac and valvular hemodynamic changes are interrelated factors that distinctly influence one another and trigger further cardiac dysfunction.

Limitations

Caution should be exercised in extrapolating the results of this ovine study to human hearts. One of the most important limitations was the duration of MR. While in patients MR progresses slowly over the course of years, these animals had isolated MR for only 12 weeks. Regardless, significant differences were found even within this short time period. Another limitation was that increasing MR was not detected over the 12-week period. This finding was likely due to the short time course and the decrease in the posterior leaflet's hole size as it healed (analysis of the posterior leaflet is reported

separately). Furthermore, although the changes in HOLE were primarily driven by MR, there were secondary changes in left ventricular dimensions, such as annular dilation, that could have affected leaflet composition. However, all of the effects on leaflet composition were either directly or indirectly caused by MR. Another limitation was the narrow range of MR in the HOLE animals. A wider range of MR, combined with more specific hemodynamic measurements, would have enabled detection of more direct correlations between hemodynamics and AML compositional changes.

Limitations in the leaflet analysis included the subjective nature of histological grading. To make this process more objective, a grading rubric was used for each characteristic, the grader was blinded to leaflet identity, and all leaflets stained for a given marker were evaluated at the same time. In addition, the surgical and histological analyses were performed at different institutions, so it was not possible to perform materials testing on these tissues or to link material properties directly to matrix changes. In the future, it will be important to analyze the remodeling and material behavior of other parts of the mitral valve, including the fibrous trigones, the chordae, and the other regions of the AML, because loading patterns across the valve are very heterogeneous.

CONCLUSIONS

Using a novel animal model of isolated mitral regurgitation, this study provides the first evidence that regurgitation alone can result in leaflet remodeling. The HOLE AML showed elevated expression of MMPs and reduced expression of type I collagen, along with greater abundance of P4H (a marker of active collagen synthesis), DCN (a proteoglycan involved in collagen fibrillogenesis), and type III collagen. Taken together,

these changes suggest an increase in matrix degradation and in collagen synthesis, particularly type III collagen synthesis. Furthermore, greater abundance of elastin in the spongiosa and fibrosa layers of the HOLE AML and higher levels of the elastin-degrading MMP9 suggest that elastin remodeling is also occurring.

This chapter, analyzing leaflet matrix remodeling in response to mitral regurgitation, opens a series of three chapters (Chapters 15-17) analyzing the mitral valve in the context of “functional” mitral regurgitation and dilated cardiomyopathy. The next two chapters (Chapter 16 and 17) address mitral valve changes in dilated cardiomyopathy. Specifically in the next chapter, changes in mitral leaflet composition and turnover in relation to changes in leaflet length with dilated cardiomyopathy.

REFERENCES

1. Singh J, Evans J, Levy D, Larson M, Freed LA, Fuller D, Lehman B, Benjamin E. Prevalence and clinical determinants of mitral, tricuspid, and aortic regurgitation (the Framingham Heart Study). *Am J Cardiol.* 1999;83(6):897-902.
2. Blondheim D, Jacobs L, Kotler M, Costacurta G, Parry W. Dilated cardiomyopathy with mitral regurgitation: decreased survival despite a low frequency of left ventricular thrombus. *Am Heart J.* 1991;122(3 Pt 1):763-771.
3. Junker A, Thyssen P, Nielsen B, Andersen P. The hemodynamic and prognostic significance of echo-Doppler-proven mitral regurgitation in patients with dilated cardiomyopathy. *Cardiology.* 1993;83(1-2):14-20.
4. Romeo F, Pelliccia F, Cianfrocca C, Gallo P, Barilla F, Cristofani R, Reale A. Determinants of end-stage idiopathic dilated cardiomyopathy: a multivariate analysis of 104 patients. *Clin Cardiol.* 1989;12(7):387-392.
5. Kunzelman KS, Reimink M, Cochran RP. Annular dilatation increases stress in the mitral valve and delays coaptation: a finite element computer model. *Cardiovasc Surg.* 1997;5(4):427-434.
6. Donal E, Levy F, Tribouilloy C. Chronic ischemic mitral regurgitation. *J Heart Valve Dis.* 2006;15(2):149-157.
7. Bolling S. Mitral valve reconstruction in the patient with heart failure. *Heart Fail Rev.* 2001;6(3):177-185.
8. Grande-Allen KJ, Borowski AG, Troughton RW, Houghtaling PL, Dipaola NR, Moravec CS, Vesely I, Griffin BP. Apparently normal mitral valves in patients with heart failure demonstrate biochemical and structural derangements: an extracellular matrix and echocardiographic study. *J Am Coll Cardiol.* 2005;45(1):54-61.
9. Borger M, Alam A, Murphy P, Doenst T, David T. Chronic ischemic mitral regurgitation: repair, replace or rethink? *Ann Thorac Surg.* 2006;81(3):1153-1161.
10. Carabello BA. Ischemic mitral regurgitation and ventricular remodeling. *J Am Coll Cardiol.* 2004;43(3):384-385.
11. Butcher J, McQuinn T, Sedmera D, Turner D, Markwald R. Transitions in early embryonic atrioventricular valvular function correspond with changes in cushion biomechanics that are predictable by tissue composition. *Circ Res.* 2007;100(10):1503-1511.
12. Grande-Allen K, Griffin B, Ratliff N, Cosgrove D, Vesely I. Glycosaminoglycan profiles of myxomatous mitral leaflets and chordae parallel the severity of mechanical alterations. *J Am Coll Cardiol.* 2003;42(2):271-277.
13. Tamura K, Jones M, Yamada I, Ferrans VJ. Wound healing in the mitral valve. *J Heart Valve Dis.* 2000;9(1):53-63.

14. Helmcke F, Nanda N, Hsiung M, Soto B, Adey C, Goyal R, Gatewood Jr R. Color Doppler assessment of mitral regurgitation with orthogonal planes. *Circulation*. 1987;75(1):175-183.
15. Nguyen TC, Itoh A, Carlhall CJ, Bothe W, Timek TA, Ennis DB, Oakes RA, Liang D, Daughters GT, Ingels NB, Jr., Miller DC. The effect of pure mitral regurgitation on mitral annular geometry and three-dimensional saddle shape. *J Thorac Cardiovasc Surg*. 2008;136(3):557-565.
16. Zhang H, Sun L, Wang W, Ma X. Quantitative analysis of fibrosis formation on the microcapsule surface with the use of picro-sirius red staining, polarized light microscopy, and digital image analysis. *J Biomed Mater Res*. 2006;76A:120-125.
17. Kinsella MG, Bressler SL, Wight TN. The regulated synthesis of versican, decorin, and biglycan: extracellular matrix proteoglycans that influence cellular phenotype. *Crit Rev Eukaryot Gene Expr*. 2004;14(3):203-234.
18. Lis Y, Burleigh MC, Parker DJ, Child AH, Hogg J, Davies MJ. Biochemical characterization of individual normal, floppy and rheumatic human mitral valves. *Biochem J*. 1987;244(3):597-603.
19. Radermecker M, Limet R, Lapiere C, Nusgens B. Increased mRNA expression of decorin in the prolapsing posterior leaflet of the mitral valve. *Interactive Cardiovascular and Thoracic Surgery*. 2003;2:389-394.
20. Willems I, Havenith M, Smits J, Daemen M. Structural alterations in heart valves during left ventricular pressure overload in the rat. *Lab Invest*. 1994;71(1):127-133.
21. Steffensen B, Häkkinen L, Larjava H. Proteolytic events of wound-healing--coordinated interactions among matrix metalloproteinases (MMPs), integrins, and extracellular matrix molecules. *Crit Rev Oral Biol Med*. 2001;12(5):373-398.
22. Koullias GJ, Korkolis DP, Ravichandran P, Psyrris A, Hatzaras I, Elefteriades JA. Tissue microarray detection of matrix metalloproteinases, in diseased tricuspid and bicuspid aortic valves with or without pathology of the ascending aorta. *Eur J Cardiothorac Surg*. 2004;26(6):1098-1103.
23. Rabkin E, Aikawa M, Stone JR, Fukumoto Y, Libby P, Schoen FJ. Activated interstitial myofibroblasts express catabolic enzymes and mediate matrix remodeling in myxomatous heart valves. *Circulation*. 2001;104(21):2525-2532.
24. Rabkin-Aikawa E, Farber M, Aikawa M, Schoen FJ. Dynamic and reversible changes of interstitial cell phenotype during remodeling of cardiac valves. *J Heart Valve Dis*. 2004;13(5):841-847.
25. Keller F, Leutert G. [Age dependence of collagen structures of the human heart]. *Z Gerontol*. 1994;27(3):186-193.
26. Timek T, Dagum P, Lai D, Liang D, Daughters G, Tibayan F, Ingels NB, Miller DC. Tachycardia-induced cardiomyopathy in the ovine heart: Mitral annular dynamic three-dimensional geometry. *J Thorac Cardiovasc Surg*. 2003;125(2):315-324.

27. Hueb A, Jatene F, Moreira L, Pomerantzeff P, Kallás E, de Oliveira S. Ventricular remodeling and mitral valve modifications in dilated cardiomyopathy: new insights from anatomic study. *J Thorac Cardiovasc Surg.* 2002;124(6):1216-1224.
28. Quick D, Kunzelman K, Kneebone J, Cochran R. Collagen synthesis is upregulated in mitral valves subjected to altered stress. *ASAIO J.* 1997;43(3):181-186.
29. Kaden JJ, Vocke DC, Fischer CS, Grobholz R, Brueckmann M, Vahl CF, Hagl S, Haase KK, Dempfle CE, Borggreffe M. Expression and activity of matrix metalloproteinase-2 in calcific aortic stenosis. *Z Kardiol.* 2004;93(2):124-130.
30. Togashi M, Tamura K, Nitta T, Ishizaki M, Sugisaki Y, Fukuda Y. Role of matrix metalloproteinases and their tissue inhibitor of metalloproteinases in myxomatous change of cardiac floppy valves. *Pathol Int.* 2007;57(5):251-259.
31. Carabello BA. Models of volume overload hypertrophy. *J Card Fail.* 1996;2(1):55-64.
32. Bursi F, Enriquez-Sarano M, Jacobsen S, Roger V. Mitral regurgitation after myocardial infarction: a review. *Am J Med.* 2006;119(2):103-112.
33. Rodriguez F, Langer F, Harrington K, Tibayan F, Zasio M, Cheng A, Liang D, Daughters G, Jr., Covell JW, Criscione J, Ingels NB, Jr., Miller DC. Importance of mitral valve second-order chordae for left ventricular geometry, wall thickening mechanics, and global systolic function. *Circulation.* 2004;110[suppl II]:II-115-II-122.

Chapter 16: Significant Changes in Mitral Valve Leaflet Matrix Composition and Turnover with Tachycardia-Induced Cardiomyopathy

In this chapter the topic of mitral valve alterations in the context of “functional” mitral regurgitation and dilated cardiomyopathy continues with a study of mitral leaflet composition and turnover in an animal model of dilated cardiomyopathy.

ABSTRACT

Background: Dilated cardiomyopathy (DCM) involves significant remodeling of the left ventricular-mitral valve (MV) complex but little is known regarding the remodeling of the mitral leaflets. The aim of this study was to assess changes in matrix composition and turnover in MV leaflets with DCM.

Methods: Radiopaque markers were implanted in 24 sheep to delineate the MV; 10 sheep underwent tachycardia-induced cardiomyopathy (TIC) while 14 sheep remained as controls (CTRL). Biplane videofluoroscopy was performed before and after TIC. Immunohistochemistry was performed on leaflet cross-sections taken from the septal, lateral, and anterior and posterior commissures attachment segments. Staining intensity was quantified within each attachment segment and leaflet region (basal, mid-leaflet, and free edge).

Results: MR increased from 0.2 ± 0.4 before TIC to 2.2 ± 0.9 after TIC ($p < 0.0002$). TIC leaflets demonstrated significant remodeling compared to CTRL including greater cell density and loss of leaflet layered structure (all $p < 0.05$). Collagen and elastic fiber turnover was greater in TIC, as was the myofibroblast phenotype (all $p < 0.05$). Compositional differences between TIC and CTRL leaflets were heterogeneous by annular segment and leaflet region, and related to regional changes in leaflet segment length with TIC.

Conclusions: This study shows that the MV leaflets are significantly remodeled in DCM with changes in leaflet composition, structure, and valve cell phenotype. Understanding how alterations in leaflet mechanics, such as those induced by DCM, drive cell-mediated remodeling of the extracellular matrix will be important in developing future treatment strategies.

The work contained in this chapter was published as:

Stephens EH, Timek TA, Daughters GT, Kuo JJ, Patton AM, Baggett LS, Ingels NB, Jr., Miller DC, Grande-Allen KJ. **Significant Changes in Mitral Valve Leaflet Matrix Composition and Turnover with Tachycardia-Induced Cardiomyopathy.** *Circulation*, 2009;120:S112-119.

INTRODUCTION

While numerous studies have demonstrated the importance of the mitral valve (MV) annulus in proper MV function and in the development of dilated cardiomyopathy (DCM),^{1,2} the MV leaflets have largely been considered bystanders in DCM. A recent study, however, demonstrated changes in the MV leaflet geometry following tachycardia-induced cardiomyopathy (TIC) that were not solely attributable to annular dilation.³ One potential explanation for these changes is that TIC altered the mechanical loads applied to the valve leaflets, which stimulated the valvular interstitial cells (VICs) to alter their phenotype and normal patterns of extracellular matrix synthesis and remodeling.⁴ Changes in the composition and arrangement of the extracellular matrix in the valve leaflets would, in turn, influence their structure and material behavior. Therefore, the objective of this study was to characterize the changes in matrix composition, matrix turnover, and VIC phenotype that occurred in mitral leaflets as a result of TIC and to relate these to leaflet segment length changes. This information should give insight into the pathogenesis of DCM and may help to improve current reparative techniques.

METHODS

All animals received humane care in accordance with the guidelines of the US Department of Health and Human Services (NIH Publ. 85-23, Revised 1985). The use of animals in this study was approved by the Stanford Medical Center Laboratory Research Animal Review Committee.

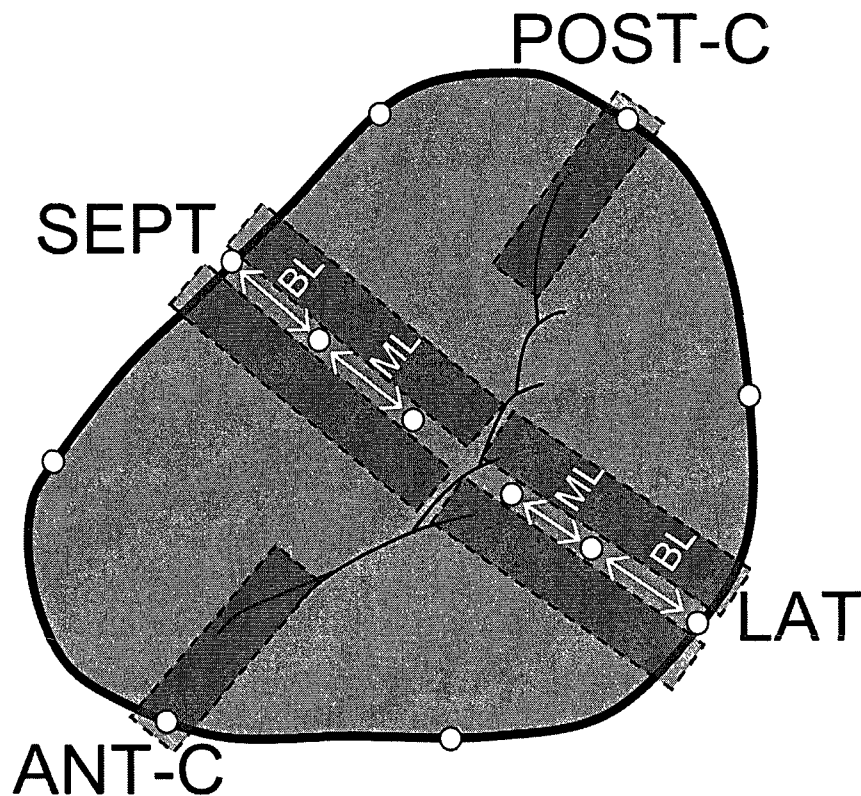


Fig. 16-1: Circles indicate the location of the implanted radiopaque markers. Gray rectangles indicate the locations from which tissue sections were taken (tissue sections were taken to either side of markers such that markers or their sutures were not included in the samples). In the case of septal segment (SEPT) and lateral segment (LAT) 2 tissue sections were analyzed and the results averaged, in the case of the anterior and posterior commissures (ANT-C, POST-C), one tissue section was taken from either side of the tantalum marker based on quality of the leaflet on each side. BL=basal leaflet, ML=mid-leaflet.

Animal Protocol

Radiopaque markers were implanted in 24 sheep to delineate the leaflet and annulus of four MV segments (Fig. 16-1): septal (SEPT), lateral (LAT), and anterior (ANT-C) and posterior commissures (POST-C). The marker implantation procedure has been described in detail previously.⁵ Ten sheep underwent a rapid-pacing protocol (TIC) for an average of 15 ± 6 days,⁵ while fourteen sheep used for an acute hemodynamic

study were utilized as histological controls (CTRL). Biplane video fluoroscopy was performed in CTRL and both before and after pacing in TIC animals. TIC-induced changes in maximum and minimum septal and lateral leaflet lengths throughout the cardiac cycle were measured for basal and mid-leaflet regions (Fig. 16-1: BL and ML, respectively). The septal-lateral diameter was measured as the maximum distance between the mid-septal and mid-lateral annular markers throughout the cardiac cycle, while the commissure-commissure diameter was measured as the maximum distance between the two commissural annular markers throughout the cardiac cycle. Although animals were not randomly assigned to groups, all animals (CTRL and pre-TIC) displayed hemodynamic parameters in the normal range and showed comparable percentage changes in annular or leaflet segment distances throughout the cardiac cycle. Mitral regurgitation was graded on a scale of 0-4 based on color Doppler regurgitant jet extent and width,⁶ as previously described.⁵ Left ventricular (LV) end-diastolic and end-systolic volume (EDV, ESV) were calculated using a space-filling analysis of epicardial markers, as described.⁵ Ejection fraction (EF) was calculated as the difference between EDV and ESV divided by EDV. These calculated EF values consistently underestimate the true EF because the calculated EDV includes LV myocardial mass, but EF calculations were only used to assess potential correlations between LV remodeling and leaflet changes amongst the TIC animals. At the end of the study, the hearts were then harvested and stored in formalin. CTRL animals were used for histological comparison only, while hemodynamic and leaflet segment length analyses compared pre-TIC and TIC data.

Histology and Immunohistochemistry

Cross-sections 3-5 mm in width were cut from insertion region (including associated myocardium) to free edge (Fig. 16-2), embedded in paraffin, and sectioned to a thickness of five microns. Sections were stained with Movat pentachrome to demonstrate the layered structure of the leaflet. Immunohistochemistry was performed for a number of extracellular matrix components and turnover proteins (Table 16-1). For each segment (LAT, SEPT, ANT-C, POST-C, Fig. 16-1), staining intensity was quantified within each leaflet region (BL, ML, and free edge) and histological layer (fibrosa, atrialis, spongiosa (spongiosa only in ML)) using ImageJ software (NIH, Bethesda, MD) (for illustration of leaflet regions and layers analyzed, see Chapter 9, Fig. 9-2). The free edge was considered a single layer. Cell density was assessed by counting

Table 16-1. Panel of Antibodies Used in IHC.

Protein	Function
<u>Collagen Turnover Proteins</u>	
Collagen I (Col I)*	Predominant collagen in valve, provides tensile strength
Collagen III (Col III)*	Reticular collagen
Matrix Metalloproteinase (MMP)-13 [†]	Collagen degradation
<u>Elastic Fiber-Related Proteins</u>	
Lysyl oxidase (LOX) [§]	Involved in collagen and elastin crosslinking
Elastin	Predominant component of elastic fibers
Matrix Metalloproteinase (MMP)-9 [‡]	Elastic fiber degradation
<u>Proteoglycans (PG) and Glycosaminoglycans (GAG)</u>	
Hyaluronan (HA) [#]	GAG providing compressibility
Decorin (DCN)*	PG involved in collagen fibrillogenesis
Biglycan (BGN)*	PG involved in collagen fibrillogenesis
<u>Valve Cell Activation</u>	
Smooth muscle alpha-actin (SMaA)**	Marker of an "activated" myofibroblast-like phenotype
Non-muscle Myosin Heavy Chain (NMM) ^{††}	Marker of an "activated" myofibroblast-like phenotype

* gift of Dr. Larry Fisher, NIH (Bethesda, MD); [†]Chemicon (Temecula, CA); [‡]Assay Designs (Ann Arbor, MI); [§]Imgenex (San Diego, CA); ^{||}Abcam (Cambridge, MA); [#]Associates of Cape Cod (Falmouth, MA); ^{**}Dakocytomation (Denmark); ^{††}Covance (Berkeley, CA).

nuclei within a defined area of the BL and ML fibrosa, as well as the free edge. Semi-quantitative grading was performed on blinded sections using a pre-determined grading rubric ranging from 0 (minimum) to 4 (maximum) for delineation between leaflet layers and diffusion of Movat-stained collagen beyond the fibrosa. Percentage differences in histological and IHC parameters between TIC and CTRL were calculated by comparing each TIC value to the average CTRL value for a given parameter.

Statistical Analysis

SigmaStat (SPSS, Chicago, IL) was used for multivariate analysis of variance (ANOVA), as described in Chapter 4. Paired t-tests were used for the statistical comparison of pre-TIC and post-TIC hemodynamics. Correlations between staining intensities of different proteins within individual leaflet layers, regions, and segments (to assess co-localization of cell activation and matrix remodeling) were calculated using a Pearson rank order test for normally distributed data and Spearman rank order correlation test for non-normally distributed data. Correlations between protein intensities and TIC-induced changes in segment lengths, EDV, ESV, and EF (to relate compositional changes, altered strain, and LV remodeling within individual animals) were similarly determined. For correlations between intensities of different proteins $p \leq 0.015$ was considered a trend and $p \leq 0.00625$ considered significant (since the intensities of 8 proteins were being compared); for correlations between intensities of proteins and TIC-induced segment length and EDV, ESV, EF changes, each protein was considered individually, therefore $p \leq 0.05$ was considered significant. Data are presented as mean and standard deviation, unless otherwise noted. Percentages for IHC are presented as

mean and standard error of the mean because of the multiple segments, layers, and/or regions involved in the statistical tests.

RESULTS

Dynamic Leaflet Changes after the Development of Dilated Cardiomyopathy

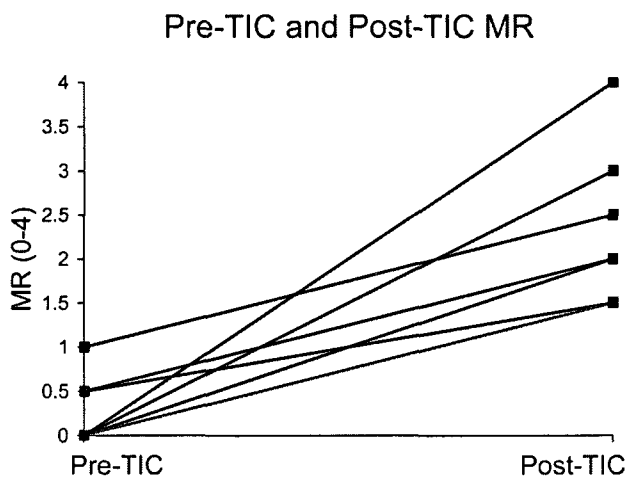


Fig. 16-2: Pre-TIC and post-TIC MR for each animal. Overall $p < 0.0002$.

Consistent with the development of DCM, the maximum annular septal-lateral diameter increased $24 \pm 9\%$ ($p < 0.0001$) in TIC compared to pre-TIC, the commissure-commissure diameter increased $9 \pm 4\%$ ($p < 0.001$), and mitral regurgitation increased from 0.2 ± 0.4 to 2.2 ± 0.9 (Fig. 16-2, $p < 0.0002$). Further characterization of annular and hemodynamic changes with TIC has been previously published.^{3,5} Leaflet segment lengths increased with TIC compared to pre-TIC for both LAT and SEPT (Table 16-2, $8 \pm 12\%$, each $p < 0.05$). In LAT and SEPT, the TIC-induced increase in the maximum mid-leaflet (ML) length was greater than that of the basal leaflet (BL) ($13 \pm 12\%$ vs.

5±10%, p=0.018) and the TIC-induced increase in the maximum ML length of LAT was greater than SEPT (14±5% vs. 5±5%, p=0.032).

Table 16-2. Pre-TIC and TIC Maximum Leaflet Segment Lengths.

(cm)	pre-TIC	TIC
SEPT		
Basal Leaflet	1.17±0.21	1.22±0.15
Mid-leaflet	1.37±0.10	1.45±0.03*
Total Leaflet	2.49±0.10	2.65±0.15*
LAT		
Basal Leaflet	0.63±0.20	0.66±0.20
Mid-leaflet	0.63±0.14	0.71±0.11*
Total Leaflet	1.26±0.28	1.36±0.23*

*p<0.05 vs. pre-TIC; data expressed as mean +/- standard deviation.

Structural Changes in TIC Leaflets

Compared with CTRL, SEPT and LAT of TIC showed greater cell density across all leaflet regions (57±17%, p=0.05 and 94±17%, p<0.001), as did ANT-C/POST-C (39±11%, p=0.05). TIC leaflets showed less delineation between valve layers compared to CTRL (Fig. 16-3A,B, -20±5%, p=0.014) with collagen more likely to be spread beyond the fibrosa layer (37±8%, p=0.002). There was also an increased incidence of muscle in TIC leaflets compared to CTRL (9 TIC vs. 2 CTRL samples, Fig. 16-3C).

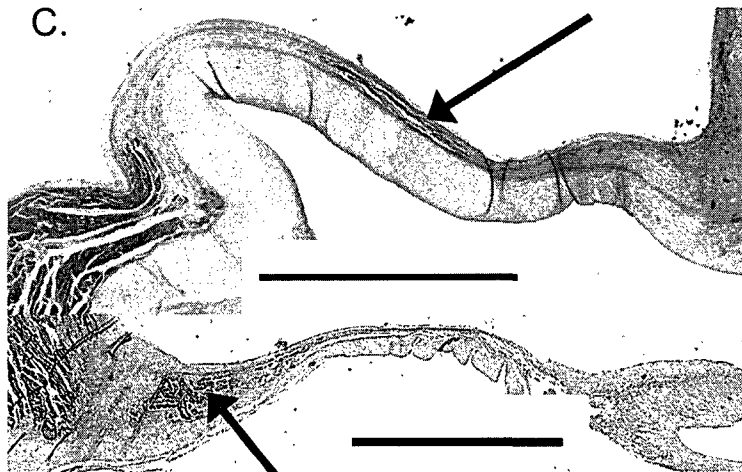
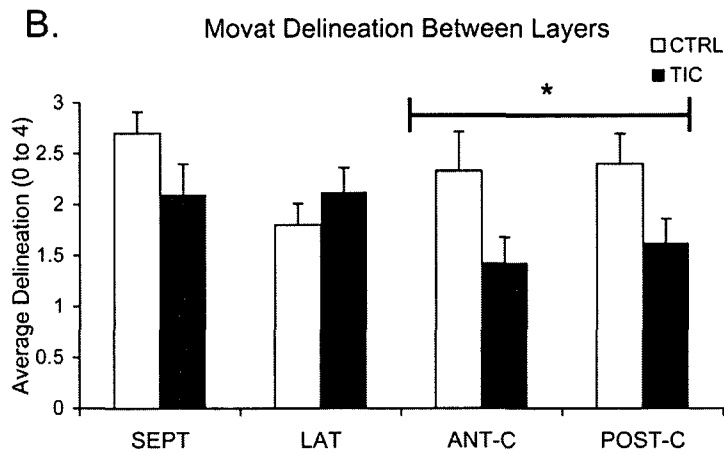
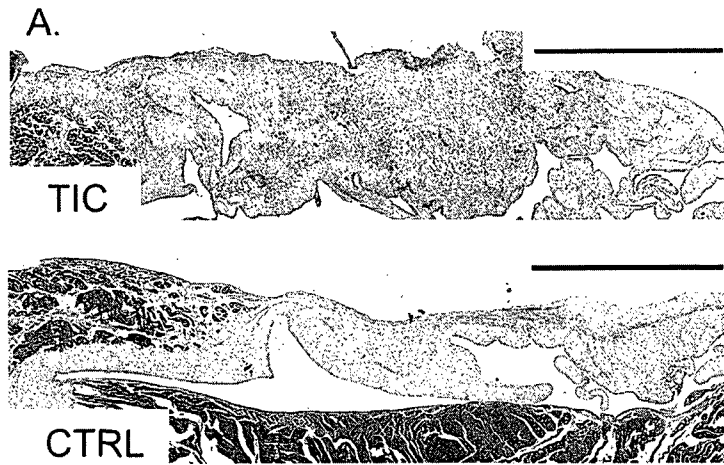


Fig. 16-3: A) Image illustrating the lack of delineation between layers in TIC (top) compared to CTRL (bottom). Samples are both LAT leaflets stained with Movat pentachrome. Scale bars represent 2 mm. B) Graph illustrating decrease in delineation in TIC compared to CTRL ($p=0.014$), $*=p=0.011$. Error bars indicate the standard error of the mean. C) Examples of muscle found considerably more often in TIC compared to CTRL (9 TIC, 2 CTRL). Arrows point to muscle, which previous studies have shown to be atrial cardiac muscle.⁷ Scale bars represent 2 mm.

Greater Collagen Turnover in TIC Leaflets

Collagen turnover was examined by staining for collagens I and III (Col I, III) and matrix metalloproteinase (MMP)-13. MMP13 in TIC ML was greater than in CTRL when all segments were considered (Fig. 16-4, $15\pm 3\%$, $p=0.005$) as well as in ANT-C

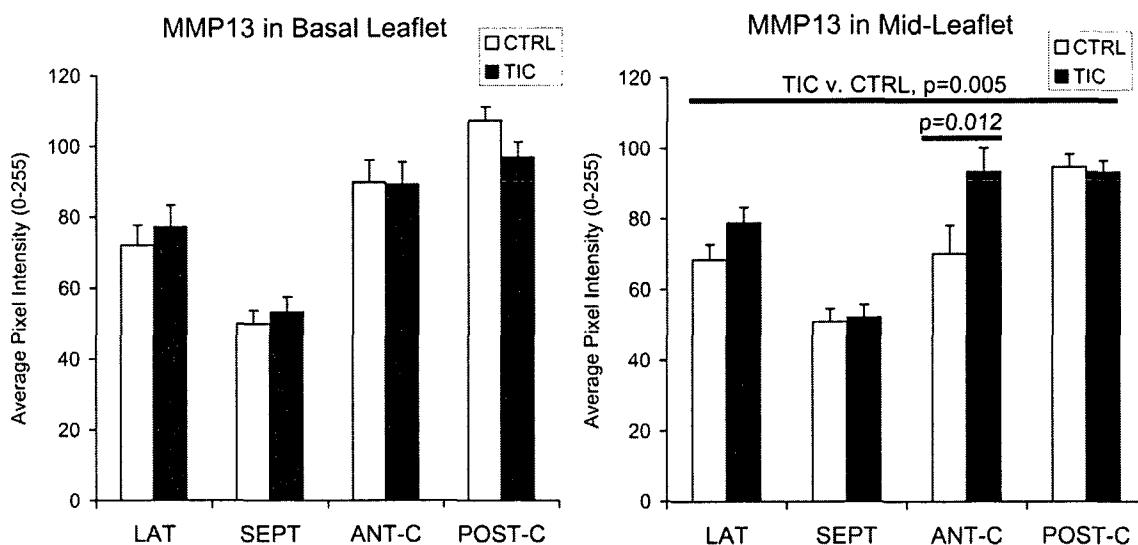


Fig. 16-4: MMP13 in basal and mid-leaflet of TIC and CTRL. In all figures, the long horizontal line indicates the comparison between groups in the ANOVA, whereas the short horizontal line indicates results of the post-hoc comparisons. Error bars indicate the standard error of the mean.

individually ($42\pm 10\%$, $p=0.012$), while no significant differences were seen in BL. MMP13 in the atrialis and fibrosa layers of TIC LAT was also greater than in CTRL ($12\pm 6\%$, $p=0.002$), while SEPT did not show such differences. Col I in TIC ML was greater than in CTRL when all segments were considered (Fig. 16-5, $9\pm 3\%$, $p=0.036$) as well as in ANT-C alone ($32\pm 8\%$, $p=0.004$), while no significant differences were seen in

BL when all segments were assessed. Col I in LAT BL ($24\pm 7\%$, $p=0.020$), the atrialis and fibrosa layers of LAT ($20\pm 4\%$, $p=0.002$), and all regions of ANT-C ($46\pm 12\%$, each

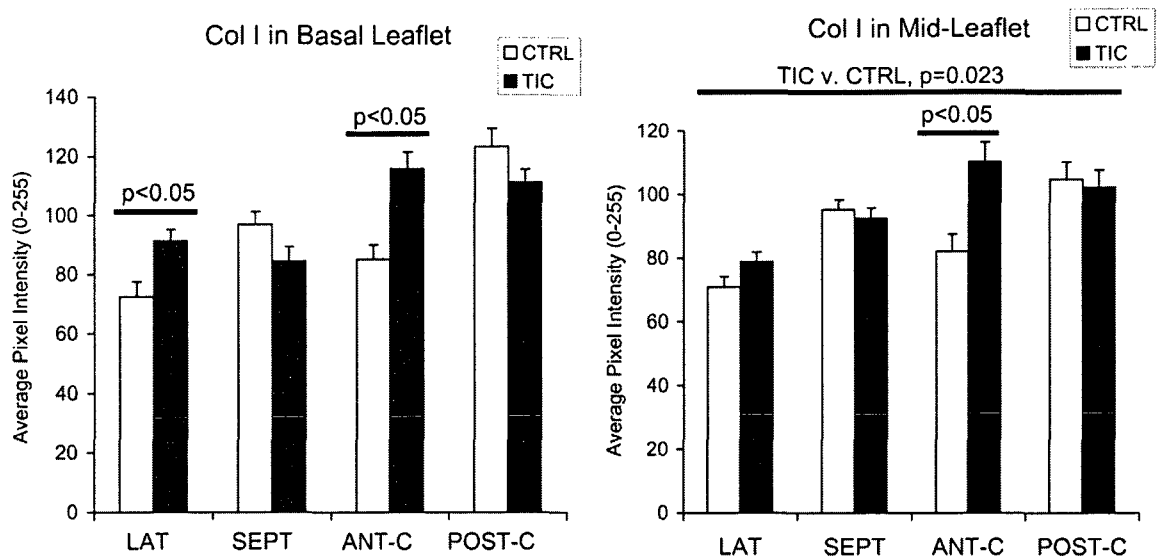


Fig. 16-5: Col I in basal and mid-leaflet of TIC and CTRL. Error bars indicate the standard error of the mean.

$p\leq 0.008$) was greater in TIC compared to CTRL. Col III in LAT BL ($14\pm 5\%$, $p=0.035$) and ANT-C fibrosa ($32\pm 7\%$, $p=0.003$) was greater in TIC compared to CTRL, but was less in SEPT across all regions ($-15\pm 6\%$, each $p\leq 0.009$). In fact, Col III in SEPT ML atrialis negatively correlated with TIC-induced changes in SEPT ML maximum and minimum length ($r=-0.671$, $p=0.021$ and $r=-0.647$, $p=0.029$). Evidence for collagen turnover was further suggested by correlations between collagens I and III with MMP13 in the ML of ANT-C and POST-C ($r=0.744-0.779$, each $p<0.015$). Lysyl oxidase (LOX), which is involved in both collagen and elastic fiber synthesis, was greater in TIC POST-

C ML compared to CTRL ($16\pm 4\%$, $p=0.012$), while no significant differences were noted in any of the BL segments.

Greater Elastic Fiber Turnover in TIC Leaflets

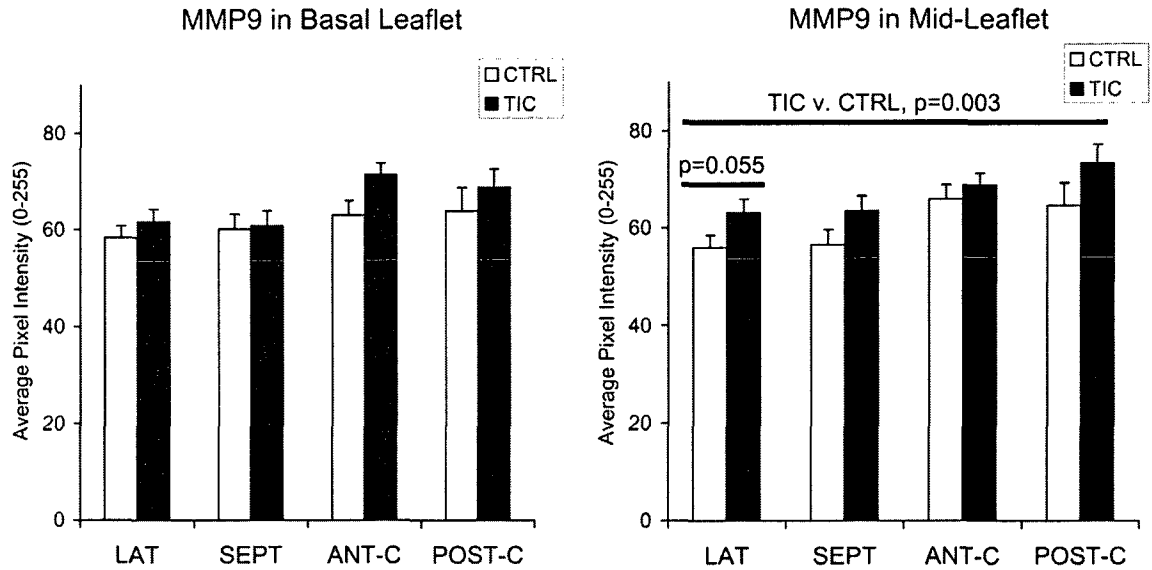


Fig. 16-6: MMP9 in basal and mid-leaflet of TIC and CTRL. Error bars indicate the standard error of the mean.

Elastic fiber turnover was examined by staining for elastin and MMP9, in addition to LOX (described above). In TIC, MMP9 in ML of all segments was greater than CTRL (Fig. 16-6, $11\pm 3\%$, $p=0.003$), but no such differences were seen in BL. MMP9 in LAT atrialis and fibrosa was also greater in TIC compared to CTRL ($7\pm 4\%$, $p=0.015$), while SEPT did not show such differences. Elastin in SEPT ML was greater in TIC ($40\pm 7\%$, $p<0.001$), while no significant differences were noted in BL. When examined by layers, the atrialis and fibrosa of both SEPT and LAT contained more elastin in TIC (atrialis:

28±9%, p<0.001; fibrosa: 25±4%, p=0.032R). This greater abundance of both elastin and MMP9 suggests elastic fiber remodeling, especially given that their degree of expression correlated with one another in certain leaflet regions (i.e., LAT ML atrialis, r=0.765, p<0.0025). Expression of elastin correlated to changes in leaflet segment length. For example, elastin in SEPT ML fibrosa positively correlated with TIC-induced changes in SEPT minimum ML length (r=0.683, p<0.007).

Proteoglycans and Glycosaminoglycans in TIC Leaflets

In TIC, the glycosaminoglycan HA in LAT ML was less than in CTRL (-11±4%, p=0.021); no significant differences were noted in any BL segments or for SEPT. The abundance of HA in LAT BL atrialis negatively correlated with TIC-induced changes in maximum BL length (r=-1.00, p=0.017). Expression of the proteoglycans BGN and DCN showed minimal changes with TIC.

Greater Valve Cell Activation in TIC Leaflets

Activation of VICs was assessed by staining for smooth muscle alpha-actin (SMaA) and non-muscle myosin (NMM), proteins indicating the contractile, highly synthetic myofibroblast phenotype.⁸ In ML, SMaA in TIC was greater than in CTRL for all segments except SEPT (Fig. 16-7, 21±3%, each p≤0.018); no significant differences were evident in BL. SMaA in POST-C free edge in TIC was also greater than in CTRL (28±6%, p=0.049). NMM in ML was greater for TIC when all segments were considered (7±2%, p=0.046), as well as in POST-C individually (13±3%, p=0.032). NMM in LAT BL (13±5%, p=0.049) was also greater in TIC.

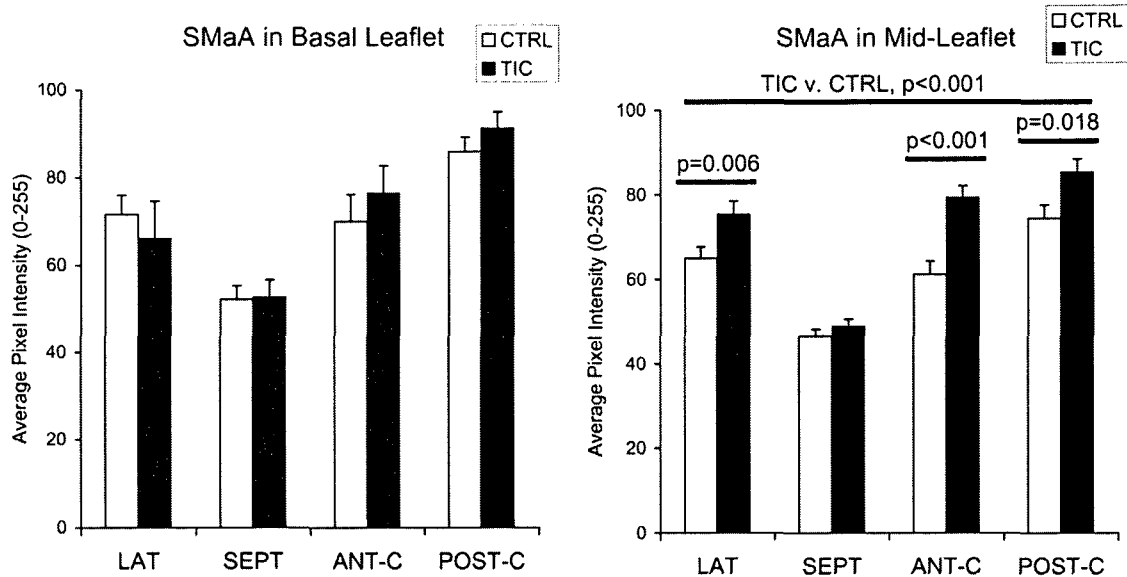


Fig. 16-7: *SMaA* in basal and mid-leaflet of TIC and CTRL. Error bars indicate the standard error of the mean.

Cell Activation and Correlations between Proteins within Leaflet Regions and Layers

There were numerous correlations between the phenotypic indicators of valve cell activation (NMM, SMAa) and matrix degradation proteins (MMP9, 13) particularly in the spongiosa and fibrosa of the different segments ($r=0.831-0.874$, $p\leq 0.002$), with strong correlation between SMAa and MMP13 in BL fibrosa across segments ($r=0.808$, $p<0.001$).

Relationship of LV Remodeling to Observed Leaflet Changes

The degree of LV remodeling, as measured by percent changes in EDV, ESV, and EF with TIC, was often predictive of leaflet changes. For instance, decreases in EF with

TIC were correlated with reductions in expression of Col I in the atrialis and fibrosa layers of LAT ML ($r=0.973$, $p<0.001$) and greater expression of Col III in ANT-C ML and BL ($r=-0.765$, $p=0.0163$). As EDV and ESV increased, SMaA and MMP13 in the ML fibrosa of ANT-C were increased (SMaA: $r=0.921-0.956$, $p\leq 0.0261$; MMP13: $r=0.858-0.861$, $p\leq 0.029$). LV remodeling also was predictive of changes in leaflet structure. For example, diffusion of collagen in LAT increased with EDV ($r=0.911$, $p=0.00115$) and cell density in LAT ML increased with both EDV and ESV ($r=0.834-0.835$, $p\leq 0.0388$). Different leaflets, however, responded in distinct ways to the LV remodeling; some changes in SEPT (i.e., MMP13 in ML fibrosa) were inversely related to EDV and ESV.

DISCUSSION

TIC leaflets demonstrated significant remodeling compared to CTRL, including greater cell density, less delineation between leaflet layers, greater collagen and elastic fiber turnover, and evidence of valve cell activation. Compositional differences between TIC and CTRL leaflets were heterogeneous by annular segment and leaflet region with extracellular matrix changes generally greater in the mid-leaflet than the basal leaflet, consistent with the magnitude of leaflet length changes in these regions. Greater expression of markers of cell activation in TIC suggests an increase in the myofibroblast population; these contractile and synthetic VICs may in part be responsible for these changes in leaflet segment length and composition with TIC. Statistical correlations provided the first *in vivo* demonstration of direct relationships between the degree of

mechanical strain and the magnitudes of phenotypic changes in VICs and valve matrix within individual animals.

Changes in Matrix Composition are Heterogeneous

TIC affected the leaflet regions heterogeneously, with greater compositional and leaflet length changes in the mid-leaflet than in the basal leaflet region. Decreased coaptation could cause the distal mid-leaflet and free edge to experience less of the compressive forces associated with coaptation, potentially increasing stresses in those regions and directly adjacent regions,¹ which could instigate larger compositional changes in the mid-leaflet than the basal leaflet. Increased stress on valves⁹ and valve cells⁴ has been shown to cause increased matrix production and valve cell activation, as found in this study. Furthermore, with a decrease in the compressive forces associated with coaptation, leaflet segment lengths should increase, particularly in the distal leaflet, as noted in this study.

In terms of layers, changes in composition between TIC and CTRL largely consisted of changes in the atrialis and fibrosa layers. Both the atrialis and fibrosa normally contain significant amounts of collagen, and given our finding of increased collagen turnover, it is logical for changes in composition to be evident in these layers. Furthermore, leaflet length changes largely correlated with compositional changes in the atrialis and fibrosa, consistent with the role these layers are thought to play in providing leaflet tensile strength.¹⁰ It is interesting to note that significant changes in elastic fiber turnover were found in the fibrosa, a layer not dominated by elastic fiber content; these changes may have been induced by increased radial deformation.

The various segments also showed significant heterogeneity in response to TIC. Compared to CTRL, LAT showed changes in valve cell activation, matrix components, and matrix remodeling proteins, such as SMaA, Col I, MMP9, and MMP13, as well as mid-leaflet thickening, but SEPT did not show these changes. Greater TIC-related changes in matrix composition in LAT compared to SEPT are consistent with greater leaflet length changes in LAT. These results corroborate previous studies of both computational modeling and animal model experiments. Kunzelman et al., in modeling the stresses of various portion of the MV after annular dilation, found that the increased stress was mostly on the lateral leaflet.¹ While changes in SEPT were less pronounced than in LAT, both the fluoroscopy and immunohistochemical results suggest that SEPT did remodel in TIC. SEPT showed increased leaflet length, cell density, and elastin in TIC compared to CTRL. Interestingly, unlike the other segments, SEPT showed a decrease in Col III. This unique remodeling pattern could imply a shift in the balance of mechanical loads between the various parts of the MV. In another recent study performed by this group, similar results of greater collagen and elastic fiber turnover were found in the septal leaflet when that leaflet was exposed to isolated regurgitation for 12 weeks.¹¹ Given the MR present in TIC and the results of this previous study, some of the changes observed in SEPT of TIC could be attributable to the regurgitation that is a part of DCM.

In terms of the commissural segments, TIC-induced changes in collagen turnover in the ANT-C resembled LAT with greater Col I, Col III, and MMP13 compared to CTRL. However, neither commissure displayed any alterations in elastic fiber turnover proteins (elastin, MMP9, and LOX) while both LAT and SEPT did. While ANT-C and

POST-C appeared to show distinct responses to TIC, further work is needed to clarify the role of the commissural remodeling in TIC.

Influence of Mitral Regurgitation and Left Ventricular Remodeling

Mitral regurgitation imposes altered hemodynamics on all of the mitral valve leaflets and commissures, including altered flow patterns,¹² in addition to the forces secondary to decreased or delayed coaptation,¹ all of which could have contributed to the changes observed in the TIC leaflets. Indeed, previous studies have documented increased collagen content in rat MV under acute increased LV pressure.¹³ However, TIC animals displayed global LV^{5, 14} and even neurohormonal¹⁵ changes in addition to MR, mimicking the clinical condition of DCM. Therefore, the leaflet changes observed with TIC are likely not solely due to MR, but could be secondary to altered forces imposed by changes in mitral annular shape and contractility,⁵ or even circulating neurohormones as documented in TIC animals.¹⁵

The predictive relationships between LV remodeling and leaflet changes observed in this study highlight how DCM results in alterations in a variety of the normal array of forces that comprise the mechanical environment of the MV. These relationships confirm that the leaflets are integral to LV structure and function. It is also important to note that these predictive relationships were unique to the different leaflets, which is consistent with the heterogeneity of the MV leaflets in relationship to LV structure, function, and response to DCM.

Changes in Phenotype and Matrix Markers Implicate Role of Myofibroblasts

The correlations between amounts and locations of valve cell activation and matrix degradation proteins, along with previous studies demonstrating the capacity of these cells for matrix synthesis and remodeling capabilities,^{8,16} provide strong evidence for the involvement of activated myofibroblasts in the matrix changes observed with TIC. These findings are consistent with the greater expression of myofibroblast markers in TIC leaflets and, more importantly, demonstrate direct relationships between magnitude of matrix remodeling, cell activation, and leaflet strain in individual animals. These results also strengthen evidence for the presumed role of VIC myofibroblasts in multiple valve diseases and remodeling processes.¹⁶ Furthermore, considering the contractile properties of valvular myofibroblasts,⁸ which have been shown to modulate leaflet stiffness,⁴ these myofibroblast cells may be responsible in part for the heterogeneous TIC-induced changes in valve geometry and strain. We speculate that, in diseases in which leaflet motion and composition are altered, the myofibroblast may be a target cell population for treatment strategies.

Implications for Human DCM

The results of this study corroborate findings in human DCM. Chaput et al. recently documented leaflet remodeling, namely increased leaflet area, in patients with functional MR¹⁷ and Grande-Allen et al. reported increased DNA, collagen, and glycosaminoglycans in valves from heart failure patients compared to controls.¹⁸ Consistent with those previous findings, this study found greater cell density and collagen in TIC ovine leaflets compared to CTRL. The increase in MMPs demonstrated in this

study is also consistent with findings of greater expression of MMPs in the ventricles of human patients with DCM.¹⁹

The compositional changes observed in this study could have functional consequences. The greater amount of collagen would be expected to make the leaflets more stiff, as observed in explanted DCM leaflets.²⁰ Computational studies have shown that such increased stiffness leads to delayed and incomplete coaptation and ultimately mitral regurgitation.²¹ Computational modeling has also demonstrated that loss of the well-defined layered structure of the leaflets would increase leaflet bending stresses.²² Greater elastic fiber turnover suggests less mature elastic fibers, which could lead to less leaflet recoil. Both the changes in stiffness and layered nature of the leaflet could worsen mitral regurgitation and lead to further adverse leaflet remodeling.¹¹ Indeed, although the study of functional MR by Chaput et al. did not examine leaflet composition, they found that remodeling of the leaflet anatomy, specifically the leaflet-to-closure area ratio, significantly correlated with MR severity, after adjusting for LV remodeling, function, and leaflet tethering.¹⁷ Their results are consistent with the speculation that the leaflet remodeling demonstrated in this study would lead to functional impairment. In the future, it will be important to demonstrate these proposed mechanisms for valve tissue dysfunction, perhaps using novel bioengineering approaches.

Limitations

One limitation in this study is the short time course. Clinically, DCM occurs over a period of years, while in this model the animals experienced DCM for only 15 days. Another limitation is the variability of immunohistochemistry, which was quantified to be

13.7% within batches. In order to limit this variability two sections were taken for SEPT and LAT and the results averaged. Additionally, for a given segment and protein, TIC and CTRL sections were stained in the same batch. Despite these limitations of short time course and variability in immunohistological analysis, significant results were found. Another limitation is that hemodynamic and leaflet length analyses were made comparing pre-TIC and TIC animals, while histological analyses compared TIC and CTRL animals. While explanted pre-TIC tissue was not available to compare to explanted TIC tissue, the authors did verify that there were no significant differences between the annular and leaflet radiopaque marker measurements of pre-TIC and CTRL animals. Another limitation was that animals were not randomized to groups. In addition, there were different numbers of animals in the TIC and CTRL groups, resulting in an unbalanced design. These numbers were due to animal loss from the TIC group, most commonly due to loss of the animal on anesthetic induction before the second set of marker and hemodynamic studies, since the animals were in florid heart failure. With respect to the lack of randomization, while each group displayed body weights and hemodynamics within a normal range, LVESP of CTRL was found to be higher than TIC ($p=0.004$), while the CTRL animals weighed less ($p=0.033$); no difference was found between CTRL and pre-TIC with respect to LVEDP or EF. The difference in LVEDP between groups could be due to a number of factors, including level of anesthetic, loading, and adrenergic drive at the time of measurement. However, given that the CTRL group in this study was exclusively used for histological comparisons between valves, and that there was no comparison of absolute differences in tissue dimensions, the authors believe that this difference does not undermine our results.

While the ovine MV has dynamics very similar to the human MV^{23,24} there are a number of anatomic differences including less redundancy in the ovine MV leaflet.^{25,26} TIC may have subtle differences compared to DCM, although studies have shown that the hemodynamics¹⁴ and neurohormonal¹⁵ changes elicited by TIC match those of human DCM. Lastly, the tantalum markers (total mass ~20mg) could have affected leaflet motion. However, studies have shown that even when enough markers are added to overload the ovine MV (total mass=184mg), MV motion does not change significantly.³ Furthermore, these markers were present in both TIC and CTRL, therefore they could not explain the differences found between TIC and CTRL. Finally, this study found a large number of correlations between MV structure, composition, and function, but further research will be required to determine causation, delineate the specific role of MR in the observed changes, and propose new therapeutic options.

CONCLUSIONS

This study shows that the MV leaflets are intimately and differentially involved in the DCM disease process, with changes in leaflet composition, structure, and valve cell phenotype. These results suggest that the MV leaflets themselves should be considered in DCM treatment strategies. Furthermore, the relationship between leaflet composition and changes in leaflet segment length suggest that changes in the extracellular matrix could be an underlying mechanism for the observed changes in leaflet motion, with the myofibroblast potentially playing an important role. The implicated link between altered leaflet strain and altered composition also reinforces the need to maintain physiological leaflet strains with appropriate annuloplasty design.

This chapter is the second of three chapters (Chapters 15-17) analyzing the mitral valve in the context of “functional” mitral regurgitation and dilated cardiomyopathy. In the next chapter, analysis of the mitral valve in dilated cardiomyopathy continues with a study analyzing matrix remodeling in the mitral annular region in relationship to changes in annular segment length.

REFERENCES

1. Kunzelman KS, Reimink MS, Cochran RP. Annular dilatation increases stress in the mitral valve and delays coaptation: a finite element computer model. *Cardiovasc Surg*. 1997; 5:427-434.
2. He S, Lemmon JD, Jr., Weston MW, Jensen MO, Levine RA, Yoganathan AP. Mitral valve compensation for annular dilatation: in vitro study into the mechanisms of functional mitral regurgitation with an adjustable annulus model. *J Heart Valve Dis*. 1999; 8:294-302.
3. Timek TA, Lai DT, Dagum P, Liang D, Daughters GT, Ingels NB, Jr., Miller DC. Mitral leaflet remodeling in dilated cardiomyopathy. *Circulation*. 2006; 114:1518-523.
4. Merryman WD, Youn I, Lukoff HD, Krueger PM, Guilak F, Hopkins RA, Sacks MS. Correlation between heart valve interstitial cell stiffness and transvalvular pressure: implications for collagen biosynthesis. *Am J Physiol*. 2006; 290:H224-231.
5. Timek TA, Dagum P, Lai DT, Liang D, Daughters GT, Tibayan F, Ingels NB, Jr., Miller DC. Tachycardia-induced cardiomyopathy in the ovine heart: Mitral annular dynamic three-dimensional geometry. *J Thorac Cardiovasc Surg*. 2003; 125:315-324.
6. Helmcke F, Nanda N, Hsiung M, Soto B, Adey C, Goyal R, Gatewood Jr R. Color Doppler assessment of mitral regurgitation with orthogonal planes. *Circulation*. 1987; 75:175-183.
7. Montiel MM. Muscular apparatus of the mitral valve in man and its involvement in left-sided cardiac hypertrophy. *Am J Cardiol*. 1970; 26:341-344.
8. Messier RH, Jr., Bass BL, Aly HM, Jones JL, Domkowski PW, Wallace RB, Hopkins RA. Dual structural and functional phenotypes of the porcine aortic valve interstitial population: characteristics of the leaflet myofibroblast. *J Surg Res*. 1994; 57:1-21.
9. Balachandran K, Konduri S, Sucusky P, Jo H, Yoganathan AP. An ex vivo study of the biological properties of porcine aortic valves in response to circumferential cyclic stretch. *Ann Biomed Eng*. 2006; 34:1655-1665.
10. Vesely I, Noseworthy R. Micromechanics of the fibrosa and the ventricularis in aortic valve leaflets. *J Biomech*. 1992; 25:101-113.
11. Stephens EH, Nguyen TC, Itoh A, Ingels NB, Jr., Miller DC, Grande-Allen KJ. The effects of hemodynamics of regurgitation alone are sufficient for mitral valve leaflet remodeling. *Circulation*. 2008; 118:S243-249.
12. Schwammenthal E, Chen C, Benning F, Block M, Breithardt G, Levine RA. Dynamics of mitral regurgitant flow and orifice area. Physiologic application of the proximal flow

- convergence method: clinical data and experimental testing. *Circulation*. 1994; 90:307-322.
13. Willems I, Havenith M, Smits J, Daemen M. Structural alterations in heart valves during left ventricular pressure overload in the rat. *Lab Invest*. 1994; 71:127-133.
 14. Wilson JR, Douglas P, Hickey WF, Lanoce V, Ferraro N, Muhammad A, Reichel N. Experimental congestive heart failure produced by rapid ventricular pacing in the dog: cardiac effects. *Circulation*. 1987; 75:857-867.
 15. Riegger A, Liebau G. The renin-angiotensin-aldosterone system, antidiuretic hormone and sympathetic nerve activity in an experimental model of congestive heart failure in the dog. *Clin Sci (Lond)*. 1982; 62:465-469.
 16. Rabkin E, Aikawa M, Stone JR, Fukumoto Y, Libby P, Schoen FJ. Activated interstitial myofibroblasts express catabolic enzymes and mediate matrix remodeling in myxomatous heart valves. *Circulation*. 2001; 104:2525-2532.
 17. Chaput M, Handschumacher MD, Tournoux F, Hua L, Guerrero JL, Vlahakes GJ, Levine RA. Mitral leaflet adaptation to ventricular remodeling: occurrence and adequacy in patients with functional mitral regurgitation. *Circulation*. 2008; 118:845-852.
 18. Grande-Allen KJ, Borowski AG, Troughton RW, Houghtaling PL, Dipaola NR, Moravec CS, Vesely I, Griffin BP. Apparently normal mitral valves in patients with heart failure demonstrate biochemical and structural derangements: an extracellular matrix and echocardiographic study. *J Am Coll Cardiol*. 2005; 45:54-61.
 19. Gunja-Smith Z, Morales AR, Romanelli R, Woessner JF, Jr. Remodeling of human myocardial collagen in idiopathic dilated cardiomyopathy. Role of metalloproteinases and pyridinoline cross-links. *Am J Pathol*. 1996; 148:1639-1648.
 20. Grande-Allen KJ, Barber JE, Klatka KM, Houghtaling PL, Vesely I, Moravec CS, McCarthy PM. Mitral valve stiffening in end-stage heart failure: evidence of an organic contribution to functional mitral regurgitation. *J Thorac Cardiovasc Surg*. 2005; 130:783-790.
 21. Kunzelman KS, Quick DW, Cochran RP. Altered collagen concentration in mitral valve leaflets: biochemical and finite element analysis. *Ann Thorac Surg*. 1998; 66:S198-205.
 22. Kunzelman KS, Cochran RP, Murphree SS, Ring WS, Verrier ED, Eberhart RC. Differential collagen distribution in the mitral valve and its influence on biomechanical behaviour. *J Heart Valve Dis*. 1993; 2:236-244.
 23. Glasson JR, Komeda M, Daughters GT, Foppiano LE, Bolger AF, Tye TL, Ingels NB, Jr., Miller DC. Most ovine mitral annular three-dimensional size reduction occurs before ventricular systole and is abolished with ventricular pacing. *Circulation*. 1997; 96:II-115-122.
 24. Ormiston JA, Shah PM, Tei C, Wong M. Size and motion of the mitral valve annulus in man. II. Abnormalities in mitral valve prolapse. *Circulation*. 1982; 65:713-719.

25. Brock R. The surgical and pathological anatomy of the mitral valve. *Br Heart J.* 1952; 14:489-513.
26. Gorman JH, 3rd., Jackson BM, Gorman RC, Kelley ST, Gikakis N, Edmunds LH, Jr. Papillary muscle discoordination rather than increased annular area facilitates mitral regurgitation after acute posterior myocardial infarction. *Circulation.* 1997; 96:II-124-127.

Chapter 17: Mitral Annular Region Ultrastructural Changes in Dilated Cardiomyopathy Correlate with Regional Remodeling

In this chapter the topic of mitral valve alterations in the context of “functional” mitral regurgitation and dilated cardiomyopathy continues with a study of mitral annular matrix remodeling in relation to annular segment length changes with dilated cardiomyopathy.

ABSTRACT

Background: The mitral annulus enlarges heterogeneously in dilated cardiomyopathy (DCM), yet the ultrastructural changes underlying this remodeling remain unknown. We studied the relationship between changes in matrix composition and regional geometric annular remodeling associated with DCM.

Methods: Radiopaque markers were inserted into 24 sheep defining four mitral annular segments: septal (SEPT), lateral (LAT), and anterior (ANT-C) and posterior commissures (POST-C); 10 sheep underwent tachycardia-induced cardiomyopathy (TIC), while 14 sheep were controls (CTRL). Biplane videofluoroscopy was performed before and after rapid pacing. Annular segment lengths were measured as distances between respective markers and were related to annular segment composition by immunohistochemistry.

Results: MR increased from 0.2 ± 0.4 to 2.2 ± 0.9 after TIC ($p < 0.0002$). For each segment, annular lengths increased with TIC (each $p < 0.001$), with the percent change in LAT greater than SEPT ($p < 0.001$). TIC annular segments showed greater collagen content overall, greater collagen and elastic fiber turnover, and greater cell activation compared to CTRL (each $p < 0.05$). Changes were heterogeneous by annular segment, with changes in LAT greater than SEPT, paralleling greater changes in LAT annular segment lengths with TIC than SEPT. Strong correlations between proteins of matrix turnover and cell activation suggest the myofibroblast phenotype may play an important role in the observed heterogeneous changes in annular composition.

Conclusions: Heterogeneous annular compositional changes with TIC corresponded with segment length changes. Matrix changes may be an underlying mechanism for annular remodeling seen in DCM.

The work contained in this chapter is under preparation for submission to *Circulation*.

INTRODUCTION

The mitral valve (MV) annulus is a major contributor to dilated cardiomyopathy (DCM). While annular dilation alone does not appear to cause mitral regurgitation (MR) in humans,¹ annular dilation and papillary muscle displacement determined regurgitation severity in DCM patients.² The role of annular dilation in MR has been confirmed in animal models³ and *in vitro* experiments.⁴ While there has been considerable analysis of DCM-induced changes in the shape and motion of the mitral annulus,^{3, 5} there is less information about the ultrastructural basis for these changes, which are presumably the result of cell-mediated remodeling of the annular extracellular matrix (ECM). Recent studies have demonstrated mitral leaflet ECM remodeling in animal models of “functional” MR⁶ and DCM,⁷ but analysis of such changes in the mitral annulus or with respect to the geometric annular changes seen in DCM has not been reported to date. Characterizing these cell-mediated ECM changes not only gives insight into the pathogenesis of the annular structural changes, but may open an avenue for early or preventative interventions.

METHODS

All animals received humane care in accordance with the guidelines of the US Department of Health and Human Services (NIH Publ. 85-23, Revised 1985). The animal protocol was approved by the Stanford Medical Center Laboratory Research Animal Review Committee.

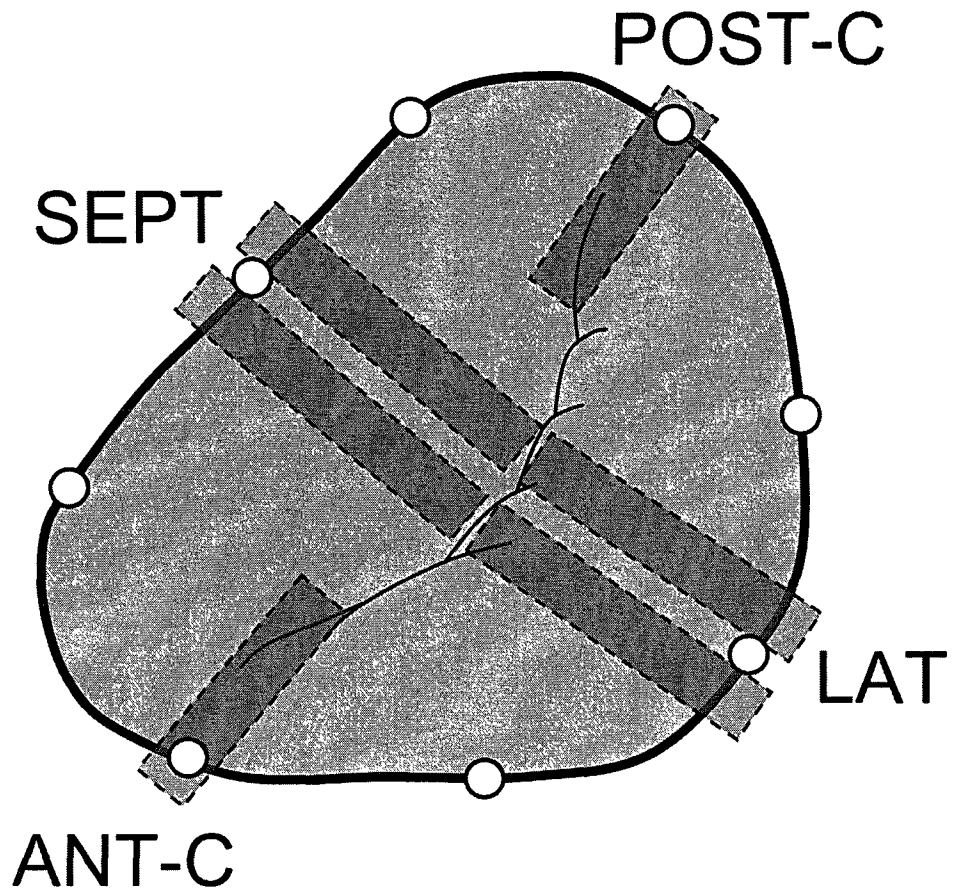


Fig. 17-1: Location of the different annular segments from which tissue sections were taken. In the case of septal segment (SEPT) and lateral segment (LAT) 2 tissue sections were analyzed, in the case of the anterior and posterior commissures (ANT-C, POST-C), one tissue section was taken from either side of the tantalum marker based on quality of the leaflet on each side.

Animal Protocol

Radiopaque markers were implanted in 24 sheep to delineate four MV annular segments (Fig. 17-1): septal (SEPT) and lateral (LAT) annulus, and anterior (ANT-C) and posterior (POST-C) commissures, as previously described in detail.⁵ Ten sheep

underwent a rapid-pacing protocol (tachycardia-induced cardiomyopathy, TIC) for an average of 15 ± 6 days,⁵ while fourteen sheep remained as controls (CTRL). Biplane video fluoroscopy (without pacing) was performed in CTRL and both before and after the rapid-pacing intervention in TIC animals. Mitral regurgitation was graded semi-quantitatively by an experienced echocardiographer on a scale of 0-4 based on size and extent of regurgitant jet. Left ventricular (LV) end-diastolic and end-systolic volumes (EDV, ESV) were calculated using space-filling analysis of epicardial markers, as described previously.⁵ The hearts were harvested and stored in formalin. CTRL animals were used for histological comparison only, while hemodynamic and annular segment length analyses compared pre-TIC and TIC data. Annular segment length was measured as the sum of the distances from the central marker in each region to the adjacent markers on either side of the central marker. TIC-induced changes in maximum (%MAX) and minimum (%MIN) annular segment length throughout the cardiac cycle were measured. The septal-lateral mitral annular diameter was measured as the maximum distance between the mid-septal and mid-lateral annular markers, while the commissure-commissure diameter was measured as the maximum distance between the two commissural annular markers throughout the cardiac cycle.

Histology and Immunohistochemistry

Cross-sections 3-5 mm wide were cut from the leaflet-annular insertion or “hinge” region at the four sites, including associated myocardium (Fig. 17-2), embedded in paraffin, and sectioned to a thickness of five microns. Sections were stained with Movat pentachrome to demonstrate the layered structure of the annular region.

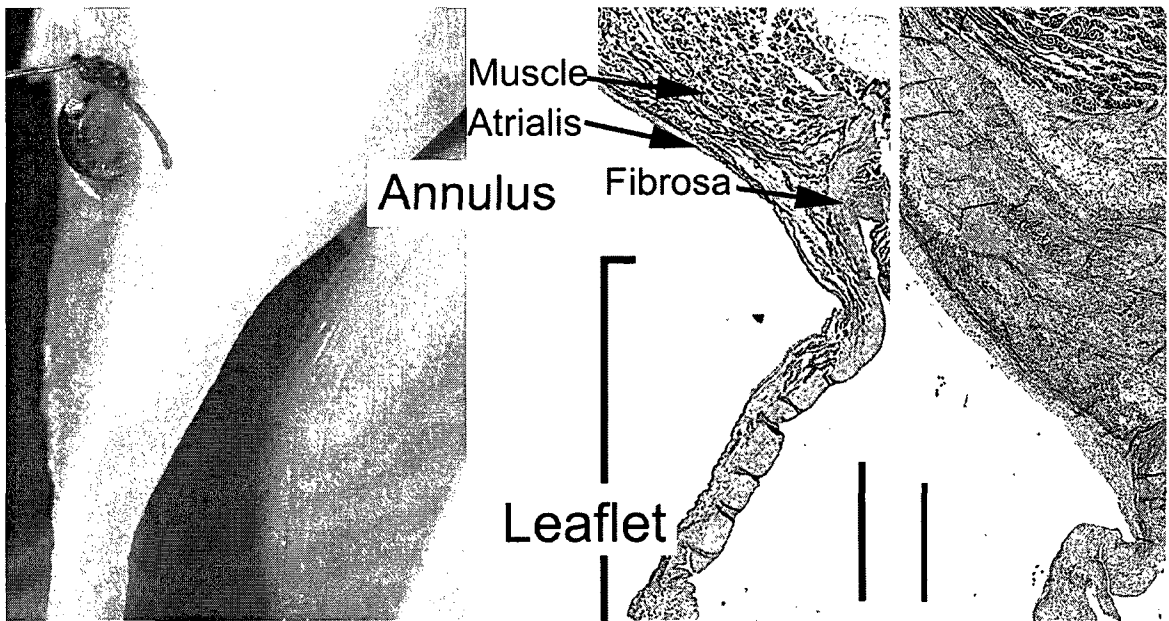


Fig. 17-2: Middle image of tissue section depicts layers of the annular region analyzed in relation to the remainder of the valve leaflet, as well as relative to the annular fluoroscopy marker demonstrated in photo of gross specimen at left. Right image illustrates representative TIC annulus showing greatly increased accumulation of collagen on the atrialis compared to control (middle). Scale bar represents 1 mm.

Immunohistochemistry (IHC) was performed for a number of ECM components and turnover proteins, as well as proteins indicating valve cell activation (Table 17-1). For each annular segment (LAT, SEPT, ANT-C, POST-C) staining intensity was quantified within each histological layer (fibrosa, atrialis, muscle, Fig. 17-2) using ImageJ software (NIH, Bethesda, MD). Analysis of blinded Movat-stained sections included semi-quantitative grading (from 0 to 4) of saffron-staining collagen in the atrialis. To determine the range of differences in histological and IHC parameters between TIC and CTRL, each TIC value was compared to the average CTRL value. The TIC leaflet analysis is reported elsewhere,⁷ see Chapter 16.

Table 17-1. Panel of Antibodies Used in IHC.

Protein	Function
<u>Collagen Turnover Proteins</u>	
Collagen I (Col I)*	Predominant collagen in valve, provides tensile strength
Collagen III (Col III)*	Reticular collagen
Matrix Metalloproteinase (MMP)-13 [†]	Collagen degradation
<u>Elastic Fiber-Related Proteins</u>	
Lysyl oxidase (LOX) [§]	Involved in collagen and elastin crosslinking
Elastin	Predominant component of elastic fibers
Matrix Metalloproteinase (MMP)-9 [‡]	Elastic fiber degradation
<u>Valve Cell Activation</u>	
Smooth muscle alpha-actin (SM α A) [#]	Marker of an "activated" myofibroblast-like phenotype
Non-muscle Myosin Heavy Chain (NMM) ^{**}	Marker of an "activated" myofibroblast-like phenotype

*gift of Dr. Larry Fisher, NIH (Bethesda, MD); [†]Chemicon (Temecula, CA); [§]Imgenex (San Diego, CA); ^{||}Abcam (Cambridge, MA); [‡]Assay Designs (Ann Arbor, MI); [#]Dakocytomation (Denmark); ^{**}Covance (Berkeley, CA).

Statistical Analysis

Multifactorial analysis of variance (ANOVA) was performed using SigmaStat (SPSS, Chicago, IL), as described in Chapter 4. Paired t-tests were used to compare pre-TIC and post-TIC hemodynamics and annular segment length changes. Correlations between factors were calculated using Pearson and Spearman tests, as described in Chapter 5. For correlations between different proteins, $p \leq 0.015$ was considered a trend and $p \leq 0.00625$ considered significant (since 8 proteins were being compared). For correlations between proteins and TIC-induced segment length and EDV/ESV changes, each protein was considered individually, therefore $p \leq 0.05$ was considered significant. Data are presented as mean and standard deviation, unless otherwise noted. Percentages for IHC are presented as mean and standard error because of the multiple segments and layers involved.

RESULTS

Development of Dilated Cardiomyopathy and Changes in Annular Dimensions

Consistent with the development of DCM, the maximum annular septal-lateral diameter increased $24\pm 9\%$ ($p<0.0001$) in TIC compared to pre-TIC, the commissure-commissure diameter increased $9\pm 4\%$ ($p<0.001$), and mitral regurgitation increased in severity from 0.2 ± 0.4 to 2.2 ± 0.9 ($p<0.0002$). Further characterization of annular and hemodynamic changes with TIC has been previously published.⁵ While the maximum and minimum annular lengths of all segments increased with TIC (each $p<0.004$), POST-C %MIN was greater than ANT-C %MIN (Table 17-2, $p<0.049$) and LAT %MAX and %MIN were greater than SEPT (each $p<0.001$).

Table 17-2. Annular Segment Length Changes with TIC.

(cm)	SEPT	LAT	ANT-C	POST-C
MAX				
Pre-TIC	2.81±0.41	3.04±0.57	2.55±0.25	2.93±0.32
TIC	2.94±0.45*	3.53±0.67*	2.90±0.25*	3.43±0.37*
% change	4.2±0.3	16.4±0.8**	14.1±0.5	17.4±0.9^
MIN				
Pre-TIC	2.59±0.42	2.65±0.59	2.26±0.23	2.60±0.30
TIC	2.71±0.42*	3.24±0.62*	2.67±0.29*	3.18±0.36*
% change	4.7±0.4	23.8±1.4**	17.7±0.6	22.8±1.1^

Data presented as mean ± standard deviation; * $p<0.05$ v. pre-TIC, ** $p<0.05$ v. SEPT, ^ $p<0.05$ v. ANT-C.

Greater Collagen Turnover in TIC Annular Region

MMP13, a collagen-degrading enzyme, was greater in TIC LAT and SEPT compared to CTRL ($22.6\pm 6.2\%$, $p=0.02$ and $9.0\pm 4.0\%$, $p=0.048$), and MMP13 expression in SEPT strongly correlated with %MIN ($r=0.84$, $p<0.001$). Col I was greater

Col I in Annular Segments of TIC and CTRL

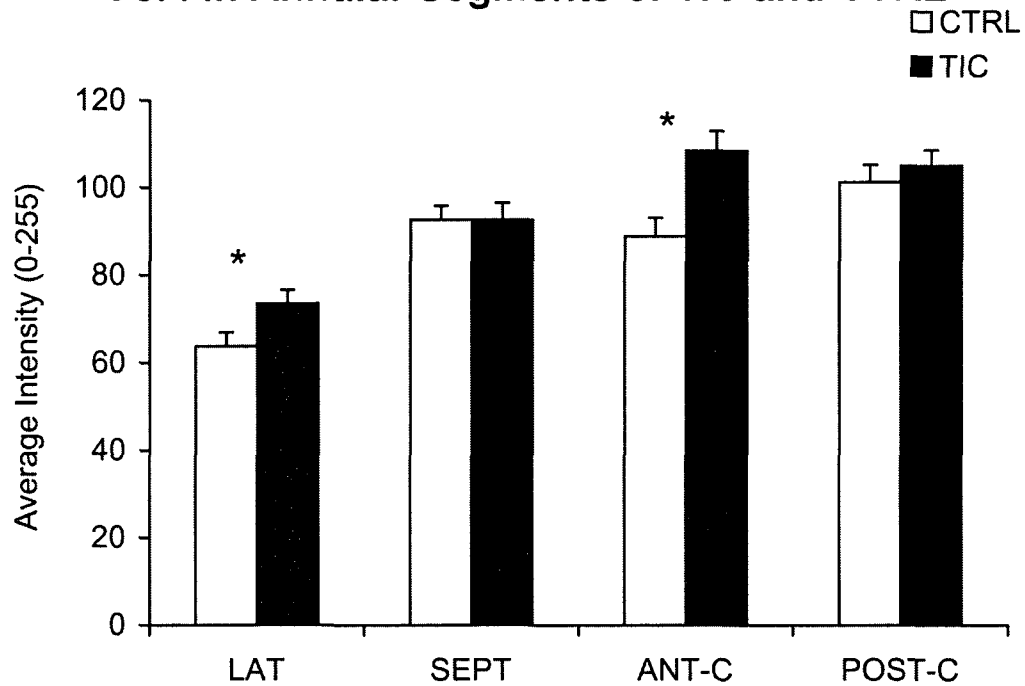
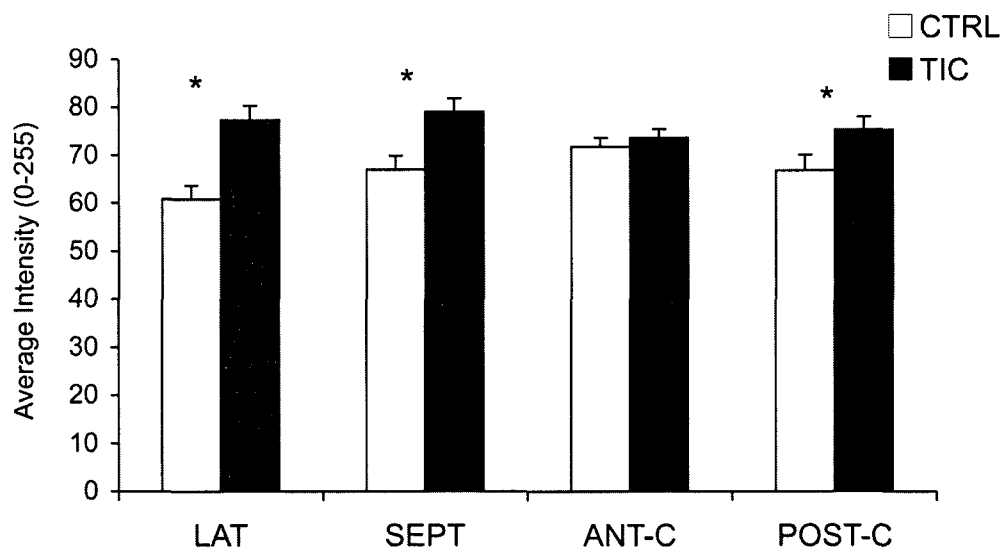


Fig. 17-3: Col I in annular segments of TIC and CTRL. * $p < 0.05$ TIC vs. CTRL for a given annular segment. Error bars indicate the standard error of the mean.

in TIC LAT (Fig. 17-3, $17.2 \pm 4.3\%$, $p = 0.042$) and ANT-C ($21.6 \pm 5.2\%$, $p = 0.004$) compared to CTRL, and Col I in the fibrosa of LAT correlated with %MAX and %MIN ($r = 0.85$, $p = 0.033$). Compared to CTRL, Col III was greater in TIC ANT-C ($14.3 \pm 4.2\%$, $p = 0.013$), but was less in TIC SEPT ($-11.6 \pm 3.0\%$, $p = 0.006$). Movat-stained sections similarly showed greater abundance of saffron-staining collagen in the atrialis layer in TIC compared to CTRL ($p = 0.0001$, Fig. 17-2).

A. MMP9 in Annular Segments of TIC and CTRL



B. NMM in Annular Segments of TIC and CTRL

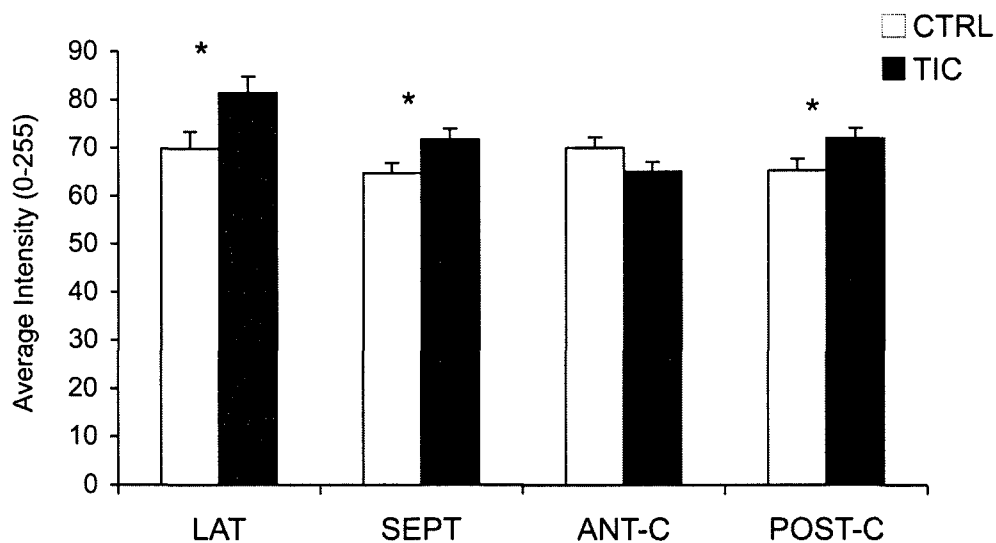


Fig. 17-4: A) MMP9 in annular segments of TIC and CTRL. B) NMM in annular segments of TIC and CTRL. * $p < 0.05$ TIC vs. CTRL for a given annular segment. Error bars indicate the standard error of the mean.

Greater Elastic Fiber Turnover in TIC Annular Region

The intensity of MMP9, a gelatinase associated with elastic fiber degradation,⁸ was significantly greater in TIC LAT, SEPT, and POST-C compared to CTRL (Fig. 17-4A, 25.4±4.9% p<0.001, 15.1±4.0%, p=0.004, and 6.8±3.8%, p=0.049) and strongly correlated with %MIN in SEPT (r=0.84, p<0.001). Compared to CTRL, elastin was greater in TIC SEPT (45.3±12.7%, p=0.017R), but was lower in TIC ANT-C (-11.9±6.9%, p=0.035). LOX, involved both in collagen and elastic fiber synthesis, was lower in TIC SEPT compared to CTRL (-11.6±3.9%, p=0.037).

Greater Cell Activation in TIC Annular Region

NMM in TIC was greater than CTRL in the annular segments LAT (Fig. 17-4B, 17.7±5.2%, p=0.024), SEPT (9.5±3.8%, p=0.03), and POST-C (9.3±3.2%, p=0.04). In LAT, SMaA was greater in TIC than in CTRL (Fig. 17-5, 16.0±4.1%, p=0.024).

Relative Changes in Composition between Annular Segments

Changes in matrix composition, matrix turnover, and cell activation in LAT with TIC were consistently greater than those of SEPT. This pattern was shown by increased expression of MMP13 (22% vs. 9% in LAT vs. SEPT), Col I (17% vs. no significant change), MMP9 (25% vs. 15%), NMM (18% vs. 10%), and SMaA (16% vs. no significant change). Greater changes in LAT vs. SEPT paralleled greater changes in annular lengths in LAT than SEPT. Similar parallels were found between %MIN in the

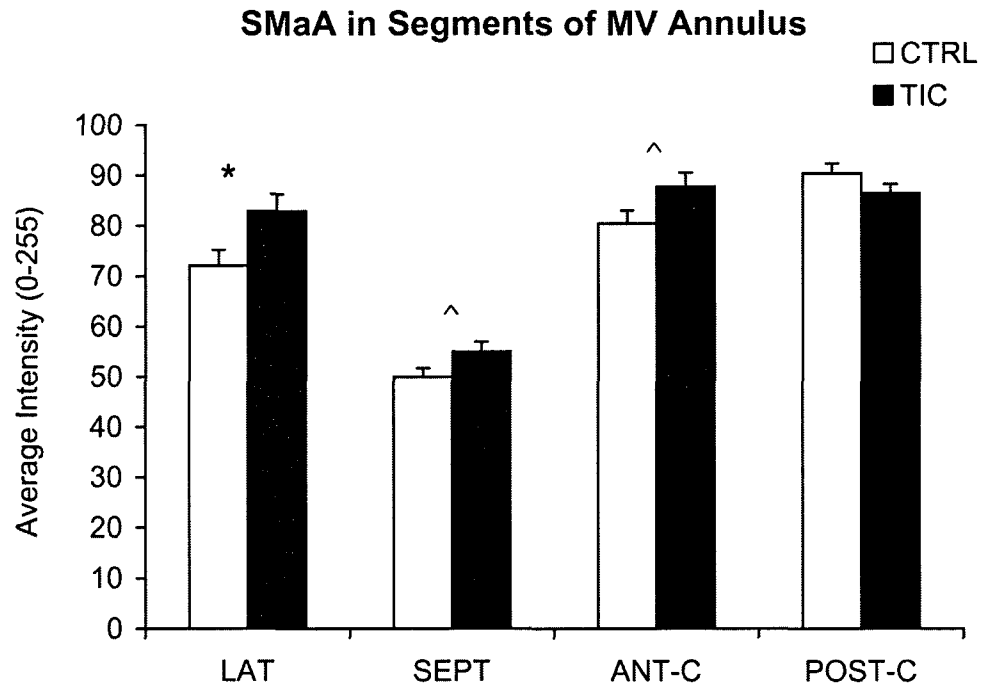


Fig. 17-5: SmaA in annular segments of TIC and CTRL. * $p < 0.05$ TIC v. CTRL, ^ $p < 0.65$ TIC vs. CTRL for a given annular segment. Error bars indicate the standard error of the mean.

commissural annular segments and changes in MMP9 and NMM expression, which were greater in POST-C with TIC but were not significantly altered in ANT-C.

Correlations between Expressions of Proteins in Annular Segments

Correlations were noted between ECM synthesis and turnover proteins and valve cell activation, suggesting a role for activated myofibroblasts in the matrix changes accompanying TIC. For example, in SEPT, NMM strongly correlated with MMP13 throughout the segments and layers of the annulus ($r=0.94$, $p=0.006$) and with Col III in the fibrosa (0.79 , $p < 0.001$). Col I correlated with SmaA in ANT-C fibrosa ($r=0.82$,

p=0.012) and NMM in POST-C atrialis (0.94, p<0.001). Correlations between SMaA and MMP13 were strong across segments in the atrialis (r=0.757, p<0.000001), fibrosa (r=0.664, p<0.000001) and muscle (r=0.742 p<0.001).

Relationship between Expression of Proteins and LV Remodeling

Degree of LV remodeling, as measured by changes in EDV and ESV, often strongly correlated with localized changes in protein expression. For instance, Col I in the muscle layer of LAT strongly correlated with changes in ESV (r=0.991, p=0.009) and SMaA in the fibrosa and muscle layers of ANT-C also strongly correlated with EDV and ESV (r=0.992, p=0.009 and r=0.919, p=0.0275). Elastin in the LAT fibrosa negatively correlated with EDV and ESV (r=-0.969, p=0.007 and r=-0.961, p=0.009) and elastin turnover indicated by MMP9 correlated with EDV in SEPT (r=0.984, p=0.016).

DISCUSSION

To further understand the underlying mechanism for annular changes associated with DCM, immunohistochemistry was used to assess the changes in matrix composition and cell phenotype changes in the annular region that accompany the development of tachycardia-induced cardiomyopathy (TIC), an animal model of DCM, and to relate those to segmental annular length change. The TIC annular region demonstrated greater collagen content overall, greater collagen turnover, greater elastic fiber turnover, and greater cell activation than CTRL. These changes were heterogeneous, with greater changes in LAT than in SEPT, which paralleled the magnitude of changes in annular length in these annular segments. Correlations between ECM synthesis and turnover

proteins and valve cell activation implicate valvular myofibroblasts in this heterogeneous remodeling.

Changes in Annular Composition with TIC in Relation to Changes in Annular Dimensions

TIC-induced changes in matrix composition, matrix turnover, and cell activation in LAT were consistently greater than those of SEPT, paralleling greater changes in annular lengths in LAT than SEPT. While correlations between matrix changes and length changes within individual segments were evident suggesting a relationship between the annular length change and matrix remodeling within that segment, regional heterogeneity was evident. For instance, matrix changes in POST-C were generally not as great as in LAT despite similar length changes with TIC, suggesting regional differences in relation to similar degrees of annular remodeling.

Implicated Role of Myofibroblasts

The strong correlations between markers for valve cell activation and matrix degradation within specific annular segments and layers imply that the activated myofibroblast phenotype is present and contributing to the heterogeneous compositional changes of the mitral annulus that accompany TIC. Indeed, this evidence of myofibroblast involvement is consistent with the known role that the myofibroblasts play in valve⁹ and connective tissue remodeling,¹⁰ as well as in the pathogenesis of other valve diseases.¹¹ Given that myofibroblasts are known to respond to their mechanical environment,¹² these cells may be an important link in the structure- function interplay

shown in this study, namely through sensing changes in annular geometry and then responding by altering matrix synthesis, which would influence local material behavior and further modify annular shape. Furthermore, the underlying tone imparted by the contractile behavior of these cells,¹³ which has been shown to alter stiffness of mitral leaflets,¹⁴ could contribute to the heterogeneity of annular segment length changes with TIC.

Role of Specific Layers in Annular Remodeling with TIC

While the muscle tissue surrounding and within the mitral annulus is presumably the primary contributor to annular contraction, and almost certainly contributed to the alterations in annular contraction found with TIC, this study demonstrated remodeling of all three layers within the annular region of MV leaflet. Additionally, many of the correlations between changes in protein expression and changes in annular lengths were present in all three layers. Although ECM changes in the atrialis and fibrosa layers of the annulus may exert less influence mechanically than the muscle layer, these findings do suggest an integral role for the insertion portion of the mitral leaflet in the process of annular remodeling with TIC. Indeed, a previous study found that ablation of the annular muscle resulted in decreased pre-systolic contraction of the annulus and altered shape of the SEPT leaflet, but no change in total annular contraction,¹⁵ suggesting that there are additional contributors to annular contraction besides the annular muscle component.

Annular Compositional Changes with TIC in the Context of LV Remodeling

The relationships between measures of LV remodeling and the annular compositional changes observed in this study highlight the global changes associated with DCM and confirm the integral role the annulus plays in maintaining LV structure and function. Simple measurements of annular segment length changes cannot account for how these global changes can influence the complex array of forces applied to the annulus as a result of alterations to the 3D configuration of the annulus,⁵ hemodynamics, and LV torsional and recoil mechanics.¹⁶ The finding that these correlations between LV remodeling and annular changes were distinct for the different annular segments again confirms the heterogeneity of the annulus in relationship to LV structure, function, and response to DCM. It is particularly interesting that correlations between EF and compositional changes appeared almost exclusively in SEPT.

Implications

Based on the observed association between altered annular length changes and abnormal annular composition, altered annular length changes imposed by an annuloplasty ring¹⁷ may similarly lead to alterations in valve cell phenotype and mitral annular composition, which could potentially cause further deterioration in MV function. Clearly further study is warranted in this arena; however, such studies could further motivate the refinement of annuloplasty design to maintain physiologic annular length changes. Furthermore, the results of this study implicate cells demonstrating the myofibroblast phenotype as contributing to the heterogeneous alterations in annular composition that underlie the annular remodeling associated with DCM. While future

studies are needed to confirm similar changes in human DCM, myofibroblasts may prove to be important therapeutic targets for prevention and treatment of the annular remodeling associated with DCM, which could have a considerable impact on its morbidity and mortality.

Limitations

While TIC is an excellent animal model for DCM, one limitation is its short time course relative to human DCM, which occurs over a period of years. Additionally, while the ovine MV has very similar dynamics to the human MV,^{18, 19} there are a number of anatomic differences such as less redundancy in the ovine MV.^{20, 21} TIC may also have subtle distinctions from DCM, although previous studies have shown that the hemodynamics²² and neurohormonal²³ changes elicited by TIC match those of human DCM. Another study limitation is the variability of immunohistochemistry, which was quantified to be 13.7% within batches. In order to limit this variability two sections were taken for SEPT and LAT and for a given segment and protein, TIC and CTRL sections were stained in the same batch. Despite these limitations of short time course and variability in immunohistological analysis, significant results were found. Another limitation is that hemodynamic and segment length analyses were made comparing pre-TIC and TIC animals, while histological analyses compared TIC and CTRL animals. While explanted pre-TIC tissue was not available to compare to explanted TIC tissue, the authors did verify that there were no significant differences between the radiopaque marker measurements of pre-TIC and CTRL animals. Additionally, the tantalum markers (total mass ~20mg) could have affected leaflet motion. However, previous studies have

shown that even when enough markers are added to overload the ovine MV (total mass=184mg), MV motion does not change significantly.²⁴ Furthermore, these markers were present in both TIC and CTRL, therefore they could not explain the differences found between TIC and CTRL. Finally, this study found a large number of correlations between MV annular structure, composition, and function, but further research will be required to determine causation.

CONCLUSIONS

In this study, heterogeneous compositional and cell phenotype changes in the mitral annular region were associated with changes in annular segmental lengths in experimental DCM, suggesting that cell-mediated alterations in annular composition may underlie annular remodeling with DCM. Furthermore, the results of this study suggest that the myofibroblast may play a key role in this annular remodeling in DCM.

This chapter is the third of three chapters (Chapters 15-17) analyzing the mitral valve in the context of “functional” mitral regurgitation and dilated cardiomyopathy. The topic of examining valves in the setting of various disease states continues in the next chapter with a study of mitral valve wound healing in response to iatrogenic injury.

REFERENCES

1. Otsuji Y, Kumanohoso T, Yoshifuku S, Matsukida K, Koriyama C, Kisanuki A, Minagoe S, Levine R, Tei C. Isolated annular dilation does not usually cause important functional mitral regurgitation: comparison between patients with lone atrial fibrillation and those with idiopathic or ischemic cardiomyopathy. *J Am Coll Cardiol.* 2002;39(10):1651-1656.
2. Aikawa K, Sheehan F, Otto C, Coady K, Bashein G, Bolson E. The severity of functional mitral regurgitation depends on the shape of the mitral apparatus: a three-dimensional echo analysis. *J Heart Valve Dis.* 2002;11(5):627-636.
3. Timek TA, Dagum P, Lai DT, Liang D, Daughters GT, Ingels NB, Miller DC. Pathogenesis of mitral regurgitation in tachycardia-induced cardiomyopathy. *Circulation.* 2001;104(12 Suppl 1):147-53.
4. He S, Lemmon JJ, Weston M, Jensen M, Levine R, Yoganathan A. Mitral valve compensation for annular dilatation: in vitro study into the mechanisms of functional mitral regurgitation with an adjustable annulus model. *J Heart Valve Dis.* 1999;8(3):294-302.
5. Timek TA, Dagum P, Lai DT, Liang D, Daughters GT, Tibayan F, Ingels NB, Miller DC. Tachycardia-induced cardiomyopathy in the ovine heart: Mitral annular dynamic three-dimensional geometry. *J Thorac Cardiovasc Surg.* 2003;125(2):315-324.
6. Dal-Bianco JP, Aikawa E, Bischoff J, Guerrero JL, Handschumacher MD, Sullivan S, Johnson B, Titus JS, Iwamoto Y, Wylie-Sears J, Levine RA, Carpentier A. Active adaptation of the tethered mitral valve: insights into a compensatory mechanism for functional mitral regurgitation. *Circulation.* 2009;120(4):334-342.
7. Stephens EH, Timek TA, Daughters GT, Kuo JJ, Patton AM, Baggett LS, Ingels NB, Miller DC, Grande-Allen KJ. Significant changes in mitral valve leaflet matrix composition and turnover with tachycardia-induced cardiomyopathy. *Circulation.* 2009;120(11 Suppl):S112-119.
8. Koullias GJ, Korkolis DP, Ravichandran P, Psyrris A, Hatzaras I, Elefteriades JA. Tissue microarray detection of matrix metalloproteinases, in diseased tricuspid and bicuspid aortic valves with or without pathology of the ascending aorta. *Eur J Cardiothorac Surg.* 2004;26(6):1098-1103.
9. Rabkin-Aikawa E, Farber M, Aikawa M, Schoen FJ. Dynamic and reversible changes of interstitial cell phenotype during remodeling of cardiac valves. *J Heart Valve Dis.* 2004;13(5):841-847.
10. Tomasek JJ, Gabbiani G, Hinz B, Chaponnier C, Brown RA. Myofibroblasts and mechano-regulation of connective tissue remodelling. *Nat Rev Mol Cell Biol.* 2002;3(5):349-363.
11. Rabkin E, Aikawa M, Stone JR, Fukumoto Y, Libby P, Schoen FJ. Activated interstitial myofibroblasts express catabolic enzymes and mediate matrix remodeling in myxomatous heart valves. *Circulation.* 2001;104(21):2525-2532.

12. Wang J, Chen H, Seth A, McCulloch CA. Mechanical force regulation of myofibroblast differentiation in cardiac fibroblasts. *Am J Physiol Heart Circ Physiol*. 2003;285(5):H1871-1881.
13. Messier RH, Jr., Bass BL, Aly HM, Jones JL, Domkowski PW, Wallace RB, Hopkins RA. Dual structural and functional phenotypes of the porcine aortic valve interstitial population: characteristics of the leaflet myofibroblast. *J Surg Res*. 1994;57(1):1-21.
14. Merryman WD, Huang HY, Schoen FJ, Sacks MS. The effects of cellular contraction on aortic valve leaflet flexural stiffness. *J Biomech*. 2006;39(1):88-96.
15. Timek TA, Lai DT, Dagum P, Tibayan F, Daughters GT, Liang D, Berry GJ, Miller DC, Ingels NB, Jr. Ablation of mitral annular and leaflet muscle: effects on annular and leaflet dynamics. *Am J Physiol Heart Circ Physiol*. 2003;285(4):H1668-1674.
16. Tibayan FA, Lai DT, Timek TA, Dagum P, Liang D, Daughters GT, Ingels NB, Miller DC. Alterations in left ventricular torsion in tachycardia-induced dilated cardiomyopathy. *J Thorac Cardiovasc Surg*. 2002;124(1):43-49.
17. Glasson JR, Green GR, Nistal JF, Dagum P, Komeda M, Daughters GT, Bolger AF, Foppiano LE, Ingels NB, Jr., Miller DC. Mitral annular size and shape in sheep with annuloplasty rings. *J Thorac Cardiovasc Surg*. 1999;117(2):302-309.
18. Glasson JR, Komeda M, Daughters GT, Foppiano LE, Bolger AF, Tye TL, Ingels NB, Jr., Miller DC. Most ovine mitral annular three-dimensional size reduction occurs before ventricular systole and is abolished with ventricular pacing. *Circulation*. 1997;96(9 Suppl):II-115-122.
19. Ormiston J, Shah P, Tei C, Wong M. Size and motion of the mitral valve annulus in man. II. Abnormalities in mitral valve prolapse. *Circulation*. 1982;65(4):713-719.
20. Brock R. The surgical and pathological anatomy of the mitral valve. *Br Heart J*. 1952;14(4):489-513.
21. Gorman JH, 3rd., Jackson BM, Gorman RC, Kelley ST, Gikakis N, Edmunds LH, Jr. Papillary muscle discoordination rather than increased annular area facilitates mitral regurgitation after acute posterior myocardial infarction. *Circulation*. 1997;96(9 Suppl):II-124-127.
22. Wilson J, Douglas P, Hickey W, Lanoce V, Ferraro N, Muhammad A, Reichek N. Experimental congestive heart failure produced by rapid ventricular pacing in the dog: cardiac effects. *Circulation*. 1987;75(4):857-867.
23. Riegger A, Liebau G. The renin-angiotensin-aldosterone system, antidiuretic hormone and sympathetic nerve activity in an experimental model of congestive heart failure in the dog. *Clin Sci (Lond)*. 1982;62(5):465-469.
24. Timek TA, Lai DT, Dagum P, Liang D, Daughters GT, Ingels NB, Miller DC. Mitral leaflet remodeling in dilated cardiomyopathy. *Circulation*. 2006;114(1 Suppl):I518-523.

RICE UNIVERSITY

**Composition, Turnover, and Mechanics of Extracellular
Matrix in Developing, Aging, and Pathological Valves**

for application in the design of age-specific tissue engineered heart valves

by
Elizabeth Humes Stephens

May 2010

VOLUME III

Chapter 18: Extracellular Matrix Remodeling in Response to Mitral Leaflet Injury

This chapter continues the topic of examining valves in the setting of various disease states with a study of mitral valve wound healing in response to iatrogenic injury.

ABSTRACT

Background: The details of valvular leaflet healing following valvuloplasty and leaflet perforation from endocarditis are poorly understood. In this study, the synthesis and turnover of valvular extracellular matrix due to healing of a critical sized wound was investigated.

Methods: 29 sheep were randomized to either CTRL (n=11) or HOLE (n=18), in which a 2.8-4.8 mm diameter hole was punched in the posterior mitral leaflet. After 12 weeks, posterior leaflets were harvested and histologically stained to localize extracellular matrix components. Immunohistochemistry was also performed to assess matrix components and markers of matrix turnover. A semi-quantitative grading scale was used to quantify differences between HOLE and CTRL.

Results: After 12 weeks the hole diameter was reduced by $71.3 \pm 25.8\%$ ($p < 0.001$). Areas of remodeling surrounding the hole contained more activated cells, greater

expression of proteoglycans and markers of matrix turnover (prolyl 4-hydroxylase, metalloproteases, and lysyl oxidase, each $p \leq 0.025$), along with fibrin accumulation and neovascularization. Two distinct remodeling regions were evident surrounding the hole, one directly bordering the hole rich in versican and hyaluronan and a second adjacent region with abundant collagen and elastic fiber turnover. The remodeling also caused reduced delineation between valve layers ($p=0.002$), more diffuse staining of matrix components and markers of matrix turnover ($p < 0.001$), and disruption of the collagenous fibrosa.

Conclusions: Acute valve injury elicited distinct, heterogeneous alterations in valvular matrix composition and structure, resulting in partial wound closure. Because these changes could also affect leaflet mechanics and valve function, it will be important to determine their impact on healing wounds.

The work contained in this chapter is under preparation for submission to *Journal of Thoracic and Cardiovascular Surgery*.

INTRODUCTION

The restoration of valvular integrity after valve perforation secondary to endocarditis or surgical procedures depends on proper valvular wound healing. Abnormal tissue growth during healing can lead to stenosis¹ and inadequate mechanical integrity of the wound can lead to valve failure.² Proper valve healing is especially important given that valve repair is generally preferred over replacement, particularly in pediatrics.³ While much is known regarding wound repair in other connective tissues, given the relatively limited vasculature in valves⁴ and large proportion of extracellular matrix (ECM) relative to cells makes valvular wound healing unique.⁵ Furthermore, valvular wound healing occurs in the presence of constant mechanical stresses on the wound site, including tension, compression, bending, and shear, that could disrupt the healing process. Previous investigations of valvular wound healing have been limited to the pathology of slicing injury and sutures in valves,^{5,6} denudation injury in a valve organ culture system,⁷ and a “scratch” wound in cultured valve cells.⁸⁻¹⁰ While hole injury is routinely used to study wound healing in other tissues,¹¹ there have been no studies, however, that examine valvular healing after the creation of a discrete mechanical hole. The aforementioned previous studies in valvular wound healing studies important insight into the formation and cellular makeup of different granulation tissues, but the role of specific ECM components in valve wound healing remains unknown.

The ECM is integrally involved in valve maintenance and function both biologically and mechanically. Turnover of collagen, which provides the valve with tensile strength,¹² occurs throughout life within normal valves¹³ and is altered in valve disease.¹⁴⁻¹⁶ Moreover, collagen synthesis within valves has been linked to mechanical

stimulation¹⁷ and therefore would likely respond to altered strain magnitudes around a wound site. Proteoglycans (PGs) and glycosaminoglycans (GAGs) not only contribute to the material behavior of the valve,¹⁸ but are also responsive to mechanical stimulation.¹⁹ PGs and GAGs are also involved in a number of cellular processes required for wound healing including cell growth and migration, growth factor regulation, and collagen fibrillogenesis.²⁰ Because ECM undergoes mechanobiological regulation, is involved in processes necessary to wound healing, and contributes to valve function, it was hypothesized that the ECM would be altered following acute valve injury and that this remodeling would promote the restoration of tissue integrity.

Given the clinical relevance of understanding valve wound repair, and the paucity of *in vivo* valve wound repair experiments, in this study a 2.8-4.8 mm diameter hole was punched in the center of the posterior leaflet of the mitral valve (PML) of sheep. Unlike a slicing injury or suture, a hole-punch creates a large defect that may not heal completely and hence could be considered representative of an exacerbated acute valve injury complete with altered hemodynamics. After 12 weeks, sections were taken from PML in the region of the hole-punch. Histology and immunohistochemistry on these sections was used to assess the quantity and distribution of PGs, GAGs, collagen, enzymes regulating matrix turnover, regional cell density, and the layered microstructure within the PML.

METHODS

Experimental Animal Protocol

All animals received humane care in accordance with the guidelines developed by the National Institutes of Health (US Department of Health and Human Services NIH Publ. 85-23, Revised 1985). Twenty-nine 1-2 year-old sheep were randomized to either control (CTRL, n=11) or experimental (HOLE, n=18) groups. A left thoracotomy and atriotomy were employed to access the mitral valve, and after establishment of cardiopulmonary bypass a 2.8-4.8 mm diameter hole was created in the central scallop of the PML of HOLE animals with an aortic hole-puncher.²¹ CTRL animals underwent the exact same operation without the hole-punch. On a weekly basis, a blinded echocardiographer performed transthoracic echocardiography and graded the MR on the basis of color Doppler regurgitant jet extent and width.²² Animals were monitored daily for signs of distress after the hole-punch procedure, but did not show any. After 12 weeks, the upper bound of range for time required for ovine valve wound healing,⁵ the MVs were harvested and fixed in formalin.

Histology and Immunohistochemistry

The PML was isolated and a 5 mm wide strip cut from annulus to free edge (Fig. 18-1A), embedded in paraffin, and sectioned to a thickness of five microns. Movat pentachrome stained sections were used to assess the characteristics of layer delineation, collagen content, and collagen diffusivity (presence of saffron-staining collagen outside of fibrosa). Masson's trichrome stain was performed to assess fibrin accumulation and neovascularization. Picrosirius red staining was performed to examine the collagen

content and alignment and infer type of collagen (red=collagen I, yellow/green=reticular collagen III²³). Immunohistochemistry (IHC) was also performed on CTRL and HOLE

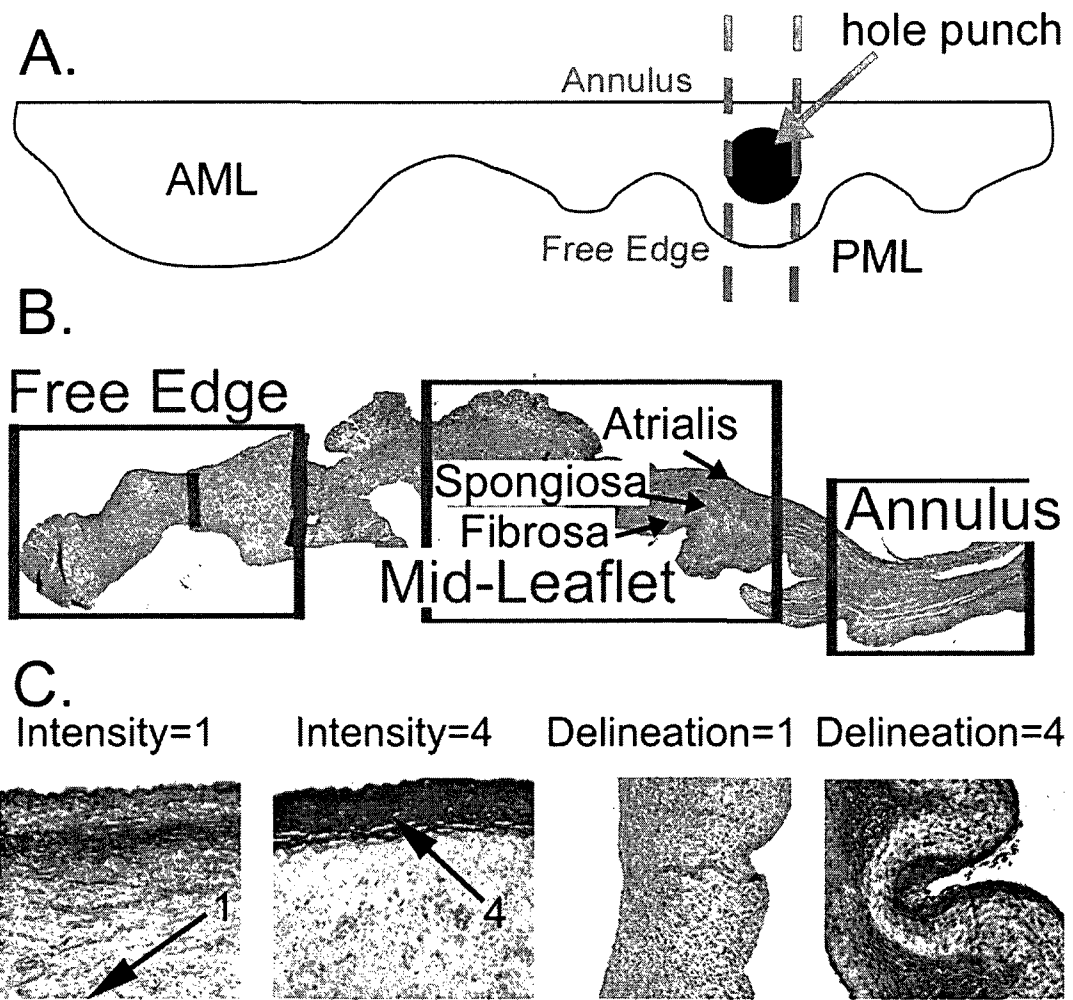


Fig. 18-1: A) Diagram showing location from which PML cross-sections were taken. AML indicates anterior leaflet of MV. Sections were cut from annulus to free edge, as indicated by the dashed lines. B) Anatomy of the normal MV posterior leaflet illustrating valve regions and histological layers in a Movat-stained section. C) Examples of grading rubrics for the characteristics staining intensity and delineation. For the characteristic delineation, “1” indicates little differentiation in intensity between layers. “4” indicates maximum for each characteristic. Separate rubrics were made for the delineation of different regions of the valve (annulus, mid-leaflet, and free edge).

with hole-punch diameters of 4-4.8 mm to demonstrate the PGs decorin and biglycan (DCN, BGN, courtesy of Dr. Larry Fisher, NIH), versican (VC, Seikagaku, Japan), and the glycosaminoglycan (GAG) hyaluronan (HA, Seikagaku); elastic fiber-related proteins elastin, fibrillin (both Abcam, Cambridge, MA), and lysyl oxidase (LOX, Imgenex, San Diego, CA, involved in crosslinking both collagen and elastin); collagen type III (Col III, courtesy of Larry Fisher, NIH) which tends to be dysregulated in remodeling tissues;²⁴ markers of collagen synthesis prolyl 4-hydroxylase (P4H, Chemicon, Temecula, CA) and heat shock protein-47 (HSP47, Abcam); markers of matrix degradation matrix metalloproteases (MMPs)-1, -2, -9, and -13 (all Assay Designs, Ann Arbor, MI, except MMP13, Chemicon); and markers of valve cell activation smooth muscle alpha-actin (SMaA, Dakocytomation, Denmark) and non-muscle myosin (NMM, Covance, Berkeley, CA). A semi-quantitative grading scale from 0 to 4 was used to assess staining intensity and delineation of stain between valve layers for all markers except SMaA and NMM in which staining was very localized. Grading was performed both for the leaflet as a whole and for the specific regions of the annulus, mid-leaflet/hole-punch region, and free edge (Fig. 18-1B, C). The hole-punch region was further subdivided into the region immediately proximal (closer to the valve annulus) and distal (closer to the free edge) to the hole.

Assessment of Cell Density, Leaflet Thickness, and Hole Closure

Cell density was determined by counting valvular interstitial cell nuclei in images (captured using a Leica DM LS2 microscope (Wetzlar, Germany)) using Image Pro software (Media Cybernetics, Bethesda, MD). Regions assessed included the annulus,

mid-leaflet, and the regions proximal and distal to the hole. Valve thickness was evaluated using Image Pro software for each of the above regions as well as the free edge. Percent hole closure (% closure) was calculated as the difference between the original hole diameter (diameter of aortic hole-punch) and final hole diameter normalized to the original hole diameter. The final hole diameter was measured as the distance between the leaflet tissues proximal and distal to the hole on the paraffin embedded tissue blocks (see Fig. 18-2A).

Statistical Analysis

Data are presented as mean and standard error of the mean, unless otherwise noted. Multifactorial analysis of variance (ANOVA) was performed using SigmaStat (SPSS, Chicago, IL), as described in Chapter 4. Correlations were calculated using Pearson and Spearman tests, as described in Chapter 5, and significance was adjusted for the number of correlations tested.

RESULTS

Remodeling in Thickened, Cell-Dense Areas Reduced Hole Diameter

MR was greater in HOLE vs. CTRL throughout the study (MR at 12 weeks: CTRL 0.5 ± 0.04 vs. HOLE 2.6 ± 0.05 , $p < 0.001$). Substantial matrix production occurred around the hole-punch reducing the hole diameter by $71.3 \pm 1.4\%$ from its original dimensions ($p < 0.001$, Fig. 18-2A). These areas of remodeling were $228 \pm 60\%$ thicker in the region proximal to the hole and $219 \pm 48\%$ thicker in the region distal to the hole

compared to adjacent leaflet regions (Fig. 18-2B). Fibrin accumulation and neovascularization was found adjacent to the hole (Fig. 18-2C-F). The thickness of the

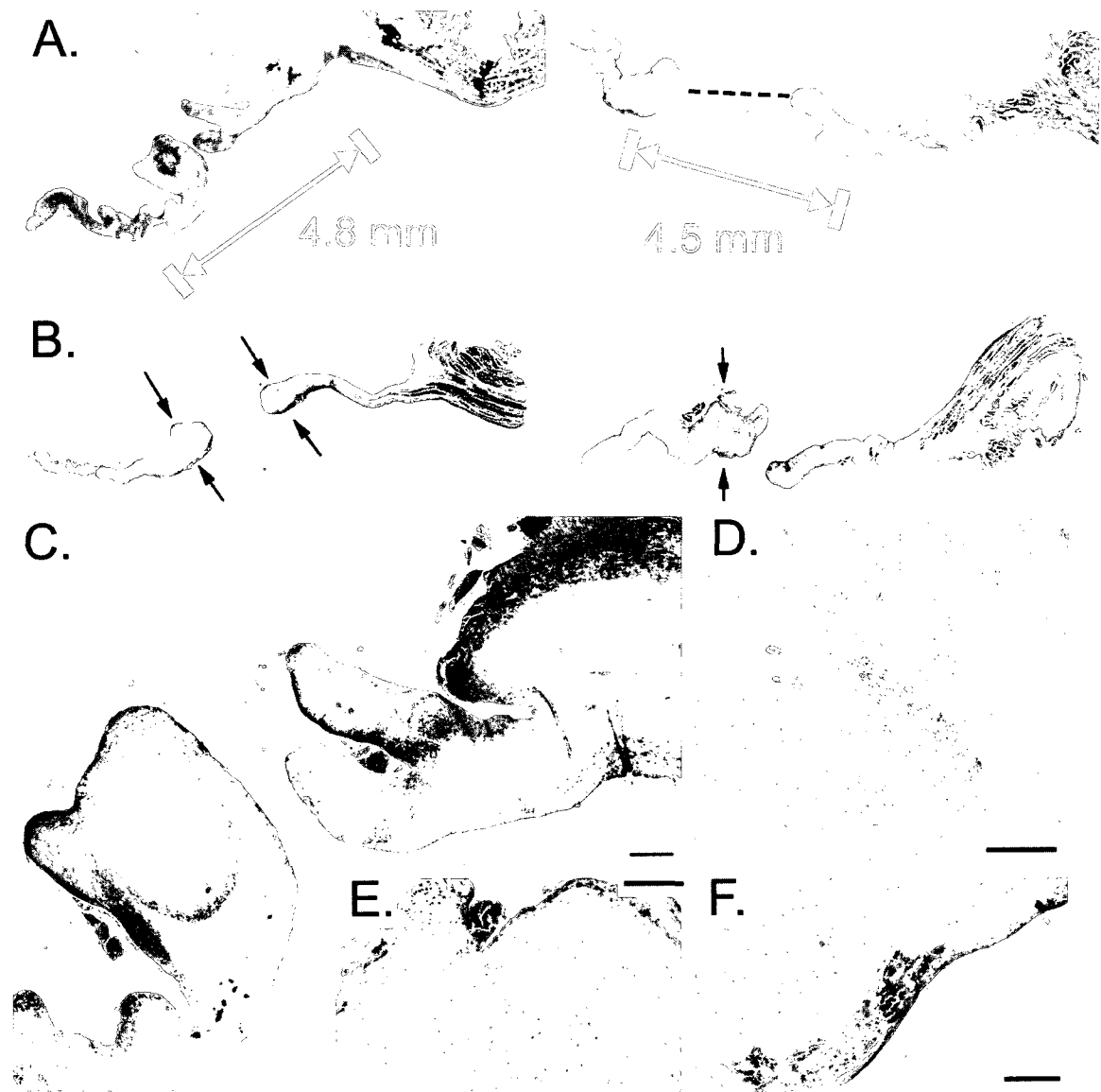


Fig. 18-2: A) Substantial areas of remodeling significantly decreased hole diameter (Movat pentachrome stain). Red block markers spanned by arrows indicate initial diameter of hole-punch; the black dashed line on the right tissue section indicates the measurement made to determine the final hole diameter. B) Areas surrounding hole-punch show significant thickening as indicated by arrows (Movat pentachrome stain). Thickening was not always symmetric around the hole, as demonstrated by right image. C) Masson's trichrome stain demonstrating accumulation of fibrin around hole. D-F) Masson's trichrome stain illustrating examples of neovascularization and fibrin accumulation adjacent to hole. Scale bars indicate 200 μm.

mid-leaflet/hole region of HOLE and CTRL positively correlated with average MR (average of MR at 6-week and 12-week time points, $r=0.54$, $p=0.007$). Average MR positively correlated with final hole diameter ($r=0.55$, $p=0.024$ (trend), see Fig. 18-3A) and, for samples with hole diameters of 4-4.8 mm, inversely correlated with % closure

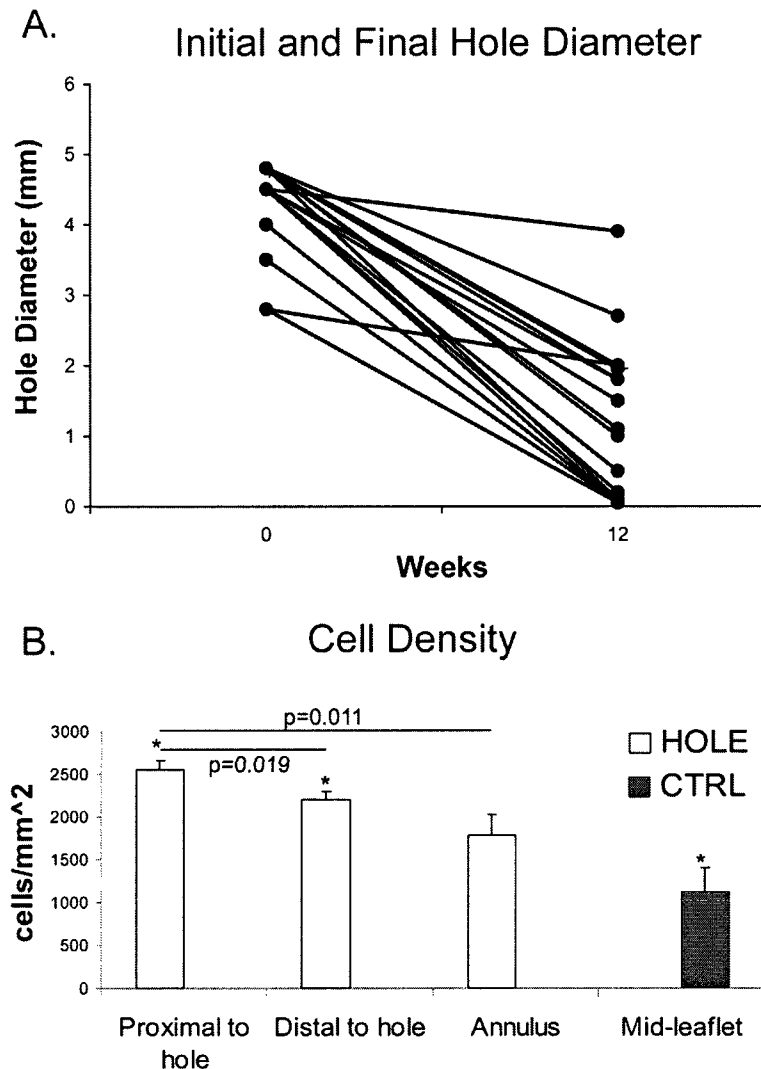


Fig. 18-3: A) Initial and final hole diameters for HOLE samples. B) Cell density was increased in areas of remodeling compared to the annulus of the same HOLE leaflet as well as compared to CTRL. $*=p<0.001$. Error bars indicate the standard error of the mean.

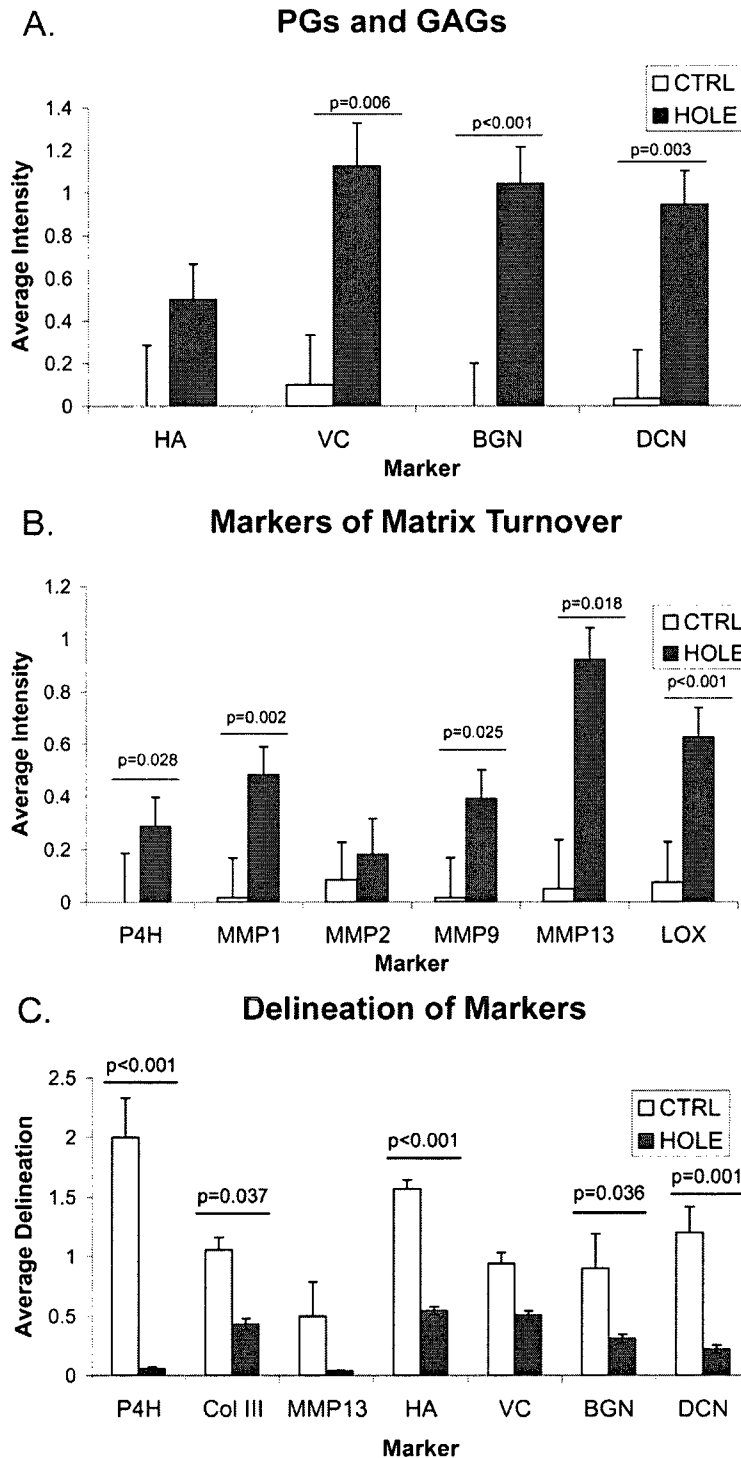


Fig. 18-4: A) Intensity of PG and GAG staining in region around hole-punch in HOLE PML versus comparable regions in CTRL. Overall $p<0.001$. B) Intensity of collagen-related marker staining in regions around hole-punch in HOLE PML versus comparable regions in CTRL. Overall $p<0.001$. C) Average delineation of markers between layers in HOLE PML compared to CTRL. Overall $p<0.001$. Error bars indicate the standard error of the mean.

($r=-0.66$, $p=0.011$). Within PMLs with hole diameters of 4-4.8 mm, cell density in the region proximal to the hole was greater than the region distal to the hole ($p=0.019$) and the annular region ($p=0.011$, Fig. 18-3B). The regions proximal and distal to the hole also had considerably higher cell densities than the mid-leaflet of CTRL PMLs ($p<0.001$).

Matrix Turnover and Cell Activation

Compared to the equivalent region in CTRL PMLs, the hole-punch region showed significantly greater expression of VC, BGN, DCN and HA (each $p\leq 0.006$, Fig. 18-4A) and markers of matrix metabolism P4H, the MMPs (1, 2, 9, 13), and LOX (each $p\leq 0.025$, Fig. 18-4B). NMM and SMaA often co-localized with the MMPs, suggesting an activated myofibroblast phenotype.

Strong and localized staining of MMPs was also noted outside the hole-punch region, such as in the atrialis layer of the annulus of many HOLE PMLs. The free edge of HOLE also showed localized expression of several matrix turnover enzymes including MMPs, most commonly MMP1 and MMP9. Several samples also demonstrated a localized increase in elastin (co-localized with MMP9 and LOX) in the leaflet free edge.

Patterns of Remodeling

Two distinct regions, each containing different ECM, were present within the remodeling tissue surrounding the hole-punch. Region 1 (R1) directly bordered the hole, whereas region 2 (R2) was adjacent to R1 but located slightly further from the hole–

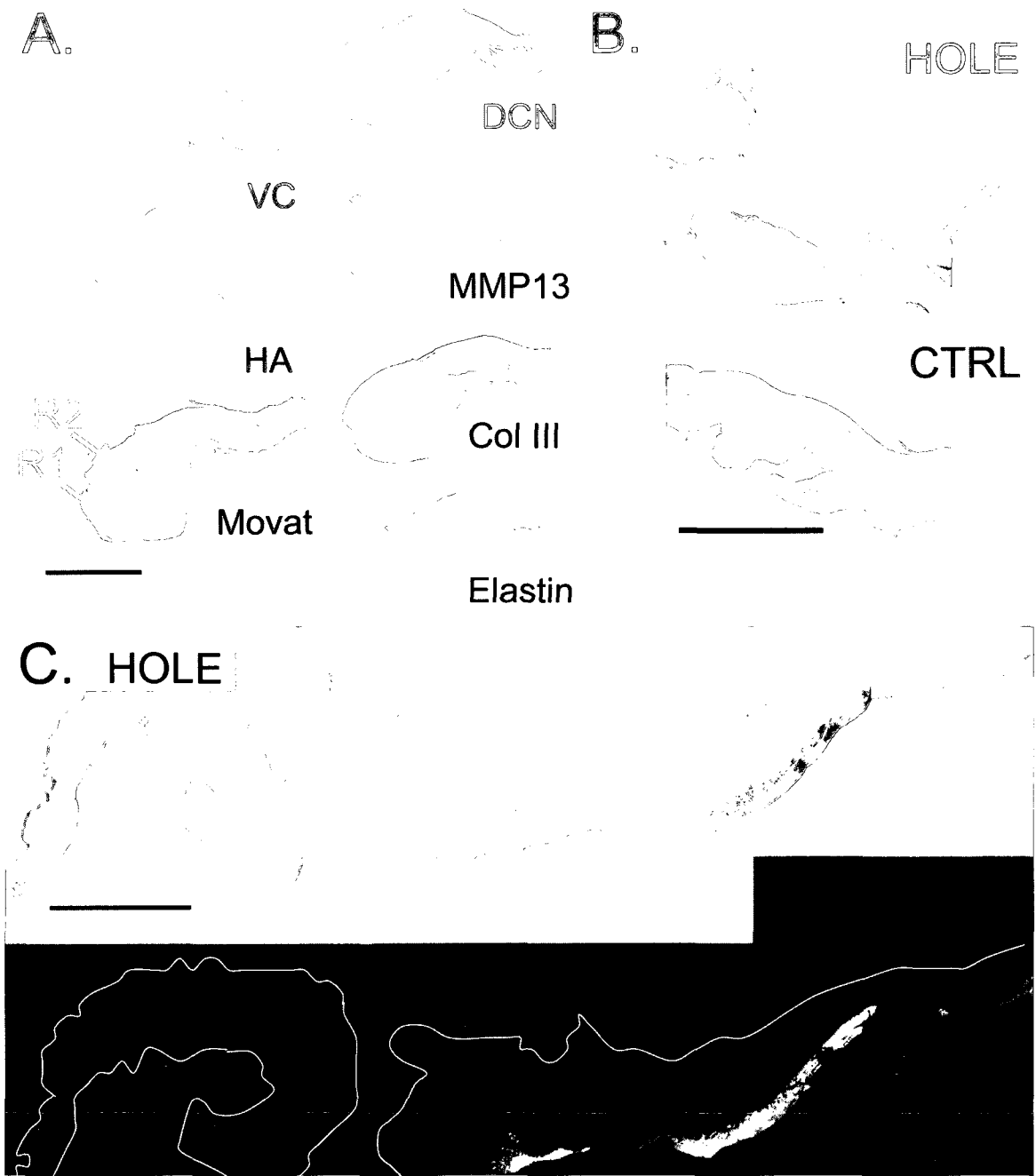


Fig. 18-5: A) Two regions of remodeling (R1, R2) were evident as indicated by the red arrows: R1=immediately adjacent to the hole, rich in VC, HA, and demonstrating alcian-blue staining in Movat-stained sections; R2=located interior to R1 relative to the hole-punch, rich in DCN, MMPs, Col III, and elastin. B) Decreased delineation (indicated by red arrow) in HOLE PML compared to CTRL. C) Visualization of picosirius red-stained tissue under polarized light demonstrates disruption of collagen backbone in HOLE PML. Scale bars for all images represent 1 mm.

punch (Fig. 18-5A). R1 was apparent in Movat-stained sections as a pocket of alcian blue staining, which was predominantly composed of VC and HA (Fig. 18-5A). VC was primarily localized to R1 while HA was more diffusely present. In contrast, R2 showed strong staining for MMPs, DCN, and to a lesser extent BGN. Elastin staining in R2 was consistently co-localized with MMP9 and LOX, suggesting elastic fiber remodeling.

Compared to samples with $\leq 60\%$ closure (n=4), those with $>90\%$ closure (n=5) had more P4H, MMP13, and Col III ($\leq 60\%$ closure 0.95 ± 0.09 , $>90\%$ closure 1.39 ± 0.11 , $p=0.009$), less PG and HA ($\leq 60\%$ closure 1.26 ± 0.07 , $>90\%$ closure 0.77 ± 0.11 , $p=0.002$), and less delineation of PGs and HA staining in the hole region ($\leq 60\%$ closure 0.64 ± 0.08 , $>90\%$ closure 0.20 ± 0.12 , $p=0.007$).

Structural and Global Leaflet Changes

The hole-punch also affected the layered structure of the PML. In the hole region, Movat-stained sections showed decreased delineation between layers (HOLE 0.6 ± 0.3 , CTRL 1.9 ± 0.3 , $p=0.002$, Fig. 18-5B) and staining for PG, HA, P4H, Col III, and MMP13 was more diffuse in the HOLE samples (Fig. 18-4C, together $p < 0.001$). Visualization of picrosirius red-stained tissues under polarized light illustrated disruption of the collagenous fibrosa in HOLE PML (Fig. 18-5C). Matrix changes in the HOLE PML, however, were not limited to the immediate vicinity of the hole-punch. PGs, Col III, and total collagen (Movat) were more diffusely present throughout the leaflet in HOLE vs. CTRL (HOLE 0.7 ± 0.1 , CTRL 1.1 ± 0.1 , $p=0.004$), and there was a reduction in overall BGN, DCN, and elastin staining (HOLE 1.39 ± 0.03 , CTRL 1.55 ± 0.05 , $p=0.037$) in HOLE vs. CTRL.

DISCUSSION

After 12 weeks, the hole-punch-wounded PML demonstrated significant remodeling that substantially reduced the hole diameter and thickened the leaflet adjacent to the hole. Areas of remodeling contained elevated densities of activated cells, abundant PGs, greater ECM turnover, fibrin accumulation, and neovascularization. Samples with greater hole closure displayed greater collagen turnover and less expression of PGs and HA. Two distinct remodeling regions surrounded the hole-punch, one directly bordering the hole that was rich in VC and HA, and a second adjacent region rich in enzymes regulating collagen and elastic fiber turnover. The remodeling also affected leaflet structure, causing reduced delineation between valve layers and disruption of the collagenous fibrosa.

Increased Collagen Turnover in Hole-Punch Region

The increase in markers of collagen synthesis (P4H, LOX), collagen degradation (MMPs), and the PGs BGN and DCN (given their role in collagen fibrillogenesis²⁰) in the mid-leaflet/hole portion of HOLE compared to CTRL indicates increased collagen fiber turnover in the hole-punch region. Increased collagen turnover is further evidenced by co-localization of markers of collagen synthesis and degradation, the positive correlation between P4H and Movat saffron-staining collagen, and the disruption of the collagen-rich fibrosa evident in picrosirius red stained sections of HOLE leaflets. Such collagen turnover has been shown to be present to a limited extent in normal porcine valves throughout development and aging,¹³ is increased in other types of non-acute valve

injury,²⁵ and appears greatly increased in this case of injury. Both MMPs and DCN have been reported to be important to dermal wound healing, and in particular scarless wound healing.²⁶⁻²⁸ The localized increase in MMPs in the annulus atriialis and free edge of HOLE found in this study likely reflect altered stress in these regions.

Cells in Remodeling Tissue Show an Activated Phenotype

The co-localization of NMM and SM α A with MMPs in the areas of remodeling suggests that these cells are myofibroblasts. These results are consistent with reports of SM α A expression by cells at the cut edges of dissected portions of the MV cultured in an organ system⁷ as well as SM α A expression in granulation tissue of a MV slice wound.⁵ Elevated SM α A expression has also been reported in chronic valve diseases as well as throughout development.^{16, 29} Therefore, the expression of SM α A by valvular cells appears to be necessary for normal valve growth and acute repair, but is also involved in remodeling responses to chronic or acute injury.

The increased cell density found surrounding the wound in this study was also observed in the slice injury study⁵ and increased cell proliferation was reported at the site of dissection in the organ culture study.⁷ This evidence for cell proliferation, in conjunction with data regarding cell migration in valve injury^{7, 30} suggests that the greater cell density local to the wound found in this study could be due to both cell migration and proliferation. It is also interesting to note that in the suture wound study healing started on the annular side of the injury and was delayed in the free edge.⁶ Correspondingly, we found significantly greater abundance of cells on the proximal side of the wound (closer

to the annulus) compared to the distal side. Areas of remodeling also demonstrated fibrin accumulation and neovascularization, consistent with previous reports.⁵

Distinct Areas of Remodeling Surrounding Hole-Punch

The existence of two regions surrounding the hole-punch (the VC/HA-rich R1 region bordering the hole and the adjacent R2 region of collagen and elastic fiber remodeling) suggests that remodeling occurs in two separate or at least temporally distinct processes. The distinct nature of these processes is supported by the strong segregation of matrix and enzyme expression. These regions are also consistent with previous studies of valve slice wounds in which two types of granulation tissue were reported, a “fibrous” variety and a “myxoid” variety that appeared to contain more PGs.⁵ The two regions demonstrated here are also reminiscent of findings in artery-vein anastomoses in which PG staining was found closer to the lumen while collagen and elastin were found deeper within the intima.³¹ HA and VC have been reported as principal components of the provisional matrix in dermal wounds^{32, 33} and elastin has also been reported to be present in dermal wounds,³⁴⁻³⁶ although neither in those studies nor in the anastomoses study³¹ were distinct regions reported. Given the myriad roles of VC and HA in cell migration,^{37, 38} their presence in the R1 remodeling region may facilitate the migration of different cell types during the repair process.⁵ Indeed, a generalized model of wound healing postulates that granulation tissue composed of HA and fibrin forms a temporary matrix into which fibroblasts and endothelial cells migrate.^{39, 40}

Characteristics of Greater Wound Closure

HOLE leaflets with greater wound closure showed more characteristics of collagen fiber turnover, less expression of hydrated PGs and GAGs, and less delineation of PGs and HA staining in the hole-punch region. One interpretation for these results could be that collagen turnover promotes wound repair better than hydrated PGs and HA; there is debate in the dermal wound literature regarding whether various PGs inhibit or promote wound healing.³² In light of the discussion of R1 and R2 above, another interpretation could be that the wounds showing greater closure are more mature, i.e., they have transitioned from a preliminary HA/VC matrix (R1) to collagen remodeling (R2). This interpretation would be consistent with previous reports of PGs increasing in abundance in valve slice wounds up to 12 weeks and collagen bundle formation increasing through 18 weeks.⁵

Limitations

The authors acknowledge that there were several limitations to this analysis. In the future, it will be important to examine the temporal changes in the distribution of the different ECM components and unique remodeling regions first addressed in this study. It should also be noted that the healing process in diseased valve tissue may be significantly different from that of normal tissues, both in terms of time course and the nature of ECM remodeling. In terms of the relevance to valve leaflet perforation in endocarditis, this model lacks the bacterial component and immunological sequelae of endocarditis. In the histological analysis, the main limitation was the subjective nature of

grading, which was combated by the use of a grading rubric and evaluating all leaflets stained for a given marker together. Variability in staining intensities between batches of IHC was avoided by staining all PML together. Although some variability remained, statistically significant differences between groups were found. Furthermore, subsequent studies in our lab have shown this semi-quantitative grading method yields results comparable to those performed using computerized methods.

The use of a hole-punch to create the acute injury, standard in dermal wound studies,⁴¹ has multiple benefits, but also some limitations. One advantage of the hole-punch injury was it simulated an exacerbated wound complete with MR. The circular geometry of the hole-punch facilitated quantifying the amount of remodeling tissue produced, but does not directly mimic the types of incisions used in valvuloplasties and may result in different forces being applied to the tissue. Future studies could further investigate the interaction of the acute injury wound healing process with the altered hemodynamics such a defect creates. Another limitation was that the final hole diameter was measured from the tissue blocks, as opposed to the intact PMLs. Furthermore, percentage closure is a limited measure of the adequacy of healing (and may simply reflect differences in the speed of healing), as successful healing has a number of components including restoration of the mechanical integrity of the tissue. Regardless, these measurements did provide a useful overview of the changes in HOLE animals.

CONCLUSIONS

This study provides a detailed characterization of valvular ECM remodeling in response to acute injury in valves in terms of a wide range of individual matrix proteins,

as well as markers of matrix synthesis and degradation. Distinct remodeling processes, including one rich in HA and VC and another related to collagen and elastic fiber turnover, were noted and may prove necessary for the restoration of valve integrity after acute injury.

This chapter, which addressed mitral valve wound healing in response to iatrogenic injury, continued the topic of examining valves in the setting of various disease states. In the next chapter, the disease of study is myxomatous mitral valve disease. In that chapter, the potential role of the mitogen-activated protein kinase (MAPK) signaling pathway in myxomatous mitral valve disease is analyzed.

REFERENCES

1. Dekker A, Black H, Von Lichtenberg F. Mitral valve restenosis: a pathologic study. *J Thorac Cardiovasc Surg.* 1968;55(3):434-446.
2. Gillinov A, Cosgrove D, Lytle B, Taylor P, Stewart R, McCarthy P, Smedira N, Muehrcke D, Apperson-Hansen C, Loop F. Reoperation for failure of mitral valve repair. *J Thorac Cardiovasc Surg.* 1997;113(3):467-473.
3. Chauvaud S, Fuzellier J, Houel R, Berrebi A, Mihaileanu S, Carpentier A. Reconstructive surgery in congenital mitral valve insufficiency (Carpentier's techniques): long-term results. *J Thorac Cardiovasc Surg.* 1998;115(1):84-92.
4. I-Ida T, Tamura K, Tanaka S, Asano G. [Blood vessels in normal and abnormal mitral valve leaflets]. *J Nippon Med Sch.* 2001;68(2):171-180.
5. Tamura K, Jones M, Yamada I, Ferrans VJ. Wound healing in the mitral valve. *J Heart Valve Dis.* 2000;9(1):53-63.
6. Tamura K, Murakami M, Washizu M. Healing of wound sutures on the mitral valve: an experimental study. *Gen Thorac Cardiovasc Surg.* 2007;55(3):98-104.
7. Lester WM, Damji A, Gedeon I, Tanaka M. Interstitial cells from the atrial and ventricular sides of the bovine mitral valve respond differently to denuding endocardial injury. *In Vitro Cellular & Developmental Biology - Animal.* 1993;29A:41-50.
8. Durbin A, Nadir N, Rosenthal A, Gottlieb AI. Nitric oxide promotes in vitro interstitial cell heart valve repair. *Cardiovasc Pathol.* 2005;14(1):12-18.
9. Fayet C, Bendeck M, Gottlieb A. Cardiac valve interstitial cells secrete fibronectin and form fibrillar adhesions in response to injury. *Cardiovasc Pathol.* 2007;16(4):203-211.
10. Gottlieb A, Rosenthal A, Kazemian P. Fibroblast growth factor 2 regulation of mitral valve interstitial cell repair in vitro. *J Thorac Cardiovasc Surg.* 2002;124(3):591-597.
11. Bedelbaeva K, Snyder A, Gourevitch D, Clark L, Zhang XM, Lefterovich J, Cheverud JM, Lieberman P, Heber-Katz E. Lack of p21 expression links cell cycle control and appendage regeneration in mice. *Proc Natl Acad Sci U S A.* 2010;107(13):5845-5850.
12. Sacks M, Yoganathan A. Heart valve function: a biomechanical perspective. *Philos Trans R Soc Lond B Biol Sci.* 2008;363(1502):1369-1391.
13. Stephens EH, Grande-Allen KJ. Age-related changes in collagen synthesis and turnover in porcine heart valves. *Journal of Heart Valve Disease.* 2007;16(6):672-682.
14. Fondard O, Detaint D, Iung B, Choqueux C, Adle-Biassette H, Jarraya M, Hvass U, Couetil JP, Henin D, Michel JB, Vahanian A, Jacob MP. Extracellular matrix remodelling in human aortic valve disease: the role of matrix metalloproteinases and their tissue inhibitors. *Eur Heart J.* 2005;26(13):1333-1341.

15. Koullias GJ, Korkolis DP, Ravichandran P, Psyrris A, Hatzaras I, Elefteriades JA. Tissue microarray detection of matrix metalloproteinases, in diseased tricuspid and bicuspid aortic valves with or without pathology of the ascending aorta. *Eur J Cardiothorac Surg.* 2004;26(6):1098-1103.
16. Rabkin E, Aikawa M, Stone JR, Fukumoto Y, Libby P, Schoen FJ. Activated interstitial myofibroblasts express catabolic enzymes and mediate matrix remodeling in myxomatous heart valves. *Circulation.* 2001;104(21):2525-2532.
17. Merryman WD, Youn I, Lukoff HD, Krueger PM, Guilak F, Hopkins RA, Sacks MS. Correlation between heart valve interstitial cell stiffness and transvalvular pressure: implications for collagen biosynthesis. *Am J Physiol Heart Circ Physiol.* 2006;290(1):H224-231.
18. Bhatia A, Vesely I. The effect of glycosaminoglycans and hydration on the viscoelastic properties of aortic valve cusps. *Conf Proc IEEE Eng Med Biol Soc.* 2005;3:2979-2980.
19. Gupta V, Grande-Allen KJ. Effects of static and cyclic loading in regulating extracellular matrix synthesis by cardiovascular cells. *Cardiovasc Res.* 2006;72(3):375-383.
20. Kinsella MG, Bressler SL, Wight TN. The regulated synthesis of versican, decorin, and biglycan: extracellular matrix proteoglycans that influence cellular phenotype. *Crit Rev Eukaryot Gene Expr.* 2004;14(3):203-234.
21. Nguyen TC, Itoh A, Carlhall CJ, Bothe W, Timek TA, Ennis DB, Oakes RA, Liang D, Daughters GT, Ingels NB, Jr., Miller DC. The effect of pure mitral regurgitation on mitral annular geometry and three-dimensional saddle shape. *J Thorac Cardiovasc Surg.* 2008;136(3):557-565.
22. Helmcke F, Nanda N, Hsiung M, Soto B, Adey C, Goyal R, Gatewood Jr R. Color Doppler assessment of mitral regurgitation with orthogonal planes. *Circulation.* 1987;75(1):175-183.
23. Zhang H, Sun L, Wang W, Ma X. Quantitative analysis of fibrosis formation on the microcapsule surface with the use of picro-sirius red staining, polarized light microscopy, and digital image analysis. *J Biomed Mater Res.* 2006;76A:120-125.
24. Lis Y, Burleigh MC, Parker DJ, Child AH, Hogg J, Davies MJ. Biochemical characterization of individual normal, floppy and rheumatic human mitral valves. *Biochem J.* 1987;244(3):597-603.
25. Stephens EH, Nguyen TC, Itoh A, Ingels NB, Jr., Miller DC, Grande-Allen KJ. The effects of mitral regurgitation alone are sufficient for leaflet remodeling. *Circulation.* 2008;118(14 Suppl):S243-249.
26. Manuel J, Gawronska-Kozak B. Matrix metalloproteinase 9 (MMP-9) is upregulated during scarless wound healing in athymic nude mice. *Matrix Biol.* 2006;25(8):505-514.
27. Järveläinen H, Puolakkainen P, Pakkanen S, Brown E, Höök M, Iozzo R, Sage E, Wight T. A role for decorin in cutaneous wound healing and angiogenesis. *Wound Repair Regen.* 2006;14(4):443-452.

28. Peled Z, Phelps E, Updike D, Chang J, Krummel T, Howard E, Longaker M. Matrix metalloproteinases and the ontogeny of scarless repair: the other side of the wound healing balance. *Plast Reconstr Surg*. 2002;110(3):801-811.
29. Aikawa E, Whittaker P, Farber M, Mendelson K, Padera RF, Aikawa M, Schoen FJ. Human semilunar cardiac valve remodeling by activated cells from fetus to adult: implications for postnatal adaptation, pathology, and tissue engineering. *Circulation*. 2006;113(10):1344-1352.
30. Durbin AD, Gotlieb AI. Advances towards understanding heart valve response to injury. *Cardiovasc Pathol*. 2002;11(2):69-77.
31. Swedberg S, Brown B, Sigley R, Wight T, Gordon D, Nicholls S. Intimal fibromuscular hyperplasia at the venous anastomosis of PTFE grafts in hemodialysis patients. Clinical, immunocytochemical, light and electron microscopic assessment. *Circulation*. 1989;80(6):1726-1736.
32. Cattaruzza S, Perris R. Proteoglycan control of cell movement during wound healing and cancer spreading. *Matrix Biol*. 2005;24(6):400-417.
33. Singer A, Clark R. Cutaneous wound healing. *N Engl J Med*. 1999;341(10):738-746.
34. Ashcroft G, Kielty C, Horan M, Ferguson M. Age-related changes in the temporal and spatial distributions of fibrillin and elastin mRNAs and proteins in acute cutaneous wounds of healthy humans. *J Pathol*. 1997;183(1):80-89.
35. Raghunath M, Höpfner B, Aeschlimann D, Lüthi U, Meuli M, Altermatt S, Gobet R, Bruckner-Tuderman L, Steinmann B. Cross-linking of the dermo-epidermal junction of skin regenerating from keratinocyte autografts. Anchoring fibrils are a target for tissue transglutaminase. *J Clin Invest*. 1996;98(5):1174-1184.
36. Zheng Q, Choi J, Rouleau L, Leask R, Richardson J, Davis E, Yanagisawa H. Normal wound healing in mice deficient for fibulin-5, an elastin binding protein essential for dermal elastic fiber assembly. *J Invest Dermatol*. 2006;126(12):2707-2714.
37. Ricciardelli C, Russell D, Ween M, Mayne K, Suwivat S, Byers S, Marshall V, Tilley W, Horsfall D. Formation of hyaluronan- and versican-rich pericellular matrix by prostate cancer cells promotes cell motility. *J Biol Chem*. 2007;282(14):10814-10825.
38. Ang L, Zhang Y, Cao L, Yang B, Young B, Kiani C, Lee V, Allan K, Yang B. Versican enhances locomotion of astrocytoma cells and reduces cell adhesion through its G1 domain. *J Neuropathol Exp Neurol*. 1999;58(6):597-605.
39. Weigel P, Fuller G, LeBoeuf R. A model for the role of hyaluronic acid and fibrin in the early events during the inflammatory response and wound healing. *J Theor Biol*. 1986;119(2):219-234.
40. Weigel P, Frost S, McGary C, LeBoeuf R. The role of hyaluronic acid in inflammation and wound healing. *Int J Tissue React*. 1988;10(6):355-365.

41. Davis T, Amare M, Naik S, Kovalchuk A, Tadaki D. Differential cutaneous wound healing in thermally injured MRL/MPJ mice. *Wound Repair Regen.* 2007;15(4):577-588.

Chapter 19: MAPK Pathway in Myxomatous Mitral Valve Disease

In this chapter the topic of examining valves in the setting of various disease states continues with a study of myxomatous mitral valve disease. Specifically in this chapter the potential role of the mitogen-activated protein kinase (MAPK) signaling pathway in myxomatous mitral valve disease is analyzed. Chapter 24, in the Appendix, also involves characterization of myxomatous mitral valves, specifically alterations in proteoglycan and glycosaminoglycan content. While that study provides important background for this chapter, I was not the lead researcher on the study and it was not considered integral to this thesis; therefore, the study was placed in the Appendix.

ABSTRACT

Background: Myxomatous mitral valve disease is known to involve altered mechanics and increased myofibroblast-like valvular interstitial cells (VICs), however, the pathways involved in the activation of these VICs in myxomatous mitral valve disease have largely not been investigated. The mitogen-activated protein kinase (MAPK) pathway is involved in myofibroblast activation and mechanotransduction, and potentially could be the pathway by which myofibroblast activation occurs in myxomatous mitral valve disease. Therefore the aim of this study was to use immunohistochemistry to determine

whether MAPK pathway markers co-localized with that of myofibroblast markers within normal and myxomatous human mitral valves.

Methods: Human mitral valve posterior leaflets (control n=5-6, myxomatous n=14-17, mean age 60-63 for all groups) were histologically stained with Movat-pentachrome and immunohistochemically stained for markers of the myofibroblast cell phenotype, including smooth muscle alpha-actin (SMaA) and non-muscle myosin (NMM); proteins involved in the mitogen-activated protein kinase (MAPK) pathway, including extracellular signal-regulated kinase (ERK)-1, -2, phosphorylated ERK (pERK); as well as transforming growth factor-beta (TGF β). Samples were also stained for the proteoglycans biglycan (BGN), decorin (DCN), and versican (VC).

Results: Myxomatous mitral valves contained greater myofibroblast marker expression relative to control mitral valves, particularly in the internal leaflet. Significant remodeling was noted in the myxomatous mitral valves, with disruption of leaflet layers and areas of elastic fiber staining in the internal leaflet where elastic fibers are normally not found. Strong co-localization was noted between proteins in the MAPK pathway, and with TGF β , NMM, and SMaA. These MAPK pathway markers, particularly ERK, co-localized with areas of elastic fiber remodeling, where it was found with VC.

Conclusions: Greater abundance of myofibroblastic cells in myxomatous mitral valve leaflets, and co-localization of MAPK pathway proteins within those leaflets suggest the involvement of MAPK pathway signaling in these phenotypic changes. Co-localization of myofibroblast markers with areas of elastic fiber remodeling suggested direct

involvement of this cell type in the pathological compositional changes present in myxomatous mitral valve disease. While further *in vitro* studies are needed to verify these findings, these results could have important implications for possible treatment strategies for myxomatous mitral valve disease.

The work contained in this chapter represents a pilot study, and will not be submitted for publication.

INTRODUCTION

Myxomatous mitral valve disease is a common valvulopathy and the etiology most frequently underlying mitral valve prolapse, which is estimated to afflict approximately 2.4% of the general population.¹ Myxomatous mitral valve disease is characterized by proliferation of the spongiosa layer and collagen and elastic fiber fragmentation,²⁻⁶ resulting in substantially decreased material strength of the valve.⁷ Previous studies have also shown the enrichment of these myxomatous mitral valves with valvular interstitial cells (VICs) expressing myofibroblast markers, including smooth muscle alpha-actin and nonmuscle myosin, along with matrix metalloproteases (MMPs) and cathepsins.⁸ Although these studies have implicated the activated myofibroblast-like VICs in myxomatous mitral valve disease,⁸ and the involvement of the mitogen-activated protein kinase (MAPK) pathway in myofibroblast activation has been studied extensively in other connective tissues⁹⁻¹² and in the context of other valve diseases,¹³⁻¹⁷ investigation of the MAPK pathway in myxomatous mitral valve disease has been largely overlooked.¹⁸ Given that myxomatous mitral valves have altered mechanics and the mechanosensitive nature of the MAPK pathway, the involvement of the MAPK pathway could be based on altered strains in myxomatous mitral valve disease.¹⁹⁻²¹ Determining the pathway by which healthy VICs are activated into pathological myofibroblast-like cells in myxomatous mitral valve disease may lead to novel treatment strategies, as well as an enhanced understanding of the pathogenesis of myxomatous mitral valve disease. *In vitro* studies have demonstrated that VICs from porcine aortic valves can be activated to demonstrate these same myofibroblast-like cell markers via the MAPK pathway.^{14, 15} Therefore, the aim of this study was to use immunohistochemistry to determine whether

MAPK pathway markers co-localized with that of myofibroblast markers within normal and myxomatous human mitral valves.

METHODS

Sample Set

Mitral valve posterior leaflets were obtained from controls at autopsy (patients not demonstrating cardiovascular disease, Table 19-1) and valves with primary myxomatous mitral valve disease surgically resected during reparative procedures. Tissues for this study were provided by St. Luke's Episcopal Hospital (Houston, TX), Ben Taub Hospital (Houston, TX), and the Cooperative Human Tissue Network. The research use of these tissues was approved by the Institutional Review Boards at all institutions. Radial strips from each leaflet were cut from the annulus to free edge and fixed in 10% formalin overnight. Fixed tissue sections were then paraffin embedded, sectioned to a thickness of 5 μ m, and mounted on glass slides according to standard procedures.

Table 19-1. Subject Demographics.

		ERK1	ERK2	pERK	TGF β	NMM	SMaA	PGs
Normal (control)	age	60.3 \pm 12	60.3 \pm 12	60.3 \pm 12	63.2 \pm 11	60.3 \pm 12	63.2 \pm 11	59.4 \pm 13
	sample #	6	6	6	5	6	5	5
	(#M/#F)	5/1	5/1	5/1	4/1	5/1	4/1	4/1
Myx	age	60.5 \pm 10	60.9 \pm 10	61.1 \pm 11	62.6 \pm 13	62.1 \pm 13	62.1 \pm 13	64.1 \pm 10
	sample #	17	16	15	14	16	16	12
	(#M/#F)	7/10	7/9	7/8	8/6	9/7	9/7	6/6

Myx=myxomatous; age is given as mean \pm standard deviation; #M/#F=number of males/number of females. *Due to the small size of some tissues, it was not possible to obtain histological sections for all stains from all subjects' tissue blocks. PGs=proteoglycans biglycan, decorin, and versican. For other abbreviations, please see the text.

Histology and Immunohistochemistry

Tissue sections were stained with Movat pentachrome to demonstrate overall leaflet structure microstructure including the leaflet layers atrialis, spongiosa, fibrosa, and ventricularis. Immunohistochemistry (IHC) was performed to demonstrate markers of the myofibroblast cell phenotype, including smooth muscle alpha-actin (SMaA, Table 19-2) and non-muscle myosin (NMM); proteins involved in the mitogen-activated protein

Table 19-2. Antibodies Used in Immunohistochemistry.

Protein	Role
<u>Myofibroblast Cell Phenotype Markers</u>	
Smooth Muscle Alpha-Actin (SMaA)*	Marker of myofibroblast cell phenotype
Non-muscle Myosin (NMM)^	Marker of myofibroblast cell phenotype
<u>Proteins in Mitogen-Activated Protein Kinase (MAPK) Pathway</u>	
Extracellular signal-regulated kinase (ERK)-1 [†]	Kinase activated by MAPK kinase (a.k.a MEK)
ERK2 [‡]	Kinase activated by MAPK kinase (a.k.a MEK)
Phosphorylated ERK1/2 (pERK)**	Activated form of ERK1, 2
<u>Growth Factors</u>	
Transforming Growth Factor-beta (TGFβ) ^{^^}	Growth factor integral to myofibroblast differentiation
<u>Proteoglycans (PG) and Glycosaminoglycans (GAG)</u>	
Decorin (DCN) ^{††}	PG involved in collagen fibrillogenesis
Biglycan (BGN) ^{††}	PG involved in collagen fibrillogenesis
Versican (VC) [‡]	PG involved elastic fiber formation, compressibility

*Dakocytomation (Denmark); ^Covance (Berkeley, CA); †Chemicon (Temecula, CA); ‡Abcam (Cambridge, MA); **Upstate (Lake Placid, NY); ^^Biovision (Mountain View, CA); ††gift of Dr. Larry Fisher, NIH (Bethesda, MD); ‡Associates of Cape Cod.

kinase (MAPK) pathway, including extracellular signal-regulated kinases (ERK)-1, -2, phosphorylated ERK1/2 (pERK); as well as transforming growth factor beta (TGFβ), which is well known to be involved in the signaling pathway leading to myofibroblast differentiation.^{11, 12, 22} The proteoglycans versican (VC), decorin (DCN), and biglycan (BGN), which are increased in myxomatous mitral valves,²³ were also examined in relation to myofibroblast and MAPK pathway markers.

RESULTS

Distribution of SMaA

In normal mitral valve posterior leaflets, SMaA staining was limited and when present was predominantly found in the atrialis layer in the annular region (Fig. 19-1A), but sometimes was also evident in the mid-leaflet atrialis layer. SMaA staining was largely located in the subendothelium but sometimes extended more interiorly into the

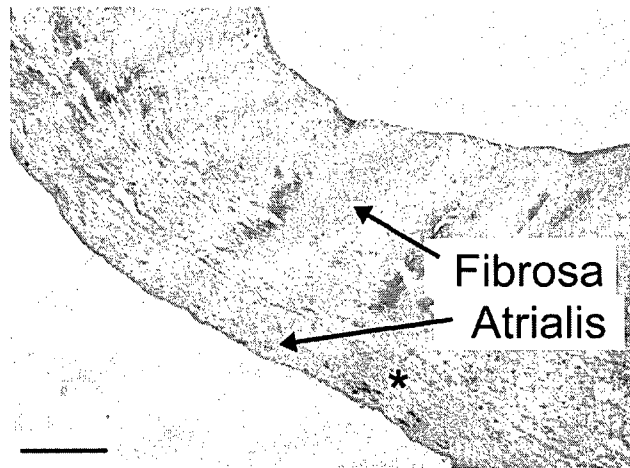


Fig. 19-1: A) Representative image illustrating the distribution of SMaA staining in control (normal) mitral valve posterior leaflets. Portion of leaflet shown is annular region. Asterisk marks punctate SMaA staining in the atrialis layer of the annular region. Scale bar represents 200 μ m.

atrialis approaching the fibrosa. Staining was also often usually linear along a small portion of the length of the leaflet. At times clusters of SMaA staining were evident characteristic of muscle fibers as opposed to myofibroblast-like valvular interstitial cells. The overall amount of SMaA staining was very limited.

In myxomatous mitral valve posterior leaflets in which layers were visible, SMaA staining was found largely in atrialis layer but usually extended more interiorly than in normal leaflets, including staining in the fibrosa and spongiosa. In some cases SMaA staining was evident throughout layers (Fig. 19-1B). The overall amount of SMaA staining in myxomatous posterior leaflets was considerably greater than in controls, more often present in the mid-leaflet and more often found interiorly compared to control. In some cases in which layers were no longer discernable, SMaA could be found diffusely throughout the interior of the internal leaflet, (Fig. 19-1C), and other times concentrated in specific areas.

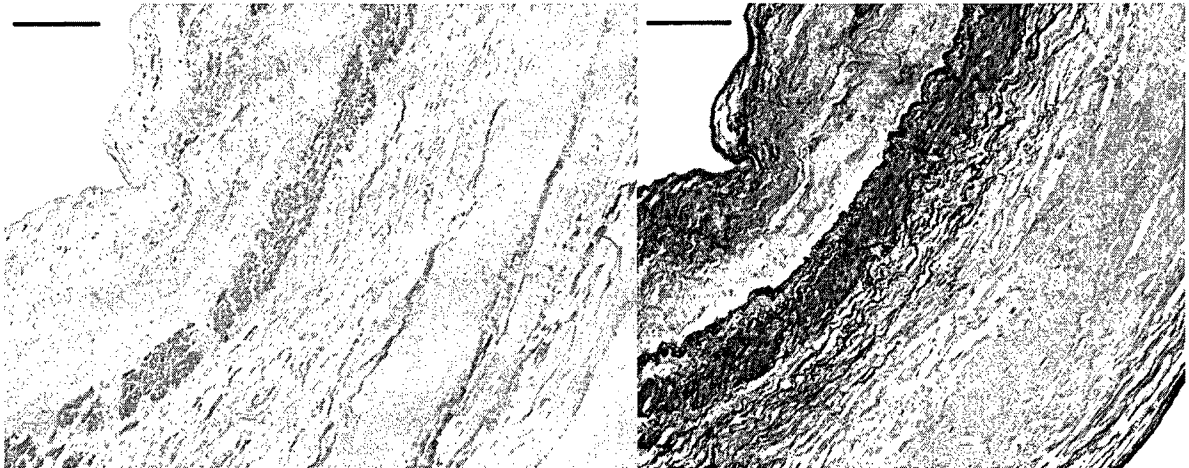


Fig. 19-1 (cont'd): B) Image illustrating SMaA staining evident throughout the leaflet layers in myxomatous mitral valve posterior leaflet. Portion of leaflet shown is annular region. Scale bar represents 200 μ m.

Co-localization of SMaA and NMM

NMM staining in both myxomatous and normal mitral valve posterior leaflets was more diffuse compared to SMaA staining. While NMM staining was predominantly

strong wherever SMaA staining was found, NMM staining was not limited to those areas of positive SMaA staining. NMM staining was also not as punctate, limited to the individual cells, as with SMaA staining.

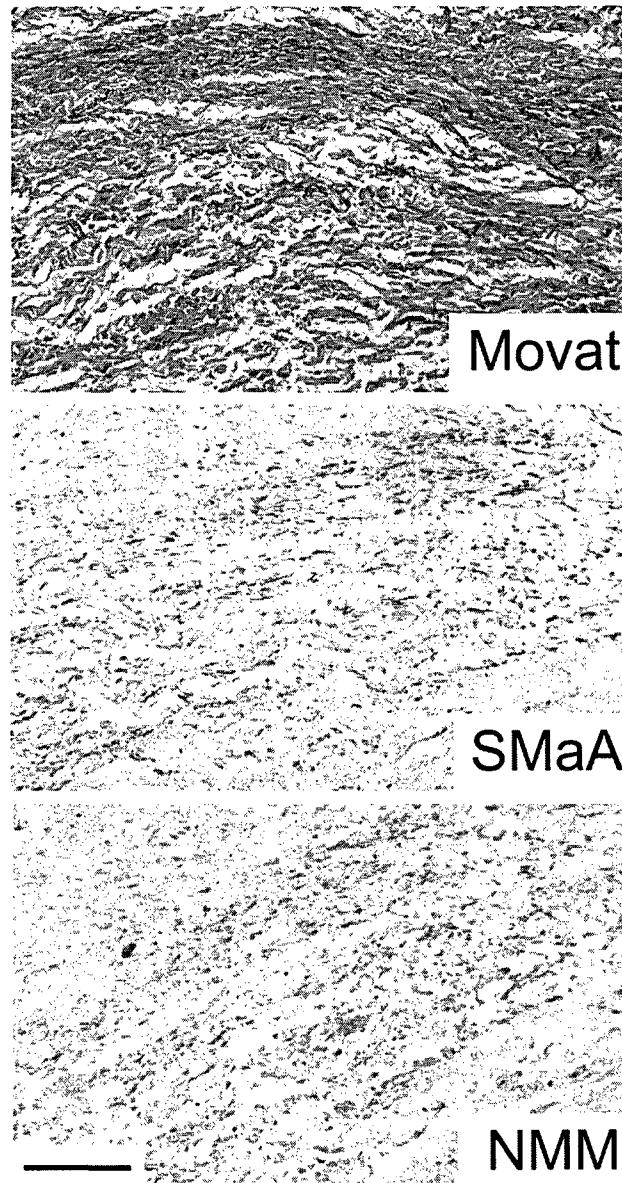


Fig. 19-1 (cont'd): C) SMaA and NMM staining in the interior region of a myxomatous mitral valve posterior leaflet in a sample in which leaflet layers were no longer distinguishable. Staining of SMaA and NMM appears abundant and distributed throughout the region. Scale bar represents 200 μ m.

Co-localization of MAPK Markers, TGF β , and Myofibroblast Markers

In myxomatous valves tight co-localization was noted between ERK1, ERK2 and pERK, with pERK staining being substantially less intense than ERK1 and ERK2. TGF β staining also appeared to co-localize with proteins in the MAPK pathway (Fig. 19-2). NMM and SMaA staining co-localized with all of the MAPK markers (Fig. 19-3). While in normal valves instances of co-localization between the MAPK markers and myofibroblast markers were noted, these were usually limited to the annulus atrialis where myofibroblast marker staining was evident (as discussed above).

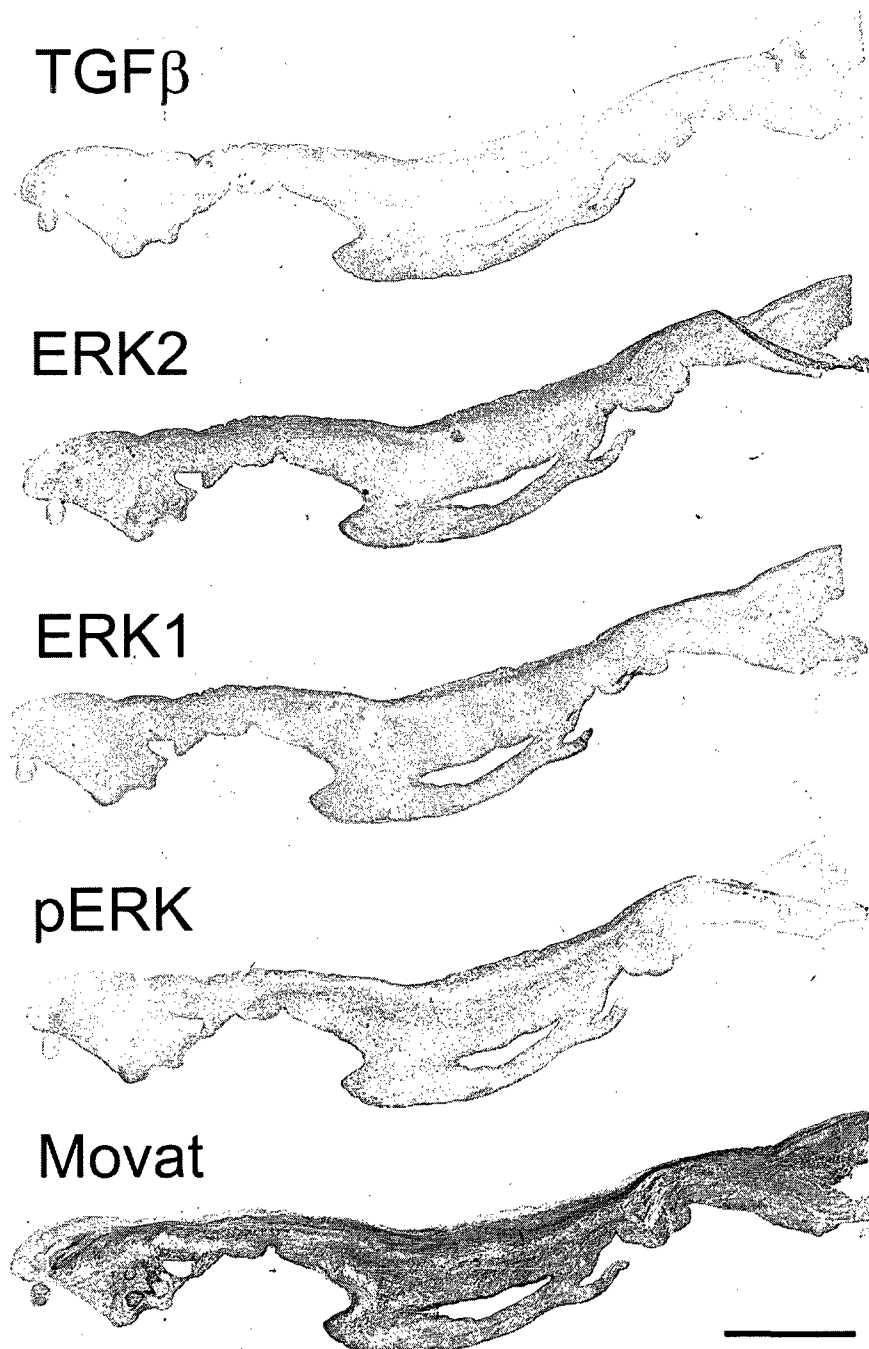


Fig. 19-2: Image illustrating the relative locations of staining for members of the MAPK pathway and TGFβ demonstrating significant co-localization throughout the leaflet. Scale bar represents 2.5 mm.

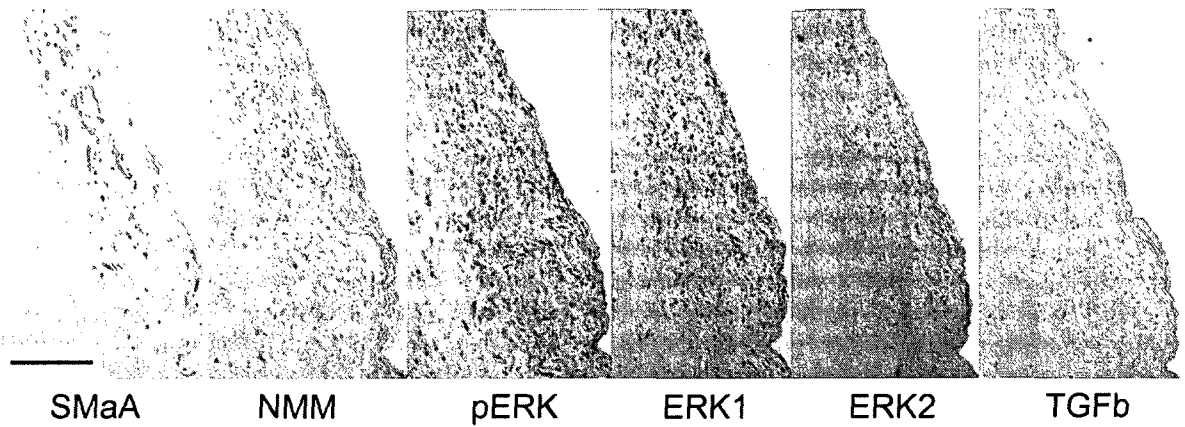


Fig. 19-3: Image depicting the relative locations of SMaA, NMM, pERK, ERK1, ERK2, and TGF β in a myxomatous mitral valve leaflet. Portion of the valve imaged is the mid-leaflet region. Scale bar represents 200 μ m.

Distribution of MAPK Markers Relative to Histological Layers

In normal mitral valve posterior leaflets ERK1, ERK2, and pERK were predominantly localized to the atrialis of the annulus with weak staining in the fibrosa, although some staining was also noted in the mid-leaflet. Some samples also showed increased expression in the free edge. In myxomatous valves ERK1 and ERK2 were not only evident in the atrialis, but this staining spread internally, where it bordered collagen staining evident in the corresponding Movat pentachrome stained section. ERK staining was particularly intense in areas of elastic fiber remodeling (Fig. 19-4) and/or bordering collagen staining, while ERK staining was usually light in collagen regions.

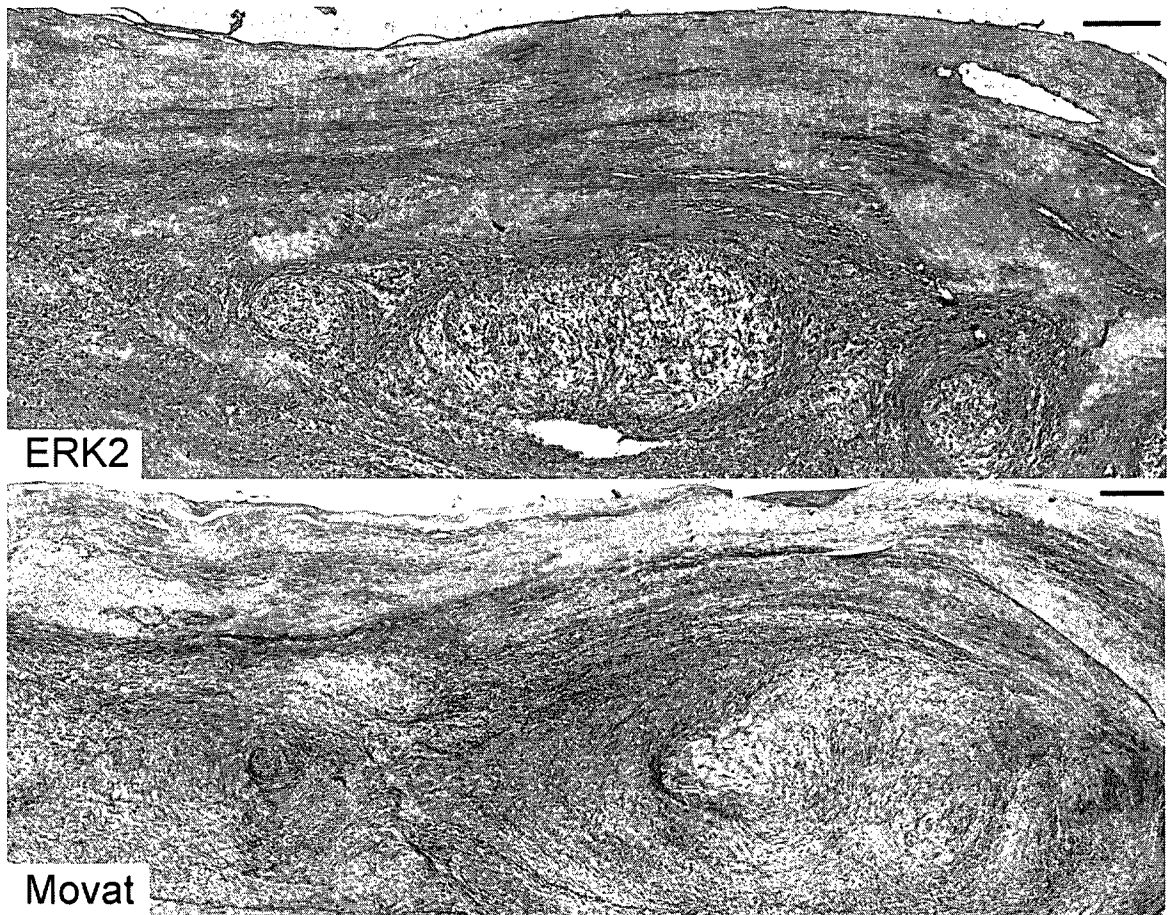


Fig. 19-4: Areas of remodeling in myxomatous leaflets showed strong co-localization of elastic fibers with ERK1 and ERK2. Although ERK2 stain is included in this figure, ERK1 stain showed similar distribution. Scale bar represents 200 μm .

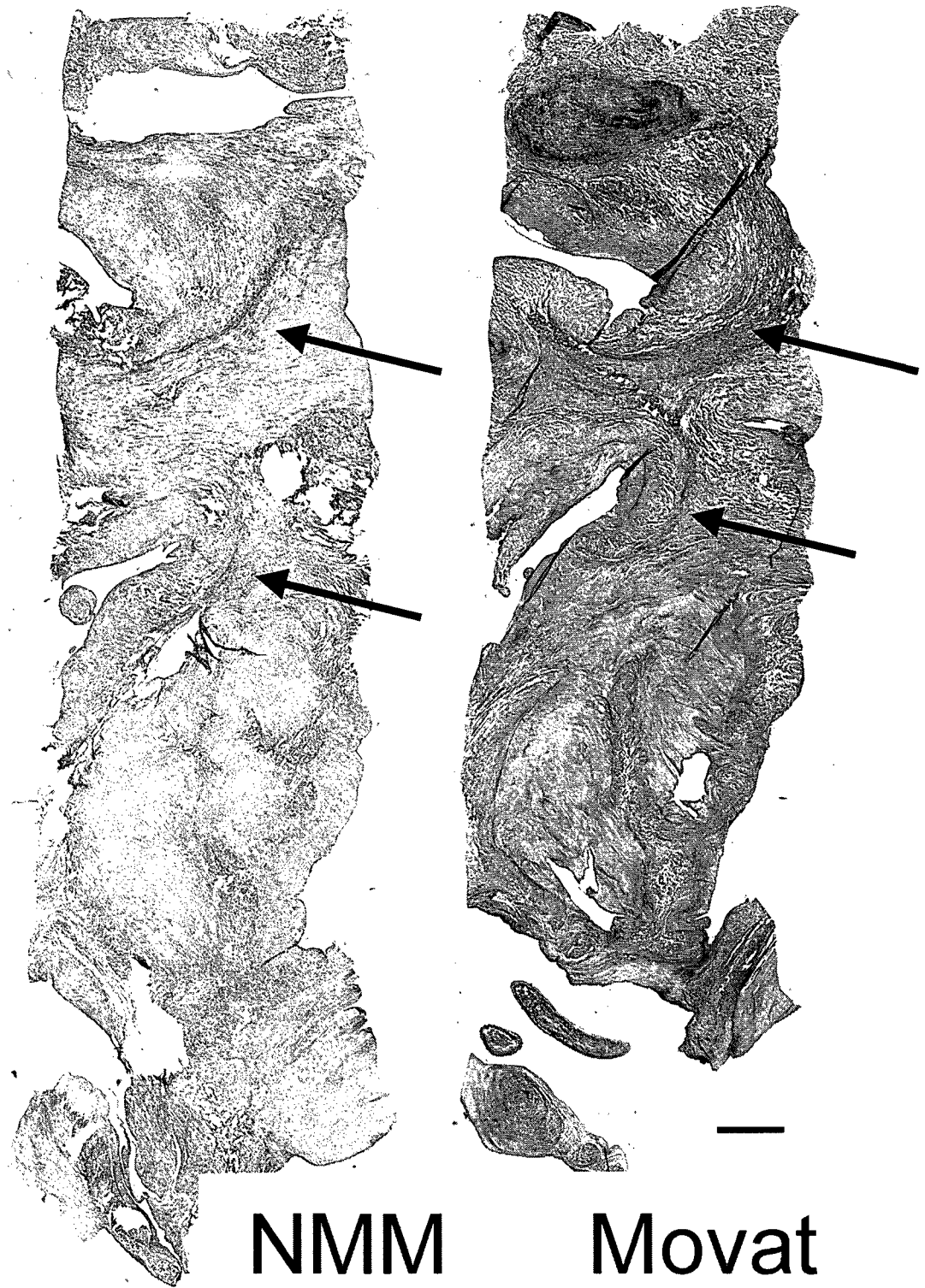


Fig. 19-5: Areas of elastic fiber remodeling in myxomatous leaflets showed strong colocalization with NMM (arrows). Scale bar represents 1 mm.

Distribution of MAPK Markers Relative to Proteoglycans

In normal valves DCN and BGN demonstrated strong co-localization. These PGs demonstrated staining in the spongiosa layer of the mid-leaflet as well as co-localization with collagen in the fibrosa layer. VC, in contrast, demonstrated strong staining intensity in the atrialis layer and little intensity in the fibrosa. Strong co-localization was noted between VC and elastic fibers, as previously reported.²³ In the posterior leaflets of myxomatous mitral valves, PG staining was increased, as previously reported.²³ The normal organization of leaflet layers was disrupted in myxomatous mitral valves making evaluation of localization of specific PGs to particular layers problematic, but VC tended to co-localize with elastic fibers both in areas in which the layers were disrupted and the atrialis when that layer was found intact. DCN usually localized with collagen and BGN localized with collagen as well as elastic fibers. In the posterior leaflets of myxomatous valves ERK2 and versican appeared to be generally localized with areas of elastic fiber remodeling (areas of elastic fibers on Movat-stained sections internal to the leaflet where elastic fibers are not normally found), bordering collagen staining on the Movat stain. These areas also showed strong NMM staining (Fig. 19-5).

DISCUSSION

Myxomatous mitral valves contained a greater number of VICs expressing myofibroblast markers relative to control mitral valves. Co-localization of proteins in the MAPK pathway with TGF β , NMM, and SMaA in myxomatous mitral valves suggested that the MAPK pathway is involved in myofibroblast activation in this disease. Co-

localization of myofibroblast markers with areas of elastic fiber remodeling suggested direct involvement of this cell type in the pathological changes present in myxomatous mitral valve disease.

MAPK Pathway in Myofibroblast Activation

Myofibroblast activation has been studied in cells derived from a number of different tissues. While multiple pathways for myofibroblast activation have been demonstrated and debate continues as to which pathways are most functionally relevant, it is proposed that there are generally three elements necessary for myofibroblast activation in tissues: 1) increased amounts of TGF β , 2) the involvement of certain specific extracellular matrix proteins, such as the extra domain A (ED-A) splice variant of fibronectin, and 3) increased extracellular stress.²⁴ The specific cell signaling pathways thought to be involved in myofibroblast activation include the smad pathway, ERK2/Ras, p38 MAPK, and Rho/c-Jun N-terminal kinase (JNK) pathways.²⁵ However, some of these pathways appear to be tissue specific. For instance, studies investigating pulmonary fibrosis suggest that the smad pathway is key to TGF β mediated SMAA transcription in pulmonary myofibroblast activation,^{26, 27} however the pathways implicated in these studies are distinct from those of smooth muscle cells.²⁸ Studies related to mechanical stress and myofibroblast activation have emphasized the importance of the fibronexus and its maturation in the myofibroblast differentiation process.²⁹ Indeed, studies in lung myofibroblast activation have shown that the downstream transcriptional effects of TGF β are closely related to focal adhesion kinase and fibronexus maturation;³⁰ therefore, there appears to be a strong interrelationship

between biological and mechanical cues in myofibroblast activation. Mechanical stress has been demonstrated to induce myofibroblast activation via the ERK2 and JNK, but not p38 pathway by some scientists in cardiac fibroblasts,³¹ but by the p38 pathway by others using rat-2 cells.^{32, 33} While the specific pathways by which myofibroblast activation occurs in different tissues continues to be debated, it is agreed that myofibroblast activation involves both biological cues and mechanical forces in the context of the cell remodeling its environment and the extracellular environment affecting the cell.

MAPK Pathway in VICs

Cushing et al. have investigated the role of fibroblast growth factor (FGF) in repressing myofibroblast activation in aortic valve VICs.^{14, 15} In the context of these studies they show that FGF signaling, at least in aortic valve VICs, appears to occur through the classical MAPK pathway (via ERK1, 2).^{14, 15} From the present study it appears that the ERK1,2 MAPK pathway may be involved in myofibroblast VIC activation in the context of myxomatous mitral valve disease. MAPK markers also demonstrated some co-localization with myofibroblast markers in the limited areas of control valves where myofibroblast markers were expressed. This could suggest that VIC myofibroblast activation generally occurs by the MAPK pathway but is simply increased with altered distribution in myxomatous mitral valve disease, but considerably more work, including *in vitro* studies, would need to be done to verify this.

MAPK Pathway in Myxomatous Mitral Valve Disease

Recent work in a canine animal model of myxomatous mitral valve disease suggested that the MAPK pathway is more active in myxomatous mitral valve disease relative to control canine mitral valves.¹⁸ In this study pERK was increased in myxomatous mitral valve disease but total ERK1,2 was not. The TGF β receptors 1,2 and latent TGF β 1 were also increased in myxomatous mitral valve disease relative to normal valves.¹⁸ This study also investigated the role of serotonergic signaling in this animal model of myxomatous mitral valve disease and found an increase in key serotonergic signaling proteins and an enzyme involved in serotonin metabolism to be decreased in myxomatous mitral valves relative to normal valves.¹⁸ The results from this study, although in a canine model of myxomatous mitral valve disease, also support the findings from the present study and the overarching hypothesis that myofibroblast VIC activation in myxomatous mitral valve disease occurs via the MAPK/ERK pathway.

Myofibroblast Phenotype and Compositional Changes in Myxomatous Mitral Valve Disease

Previous studies have demonstrated altered matrix composition of myxomatous mitral valves relative to age-matched normal mitral valves, including greater water content, more DNA, and an increase in GAGs, particularly 6-sulfated chondroitin.³⁴ We previously showed that the abundance of the proteoglycans DCN, VC, and BGN were all increased in myxomatous mitral valves relative to control.²³ Studies have reported increased collagen content, particularly collagen type III, in myxomatous mitral valves,³⁵ as well as collagen fragmentation,^{2, 3, 6, 8} although the ability of VICs to synthesize

collagen was retained in VICs within myxomatous mitral valves.⁸ Elastic fibers in myxomatous mitral valves have also been shown to be increased and fragmented relative to normal mitral valves.^{3, 6, 8, 36} These findings of elastic and collagen fiber fragmentation are consistent with reports of myxomatous mitral valves enriched in myofibroblast-like VICs expressing the gelatinase enzymes MMP2, 9 and the collagenase enzymes MMP1 and 13.⁸ In fact, previous studies have observed that VICs expressing myofibroblast markers and MMP13 were localized to areas of myxoid stroma with fragmented elastic fibers and loosely arranged collagen fibers,⁸ suggesting a direct link between the myofibroblast-like VIC and the compositional changes observed in myxomatous mitral valve disease. These previous observations of VICs expressing myofibroblast markers in areas of myxoid remodeling are consistent with the observations of strong NMM staining in areas of elastic fiber remodeling in the present study.

Myofibroblast Phenotype in Valvulopathies

The myofibroblast-like VIC has not only been implicated in the pathogenesis of myxomatous mitral valve disease, but other valve diseases including calcific aortic valve disease and functional mitral regurgitation. In calcific aortic valve disease, VICs expressing SMAA have been demonstrated to be present early in the calcification process;³⁷⁻³⁹ TGF β signaling has also been shown to increase calcification of VICs in culture⁴⁰⁻⁴³ and be greater in calcified aortic valves relative to control.⁴⁴ Mitral valve compositional changes in ovine models of functional mitral regurgitation also have implicated the VIC myofibroblast-like cell phenotype in the pathogenesis of these valve diseases.^{45, 46} Therefore this myofibroblast-like activation of VICs, and the pathway(s)

by which it occurs, is not only important to understand because of its potential role in myxomatous mitral valve disease, but because of its implicated role in other valve diseases. To this end our laboratory has been pursuing means of separating this VIC subpopulation from normal and myxomatous mitral valves for further *in vitro* study.⁴⁷

Implications

While this study does not directly demonstrate a causative link between the MAPK pathway and myofibroblast activation in myxomatous mitral valve disease, the association of MAPK markers and myofibroblast phenotype markers and matrix remodeling in this study is compelling and deserves further attention. More in depth analysis of elastic remodeling, such as the gelatinases MMP2 and 9 as well as lysyl oxidase, and its association with myofibroblastic activation would be informative. Similarly, further analysis is warranted to understand how PGs such as versican, which are known to be increased in myxomatous mitral valve disease,²³ relate to these phenotypic changes and potentially signaling pathways. Further verification of the pathway by which myofibroblast activation occurs in myxomatous mitral valves, such as using *in vitro* cell culture-based studies, would provide a signaling mechanism of activation for this cell-type thought to be an effector of the deleterious changes in myxomatous mitral valve disease. Moreover, verification and further elucidation of this pathway of activation could open opportunities for pathway and protein-specific molecular treatment strategies for this widespread, debilitating disease.

Limitations and Future Studies

Limitations of this study include difficulty in identifying the distinct characteristic leaflet layers within the myxomatous valve sections, lack of female patients in the control group, and overall small number of control sections. Future analysis quantifying staining intensity would strengthen the observations of this study. Most importantly, this study is limited in that it only demonstrates an associative relationship between MAPK pathway markers and the myofibroblast-cell phenotype by co-localization of marker staining, which in conjunction with previous *in vitro* studies suggests a causal relationship, however, further study confirming and elucidating a causative relationship is warranted. Such future studies investigating the role of this MAPK pathway could involve both normal VICs and VICs isolated from myxomatous mitral valves, as well as manipulation of the myofibroblast-like subpopulation of normal VICs. Additional pathways may also be involved in the activation of VICs and should be investigated.

CONCLUSIONS

In summary, the co-localization of MAPK pathway markers, myofibroblast markers, and areas of matrix remodeling in myxomatous mitral valves suggested that the deleterious compositional changes that occur in myxomatous mitral valve disease could occur via MAPK-pathway dependent myofibroblast activation of VICs. While further *in vitro* studies remain to be performed demonstrated a direct, causative relationship between MAPK signaling and valve compositional changes, these findings could lead to novel treatment strategies for myxomatous mitral valve disease.

This chapter, which analyzed the mitogen-activated protein kinase (MAPK) signaling pathway in myxomatous mitral valve disease, continued the topic of valve alterations in various disease states. It should be noted that Chapter 24 in the Appendix also analyzes valve changes in myxomatous mitral valve disease (specifically characterizing changes in proteoglycan and glycosaminoglycan content), and provides important context for the present study. As stated in the preface, that study was placed in the Appendix because I was not the lead researcher on the study and it was not considered integral to this thesis. The next two chapters (Chapters 20 and 21) move from studying myxomatous mitral valves to characterization of valve alterations in calcific aortic valve disease. Specifically in the next chapter a study analyzing proteoglycan and glycosaminoglycan content relative to calcified nodules is presented.

REFERENCES

1. Freed LA, Levy D, Levine RA, Larson MG, Evans JC, Fuller DL, Lehman B, Benjamin EJ. Prevalence and clinical outcome of mitral-valve prolapse. *N Engl J Med.* 1999;341(1):1-7.
2. Olsen EG, Al-Rufaie HK. The floppy mitral valve. Study on pathogenesis. *Br Heart J.* 1980;44(6):674-683.
3. Nasuti JF, Zhang PJ, Feldman MD, Pasha T, Khurana JS, Gorman JH, 3rd, Gorman RC, Narula J, Narula N. Fibrillin and other matrix proteins in mitral valve prolapse syndrome. *Ann Thorac Surg.* 2004;77(2):532-536.
4. Akhtar S, Meek KM, James V. Ultrastructure abnormalities in proteoglycans, collagen fibrils, and elastic fibers in normal and myxomatous mitral valve chordae tendineae. *Cardiovasc Pathol.* 1999;8(4):191-201.
5. Akhtar S, Meek KM, James V. Immunolocalization of elastin, collagen type I and type III, fibronectin, and vitronectin in extracellular matrix components of normal and myxomatous mitral heart valve chordae tendineae. *Cardiovasc Pathol.* 1999;8(4):203-211.
6. Tamura K, Fukuda Y, Ishizaki M, Masuda Y, Yamanaka N, Ferrans VJ. Abnormalities in elastic fibers and other connective-tissue components of floppy mitral valve. *Am Heart J.* 1995;129(6):1149-1158.
7. Barber J, Kasper F, Ratliff N, Cosgrove D, Griffin B, Vesely I. Mechanical properties of myxomatous mitral valves. *J Thorac Cardiovasc Surg.* 2001;122(5):955-962.
8. Rabkin E, Aikawa M, Stone JR, Fukumoto Y, Libby P, Schoen FJ. Activated interstitial myofibroblasts express catabolic enzymes and mediate matrix remodeling in myxomatous heart valves. *Circulation.* 2001;104(21):2525-2532.
9. Yang M, Huang H, Li J, Li D, Wang H. Tyrosine phosphorylation of the LDL receptor-related protein (LRP) and activation of the ERK pathway are required for connective tissue growth factor to potentiate myofibroblast differentiation. *Faseb J.* 2004;18(15):1920-1921.
10. Furukawa F, Matsuzaki K, Mori S, Tahashi Y, Yoshida K, Sugano Y, Yamagata H, Matsushita M, Seki T, Inagaki Y, Nishizawa M, Fujisawa J, Inoue K. p38 MAPK mediates fibrogenic signal through Smad3 phosphorylation in rat myofibroblasts. *Hepatology.* 2003;38(4):879-889.
11. Liu P, Zhang C, Feng J, Zhao Y, Wang X, Yang J, Zhang M, Wang X, Zhang Y. Cross-Talk Among Smad, MAPK, and Integrin Signaling Pathways Enhances Adventitial Fibroblast Functions Activated by Transforming Growth Factor {beta}1 and Inhibited by Gax. *Arterioscler Thromb Vasc Biol.* 2008(Epub Jan 10).
12. Hu Y, Peng J, Feng D, Chu L, Li X, Jin Z, Lin Z, Zeng Q. Role of extracellular signal-regulated kinase, p38 kinase, and activator protein-1 in transforming growth factor-beta1-

- induced alpha smooth muscle actin expression in human fetal lung fibroblasts in vitro. *Lung*. 2006;184(1):33-42.
13. Gu X, Masters KS. Role of the MAPK/ERK pathway in valvular interstitial cell calcification. *Am J Physiol Heart Circ Physiol*. 2009;296(6):H1748-1757.
 14. Cushing MC, Liao J, Jaeggli MP, Anseth KS. Material-based regulation of the myofibroblast phenotype *Biomaterials*. 2007;28:3378-3387.
 15. Cushing MC, Mariner PD, Liao JT, Sims EA, Anseth KS. Fibroblast growth factor represses Smad-mediated myofibroblast activation in aortic valvular interstitial cells. *Faseb J*. 2008;22(6):1769-1777.
 16. Pho M, Lee W, Watt D, Laschinger C, Simmons C, McCulloch C. Cofilin is a marker of myofibroblast differentiation in cells from porcine aortic cardiac valves. *Am J Physiol Heart Circ Physiol*. 2008;294(4):H1767-1778.
 17. Xu J, Jian B, Chu R, Lu Z, Li Q, Dunlop J, Rosenzweig-Lipson S, McGonigle P, Levy RJ, Liang B. Serotonin mechanisms in heart valve disease II: the 5-HT₂ receptor and its signaling pathway in aortic valve interstitial cells. *Am J Pathol*. 2002;161(6):2209-2218.
 18. Disatian S, Orton EC. Autocrine serotonin and transforming growth factor beta 1 signaling mediates spontaneous myxomatous mitral valve disease. *J Heart Valve Dis*. 2009;18(1):44-51.
 19. MacKenna D, Dolfi F, Vuori K, Ruoslahti E. Extracellular signal-regulated kinase and c-Jun NH₂-terminal kinase activation by mechanical stretch is integrin-dependent and matrix-specific in rat cardiac fibroblasts. *J Clin Invest*. 1998;101(2):301-310.
 20. Gruden G, Zonca S, Hayward A, Thomas S, Maestrini S, Gnudi L, Viberti GC. Mechanical stretch-induced fibronectin and transforming growth factor-beta₁ production in human mesangial cells is p38 mitogen-activated protein kinase-dependent. *Diabetes*. 2000;49(4):655-661.
 21. Lammerding J, Kamm RD, Lee RT. Mechanotransduction in cardiac myocytes. *Ann N Y Acad Sci*. 2004;1015:53-70.
 22. Hinz B. Formation and function of the myofibroblast during tissue repair. *J Invest Dermatol*. 2007;127(3):526-537.
 23. Gupta V, Barzilla JE, Mendez JS, Stephens EH, Lee EL, Collard CD, Laucirica R, Weigel PH, Grande-Allen KJ. Abundance and location of proteoglycans and hyaluronan within normal and myxomatous mitral valves. *Cardiovasc Pathol*. 2009;18(4):191-197.
 24. Tomasek JJ, Gabbiani G, Hinz B, Chaponnier C, Brown RA. Myofibroblasts and mechano-regulation of connective tissue remodelling. *Nat Rev Mol Cell Biol*. 2002;3(5):349-363.
 25. Sousa AM, Liu T, Guevara O, Stevens J, Fanburg BL, Gaestel M, Toksoz D, Kayyali US. Smooth muscle alpha-actin expression and myofibroblast differentiation by TGFbeta are dependent upon MK2. *J Cell Biochem*. 2007;100(6):1581-1592.

26. Ramirez AM, Shen Z, Ritzenthaler JD, Roman J. Myofibroblast transdifferentiation in obliterative bronchiolitis: tgf-beta signaling through smad3-dependent and -independent pathways. *Am J Transplant.* 2006;6(9):2080-2088.
27. Hu B, Wu Z, Liu T, Ullenbruch MR, Jin H, Phan SH. Gut-enriched Kruppel-like factor interaction with Smad3 inhibits myofibroblast differentiation. *Am J Respir Cell Mol Biol.* 2007;36(1):78-84.
28. Hinz B, Phan SH, Thannickal VJ, Galli A, Bochaton-Piallat ML, Gabbiani G. The myofibroblast: one function, multiple origins. *Am J Pathol.* 2007;170(6):1807-1816.
29. Hinz B. Masters and servants of the force: The role of matrix adhesions in myofibroblast force perception and transmission. *Eur J Cell Biol.* 2006;85:175-181.
30. Thannickal VJ, Lee DY, White ES, Cui Z, Larios JM, Chacon R, Horowitz JC, Day RM, Thomas PE. Myofibroblast differentiation by transforming growth factor-beta1 is dependent on cell adhesion and integrin signaling via focal adhesion kinase. *J Biol Chem.* 2003;278(14):12384-12389.
31. MacKenna DA, Dolfi F, Vuori K, Ruoslahti E. Extracellular signal-regulated kinase and c-Jun NH2-terminal kinase activation by mechanical stretch is integrin-dependent and matrix-specific in rat cardiac fibroblasts. *J Clin Invest.* 1998;101(2):301-310.
32. Wang J, Fan J, Laschinger C, Arora PD, Kapus A, Seth A, McCulloch CA. Smooth muscle actin determines mechanical force-induced p38 activation. *J Biol Chem.* 2005;280(8):7273-7284.
33. Wang J, Zohar R, McCulloch CA. Multiple roles of alpha-smooth muscle actin in mechanotransduction. *Exp Cell Res.* 2006;312(3):205-214.
34. Grande-Allen K, Griffin B, Ratliff N, Cosgrove D, Vesely I. Glycosaminoglycan profiles of myxomatous mitral leaflets and chordae parallel the severity of mechanical alterations. *J Am Coll Cardiol.* 2003;42(2):271-277.
35. Cole WG, Chan D, Hickey AJ, Wilcken DE. Collagen composition of normal and myxomatous human mitral heart valves. *Biochem J.* 1984;219(2):451-460.
36. Lis Y, Burleigh MC, Parker DJ, Child AH, Hogg J, Davies MJ. Biochemical characterization of individual normal, floppy and rheumatic human mitral valves. *Biochem J.* 1987;244(3):597-603.
37. Tanaka K, Sata M, Fukuda D, Suematsu Y, Motomura N, Takamoto S, Hirata Y, Nagai R. Age-associated aortic stenosis in apolipoprotein E-deficient mice. *J Am Coll Cardiol.* 2005;46(1):134-141.
38. Otto CM, Kuusisto J, Reichenbach DD, Gown AM, O'Brien KD. Characterization of the early lesion of 'degenerative' valvular aortic stenosis. Histological and immunohistochemical studies. *Circulation.* 1994;90(2):844-853.

39. O'Brien KD, Reichenbach DD, Marcovina SM, Kuusisto J, Alpers CE, Otto CM. Apolipoproteins B, (a), and E accumulate in the morphologically early lesion of 'degenerative' valvular aortic stenosis. *Arterioscler Thromb Vasc Biol.* 1996;16(4):523-532.
40. Mohler ER, 3rd, Chawla MK, Chang AW, Vyavahare N, Levy RJ, Graham L, Gannon FH. Identification and characterization of calcifying valve cells from human and canine aortic valves. *J Heart Valve Dis.* 1999;8(3):254-260.
41. Osman L, Yacoub MH, Latif N, Amrani M, Chester AH. Role of human valve interstitial cells in valve calcification and their response to atorvastatin. *Circulation.* 2006;114(1 Suppl):I547-552.
42. Benton JA, Kern HB, Anseth KS. Substrate properties influence calcification in valvular interstitial cell culture. *J Heart Valve Dis.* 2008;17(6):689-699.
43. Clark-Greuel JN, Connolly JM, Sorichillo E, Narula NR, Rapoport HS, Mohler ER, 3rd, Gorman JH, 3rd, Gorman RC, Levy RJ. Transforming growth factor-beta1 mechanisms in aortic valve calcification: increased alkaline phosphatase and related events. *Ann Thorac Surg.* 2007;83(3):946-953.
44. Jian B, Narula N, Li QY, Mohler ER, 3rd, Levy RJ. Progression of aortic valve stenosis: TGF-beta1 is present in calcified aortic valve cusps and promotes aortic valve interstitial cell calcification via apoptosis. *Ann Thorac Surg.* 2003;75(2):457-465; discussion 465-456.
45. Stephens EH, Timek TA, Daughters GT, Kuo JJ, Patton AM, Baggett LS, Ingels NB, Miller DC, Grande-Allen KJ. Significant changes in mitral valve leaflet matrix composition and turnover with tachycardia-induced cardiomyopathy. *Circulation.* 2009;120(11 Suppl):S112-119.
46. Stephens EH, Nguyen TC, Itoh A, Ingels NB, Jr., Miller DC, Grande-Allen KJ. The effects of mitral regurgitation alone are sufficient for leaflet remodeling. *Circulation.* 2008;118(14 Suppl):S243-249.
47. Stephens EH, Huynh TN, Cieluch JD, Grande-Allen KJ. Fibronectin-based isolation of valve interstitial cell subpopulations: relevance to valve disease. *J Biomed Mater Res A.* 2010;92(1):340-349.

Chapter 20: Differential Proteoglycan and Hyaluronan

Distribution in Calcified Aortic Valves

In this chapter the topic of examining valves in the setting of various disease states continues with the first of two chapters (Chapters 20 and 21) related to calcific aortic valve disease. Specifically in this chapter, analysis of proteoglycan and glycosaminoglycan content relative to calcified nodules is presented.

ABSTRACT

Background: While the prevalence of calcified aortic valve disease continues to rise and no pharmacological treatments exist, little is known regarding the pathogenesis of the disease. Proteoglycans and the glycosaminoglycan hyaluronan are involved in calcification in atherosclerosis and their characterization in calcified aortic valves may lend insight into the pathogenesis of the disease.

Methods: 14 calcified aortic valves removed during valve replacement surgery were immunohistochemically stained for the proteoglycans (PGs) decorin, biglycan, and versican, as well as the glycosaminoglycan hyaluronan. Staining intensity was evaluated in the following regions of interest: center of calcified nodule, edge of nodule, tissue directly surrounding nodule; center and tissue surrounding small “prenodules”; and fibrosa layer of normal regions of the leaflet distanced from the nodule.

Results: Decorin, biglycan, and versican, as well as hyaluronan, were abundantly present immediately surrounding the calcified nodules, but minimal within the nodule itself. Expression of decorin and biglycan in and surrounding prenodules was greater than in the edge and center regions of mature nodules. The levels of expression of the PGs and hyaluronan highly correlated with one another in the different regions of the valve.

Conclusions: The PGs decorin, biglycan, and versican, as well as the glycoasminoglycan hyaluronan, demonstrated distinctive localization relative to mature nodules within calcified aortic valves, where they likely mediate lipid retention, cell proliferation, and extracellular matrix remodeling, and motivate further study. Comparisons between expression of these components in mature nodules and prenodules suggest distinct roles for these components in nodule progression, especially in the tissues surrounding the nodules. Comparisons between expression of these components in mature nodules and prenodules suggest distinct roles for these components in nodule progression, especially in the tissues surrounding the nodules.

The work contained in this chapter is under review by the journal *Cardiovascular Pathology*:

Stephens EH, Saltarelli JG, Baggett LS, Nandi I, Kuo JJ, Davis AR, Olmstead-Davis EA, Reardon MJ, Morrisett JD, Grande-Allen KJ. **Differential Proteoglycan and Hyaluronan Distribution in Calcified Aortic Valves. *Cardiovasc Pathology*, under review.**

INTRODUCTION

The prevalence of calcific aortic valve disease (CAVD) is rising and represents the second most common indication for cardiac surgery in elderly patients.¹ CAVD is associated with aging,¹ male gender² metabolic syndrome,³ and is only treatable by surgical replacement of the stenotic valve with a mechanical, bioprosthetic or biological valve.⁴ CAVD is marked by lipid retention and monocyte infiltration in its early sclerotic stage, resulting in leaflet thickening, whereas the later stenotic stage is characterized by thickened, stiff, calcified leaflets containing heterotopic bone.⁵ At the present time, there are no pharmacological therapies designed expressly for the treatment of CAVD, largely due to our limited understanding of the disease mechanisms. The use of statins initially appeared promising as a means of preventing or reversing CAVD in patients, based on the ability of these lipid-lowering drugs to reduce valve calcification *in vitro*^{6, 7} and in animal models,⁸⁻¹¹ but unfortunately that promise has not translated to a significant improvement in prospective clinical trials.¹²⁻¹⁴ For these reasons, numerous investigators are examining calcified heart valve lesions and valve cells to determine the roles of osteogenic and inflammation-related genes, various extracellular matrix components, matrix remodeling enzymes, lipids, oxidative stress, and mechanical stress.^{11, 15-18}

A potential role of the extracellular matrix in the initiation and progression of CAVD is suggested by early valve lesions specifically developing within the unique extracellular matrix composition of the fibrosa layer within the leaflet. This layer contains highly aligned collagen as well as the proteoglycans (PGs) decorin and biglycan.^{19, 20} A PG consists of a core protein covalently linked to at least one

glycosaminoglycan (GAG) chain; with the exception of hyaluronan (HA), all GAGs exist *in vivo* as components of PGs. The small leucine-rich PGs decorin and biglycan are themselves interesting because these PGs mediate collagen fibrillogenesis²¹ and sequester transforming growth factor-beta (TGF β),²² and their GAG chains are well known to bind to lipids and lipoproteins in the progression of atherosclerosis.²³ HA also demonstrates the ability to retain lipids.^{24, 25} In atherosclerosis, lipid retention and oxidation triggers inflammation, the proliferation and transdifferentiation of smooth muscle cells, angiotensin receptor activation, and free radical formation, among other processes;^{16, 23, 26, 27} similar mechanisms may occur in aortic valve sclerosis. Intriguingly, O'Brien et al. suggested that biglycan and decorin are co-localized with apolipoprotein-E and apolipoprotein-B in these lipid-rich valve lesions,²⁸ but this notion was never fully explored. The ability of HA to attract and promote the accumulation of monocytes in atherosclerosis suggests an additional potential role for these GAGs in the chronic inflammation of valve disease.^{29, 30} Finally, HA has also been shown to be an effective medium for the delivery of bone morphogenic protein (BMP)-2,^{31, 32} which mediates both normal bony ossification and abnormal heterotopic ossification in many tissues including heart valves.¹⁶ The PGs decorin, biglycan, and versican, as well as all four classes of GAGs, are found in varying abundance in heart valves,^{33, 34} and have been studied in bioprosthetic aortic valves³⁵ and myxomatous mitral valves,³⁶ but have received little attention regarding CAVD.

Therefore, the purpose of this study was to assess the location and abundance of specific PGs and the GAG HA relative to calcific nodules in diseased aortic valves. Such

characterization could improve our understanding of this common valve disease and contribute towards developing novel treatments.

METHODS

Tissue Procurement and Decalcification

Calcified aortic valves that were removed during valve replacement surgery and did not show signs of rheumatic disease were obtained from Baylor College of Medicine (BCM) and Cooperative Human Tissue Network (CHTN) (n=14, mean age 65±15, 80% male). The Institutional Review Board at each institution approved the research use of these tissues. The 10 calcified aortic valves obtained from BCM were either stored in 50% glycerol in phosphate-buffered saline (PBS) at -20°C or in RNAlater (Applied Biosystems, Foster City, CA) at -80°C. Prior to histological processing, glycerol or RNAlater was removed by dialyzing overnight in fresh PBS. Afterwards, several two to three millimeter radial strips were cut from each leaflet and placed into 10% formic acid at room temperature for 12-24 hours (depending on level of calcification) to decalcify the sections allowing routine paraffin embedding; it has been previously shown that formic acid treatment decalcifies tissues without damaging antigenicity.^{37, 38} Once an appropriate level of decalcification was achieved, as determined by palpation, diseased valves were embedded in paraffin and sectioned according to routine procedures. The 4 specimens obtained from the CHTN were already decalcified and embedded in paraffin and were similarly sectioned. The exact method of decalcification for the CHTN samples is undetermined; however, the CHTN stained tissues could not be distinguished from samples from BCM.

Histology and Immunohistochemistry

Sections were stained with Movat pentachrome to demonstrate the heterogeneous microstructure of the leaflet. Immunohistochemistry (IHC) was performed to localize the PGs decorin, biglycan and versican within the valve tissues using antibodies against their respective core proteins. Briefly, tissue slides were processed through a series of graded alcohols and hydrated to water. All slides were pretreated with chondroitinase ABC (200 mU/ml, 37°C, 1 hour) to remove the GAG chains from the PG core proteins. Sections were blocked with 10% goat-serum (Sigma, St. Louis, MO), then incubated with primary antibodies against PGs overnight at 4°C. The rabbit anti-human decorin (LF-136, dilution 1:800) and biglycan antibodies (LF-51, dilution 1:2000) were generously provided by Larry Fisher, Ph.D., NIH, Bethesda, MD;³⁹ the murine antibody against mammalian versican (clone 2-B-1, dilution 1:5000) was purchased from Associates of Cape Code (East Falmouth, MA). After rinsing in PBS, biotinylated secondary antibodies were applied (goat anti-mouse or anti-rabbit IgG, Jackson ImmunoResearch Inc., West Grove, PA) for 1 hour at room temperature. Positive staining was demonstrated by a chromogen reaction using Vectastain Elite ABC and diaminobenzidine kits (Vector Laboratories, Burlingame, CA). The presence of HA was demonstrated by histochemical binding to an HA binding protein (HABP),⁴⁰ which contains the “link” domain protein that normally binds HA to aggrecan in the formation of an aggrecan aggregate. This HA staining procedure required blocking with 2% fetal bovine serum, treating with biotinylated HABP (exactly as described by Lara et al.⁴⁰), then performing

chromogenic detection as described above. All samples were counterstained with hematoxylin. To minimize variability, multiple samples were taken from a given patient's valve. Negative controls for all markers were performed in the absence of the primary antibody or HABP.

Analysis of Immunohistochemical Staining

Several regions of the radially oriented leaflet sections stained for PGs and HA were evaluated to quantify the 8-bit intensity of brown staining using ImageJ software (NIH, Bethesda, MD). Because the binding of lipids by GAGs and PG is speculated to be an early event in the progression of CAVD,⁴¹ calcified nodules were categorized as large and presumably mature ("nodule") or small and presumably early-stage ("prenodule"). Prenodules were identified as subsidiary, substantially smaller nodules (typically $\leq 1/2$ of leaflet cross-sectional width), which were not continuous with the main nodule; prenodules were generally located closer to the annulus than was the main nodule. Regions of interest were identified in the nodule center (innermost 2/3), edge (outermost 1/3), and surrounding tissue; in the prenodule center and surrounding tissue; and in the fibrosa layer of a normal-appearing region of the same leaflet far away from the nodules.

Statistical Analysis

Statistical analysis of data was performed using SAS (Cary, NC). A multifactorial analysis of variance (ANOVA) test was used with the level of significance set at 0.05. Multiple comparisons of group means were performed using the Tukey-

Kramer method for controlling maximum experimentwise error rate. Correlations between staining intensities of different proteins within individual leaflet regions (to assess protein co-localization) were calculated using Pearson Product Moments. For correlations between intensities of different matrix components, the level of significance was reduced to 0.0125 to account for 4 markers being considered.

RESULTS

As expected from numerous previous pathological descriptions,^{4, 5, 26, 33} the Movat pentachrome staining showed that the diseased aortic valves contained large calcific nodules, often occupying approximately one-third of the full radial length. The calcifications were stained dark purple by the Voerhoff's hematoxylin component of the Movat stain, making it straightforward to localize the boundaries of the nodules and thus identify nodule center, edge, and surrounding tissue. All 14 diseased valves had mature nodules, whereas only 7 of the valves had prenodules (Fig. 20-1). The distal regions of most valve leaflets (far away from the nodules) demonstrated a normal appearing layered structure in which the fibrosa layer (stained yellow by the saffron component of the Movat stain) could be identified.

The proteoglycans and HA demonstrated greatest expression in the valve tissue immediately surrounding the mature nodules (Fig. 20-2; overall ANOVA $p < 0.0001$ for decorin, biglycan, and versican; $p = 0.0104$ for HA). There was often a distinct border of

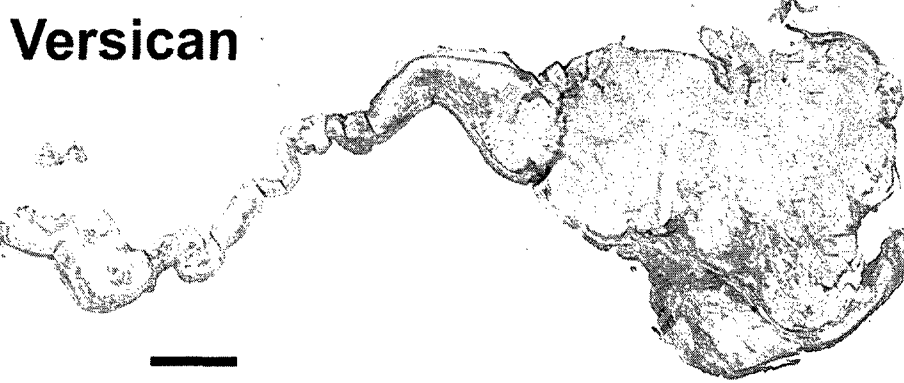
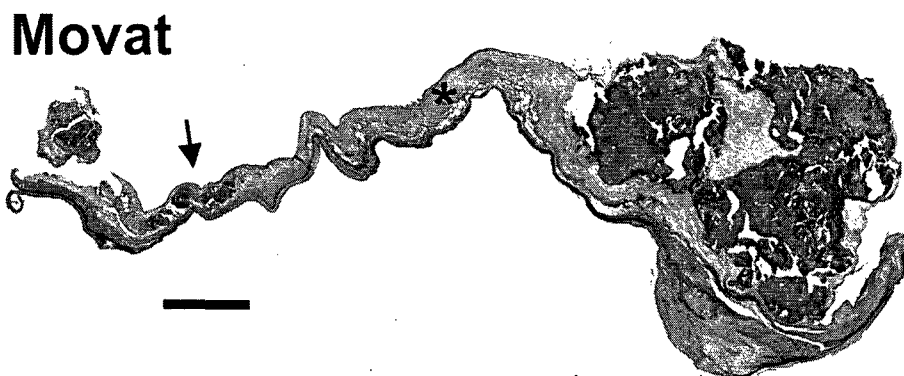
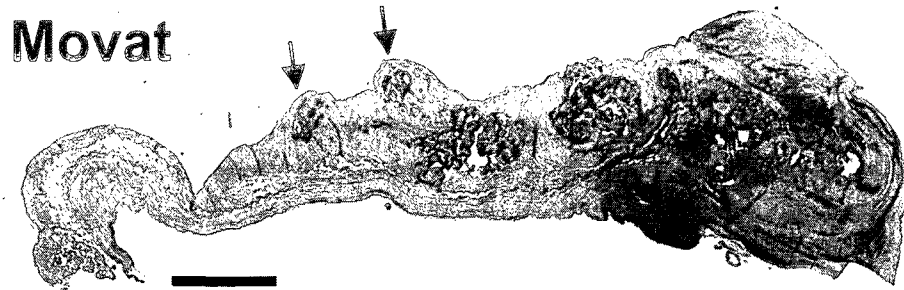
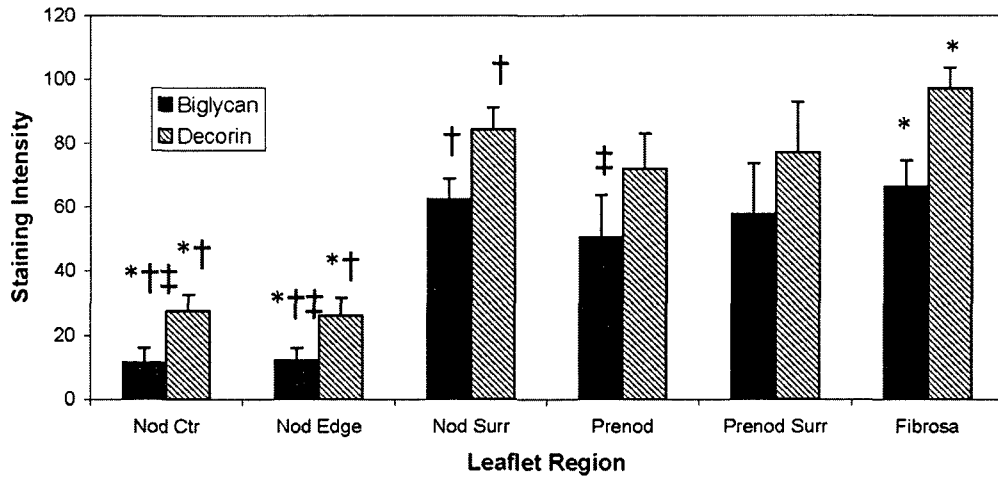


Fig. 20-1: Upper two images: Movat pentachrome stain of two calcified aortic valves showing large nodules at the distal end and small prenodules (indicated by arrows) more proximal to the annular edge of the leaflet. Lower two images: one of the same calcified valve stained for hyaluronan (HA) and versican. Asterisk indicates normal fibrosa; scale bars=1 mm.

Small Proteoglycan Expression



Versican and Hyaluronan Expression

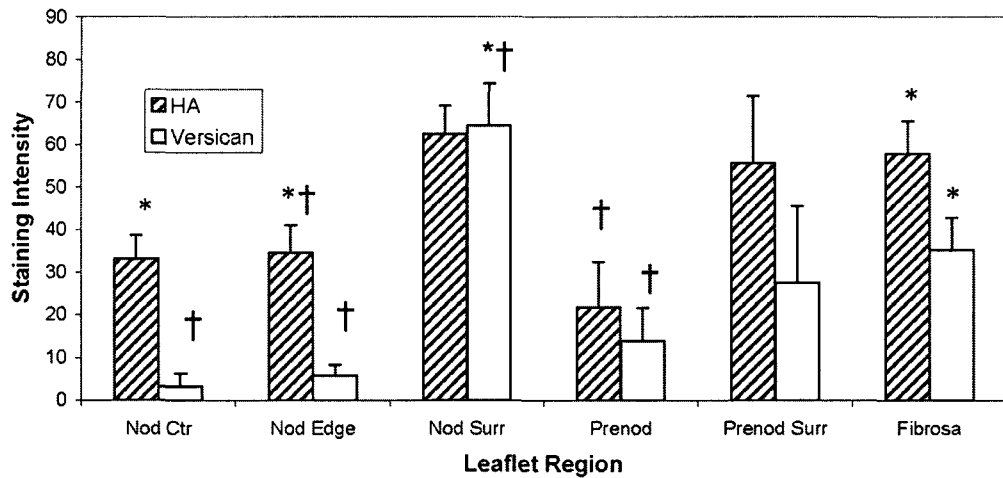


Fig. 20-2: Intensities of staining for PGs and HA in different regions of calcified aortic valves. Error bars indicate standard error of the mean. † $p < 0.05$ compared to Nod Surr. * $p < 0.05$ compared to Fibrosa. ‡ $p < 0.05$ compared to Prenod. Nod Ctr = innermost 2/3 of the large nodule. Nod Edge = outer 1/3 of the large nodule. Nod Surr = tissue immediately surrounding the large nodule. Prenod = prenodule. Prenod Surr = tissue immediately surrounding the prenodule.

expression ending at the nodule, although in some valves there was some degree of PG and HA expression within the nodule as well. Versican and HA expression in the tissue immediately surrounding the nodule was significantly greater than in the nodule edge

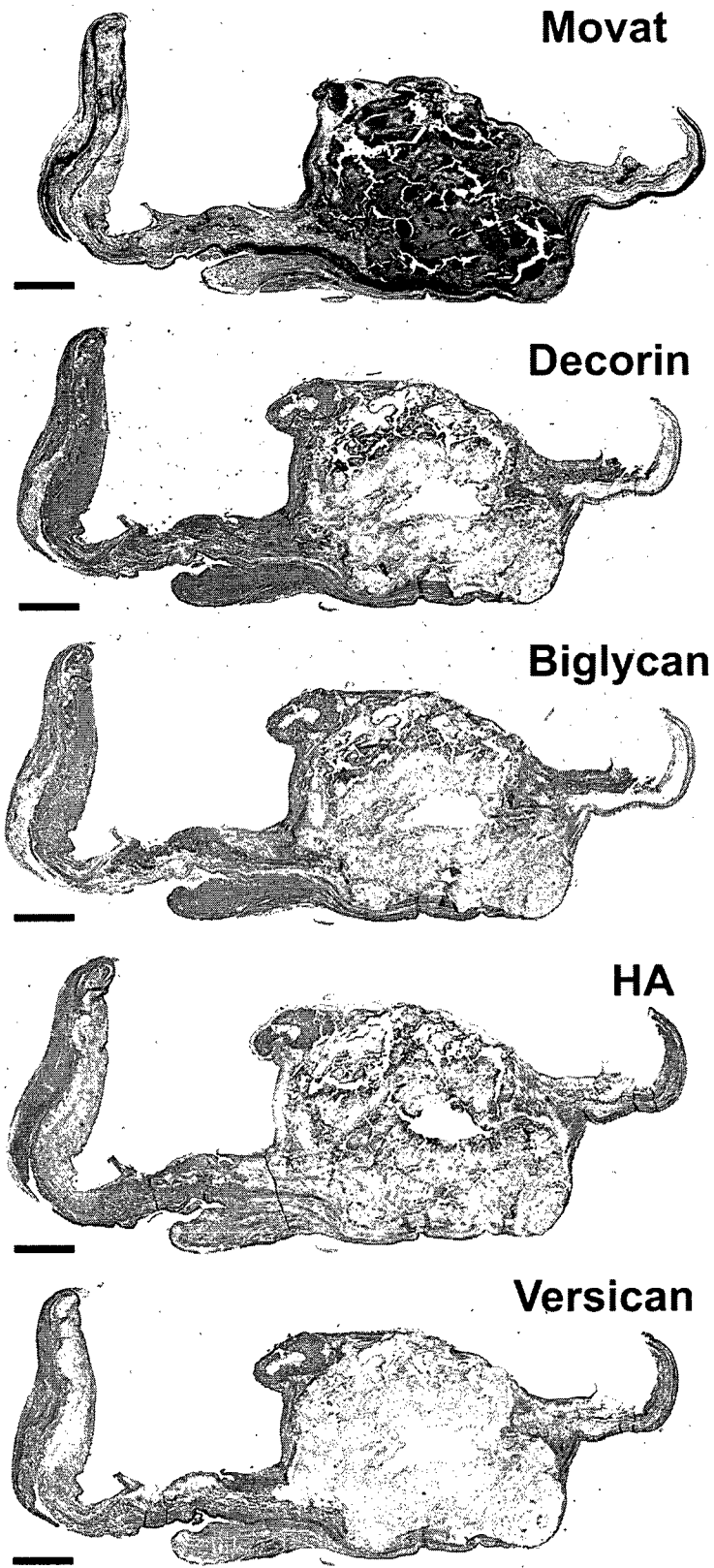


Fig. 20-3: Calcified valve stained with Movat pentachrome and histochemically stained for decorin, biglycan, hyaluronan (HA), and versican. Scale bars=1 mm.

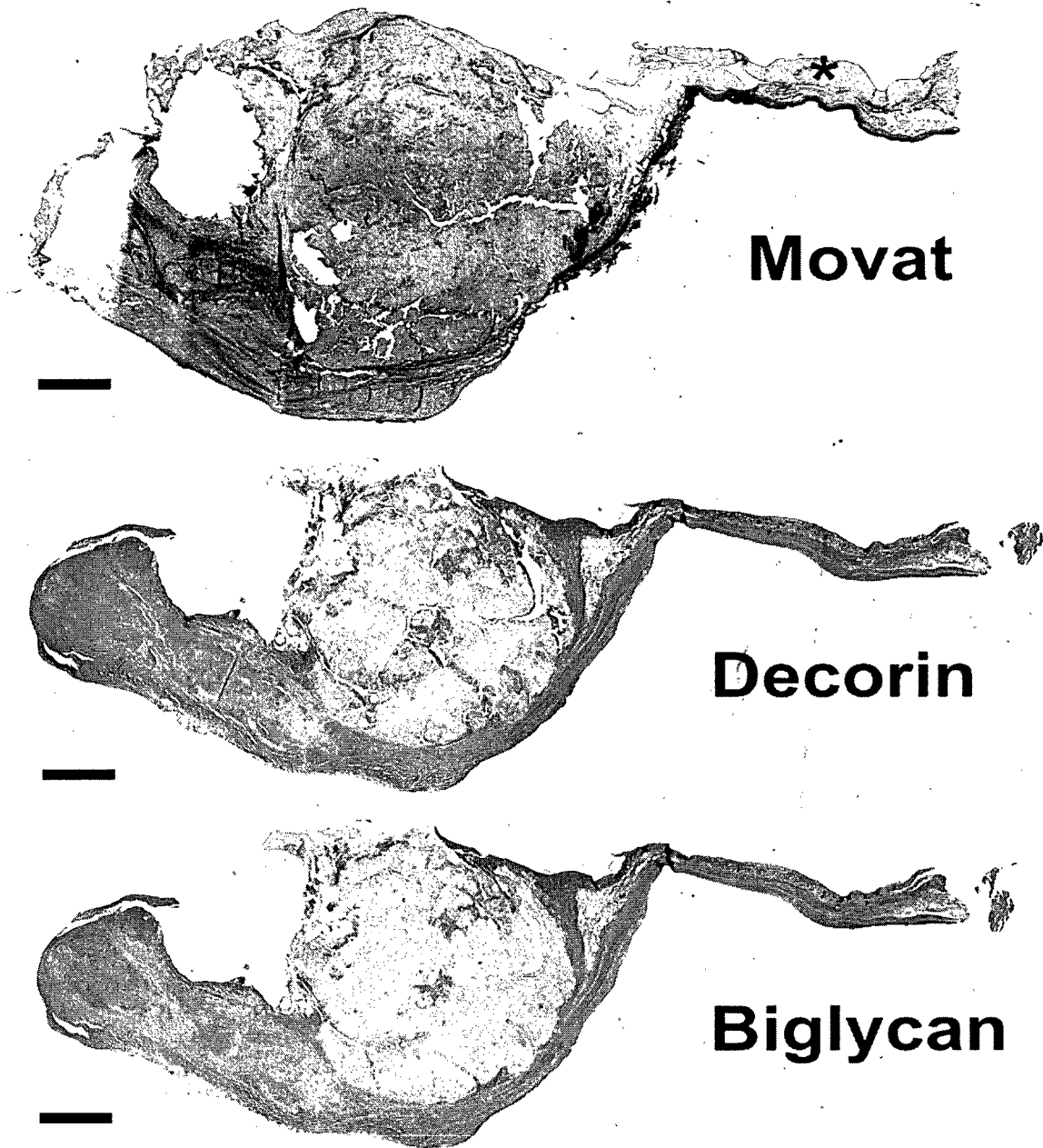


Fig. 20-4: Calcified valve stained with Movat pentachrome and immunohistochemically stained for decorin and biglycan. Asterisk indicates normal fibrosa; scale bars=1 mm.

and prenodule (Fig. 20-1 to 20-3). Versican expression surrounding the nodule was also greater than in the nodule center and in the normal fibrosa; versican expression in the nodule center and edge was lower than in the distal normal fibrosa. While strong

versican expression often directly abutted the nodule, HA expression often tapered off, being externally high and then decreasing approaching the edge of the nodule. Versican expression in the nodule center and edge was also lower than in the distal normal fibrosa. Expression of biglycan within the center and edge of the nodule was significantly lower than in the tissue surrounding the nodule, in the pre-nodule, and in the distal normal fibrosa (Fig. 20-3, 20-4). Expression of decorin showed a similar regional pattern with expression being significantly lowest in the nodule edge and center. The expression of decorin and biglycan within and surrounding pre-nodules was also greater than in the edge and center regions of mature nodules.

The levels of expression of the different PGs and HA were highly correlated with each other in different regions of the diseased aortic valves. In the tissue immediately surrounding the nodule, biglycan expression was positively correlated with expression of versican ($r=0.80$, $p=0.0003$) and HA ($r=0.71$, $p<0.002$). HA and versican were also correlated in this same region ($r=0.79$, $p=0.004$). Decorin and biglycan were positively correlated in the edge (outermost 1/3) of the nodule ($r=0.64$, $p<0.008$), and even more strongly correlated in the tissue surrounding the pre-nodule ($r=0.98$, $p=0.0005$). Interestingly, in the pre-nodule, biglycan was negatively correlated with HA ($r=-0.95$, $p<0.004$). No other significant correlations were found between the various PGs or HA in the center (inner 2/3) of the nodule nor in the distal fibrosa.

DISCUSSION

In this study, we showed that the PGs versican, decorin, and biglycan, as well as the GAG HA, which are normally abundant in distinct regions of the aortic valve, are richly

present within the tissue immediately surrounding the calcified nodules, but generally absent from the nodules. We also found that versican and HA are strongly abundant in the vicinity of the larger nodules, but less so in the smaller “prenodules.” These differences in the distribution of small leucine-rich PGs and the large, hydrated PG and GAG suggest that distinctive remodeling processes are occurring throughout the diseased aortic valve leaflets.

The small leucine-rich PGs decorin and biglycan were abundant throughout the calcified aortic valve leaflets, where they were likely involved with active pathological remodeling in the tissue surrounding the nodules. In normal human aortic valves, decorin and biglycan are ubiquitously distributed,⁴² yet frequently co-localized with collagen, which would support their role in collagen fibrillogenesis.⁴³ The core proteins of these small PGs are also able to bind to growth factors such as TGF β and epidermal growth factor, and thus could influence cell proliferation. In addition, the chondroitin sulfate GAG chains on these PGs are known to bind to lipids and retain them within the local region of the calcific nodule, thereby facilitating the ability of oxidized lipids to initiate further pathological remodeling.⁴⁴ The ability of these GAG chains to bind lipids is influenced by their fine structure, meaning their chain length, the extent and pattern of sulfation, and the isoform of the uronic acid moiety.^{45, 46} As we could not determine by immunohistochemical detection of the PG core proteins whether or not there were differences in the fine structure of the GAG chain, it will be important to examine these small PGs and their GAG chains in the future to discern if the GAG chains in the tissue surrounding the nodule show enhanced lipid binding properties.

The novel finding of the PG versican and HA in the tissue surrounding the calcific nodule further underscores the active remodeling occurring with this area. Versican is a very large PG that contains a multi-domain core protein from which emanates 15-20 very long chondroitin sulfate GAG chains. The G1 domain of the versican core protein is known to destabilize adhesive contacts⁴⁷ and has another region that promotes binding to HA to create a versican aggregate.⁴⁸ The G3 domain is also multifunctional, and contains an epidermal growth factor-like region that promotes cell proliferation.⁴⁹ The GAG chains attached to the center of the core protein imbue the PG with substantial hydration. As a result, the overall versican PG has considerable capability to swell tissues and influence regional cell proliferation and migration. Normally, versican is primarily located within the central spongiosa layer of aortic valves,^{19, 20} where it is believed to aid in the tissue's resistance to cyclic compression and where it can provide lubrication to the outer fibrosa and ventricular layers. Similarly to decorin and especially biglycan, the GAG chains on versican could also bind lipids, as is demonstrated in atherosclerosis.⁵⁰ Versican is linked with numerous additional pathological processes in atherosclerosis as well, including interactions with inflammatory cells and cytokines, roles in platelet aggregation, interference (specific and nonspecific) with normal extracellular matrix assembly, and upregulating cell proliferation.⁵⁰ Recently, it was found that the genes for versican, biglycan, and several enzymes involved in GAG chain assembly (such as xylosyltransferase-I, β -1,4-N-acetylgalactosaminyltransferase) were upregulated in mesenchymal stem cells cultured in osteogenic medium, and that the expression of these genes was strongly and temporally associated with expression of alkaline phosphatase and osteopontin as well as von Kossa

staining for mineralization.⁵¹ Taken together, there is growing evidence pointing towards active roles of these PGs in the progression of CAVD.

The well recognized abilities of HA to influence cell and tissue behavior are also likely to play roles in the tissue surrounding the calcific nodules. HA is normally a linear chain of repeating, unmodified disaccharide units that exists as a distinct molecule thousands of disaccharides long – yielding a potential length up to 10 μm measured end to end. HA can account for up to 50%-60% of all valve GAGs³⁴⁻³⁶ and is secreted by valvular interstitial cells (VICs).^{52, 53} In normal heart valves, HA is attributed with many of the same biophysical characteristics as is versican, namely to promote tissue hydration, lubrication, and resistance to compression.¹⁹ However, HA is abundant in atherosclerotic lesions,⁵⁴ and based on selected other similarities between atherosclerosis and CAVD it is compelling to consider what factors influence HA regulation in atherosclerosis. Atherosclerotic lesions stain strongly for TGF β , as well as for PDGF-AB⁵⁴ and both have been shown to regulate HA synthesis (as well as PG synthesis and GAG chain fine structure⁵⁵) by numerous cell types.⁵⁶ VICs treated with TGF β also upregulate HA secretion.⁵³ HA has been implicated in tissue responses to injury including monocyte adhesion and activation and the proliferation and migration of vascular smooth muscle cells and leukocytes.^{54, 57} Proliferating vascular smooth muscle cells and fibroblasts synthesize more HA,⁵⁷ often as cables that bind and retain monocytes.⁵⁸ HA also demonstrates the ability to retain lipids,^{24, 25} leading to the development of sclerotic lesions.

Other potential therapeutic targets for atherosclerosis, and potentially for CAVD, include the three HA synthases (HAS-1, HAS-2, and HAS-3) and the HA receptors on

the cell surface, namely CD44, RHAMM (the receptor for hyaluronic acid mediated motility), and HARE (HA receptor for endocytosis). It is known that in general, HA ligation to CD44 mediates leukocyte, monocyte, and macrophage recruitment, the production of several inflammatory mediators, vascular cell activation,^{24, 58} tyrosine kinase activity of p185^{HER-2} and src and the activation of Rho and Rac-1. CD44-null mice crossed with apolipoprotein-E null mice had less atherosclerosis than the uncrossed apolipoprotein-E null mice, despite equivalent cholesterol levels.²⁴ Binding of HA to RHAMM activates downstream signaling via src and Ras.⁵⁸ *In vitro*, the addition of low molecular weight HA caused a CD44-dependent upregulation of smooth muscle cell proliferation (an effect also reported in VICs⁵⁹) and VCAM-1 synthesis;²⁴ other HA receptors may also be involved in early lesion development.²⁴ *In vivo*, these low molecular weight HA fragments would be generated by hyaluronidases such as Hyal-1 and Hyal-2.⁶⁰ Taken together, the various factors that promote the formation of an HA-rich matrix likely regulate sclerotic lesion development and inflammatory responses in heart valves as well as vessels, although the roles of HA receptors, synthases, and degrading enzymes in CAVD are presently unknown.

The differences in abundance and correlations between the small PGs and the larger, hydrated versican and HA across the diseased leaflets suggests the presence of distinctive remodeling mechanisms. Each of the examined PGs and HA were more abundant surrounding the nodules compared to the interior of the nodule, which suggest that these molecules are not involved in mineralization. Decorin and biglycan, in particular, were also significantly more abundant in the pre-nodule and region surrounding the pre-nodule compared to the main nodule edge and center. This pattern suggests that

these components are expressed and accumulate early in nodule formation, but then as the nodule matures and becomes more mineralized, their expression within the nodule is reduced and they are more involved in the remodeling of the surrounding tissue. Versican and HA, in contrast, were negatively correlated with decorin and biglycan in the prenodule, suggesting that they are less involved in the early nodule formation and more involved in remodeling surrounding the mineralized tissues. It may be that versican and HA are subjected to some form of paracrine regulation that is distinctive between the prenodules and large mineralized nodules. Others have similarly shown that smaller calcific nodules are more highly vascularized than are larger nodules.⁶¹ The presence of HA and versican surrounding the larger nodules might be a way to promote improved diffusion of nutrients and oxygen through these valve regions, since diffusion would be enhanced with more highly hydrated tissues.

CONCLUSIONS

In conclusion, we have shown that the PGs decorin, biglycan, and versican, and the GAG HA demonstrate distinctive patterns of expression in the vicinity of large and small nodules in calcified aortic valves. The diverse biological and biophysical functions of these extracellular matrix molecules, and the complexities of their regulation, make them compelling subjects for future investigations of the development and treatment of CAVD.

In this chapter, which analyzed proteoglycan and glycosaminoglycan content relative to calcified nodules, the topic of examining valves in the setting of various disease states continued. The next chapter contains the second of these two studies on calcific aortic valve disease, in which markers of hypoxia, hyaluronan homeostasis, brown adipocytes, and osteogenesis and chondrogenesis were analyzed relative to calcified nodules.

REFERENCES

1. Stewart BF, Siscovick D, Lind BK, Gardin JM, Gottdiener JS, Smith VE, Kitzman DW, Otto CM. Clinical factors associated with calcific aortic valve disease. *J Am Coll Cardiol*. 1997;29(3):630-634.
2. Owens DS, Katz R, Takasu J, Kronmal R, Budoff MJ, O'Brien KD. Incidence and Progression of Aortic Valve Calcium in the Multi-Ethnic Study of Atherosclerosis (MESA). *Am J Cardiol*. 105(5):701-708.
3. Katz R, Wong ND, Kronmal R, Takasu J, Shavelle DM, Probstfield JL, Bertoni AG, Budoff MJ, O'Brien KD. Features of the metabolic syndrome and diabetes mellitus as predictors of aortic valve calcification in the Multi-Ethnic Study of Atherosclerosis. *Circulation*. 2006;113(17):2113-2119.
4. Schoen FJ. Cardiac valves and valvular pathology: update on function, disease, repair, and replacement. *Cardiovasc Pathol*. 2005;14(4):189-194.
5. Mohler ER, 3rd, Gannon F, Reynolds C, Zimmerman R, Keane MG, Kaplan FS. Bone formation and inflammation in cardiac valves. *Circulation*. 2001;103(11):1522-1528.
6. Wu B, Elmariah S, Kaplan FS, Cheng G, Mohler ER, 3rd. Paradoxical effects of statins on aortic valve myofibroblasts and osteoblasts: implications for end-stage valvular heart disease. *Arterioscl Thromb Vasc Biol*. 2005;25(3):592-597.
7. Osman L, Yacoub MH, Latif N, Amrani M, Chester AH. Role of human valve interstitial cells in valve calcification and their response to atorvastatin. *Circulation*. 2006;114(1 Suppl):I547-552.
8. Rajamannan NM, Subramaniam M, Caira F, Stock SR, Spelsberg TC. Atorvastatin inhibits hypercholesterolemia-induced calcification in the aortic valves via the Lrp5 receptor pathway. *Circulation*. 2005;112(9 Suppl):I229-234.
9. Rajamannan NM, Subramaniam M, Springett M, Sebo TC, Niekrasz M, McConnell JP, Singh RJ, Stone NJ, Bonow RO, Spelsberg TC. Atorvastatin inhibits hypercholesterolemia-induced cellular proliferation and bone matrix production in the rabbit aortic valve. *Circulation*. 2002;105(22):2660-2665.
10. Rajamannan NM, Subramaniam M, Stock SR, Stone NJ, Springett M, Ignatiev KI, McConnell JP, Singh RJ, Bonow RO, Spelsberg TC. Atorvastatin inhibits calcification and enhances nitric oxide synthase production in the hypercholesterolaemic aortic valve. *Heart (British Cardiac Society)*. 2005;91(6):806-810.
11. Caira FC, Stock SR, Gleason TG, McGee EC, Huang J, Bonow RO, Spelsberg TC, McCarthy PM, Rahimtoola SH, Rajamannan NM. Human degenerative valve disease is associated with up-regulation of low-density lipoprotein receptor-related protein 5 receptor-mediated bone formation. *J Am Coll Cardiol*. 2006;47(8):1707-1712.
12. Rossebo AB, Pedersen TR, Boman K, Brudi P, Chambers JB, Egstrup K, Gerds E, Gohlke-Barwolf C, Holme I, Kesaniemi YA, Malbecq W, Nienaber CA, Ray S, Skjaerpe

- T, Wachtell K, Willenheimer R. Intensive lipid lowering with simvastatin and ezetimibe in aortic stenosis. *N Engl J Med.* 2008;359(13):1343-1356.
13. Cowell SJ, Newby DE, Prescott RJ, Bloomfield P, Reid J, Northridge DB, Boon NA. A randomized trial of intensive lipid-lowering therapy in calcific aortic stenosis. *N Engl J Med.* 2005;352(23):2389-2397.
 14. Moura LM, Ramos SF, Zamorano JL, Barros IM, Azevedo LF, Rocha-Goncalves F, Rajamannan NM. Rosuvastatin affecting aortic valve endothelium to slow the progression of aortic stenosis. *J Am Coll Cardiol.* 2007;49(5):554-561.
 15. Miller JD, Chu Y, Brooks RM, Richenbacher WE, Pena-Silva R, Heistad DD. Dysregulation of antioxidant mechanisms contributes to increased oxidative stress in calcific aortic valvular stenosis in humans. *J Am Coll Cardiol.* 2008;52(10):843-850.
 16. O'Brien KD. Pathogenesis of calcific aortic valve disease: a disease process comes of age (and a good deal more). *Arterioscl Thromb Vasc Biol.* 2006;26(8):1721-1728.
 17. Monzack EL, Gu X, Masters KS. Efficacy of simvastatin treatment of valvular interstitial cells varies with the extracellular environment. *Arterioscler Thromb Vasc Biol.* 2009;29(2):246-253.
 18. Sucusky P, Padala M, Elhammali A, Balachandran K, Jo H, Yoganathan AP. Design of an ex vivo culture system to investigate the effects of shear stress on cardiovascular tissue. *J Biomech Eng.* 2008;130(3):035001.
 19. Stephens EH, Chu CK, Grande-Allen KJ. Valve proteoglycan content and glycosaminoglycan fine structure are unique to microstructure, mechanical loads, and age: relevance to an age-specific tissue engineered heart valve. *Acta Biomaterialia.* 2008;4:1148-1160.
 20. Latif N, Sarathchandra P, Taylor PM, Antoniw J, Yacoub MH. Localization and pattern of expression of extracellular matrix components in human heart valves. *J Heart Valve Dis.* 2005;14(2):218-227.
 21. Reed CC, Iozzo RV. The role of decorin in collagen fibrillogenesis and skin homeostasis. *Glycoconj J.* 2002;19(4-5):249-255.
 22. Kresse H, Schonherr E. Proteoglycans of the extracellular matrix and growth control. *J Cell Physiol.* 2001;189(3):266-274.
 23. Nakashima Y, Fujii H, Sumiyoshi S, Wight TN, Sueishi K. Early human atherosclerosis: accumulation of lipid and proteoglycans in intimal thickenings followed by macrophage infiltration. *Arterioscler Thromb Vasc Biol.* 2007;27(5):1159-1165.
 24. Cuff CA, Kothapalli D, Azonobi I, Chun S, Zhang Y, Belkin R, Yeh C, Secreto A, Assoian RK, Rader DJ, Pure E. The adhesion receptor CD44 promotes atherosclerosis by mediating inflammatory cell recruitment and vascular cell activation. *J Clin Invest.* 2001;108(7):1031-1040.

25. Seike M, Ikeda M, Matsumoto M, Hamada R, Takeya M, Kodama H. Hyaluronan forms complexes with low density lipoprotein while also inducing foam cell infiltration in the dermis. *J Dermatol Sci*. 2006;41(3):197-204.
26. O'Brien KD, Reichenbach DD, Marcovina SM, Kuusisto J, Alpers CE, Otto CM. Apolipoproteins B, (a), and E accumulate in the morphologically early lesion of 'degenerative' valvular aortic stenosis. *Arterioscler Thromb Vasc Biol*. 1996;16(4):523-532.
27. Chang MY, Potter-Perigo S, Tsoi C, Chait A, Wight TN. Oxidized low density lipoproteins regulate synthesis of monkey aortic smooth muscle cell proteoglycans that have enhanced native low density lipoprotein binding properties. *J Biol Chem*. 2000;275(7):4766-4773.
28. O'Brien KD, Otto CM, Reichenbach DD, Alpers CE, Wight TN. Regional accumulation of proteoglycans in lesions of "degenerative" valvular aortic stenosis and their relationship to apolipoproteins. *Circulation*. 1995;92(suppl I):I-612.
29. de la Motte CA, Hascall VC, Drazba J, Bandyopadhyay SK, Strong SA. Mononuclear leukocytes bind to specific hyaluronan structures on colon mucosal smooth muscle cells treated with polyinosinic acid:polycytidylic acid: inter-alpha-trypsin inhibitor is crucial to structure and function. *Am J Pathol*. 2003;163(1):121-133.
30. Bobik A, Agrotis A, Kanellakis P, Dilley R, Krushinsky A, Smirnov V, Tararak E, Condron M, Kostolias G. Distinct patterns of transforming growth factor-beta isoform and receptor expression in human atherosclerotic lesions. Colocalization implicates TGF-beta in fibrofatty lesion development. *Circulation*. 1999;99(22):2883-2891.
31. Itoh S, Matubara M, Kawauchi T, Nakamura H, Yukitake S, Ichinose S, Shinomiya K. Enhancement of bone ingrowth in a titanium fiber mesh implant by rhBMP-2 and hyaluronic acid. *J Mater Sci Mater Med*. 2001;12(7):575-581.
32. Kim HD, Valentini RF. Retention and activity of BMP-2 in hyaluronic acid-based scaffolds in vitro. *J Biomed Mater Res*. 2002;59(3):573-584.
33. Otto CM, Kuusisto J, Reichenbach DD, Gown AM, O'Brien KD. Characterization of the early lesion of 'degenerative' valvular aortic stenosis. Histological and immunohistochemical studies. *Circulation*. 1994;90(2):844-853.
34. Grande-Allen KJ, Calabro A, Gupta V, Wight TN, Hascall VC, Vesely I. Glycosaminoglycans and proteoglycans in normal mitral valve leaflets and chordae: association with regions of tensile and compressive loading. *Glycobiology*. 2004;14(7):621-633.
35. Grande-Allen KJ, Mako WJ, Calabro A, Shi Y, Ratliff NB, Vesely I. Loss of chondroitin 6-sulfate and hyaluronan from failed porcine bioprosthetic valves. *J Biomed Mater Res*. 2003;65(2):251-259.
36. Grande-Allen KJ, Griffin BP, Ratliff NB, Cosgrove DM, Vesely I. Glycosaminoglycan profiles of myxomatous mitral leaflets and chordae parallel the severity of mechanical alterations. *J Am Coll Cardiol*. 2003;42(2):271-277.

37. Athanasou NA, Quinn J, Heryet A, Woods CG, McGee JO. Effect of decalcification agents on immunoreactivity of cellular antigens. *J Clin Pathol*. 1987;40(8):874-878.
38. McCormick D, Chong H, Hobbs C, Datta C, Hall PA. Detection of the Ki-67 antigen in fixed and wax-embedded sections with the monoclonal antibody MIB1. *Histopathology*. 1993;22(4):355-360.
39. Fisher LW, Stubbs JT, 3rd, Young MF. Antisera and cDNA probes to human and certain animal model bone matrix noncollagenous proteins. *Acta Orthop Scand Suppl*. 1995;266:61-65.
40. Lara SL, Evanko SP, Wight TN. Morphological evaluation of proteoglycans in cells and tissues. *Methods Mol Biol*. 2001;171:271-290.
41. Grande-Allen KJ, Osman N, Ballinger ML, Dadlani H, Marasco S, Little PJ. Glycosaminoglycan synthesis and structure as targets for the prevention of calcific aortic valve disease. *Cardiovasc Res*. 2007;76(1):19-28.
42. Latif N, Sarathchandra P, Taylor PM, Antoniow J, Yacoub MH. Localization and Pattern of Expression of Extracellular Matrix Components in Human Heart Valves. *J Heart Valve Dis*. 2005;14:218-227.
43. Reed CC, Iozzo RV. The role of decorin in collagen fibrillogenesis and skin homeostasis. *Glycoconj J*. 2002;19(4-5):249-255.
44. Camejo G, Hurt-Camejo E, Wiklund O, Bondjers G. Association of apo B lipoproteins with arterial proteoglycans: pathological significance and molecular basis. *Atherosclerosis*. 1998;139(2):205-222.
45. Camejo G, Hurt-Camejo E, Olsson U, Bondjers G. Proteoglycans and lipoproteins in atherosclerosis. *Curr Opin Lipidol*. 1993;4:385-391.
46. Ballinger ML, Nigro J, Frontanilla KV, Dart AM, Little PJ. Regulation of glycosaminoglycan structure and atherogenesis. *Cell Mol Life Sci*. 2004;61(11):1296-1306.
47. Yang BL, Zhang Y, Cao L, Yang BB. Cell adhesion and proliferation mediated through the G1 domain of versican. *J Cell Biochem*. 1999;72(2):210-220.
48. Matsumoto K, Shionyu M, Go M, Shimizu K, Shinomura T, Kimata K, Watanabe H. Distinct interaction of versican/PG-M with hyaluronan and link protein. *J Biol Chem*. 2003;278(42):41205-41212.
49. Zhang S, Chang MC, Zylka D, Turley S, Harrison R, Turley EA. The hyaluronan receptor RHAMM regulates extracellular-regulated kinase. *J Biol Chem*. 1998;273(18):11342-11348.
50. Wight TN, Merrilees MJ. Proteoglycans in atherosclerosis and restenosis: key roles for versican. *Circ Res*. 2004;94(9):1158-1167.

51. Muller B, Prante C, Gastens M, Kuhn J, Kleesiek K, Gotting C. Increased levels of xylosyltransferase I correlate with the mineralization of the extracellular matrix during osteogenic differentiation of mesenchymal stem cells. *Matrix Biol.* 2008;27(2):139-149.
52. Gupta V, Werdenberg JA, Blevins TL, Grande-Allen KJ. Synthesis of glycosaminoglycans in differently loaded regions of collagen gels seeded with valvular interstitial cells. *Tissue engineering.* 2007;13(1):41-49.
53. Jian B, Narula N, Li QY, Mohler ER, 3rd, Levy RJ. Progression of aortic valve stenosis: TGF-beta1 is present in calcified aortic valve cusps and promotes aortic valve interstitial cell calcification via apoptosis. *Ann Thorac Surg.* 2003;75(2):457-465; discussion 465-456.
54. Evanko SP, Raines EW, Ross R, Gold LI, Wight TN. Proteoglycan distribution in lesions of atherosclerosis depends on lesion severity, structural characteristics, and the proximity of platelet-derived growth factor and transforming growth factor-beta. *Am J Pathol.* 1998;152(2):533-546.
55. Kinsella MG, Bressler SL, Wight TN. The regulated synthesis of versican, decorin, and biglycan: extracellular matrix proteoglycans that influence cellular phenotype. *Crit Rev Euk Gene Exp.* 2004;14(3):203-234.
56. Allison DD, Grande-Allen KJ. Review. Hyaluronan: a powerful tissue engineering tool. *Tissue Eng.* 2006;12(8):2131-2140.
57. Evanko SP, Angello JC, Wight TN. Formation of hyaluronan- and versican-rich pericellular matrix is required for proliferation and migration of vascular smooth muscle cells. *Arterioscl Thromb Vasc Biol.* 1999;19(4):1004-1013.
58. Wilkinson TS, Bressler SL, Evanko SP, Braun KR, Wight TN. Overexpression of hyaluronan synthases alters vascular smooth muscle cell phenotype and promotes monocyte adhesion. *J Cell Physiol.* 2006;206(2):378-385.
59. Masters KS, Shah DN, Leinwand LA, Anseth KS. Crosslinked hyaluronan scaffolds as a biologically active carrier for valvular interstitial cells. *Biomaterials.* 2005;26(15):2517-2525.
60. Csoka AB, Frost GI, Stern R. The six hyaluronidase-like genes in the human and mouse genomes. *Matrix Biol.* 2001;20(8):499-508.
61. Charest A, Pepin A, Shetty R, Cote C, Voisine P, Dagenais F, Pibarot P, Mathieu P. Distribution of SPARC during neovascularisation of degenerative aortic stenosis. *Heart.* 2006;92(12):1844-1849.

Chapter 21: Hyaluronan Turnover and Hypoxic Brown Adipocytes are Co-localized with Endochondral Ossification in Calcified Aortic Valves

This chapter contains the second of two studies on calcific aortic valve disease (Chapters 20 and 21). In this chapter markers of hypoxia, hyaluronan homeostasis, brown adipocytes, and osteogenesis and chondrogenesis were analyzed relative to calcified nodules.

ABSTRACT

Background: While calcified aortic valve disease is the most common adult heart valve disease and incurs a substantial burden on today's society, little is known regarding the mechanisms involved in the pathogenesis of this disease. The aim of this study was to assess markers related to hypoxia, hyaluronan homeostasis, brown fat, and bone/cartilage formation in different regions of valves with calcified nodules. Characterization of these markers' expression both relative to nodules at different stages in development as well as relative to other markers could lend insight into the mechanisms involved in nodule formation in CAVD.

Methods: 14 calcified aortic valves removed during valve replacement surgery were immunohistochemically stained for markers from different mechanistic families potentially involved in nodule formation: hypoxia/brown fat, hyaluronan homeostasis,

and ossification. Staining intensity was evaluated in the following regions of interest: center of calcified nodule (NodCtr), edge of nodule (NodEdge), tissue directly surrounding nodule (NodSurr); center and tissue surrounding small “prenodules” (PreNod, PreNodSurr); and fibrosa layer of normal regions of the leaflet distanced from the nodule (CollFibr).

Results: Region-specific localization of markers from the different mechanistic families was evident, with strong correlations between markers from the different mechanistic families that were distinct with respect to region. Osteogenic markers were found to primarily localize to the nodule, along with markers related to hyaluronan turnover and hypoxia. Markers of brown fat cells were found to co-localize with markers of hypoxia. In NodCtr as well as NodSurr, the expression of hyaluronidase-1, which degrades hyaluronan, strongly correlated with both markers of brown fat and ossification markers. In NodEdge, however, the marker of hyaluronan synthesis, HAS-2, demonstrated strongly correlated with markers of brown fat, hypoxia, and ossification. Tumor necrosis factor- α stimulated gene-6 (TSG-6) protein, which when bound to hyaluronan will promote ossification, strongly correlated with ossification markers and hyaluronidase in the regions surrounding the nodules (NodSurr, PreNodSurr).

Conclusions: This study demonstrates for the first time a role for hyaluronan homeostasis and the promotion of hypoxia by brown fat cells in calcific aortic valve disease. Interactions between markers from the different mechanistic families were heterogeneous relative to calcific nodules, suggesting distinct roles for these mechanisms

within the complex microanatomy of nodule pathogenesis. Future work examining causative relationships between these factors will expand upon the associative findings demonstrated in this study.

The work contained in this chapter is in preparation for submission to *Cardiovascular Pathology*.

INTRODUCTION

Valve disease is widely prevalent in our society, with valve replacement or repair in almost 100,000 people in the United States¹ and 275,000 people worldwide each year.² The most common heart valve disease is calcific aortic valve disease (CAVD), also known as calcific aortic stenosis. CAVD is associated with aging and the obesity-driven metabolic syndrome and thus is predicted to become an ever increasing clinical problem in the U.S. population³ whose treatment will represent substantial health care costs. Despite these statistics, there are no treatments for CAVD other than surgical aortic valve replacement, nor are there any medications that specifically target CAVD. Moreover, investigators have only begun to explore possible mechanisms for the progression of CAVD in the last several years.

Several previous mechanistic studies of the development and progression of CAVD have related to the deposition of calcific nodules, which is a hallmark of the advanced valvular sclerotic lesion, and which cause the leaflets to become stiff and the valve stenotic. These nodules, which may appear as hydroxyapatite crystals and show characteristics of heterotopic bone,⁴ are found in association with lipids both in human valves and in animal models. Calcified aortic valve leaflets also contain osteoblast-like cells⁵ and an abundance of several osteogenic mediators, including bone morphogenic protein-2 (BMP-2).^{6, 7} Investigations of heterotopic bone formation in a mouse muscle model⁸ have shown associations between overproduction of BMP-2, rapid production of brown fat cells that stimulate hypoxic conditions, and heterotopic endochondral ossification. In this model, three days after the delivery of excess BMP-2 to the muscle, gene expression was strongly upregulated for several markers that are also reportedly

elevated in either atherosclerosis or CAVD, including CD44, E-selectin, apolipoprotein E, cyclooxygenase-2, prostaglandins, and the small proteoglycan decorin.⁹ Expression of many of these markers is regulated by the inflammatory cytokine tumor necrosis factor- α (TNF- α), which is intriguing because the TNF- α stimulated gene-6 protein (TSG-6) provides a mechanistic link between BMP-2 and the glycosaminoglycan hyaluronan (HA).

Due to the complex ability of HA to bind to lipids and monocytes,^{10, 11} the many regulators of HA homeostasis (synthases, receptors, and degrading enzymes) have been strongly associated with the progression of atherosclerosis,^{10, 12-14} and these same regulators may potentially impact CAVD as well. HA can also bind to TSG-6 through a Link-protein-like domain; TSG-6 binds to BMP-2 through this same domain, thereby inhibiting BMP-2 mediated ossification.¹⁵ In the presence of HA, the TSG-6 Link domain is bound to HA, and therefore TSG-6 cannot inhibit BMP-2. Perhaps for this reason, HA has been shown to be a very efficient carrier of BMP-2 promoting the mineralization of tissue engineered bone and bony ingrowth into implants.^{16, 17}

The purpose of this study was to investigate the relationships between BMP-2, hypoxia, HA regulation, and endochondral ossification by performing immunohistochemistry on calcified aortic valves. The two primary hypotheses examined were first, that BMP-2-potentiated hypoxia, as demonstrated by markers of brown adipocytes, would be associated with markers for bone and chondrocytes. The second hypothesis was that in leaflet regions demonstrating overall HA synthesis, TSG-6 would be unable to bind to BMP-2 and thus BMP-2 could promote calcification, but otherwise TSG-6 could bind and inhibit BMP-2 activity.

METHODS

Tissue Procurement and Decalcification

[For a complete description of Tissue Procurement and Decalcification for this study, please see Chapter 20]

Calcified aortic valves that were removed during valve replacement surgery and did not show signs of rheumatic disease were obtained from Baylor College of Medicine (BCM) and Cooperative Human Tissue Network (CHTN) (n=14, 80% male, mean age 65±15). After decalcification, diseased valves were embedded in paraffin and sectioned according to routine procedures.

Histology and Immunohistochemistry

Sections were stained with Movat pentachrome to demonstrate the general microstructure of the leaflet. Sections were also stained immunohistochemically for a range of proteins related to osteogenesis and chondrogenesis, hyaluronan homeostasis, and hypoxia (Table 21-1). Briefly, sections were deparaffinized using xylene and then were rehydrated using a decreasing gradient of ethanol. Hydrated sections underwent citrate buffer-based antigen retrieval (Antigen Decloaker, Biocare Medical, Concord, CA) or enzymatic pre-treatment appropriate for each antibody. Sections were blocked with 10% goat-serum (Sigma, St. Louis, MO), then incubated with primary antibodies at 37°C for one hour. After rinsing in PBS, biotinylated secondary antibodies were applied (goat anti-mouse or anti-rabbit IgG, Jackson ImmunoResearch Inc., West Grove, PA) for

Table 21-1. Antibodies Used in Immunohistochemistry.

Protein	Function
Hyaluronan (HA)-related	
Hyaluronan receptor for endocytosis (HARE) ^a	HA clearance from bloodstream
Hyaluronan synthase-2 (HAS-2) ^b	HA synthesis
CD168 ^c	Receptor for HA mediated motility
Hyaluronidase-1 (Hyal-1) ^d	HA degrading endolyase
Hypoxia-related	
Uncoupling protein-1 (UCP-1) ^e	Identifies brown adipocytes
Peroxisome proliferator-activated receptor γ , co-activator 1 α (PGC-1 α) ^f	Identifies newly differentiated brown adipocytes
Hypoxia inducible factor-1 (HIF-1 α) ^g	Expressed in the setting of oxygen deprivation
Ossification-related	
Bone morphogenic protein-2 (BMP-2) ^h	Involved in osteoblast cell differentiation
S-100 ⁱ	Identifies chondrocytes
Tumor necrosis factor α simulated gene-6 protein (TSG-6) ^j	Inhibits BMP-2 mediated ossification
Periostin ^k	Osteoblast specific factor

^agift from Dr. Paul Weigel, University of Oklahoma Health Science Center (Oklahoma City, OK); ^bgift from Dr. Melanie Simpson, University of Nebraska (Lincoln, NE); ^cLeica Microsystems (St. Louis, MO); ^dAbnova (Nieuhi, Taipei, Taiwan); ^eChemicon/Millipore International (Billerica, ME); ^fEMD/Calbiochem (Gibbstown, NJ); ^gR&D Systems (Minneapolis, MN); ^hLifespan Biosciences (Seattle, WA); ⁱThermoFisher Scientific (Fremont, CA); ^jSanta Cruz Biotechnology (Santa Cruz, CA).

1 hour at room temperature. Positive staining was demonstrated by a chromogen reaction using Vectastain Elite ABC and diaminobenzidine kits (Vector Laboratories, Burlingame, CA). All samples were counterstained with hematoxylin. To minimize variability, multiple samples were taken from a given patient's valve. Negative controls for all markers were performed in the absence of the primary antibody.

Analysis of Immunohistochemical Staining

Several regions of the radially oriented leaflet sections were evaluated to quantify the 8-bit intensity of brown staining using ImageJ software (NIH, Bethesda, MD). Calcified nodules were categorized as large and presumably mature ("nodule") or small and presumably early-stage ("prenodule"). Prenodules were identified as subsidiary, substantially smaller nodules (typically $\leq 1/2$ of leaflet height), which were not continuous

with the main nodule; prenODULES were generally located closer to the annulus than was the main nodule. Regions of interest were identified (Fig. 21-1) in the nodule center (NodCtr, innermost 1/3), edge (NodEdge, outermost 1/3), and surrounding tissue (NodSurr); in the prenodule center (PreNod) and surrounding tissue (PreNodSurr); and in the fibrosa layer of a normal-appearing region of the same leaflet far away from the nodules (CollFibr).

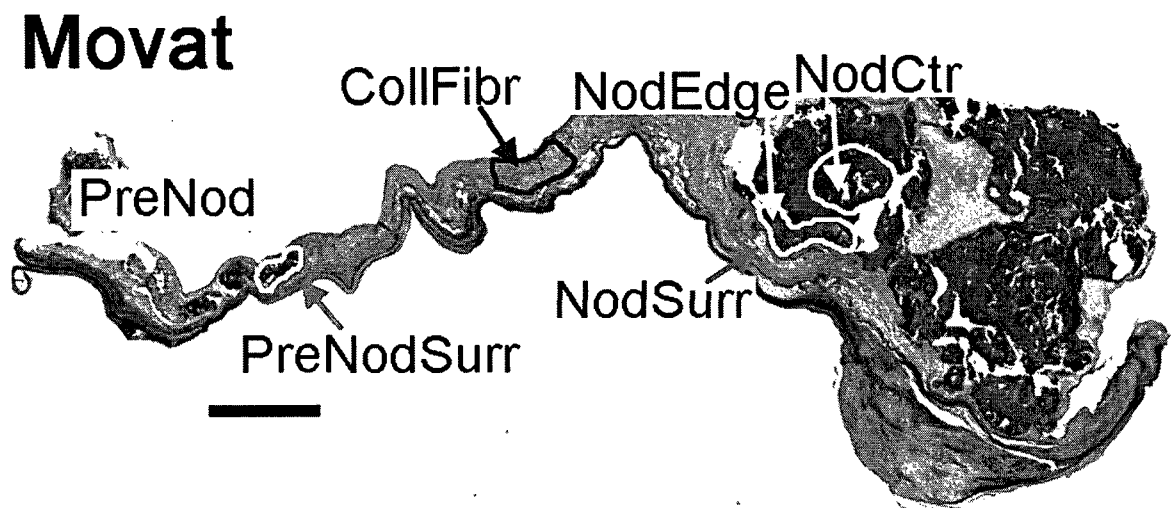


Fig. 21-1: Representative Movat stained section illustrating different regions analyzed: NodCtr=nodule center, NodEdge=outermost edge of nodule, NodSurr=region surrounding nodule, PreNod=prenodule center, PreNodSurr=region surrounding prenodule, CollFibr=collagenous fibrosa from normal-appearing portion of leaflet. Scale bar indicates 1 mm.

Statistical Analysis

Statistical analysis of data was performed using SAS (Cary, NC). Correlations between staining intensities of different proteins within individual leaflet regions (to assess protein co-localization) were calculated using Pearson Product Moments. For correlations between intensities of different matrix components, the level of significance

was reduced to 0.0045 to account for 11 markers being considered. Correlations for which $p < 0.01$ were considered trends.

RESULTS

Co-localizations between Markers

BMP-2 was primarily demonstrated within the calcific nodule (meaning both NodCtr and NodEdge, unless otherwise noted), with some staining in NodSurr as well. BMP-2 was often co-localized with staining for Hyal-1 (Fig. 21-2) and to a lesser extent HIF-1 α (Fig. 21-3). HIF-1 α staining was generally observed inside the nodule as well (where usually staining in NodCtr appeared stronger than NodEdge), and was usually co-localized with S-100, BMP-2, and PGC-1 α (Fig. 21-3). TSG-6 was often localized to the inside of the nodule (with PGC-1 α and UCP-1), but could also be found in NodSurr; TSG-6 was partly co-localized with BMP-2. Similarly, Hyal-1 and HAS-2 were most often demonstrated within the nodule, but were also found in NodEdge, where Hyal-1 was often co-localized with TSG-6. Periostin was predominantly localized to within and immediately adjacent to the nodule than in the remainder of the leaflet tissue (Fig. 21-4).

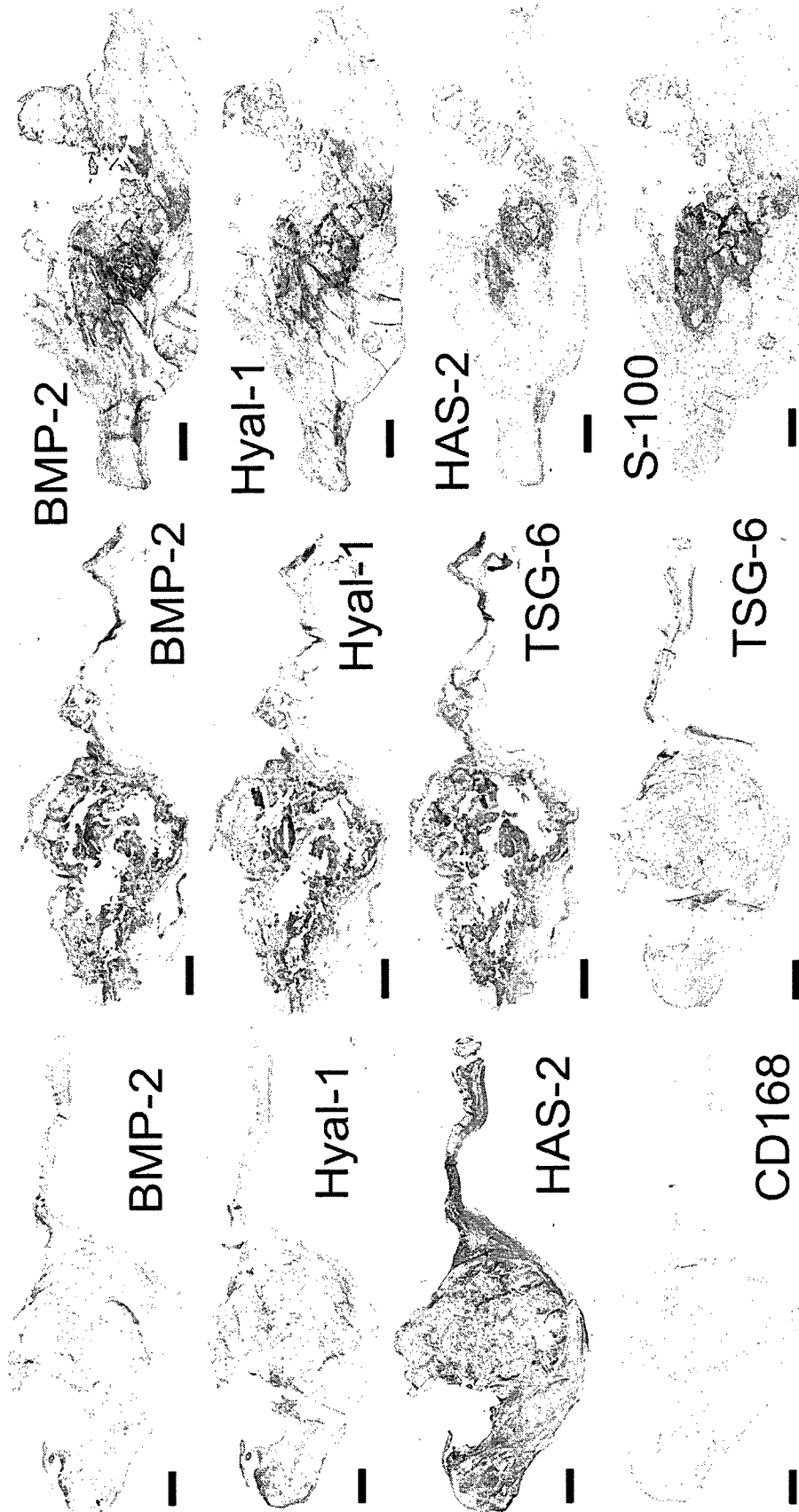


Fig. 21-2: Co-localization of BMP-2, Hyal-1, HAS-2, and CD168 relative to nodules within calcified aortic valves. Scale bars indicate 1 mm.

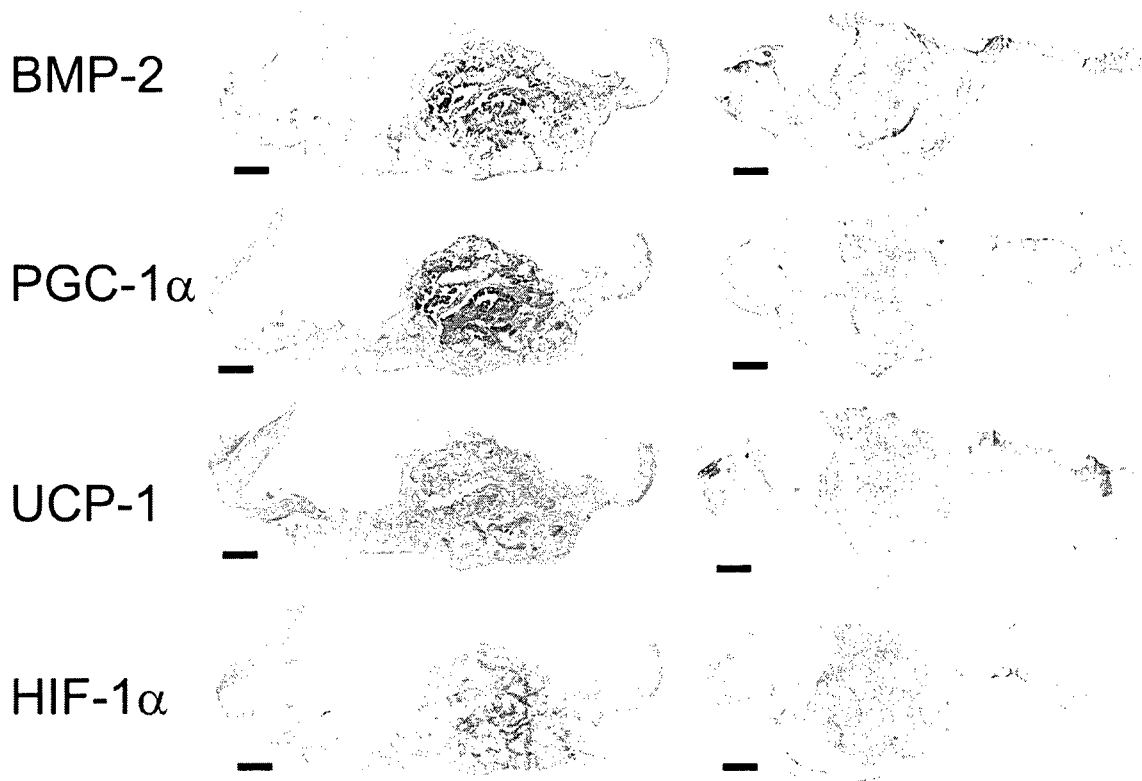


Fig. 21-3: Co-localization of BMP-2, PGC-1 α , UCP-1, and HIF-1 α relative to nodules in calcified aortic valves. Scale bars indicate 1 mm.

Correlations within Mechanistic Families

There were numerous correlations among markers in the same mechanistic family, which was to be expected (Table 21-2). For the regulators of HA, CD168 was significantly and very strongly associated with Hyal-1 in NodSurr; this same association, albeit less strong, was also a trend in CollFibr. HARE was also significantly associated



Fig. 21-4: *Periostin staining relative to nodules in calcified aortic valves demonstrating stronger staining in the center of and at the edge of nodules relative to surrounding tissues. Scale bars indicate 1 mm.*

with Hyal-1 in CollFibr. For hypoxic regulators, HIF-1 α was strongly associated with markers for brown fat differentiation (PGC-1 α in NodEdge and UCP-1 in PreNodSurr); a less strong link with UCP-1 was also suggested as a trend in NodSurr. PGC-1 α and UCP-1 were also associated in NodCtr. Finally, there were numerous associations between the markers of endochondral ossification; BMP-2, S-100, and TSG-6 were all significantly associated with each other in NodSurr. TSG-6 had trends of association with S-100 in NodEdge and BMP-2 in PreNodSurr. Periostin was also significantly and strongly associated with TSG-6 in NodCtr.

Correlations between Mechanistic Families

The findings of correlations between markers from different mechanistic families suggest interactions between these agents in distinct regions of the leaflet (Table 21-3). Correlations between these markers were unique depending on the different regions

Table 21-2. Correlations within Mechanistic Families.

Marker 1	Marker 2	Region	r	P
Hyaluronan Regulation				
CD168	Hyal-1	NodSurr	0.889	<0.0001
CD168	Hyal-1	CollFibr	0.596	<i>0.0091</i>
HARE	Hyal-1	CollFibr	0.798	<0.0001
Hypoxia				
HIF-1 α	UCP-1	NodSurr	0.631	<i>0.0050</i>
HIF-1 α	PGC-1 α	NodEdge	0.849	<0.0001
HIF-1 α	UCP-1	PreNodSurr	0.880	0.0039
PGC-1 α	UCP-1	NodCtr	0.721	0.0024
Endochondral Ossification				
BMP-2	S-100	NodSurr	0.716	0.0008
BMP-2	TSG-6	NodSurr	0.668	0.0025
BMP-2	TSG-6	PreNodSurr	0.873	<i>0.0102</i>
S-100	TSG-6	NodSurr	0.674	0.0022
S-100	TSG-6	NodEdge	0.585	<i>0.0086</i>
Periostin	TSG-6	NodCtr	0.856	0.0008

NodSurr=tissue surrounding nodule, NodEdge=edge of nodule, PreNodSurr=tissue surrounding prenodule, NodCtr=center of nodule, CollFibr=normal appearing fibrosa far from nodules.

Non-italicized p-values are significant correlations ($p < 0.0045$).

Italicized p-values are trends ($p \leq 0.01$).

suggesting distinct processes relative to the microstructure of the nodule. In NodCtr, HA degradation (Hyal-1) strongly correlated with markers of brown fat differentiation (UCP-1 and PGC-1 α), and had a trend of association with chondrogenic differentiation (S-100). S-100 was also significantly correlated with UCP-1 in this region, as was BMP-2 and PGC-1 α . In contrast to NodCtr, in NodEdge HA synthesis (HAS-2) was significantly associated with the brown fat marker PGC-1 α and marker of hypoxia HIF-1 α , as well as a trend of association with BMP2. Chondrogenic differentiation and hypoxia were also linked by a significant moderate association between S-100 and UCP-1 in NodEdge. In this region periostin demonstrated a trend of association with HAS-2, HIF-1 α , and PGC-1 α .

Table 21-3. Correlations between Different Mechanistic Families.

Region	Marker 1	Marker 2	r	P
NodSurr				
	BMP-2	Hyal-1	0.772	0.0002
		CD168	0.695	0.0014
		UCP-1	0.608	<i>0.0075</i>
	CD168	S-100	0.797	0.0001
		TSG-6	0.741	0.0004
		UCP-1	0.662	0.0028
	Hyal-1	S-100	0.813	<0.0001
		UCP-1	0.716	0.0008
		TSG-6	0.700	0.0012
	S-100	UCP-1	0.672	0.0022
	TSG-6	UCP-1	0.634	<i>0.0047</i>
NodEdge (Outer 1/3)				
	BMP-2	HAS-2	0.587	<i>0.0083</i>
	HAS-2	HIF-1 α	0.730	0.0004
		PGC-1 α	0.744	0.0004
		Periostin	0.702	<i>0.0051</i>
	HIF-1 α	Periostin	0.667	<i>0.0092</i>
	PGC-1 α	Periostin	0.693	<i>0.0086</i>
	S-100	UCP-1	0.662	0.0020
NodCtr (Inner 1/3)				
	Hyal-1	UCP-1	0.900	<0.0001
		PGC-1 α	0.734	0.0019
		S-100	0.641	<i>0.0075</i>
	S-100	UCP-1	0.704	0.0023
	BMP-2	PGC-1 α	0.701	0.0036
PreNod				
	BMP-2	Hyal-1	0.912	0.0042
	HARE	S-100	0.902	<i>0.0055</i>
	Hyal-1	S-100	0.932	0.0023
		TSG-6	0.922	<i>0.0089</i>
PreNodSurr				
	Hyal-1	BMP-2	0.937	0.0018
		TSG-6	0.957	0.0007
CollFibr				
	UCP-1	CD168	0.673	0.0022
		Hyal-1	0.743	0.0003
		S-100	0.612	<i>0.0069</i>
	HARE	S-100	0.666	0.0035
	PGC-1	Periostin	0.761	0.0010

NodSurr=tissue surrounding nodule, NodEdge=edge of nodule,
 NodCtr=center of nodule, PreNod=center of prenodule,
 PreNodSurr=tissue surrounding prenodule,
 CollFibr=normal appearing fibrosa far from nodules.
 Non-italicized p-values are significant correlations ($p < 0.0045$).
 Italicized p-values are trends ($p \leq 0.01$).

Far more significant correlations were found between mechanistic families in NodSurr. Significant interactions between HA regulation and endochondral ossification were demonstrated by correlations of BMP-2, TSG-6, and S-100 with Hyal-1 and CD168. Specifically, Hyal-1 showed strong correlations with the brown fat marker UCP-1, as well as BMP2. Significant interactions between hypoxic regulation and HA regulation were also shown by correlations of UCP-1 with CD168. Links between UCP-1 and endochondral ossification were more moderate, with only a significant correlation with S-100. TSG-6 demonstrated a trend of associations with BMP-2 and HYAL-1.

In PreNod and PreNodSurr, the number of correlations between mechanistic families was smaller, but the correlations were extremely strong. Within the PreNod, endochondral ossification and HA regulation showed strong associations with Hyal-1 strongly correlating with the ossification markers S-100 and BMP-2, HARE associating with S-100, and a correlation trend evident between TSG-6 and Hyal-1. In PreNodSurr, Hyal-1 was significantly correlated with BMP-2 and TSG-6.

In CollFibr, several moderate correlations between mechanistic families were present. Hypoxic regulation (UCP-1) was significantly correlated with HA regulation (CD168, Hyal-1). Links between hypoxic regulation and endochondral ossification were also demonstrated by a significant correlation between PGC-1 α and periostin, and a correlation trend between UCP-1 and S-100. Finally, HA regulation (HARE) was linked with endochondral ossification (S-100).

DISCUSSION

This work provides evidence indicating the presence of hypoxia and brown fat driven mechanisms within calcified aortic valves, as well as mechanisms linked to hyaluronan balance and TSG-6, a molecule that can either promote or suppress BMP-2-induced calcification depending on the presence or absence of HA. These results support the proposed hypotheses and also highlight the role of Hyal-1, which was strongly linked with both hypoxic and endochondral ossification markers. The mechanistic roles of brown fat and hyaluronan regulation have not been previously investigated in CAVD.

Role for Hypoxia and Brown Fat in Calcification

The demonstration of two markers signifying the differentiation of brown fat cells, UCP-1 and PGC-1 α , that were found together with HIF-1 α within and surrounding the nodules of these calcified aortic valves provides a tantalizing new direction for investigation of disease mechanisms and possibly the development of novel therapies. In murine models of heterotopic ossification within muscle, brown adipocytes begin to accumulate with 24 hours of delivery of adenovirus transduced cells expressing BMP2.^{8, 18} These brown adipocytes generated hypoxic stress within the muscle tissue⁸ and expressed vascular endothelial growth factor,¹⁸ thus driving the early stages of heterotopic endochondral ossification. Lowering oxygen tension within soft tissue creates the correct environment for chondrogenesis, and promoting the formation of new blood vessels aids in the delivery of osteoblastic progenitor cells; together these steps are critical to the differentiation of cartilage and the transition to bone. Furthermore, many of the novel correlations between the markers for brown fat, hypoxia, and endochondral

ossification were present in the nodule region but not present in the normal collagenous fibrosa, thus corroborating our hypothesis that these agents are relevant to the nodule formation. Interestingly, these correlations were completely absent from the prenodule region, which suggests that differential remodeling is occurring between the smaller and larger nodules.

Correlations between brown fat-generated hypoxia and HA turnover also suggest future research directions. Although more precise details regarding the interactions of these mechanisms cannot be determined using immunohistochemistry, we speculate that hypoxia promotes HA synthesis in the nodule boundary (NodEdge). More towards the interior of the nodule (NodCtr), the action of hyaluronidases would generate HA fragments that may aid in promoting the differentiation of brown fat cells. Others have also reported the involvement with HA and the balance between HAS-2 and hyaluronidase in the differentiation of pre-adipocytes and mature adipocytes.^{19, 20} Interestingly, TSG-6 is also expressed during the process of adipocyte maturation.²¹ The production of low molecular weight HA chains by hyaluronidases has also been shown to induce unique effects on chondrocytes in a variety of previous reports;²² the presence of HA was also found to promote chondrogenic differentiation of adipose derived stem cells *in vitro*.²³ As noted above, these relationships between HA, brown fat, and hypoxia were primarily present in the nodules and surrounding tissues, but generally absent in the normal-appearing fibrosa, with the exception of a correlation between Hyal-1 and UCP-1.

Role for HA Regulation in Calcification

Our hypothesis that HA homeostasis could affect TSG-6 to either promote or inhibit BMP-2 mediated calcification was supported by correlations between HA homeostasis markers, ossification markers, and TSG-6 that were unique depending on leaflet region. While Hyal-1 demonstrated correlations with markers of brown fat and ossification in PreNod and NodCtr, as well as NodSurr and PreNodSurr, no such correlations were evident in NodEdge. In contrast, in NodEdge HAS-2 showed strong correlations with these same markers of brown fat and ossification. Furthermore, TSG-6 was associated with Hyal-1 and BMP-2 in NodSurr. This association of TSG-6 with BMP-2 could indicate TSG-6 inhibiting BMP-2 in promoting ossification, and may be related to Hyal-1 whose degradation of HA would allow TSG-6 to bind BMP-2. In NodEdge, however, HAS-2 appeared to be more active in ossification as demonstrated by numerous correlations with other markers. In the future, it will be important to investigate this hypothesis further, especially by assessing the activity of the other HA synthases (HAS-1 and HAS-3) in addition to HAS-2.

We speculate, as shown in Figure 21-5, that the presence of newly synthesized HA at the nodule boundary (NodEdge), as opposed to HA degraded by Hyal-1, would have competed with BMP-2 for the same binding site on TSG-6, and as a result more BMP-2 would have been free to promote calcification and growth of the nodule at the boundary. In the other regions, the degraded HA may not have been able to bind to TSG-6; the binding of HA to the glycoprotein hyaluronectin, a hyaladherin, was previously reported to be size dependent with smaller fragments (from 10 to <60 disaccharides) having lower binding affinity to hyaluronectin.²⁴ Absent or reduced

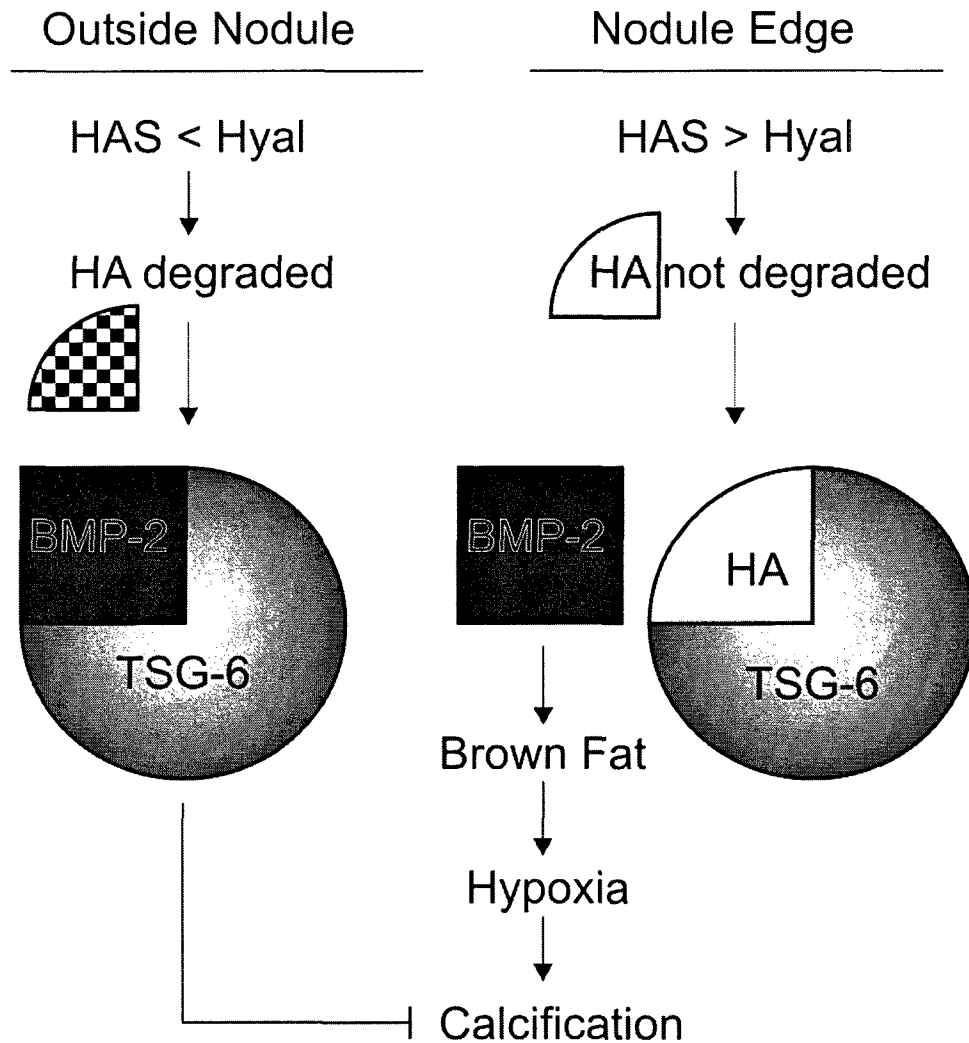


Fig. 21-5: Hypothesized mechanism for inhibition of calcification outside of the nodule, in comparison to calcification processes occurring at the nodule edge. Outside of the nodule Hyal-1 appears more active than HAS-2, leading to net HA degradation. Therefore HA does not displace BMP-2 from binding TSG-6. BMP-2, while bound to TSG-6, is not able to promote calcification in the region outside of the nodule. However, at the nodule edge, HAS-2 appears more active than Hyal-1, resulting in net HA synthesis. This HA displaces BMP-2 such that BMP-2 is able to promote calcification in the nodule edge region.

binding between HA fragments and TSG-6 would thus allow the sequestration of BMP-2 and inhibit new calcification deep within the mature nodule (NodCtr), within the prenodule, and in the tissues surrounding the nodule (NodSurr, PreNodSurr). Hyaluronidases have not been previously investigated in calcified aortic valves, but with

regards to atherosclerosis their ability to generate low molecular weight HA has been linked with proliferation of smooth muscle cells (an effect also reported in valvular interstitial cells²⁵) and VCAM-1 synthesis *in vitro*.¹² In three-dimensional *in vitro* cultures of chick limb-bud mesenchymal cells or cartilage slices, the addition of hyaluronidase promoted increased mineral accumulation.^{26,27} HA itself appears to have a complicated relationship with calcification, with some reports suggesting that HA promotes the late osteogenic differentiation of cells²⁸ while others have integrated HA into biomaterial scaffolds and found either enhancement²⁹ or prevention³⁰ of mineralization. Although there have been no published investigations of the HA synthases in heart valves, the signaling pathways regulating the activity of HAS-1, HAS-2, and HAS-3 represent therapeutic targets for atherosclerosis³¹ and potentially should be investigated for CAVD as well.

The results also showed roles for the HA binding receptors CD168 and HARE in NodSurr and PreNodSurr, respectively. This work was the first demonstration of CD168, also known as RHAMM (receptor for hyaluronic acid mediated motility) in heart valves. Our group has previously demonstrated the presence of HARE (HA receptor for endocytosis) in normal and myxomatous mitral valves,³² but its role in those valves as in these calcified valves is uncertain. In the kidney, HARE enables the clearance of HA and selected galactosaminoglycan proteoglycans from the bloodstream and is thought to be associated with HA turnover.³³ The binding of HA to HARE causes phosphorylation of extracellular signal-regulated kinases 1 and 2 (ERK1/2) in a dose- and time-dependent manner.³⁴ Moreover, the presence of HARE in heart valves is rather unique since this receptor is not found in other cardiovascular tissues. The finding that HARE is highly

correlated with the abundance of S-100 suggests that these diseased valves may have alterations in HA metabolism or intracellular signaling. Interestingly, the distribution of CD44 was unremarkable and did not show profound correlations with valve calcification (data not shown), despite its well known roles in inflammatory mediation in atherosclerosis^{10, 12} and in regulating tyrosine kinase activity of p185^{HER-2} and src and the activation of Rho and Rac-1. CD44 was primarily involved with other HA regulatory mediators in the normal collagenous fibrosa.

Distinctions among Nodule Regions and Prenodules

The specificity and strength of the correlations between different mechanistic families was rather distinct between the inside and outside of the nodules, as well as between the nodules and prenodules. Although these overall mechanistic interactions tended to occur in almost every region, the specific markers involved tended to vary across the microanatomy. Correlations involving Hyal-1 were found in all nodule regions (NodCtr, PreNod) and surrounding tissues (NodSurr, PreNodSurr) except for NodEdge, where HAS-2 and HIF-1 α correlations were found. NodSurr had the greatest numbers of correlations between mechanistic families, suggesting that more active cell-mediated remodeling was occurring within that region. PreNod and PreNodSurr were characterized by many very strong correlations between HA regulation and endochondral ossification, but no interactions between these mechanisms and the hypoxic/brown fat mechanism, which suggests that the prenodules are undergoing remodeling that is distinctive from the mature nodules and may represent an earlier stage of the nodule maturity. Indeed, others have noted that smaller nodules have a greater degree of

neovascularization compared with large nodules,³⁵ which perhaps counters the brown-fat-generated hypoxic conditions in the prenodules.

Limitations

Although numerous correlations between different remodeling mechanisms were highly significant, the heterogeneous nature of the microstructural remodeling amongst the leaflet samples made it difficult to demonstrate significant differences in the abundance of the various markers through an analysis of variance. As a result, the work was primarily descriptive. In the future, it may be useful to examine the interactions between these mechanisms in well-controlled animal or *in vitro* models.

CONCLUSIONS

This research demonstrated the first evidence that the regulation of HA turnover, as well as the promotion of hypoxic conditions by brown fat cells, is associated with endochondral ossification in calcific aortic stenosis. Additionally, the interactions between these mechanisms vary between large and small nodules and between the nodules and their surrounding tissues, with the tissues surrounding the nodules showing the greatest active remodeling. Further investigation of these regulatory and remodeling mechanisms, and their interactions with other pathways such as *wnt*, may offer insight into novel medical therapies that could intervene in numerous important pathological processes within the progression of this disease.

This chapter, which analyzed markers of hypoxia, hyaluronan homeostasis, brown adipocytes, and osteogenesis and chondrogenesis relative to calcified nodules, completes the set of two studies on calcific aortic valve disease (Chapters 20 and 21), as well as the portion of the thesis analyzing valve alterations in various diseased states (Chapters 13-21). Among other purposes, these studies analyzing valves in diseased states were intended to develop negative design criteria for a tissue engineered heart valve, which could be combined with the studies of normal valves (Chapters 2-12) providing positive design criteria for such a valve. The next chapter presents preliminary work towards the development of a tissue engineered heart valve. In this study, functionalized poly(ethylene) glycol hydrogels were used to investigate age- and valve-region-specific responses of mitral valvular interstitial cells to substrate stiffness. In the future, these functionalized poly(ethylene) glycol hydrogels can potentially serve as scaffolds for a tissue engineered heart valve.

REFERENCES

1. American Heart Association. *Heart Disease and Stroke Statistics - 2004 Update*. Dallas: American Heart Association; 2004.
2. Rabkin E, Schoen FJ. Cardiovascular tissue engineering. *Cardiovasc Pathol*. 2002;11(6):305-317.
3. Katz R, Wong ND, Kronmal R, Takasu J, Shavelle DM, Probstfield JL, Bertoni AG, Budoff MJ, O'Brien KD. Features of the metabolic syndrome and diabetes mellitus as predictors of aortic valve calcification in the Multi-Ethnic Study of Atherosclerosis. *Circulation*. 2006;113(17):2113-2119.
4. Mohler ER, 3rd, Chawla MK, Chang AW, Vyavahare N, Levy RJ, Graham L, Gannon FH. Identification and characterization of calcifying valve cells from human and canine aortic valves. *J Heart Valve Dis*. 1999;8(3):254-260.
5. Mohler ER, 3rd, Gannon F, Reynolds C, Zimmerman R, Keane MG, Kaplan FS. Bone formation and inflammation in cardiac valves. *Circulation*. 2001;103(11):1522-1528.
6. Durbin AD, Gotlieb AI. Advances towards understanding heart valve response to injury. *Cardiovasc Pathol*. 2002;11(2):69-77.
7. Jian B, Narula N, Li QY, Mohler ER, 3rd, Levy RJ. Progression of aortic valve stenosis: TGF-beta1 is present in calcified aortic valve cusps and promotes aortic valve interstitial cell calcification via apoptosis. *Ann Thorac Surg*. 2003;75(2):457-465; discussion 465-456.
8. Olmsted-Davis E, Gannon FH, Ozen M, Ittmann MM, Gugala Z, Hipp JA, Moran KM, Fouletier-Dilling CM, Schumara-Martin S, Lindsey RW, Heggeness MH, Brenner MK, Davis AR. Hypoxic adipocytes pattern early heterotopic bone formation. *Am J Pathol*. 2007;170(2):620-632.
9. O'Brien KD. Pathogenesis of calcific aortic valve disease: a disease process comes of age (and a good deal more). *Arterioscl Thromb Vasc Biol*. 2006;26(8):1721-1728.
10. Wilkinson TS, Bressler SL, Evanko SP, Braun KR, Wight TN. Overexpression of hyaluronan synthases alters vascular smooth muscle cell phenotype and promotes monocyte adhesion. *J Cell Physiol*. 2006;206(2):378-385.
11. Seike M, Ikeda M, Matsumoto M, Hamada R, Takeya M, Kodama H. Hyaluronan forms complexes with low density lipoprotein while also inducing foam cell infiltration in the dermis. *J Dermatol Sci*. 2006;41(3):197-204.
12. Cuff CA, Kothapalli D, Azonobi I, Chun S, Zhang Y, Belkin R, Yeh C, Secreto A, Assoian RK, Rader DJ, Pure E. The adhesion receptor CD44 promotes atherosclerosis by mediating inflammatory cell recruitment and vascular cell activation. *J Clin Invest*. 2001;108(7):1031-1040.

13. Raj T, Kanellakis P, Pomilio G, Jennings G, Bobik A, Agrotis A. Inhibition of fibroblast growth factor receptor signaling attenuates atherosclerosis in apolipoprotein E-deficient mice. *Arterioscler Thromb Vasc Biol.* 2006;26(8):1845-1851.
14. Jain M, He Q, Lee WS, Kashiki S, Foster LC, Tsai JC, Lee ME, Haber E. Role of CD44 in the reaction of vascular smooth muscle cells to arterial wall injury. *J Clin Invest.* 1996;98(3):877.
15. Tsukahara S, Ikeda R, Goto S, Yoshida K, Mitsumori R, Sakamoto Y, Tajima A, Yokoyama T, Toh S, Furukawa K, Inoue I. Tumour necrosis factor alpha-stimulated gene-6 inhibits osteoblastic differentiation of human mesenchymal stem cells induced by osteogenic differentiation medium and BMP-2. *Biochem J.* 2006;398(3):595-603.
16. Itoh S, Matubara M, Kawauchi T, Nakamura H, Yukitake S, Ichinose S, Shinomiya K. Enhancement of bone ingrowth in a titanium fiber mesh implant by rhBMP-2 and hyaluronic acid. *J Mater Sci Mater Med.* 2001;12(7):575-581.
17. Kim HD, Valentini RF. Retention and activity of BMP-2 in hyaluronic acid-based scaffolds in vitro. *J Biomed Mater Res.* 2002;59(3):573-584.
18. Dilling CF, Wada A, Lazard Z, Salisbury E, Gannon F, Vadakkan T, Gao L, Hirschi K, Dickinson M, Davis AR, Olmsted-Davis E. Vessel formation is induced prior to the appearance of cartilage in BMP2-mediated heterotopic ossification. *J Bone Miner Res.* 2009;in press.
19. Allingham PG, Brownlee GR, Harper GS, Pho M, Nilsson SK, Brown TJ. Gene expression, synthesis and degradation of hyaluronan during differentiation of 3T3-L1 adipocytes. *Arch Biochem Biophys.* 2006;452(1):83-91.
20. Zizola CF, Julianelli V, Bertolesi G, Yanagishita M, Calvo JC. Role of versican and hyaluronan in the differentiation of 3T3-L1 cells into preadipocytes and mature adipocytes. *Matrix Biol.* 2007;26(6):419-430.
21. Guo XR, Ding SL, Pan XQ, Gong HX, Fei L, Ni YH, Chen RH. [Expression of TSG-6 gene during 3T3-L1 preadipocyte differentiation and regulative role of tumor necrosis factor-alpha]. *Zhonghua Er Ke Za Zhi.* 2004;42(5):344-347.
22. Stern R, Asari AA, Sugahara KN. Hyaluronan fragments: an information-rich system. *Eur J Cell Biol.* 2006;85(8):699-715.
23. Wu SC, Chang JK, Wang CK, Wang GJ, Ho ML. Enhancement of chondrogenesis of human adipose derived stem cells in a hyaluronan-enriched microenvironment. *Biomaterials.* 2010;31(4):631-640.
24. Courel MN, Maingonnat C, Tranchepain F, Deschrevel B, Vincent JC, Bertrand P, Delpech B. Importance of hyaluronan length in a hyaladherin-based assay for hyaluronan. *Anal Biochem.* 2002;302(2):285-290.
25. Masters KS, Shah DN, Leinwand LA, Anseth KS. Crosslinked hyaluronan scaffolds as a biologically active carrier for valvular interstitial cells. *Biomaterials.* 2005;26(15):2517-2525.

26. Boskey AL, Stiner D, Binderman I, Doty SB. Effects of proteoglycan modification on mineral formation in a differentiating chick limb-bud mesenchymal cell culture system. *J Cell Biochem.* 1997;64(4):632-643.
27. Smetana K, Jr., Stol M, Novak M. Artificial mineralization in vitro--a model of tissue mineralization. *Folia Biol (Praha).* 1993;39(1):23-28.
28. Zou L, Zou X, Chen L, Li H, Mygind T, Kassem M, Bunker C. Effect of hyaluronan on osteogenic differentiation of porcine bone marrow stromal cells in vitro. *J Orthop Res.* 2008;26(5):713-720.
29. Lisignoli G, Toneguzzi S, Zini N, Piacentini A, Cristino S, Tschon M, Grassi F, Fini M, Giardino R, Maraldi NM, Facchini A. Hyaluronan-based biomaterial (Hyaff-11) as scaffold to support mineralization of bone marrow stromal cells. *Chir Organi Mov.* 2003;88(4):363-367.
30. Ohri R, Hahn SK, Hoffman AS, Stayton PS, Giachelli CM. Hyaluronic acid grafting mitigates calcification of glutaraldehyde-fixed bovine pericardium. *J Biomed Mater Res A.* 2004;70(2):328-334.
31. Marzoll A, Nagy N, Wordehoff L, Dai G, Fries S, Lindner V, Grosser T, Fischer JW. Cyclooxygenase inhibitors repress vascular hyaluronan-synthesis in murine atherosclerosis and neointimal thickening. *J Cell Mol Med.* 2009;13(9B):3713-3719.
32. Gupta V, Barzilla JE, Mendez JS, Stephens EH, Lee EL, Collard CD, Laucirica R, Weigel PH, Grande-Allen KJ. Abundance and location of proteoglycans and hyaluronan within normal and myxomatous mitral valves. *Cardiovasc Pathol.* 2009;18(4):191-197.
33. Zhou B, McGary CT, Weigel JA, Saxena A, Weigel PH. Purification and molecular identification of the human hyaluronan receptor for endocytosis. *Glycobiology.* 2003;13(5):339-349.
34. Kyosseva SV, Harris EN, Weigel PH. The hyaluronan receptor for endocytosis (HARE) mediates hyaluronan-dependent signal transduction via extracellular signal-regulated kinases. *J Biol Chem.* 2008;283(22):15047-55.
35. Charest A, Pepin A, Shetty R, Cote C, Voisine P, Dagenais F, Pibarot P, Mathieu P. Distribution of SPARC during neovascularisation of degenerative aortic stenosis. *Heart.* 2006;92(12):1844-1849.

Chapter 22: Age- and Valve-Region-Specific Responses of Mitral Valvular Interstitial Cells to Substrate Stiffness

While the studies in the earlier portions of the thesis addressed developing positive design criteria (by analyzing normal valves, Chapters 3-12) and negative design criteria (by analyzing valves in various diseased states, Chapters 13-21) for a tissue engineered heart valve, this chapter presents preliminary work in constructing a tissue engineered heart valve. In this chapter functionalized poly(ethylene) glycol hydrogels, which potentially can serve as scaffolds for a tissue engineered heart valve, were used to investigate age- and valve-region-specific responses of mitral valvular interstitial cells to substrate stiffness.

ABSTRACT

Background: While work has been performed developing scaffolds for a tissue engineered heart valve (TEHV) with proper mechanical properties, little attention has been paid to the role of scaffold stiffness in influencing valvular interstitial cell (VIC) phenotype, and resultant matrix synthesis. Additionally, recent studies suggest the need for an age-specific TEHV. Given that different aged VICs reside in matrices with different stiffnesses, we hypothesized that there may be an age-specific response of VICs to substrate stiffness. Similarly, VICs derived from regions of the mitral valve (MV) known to have different stiffnesses may display distinct responses to substrate stiffness.

Methods: To test these hypotheses, 6-week, 6-month, and 6-year-old porcine VICs from the anterior center of the mitral valve (MVAC) and the posterior mitral leaflet (PML) were seeded onto poly(ethylene) glycol (PEG) hydrogels of different stiffnesses and stained for markers of VIC activation (smooth muscle alpha-actin (SMaA) and collagen synthesis (heat shock protein-47 (HSP47) and prolyl 4-hydroxylase (P4H)).

Results: While 6-week-old MVAC VICs demonstrated decreased SMaA, P4H, and HSP47 on stiffer gels, 6-week-old PML VICs only demonstrated decreased HSP47. While 6-month-old MVAC VICs demonstrated no differences in marker expression when seeded on the two stiffnesses, 6-month-old PML VICs demonstrated decreased SMaA, P4H, and HSP47 on the stiffer gels. 6-year-old MVAC VICs demonstrated decreased P4H and HSP47 on the stiffer gels, while 6-year-old PML VICs demonstrated decreased P4H and increased HSP47 on the stiffer gels.

Conclusions: The results from this study demonstrated both age-specific and valve-region-specific responses of VICs to substrate stiffness. These findings should be taken into consideration in the design of an age-specific tissue engineered heart valve, as well as future investigations into heart valve mechanobiology.

The work contained in this chapter is under review by the journal *Biomaterials*:

Stephens EH, Durst CA, West JL, Grande-Allen KJ. **Age- and Valve-Region Specific Response of Mitral Valvular Interstitial Cells to Substrate Stiffness. *Biomaterials*, under review.**

INTRODUCTION

Valve disease affects a large portion of the population: 1-2% of 26-84 year-olds are afflicted by mitral valve disorders and approximately 1% of the population have a bicuspid aortic valve.² Valve disease incurs significant morbidity and mortality, requiring over 100,000 surgeries in the U.S. each year.³ While mechanical and bioprosthetic valves are currently used as surgical replacements for diseased valves, they are suboptimal in terms of complications and long-term durability. A tissue engineered heart valve made of autologous cells, however, could provide a much improved treatment option for the many afflicted by valve disease. Such a valve would be especially advantageous for the pediatric population, in which complications and durability of mechanical and bioprosthetic valve replacements are particularly problematic. Additionally, these valve replacements do not grow with the child; therefore, even if issues related to anti-coagulation, calcification, and long-term durability were resolved, these patients would still require surgeries every few years to replace their outgrown valves. A tissue engineered heart valve, however, could be designed to grow with the patient and after initial implantation additional re-operations could be avoided.

Ongoing work in a number of laboratories toward the development of a tissue engineered heart valve covers topics ranging from assessment of potential cell sources, design of bioreactors for mechanical conditioning of tissue engineered constructs, and optimization of scaffold technology. While developing a scaffold with material properties that can withstand physiologic pressures and flows has been extensively investigated,⁴ the role of scaffold stiffness in affecting valvular interstitial cell (VIC) phenotype has largely not been studied, with the exception of preliminary investigations

into the role of stiffness in VIC calcification.⁵ It is well known that cells of many types respond to substrate stiffness;⁶ stiffness affects cell proliferation, matrix production, and even cell differentiation,⁶ all properties that would be important in the long-term success of a tissue engineered heart valve.

Recent work demonstrating significant changes in valve composition⁷⁻⁹ and material properties with age¹⁰ suggests the need for an age-specific tissue engineered heart valve. Given that different aged VICs reside in valves with distinct stiffnesses,¹⁰ it was hypothesized that there may be an age-related response of VICs to substrate stiffness. Similarly, different regions of the MV have different stiffnesses,¹¹ therefore the VICs from these distinct regions may also respond to substrate stiffness differently. In order to test this hypothesis, different aged VICs and VICs from different regions of the MV from the same hearts were cultured on poly(ethylene) glycol (PEG) hydrogels of different stiffnesses for 48 hours and VIC expression of cell phenotype and collagen synthesis markers was assessed using immunocytochemistry (ICC).

PEG hydrogels were chosen for this experiment based on their promise as a potential platform for the design of scaffolds for tissue engineered heart valves. PEG hydrogels are extremely hydrophilic, providing prevention against protein adsorption, a critical step in the immunogenicity and degradation of bioprosthesis.¹² PEG hydrogels are also highly permeable allowing the exchange of nutrients and waste materials.¹³ Their stiffness can be regulated by changing the molecular weight and concentration of PEG.¹⁴ However, one of the factors that makes these gels particularly attractive is the ability to customize them by conjugating to the PEG backbone various peptides, including cell ligands and growth factors, as well as incorporating enzyme degradable

sequences allowing tunability of the degradation rate of the hydrogel. This designer biofunctionality makes PEG hydrogels ideal for the tissue engineering of heart valves. In the present study PEG hydrogels were conjugated with an Arg-Gly-Asp-Ser (RGDS) peptide, enabling VIC attachment to the hydrogel, and methacrylated heparin, which is necessary for normal VIC morphology.^{15, 16} These functionalized PEG hydrogels of different stiffnesses were formulated to keep the concentration of biological cues constant, thus isolating the effect of stiffness on VIC phenotype.

METHODS

Preparation and Purification of PEG-Diacrylate (PEG-DA)

PEG-diacrylate (PEG-DA) of 3400 Da MW was synthesized from PEG (Sigma-Aldrich, St. Louis, MO, unless otherwise indicated all reagents used were obtained from Sigma-Aldrich) as previously described.¹⁴ Briefly, 0.014 moles of 3400 Da MW PEG dissolved in anhydrous dichloromethane was combined under anhydrous conditions with 0.028 moles of triethyl amine. The solution was allowed to mix for 5 minutes before the addition of 0.056 moles acryloyl chloride. The solution was allowed to react overnight (Fig. 22-1). The following day 56 mL of 2 M K_2CO_3 was added and the solution shook vigorously. The reaction vessel was then allowed to sit overnight allowing the two phases to separate (the upper aqueous phase consisting of triethyl amine-Cl and lower organic phase consisting of PEG-DA). The lower organic phase containing PEG-DA was then drained and the upper aqueous phase discarded. Anhydrous $MgSO_4$ (Fisher) was added to the organic phase and the solution was filtered. PEG-DA was precipitated out of solution using diethyl ether (Fisher). The resulting precipitate was dried under vacuum

and stored at -20°C under argon until use. ^1H NMR analysis revealed $>95\%$ acrylation (Fig. 22-2). ^1H NMR spectra of all PEG components were taken at 25°C on a Varian 800 MHz Inova NMR spectrometer (Palo Alto, CA) equipped with a 5 mm inverse HCN cold probe. Samples were prepared in $600\ \mu\text{L}$ D_2O w/ $28\ \mu\text{M}$ 3-(Trimethylsilyl)propionic acid (TSP) added as a proton standard. Proton 1D spectra were acquired using a 90° pulse, a 3 second acquisition time, and a 3 second recycle delay for a total interpulse delay of 6 seconds; 32 transients were collected. The spectra were processed using the VNMRJ2.2D software (Varian).

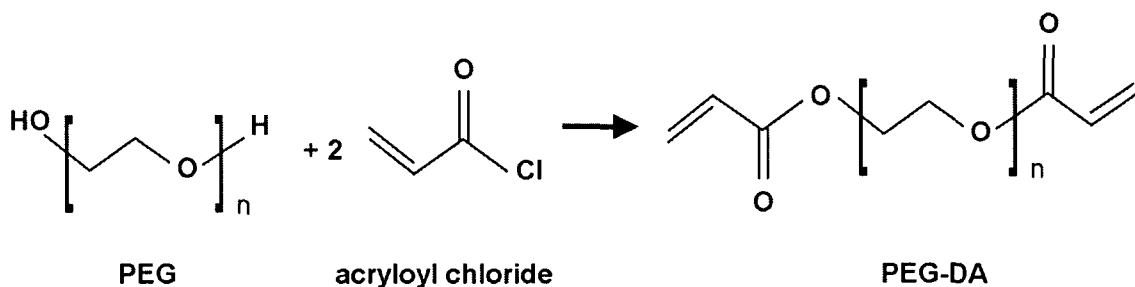


Fig. 22-1: PEG-DA reaction schematic. PEG is reacted with acryloyl chloride in a 2 acryloyl chloride:1 PEG molar ratio. The product contains acrylate groups that allow crosslinking of the PEG polymers into hydrogels.

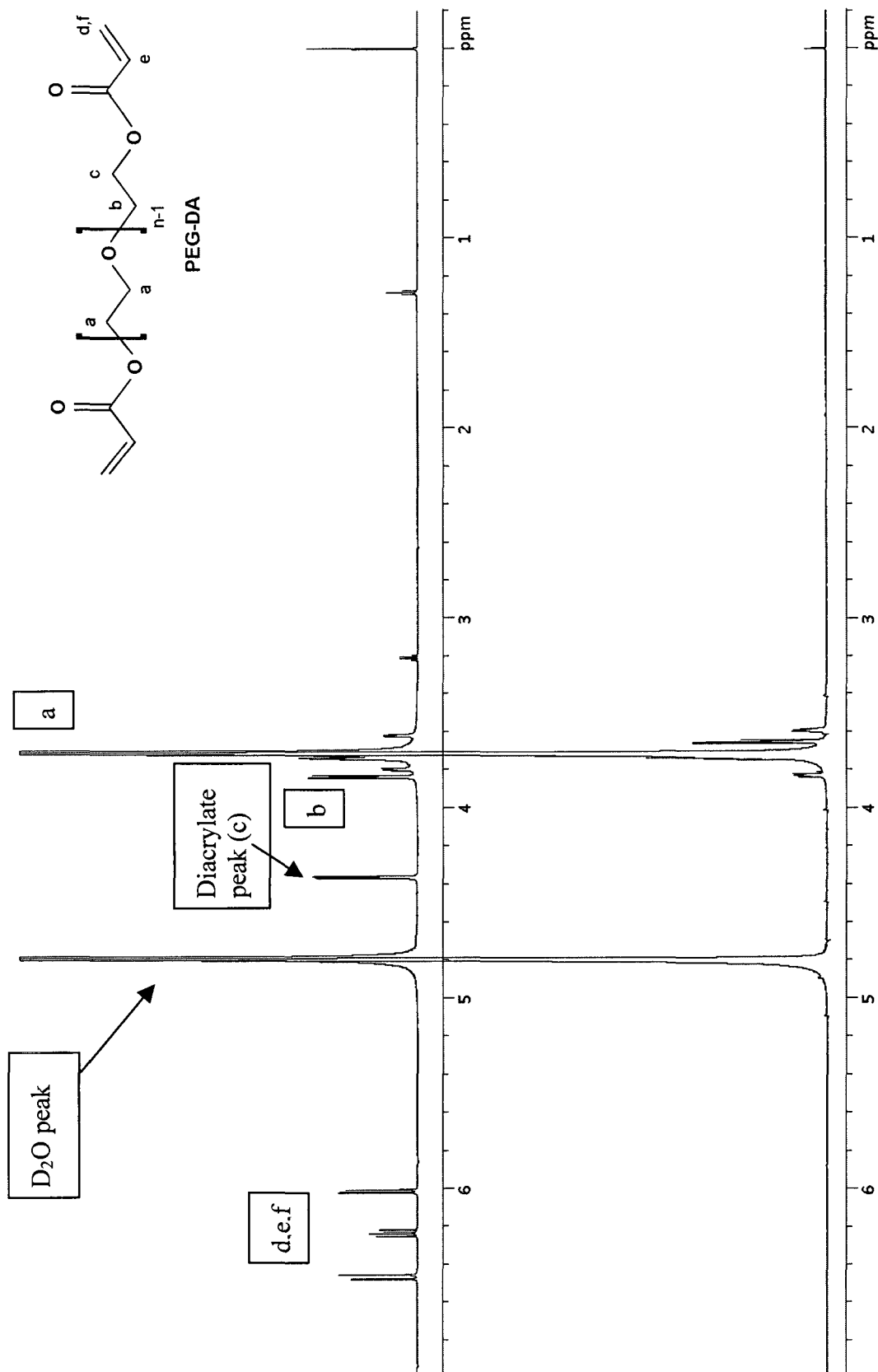


Fig. 22-2: ¹H NMR of PEG-DA. The spectra for PEG-DA is shown in the top panel, along with the PEG-DA structure labeled with the protons that correspond to the spectra peaks; unmodified PEG is shown in the bottom panel. Additional 2D experiments using an 800MHz magnet confirmed no detectable unconjugated PEG in the PEG-DA product (>95% acrylation).

Preparation and Purification of PEG-RGDS and PEG-WRGDS

The Arg-Gly-Asp-Ser (RGDS) peptide (Bachem, Bubendorf, Switzerland), which allows cell adhesion to PEG hydrogels, was attached to hetero-bifunctional PEG (PEG-SCM, Laysan Bio, Arab, AL) by reacting the peptide PEG-SCM and catalyst diisopropylamine in dimethyl sulfoxide (DMSO) (1.2 M RGDS : 1.0 M PEG-SCM : 2.0 M diisopropylamine). Briefly, the 20 mg of the RGDS peptide was dissolved in DMSO. The base catalyst diisopropylamine was added to the RGDS solution in a 2 diisopropylamine: 1.2 RGDS molar ratio. Then PEG-SCM dissolved in DMSO was added drop-wise to the RGDS/diisopropylamine solution in a 1 PEG-SCM: 1.2 RGDS molar ratio (Fig. 22-3). The resulting solution was vortexed and placed on an orbital shaker overnight. The next day the solution was placed on ice and ultrapure water was added to double the reaction volume. The resulting solution was then dialyzed against ultrapure water using a 1000 MWCO membrane (Spectrum Laboratories, Rancho Dominguez, CA) and lyophilized to dryness. The product was stored at -20°C under argon until use. The Tryp-Arg-Gly-Asp-Ser (WRGDS) peptide (GenScript, Piscataway, NJ) was attached to PEG-SCM and purified in the same manner. Percent conjugation was evaluated using gel permeation chromatography. Samples were dissolved in dimethylformamide with 0.1% ammonium acetate at a concentration of ~2 mg/ml, run on a PLgel column (5 µm, 500 Å, Polymer Laboratories, Shropshire, UK), with an evaporative light scattering detector (Polymer Laboratories), and resultant peak areas analyzed using PL ELS 1000 software (Polymer Laboratories). Evaluation of PEG-

RGDS by gel permeation chromatography revealed 81% conjugation (Fig. 22-4). Similarly, evaluation of PEG-WGRDS by NMR revealed 83% conjugation (Fig. 22-5).

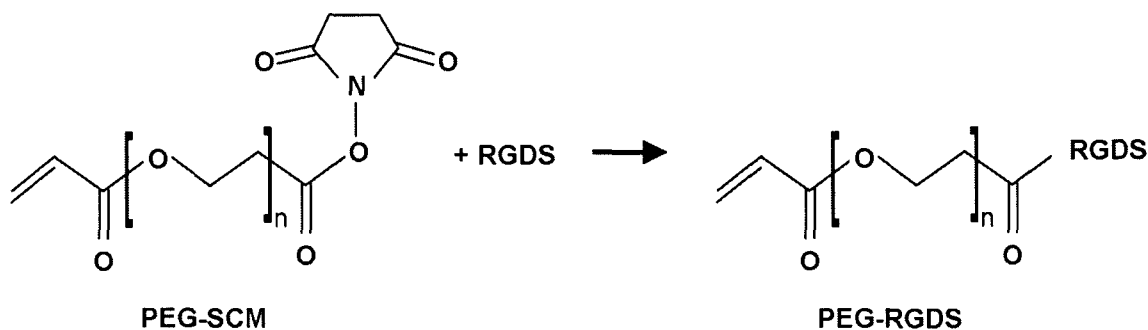


Fig. 22-3: PEG-RGDS reaction schematic. PEG-SCM is reacted with RGDS peptide yielding PEG-RGDS. Incorporation of PEG-RGDS in PEG hydrogels allows cell adhesion. The reaction schematic for PEG-WRGDS is equivalent.

Preparation and Purification of Methacrylated Heparin

Methacrylated heparin was synthesized as published previously.¹⁵ Briefly, a 10 mg/ml solution of heparin dissolved in ultra pure water was reacted with 40 fold molar excess methacrylic anhydride. The pH of the solution was adjusted to 7.5 using 4M NaOH and stirred for 24 hours. Methacrylated heparin was then precipitated using cold 95% ethanol. The precipitate was then filtered, dried, and dialyzed against ultra pure water using a 1000 MWCO membrane (Spectrum Laboratories). The product was then lyophilized and stored at -20°C under argon until use. ¹H NMR analysis revealed 5% methacrylation per disaccharide (Fig. 22-6).

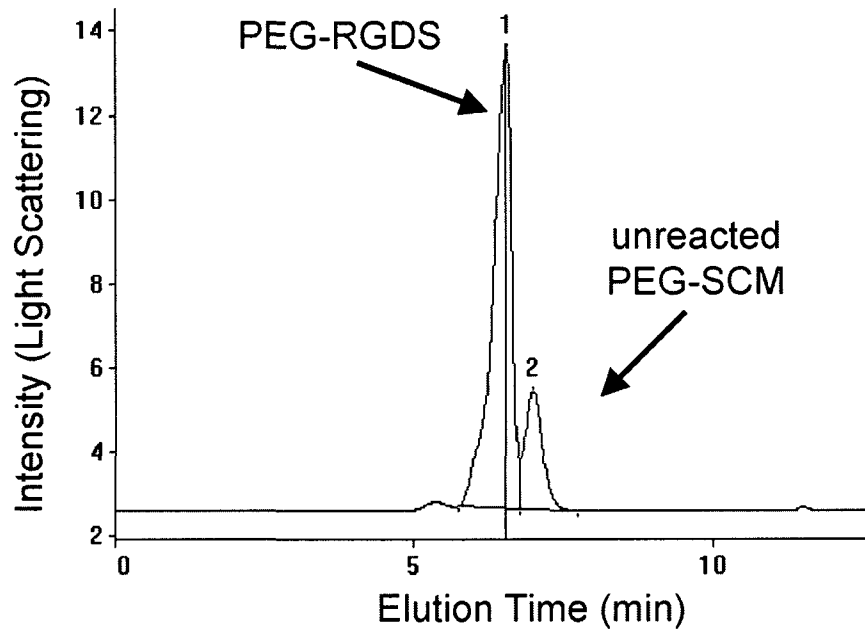


Fig. 22-4: Gel permeation chromatography of PEG-RGDS. The conjugated product, with its higher molecular weight elutes faster from the column and appears as the first peak (1), while the unconjugated PEG-SCM elutes later and appears as the second peak (2). Analysis of the areas under the curves revealed 81% conjugation.

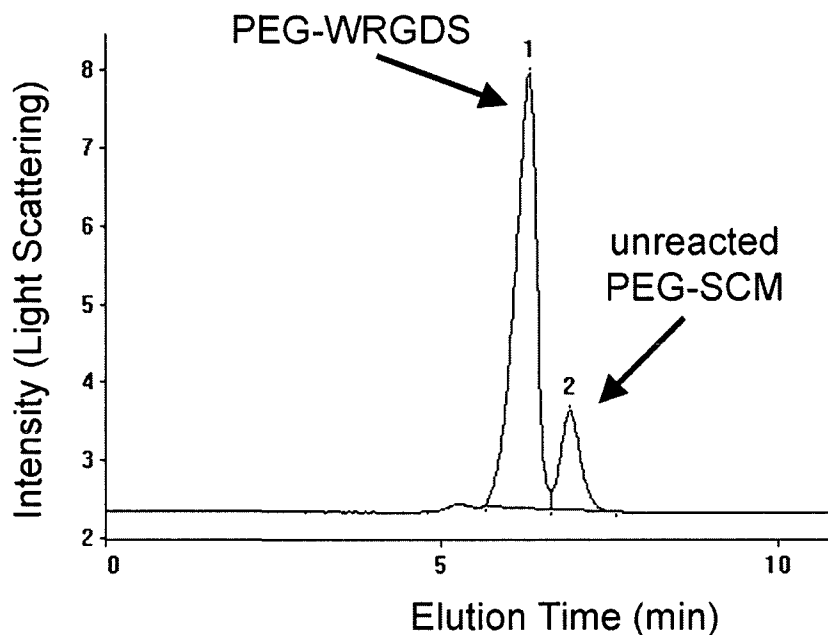


Fig. 22-5: Gel permeation chromatography of PEG-WRGDS. The conjugated product, with its higher molecular weight, elutes faster from the column and appears as the first peak (1), while the unconjugated PEG-SCM elutes later and appears as the second peak (2). Analysis of the areas under the curves revealed 81% conjugation.

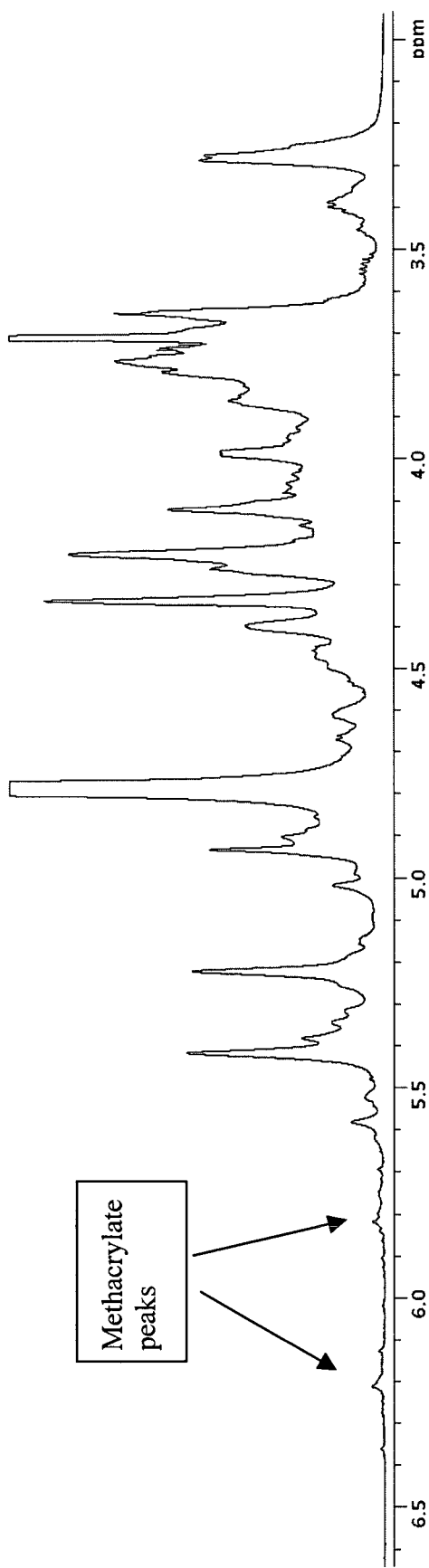


Fig. 22-6: ^1H NMR of methacrylated heparin. Analysis revealed 5% acrylation per disaccharide repeat.

Polymerization of Functionalized PEG Hydrogels

Functionalized PEG hydrogels were synthesized by dissolving the appropriate amounts of PEG-RGDS, methacrylated heparin, and PEG-DA in phosphate-buffered saline. Then 10 $\mu\text{L}/\text{mL}$ 2,2-dimethoxy-2-phenyl-acetophenone (300 mg/mL in 1-vinyl-2-pyrrolidone) was added and the solution was poured between two sterile glass slides separated by a 0.4 mm spacer and exposed to UV light for 2 minutes (365 nm, 10 mW/cm²). Hydrogels were then removed from the mold and soaked in phosphate-buffered saline with 2% antibiotic (Mediatech, Herndon, VA) for at least 24 hours allowing the hydrogels to swell to equilibrium and any unreacted reagents to diffuse out of the hydrogels. Hydrogel thickness was optically measured using a Leica DFC 320 CCD camera (Wetzlar, Germany) and ImagePro acquisition software (Media Cybernetics, Bethesda, MD). Hydrogel thicknesses were determined from the acquired images using ImageJ software (NIH, Bethesda, MD).

Quantification of Methacrylated Heparin in Functionalized PEG Hydrogels

The concentration of methacrylated heparin in polymerized, swollen gels was determined using an uronic acid assay, as described by Blumenkrantz and Asboe-Hansen.¹⁷ Briefly, hydrogels were hydrolyzed by reacting them with 0.1N NaOH for 34 hours at 37°C. The solutions were then neutralized using 0.1 N HCl. An aliquot was then added to cold sulfuric acid tetraborate (12.5 mM sodium tetraborate in sulfuric acid). The solution was heated at 100°C for 5 minutes, and then cooled in a room temperature water bath for 5 minutes. Half of the solution was transferred to separate tubes to serve as blanks in the assay, while 10 μl of hydroxyphenyl (0.15% m-hydroxyphenol in 0.5%

NaOH) was added to samples. Samples and blanks were aliquoted in triplicate into a 96-well plate and read on a spectrophotometer (SpectraMax M2, Molecular Devices, Sunnyvale, CA, absorbance read at 532 nm with background subtraction of 750 nm). A standard curve of methacrylated heparin was similarly created allowing quantification of the amount of methacrylated heparin in the polymerized, functionalized PEG hydrogels.

Quantification of PEG-RGDS in Functionalized PEG Hydrogels

Quantification of the amount of RGDS in the polymerized, swollen functionalized PEG hydrogels was performed utilizing tryptophan (which was detected by its absorbance at 280 nm) in the RGDS peptide (WRGDS). PEG-DA/PEG-WRGDS/methacrylated heparin hydrogels were synthesized in the same manner as described above and biopsy punches taken from these swollen gels were read on a spectrophotometer (SpectraMax M2). The absorbance of these samples at 280 nm was then compared to a PEG-WRGDS standard curve and the amount of PEG-WRGDS in the hydrogels calculated.

Optimization of Functionalized PEG Hydrogels

Optimization studies were performed to determine the concentrations of PEG-RGDS and methacrylated heparin in the pre-polymer solution necessary to yield equivalent amounts of PEG-RGDS and methacrylated heparin in the swollen, polymerized gels of the two different weight-volume fractions of PEG-DA. The concentration of methacrylated heparin in polymerized, swollen gels was determined using an uronic acid assay, as described above determined that 9.0 mg/ml of

methacrylated heparin in the pre-polymer hydrogel solution for the 5% weight-volume PEG-DA hydrogel and 10.6 mg/ml of methacrylated heparin in the solution for the 15% weight-volume PEG-DA hydrogel yielded equivalent concentrations of methacrylated heparin in the polymerized, swollen gels of the different PEG-DA weight-volume fractions (Fig. 22-7). Optimization studies utilizing tryptophan (described above), determined that 7.49 mg/ml of PEG-RGDS in the pre-polymer solutions for both weight-volume PEG-DA hydrogels yielded equivalent final concentrations of PEG-RGDS in the swollen, polymerized gels (Fig. 22-8).

Concentration of Methacrylated Heparin in Gels

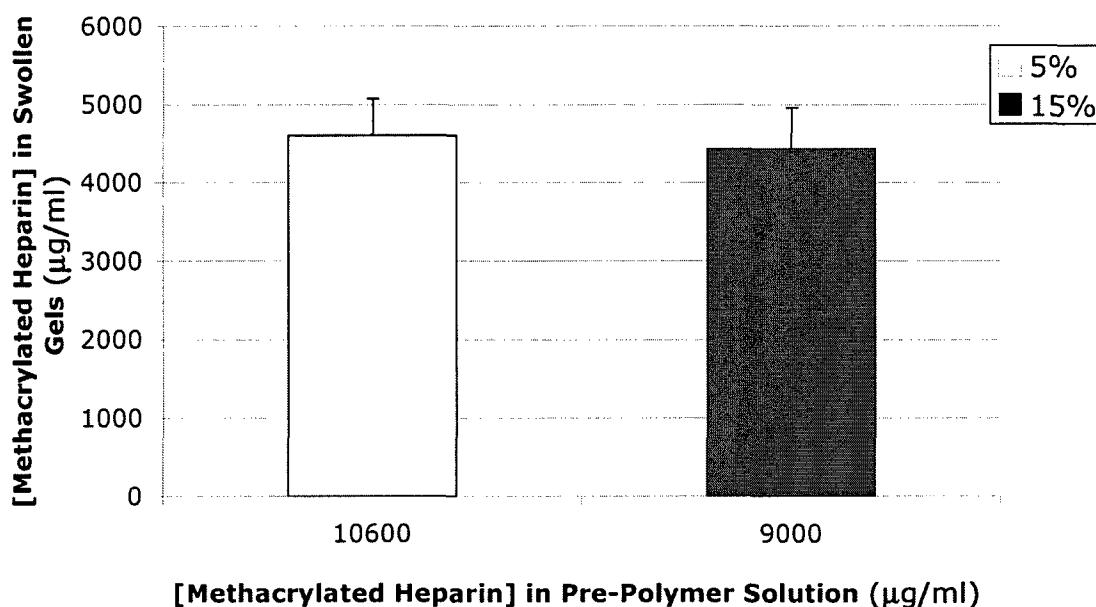


Fig. 22-7: Concentration of methacrylated heparin in different weight-volume fraction PEG swollen gels as determined by uronic acid assay. Error bars on all graphs indicate standard error of the mean.

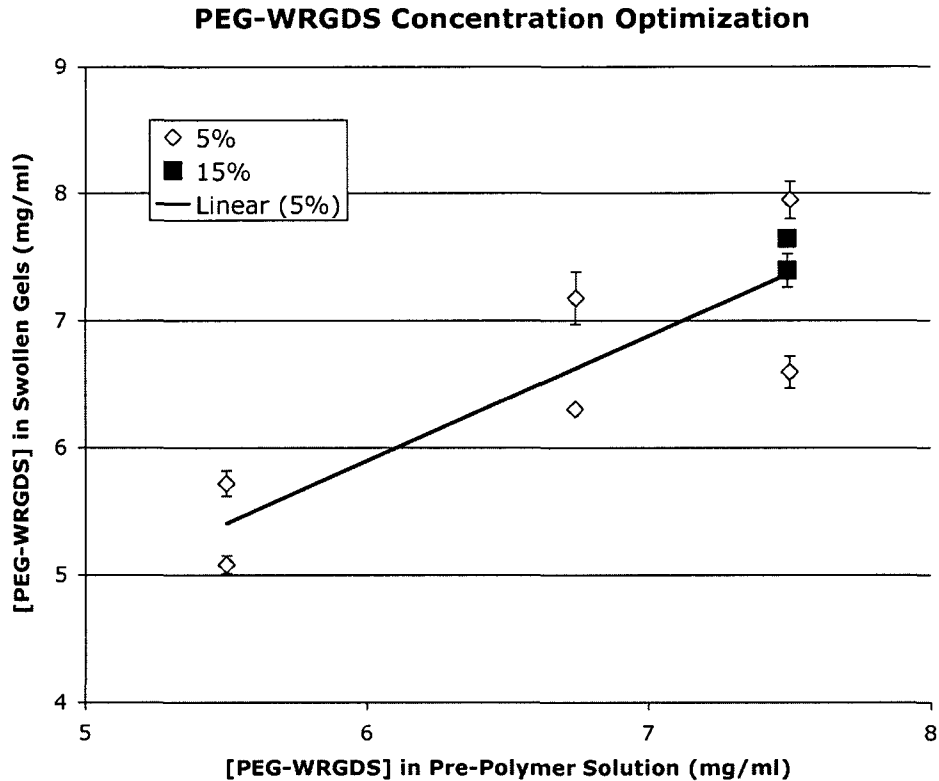


Fig. 22-8: Optimization of PEG-WRGDS in different weight-volume fraction PEG swollen gels by varying concentration of PEG-WRGDS in the pre-polymer solutions. Concentration of PEG-WRGDS was determined by absorption at 280 nm.

Determination of Elastic Modulus of Functionalized PEG Hydrogels

Strips of each weight-volume fraction PEG hydrogel (5 mm in width) were uniaxially tensile tested using an EnduraTec ELF 3200 (Bose, Eden Prairie, MN). The strain-rate was 10 mm/sec and load-elongation data recorded until failure occurred. Displacement was converted to strain based on the initial hydrogel length between grips. The elastic modulus was determined as the slope of the least-squares linear fit to the stress-strain curve.

Cell Culture and Cell Seeding onto PEG

Mitral valves were dissected from hearts from 6-week, 6-month, and 6-year-old pigs obtained from an abattoir (6-week and 6-month-old from Fisher Ham and Meat, Spring, TX; 6-year old from Animal Technologies, Tyler, TX). Valvular interstitial cells (VICs) were isolated from the anterior leaflet center (MVAC) and the posterior leaflet (PML) from the same hearts according to previously published protocols;¹⁸ previous studies have demonstrated that the MVAC is stiffer than the PML.¹¹ Cells were cultured in medium containing 10% bovine growth serum (HyClone, Logan, UT) and 2% antibiotic/antimycotic (Mediatech). Media was changed every 2-3 days and cells were passaged after reaching 80-90% confluence. Experiments were performed on cells from passage 5-6. Cells were seeded onto functionalized PEG hydrogels at a cell density of 6,000 cells/cm² and maintained in 10% serum media with 2% antibiotic/antimycotic.

Immunocytochemistry

After 48 hours of culture the gels were fixed by incubation in 10% formaldehyde in PBS for 30 minutes at room temperature. Samples of dimensions 4 mm x 6 mm were cut from cell-seeded gels and transferred to the wells of an 8-well cover glass chamber (LabTek II, Nalge Nunc International, Naperville, IL) for immunocytochemical (ICC) staining and subsequent imaging. ICC was performed for markers of collagen synthesis prolyl 4-hydroxylase (P4H, Chemicon, Temecula, CA), heat shock protein 47 (HSP47, Assay Designs, Ann Arbor, MI), as well as markers related to valve cell phenotype vimentin (Dakocytomation, Denmark) and smooth muscle alpha-actin (SMaA, Dakocytomation), with AlexaFluor 488 secondary antibodies (Invitrogen Molecular

Probes, Eugene, OR). Stained gels were imaged using LSM 5 LIVE 5 DuoScan (Zeiss, Oberkochen, Germany) and staining intensity and as well as cell morphology (area and circularity) were quantified using ImageJ software.

Statistical Analysis

Multifactorial analysis of variance to compare differences between subpopulations was performed using SigmaStat (SPSS, Chicago, IL), as described in Chapter 4.

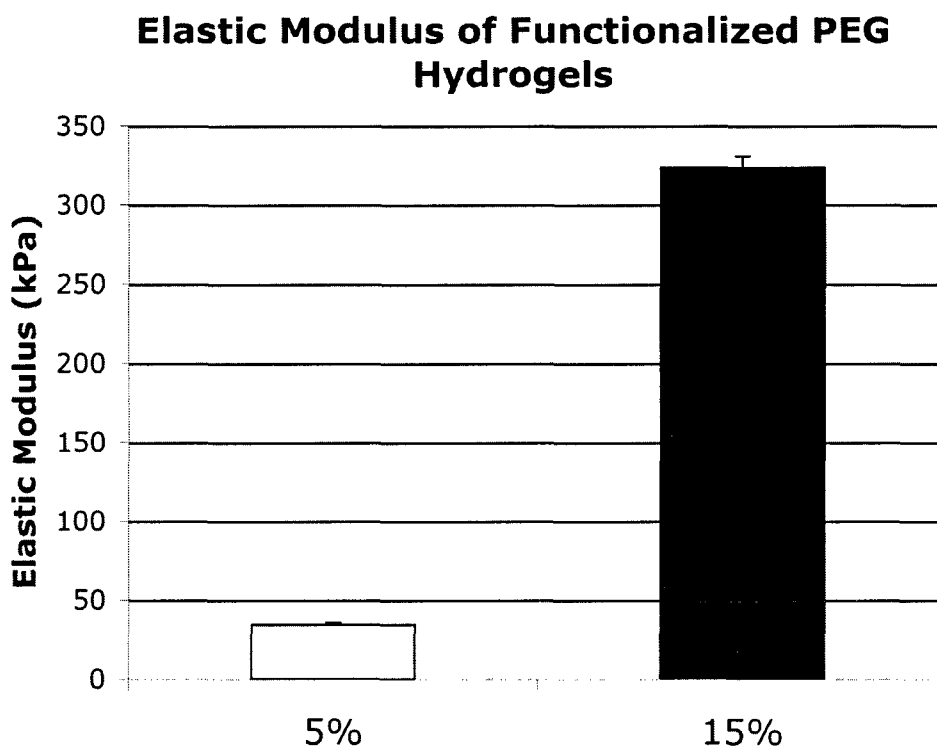
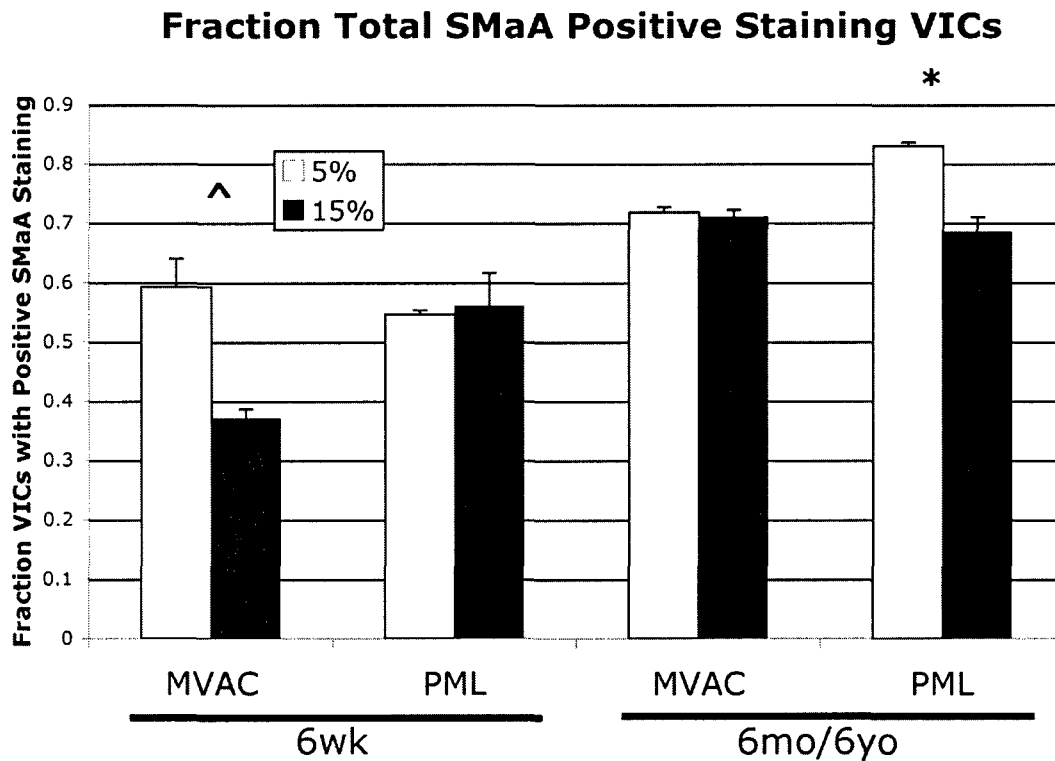


Fig. 22-9: Stiffness of different weight-volume fraction functionalized PEG gels as determined by uniaxial tensile testing.

RESULTS

Stiffness of Different Weight-Volume Fraction Functionalized PEG Hydrogels

Uniaxial testing revealed that functionalized 5% weight-volume PEG gels had a mean modulus of 34.5 kPa while functionalized 15% weight-volume PEG gels had a mean modulus of 323.3 kPa (Fig. 22-9).



*Fig. 22-10: Fraction of VICs displaying positive SMaA staining on gels of different stiffnesses, * $p=0.06$, ^ $p=0.1$ 5% vs. 15% gels.*

SMaA Expression of VICs on Gels of Different Stiffnesses

Not all VICs stained positively for SMaA, as expected. Analysis of the fraction of VICs expressing SMaA (SMaA+ VICs) on the different gels revealed a trend towards decreased SMaA+ VICs on the 15% gels compared to the 5% in the 6-week-old MVAC

VICs (Fig. 22-10, $p=0.1$), but no difference between gels for 6-week-old PML VICs. 6-month and 6-year-old MVAC VICs did not display a difference in the fraction of SMAA+ VICs between gels, but 6-month and 6-year-old PML VICs showed a trend toward decreased SMAA + VICs on the 15% gels relative to the 5% gels ($p=0.06$). Analysis of the intensity of SMAA stain in SMAA+ VICs on the different gels revealed a trend towards decreased intensity in SMAA+ VICs for 6-week-old MVAC VICs (Fig. 22-11, $p=0.087$), but no difference for 6-week-old PML VICs. 6-month-old MVAC demonstrated no change in SMAA intensity in MVAC VICs, but decreased SMAA intensity in PML VICs ($p<0.05$). No difference in SMAA intensity between gels was evident for 6-year-old MVAC VICs or 6-year-old PML VICs.

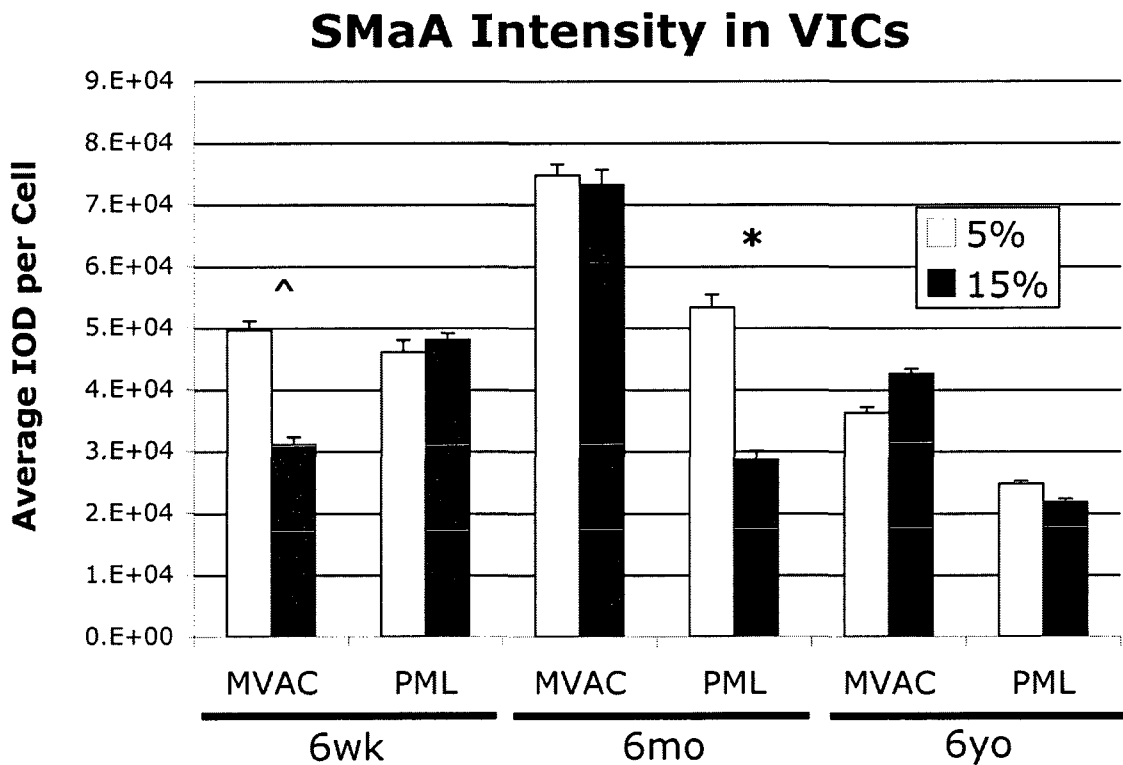


*Fig. 22-11: SMAA staining intensity for positive SMAA staining VICs on gels of different stiffnesses, * $p<0.05$, ^ $p=0.087$ 5% vs. 15% gels.*

P4H Expression of VICs on Gels of Different Stiffnesses

Analysis of P4H intensity, which was expressed by all VICs, demonstrated decreased intensity in 6-week-old MVAC VICs on the 15% gels relative to the 5% gels ($p < 0.05$), but no difference between gels for 6-week-old PML VICs. 6-month-old MVAC VICs demonstrated no difference in P4H intensity between gels, but 6-month-old PML VICs demonstrated decreased intensity on the 15% gels relative to the 5% gels (Fig. 22-12, $p < 0.05$). 6-year-old MVAC and PML VICs both demonstrated decreased P4H intensity on the 15% gels relative to the 5% gels (MVAC $p < 0.05$, PML $p < 0.085$ (trend)).

P4H Intensity in VICs

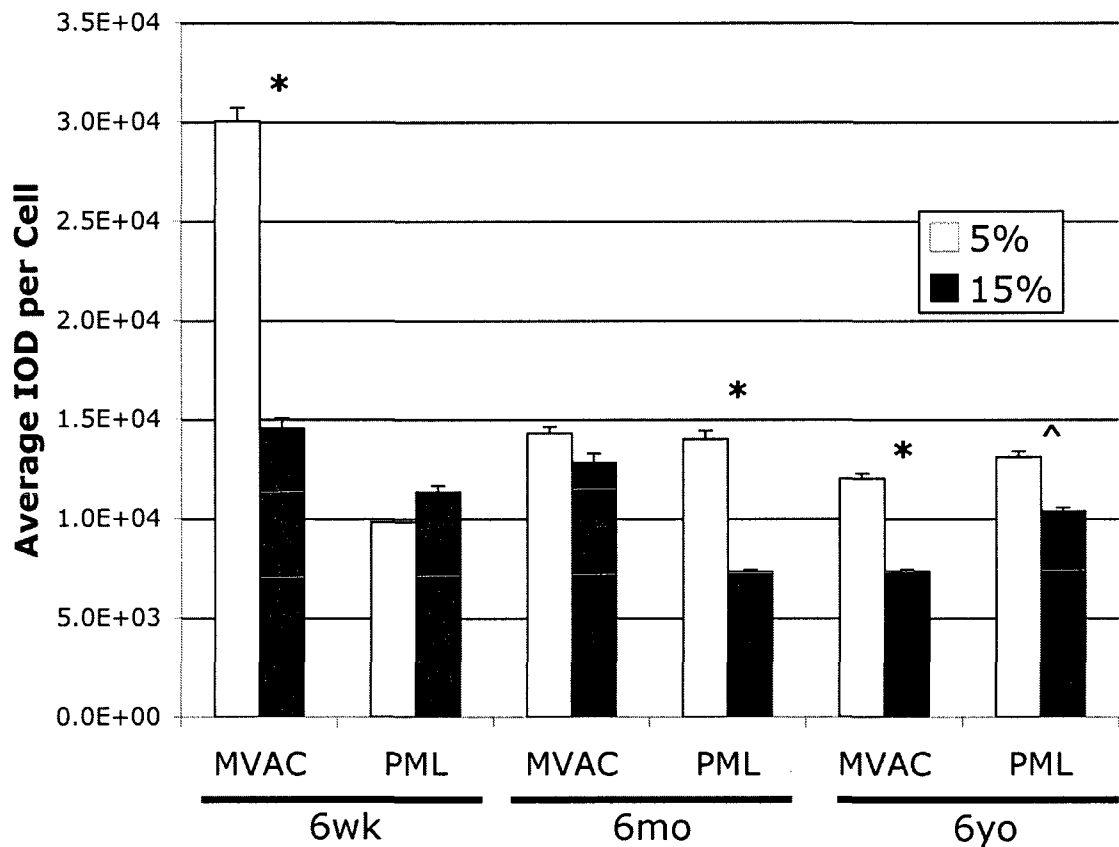


Fig. 22-12: P4H staining intensity of VICs on gels of different stiffnesses, $*p < 0.05$, $^{\wedge}p < 0.085$ 5% vs. 15% gels.

HSP47 Expression of VICs on Gels of Different Stiffnesses

Analysis of HSP47 intensity, which was expressed by all VICs, demonstrated decreased intensity in both 6-week-old MVAC and PML VICs on the 15% gels relative to the 5% gels (Fig. 22-13, both $p < 0.05$). 6-month-old MVAC VICs demonstrated no difference in HSP47 intensity between gels, but 6-month-old PML VICs demonstrated decreased HSP47 intensity on the 15% gels relative to the 5% gels ($p < 0.05$). 6-year-old MVAC demonstrated no difference in HSP47 intensity between gels, but 6-year-old PML VICs demonstrated increased HSP47 intensity on the 15% gels relative to the 5% gels ($p < 0.05$).

HSP47 Intensity in VICs

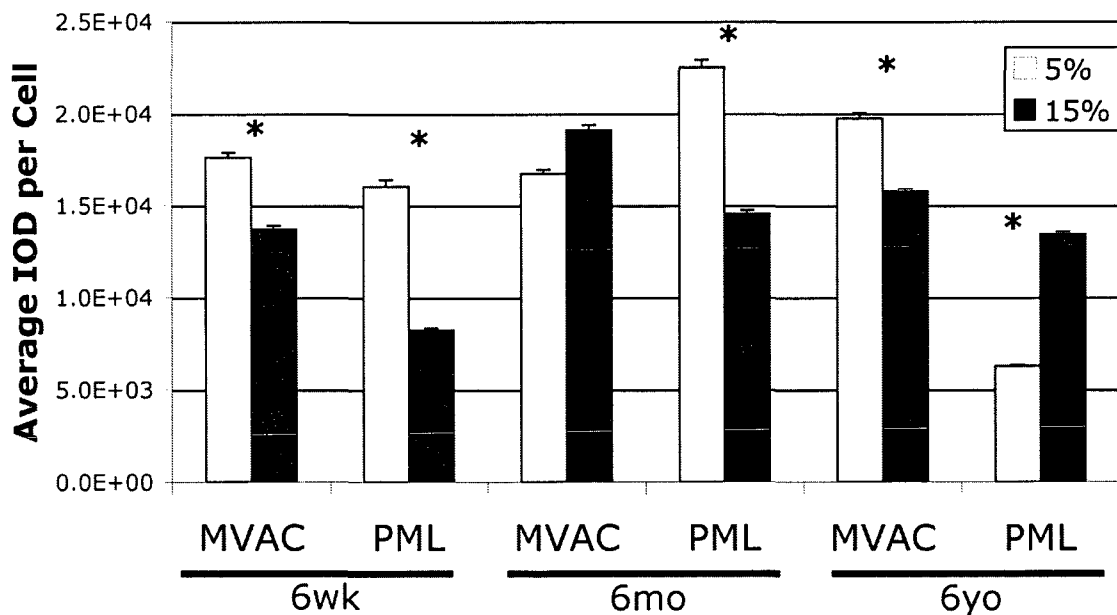


Fig. 22-13: HSP47 staining intensity of VICs on gels of different stiffnesses, $*p < 0.05$ 5% vs. 15% gels.

VIC Morphology on Gels of Different Stiffnesses

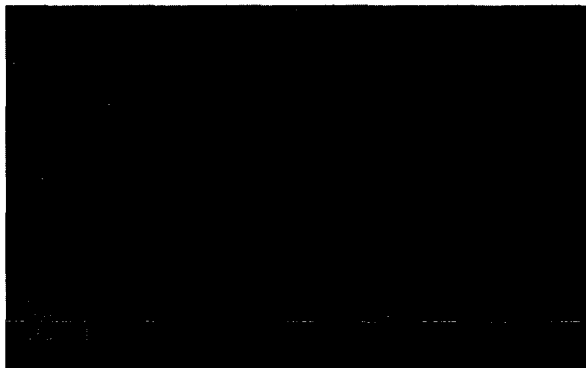
For both MVAC and PML VICs of each age and on each gel, two populations of VICs were noted: one with a spindle-shaped cell morphology, and a second with a cuboidal cell morphology (Fig. 22-14). Analysis of staining intensity of cuboidal and spindle-shaped subpopulations revealed that for given age- and valve-region VICs that responded to substrate stiffness, both subpopulations demonstrated a response (data not shown). Cell morphology analysis of vimentin-stained VICs revealed decreased cell area of 6-month-old PML VICs on the 15% gels relative to the 5% gels ($p < 0.02$). No difference was noted in circularity between VICs on PEG hydrogels of different stiffnesses.



6 wk



6 mo



6 yo

Fig. 22-14: Images of vimentin-stained VICs from each age group demonstrating two distinct VIC morphologic sub-populations: spindle-shaped cells and cuboidal cells. These distinct sub-populations were evident for VICs isolated from both MVAC and PML and on PEG gels of both stiffnesses. Shown here are MVAC VICs on 15% PEG gels. Scale bars indicate 50 μm .

DISCUSSION

In this study, mitral VICs grown on functionalized PEG hydrogels demonstrated both age-specific and valve-region specific (MVAC vs. PML) responses to substrate stiffness. While 6-week-old MVAC VICs on the gels of different stiffnesses demonstrated differences in SMAA, P4H, and HSP47 expression, 6-week-old PML VICs only demonstrated altered HSP47 expression. In contrast, 6-month-old MVAC VICs demonstrated no differences in marker expression on the gels of different stiffnesses, while 6-month-old PML VICs demonstrated differences in SMAA, P4H, and HSP47 expression. 6-year-old MVAC and PML VICs displayed a more complex response to the gels of different stiffnesses: 6-year-old MVAC VICs demonstrated no difference in SMAA intensity between the two gels, but decreased P4H and HSP47 on the stiffer gels. 6-year-old PML VICs also demonstrated no difference in SMAA intensity between the two gels, but decreased P4H and increased HSP47 intensity on the stiffer gels. These results underscore the range of unique phenotypes found in valvular cells depending on anatomic region and age.

Previous Studies of VICs and Substrate Stiffness

While the response of cells to substrate stiffness has been studied extensively in cell-types from many other tissues (see excellent review by Nemir, et al.⁶), very limited investigation has been performed on the response of VICs to substrate stiffness. Furthermore, no published studies to date have examined the response of MV VICs to

substrate stiffness and no studies have investigated a potential age-specific or valve region-specific response of VICs to substrate stiffness.

Work in fibroblasts from different tissues examining cell phenotype and morphology changes in response to substrate stiffness has documented increased actin fibers in response to increased substrate stiffness,⁶ appearance of stress fibers on stiffnesses 10 kPa and above,¹⁹ and an increase in cell spreading that was maximum on substrate stiffnesses of 8-10 kPa.^{19, 20} However, all of these studies were performed within a range of substrate stiffnesses that was much lower (i.e. 1 kPa to 100 kPa⁶) than the stiffnesses used in the present study. While the *in vivo* stiffness of the MVAC continues to be debated,^{21, 22} and the *in vivo* stiffness of the PML remains to be determined, these stiffnesses are certainly considerably greater than the 1-10 kPa range of substrate stiffness commonly utilized in fibroblast experiments. The two gel stiffnesses used in this study were chosen to be in the same general range that could be consistent with *in vivo* stiffnesses of the MVAC and PML, and yet two stiffnesses that were different enough to potentially elicit age- and valve-region specific VIC responses.

In the context of aortic valve (AV) calcification, three studies have analyzed the effect of substrate stiffness on the calcification potential and activation of porcine AV VICs. In a study by Benton et al.,²³ 10% 4.6 kDa PEG-dimethacrylate (PEG-DM) hydrogels (compressive modulus of ~100 kPa) were functionalized with fibronectin or fibrin. The calcification potential of AV VICs cultured on these surfaces was then compared to AV VICs cultured on unmodified tissue culture polystyrene (TCPS, much stiffer substrate), as well as TCPS coated with fibrin and fibronectin.²³ Cells were seeded at confluence (allowing cell-to-cell interaction) and cultured for 6 days on their respective

substrates before assaying for markers of VIC activation (SMaA) and calcification.²³ One of the key findings of this study was that the response of VICs to substrate stiffness differed depending on the matrix coating the substrate. AV VICs cultured on fibronectin-coated TCPS and fibronectin-functionalized PEG both did not show increases in calcification markers relative to controls, but VICs cultured on fibrin-coated TCPS showed increases in calcification markers while VICs cultured on fibrin-coated PEG did not.²³ In another study of AV VIC calcification potential using collagen gels of different stiffnesses, Yip et al.⁵ found that porcine AV VICs did not display any difference in calcification potential with varying substrate stiffness in normal media, but in calcification media AV VICs developed different types of calcific nodules depending on the stiffness of the collagen gels. In an earlier study by Pho et al.,²⁴ SMaA expression in AV VICs was increased on stiffer collagen gels; however, unlike in the study by Yip et al. in which collagen gels stiffness was varied by altering the gel thickness, in the study by Pho et al. stiffness was varied by altering collagen concentration. Therefore, in the study by Pho et al. VICs on the gels of different stiffnesses were also exposed to different concentrations of collagen fibers, and the potential difference in biological cues given to the VICs on the different substrates may have confounded their results.²⁴

Age-Specific and Valve-Region Specific Responses of VICs to Substrate Stiffness

In the present study both age-specific and region-specific responses of VICs to different substrate stiffnesses were evident. Based on *ex vivo* experiments of material properties of different aged porcine MVs and different regions within the porcine MV (MVAC vs. PML), one would expect the 6-week-old VICs to be accustomed to a less

stiff substrate relative to 6-month and 6-year-old VICs. Similarly, given studies demonstrating that MVAC tissues are stiffer than PML tissues,¹¹ one would expect VICs isolated from the MVAC to be accustomed to a stiffer substrate than VICs isolated from the PML. Unfortunately, the actual *in vivo* stiffness of the MVAC remains unclear, with only a few reports citing vastly differing values,^{21, 22} and no reports exist citing values for the *in vivo* stiffnesses of different aged MVAC and PML. Potentially, the results from this study could be explained by differences in “optimal” stiffness for each VIC population assessed. Just as “optimal” stiffnesses have been demonstrated for stem cell lineage specification and the expression of associated cellular markers,²⁵ in VICs expression of myofibroblast phenotype and collagen synthesis markers may reach a maximum at a certain stiffness, and this stiffness could be unique for each VIC population. Based on the mechanical testing studies cited above, potentially the “optimal” stiffness for 6-week-old PML would be less than 6-month-old PML and 6-week-old MVAC. Where the stiffnesses of the 5% and 15% gels used in this study fall upon this hypothetical marker expression-stiffness curve for a particular VIC population could explain whether differences in marker expression were observed for that VIC population seeded on the 5% and 15% gels (Fig. 22-15). Clearly, substantial future work is needed to investigate this hypothesis further; nevertheless, the results from this study demonstrate that there are age- and valve region-specific responses of VICs to substrate stiffness.

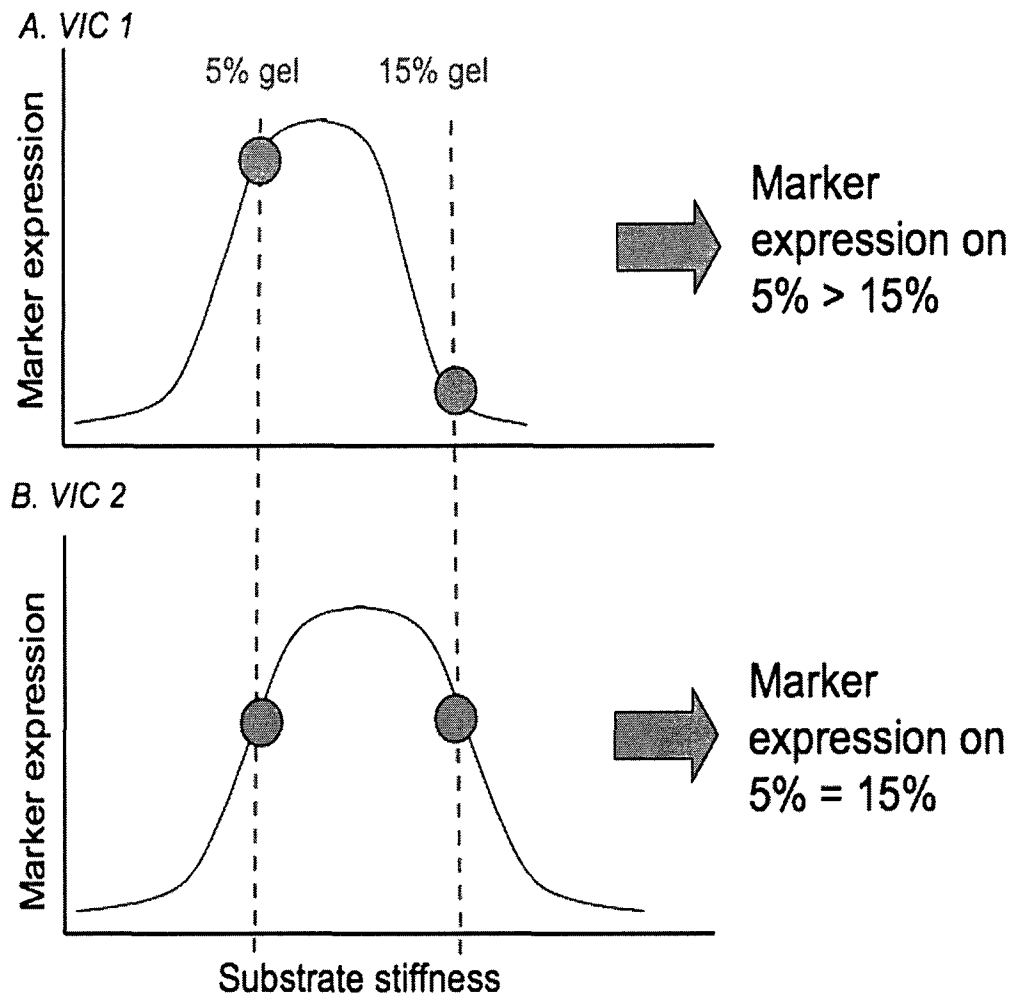


Fig. 22-15: Schematic illustrating how differences or lack of differences in marker expression between VICs seeded on 5% and 15% gels observed in this study may relate to a hypothetical marker expression-substrate stiffness continuum. These curves could be distinct for each VIC population (i.e., age and valve-region). A) The stiffnesses of the 5% and 15% gels fall on the marker expression-substrate stiffness curve such that marker expression of VICs on the 5% gels is greater than on the 15% gels. B) The stiffnesses of the 5% and 15% gels fall on the marker expression-substrate stiffness curve such that marker expression of VICs on the 5% gels is equal to the marker expression of VICs on the 15% gels.

In terms of specific protein expression, SMAA expression and proportion of SMAA⁺ cells generally paralleled changes in collagen synthesis markers in 6-week-old and 6-month-old MVAC and PML VICs. However, in 6-year-old VICs changes were evident in markers of collagen synthesis despite no detectable change in SMAA intensity.

Benton et al. similarly found a disparity between changes in SMaA expression and calcification potential in studying AV VICs, where on some surfaces no change in SMaA expression was noted, while markers of calcification demonstrated significant changes.²³ While the results for HSP47 largely paralleled those of P4H, in 6-year-old PML VICs P4H expression was decreased on 15% gels relative to 5% gels, while HSP47 was increased. Previous studies have shown that HSP47 can be induced by mechanical stress in tendon cells independent of collagen synthesis.²⁶ Additionally, transforming growth factor-beta (TGF β) in fibroblasts induces HSP47,²⁷ and VICs on heparin-coated surfaces produce more TGF β , which is then bound by heparin, allowing this growth factor to modulate VIC cell phenotype.²⁸ Certain enzymes, such as lysyl hydroxylase 2, also have demonstrated differential regulation of HSP47 and P4H in dermal fibroblasts.²⁹ Therefore, there is the potential for HSP47 to show distinct changes in response to substrate stiffness relative to P4H.

While the decrease in SMaA in some of the VIC populations on stiffer gels in this study at first glance may appear to contradict the findings of Pho et al.,²⁴ it should be noted that there were substantial differences between these studies. In the study by Pho et al. AV VICs were studied, cells were seeded near confluence allowing cell-cell interactions, collagen gels were used as substrates, and collagen concentrations (and therefore cell-matrix signaling) between the gels of different stiffnesses varied.²⁴ Furthermore, the stiffer gel in the study by Pho et al. was considerably less stiff than the 15% PEG gel used in the present study.²⁴ Work by Engler et al.²⁵ has demonstrated that for stem cells there exists a stiffness at which there is a maximum in myofibroblast marker expression, and above this stiffness myofibroblast marker expression actually

decreases, which would be consistent with the findings of this study. Differences in the results between the Pho, et al. study and the present study may also be influenced by the matrix components used in the substrates of different stiffnesses. In studying the calcification potential of AV VICs in response to substrate stiffness, Benton found that AV VICs responded to the same substrate stiffness differently depending on what matrix component coated the surface.²³ Additionally, studies have demonstrated differences in AV and MV VICs in response to growth factors,^{30, 31} therefore, VICs from the AV and MV may also demonstrate distinct responses to substrate stiffness.

VIC Subpopulations

Distinct VIC subpopulations, including the spindle-shaped and cuboidal cell morphologies evident in this study, have been previously documented.^{32, 33} The spindle-shaped cells demonstrate qualities similar to fibroblasts, while those with cuboidal morphology are similar to myofibroblasts and are associated with valve remodeling and various valve pathologies.³²⁻³⁶ These subpopulations also demonstrate differences in adhesion to different substrates and matrix components, such as fibronectin.^{37, 38} In the present study, when a difference in marker expression in VICs between the gels of different stiffnesses was evident, both subpopulations appeared to display this difference. Recent advancements in the isolation of these subpopulations could allow a more in-depth investigation of these subpopulations with respect to substrate stiffness.^{37, 38}

Implications

The age- and region-specific differences of VICs in response to substrate stiffness observed in this study should be taken into consideration in selecting cell

sources for tissue engineered heart valves. These results suggest that substrate stiffness should be carefully orchestrated in the context of specific VIC populations to optimize cell phenotype and matrix production. Furthermore, in light of the fact that these different VIC populations (from different aged valves and from different regions) reside in matrices of different stiffnesses, these results suggest that the *in vivo* mechanical environment in which VICs reside has a profound, fundamental impact on the responsiveness of VICs to their external environment (i.e., their baseline intracellular signaling framework), even in the *ex vivo* setting.

Limitations and Future Studies

While the results of this study provide fundamental knowledge regarding how MV VICs respond to substrate stiffness, substantial work remains in this area and certain study limitations should be noted. While the concentrations of biological cues presented to these cells (RGDS and methacrylated heparin) were carefully orchestrated to be the same between the two substrates, there may be differences in how different aged VICs and VICs from different valve regions respond to the same concentration of these biological cues (for example, if cultured on tissue culture plastic). Future studies investigating this further, and perhaps assessing differences in how these cells interact with their substrate (i.e., expression of integrins) would add insight in this area. Additionally, the mechanism(s) by which these cells respond differently to their substrate warrants investigation. For instance, while PEG is highly hydrophilic and does not adsorb proteins, heparin is known to bind growth factors.²⁸ Therefore, differences in amounts or types of growth factors produced by these different VICs in response to

different substrates could then be sequestered by heparin in the gels and propagate changes in VIC phenotype. Future investigation into inherent differences between these VIC populations could also lend insight into the results found in this study. Ultimately, a larger range of substrate stiffnesses, including stiffnesses that match those in which these different VICs reside *in vivo* could allow the determination of an “optimal” substrate stiffness for each VIC population. However, this has been difficult given limited, conflicting reports regarding the *in vivo* stiffnesses of the MVAC,^{21, 22} and no *in vivo* studies of the PML. The goal of this set of experiments was to first determine whether there were age- and valve-region specific responses to substrate stiffness.

CONCLUSIONS

In this study, for the first time the response of MV VICs to substrate stiffness has been investigated. VIC populations taken from different regions of the same MV and VICs of different ages cultured on PEG hydrogels of different stiffnesses demonstrated age- and valve-region-specific responses to substrate stiffness. These findings should be taken into consideration in the design of an age-specific tissue engineered heart valve and in future investigations of heart valve mechanobiology.

This chapter, which analyzed the response of mitral valvular interstitial cells from different aged valves and different valve regions to substrate stiffness, also involved the development of functionalized poly(ethylene) glycol hydrogels that potentially can serve as scaffolds for a tissue engineered heart valve. Therefore, this

chapter not only built upon earlier findings in this thesis (i.e., that different aged valves and valve regions demonstrated differences in matrix and material properties, suggesting that the valvular interstitial cells may behave differently), but brought these insights to bear upon preliminary work towards engineering a valve replacement. This chapter concludes the studies portion of the thesis (Chapters 2-22). In the next chapter key findings from this thesis work will be briefly summarized, contributions that this thesis makes to our understanding of valve mechanobiology will be highlighted, and future directions will be outlined. Additionally, the insight that this thesis work provides for tissue engineered heart valve design will be discussed.

REFERENCES

1. Nilasaroya A, Poole-Warren LA, Whitelock JM, Jo Martens P. Structural and functional characterisation of poly(vinyl alcohol) and heparin hydrogels. *Biomaterials*. 2008;29(35):4658-4664.
2. Rosamond W, Flegal K, Friday G, Furie K, Go A, Greenlund K, Haase N, Ho M, Howard V, Kissela B, Kittner S, Lloyd-Jones D, McDermott M, Meigs J, Moy C, Nichol G, O'Donnell C, Roger V, Rumsfield J, Sorlie P, Steinberger J, Thom T, Wasserthiel-Smoller S, Hong Y, Subcommittee for AHASCaSS. Heart Disease and Stroke Statistics—2007 Update: A Report From the American Heart Association Statistics Committee and Stroke Statistics Subcommittee. *Circulation*. 2007;115(6):e69-171.
3. American Heart Association. *Heart Disease and Stroke Statistics -- 2008 Update*. Dallas, TX 2008.
4. Taylor PM. Biological matrices and bionanotechnology. *Philos Trans R Soc Lond B Biol Sci*. 2007;362(1484):1313-1320.
5. Yip CY, Chen JH, Zhao R, Simmons CA. Calcification by valve interstitial cells is regulated by the stiffness of the extracellular matrix. *Arterioscler Thromb Vasc Biol*. 2009;29(6):936-942.
6. Nemir S, West JL. Synthetic Materials in the Study of Cell Response to Substrate Rigidity. *Ann Biomed Eng*. 2009;38(1):2-20.
7. Stephens EH, Chu CK, Grande-Allen KJ. Valve proteoglycan content and glycosaminoglycan fine structure are unique to microstructure, mechanical load and age: Relevance to an age-specific tissue-engineered heart valve. *Acta Biomater*. 2008;4(5):1148-1160.
8. Stephens EH, Grande-Allen KJ. Age-related changes in collagen synthesis and turnover in porcine heart valves. *J Heart Valve Dis*. 2007;16(6):672-682.
9. Aikawa E, Whittaker P, Farber M, Mendelson K, Padera RF, Aikawa M, Schoen FJ. Human semilunar cardiac valve remodeling by activated cells from fetus to adult: implications for postnatal adaptation, pathology, and tissue engineering. *Circulation*. 2006;113(10):1344-1352.
10. Stephens EH, de Jonge N, McNeill MP, Durst CA, Grande-Allen KJ. Age-related changes in material behavior of porcine mitral and aortic valves and correlation to matrix composition. *Tissue Eng*. 2010;16(3):867-878.
11. Kunzelman KS, Cochran RP. Stress/strain characteristics of porcine mitral valve tissue: parallel versus perpendicular collagen orientation. *J Card Surg*. 1992;7(1):71-78.
12. Gombotz W, Wang G, Horbett T, Hoffman A. Protein adsorption to poly(ethylene oxide) surfaces. *J Biomed Mater Res*. 1991;25(12):1547-1562.
13. Zheng S, Liu Y, Palumbom F, Luo Y, Prestwich G. In situ crosslinkable hyaluronan hydrogels for tissue engineering. *Biomaterials*. 2004;25(7-8):1339-1348.

14. Hahn M, McHale M, Wang E, Schmedlen R, West J. Physiologic pulsatile flow bioreactor conditioning of poly(ethylene glycol)-based tissue engineered vascular grafts. *Ann Biomed Eng.* 2007;35(2):190-200.
15. Cushing MC, Liao J, Jaeggli MP, Anseth KS. Material-based regulation of the myofibroblast phenotype *Biomaterials.* 2007;28:3378-3387.
16. Masters KS, Shah DN, Walker G, Leinwand LA, Anseth KS. Designing scaffolds for valvular interstitial cells: cell adhesion and function on naturally derived materials. *J Biomed Mater Res A.* 2004;71(1):172-180.
17. Blumenkrantz N, Asboe-Hansen G. New method for quantitative determination of uronic acids. *Anal Biochem.* 1973;54(2):484-489.
18. Stephens EH, Carroll JL, Grande-Allen KJ. The use of collagenase III for the isolation of porcine aortic valvular interstitial cells: rationale and optimization. *J Heart Valve Dis.* 2007;16(2):175-183.
19. Yeung T, Georges PC, Flanagan LA, Marg B, Ortiz M, Funaki M, Zahir N, Ming W, Weaver V, Janmey PA. Effects of substrate stiffness on cell morphology, cytoskeletal structure, and adhesion. *Cell Motil Cytoskeleton.* 2005;60(1):24-34.
20. Solon J, Levental I, Sengupta K, Georges PC, Janmey PA. Fibroblast adaptation and stiffness matching to soft elastic substrates. *Biophys J.* 2007;93(12):4453-4461.
21. Krishnamurthy G, Itoh A, Bothe W, Swanson JC, Kuhl E, Karlsson M, Miller DC, Ingels NB, Jr. Stress-strain behavior of mitral valve leaflets in the beating ovine heart. *J Biomech.* 2009.
22. Sacks MS, Enomoto Y, Graybill JR, Merryman WD, Zeeshan A, Yoganathan AP, Levy RJ, Gorman RC, Gorman JH, 3rd. In-vivo dynamic deformation of the mitral valve anterior leaflet. *Ann Thorac Surg.* 2006;82(4):1369-1377.
23. Benton JA, Kern HB, Anseth KS. Substrate properties influence calcification in valvular interstitial cell culture. *J Heart Valve Dis.* 2008;17(6):689-699.
24. Pho M, Lee W, Watt D, Laschinger C, Simmons C, McCulloch C. Cofilin is a marker of myofibroblast differentiation in cells from porcine aortic cardiac valves. *Am J Physiol Heart Circ Physiol.* 2008;294(4):H1767-1778.
25. Engler AJ, Sen S, Sweeney HL, Discher DE. Matrix elasticity directs stem cell lineage specification. *Cell.* 2006;126(4):677-689.
26. Pan H, Halper J. Regulation of heat shock protein 47 and type I procollagen expression in avian tendon cells. *Cell Tissue Res.* 2003;311(3):373-382.
27. Sasaki H, Sato T, Yamauchi N, Okamoto T, Kobayashi D, Iyama S, Kato J, Matsunaga T, Takimoto R, Takayama T, Kogawa K, Watanabe N, Niitsu Y. Induction of heat shock protein 47 synthesis by TGF-beta and IL-1 beta via enhancement of the heat shock

- element binding activity of heat shock transcription factor 1. *J Immunol.* 2002;168(10):5178-5183.
28. Cushing MC, Liao JT, Anseth KS. Activation of valvular interstitial cells is mediated by transforming growth factor-beta1 interactions with matrix molecules. *Matrix Biol.* 2005;24(6):428-437.
 29. Wu J, Reinhardt DP, Batmunkh C, Lindenmaier W, Far RK, Notbohm H, Hunzelmann N, Brinckmann J. Functional diversity of lysyl hydroxylase 2 in collagen synthesis of human dermal fibroblasts. *Exp Cell Res.* 2006;312(18):3485-3494.
 30. Walker GA, Masters KS, Shah DN, Anseth KS, Leinwand LA. Valvular myofibroblast activation by transforming growth factor-beta: implications for pathological extracellular matrix remodeling in heart valve disease. *Circ Res.* 2004;95(3):253-260.
 31. Liu AC, Gotlieb AI. Transforming growth factor-beta regulates in vitro heart valve repair by activated valve interstitial cells. *Am J Pathol.* 2008;173(5):1275-1285.
 32. Taylor PM, Batten P, Brand NJ, Thomas PS, Yacoub MH. The cardiac valve interstitial cell. *Int J Biochem Cell Biol.* 2003;35(2):113-118.
 33. Messier RH, Jr., Bass BL, Aly HM, Jones JL, Domkowski PW, Wallace RB, Hopkins RA. Dual structural and functional phenotypes of the porcine aortic valve interstitial population: characteristics of the leaflet myofibroblast. *J Surg Res.* 1994;57(1):1-21.
 34. Rabkin E, Aikawa M, Stone JR, Fukumoto Y, Libby P, Schoen FJ. Activated interstitial myofibroblasts express catabolic enzymes and mediate matrix remodeling in myxomatous heart valves. *Circulation.* 2001;104(21):2525-2532.
 35. Rabkin-Aikawa E, Farber M, Aikawa M, Schoen FJ. Dynamic and reversible changes of interstitial cell phenotype during remodeling of cardiac valves. *J Heart Valve Dis.* 2004;13(5):841-847.
 36. Stephens EH, Timek TA, Daughters GT, Kuo JJ, Patton AM, Baggett LS, Ingels NB, Miller DC, Grande-Allen KJ. Significant changes in mitral valve leaflet matrix composition and turnover with tachycardia-induced cardiomyopathy. *Circulation.* 2009;120(11 Suppl):S112-119.
 37. Blevins TL, Carroll JL, Raza AM, Grande-Allen KJ. Phenotypic characterization of isolated valvular interstitial cell subpopulations. *J Heart Valve Dis.* 2006;15(6):815-822.
 38. Stephens EH, Huynh TN, Cieluch JD, Grande-Allen KJ. Fibronectin-based isolation of valve interstitial cell subpopulations: relevance to valve disease. *J Biomed Mater Res A.* 2010;92(1):340-349.

Chapter 23: Conclusions

In this chapter key findings from this thesis work are briefly summarized, contributions that this thesis makes to our understanding of valve mechanobiology highlighted, and future directions outlined. Additionally, the insight that this thesis work provides for tissue engineered heart valve design is discussed.

A. Summary of Principal Findings and their Implications

In this section the main findings from this body of work are highlighted, along with their implications.

i. Age-Related Changes in Valves

This body of work demonstrated significant changes in valve matrix composition, structure, and material properties with age, both throughout fetal and postnatal life. Furthermore, a direct relationship between compositional/structural changes and material properties changes was demonstrated. These results have implications for our understanding of certain valve pathologies, cardiac mechanics, and aging, as well as the design of a tissue engineered heart valve (TEHV). A number of valve diseases show increased prevalence in certain age groups; potentially, these pathologies could relate to abnormalities of the aging process. Therefore, understanding how valves normally age could lend insight into some of these pathologies. This need for greater understanding applies not only to postnatal valve pathologies, but to congenitally diseased valves as

well. The results from these studies with respect to aging also provide insight into cardiac physiology. As cardiac hemodynamics change throughout fetal and postnatal life, valve composition, structure, and material properties change as well, with the material properties likely affecting hemodynamics and function, the mechanoenvironment affecting valve composition and structure, and valve composition and structure affecting material properties. Therefore, these results suggest a dynamic interplay between structure and function within valves throughout life. Lastly, given the age-related differences demonstrated in these studies, an optimal TEHV would be age-specific with specific composition, structure, and material properties that are appropriate for a normal valve of that age. These studies provide a baseline for the design of such a TEHV.

ii. Valve and Valve-Region Heterogeneity

This work also demonstrated structural and compositional differences between valves and valve regions, and similar to the age-related results, correlated these to differences in material properties. This evidence for valve and valve-region heterogeneity adds to our understanding of cardiac physiology as well as informs the design of a TEHV. In terms of cardiac physiology, the mitral and aortic valves (MV, AV) are exposed to different mechanical environments; the observed compositional, structural, and material property differences likely allow the valves and valve regions to function properly within their respective mechanoenvironments, and likely are even at least partly determined by that mechanoenvironment. Therefore, these findings provide further insight into the relationship between structure and function in the valve. These

results also have applications in the design of a TEHV; specifically, the valve and valve-region heterogeneity demonstrated in this body of work suggests that in order to faithfully emulate native valves, TEHVs should be developed with the specific properties of a particular valve, complete with regional heterogeneity. Furthermore, the compositional, structural, and material property characterization contained in this body of work provides baseline design criteria for such a TEHV.

iii. Normal Valve Physiology

The studies of normal MV physiology expounded upon the above studies of valve-region heterogeneity by examining the regional compositional and structural heterogeneity of the MV leaflets and annulus around the full circumference of the valve in the context of the *in vivo* strains experienced by each region. These studies demonstrated significant structural and compositional differences between the commissural leaflets, the posterior leaflet, and the anterior leaflet that related to the *in vivo* strains of these regions. Additionally, the MV annulus was characterized and similarly found to vary along the circumference of the MV in a manner that correlated with the strains experienced by each region. These studies demonstrated the complexity of the MV, and provided further characterization necessary for the design of a tissue engineered MV. In particular, these studies provided much needed characterization of the junction of the MV annulus and the myocardium that is required for the continuity between the MV leaflets and the rest of the heart. The structure and mechanics of this interface will be important to consider in the design of a tissue engineered MV. These

studies additionally provided insight into the relationship between structure and function in the *in vivo* MV.

iv. Involvement of Valves in Acquired Cardiac Diseases

This work demonstrated that the MV is affected by and involved in “functional” mitral regurgitation and dilated cardiomyopathy (DCM), both diseases commonly considered to predominantly involve abnormalities in the left ventricle and to spare the MV. Additionally, these studies demonstrated a relationship between altered leaflet strains and composition, suggesting that altered strain may have played a role in the compositional changes. Furthermore, results from these studies implicated the valvular interstitial cell (VIC) myofibroblast phenotype in both the compositional and mechanical changes. These studies have important potential implications for our understanding of “functional” mitral regurgitation and DCM, their pathogenesis, as well as potential treatments. In the context of “functional” mitral regurgitation, the compositional changes observed suggested that mitral regurgitation (MR) induced leaflet remodeling that could worsen the regurgitation, thereby providing a potential mechanism for the clinically observed “MR begets MR.” The results from the DCM studies suggest that altered strain could have caused the changes in MV composition; if this supposed mechanism is correct, and these compositional changes were found to be detrimental, it would further motivate the refinement of annuloplasty design to retain or restore normal physiological MV strains. The study examining the MV annulus in particular provides a potential mechanism for the annular dilation critical to DCM pathogenesis; further work in this area could potentially lead to novel treatments involving modification of the

extracellular matrix and/or valve cells. Nonetheless, overall these studies demonstrated that the MV is involved in these cardiac diseases and suggest that the MV should be taken into consideration for understanding the pathophysiology of these diseases and for providing context for various repair strategies.

v. Acquired Valve Disease

In calcific aortic valve disease, this body of work demonstrated that proteoglycans, hyaluronan homeostasis, and hypoxia are associated with nodule formation. Furthermore, results suggested that these matrix components and mechanisms interact with one another within the calcification process, and that the interactions between these factors were different within the various regions within and surrounding mature and preliminary nodules. The results with respect to hyaluronan homeostasis in particular suggest a novel mechanism that could underlie the pathogenesis of calcific aortic valve disease. The observed regional heterogeneity in matrix composition and interaction of matrix regulators relative to mature and preliminary nodules also provides understanding into the progression of nodule formation. While further studies are needed to demonstrate and elucidate the causal relationship between these factors *in vitro* and *in vivo*, as well as the time dependent nature of nodule formation, the studies contained in this work can lay groundwork for future investigations that could ultimately lead to novel therapeutics for this widespread disease.

In myxomatous mitral valve disease, this work characterized the specific proteoglycans increased in these diseased valves (see Chapter 24 in the Appendix) and demonstrated that the mitogen-activated protein kinase (MAPK) pathway is likely a

signaling mechanism for the increased number of activated myofibroblast-like VICs in the disease. Additionally, this work demonstrated correlations between myofibroblast markers and regional extracellular matrix disarray, suggesting that these myofibroblasts are involved in the matrix dysregulation that leads to the deterioration in valve function. Although the studies of the MAPK pathway in this body of work are limited to documenting associations between factors, further study regarding this pathway could lead to therapeutics that target the MAPK pathway for the treatment of myxomatous mitral valve disease.

In terms of the iatrogenic valvulopathy of a surgical wound, this body of work demonstrated that two distinct regions of remodeling are present in normal wound healing. This work characterized these regions in terms of specific matrix components, VIC phenotype, and microstructural changes. This characterization of normal valve wound healing could provide insight into the mechanisms that underlie abnormal wound healing. These studies could also provide insight into how to improve the healing process after valve repair surgeries.

vi. Congenital Valve Disease

With respect to congenital valve disease, this work characterized the specific matrix abnormalities found in congenitally diseased semilunar valves. These valves demonstrated significant alterations related to collagen and elastic fiber turnover that were distinct depending on pathology. Plaques evident on these valves similarly displayed altered matrix composition and turnover; furthermore, the relatively normal-appearing regions underlying the plaques displayed alterations that could relate to the

development of these plaques. The characterization of these congenitally diseased valves contained in this work may lend insight into disease pathogenesis, as well as pave the way for more specific pathological diagnoses of these valves, with potential prognostic and therapeutic implications. Furthermore, analysis of VICs isolated from these diseased valves revealed alterations in phenotypic markers as well as general cell morphology. These results suggest inherent abnormalities in VICs contained within congenitally diseased valves that likely relates to the altered composition of the leaflet itself, as well as has implications for autologous cell sources for a TEHV for this population.

vii. Structure-Function Relationship in the Valve

A number of the studies within this body of work demonstrated significant correlations between the observed structural and compositional differences (whether between valves, valve regions, or different ages), and functional differences (such as differences in strains, material properties, or the hemodynamic environment). The demonstration of such a relationship between structure and function has a number of important implications. For example, in instances in which the strain of the leaflet has been altered, such as in the placement of an annuloplasty ring, the composition of the valve may be affected, which could potentially alter valve mechanics and ultimately valve function. As another example, when various disease processes or aging affects valve composition, the material properties of the valve may be altered, which similarly could result in altered valve function. These studies demonstrating a link between structure and function also have implications for a TEHV, since these studies provide design criteria in terms of valve composition and structure in order to create a valve with

the material properties desired. In addition, these studies suggest that physiologic flow loops or other means of imposing physiologic, regionally heterogeneous strains on a TEHV construct could provide an important mechanical stimulus enabling the TEHV to remodel to generate structural, composition, and even material properties that are more similar to the native valve.

viii. Valvular Interstitial Cells

While analysis of VIC cell phenotype comprised a portion of a number of valve composition studies, in terms of experiments whose focus was on VICs, this body of work demonstrated that VICs appear to act within a dynamic VIC-collagen functional unit within the valve. This finding has a number of implications. First, it provides a mechanism for leaflet force generation, and potentially for leaflet stiffness modulation evident *in vivo*. Secondly, it provides a potential framework for understanding valvulopathies (i.e., any part of that functional unit can be perturbed and contribute to valvulopathies). Thirdly, it further emphasizes the importance of VICs, and suggests their necessary inclusion in a TEHV (as opposed to an acellular scaffold), at the very least for baseline valve tonus.

Additionally this body of work showed that VICs demonstrate an age- and valve-region-specific response to substrate stiffness. This age-specific response to substrate stiffness will need to be taken into consideration as designs of age-specific TEHVs are developed.

ix. Methods

This body of work included the development of a number of methods related to the study of valve physiology and pathology. First, the method for enzymatic isolation of VICs was optimized for porcine valves of different ages. Another study explored the use of differential adhesion of VICs to tissue culture polystyrene (TCP) and fibronectin (FN) as a means for isolating the VIC myofibroblast subpopulation. Results from that study demonstrated that differential adhesion to FN yielded a subpopulation with enhanced expression of myofibroblast-related markers. The subsequent functional characterization of this VIC subpopulation revealed that these cells also contracted and remodeled collagen gels in a manner consistent with myofibroblasts. Based on these results, differential adhesion of VICs to FN may be a useful means for studying the VIC myofibroblast subpopulation, a cell-type implicated in valve pathologies but previously difficult to study because there were no means for isolating this population. Another method developed in the context of this body of work was the radius of transition curvature. This parameter quantifies the acuteness of the transition region of a stress-strain (or tension-strain) curve from the low stress to high stress region. In valves, during this transition region collagen fibers align and begin bearing load, therefore a lower radius of transition curvature suggests that collagen fibers are more aligned or more homogeneously crimped compared to a higher radius of transition curvature, although additional study remains to verify this. The radius of transition curvature could be a useful parameter to characterize stress-strain curves of all types of biological tissues and engineered constructs possessing a biphasic shape. Another method developed within the body of this work was a strain-load device that fits within the stage of a confocal

microscope. This device allows the visualization of valve microstructure during various manipulations, such as addition of various vasoactive agents or manual strain of the tissue, while simultaneously measuring load. Lastly, the feasibility of poly(ethylene) glycol (PEG)-RGDS-methacrylated heparin hydrogels as a platform for a TEHV was demonstrated. These hydrogels are a promising scaffold material providing flexibility in design parameters including scaffold stiffness, proteins or peptides presented to the seeded cells, and size and shape of the construct. An additional key advantage of a PEG-based scaffold is that PEG hydrogels themselves are bio-inert and therefore immunocompatible.

B. Unique Contributions to the Literature

While the specific unanswered questions that each study addresses have been discussed within each chapter, in this section certain key ways in which this body of work provides unique contributions to our current understanding of valve physiology and pathology are highlighted. Within this section, select previous studies relevant to a given topic have been referenced; for more complete discussions of previous work in a given area and accompanying references, please see individual chapters.

i. Age-Related Changes in Valves

While compositional changes with aging, predominantly related to embryological development as well as some analysis of changes in the elderly, have been previously studied, this body of work provides important additional insight into valve aging later in

life as well as novel insight into the changes that occur during fetal and earlier postnatal life. In terms of the older age groups, this body of work characterized both AV and MV from the same animals, and demonstrated that the aging process is distinct within the different valves; the aging process is even distinct within different regions of the MV. Additionally, this work provides characterization of changes in material properties with late postnatal aging, which was heretofore lacking.

In terms of the earlier age groups, the results from this body of work demonstrate that significant changes in valve composition, structure, and material properties are not limited to the elderly, but occur throughout postnatal life. Similarly, the results from fetal and perinatal valves demonstrate that changes in valve composition and structure are not limited to the early fetal period of valvulogenesis. In sum, the age-related results from this body of work suggest that valve aging occurs throughout life.

li. Valve and Valve-Region Heterogeneity

While previous studies had examined differences between various regions of the MV in terms of composition and material properties,^{1, 2} there were no previous investigations of differences between AV and the regions of the MV from the same animals. Furthermore, the differences in material properties among these valves and valve regions had never before been directly related to compositional and structural differences within the same valve samples. Additionally, the examination of the aging process in terms of composition and material properties of these different regions of the MV and AV represents a unique contribution to the literature.

ii. Normal Valve Physiology

It has been well documented that valves respond to alterations in strain in previous *in vitro* experiments,^{3, 4} and various studies (including early studies comprising this body of work) have demonstrated that valve matrix undergoes constant remodeling. However, the idea that the degree of strain experienced by certain regions in the normal valve *in vivo* could be related to collagen turnover in that region had not been explored prior to this body of work.

An additional novel component to the normal valve physiology studies was the characterization of the mitral annulus and commissural leaflets. While the mitral annulus has been implicated in a number of diseases, including DCM and “functional” mitral regurgitation, the composition and structure of this critical junction connecting the valve to the remainder of the heart has largely been overlooked. Similarly, prior compositional and structural studies of the MV leaflets have overlooked the commissural leaflets.

iii. Involvement of Valves in Acquired Cardiac Diseases

Heretofore, both “functional” mitral regurgitation and DCM were thought to be ventricular diseases, therefore MV composition and structure in these diseases largely had not been studied. While MV geometry and closing dynamics have been studied with respect to the degree of regurgitation in these diseases, the leaflets themselves were largely thought to be normal and the regurgitation due to geometric changes in the ventricle to which the valve was anchored. This body of work, expounding upon studies by Grande-Allen et al.,⁵ provides novel insight into these diseases by demonstrating that valve structure and matrix composition are significantly altered in this disease. These

results suggest that “functional” mitral regurgitation and DCM are diseases of the MV as well as the ventricle. Furthermore, novel studies in which *in vivo* leaflet strains were directly correlated to regional leaflet composition implicated a role for altered strain in the context of these diseases. These results further elucidated the relationship between structure and function in the valve. Moreover, these studies add to a growing body of evidence that the valves are not passive, but are actively involved in normal cardiac function as well as pathologies.

iv. Acquired Valve Disease

While a number of researchers are actively investigating the process of calcification of the aortic valve, the examination of the potential role for hypoxia and hyaluronan metabolism in this process represents a unique contribution to the literature. Additionally, the consideration of the regional heterogeneity of the calcification process, i.e., evaluation of protein expression within the nodules, at the edge of the nodule, and immediately surrounding the nodule, as well as in “prenodules,” represents a novel advance in understanding the calcification process. In terms of myxomatous mitral valve disease, while increased numbers of myofibroblast-like VICs have been demonstrated in the disease, and the MAPK pathway has been investigated in the context of calcific aortic valve disease, the role of the MAPK pathway in myxomatous mitral valve disease is a novel contribution of this body of work.

With respect to wound healing in valves, previous *in vivo* studies have been limited to pathological studies of valve slice and suture wounds.^{6,7} In this body of work a systematic study was undertaken to investigate *in vivo* matrix remodeling, specific

matrix composition, and VIC phenotype in response to iatrogenic injury, providing further characterization of the normal *in vivo* wound healing process in the valve.

v. Congenital Valve Disease

The majority of previous studies of congenital valve diseases have examined either their gross anatomical configurations (i.e., number and attachments of leaflets), or the embryological processes leading to these congenitally malformed valves. Furthermore, standard pathological examination of congenitally diseased valves involves broad categorizations, such as “dysplastic,” that are often based on gross anatomical examination. However, the studies contained in this body of work provide novel information as to the specific matrix components that are dysregulated in congenital valve disease and also provide more detailed characterization of the microstructural changes. Furthermore, these studies also examined the VICs from congenitally diseased valves, which had not previously been done.

vi. Structure-Function Relationship in the Valve

The examination of structure in relation to function, which was performed in a number of studies, is another area in which this body of work makes novel contributions to the literature. While the relationship between stresses and/or strains and valve composition has been studied *in vitro*, this relationship had not been previously studied *in vivo*, nor have direct correlations been made between regional strains and composition within the same heart. Results from this body of work suggest that strains play a role in determining valve structure and function both in the healthy leaflet and in different

valvulopathies. Similarly, while the material properties of valves have been studied for decades, the direct relationship between these material properties and valve composition and structure has largely been overlooked, and certainly this relationship in the context of different aged valves never had been addressed previously.

Lastly, consideration of the material properties of a TEHV scaffold with respect to valvular cell phenotype is a novel investigation. While certainly much effort has been applied toward developing a TEHV with sufficient strength to withstand *in vivo* hemodynamics, the role of the material properties of the TEHV in determining valvular cell phenotype, which could effect the subsequent matrix production and matrix remodeling potential of the VICs, has received very little attention.

vii. Valvular Interstitial Cells

Previous studies have demonstrated VICs in proximity to collagen within fixed valve specimens,^{8, 9} however this body of work demonstrated, for the first time, VICs functionally interacting with collagen in *ex vivo* leaflets. Furthermore, this work demonstrated a functional role for integrins in the leaflet; previously integrins on VICs have only been documented using flow cytometry on enzymatically isolated VICs or via immunohistochemistry of valve sections.^{10, 11} This work specifically identified the $\alpha_2\beta_1$ integrin as an important receptor by which VICs interact with collagen, a receptor necessary for force generation in the valve. While force generation in the valve has been studied previously,^{8, 12-17} the investigation of the microstructure and molecular mechanisms that underlie force generation in the valve contained in this body of work is unique.

The study of differences between VICs from different aged valves, as well as VICs from different regions of the MV that undergo different loading patterns, is relatively novel. Furthermore, the demonstration of age- and valve-region specific differences in the response of VICs to substrate stiffness by this body of work represents a unique contribution to the valve literature.

viii. Methods

Of the various methods developed within this body of work, the development of the radius of transition curvature was particularly novel, and could be applied to stress-strain curves of many types of biological and engineered materials. While additional studies remain to verify that the radius of curvature in valves corresponds to collagen alignment and crimp, this is a useful parameter to quantify differences between stress-strain curve shapes that may have a variety of meanings in the context of different tissues. The strain-load device was also a novel development in allowing real-time visualization of microstructural changes in relationship to macrostructural tissue mechanics. Lastly, further development of the PEG-RGDS-methacrylated heparin builds upon considerable work previously done in the area of PEG scaffolds, but will be particularly important moving forward in the development of a TEHV.

C. Unifying Themes

The studies that embody this thesis are quite varied, and in some respects could appear disparate; however, there are several broad underlying themes that unify this body

of work. While some of these themes have been touched upon in earlier sections, they warrant specific discussion, which is done in the following section. Figure 23-1 illustrates these themes in relationship to the various valve components.

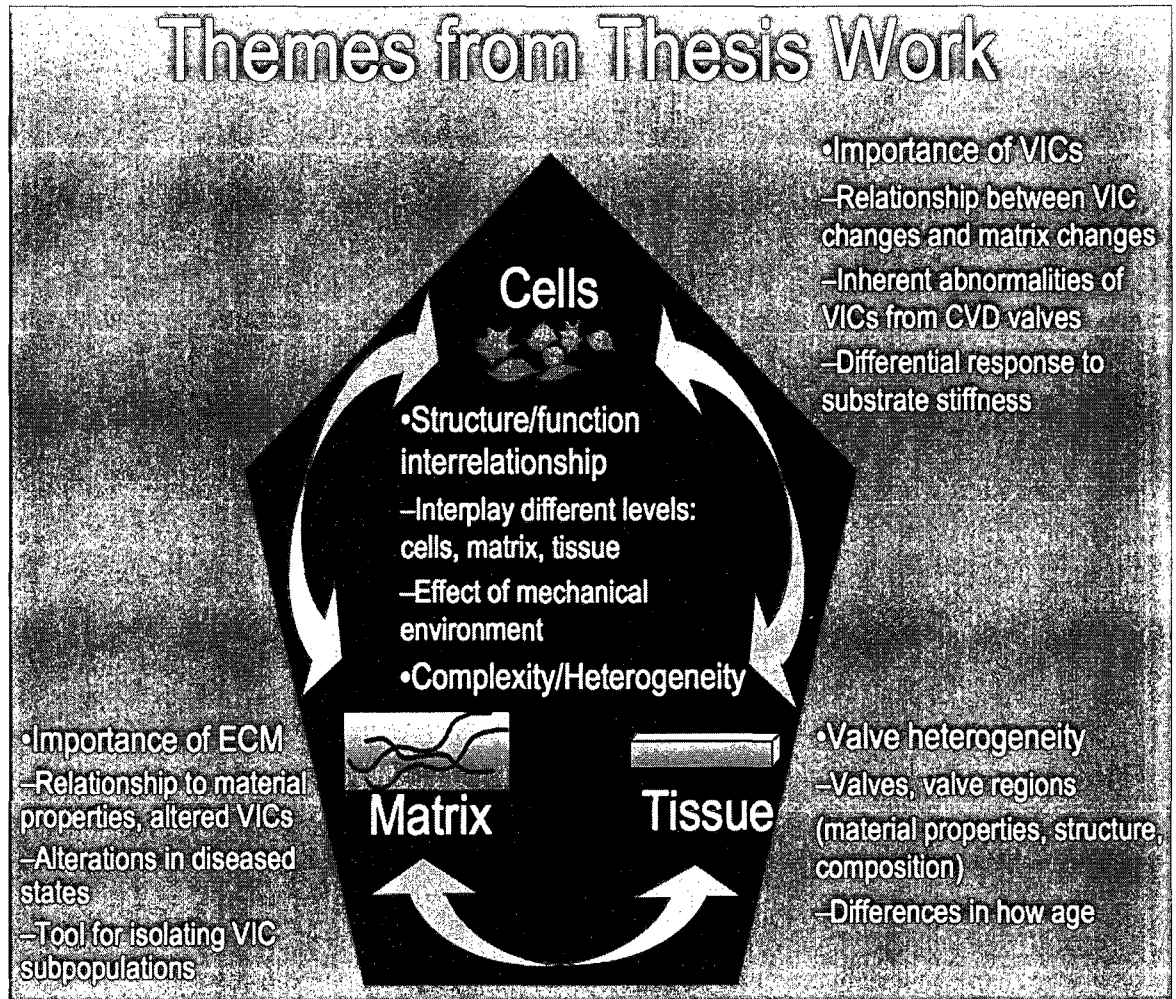


Fig. 23-1: Schematic illustrating key themes underlying this thesis work in relation to components of heart valves. ECM=extracellular matrix; CVD=congenital valve disease.

i. Importance of the Extracellular Matrix

The importance of the extracellular matrix was a constant thread running through a number of the studies. Not only did this body of work characterize the composition and

structure of the extracellular matrix in various valves and valve regions of different ages, but it showed that matrix remodeling occurs throughout life. Moreover, this thesis work demonstrated the role of this extracellular matrix in the material properties of the valve samples examined. This body of work also demonstrated the interrelationship between the extracellular matrix and strains in both normal and diseased states. These results, again, point to the dynamic nature of the extracellular matrix. In fact, the dynamic myofiber coupling seen in ventricular myocardial strains (Chapter 26 of the Appendix) implicates a dynamic role of extracellular matrix in cardiac mechanics. Results within this thesis also show that the valve extracellular matrix is altered in diseases previously thought to spare the valve leaflets; these matrix alterations could explain some of the functional problems in these diseases and points to the potential importance of restoring the extracellular matrix in treating these diseases. In relation to VICs, this thesis showed alterations in VICs were associated with changes in the extracellular matrix. The extracellular matrix (fibronectin) was also used in one of the methods developed in this thesis as a tool for isolating of VIC subpopulations. Given that the extracellular matrix is altered in myxomatous mitral valve disease, a disease in which the myofibroblast-like VIC is enriched, this altered extracellular matrix was used for isolating these cell types. In the course of assessing this isolation technique, it was also observed that fibronectin could be used to modulate the myofibroblast VIC phenotype. Lastly, this body of work demonstrated a dynamic, functional relationship between VIC and the extracellular matrix component collagen at the microstructural level.

ii. Importance of Valvular Interstitial Cells

A second underlying theme that unified this body of work was the role of the VIC in valve function and disease. As alluded to above, VICs were associated with both matrix remodeling that occurs in normal valves throughout life and alterations in matrix in various diseased states. In particular, the myofibroblast VIC phenotype appeared central to this remodeling in both normal and diseased states. In terms of the myofibroblast VIC phenotype, this body of work demonstrated that the VIC myofibroblast phenotype shows differential expression at various times during fetal development as well as postnatal life. This phenotype was also enhanced in a number of diseased states. Furthermore, the results suggested that the VIC myofibroblast phenotype could have played a role in both the observed changes in composition and strains, and even act as a link between these two components. Given the potential importance of this VIC subpopulation, as evident both in the aforementioned studies within this work and in other studies, a method for isolating this important VIC subpopulation was developed. An additional study examined the pathway potentially responsible for the differentiation of VIC into the VIC myofibroblast phenotype in myxomatous mitral valve disease.

Other key findings of this thesis also centered on VICs. Importantly in the study of congenitally diseased valves it was shown that VICs in these valves have altered markers of collagen synthesis, cellular activation, and cellular morphology. Similar to the other valvulopathies studied, these VIC phenotypic changes in congenitally diseased valves could be important to the disease's pathogenesis and potential novel therapeutics. These findings also have significant ramifications for cell source decisions for TEHVs for this patient population. The study investigating the VIC-integrin-collagen unit also

centered on VICs. This study showed the importance of VICs functionally interacting with collagen and potentially modulating leaflet stiffness *in vivo*. Lastly, this body of work documented an age- and valve-region-specific response of VICs to substrate stiffness, which will be important to take into consideration for the design of age-specific TEHVs.

iii. Importance of the Valve Mechanical Environment

Another theme woven throughout this body of work was the role of the valve's mechanical environment in determining valve composition and structure in both normal and diseased valves. This relationship was evident, for instance, in analysis of perinatal changes in valve composition and hemodynamics, as well as mitral leaflet strains and composition in normal and diseased states. The importance of the mechanical environment was also evident in relationship to VICs in the study demonstrating that substrate stiffness affected VIC phenotype, and that this response of VICs to substrate stiffness was dependent upon age and valve region. Further understanding of the interaction between the valve and its mechanical environment could aid both our understanding of valve diseases, as well as how to use mechanical stimulation to create the composition desired in a TEHV.

iv. Structure-Function Relationship

Another recurring theme was the interrelation between valve composition and structure and valve function. For instance, valve composition and structure, for a variety of valves and valve regions of different ages, were demonstrated to correlate to material

properties as well as measured strains. Examination of the valve microstructure revealed the VIC-integrin-collagen functional unit that underlies valve force generation. Throughout these studies significant interactions were evident between the different valve components (cells, matrix, and tissue), as well as between these components and the valve's mechanical environment; these complex interrelationships likely are important determinants of overall valve function. Continued study to better understand these relationships between structure and function will be essential to obtaining the ultimate goal: maintaining or restoring proper valve function.

v. Valve Heterogeneity

Throughout this body of work heterogeneity was apparent at multiple levels and in multiple parameters. Heterogeneity in valve composition and material properties was apparent among different regions of the MV, between the MV and AV as well as the AV and PV, and between different ages. These different valves and valve regions also were distinct in how their compositions changed with age. Heterogeneity was also observed in terms of regional valve structure, such as the mitral annular insertion structure. Strains among different regions of the MV, both along the annular circumference and along the length of the leaflet, were also heterogeneous. Similarly, heterogeneity in VICs was evident in their adhesive properties (i.e., to fibronectin), among VIC subpopulations isolated by differential adhesion, and among VICs from different valve regions and ages in terms of their response to substrate stiffness. These multiple levels of heterogeneity (at the level of the tissue, matrix, and cells) reveal the complexity of the valves, and present

a substantial challenge for the ultimate goal of developing TEHVs that closely mimic native valves at various ages.

D. Future Directions

While this body of work addresses many previously unanswered questions, a considerable number of questions remain or arise from these studies that should be addressed in the future. This section will discuss several potential future studies that could build upon the knowledge obtained from this body of work.

i. Age-Related Changes in Valves

While age-related compositional and structural differences were demonstrated in this body of work, future studies are warranted to elucidate the mechanisms by which these differences are created. Factors such as signaling molecules, potentially interacting with mechanical and hemodynamic cues, likely are important determinants.

Examination of how VICs from different aged valves are different is also warranted. Because the matrix composition that the VICs produce and material properties of the valves in which the VICs reside differs with age, there are also likely age-related differences in the VICs themselves. Such differences would likely impact their use as a cell-source for age-specific TEHVs. Furthermore, additional examination is warranted regarding how VICs of different aged valves interact and respond to their environment, including both the material properties (i.e., stiffness) and the biological cues of that environment. For instance, these VICs from different aged valves could

express different arrays of integrins or secrete differing amounts or types of growth factors in response to mechanical and biological cues from their environment. Further elucidation of the age-specific nature of VIC-extracellular matrix/substrate interaction will be important in the development of an age-specific TEHV.

ii. Valve and Valve-Region Heterogeneity

While regional heterogeneity within the MV has been examined in this body of work and related to differences in material, regional heterogeneity in the AV has been largely overlooked. Various regions of the AV are known to undergo different loading patterns, therefore it is likely that these regions have different matrix components, structures, and material properties. Preliminary work was performed within this thesis in this area, but further investigation is needed, particularly addressing whether these regions undergo distinct age-related changes.

iii. Involvement of Valves in Acquired Cardiac Diseases

While the series of studies presented here provide an important foundation for understanding the role of the MV in acquired cardiac diseases, these studies should be expounded upon by demonstrating a functional role for the observed MV compositional and structural changes in terms of cardiac dynamics as well as altered MV material properties. Furthermore, these changes should optimally be demonstrated in humans. Lastly, given the involvement of the MV in “functional” mitral regurgitation and DCM, it would be interesting to investigate whether the specific MV matrix and structural alterations found in “functional” mitral regurgitation and DCM in this body of work were

similarly altered in the MV in ischemic mitral regurgitation and other cardiomyopathies, or whether the valve pathologies of each of these diseases are distinct.

iv. Acquired Valve Disease

While the studies in this body of work investigating valve changes in myxomatous mitral valve disease and calcific aortic valve disease showed associations suggestive of mechanisms for the pathogenesis of these diseases, work *in vitro* is warranted to demonstrate a causative role for certain factors, such as hypoxia in calcific aortic valve disease, and even signaling pathways involved in the pathogenesis of these diseases. Further elucidation of these pathways would allow for potential novel therapeutic interventions for these diseases.

v. Congenital Valve Disease

While much is still to be learned regarding congenital valve disease, one finding that particularly warrants subsequent investigation is how the VICs from congenitally diseased valves differ from similarly aged normal valves. While preliminary work within this thesis addresses this question, more information in this area could both aid in the understanding of congenital valve disease pathogenesis. Moreover, such studies could lead to the development of methods to modulate the congenitally diseased VIC phenotype sufficiently *in vitro* such that the patient's own cells could be used in a TEHV. This approach would be particularly advantageous to the patient by avoiding the immune response to foreign cells. Additionally, further characterization of the different types of congenital valve disease, as well as the mechanisms behind the pathogenesis of these

different diseases, should be pursued. Clearly, a greater number of patients with age-matched controls would be necessary for such further study, and the confounding factor of hemodynamics should be addressed, since this is often altered in congenital valve disease.

vi. Structure-Function Relationship in the Valve

A number of studies within this body of work suggested an interaction between structure and function, however further investigation is needed to better understand and characterize this interaction. *In vitro* experiments in which a single variable can be isolated and carefully manipulated would aid in this regard. Once this interrelationship and its dynamics are better understood, it would be interesting to investigate whether this coupling between structure and function is disrupted in various diseased states.

vii. Valvular Interstitial Cells

A number of studies could potentially follow from the work on VICs contained in this thesis. For instance, further characterization of the proposed VIC-collagen-integrin functional unit is warranted, along with studies assessing how various factors affect that functional unit. Additionally, a number of studies within this body of work suggested that VIC myofibroblasts may have played a role in the compositional and mechanical changes observed; further research should be pursued to verify this role and elucidate the mechanism for these changes. Lastly, given the regional, valve, and age-specific compositional differences demonstrated in this body of work, it would follow to characterize the VICs within these regions and valves of different ages to understand how

these differences came about. The results of such a study might also have implications for VIC cell sources, or even the manipulation of cells other than VICs, for the use in TEHVs that are age and valve-specific.

viii. Methods

A number of future studies could be performed using the methods developed in this body of work. First and foremost, further investigation is needed to understand what factors the radius of transition curvature actually measures in valves. Once this validation has been done, the investigation of the use of these parameters in other tissues could be performed. Additional study is also warranted to further understand the mechanism that underlies the isolation of the VIC myofibroblast subpopulation using differential FN adhesion, and to further characterize that subpopulation. Perhaps most importantly for the ultimate goal of a TEHV, further work remains to continue to develop the PEG-RGDS-methacrylated heparin hydrogels. Future work could include incorporation of features such as regional heterogeneity and anisotropy in material properties, regional heterogeneity in peptide ligands and cell types, layering, mechanical conditioning, and incorporating degradable peptide sequences. Clearly, much of this thesis was working towards this TEHV frontier. PEG-RGDS-methacrylated heparin hydrogels can serve as a platform upon which many of the findings of this thesis can be implemented as we strive to engineer a physiologic, age-specific, valve-specific TEHV. The implementation of this thesis work as it relates to TEHV design is covered in the subsequent section.

E. Design Criteria for a Tissue Engineered Heart Valve

i. Overview

As stated in the Abstract and Background, the overarching goal of this thesis work was to study valve mechanobiology in normal states, including normal aging, as well as diseased states, to inform design criteria for a TEHV. In this section first the insight that this thesis contains with respect to the final characteristics desired in this TEHV will be discussed. Then, considering that different approaches are being proposed for obtaining this end-product, these approaches to constructing a TEHV will be briefly outlined, followed by a discussion of how this thesis work informs each of those approaches. Lastly, the remaining data required with respect to developing TEHV design criteria will be summarized.

ii. Insight of Thesis Work into Tissue Engineered Heart Valve Characteristics

Regardless of the approach taken to construct the TEHV end-product, this thesis has substantial insight into the characteristics that the ideal TEHV should ultimately possess. Overall the goal in the design of a TEHV is to construct a heart valve with physiologic function that is capable of growth with the patient, in the case of the pediatric population, the ability to effectively remodel and adapt to the valve's changing *in vivo* mechanoenvironment, and lastly immunocompatibility. Therefore this TEHV needs to be dynamic, remodeling throughout life, and responsive to its mechanical environment. Based on this thesis work, TEHVs need to be designed to be age-specific and valve-

specific, with regional heterogeneity, layer specific matrix composition, and accompanying differences in material properties. The insights that this thesis has on these various features are discussed below.

A. Age-Specific, Valve-Specific Design Criteria for Tissue Engineered Heart Valves

One of the key contributions that this thesis work makes to TEHV design is that TEHVs should be both age-specific and valve-specific. The data contained in this thesis demonstrating substantial changes in valves with age and differences between the different valves, implies that one TEHV design will not suit all valves or patients of all ages. This concept of an age-specific, valve-specific TEHV fundamentally changes the TEHV paradigm. Issues related to the age-specific and valve-specific aspects of different TEHV components are discussed in the following sections, but this fundamental shift in thinking deserved special attention before detailed discussion of specific TEHV features.

B. Cellular Component of a Tissue Engineered Heart Valve

This thesis demonstrated the importance of the cellular component of valves in normal valve mechanobiology. VICs affect valve material properties, providing baseline tonus and affecting valve flexural stiffness,¹⁸ as well as potentially imparting dynamic stiffness modulation as shown in this thesis. This thesis work also showed that VICs are involved in normal collagen turnover throughout life; this collagen turnover is likely part of important repair processes that maintain valve durability. It was also demonstrated in this thesis that VICs play a role in remodeling valves in response to altered strains in

diseased states. Given the importance of VICs in normal valve mechanobiology, their incorporation, or the incorporation of cells with similar characteristics, in a TEHV will be essential. In a TEHV, the cellular component is what enables the TEHV to be a dynamic structure, to remodel in response to alterations in the mechanoenvironment, grow with the patient, and even undergo the normal repair processes in response to the repeated loading that the valve experiences, which are likely necessary for long-term durability.

C. Material Properties of a Tissue Engineered Heart Valve

In terms of the material properties desired in a TEHV, they should be specific for the age of the patient and the valve it will be replacing. For all age groups and valves, the TEHV will need to exhibit anisotropy, with the stiffness greater and extensibility less in the circumferential direction compared to the radial direction. Based on this thesis work, the stiffness of the TEHV designed for an older adult patient should be greater and extensibility less than a TEHV designed for a younger adult or child. In terms of differences between a TEHV designed to replace an AV compared to a MV, the MV TEHV should be stiffer. These material properties will also need to vary among the different valve regions. For instance, the anterior center region of the MV (MVAC) circumferential stiffness should be greater than that of the MV free edge region (MVF).

D. Macrostructure and Matrix Composition of a Tissue Engineered Heart Valve

As demonstrated in this thesis, the material properties of valves are integrally linked to the valve's macrostructure and matrix composition. Therefore, in terms of the

corresponding matrix composition of these age-specific and valve-specific TEHV, valves designed for older patients should have thicker leaflet layers, with more collagen throughout the layers, but particularly in the fibrosa and ventricularis layers. Ideally, this collagen should have a crimped conformation allowing the extensibility seen in native valves. The MVAC should consist almost exclusively of collagen, while the corresponding annular region of the AV should have a fibrosa that occupies $\sim 1/3$ of the leaflet thickness. In the MVF, the predominant matrix component should be proteoglycans and glycosaminoglycans (GAGs); the fibrosa layer should occupy less than $\sim 1/4$ of the leaflet thickness. In terms of specific types of GAGs that should comprise these leaflets, the MVAC should have more 4-sulfated GAGs, especially 4-sulfated iduronate and hypersulfated GAGs than the MVF. The AV should have high total amounts of GAGs relative to the MVAC, especially glucuronate and hyaluronan, with a high 6:4 sulfation ratio. Overall with age the MV and AV TEHVs should have increased hyaluronan, decreased unsulfated glucuronate and 6-sulfated glucuronate, and a decrease in the chondroitin sulfate:dermatan sulfate ratio. In terms of valve and valve-region specific aging, with age the MVAC should have less 6-sulfated GAGs and more 4-sulfated iduronate, while the MVF should have less 4-sulfated GAGs and more 6 sulfated GAGs. With age the AV should have less 6-sulfated and more 4-sulfated GAGs, particularly 4-sulfated iduronate. In terms of other matrix components, this thesis work demonstrated that overall the AV should have greater expression of collagen-related markers than the MV. There were also significant differences in the expression of these markers between the corresponding layers of the AV and MV. For instance collagen-

turnover in the spongiosa of the AV was higher than other AV layers, while in the MV collagen-turnover was highest in the inflow ventricularis layer.

E. Heterogeneity within a Tissue Engineered Heart Valve

As discussed briefly in the sections on TEHV material properties and macrostructure and matrix composition, these TEHVs should demonstrate heterogeneity at multiple levels. The layers within the TEHV should be designed with distinct matrix compositions, and the MVAC and MVF should be designed to have different material properties and corresponding matrix compositions. This thesis also demonstrated that the MV commissural leaflets have unique compositions, and preliminary work assessing AV regional GAG composition suggests that the AV may similarly have regional differences in GAG composition. Regional variation in AV composition was also demonstrated in terms of markers of collagen synthesis, with greater expression of these markers in the free edge region compared to the annular region. These elements of heterogeneity should also be taken into consideration in the design of a TEHV. With regards to the MV, this thesis work characterized the structure of the MV leaflet annular insertion region and found it to be distinct depending on the location around the mitral annulus. This attachment between the leaflet and the myocardium is important both for integrity of the leaflet/annular complex and for preventing the potential complication of annular dilation. Careful design of this attachment region will be crucial for long-term durability and function of a TEHV.

iii. Different Approaches for Constructing a Tissue Engineered Heart Valve

While the end goal is to create a TEHV with the features outlined above (physiologic function, capability for growth and remodeling, and immunocompatibility), this end-product can be arrived at via different avenues. In the following section different approaches for obtaining the desired features will be discussed in turn. In the subsequent section (part “iv”), the insight that this thesis brings to bear on these different approaches to obtaining these features will be discussed.

A. Macrostructure and Material Properties for Physiologic Function

Proper physiologic valve function depends on a number of factors, but most importantly in terms of a TEHV are the material properties of the valve. These include its tensile strength, flexural properties, ability to withstand shear stress, and ultimately the durability of the TEHV to bear the repeated, complex loading that the valve experiences thousands of times a day for years on end. As demonstrated in this thesis work, as well as by previous researchers, the material properties of a valve depend on its complex macrostructure, including its layered leaflet structure. Additionally, this thesis work, as discussed above, demonstrated substantial regional heterogeneity in valve composition, structure, and material properties that will likely need to be emulated in order to obtain physiologic function of a TEHV. However, these desired macrostructural features of a layered structure with regional heterogeneity could be obtained using a number of different strategies. In the following paragraphs three strategies that appear most promising will be summarized.

The first strategy for obtaining the desired macrostructure and material properties would be to construct the valve using the desired matrix components with patterning that mimics the native valve's macrostructure. This could be accomplished using a matrix layering approach: a glycosaminoglycan/proteoglycan-rich layer to simulate the spongiosa, an elastic fiber-rich layer to simulate the ventricularis of the AV and the atrialis and ventricularis in the MV, and a collagen-rich layer simulating the fibrosa layer. Indeed Shi et al. have illustrated the potential for using such an approach;¹⁹ in their outlined strategy, collagen fiber bundles would be layered with cross-linked hyaluronan; smooth muscle cells would then be utilized, seeded on top of the hyaluronan layer, to create a layer of elastin.¹⁹ A challenge with this approach would be how to create sufficient integration between the layers to prevent layer dehiscence. Another limitation to this approach is that native leaflet layers are not comprised of one component; for instance, collagen is present in the ventricularis. It will be a challenge to design a matrix layering approach in which these layers themselves are composites of these different components and more accurately resemble the matrix composition of native leaflet layers. A strategy related to this matrix layering approach is the use of decellularized valves. The advantage of this approach is that the complex macrostructure, including the correct matrix components and even the anisotropic material properties, are already in place. However, this approach has been severely limited by the inability to remove all the immunogenic cellular components²⁰ (see part "B" of this section), and so is not discussed in depth.

The second strategy would be to use a bottom-up approach and seed the appropriate VICs in the appropriate locations in a TEHV construct. Based on inherent

differences between VICs of different ages, valves, and regions, and based on the hypothesis that these cells would contain the proper information to synthesize the appropriate matrix, this approach would rely on the cells to synthesize the necessary matrix and macrostructure for physiologic valve function. With this strategy, the cells would need a preliminary construct in which to be seeded and culture conditions that would support the appropriate synthesis of matrix components by these cells. Likely, this would entail a degradable scaffold that would provide initial support and degrade at a rate inversely proportional to the amount of matrix synthesized by the cells. A PEG scaffold with an MMP degradable sequence,²¹ for instance, could be used for such an application. Considerations would need to be made of what mechanical stimulation these cells might need and what input from the scaffold (i.e., certain matrix components and/or preliminary macrostructure) these cells might need to be encouraged to synthesize the correct matrix and form the correct native valve macrostructure.

A third approach to obtaining the desired macrostructure of a TEHV would be to rely on the appropriate mechanical stimulation. We know that VICs and valve tissue overall are responsive to their mechanical environment, and as demonstrated in this thesis, there is a strong link between the mechanical forces that the valve experiences *in vivo* and its matrix composition and structure. It may be that the mechanical cues are central to the development of proper macrostructure and material properties in a TEHV. In this approach, the focus would be on developing a bioreactor that faithfully simulated the *in vivo* hemodynamics that the valve experiences. A preliminary TEHV construct would then be placed in this bioreactor, and given the correct mechanical cues, induced to remodel and create the proper macrostructure and material properties. Key questions

with this approach include what the initial construct would need to be comprised of, including what cells would need to be used (i.e., VICs, or whether all cell types would respond appropriately), and what type of initial macrostructure is necessary.

While these different strategies have been presented as three independent approaches used in isolation, most likely a combination of these strategies is necessary, and in fact there is considerable overlap between these approaches. As discussed in the bottom-up VIC approach, these cells would likely need the mechanical stimulation that is central to the third mechanoenvironment-based approach, as well as some initial macrostructure or matrix cues central to the first matrix layering approach. Similarly, the first matrix layering approach would still need cells to remodel the matrix and maintain TEHV durability (as discussed below). And in the third mechanoenvironment-based approach, an initial construct seeded with cells would have to be placed in this carefully designed mechanical environment, harkening back to the first and second approaches. Common to both the bottom-up VIC approach and the mechanoenvironment-based approach is the need for a scaffold.

B. Capability for Growth and Remodeling

The capability of a TEHV to grow and remodel relies on cells. Key features of the cells used in a TEHV include: 1) responsive to the mechanoenvironment and properly remodel the valve in response to changes in that environment, and 2) age appropriately, facilitating the normal growth and aging process to occur in the TEHV. Different approaches can be used to obtain these features. VICs seem the optimal choice in that they would theoretically have built-in the ability to respond appropriately to the

mechanoenvironment and facilitate normal valve growth and aging. However, as demonstrated in this thesis work, congenitally diseased valves contain VICs that are abnormal and would not be appropriate cell sources for a TEHV. Other issues, such as difficulty in procuring autologous VICs, make VICs a less attractive option. An alternative approach is to condition non-valve cells to act like VICs in terms of responding to the mechanoenvironment and facilitating valve growth and remodeling. Concerns related to this approach include how to ensure that these non-valve cells maintain their VIC-like features long-term, as well as how to condition these cells to function like VICs.

C. Immunocompatibility

The immunocompatibility desired in a TEHV also can be obtained via various approaches, and in part depends on other aspects of a given TEHV's design strategy. Generally, issues concerning immunocompatibility can be divided into those related to the scaffold or matrix being employed and those related to cell sources. With respect to scaffolds and matrices being utilized to create the TEHV macrostructure, if a natural 3D matrix is used, the key for making this scaffold immunocompatible is complete removal of cellular components. As mentioned above, this task has proven exceedingly difficult. Strategies include various detergents, enzymatic digestions, and freeze drying techniques.²⁰ With these decellularization strategies, the goal is to completely remove the cells and any cellular debris while preserving as much of the matrix as possible, and in the process create a porous enough scaffold for successful cell seeding. If a matrix layering approach is being employed, careful purification of these components is

essential for immunocompatibility of the scaffold. The advantage of a polymeric scaffold in this regard is that it can be inherently immunocompatible (without any immunogenic components). However, polymeric scaffolds can allow protein adsorption once implanted in the body, which can lead to activation of the coagulation cascade and device complications. The possibility of toxic metabolites in the case of degradable polymeric scaffolds should also be considered. The key advantage of PEG scaffolds is that their extreme hydrophilicity prevents protein adsorption; therefore, these scaffolds are biocompatible.

The second component of a TEHV that affects its immunocompatibility is the cell source. Of course, optimally an autologous cell source is preferred, and based on the hypothesis that VICs have an inherent capability to respond to their mechanoenvironment and synthesize appropriate matrix for a TEHV, autologous VICs would be ideal. However, in cases in which VICs from a patient are abnormal, or given the difficulty in procuring VICs from a given patient, autologous VICs may not be an option. In these cases the question becomes whether it is better to use another autologous cell source from a patient, such as dermal fibroblasts, or whether the inherent capabilities of VICs procured from a human or animal valve outweigh the disadvantage of their potential immunogenicity.

iv. Application of Thesis Work in Relation to Different Tissue Engineered Heart Valve Approaches

The data contained in this thesis can inform each of the approaches to constructing a TEHV with the desired macrostructure and material properties, as well as the issues of designing a TEHV with remodeling/growth potential and immunocompatibility. Each of these topics is discussed in the subsequent section.

A. Insights into Different Approaches for Obtaining Macrostructure and Material Properties for Physiologic Function

In terms of the matrix layering based approach to constructing a TEHV, this thesis work demonstrates that these layers' composition and thickness, particularly of the collagenous fibrosa layer, should be substantially different based on valve region as well as age. Ideally, the fibrosa layer should be created with the collagen in a crimped conformation, since that would allow the extensibility seen in native valves. Potentially, modifying the degree of collagen crimp within this construct could be used to create the specific extensibility desired in the TEHV. In order to create the desired stiffness, collagen content could be varied as well as the degree of crosslinking. While one of the age-related changes observed in this thesis was changes in delineation between the layers, it remains a challenge how variations in leaflet layer delineation could be created using this approach. Another consideration with this approach, and the other approaches, is how the leaflet insertion into the myocardium should be designed.

In terms of using a decellularized valve to create the desired valve macrostructure, this thesis and previous studies have shown that the valve's anisotropic material

properties, regional heterogeneity, and layered leaflet structure are key to proper valve function. The advantages of this approach, as discussed above, are that these properties are already built into the scaffold. An additional advantage to this approach is that different aged valves could be decellularized, providing an easy means for modifying the basic TEHV design with age-specific features such that the TEHV could be specific for any age. Given the substantial changes in valve macrostructure, matrix, and material properties in valves with aging demonstrated in this thesis, this is a key advantage to this approach. The major limitation, however, as discussed above, is the decellularization process.

In terms of the cell-based approach for constructing the macrostructure desired in a TEHV, this thesis work suggests that the specific cell type used will be crucial. Given the demonstration that VICs from different aged valves and different valve regions possess inherent differences in their synthetic and phenotypic response to substrate stiffness, the initial scaffold used in this approach will be important. Furthermore, given these inherent differences between VICs of different valve regions, utilizing different VIC populations in different regions of the preliminary TEHV scaffold results in a macrostructure with the regional heterogeneity desired. Similarly, utilizing appropriately aged VICs within this approach could lead to the formation of a TEHV that reflects age-related differences in macrostructure and material properties desired.

With respect to the mechanoenvironment-based approach, this thesis work suggests that the mechanoenvironment closely relates to normal valve composition, structure, and VIC phenotype. Therefore, creating the correct mechanoenvironment could be a powerful tool for inducing the desired macrostructure and material properties.

This strategy requires an initial TEHV construct complete with cells, and so it would likely be combined with other strategies.

B. Capability for Growth and Remodeling

In terms of the various approaches for designing a TEHV capable of growth and remodeling (i.e., VICs vs. non-valve cells), this thesis work showed that VICs display the key traits desired for a cell source in a TEHV capable of remodeling, including demonstrating remodeling in association with altered strains in diseased states. However, this thesis did not directly demonstrate VICs facilitating valve growth. In terms of cell sources for a TEHV, this thesis work only involved VICs; therefore it remains to be seen whether non-valve cells can be induced to possess similar traits. It should be noted that I performed preliminary work (not included in this thesis) demonstrating the capability of dermal fibroblasts to express myofibroblast markers in response to TGF β similar to VICs (as also demonstrated by Narine et al.²²), suggesting that this cell type might have potential for use in a TEHV. However, much more remains to be done in that regard.

C. Immunocompatibility

With respect to scaffolds and immunocompatibility issues, this thesis has demonstrated the feasibility of PEG-RGDS-methacrylated heparin scaffolds (similar to those used by Cushing et al.²³), for use in a TEHV. As stated earlier, one of the main advantages of these PEG-based scaffolds is that they are immunocompatible.

In terms of cell sources and their accompanying immunocompatibility issues, this thesis work has demonstrated inherent abnormalities in VICs isolated from congenitally

diseased valves. Therefore, in the case of a patient with a congenitally diseased valve, we could either modulate the phenotype of the VICs from that patient, or use an alternative autologous cell source, such as dermal fibroblasts, and promote the differentiation of those cells into VIC-like cells. As stated above, I have done preliminary studies showing that such modulation of dermal fibroblasts is feasible; the disadvantage of using an alternative cell type is that these cells may be missing some of the inherent information allowing them to form matrix and macrostructure of native valves, respond appropriately to the mechanical environment, and remodel the matrix around them accordingly. This would be particularly disadvantageous when using a bottom-up, cell-based TEHV approach. This thesis work has developed a method for separating VIC subpopulations from myxomatous human valves. In cases of valve disease in which some of the VICs are normal, it may be possible to isolate that subpopulation and use it to seed a TEHV.

While autologous VICs certainly are ideal in terms of immunocompatibility, they may not be an optimal cell source because of difficulty in harvesting these cells. Of course, in cases in which multiple surgical interventions are planned and the native valve has normal morphology, it may be possible to harvest VICs from that patient during the first surgical intervention, (either by surgical removal of the native valve and placement of a mechanical or bioprosthetic valve until the next surgical intervention, or if the native valve can remain until the second surgical intervention, harvesting a very small portion of the valve such that valve function is not impaired), and in the interim grow the TEHV using the patient's VICs that could then be surgically implanted during the second operation. Therefore, in the future cell source decisions may need to be patient-specific, made in coordination with the overall treatment plan.

v. Remaining Data Required

A. Cellular Component of a Tissue Engineered Heart Valve

While the data contained in this thesis addresses many aspects of TEHV design, multiple questions remain. Those include unanswered questions with respect to the cellular component of a TEHV, its growth and remodeling, its macrostructure and material properties, as well as the different approaches for constructing the desired TEHV end-product.

In terms of remaining questions related to the cellular component of a TEHV, one of the largest questions is: what cell phenotype is optimum? While the myofibroblast VIC subpopulation has been implicated in a number of valve diseases,²⁴ it has also been observed in remodeling in TEHV²⁵ and in this thesis was observed in association with normal collagen turnover. Therefore some expression of myofibroblast markers in this optimum cell phenotype may be desired so that remodeling, particularly during initial formation of a TEHV, can occur. However, long-term expression of myofibroblast markers in a TEHV, or cells that do not appropriately become activated and then become quiescent in response to the mechanoenvironment, may prove detrimental. Better understanding of the regulators and signaling pathways governing cell activation would be helpful in this regard. Time-dependent control of cell activation, should it be considered necessary, could prove particularly challenging. A subsidiary question is: what is the desired cell phenotype for different aged valves?

Other issues that remain with respect to the cellular component of a TEHV include how the desired cell phenotype can be maintained long-term. This issue of long-term stability of cell phenotype is particularly a concern if non-valve cells are used after having been treated or conditioned in some manner to more closely resemble VICs. It will be important to determine what cues these cells need in order to remain in that phenotypic niche. Of course, if stem cells are being used, there is the concern of de-differentiation and tumorigenic potential.

Another remaining question with respect to cell sources in a TEHV is whether some of the VICs within congenitally diseased valves are normal. As discussed above, this thesis work has demonstrated that, as a group, VICs isolated from congenitally diseased valves are abnormal, which precludes their use in a TEHV. However, if a subpopulation of VICs from congenitally diseased valves is normal, this subpopulation could potentially be isolated and used for an autologous TEHV. The advantage of this approach is that it avoids the challenges related to how to make non-valve cells behave like VICs and maintain those characteristics long-term. Similar questions could be asked of adult acquired valve diseases. For instance, in a myxomatous mitral valve that needs replacing, could the normal subpopulation be isolated, such as by using differential adhesion to fibronectin as developed in this thesis, and seeded into a TEHV?

Lastly, much remains to be learned about valvular endothelial cells, their role in normal valve mechanobiology, and how to incorporate them into a TEHV.

B. Growth and Remodeling in a Tissue Engineered Heart Valve

Additional questions also remain regarding growth and remodeling in a TEHV. While VICs demonstrated remodeling potential in this thesis, VICs were not directly observed facilitating valve growth. Therefore, further work is needed to understand the processes governing valve growth and the role that VICs play. For instance, if VICs from a young child are used to construct a TEHV, and that TEHV is implanted back into that child, will those VICs inherently “know” how to create a valve of the right size and material properties as the child grows? Or is growth mechanically induced? Can non-valve cells be used and growth occur in a TEHV? Clearly, these questions relate to the more basic issue of understanding what induces growth in valves and what prevents too much growth.

Another question related to growth and remodeling in a TEHV is whether the remodeling processes in a valve are different at different ages. While this thesis demonstrated that valve remodeling occurs throughout life, there could be differences in these processes. A subsidiary question is: how would these differences be incorporated into a TEHV?

C. Macrostructure and Material Properties of a Tissue Engineered Heart Valve

With respect to TEHV macrostructure and material properties, knowledge of what range of strains a valve experiences *in vivo* would aid in the testing of TEHV constructs, since we would know what portion of the stress-strain curve was most important to emulate. Similarly, knowledge of the *in vivo* stiffness of valves of different ages would

help us refine our TEHV design and evaluate TEHV constructs. This knowledge of *in vivo* stiffness would also aid in evaluating how VIC phenotype changes in response to substrate stiffness within a physiologically meaningful range of stiffnesses (in the current thesis work experiments were performed using different stiffnesses, but it is unclear where those stiffnesses lie relative to *in vivo* valve stiffness) and what other biological cues might be necessary to combine with the mechanical input of scaffold stiffness to obtain the VIC phenotype desired. Other material property data that would be useful includes biaxial tensile testing of fresh leaflets in which cells have been kept alive, given evidence that *in vivo* stiffness of the MV leaflets exceeds *ex vivo* stiffness (in which cells have not been kept alive)^{26, 27} and the suggestion that VICs may play an important role in valve material properties (evident in both this thesis work and in work by Merryman et al.¹⁸). Similarly, flexural stiffness data for freshly excised valves of different ages is needed. These sets of data would also be useful for evaluation of TEHV constructs.

In terms of information still needed regarding valve macrostructure, further regional characterization of AV composition and structure of different ages would provide necessary information regarding the regional heterogeneity of the AV. This thesis work provided limited preliminary data for regional GAG composition of aged AV and some analysis of heterogeneity of matrix components along the length of the AV leaflet, but a more complete analysis of regional matrix composition and valve macrostructure of the AV is lacking. Furthermore, analysis of the pulmonic valve in these respects is completely lacking, even though there is substantial clinical motivation for a tissue engineered pulmonic valve.

D. Different Approaches for Constructing a Tissue Engineered Heart Valve

A number of unanswered questions remain with respect to different strategies for constructing a TEHV. In the context of using a matrix layering strategy, it remains to be determined how these layers can be constructed to integrate with one another, as well as how to create regional heterogeneity (other than by varying layer thickness). Yet another issue to be addressed using this approach is how to create layers that are a heterogeneous blend of different matrix components, more reflective of the native valve, or how to create the crimped collagen conformation seen in the native valve. In the context of the bottom-up VIC approach, it remains to be determined what matrix signals and macrostructure are necessary to prompt VICs to produce the right macrostructure and material properties. In the mechanoenvironment-based approach it is unclear whether non-valve cells can be induced by a valve-specific mechanoenvironment to create valve macrostructure and material properties, and how closely the initial TEHV construct must resemble a valve for the remodeling process to be successful. For many of these approaches, questions regarding the scaffold remain. For instance, continued work is needed to tailor the degradation rate of a degradable TEHV scaffold such that lost matrix is immediately replaced by newly synthesized matrix, without a decline in material properties.

E. General Considerations

In terms of more general considerations, we need design criteria obtained from human valves. While the data in this thesis using animal models provides a starting point, and both pig and sheep are considered relatively good animal models for human

heart valve mechanobiology,²⁸⁻³² the ovine MV is known to have less redundancy than the human MV^{33, 34} and there may be other species-specific differences that prove important. Therefore, we need data on valve composition and material properties of different aged human valves.

Another more general question that remains to be answered is whether a TEHV with properties of an elderly valve would function better in an elderly patient than a TEHV with properties of a middle-aged adult. In other words, we are assuming that the matrix and material property changes evident in elderly valves enable them to withstand the altered hemodynamics that accompanies this aging process, but it may be that these normal aging changes in valves in fact are detrimental to valve function.

An additional more general consideration with respect to TEHV design is which of the features we observe in a native valve are necessary for proper valve function. In other words, just because a feature is evident in a native valve does not necessarily mean it needs to be emulated in a TEHV. Furthermore, given the incredible complexity and heterogeneity of native valves, it is likely nearly impossible to perfectly emulate a native valve in every respect. Moving forward, it will be important to determine which are the key features of native valves that allow proper valve function and long-term durability.

F. Conclusion

In summary, this thesis work provides foundational knowledge in valve mechanobiology that will be necessary in the continued pursuit of developing a physiologic TEHV. Key insights into valve aging and heterogeneity; how the VICs,

matrix, and tissue mechanics interact with one another; and the role of VICs and the matrix in determining proper valve function will be particularly important as the field moves forward. Additionally, in the course of these studies, insights into a variety of valve diseases, including both congenital and acquired valve disease, and the involvement of valves in cardiac diseases, provide insight into pathogenesis of these diseases as well as potential targets for therapeutic interventions.

REFERENCES

1. Kunzelman KS, Cochran RP. Stress/strain characteristics of porcine mitral valve tissue: parallel versus perpendicular collagen orientation. *J Card Surg.* 1992;7(1):71-78.
2. Grande-Allen KJ, Calabro A, Gupta V, Wight TN, Hascall VC, Vesely I. Glycosaminoglycans and proteoglycans in normal mitral valve leaflets and chordae: association with regions of tensile and compressive loading. *Glycobiology.* 2004;14(7):621-633.
3. Balachandran K, Konduri S, Sucusky P, Jo H, Yoganathan AP. An ex vivo study of the biological properties of porcine aortic valves in response to circumferential cyclic stretch. *Ann Biomed Eng.* 2006;34(11):1655-1665.
4. Balachandran K, Sucusky P, Jo H, Yoganathan AP. Elevated cyclic stretch alters matrix remodeling in aortic valve cusps: implications for degenerative aortic valve disease. *Am J Physiol Heart Circ Physiol.* 2009;296(3):H756-764.
5. Grande-Allen KJ, Borowski AG, Troughton RW, Houghtaling PL, Dipaola NR, Moravec CS, Vesely I, Griffin BP. Apparently normal mitral valves in patients with heart failure demonstrate biochemical and structural derangements: an extracellular matrix and echocardiographic study. *J Am Coll Cardiol.* 2005;45(1):54-61.
6. Tamura K, Jones M, Yamada I, Ferrans VJ. Wound healing in the mitral valve. *J Heart Valve Dis.* 2000;9(1):53-63.
7. Tamura K, Murakami M, Washizu M. Healing of wound sutures on the mitral valve: an experimental study. *Gen Thorac Cardiovasc Surg.* 2007;55(3):98-104.
8. Filip D, Radu A, Simionescu M. Interstitial cells of the heart valve possess characteristics similar to smooth muscle cells. *Circulation Research.* 1986;59(3):310-320.
9. Huang H, Liao J, Sacks M. In-situ deformation of the aortic valve interstitial cell nucleus under diastolic loading. *J Biomech Eng.* 2007;129(6):880-889.
10. Latif N, Sarathchandra P, Taylor P, Antoniow J, Yacoub M. Molecules mediating cell-ECM and cell-cell communication in human heart valves. *Cell Biochem Biophys.* 2005;43(2):275-287.
11. Wiester L, Giachelli C. Expression and function of the integrin alpha9beta1 in bovine aortic valve interstitial cells. *J Heart Valve Dis.* 2003;12(5):605-616.
12. Chester A, Misfeld M, Yacoub M. Receptor-mediated contraction of aortic valve leaflets. *J Heart Valve Dis.* 2000;9(2):250-254.
13. Pompilio G, Rossoni G, Sala A, Polvani GL, Berti F, Dainese L, Porqueddu M, Biglioli P. Endothelial-dependent dynamic and antithrombotic properties of porcine aortic and pulmonary valves. *Ann Thorac Surg.* 1998;65(4):986-992.

14. Wassenaar C, Bax WA, van Suylen RJ, Vuzevski VD, Bos E. Effects of cryopreservation on contractile properties of porcine isolated aortic valve leaflets and aortic wall. *J Thorac Cardiovasc Surg.* 1997;113(1):165-172.
15. Bowen I, Marr C, Chester A, Wheeler-Jones C, Elliott J. In-vitro contraction of the equine aortic valve. *J Heart Valve Dis.* 2004;13(4):593-599.
16. Sonnenblick E, Napolitano L, Daggett W, Cooper T. An intrinsic neuromuscular basis for mitral valve motion in the dog. *Circ Res.* 1967;21(1):9-15.
17. Kershaw J, Misfeld M, Sievers H, Yacoub M, Chester A. Specific regional and directional contractile responses of aortic cusp tissue. *J Heart Valve Dis.* 2004;13(5):798-803.
18. Merryman WD, Huang HY, Schoen FJ, Sacks MS. The effects of cellular contraction on aortic valve leaflet flexural stiffness. *J Biomech.* 2006;39(1):88-96.
19. Shi Y, Ramamurthi A, Vesely I. Towards tissue engineering of a composite aortic valve. *Biomed Sci Instrum.* 2002;38:35-40.
20. Brody S, Pandit A. Approaches to heart valve tissue engineering scaffold design. *J Biomed Mater Res B Appl Biomater.* 2007;83(1):16-43.
21. Leslie-Barbick JE, Moon JJ, West JL. Covalently-immobilized vascular endothelial growth factor promotes endothelial cell tubulogenesis in poly(ethylene glycol) diacrylate hydrogels. *J Biomater Sci Polym Ed.* 2009;20(12):1763-1779.
22. Narine K, DeWever O, Cathenis K, Mareel M, Van Belleghem Y, Van Nooten G. Transforming growth factor-beta-induced transition of fibroblasts: a model for myofibroblast procurement in tissue valve engineering. *J Heart Valve Dis.* 2004;13(2):281-289; discussion 289.
23. Cushing MC, Liao J, Jaeggli MP, Anseth KS. Material-based regulation of the myofibroblast phenotype. *Biomaterials.* 2007;28:3378-3387.
24. Rabkin E, Aikawa M, Stone JR, Fukumoto Y, Libby P, Schoen FJ. Activated interstitial myofibroblasts express catabolic enzymes and mediate matrix remodeling in myxomatous heart valves. *Circulation.* 2001;104(21):2525-2532.
25. Rabkin-Aikawa E, Farber M, Aikawa M, Schoen FJ. Dynamic and reversible changes of interstitial cell phenotype during remodeling of cardiac valves. *J Heart Valve Dis.* 2004;13(5):841-847.
26. Krishnamurthy G, Itoh A, Bothe W, Swanson JC, Kuhl E, Karlsson M, Miller DC, Ingels NB, Jr. Stress-strain behavior of mitral valve leaflets in the beating ovine heart. *J Biomech.* 2009.
27. Sacks MS, Enomoto Y, Graybill JR, Merryman WD, Zeeshan A, Yoganathan AP, Levy RJ, Gorman RC, Gorman JH, 3rd. In-vivo dynamic deformation of the mitral valve anterior leaflet. *Ann Thorac Surg.* 2006;82(4):1369-1377.

28. Crick S, Sheppard M, Ho S, Gebstein L, Anderson R. Anatomy of the pig heart: comparisons with normal human cardiac structure. *J Anat.* 1998;193:105-119.
29. Sands MP, Rittenhouse EA, Mohri H, Merendino KA. An anatomical comparison of human pig, calf, and sheep aortic valves. *Ann Thorac Surg.* 1969;8(5):407-414.
30. Sim EK, Muskawad S, Lim CS, Yeo JH, Lim KH, Grignani RT, Durrani A, Lau G, Duran C. Comparison of human and porcine aortic valves. *Clin Anat.* 2003;16(3):193-196.
31. Glasson JR, Komeda M, Daughters GT, Foppiano LE, Bolger AF, Tye TL, Ingels NB, Jr., Miller DC. Most ovine mitral annular three-dimensional size reduction occurs before ventricular systole and is abolished with ventricular pacing. *Circulation.* 1997;96(9 Suppl):II-115-122.
32. Ormiston J, Shah P, Tei C, Wong M. Size and motion of the mitral valve annulus in man. II. Abnormalities in mitral valve prolapse. *Circulation.* 1982;65(4):713-719.
33. Brock R. The surgical and pathological anatomy of the mitral valve. *Br Heart J.* 1952;14(4):489-513.
34. Gorman JH, 3rd., Jackson BM, Gorman RC, Kelley ST, Gikakis N, Edmunds LH, Jr. Papillary muscle discoordination rather than increased annular area facilitates mitral regurgitation after acute posterior myocardial infarction. *Circulation.* 1997;96(9 Suppl):II-124-127.

Appendix

Chapter 24: Abundance and Location of Hyaluronan and Proteoglycans within Myxomatous Mitral Valves

In this chapter the topic of examining valves in the setting of various disease states (the subject of Chapters 13-21) continues with a study of myxomatous mitral valve disease (also the subject of Chapter 19). Specifically in this chapter alterations in proteoglycan and glycosaminoglycan content in myxomatous mitral valves are analyzed. While this study certainly adds to our understanding of myxomatous mitral valve disease and serves as background for the study analyzing the mitogen-activated protein kinase (MAPK) signaling pathway in myxomatous mitral valves (Chapter 19), I was not the lead researcher on this study and it was not considered integral to this thesis; therefore, this study was placed in the Appendix.

ABSTRACT

Background: Extracellular matrix changes occur in many heart valve pathologies. For example, myxomatous mitral valves are reported to contain excess proteoglycans (PGs) and hyaluronan (HA). However, it is unknown which specific PGs are altered in myxomatous valves. Because PGs perform varied functions in connective tissues, this study was designed to identify and localize three matrix-associated PGs as well as HA and the HA receptor for endocytosis (HARE) within myxomatous and normal mitral valves.

Methods: Human mitral posterior leaflets (control n=6-9, myxomatous n=14-21, mean age 61 for all groups) were histochemically stained for PG core proteins, HA, and HARE. Stain intensity was semi-quantitatively graded to determine differences in marker abundance between normal and myxomatous valves. The PGs were localized to different regions of the leaflet by correspondence to parallel Movat stained sections.

Results: The PGs decorin, biglycan and versican were more abundant in myxomatous valves than in normal controls ($p<0.03$). There was a gender effect on PG presence but no age related trends were observed. HA and HARE were distributed throughout all valves. There was no significant difference in HA between groups, but HARE expression was reduced in myxomatous valves compared to normal controls ($p<0.002$).

Conclusions: Excess decorin, biglycan and versican may be associated with the remodeling of other matrix components in myxomatous mitral valves. Decreased expression of HARE in myxomatous valves suggests that HA metabolism could be altered in myxomatous mitral valve disease. These findings contribute towards elucidating the pathogenesis of myxomatous mitral valve disease and developing potential new therapies.

The work contained in this chapter was published as:

Gupta V, Barzilla JE, Stephens EH, Mendez JS, Lee E, Collard CD, Weigel P, Grande-Allen KJ. **Abundance and Location of Hyaluronan and Proteoglycans within Myxomatous Mitral Valves.** *Cardiovascular Pathology*, 2009;18(4):191-197.

INTRODUCTION

Myxomatous mitral valve disease is a common valve abnormality with an incidence of 2.4-5%.¹ Myxomatous degeneration is the most common cause of mitral regurgitation in older patients,² but the cause and progression of myxomatous disease remains unclear. Myxomatous mitral valves are characterized by floppy leaflets and elongated or ruptured chordae tendineae, which have profoundly weakened material behavior compared to normal valve tissues.³ Previous histological studies of myxomatous valves have revealed collagen disruption,⁴ elastic fiber fragmentation,⁵ and the accumulation of matrix metalloproteinases and glycosaminoglycans (GAGs).⁶ Currently, the only treatment for this disease is surgical repair; no medical therapies are available to treat the matrix changes associated with myxomatous degeneration. Although there are a number of different theories regarding the pathogenesis of myxomatous mitral valve disease, including the diminished healing response of aging valve tissue to mechanical stress,² genetic abnormalities,⁷ collagen and matrix dissolution⁶ or abnormal accumulation of proteoglycans (PGs),⁸ there is no consensus as to the mechanism of myxomatous degeneration. It is, however, evident by histological examination that GAGs and PGs, as a general matrix class, are abnormally distributed within myxomatous mitral valves, but exactly which PGs are overabundant within myxomatous valves has not been previously investigated.

Given the diverse nature of different PGs and their associated GAG chains, and their functions in mediating extracellular matrix organization,⁹ it is compelling to ask which specific PG or PGs could be involved in the remodeling and resultant dysfunction of myxomatous mitral valves. PGs consist of at least one GAG chain attached to a core

protein. All GAG types exist as components of a PG, except for hyaluronan (HA), which is unsulfated and frequently present as a free molecule, although HA may be non-covalently bound to the core protein of some of the larger hyalectin PGs through a link protein, also known as HA binding protein (HABP). The diverse group of PGs, as well as HA, performs many functions related to the growth, development and pathology of tissues,¹⁰ and likely performs many such roles in heart valves as well. It has been shown that three particular PGs (decorin, biglycan, and versican) are present in the mitral valve and that their relative abundance varies according to the type of loading experienced by specific valve regions.¹¹ In the regions that experienced tension, the small leucine-rich PGs decorin and biglycan were more abundant; these PGs mediate collagen fibrillogenesis¹² and sequester transforming growth factor-beta.¹³ The large hyalectin PG versican was also found in the mitral valve; versican can aggregate with HA¹⁴ to provide hydrated compressive resistance to tissues. Versican often co-localizes with elastic fibers and numerous cell associated molecules to regulate cell adhesion, proliferation and migration.¹⁴ We have previously reported that there are elevated concentrations of selected GAG classes within myxomatous mitral valve chordae and posterior leaflets as compared to normal control tissues,¹⁵ but have not investigated specific classes of PGs within these valves. Therefore, the primary purpose of this study was to assess the location and abundance of specific PGs and the GAG HA within myxomatous and normal mitral valves to improve our understanding of this common valve disease and contribute towards developing novel treatments for this disease.

The secondary purpose of this study was an initial step towards investigating the mechanisms of turnover of PGs and GAGs, including HA, within heart valves.

Understanding how the synthesis and degradation of PGs and GAGs are regulated within these tissues is important not only for myxomatous mitral valve disease but also for calcific aortic valve disease¹⁶ and the design of bioprosthetic valves. In addition, understanding this regulation may lead to the development of novel medical therapies for valve disease or offer opportunities for earlier intervention. Because gaining this knowledge will be a profound undertaking, in this particular study we only investigated the potential for the turnover of HA in mitral valves via the HA receptor for endocytosis or HARE.¹⁷ HARE, a.k.a. stabilin-2, is a cell receptor that enables the scavenging and clearance of HA and other GAGs from the blood.¹⁸ Most abundant in lymph nodes, spleen, and liver, HARE has also been found in the heart valves of mice,¹⁹ but is absent from any other cardiovascular tissues. Based on the previously reported excess of HA in myxomatous tissues it was speculated that the abundance of HARE in human myxomatous heart valves, might be different from that of control valves. Therefore, in this study the abundance of specific PGs, HA, and HARE within normal and myxomatous mitral valves was measured using histochemical techniques.

METHODS

Tissue Procurement

Normal control mitral valve posterior leaflets were obtained after autopsy. Control subjects demonstrating any cardiovascular disease were excluded from this study. Myxomatous mitral valve posterior leaflets were surgically resected from patients undergoing a surgical repair procedure to correct mitral regurgitation resulting from primary myxomatous degeneration (all had regurgitation grades of 3+/4+). The

demographic makeup of all groups is shown in Table 24-1. Tissues for this study were provided by the Cleveland Clinic Foundation (Cleveland, OH), St. Luke's Episcopal Hospital (Houston, TX), Ben Taub Hospital (Houston, TX), and the Cooperative Human Tissue Network. The research use of these tissues was approved by the Institutional Review Boards at all institutions. Radially oriented segments of the leaflets were cut from the annulus to free edge and fixed immediately in 10% formalin to minimize autolysis. After overnight fixation, the tissue sections were paraffin embedded, cut in 5 μ m full thickness sections, and mounted on glass slides according to standard procedures.

Table 24-1. Subject Demographics.

Group	Subjects*	Gender (M/F)	Age (years)
PGs			
Normal	9	7/2	61 \pm 15
Myxomatous	17	9/8	61 \pm 10
HA			
Normal	8	6/2	61 \pm 15
Myxomatous	14	5/9	61 \pm 11
HARE			
Normal	6	5/1	60 \pm 12
Myxomatous	21	9/12	61 \pm 12

Data represented as mean \pm standard deviation.

*Due to the small size of some tissues, it was not possible to obtain histological sections for all stains from all subjects' tissue blocks.

Histochemistry

Immunohistochemistry (IHC) was performed to localize the PGs decorin, biglycan and versican within the valve tissues using antibodies against their respective core proteins, as described in Chapter 20. A set of mitral valves was also stained for HARE and HA. The immunohistochemical staining for HARE was performed as for PGs

except that the pretreatment was performed using 0.1 N HCl for 15 minutes at 37°C and the mAb159 antibodies for human HARE were developed in Dr. Weigel's laboratory.¹⁷ The presence of HA was demonstrated by histochemical binding to an HA binding protein (HABP),²⁰ which contains the "link" domain protein that normally binds HA to aggrecan in the formation of an aggrecan aggregate. This HA staining procedure required blocking with 2% fetal bovine serum, treating with biotinylated HABP (exactly as described by Lara et al.²⁰), then performing chromogenic detection as described above. To minimize variability, all normal and myxomatous tissues were stained together in one batch.

Negative controls for all markers were performed in the absence of the primary antibody. After staining, samples were blinded and graded on a scale of 0-4 to evaluate overall intensity. Grade "0" was chosen for no staining, "1" for weak stain in <50% of tissue, "2" for weak stain in >50% of tissue or strong stain in <10% of tissue, "3" for strong stain in >10% but <50% of tissue and "4" for strong stain in >50% of tissue.⁶ Between 1 to 3 sections of a given valve sample were stained for a given marker and the staining intensity of all tissue sections was graded twice. Replicates were averaged and the staining and grading variability was calculated to be less than 15%.

Localization

Parallel sections of the posterior leaflets were also stained with Movat pentachrome to co-localize the different PGs, which stained blue/green, with collagen and elastin, which were stained yellow and black, respectively. Mapping the ECM composition of these sections also enabled the comparison of PG localization between the

deep spongiosa layer and the more superficial atrialis and fibrosa layers of the mitral valve.

Statistical Analysis

A one-way ANOVA (SigmaStat, San Jose, CA) was used to compare immunohistochemical data between the normal and myxomatous valve groups. A two-way ANOVA with post hoc Tukey testing was performed to examine the effect of gender by choosing factor 1 as valve condition (normal vs. myxomatous) and factor 2 as gender (male vs. female). A Spearman rank order correlation was performed to determine if there were any age related trends in the data. In all cases, the level of significance was chosen as 0.05.

RESULTS

IHC for Decorin, Biglycan, and Versican

Myxomatous valve sections showed overall higher PG staining intensity, with significantly greater abundance of decorin ($p < 0.001$), biglycan ($p < 0.003$) and versican ($p < 0.03$) as compared to normal valves (Figs. 24-1 and 24-2). The staining intensity of versican in the myxomatous mitral valves was almost a full grade stronger than in the normal valves and the staining intensities of decorin and biglycan were more than a full grade stronger in the myxomatous valves. The negative control grading for PG staining was found as 0.16 ± 0.28 (mean \pm standard deviation, $n=24$) for normal valves and 0.07 ± 0.24 (mean \pm standard deviation, $n=22$) for myxomatous valves.

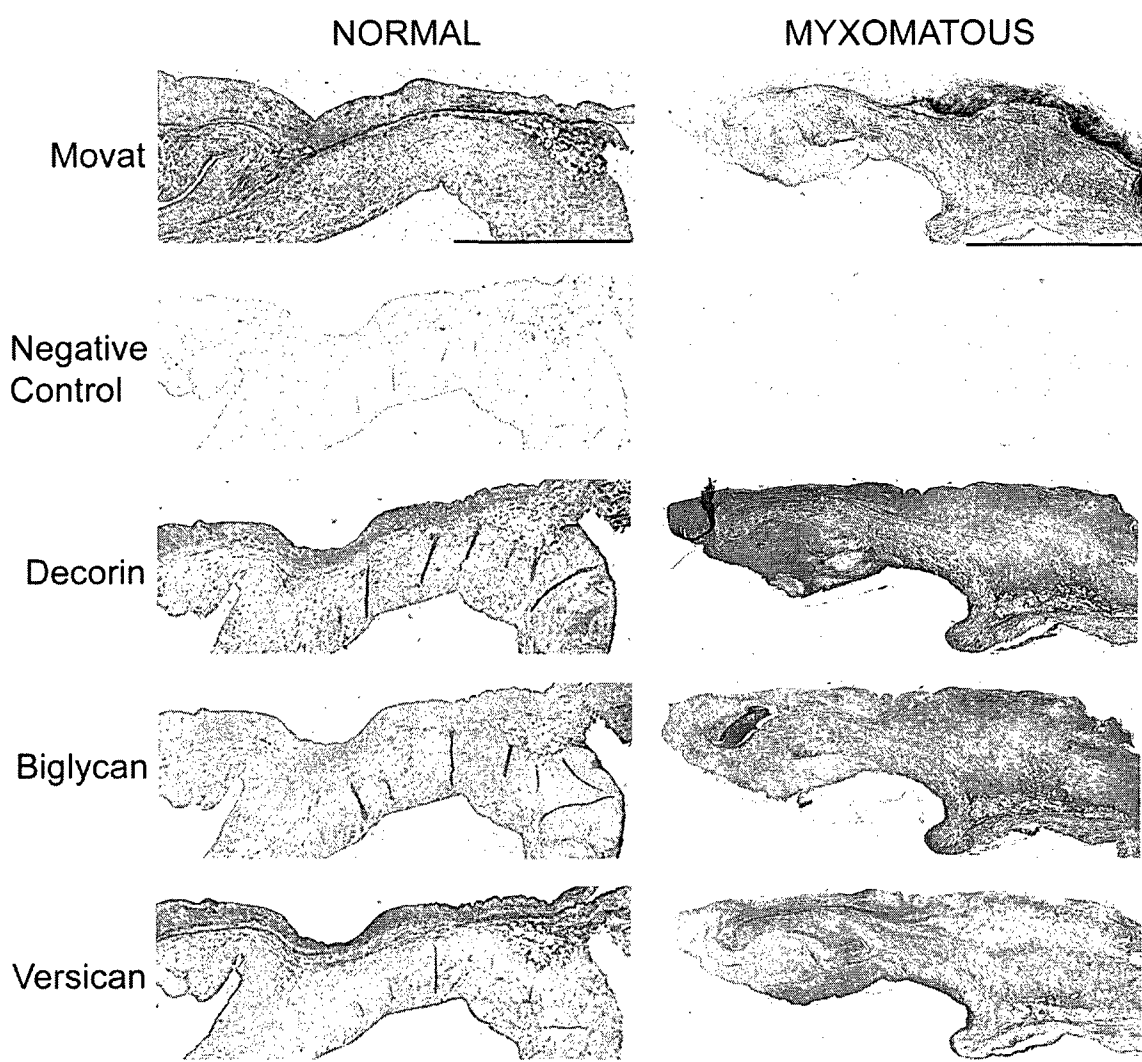


Fig. 24-1: Normal and myxomatous valve sections immunohistochemically stained for the core proteins of decorin, biglycan and versican. The scale bar for each valve represents 1 mm. Images of the same valve stained with Movat pentachrome are provided to demonstrate the leaflet's layered microstructure.

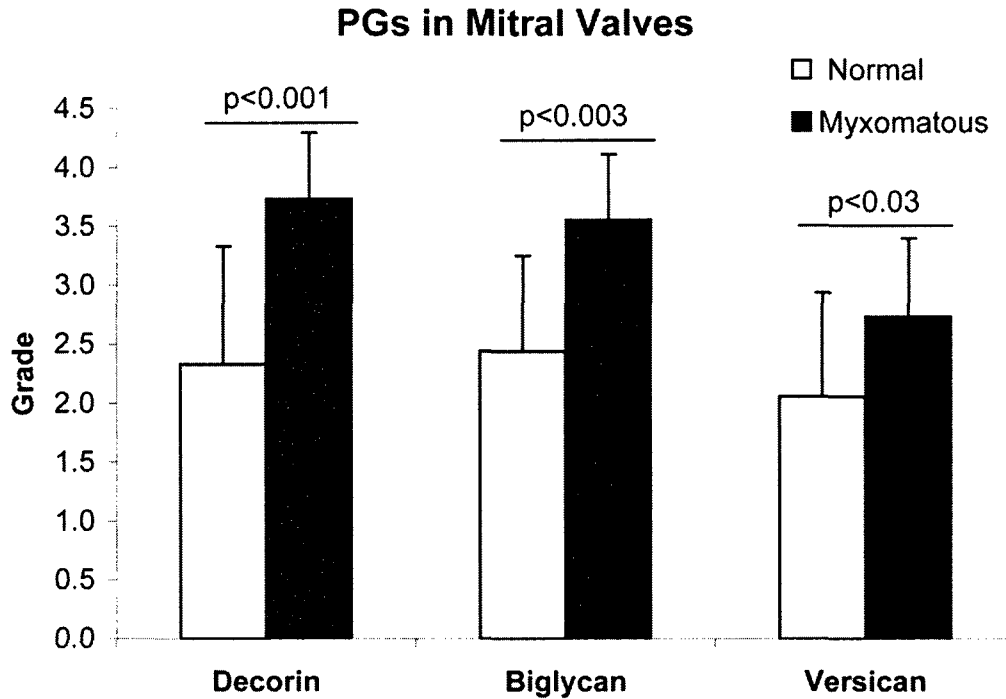


Fig. 24-2: Abundances of decorin, biglycan and versican in normal and myxomatous mitral valves. Grading was performed on immunohistochemically stained valve sections using a scale of 0 to 4. Data represented as mean \pm standard deviation.

IHC for HA and HARE

There was no significant difference found in HABP staining for HA between normal and myxomatous valves (Figs. 24-3 and 24-4). However, there was almost one full grade less HARE expression in myxomatous valves than in normal valves ($p<0.002$). The negative control grading for HA staining was 0.22 ± 0.42 (mean \pm standard deviation, $n=24$) and for HARE staining was 0.13 ± 0.35 (mean \pm standard deviation, $n=20$).

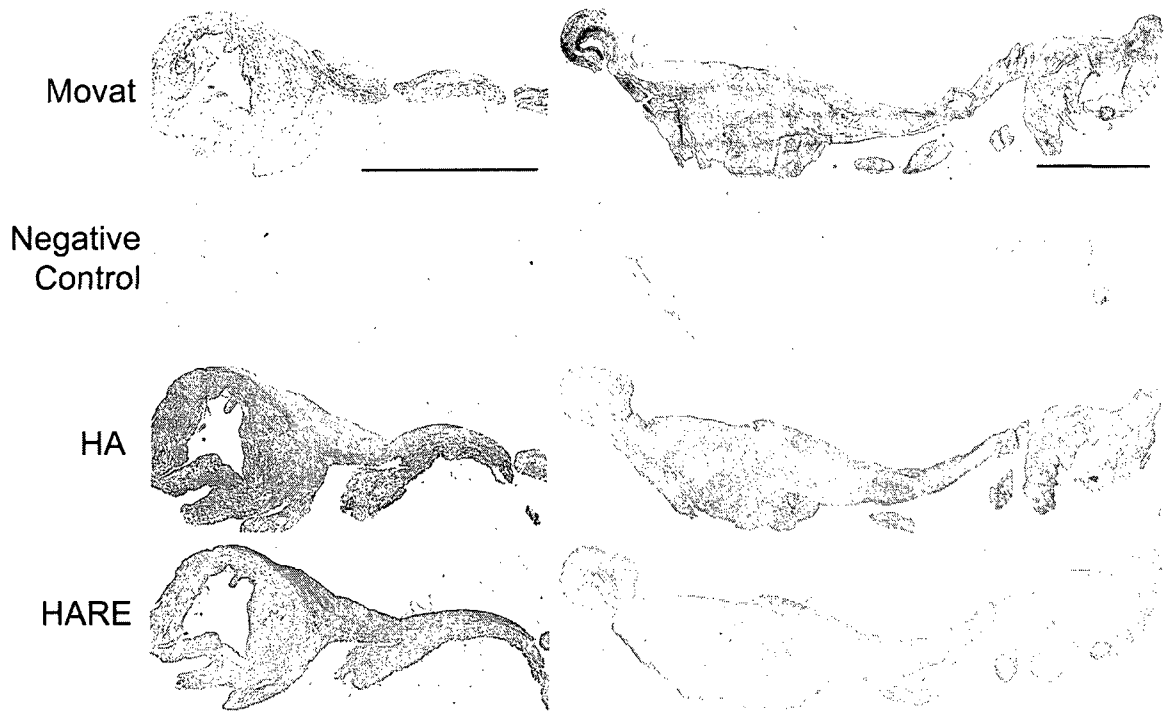


Fig. 24-3: Normal and myxomatous valve sections histochemically stained for HA and HARE. The scale bar for each valve represents 500 μm . Images of the same valve stained with Movat pentachrome are provided to demonstrate the leaflet's layered microstructure.

Co-localization of Specific PGs and Other Extracellular Matrix Components

Comparison of Movat Pentachrome stained valve tissues with the histochemically stained tissues revealed many interesting patterns regarding the location of PGs. The Movat stain demonstrated the three layers of the normal mitral valve: the collagen-rich fibrosa (upper outer layer), the PG-rich spongiosa (deep inner layer), and the atrialis (lower outer layer), which contains several thin layers of elastic fibers (Fig. 24-1). It was

HA and HARE in Mitral Valves

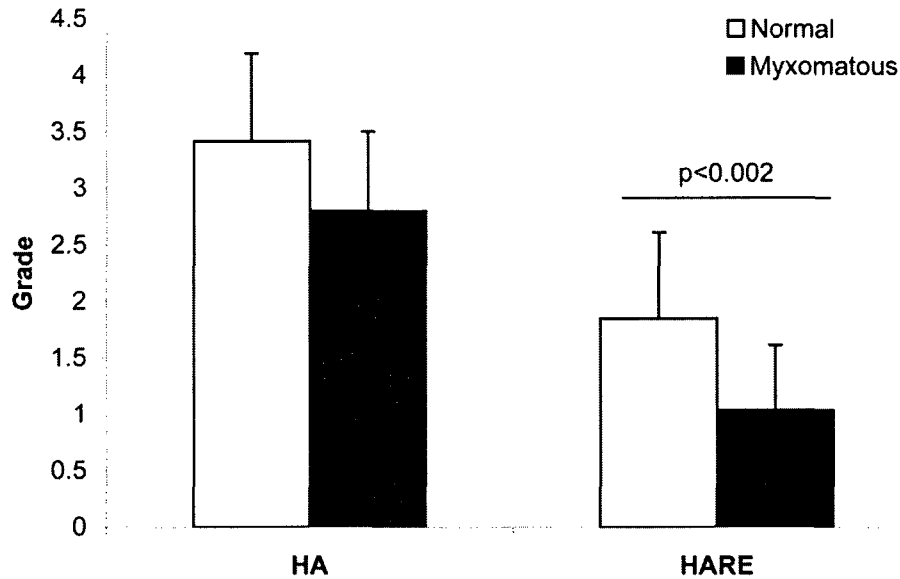


Fig. 24-4: Abundances of HA and HARE in normal and myxomatous mitral valves. Grading was performed on histochemically stained valve sections using a scale of 0 to 4. Data represented as mean \pm standard deviation.

difficult to distinguish the layered structure in Movat stains of myxomatous valves as these valves were deformed, irregularly shaped and had disorganized ECM. In both normal and myxomatous valve sections, staining for decorin was co-localized with collagen (Fig. 24-1). However, biglycan was found in locations that also stained strongly for both collagen and elastin. Interestingly, versican staining corresponded to leaflet regions that were rich in PG and elastic fibers for both normal and myxomatous valves.

HA staining was found to be greater in the presence of elastin but lower in the presence of collagen (Fig. 24-3). Similarly, HARE binding was strong in elastin rich regions (Fig. 24-3).

Effect of Gender and Age on Abundance of PGs

Of all the PGs, only the abundance of versican had any relation to gender. This association with gender was found in both normal and myxomatous valves. Interestingly, versican staining was stronger for females (compared to males) in normal controls (male 1.7 ± 0.5 vs. female 3.2 ± 1.1 ; $p < 0.01$) but showed a trend of being lower in myxomatous valves (male 3.0 ± 0.7 vs. female 2.4 ± 0.5 ; $p = 0.07$). Also, when data describing the abundance of each PG were grouped together, myxomatous valves from males showed a trend of greater PG abundance than found in valves from females (3.5 ± 0.6 vs. 3.1 ± 0.8 , $p = 0.06$). There was no significant correlation between age and the abundance of specific PGs. However, HARE expression in normal valves significantly increased with age ($R^2 = 0.62$; Spearman correlation, $p < 0.001$).

DISCUSSION

This study demonstrated differences in the abundance and localization of specific PGs within normal and myxomatous mitral valves. Decorin, biglycan and versican, three PGs previously found in normal mitral valves,¹¹ were present in significantly greater abundance in myxomatous valves. We did not find significant differences in the presence of HA within normal and myxomatous valve sections, although the abundance of HARE was stronger in normal valves. This is the first study to demonstrate the presence of HARE in human heart valves.

The stronger immunohistochemical staining for all three PGs within myxomatous valves was unexpected, given our previous analysis of GAGs using fluorophore-assisted carbohydrate electrophoresis (FACE).¹⁵ FACE analysis showed

that myxomatous valves are particularly rich in 6-sulfated GAGs, which are strongly associated with the PG versican,²¹ but not decorin or biglycan. We speculate that these differences between the FACE and immunohistochemical results arose because FACE measures GAGs, whereas these valve samples were stained for the core proteins of the different PGs. The amount, type, or sulfation pattern of the GAGs associated with the different PGs may be responsible for these differences. More specifically, decorin and biglycan have 1 and 2 GAG chains respectively, so their GAG content may represent only a small percentage of total leaflet GAGs measured by FACE, even if their core proteins are shown to be abundant within the tissues. Versican, in contrast, contains 15-20 GAG chains and hence the numerous GAGs from versican may be disproportionately abundant in a FACE analysis. The relative amount of GAG per PG may also explain the location of these PGs within the different layers of the valve. Versican immunostaining was strong in areas of the leaflet that also stained strongly with alcian blue from the Movat pentachrome stain, indicating an abundance of GAGs, but decorin and biglycan were not strongly stained in the blue regions. There are also significant differences in the preparation of the tissue between these two methods. In the future, it will be important to confirm these patterns of PG abundance using biochemical methods such as western blotting.

Although there has been very little investigation of the upregulation of specific types of PGs in myxomatous valves, our results are consistent with a previous report showing increased decorin gene expression in myxomatous leaflets.²² In this study, decorin was strongly co-localized with collagen fibers in both normal and myxomatous valves; localization of decorin with collagen fibers has also been shown by others.^{12, 23}

This co-localization is understandable given that decorin is known to regulate collagen fibrillogenesis.¹² Biglycan, which is a small leucine-rich PG closely related to decorin, was found in both collagen and elastin rich regions of the leaflets. Biglycan has been shown to bind to tropoelastin and may influence elastic fiber formation.²⁴ Versican, which was strongly co-localized with elastic fibers, has been shown to bind to fibulin and fibrillin, microfibrillar proteins that are components of elastic fibers.¹⁴ Interestingly, abnormal fibrillin distribution has been proposed as a factor in the development of myxomatous degeneration.⁴ Collagen and elastin fragmentation has been shown before during myxomatous remodeling^{4, 5} and the link between PGs and these ECM fibrous protein may explain the compensatory mechanism during myxomatous valve remodeling. The fact that each of these three proteoglycans – each of which is differentially regulated and likely to perform a distinct function within the ECM – was more abundant demonstrates the complexity of matrix changes in myxomatous valve remodeling. These numerous matrix changes suggest that there may not be a single primary cause of myxomatous degeneration.

We did not find significant differences in HA staining between normal and myxomatous leaflets, which is consistent with our previous biochemical findings using FACE.¹⁵ Although our previous FACE analyses demonstrated elevated amounts of HA in myxomatous chordae, that study also showed that the myxomatous posterior leaflets did not contain more HA than normal posterior leaflets.

This is the first study to demonstrate the presence of HARE in human heart valves. Previously, HARE has been found in the heart valves of mice.¹⁹ HARE is a cell receptor that enables the clearance of HA and thought to be associated with HA

turnover.¹⁸ In addition, it was recently demonstrated that the binding of HA to HARE causes phosphorylation of extracellular signal-regulated kinases 1 and 2 (ERK1/2) in a dose- and time-dependent manner.²⁵ The finding of less HARE expression in myxomatous mitral valves suggests that diseased valves may have alterations in HA metabolism or intracellular signaling. In general, the demonstration of HARE in these tissues opens new avenues for research into the turnover and function of HA in valve remodeling and pathology. HA also interacts with other receptors such as CD44, which have been previously demonstrated in heart valves,²⁶ and the receptor for HA-mediated motility (RHAMM) during cell migration and ECM remodeling.²⁷ HA turnover is also regulated by enzymes such as the HA synthases and hyaluronidases.²⁸ Any one or more of these receptors and enzymes may regulate the abundance and activity of HA during myxomatous degeneration, and should be examined in greater detail in future studies.

Other limitations of this study included our difficulty in identifying the distinct characteristic leaflet layers within the myxomatous valve sections, which restricted us to PG localization based on collagen or elastin as opposed to layers. In addition, some of the valve sections showed clear “onlays” or superficial plaques²⁹ that were not part of any valve layer, but stained for PGs. Compared to rest of the valve section, onlays in normal valve sections (n=3) tended to stain strongly for decorin and versican whereas in myxomatous valve sections (n=4) onlays stained stronger only for biglycan. In another investigation, myxomatous valve onlays have been shown to contain similar amount of GAGs and collagen compared to rest of the valve.²⁹

CONCLUSIONS

In summary, the PGs decorin, biglycan and versican were significantly more abundant in myxomatous mitral valves compared to normal valves, a difference that may either contribute to or be a consequence of the valve remodeling. Although HA expression was unaltered between two leaflet groups, HARE expression was lower in myxomatous valves, suggesting that HA homeostasis may be altered in myxomatous mitral valve disease. In the future, it will be important to investigate the regulation of matrix synthesis and degradation within these diseased valves in order to identify the regulatory molecules or cell population(s) responsible for valve remodeling. Such information will be essential for the development of medical therapies to target the responsible agents and would provide a platform to treat myxomatous degeneration without requiring valve surgery.

This chapter, which characterized alterations in proteoglycan and glycosaminoglycan content in myxomatous mitral valves, provided important background for the analysis of mitogen-activated protein kinase (MAPK) signaling pathway in myxomatous mitral valves in Chapter 19. While this study certainly adds to our understanding of myxomatous mitral valve disease, I was not the lead researcher on the study and it was not considered integral to this thesis; therefore, this study was placed in the Appendix.

REFERENCES

1. Freed LA, Acierno JS, Jr., Dai D, Leyne M, Marshall JE, Nesta F, Levine RA, Slangenaupt SA. A locus for autosomal dominant mitral valve prolapse on chromosome 11p15.4. *Am J Hum Genet.* 2003;72(6):1551-1559.
2. Collins P, Cotton RE, Duff RS. Symptomatic mitral myxomatous transformation in the elderly. *Thorax.* 1976;31(6):765-770.
3. Barber JE, Kasper FK, Ratliff NB, Cosgrove DM, Griffin BP, Vesely I. Mechanical properties of myxomatous mitral valves. *J Thorac Cardiovasc Surg.* 2001;122(5):955-962.
4. Nasuti JF, Zhang PJ, Feldman MD, Pasha T, Khurana JS, Gorman JH, 3rd, Gorman RC, Narula J, Narula N. Fibrillin and other matrix proteins in mitral valve prolapse syndrome. *Ann Thorac Surg.* 2004;77(2):532-536.
5. Akhtar S, Meek KM, James V. Ultrastructure abnormalities in proteoglycans, collagen fibrils, and elastic fibers in normal and myxomatous mitral valve chordae tendineae. *Cardiovasc Pathol.* 1999;8(4):191-201.
6. Rabkin E, Aikawa M, Stone JR, Fukumoto Y, Libby P, Schoen FJ. Activated interstitial myofibroblasts express catabolic enzymes and mediate matrix remodeling in myxomatous heart valves. *Circulation.* 2001;104(21):2525-2532.
7. Trochu JN, Kyndt F, Schott JJ, Gueffet JP, Probst V, Benichou B, Le Marec H. Clinical characteristics of a familial inherited myxomatous valvular dystrophy mapped to Xq28. *J Am Coll Cardiol.* 2000;35(7):1890-1897.
8. Olsen EG, Al-Rufaie HK. The floppy mitral valve. Study on pathogenesis. *Br Heart J.* 1980;44(6):674-683.
9. Kinsella MG, Bressler SL, Wight TN. The regulated synthesis of versican, decorin, and biglycan: extracellular matrix proteoglycans that influence cellular phenotype. *Crit Rev Eukaryot Gene Expr.* 2004;14(3):203-234.
10. Wight TN, Heinegard D, Hascall VC. *Proteoglycans: Structure and Function.* New York: Plenum Press; 1991.
11. Grande-Allen KJ, Calabro A, Gupta V, Wight TN, Hascall VC, Vesely I. Glycosaminoglycans and proteoglycans in normal mitral valve leaflets and chordae: association with regions of tensile and compressive loading. *Glycobiology.* 2004;14(7):621-633.
12. Reed CC, Iozzo RV. The role of decorin in collagen fibrillogenesis and skin homeostasis. *Glycoconj J.* 2002;19(4-5):249-255.
13. Kresse H, Schonherr E. Proteoglycans of the extracellular matrix and growth control. *J Cell Physiol.* 2001;189(3):266-274.

14. Wight TN. Versican: a versatile extracellular matrix proteoglycan in cell biology. *Curr Opin Cell Biol.* 2002;14(5):617-623.
15. Grande-Allen KJ, Griffin BP, Ratliff NB, Cosgrove DM, Vesely I. Glycosaminoglycan profiles of myxomatous mitral leaflets and chordae parallel the severity of mechanical alterations. *J Am Coll Cardiol.* 2003;42(2):271-277.
16. Grande-Allen KJ, Osman N, Ballinger ML, Dadlani H, Marasco S, Little PJ. Glycosaminoglycan synthesis and structure as targets for the prevention of calcific aortic valve disease. *Cardiovasc Res.* 2007;76(1):19-28.
17. Zhou B, Weigel JA, Fauss L, Weigel PH. Identification of the hyaluronan receptor for endocytosis (HARE). *J Biol Chem.* 2000;275(48):37733-37741.
18. Zhou B, McGary CT, Weigel JA, Saxena A, Weigel PH. Purification and molecular identification of the human hyaluronan receptor for endocytosis. *Glycobiology.* 2003;13(5):339-349.
19. Falkowski M, Schledzewski K, Hansen B, Goerdts S. Expression of stabilin-2, a novel fasciclin-like hyaluronan receptor protein, in murine sinusoidal endothelia, avascular tissues, and at solid/liquid interfaces. *Histochem Cell Biol.* 2003;120(5):361-369.
20. Lara SL, Evanko SP, Wight TN. Morphological evaluation of proteoglycans in cells and tissues. *Methods Mol Biol.* 2001;171:271-290.
21. Schonherr E, Jarvelainen HT, Sandell LJ, Wight TN. Effects of platelet-derived growth factor and transforming growth factor-beta 1 on the synthesis of a large versican-like chondroitin sulfate proteoglycan by arterial smooth muscle cells. *J Biol Chem.* 1991;266(26):17640-17647.
22. Radermecker MA, Limet R, Lapiere CM, Nusgens B. Increased mRNA expression of decorin in the prolapsing posterior leaflet of the mitral valve. *Interact Cardiovasc Thorac Surg.* 2003;2(3):389-394.
23. Scott JE. Proteoglycan-fibrillar collagen interactions. *Biochem J.* 1988;252(2):313-323.
24. Reinboth B, Hanssen E, Cleary EG, Gibson MA. Molecular interactions of biglycan and decorin with elastic fiber components: biglycan forms a ternary complex with tropoelastin and microfibril-associated glycoprotein 1. *J Biol Chem.* 2002;277(6):3950-3957.
25. Kyosseva SV, Harris EN, Weigel PH. The hyaluronan receptor for endocytosis (HARE) mediates hyaluronan-dependent signal transduction via extracellular signal-regulated kinases (ERK). 2008 (submitted).
26. Hellstrom M, Johansson B, Engstrom-Laurent A. Hyaluronan and its receptor CD44 in the heart of newborn and adult rats. *Anat Rec A Discov Mol Cell Evol Biol.* 2006;288(6):587-592.
27. Savani RC, Cao G, Pooler PM, Zaman A, Zhou Z, DeLisser HM. Differential involvement of the hyaluronan (HA) receptors CD44 and receptor for HA-mediated

motility in endothelial cell function and angiogenesis. *J Biol Chem.* 2001;276(39):36770-36778.

28. Allison DD, Grande-Allen KJ. Review. Hyaluronan: a powerful tissue engineering tool. *Tissue Eng.* 2006;12(8):2131-2140.
29. McDonald PC, Wilson JE, McNeill S, Gao M, Spinelli JJ, Rosenberg F, Wiebe H, McManus BM. The challenge of defining normality for human mitral and aortic valves: geometrical and compositional analysis. *Cardiovasc Pathol.* 2002;11(4):193-209.

Chapter 25: The Myocardium Overlying the Papillary Muscle Contributes to the Antero-Lateral Left Ventricular Wall Deformation Continuum

In this series of two chapters (Chapters 25 and 26), analysis of left ventricular myocardial mechanics using transmural beadsets is presented. While these chapters provide important insight into cardiac mechanics and left ventricular heterogeneity in transmural strains in particular, these studies do not directly relate to the overarching goals of this thesis. Therefore, these studies have been included in the Appendix. In the first of these two studies, analysis of transmural strains at end-diastole and end-systole at sites across the left ventricle demonstrates an antero-lateral continuum in transmural strain profiles.

ABSTRACT

Background: Previous studies of transmural left ventricular (LV) strains suggested that the myocardium overlying the papillary muscle displays depressed deformation, suggesting significant regional heterogeneity. However, these comparisons were made using different hearts, one group in which an anterior region was studied and another in which the region overlying the papillary muscle was studied. We wanted to extend these

studies by examining three equatorial regions in the same heart, during the same heart beat. Therefore, we compared the transmural strains in the LV myocardium overlying the antero-lateral papillary muscle (PAP) to regions on the same transverse equatorial plane located directly anteriorly (ANT) and laterally (LAT).

Methods: Transmural radiopaque beadsets were placed into ten sheep in three locations (ANT, LAT, and PAP) along the equatorial LV wall. Biplane videofluoroscopy was performed allowing the *in vivo* measurement of radial, circumferential, and longitudinal strains at each of three LV wall depths (subepicardial, midwall, and subendocardial) in the three locations for each heart beat. Myofiber angle measurements at each depth in each location from histological sections post-mortem allowed transformation of these strains into fiber and cross-fiber strains.

Results: LAT normal longitudinal and radial strains, as well as major principal strains, were less than ANT, while those of PAP were intermediate. Subepicardial and midwall myofiber angles of LAT, PAP, and ANT were not significantly different, but PAP subendocardial myofiber angles were significantly higher. Subepicardial and midwall myofiber strains of ANT, PAP, and LAT were not significantly different, but PAP subendocardial myofiber strains were less. Transmural gradients in circumferential and radial normal strains, and major principal strains, were evident in each region.

Conclusions: The three main findings of this study were: 1) PAP strains are largely consistent with adjacent free wall regions, 2) there is a continuum of strains across the anterolateral equatorial LV despite similarities in myofibers, and 3) transmural strain gradients were evident in all regions. These findings point to the heterogeneity of the LV, and suggest that regional differences in myofiber coupling may constitute the basis for such heterogeneity.

The work contained in this chapter is under preparation for submission to *American Journal of Physiology-Heart and Circulatory Physiology*.

INTRODUCTION

The mitral valve (MV) papillary muscles are important for normal LV function as part of the subvalvular apparatus,¹⁻⁶ and have been implicated in a number of disease states.⁷⁻¹⁵ The importance of the chordal-papillary complex to cardiac function has been highlighted by experimental studies in which chordal severing resulted in substantial decreases in LV function,¹⁻⁶ as well as worsened LV function and clinical outcomes in patients with MV replacement without chordal preservation relative to those with chordal preservation.¹⁶⁻²¹ Additional experimental studies suggest that the papillary muscles may be key to decreased LV function after chordal severing.^{22, 23} Papillary muscle dysfunction⁹⁻¹⁵ and/or displacement^{7, 8} have also been implicated in functional mitral regurgitation (MR), and has inspired papillary re-location techniques as part of functional MR treatment.²⁴⁻²⁷

Although the importance of the papillary muscles has been well established, questions remain regarding their functional integration into the LV myocardium. The papillary muscles structurally link the MV to the LV myocardium within the valvular-ventricular complex. While the LV myocardium is known to be composed of sheets of complex but largely helically arranged fibers,^{28, 29} fibers within the papillary muscles themselves are highly aligned in the direction of tension^{30, 31} and there is an abrupt change in myofiber angle from the LV compacta to the papillary muscles, particularly in the last 1-2 mm of the subendocardial LV wall.^{30, 31} Functionally, papillary muscle

contraction appears to occur in concert with LV contraction, shortening during ejection and lengthening during diastole.³² Recent studies analyzing transmural myocardial strains overlying the papillary muscles have raised the question of whether the myocardium overlying the papillary muscles is unique relative to adjacent regions of LV myocardium. Holmes et al.³⁰ in a study of dogs found decreased deformation in regions overlying the antero-lateral papillary muscle compared to more anteriorly located LV. However, these findings were derived from comparisons between different hearts. We wanted to extend these studies by examining three equatorial regions in the same heart, during the same heart beat.

METHODS

All animals received humane care in compliance with the “Principles of Laboratory Animal Care” formulated by the National Society for Medical Research and the *Guide for the Care and Use of Laboratory Animals* prepared by the National Academy of Sciences and published by the National Institutes of Health (U.S. Department of Health and Human Services, NIH Publication 85-23, Revised 1985). This study was approved by the Stanford Medical Center Laboratory Research Animal Review Committee and was conducted according to Stanford University policy.

Surgical Transmural Beadset Placement

The methods for the surgical placement of the transmural beadsets and data acquisition have been described in detail elsewhere³³⁻³⁵ and therefore, are only summarized herein. Ten adult Dorsett hybrid sheep (52±4 kg) were pre-medicated with Ketamine (25mg/kg intramuscularly) for venous and arterial catheter placement and monitoring. Anesthesia was induced and maintained with inhalational isoflurane (1.5-2.5%) and supplemental oxygen. Through a left thoracotomy, the pericardium was opened and the heart was confirmed to have no more than mild insufficiency in the aortic and mitral valves by epicardial color Doppler echocardiography (Sonos 5500, Hewlett-Packard, Palo Alto, CA). Thirteen miniature tantalum radiopaque subepicardial markers were implanted to silhouette the LV: 4 markers spaced equally along the longitudinal meridians of 3 transverse planes (basal, equatorial, and apical, Fig. 25-1A) and one marker located on the LV apex. Diastolic LV wall thickness was measured by epicardial echocardiography in three adjacent segments on the equatorial level (Fig. 25-1C): anterior wall (ANT), LV wall over the antero-lateral papillary muscle (PAP) and mid-lateral wall between the antero-lateral and postero-medial papillary muscles (LAT). This wall thickness was then used to determine the implantation depth for 3 transmural beadsets (Fig. 25-1B). A plexiglass template was used guide insertion of the beadsets, perpendicular to the LV wall, at each of the three locations, in a manner similar to those

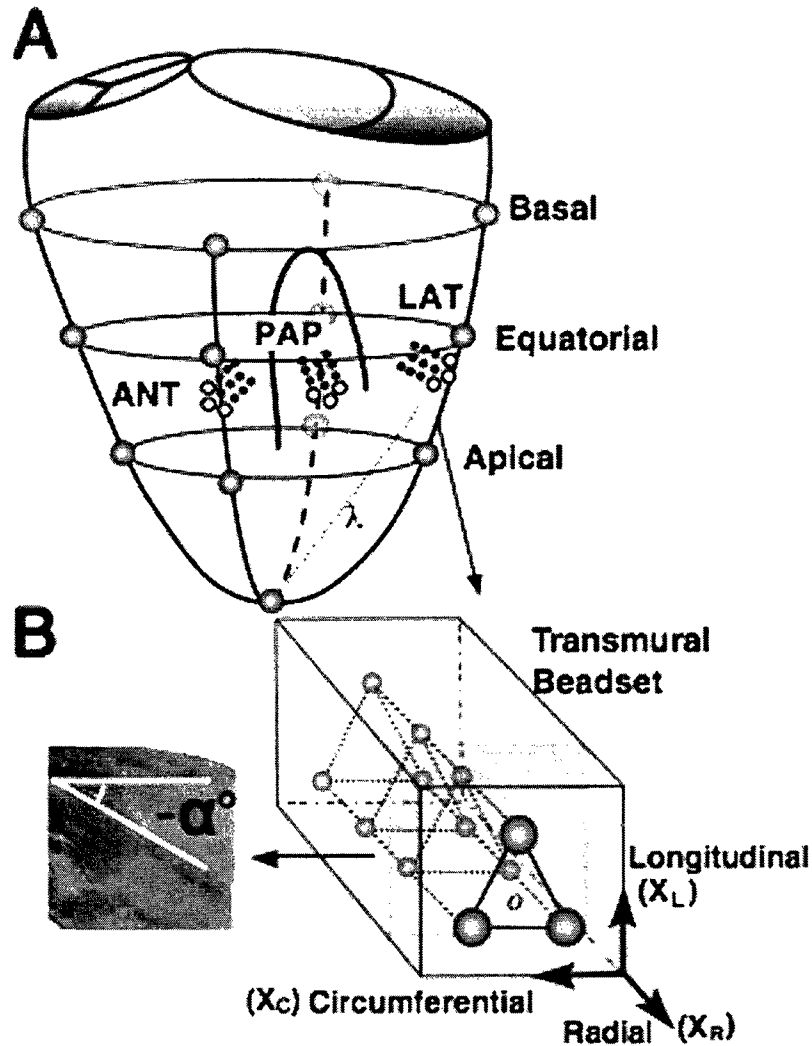


Fig. 25-1: A) Locations of markers silhouetting the LV: 4 markers spaced equally along the longitudinal meridians of 3 transverse planes (basal, equatorial, and apical), and one marker located at the LV apex. Three transmural beadsets are shown placed in specific LV regions: anterior (ANT), LV overlying the antero-lateral papillary muscle (PAP), and lateral (LAT), as determined by epicardial echocardiography. B) Close-up of one of the three transmural beadsets. Markers were spaced evenly from endocardium to epicardium in a column oriented normal to the epicardial tangent plane. The deepest (subendocardial) beads were implanted at 90% of the echocardiographically determined end-diastolic wall thickness. For each videographic frame, a local coordinate system was defined with the origin (O) at the center of the epicardial equilateral triangle of beads, the radial (X_R) axis defined as 180 degrees from the LV chamber, the longitudinal (X_L) axis defined at the intersection of X_R and the long axis (λ) in the epicardial tangent plane, and the circumferential (X_C) axis orthogonal to the previously defined axes. Myofiber angle (α) was defined relative to the circumferential (X_C) axis.

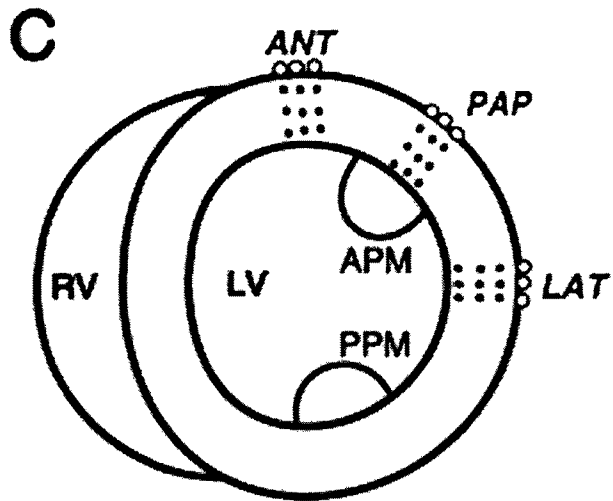


Fig. 25-1 (cont'd): C) Diagram of LV transverse equatorial short-axis plane as viewed from the LV apex illustrating the location of the three transmurular beadsets (ANT, PAP, and LAT) relative to the antero-lateral (APM) and postero-medial papillary muscles (PPM). RV=right ventricle, LV=left ventricle.

previously described.^{34,36} The deepest (subendocardial) beads were implanted at 90% of the echocardiographically determined end-diastolic wall thickness and two additional 0.7mm beads were placed to span the myocardium. For each column a fourth 1.7 mm bead was sutured onto the overlying epicardium. In order to compare the pure LV wall motion in all segments, the deepest beads of PAP were adjusted at the same level as ANT and LAT and did not penetrate into the papillary muscle. Upon study completion the hearts were excised and thoroughly examined to confirm correct bead placement with magnetic resonance imaging and histological examination.

***In Vivo* Marker Data Acquisition**

Immediately after the operation, animals were transferred to the catheterization laboratory and studied in the right decubitus position with the chest open. Two micromanometer-tipped pressure transducers (model MPC-500; Millar Instruments, Houston, TX) were calibrated and inserted into the LV and ascending aorta via carotid artery catheters. Simultaneous biplane videofluoroscopic images of markers (60 Hz, Philips Medical Systems, Pleasanton, CA), ECG, LV pressure (LVP) and aortic pressure were recorded during three consecutive heart beats in normal sinus rhythm with ventilation transiently arrested at end-expiration, as previously described.³⁴ Data from the two 2D videofluoroscopic views were merged using 3D helical phantom image data and custom software,³⁷ thus yielding the 3D coordinates of each marker centroid every 16.7 msec. The accuracy of these 3D reconstructions has previously been shown to be 0.1 ± 0.3 mm.³⁸

Quantitative Analysis of Myofiber Angle

At the end of the study the animals were euthanized by intravenous administration of KCl (80 mEq) under 5% isoflurane. LVP was adjusted to match *in vivo* LV end-diastolic pressure with left atrial exsanguination. While the pressure was maintained, the hearts were fixed *in situ* with 300 ml of 5% buffered glutaraldehyde into the left coronary artery balloon catheter (Guidant, AguiTrac Peripheral Catheter, Santa Clara, CA). The

hearts were then excised and stored in 10% formalin for 48 hours. A LV long axis was defined as the line passing through the LV apex and mid-anterior mitral leaflet. Each transmural beadset was excised surrounded by a rectangular cuboid, with a 15 x 15 mm square face, whose sides paralleled the local circumferential (X_C), longitudinal (X_L) and radial (X_R) lines (Fig. 25-1B). Each block was sliced into sequential 1-mm-thick sections parallel to the epicardial plane (X_C - X_L) from the epicardium to endocardium, providing a series of slices for measurement of myofiber angle (α). The myofiber angle, α , defined as the average angle between the local muscle fiber axis (X_f) and circumferential axis (X_C), was determined at 20, 50 and 80% depths using MATLAB 2007b (The Mathworks, Inc, Natick, MA), as described previously.^{33, 39}

Analysis of Strains

The three transmural beadsets permitted 3D LV wall deformation measurements in the ANT, PAP, and LAT regions. The analysis of normal, principal, fiber and cross-fiber strains have been described in detail previously.^{33, 34} Briefly, for each transmural beadset in each videographic frame a local, orthogonal coordinate system (Fig. 25-1B) was defined relative to the three beads sewn on the epicardium. The origin of this coordinate system (O) was defined as the center of this equilateral triangle of beads in the epicardial tangent plane, the radial (X_R) axis was defined as 180 degrees from the LV chamber, the longitudinal (X_L) axis was defined at the intersection of X_R and the long

axis (λ , through the origin (O) and the LV apex marker, Fig. 25-1A) in the epicardial tangent plane, and the circumferential (X_C) axis defined as orthogonal to the previously defined axes (X_R and X_L).

Each cardiac cycle for each beat was visualized by pressure-volume loop for concrete timing definition of end-diastole (ED) as undeformed state (reference), and end-systole (ES) as the deformed state.

For each beat, the displacement of the beads relative to ED was characterized by a continuous polynomial position field with quadratic dependence in E_R and linear dependence in E_L and E_C using least-squares fits.⁴⁰ As described previously,^{34, 35} the material gradient of the position field is the local deformation gradient tensor (\mathbf{F}) and the Lagrangian strain (\mathbf{E}) is then calculated as $\mathbf{E}=(\mathbf{F}^T\mathbf{F}-\mathbf{I})/2$, where \mathbf{I} is the identity tensor. In terms of the coordinate system used in this study (X_C , X_L , and X_R), the three normal strains (E_{CC} , E_{LL} , and E_{RR}) measure local elongation or shortening along the circumferential (E_{CC}), radial (E_{RR}), and longitudinal (E_{LL}) axes. The three shear strains (E_{CL} , E_{LR} , and E_{CR}) represent angle changes between orthogonally oriented axes. The major principal strain (E_1) was calculated as the maximum eigenvalue of \mathbf{E} . Strains were interpolated along the central axis of each transmural bead column at 1% increments of wall depth from the epicardium to the most subendocardial bead. The four beads are approximately located at depths of 0%, 30%, 60%, and 90% of wall depth at ED, where 0% is at the epicardium and 100% is at the endocardium. The three depths chosen for

detailed strain analysis were defined as 20% (subepicardium), 50% (midwall), and 80% (subendocardium) of the depth of the deepest bead measured from the epicardial surface as each time point, which approximately represents transmural depths of 18%, 45%, and 72%.³⁴

The myofiber angles (α) calculated at each depth were used to express myocardial strains at each depth in terms of myofiber (E_{fiber}) and cross-fiber (E_{cross}) strains. The strain tensor at a given depth was transformed from the local myocardium coordinate system (X_R , X_L , and X_C) into that relative to myofiber axis (X_f) and the perpendicular axis to X_f (X_c) at a given depth in planes parallel to the epicardial tangent plane.

Statistical Analysis

Data are reported as mean \pm standard deviation. Comparisons between groups (LV location: ANT, LAT, PAP; transmural depth: subepicardium, midwall, subendocardium) were performed using 2 way repeated measures (RM) ANOVA with a Bonferroni correction using SigmaStat (version 3.5, SPSS, Inc. Chicago, IL). Significance level was set at $p=0.05$.

RESULTS

Hemodynamic data for the animals are reported in Table 25-1. The normal strains E_{LL} and E_{RR} were significantly different between the ANT and LAT regions (Table 25-2),

Table 25-1. Hemodynamics.

Body weight (kg)	54	± 7
Heart rate (beats/min)	90	± 9
ESLVP (mmHg)	83	± 7
LVESV (mL)	84	± 12
LVEDV (mL)	122	± 15
dP/dt _{max} (mmHg/s)	1,270	± 80

N=10, data mean ± SD. ESLVP=end systolic LV pressure,
LVESV=LV end systolic volume, LVEDV=LV end diastolic volume.

with LAT E_{LL} and E_{RR} at all transmural depths (except subepicardial E_{RR}) significantly less than those of ANT. No significant differences were found between ANT and LAT in E_{cc} . PAP normal strains, especially E_{RR} , were largely intermediate between those of ANT and LAT at each depth (ANT>PAP>LAT), with the exception of PAP subendocardial E_{cc} which was less than both ANT and LAT. LAT E_{cc} was significantly greater than E_{LL} ($p<0.001$), whereas E_{cc} and E_{LL} were comparable in ANT, as was true in PAP. A transmural gradient of strain (subendocardium>midwall>subepicardium) was evident in E_{cc} for all regions, E_{RR} for ANT and PAP, and a partial transmural gradient (subendocardium>subepicardium) was evident in LAT E_{RR} . E_{LL} demonstrated a partial transmural gradient (subendocardium>subepicardium) in ANT and PAP.

Table 25-2. Normal Strains.

Normal Strain		ANT	PAP	LAT
E _{CC}	Subepi	-0.08 ± 0.03	-0.07 ± 0.03	-0.07 ± 0.02
	Midwall	-0.14 ± 0.03	-0.11 ± 0.03	-0.13 ± 0.03
	Subendo	-0.20 ± 0.04	-0.16 ± 0.04[#]	-0.19 ± 0.04
E _{LL}	Subepi	-0.07 ± 0.03	-0.06 ± 0.03	-0.02 ± 0.04 ^{#§}
	Midwall	-0.09 ± 0.02	-0.09 ± 0.03	-0.02 ± 0.03 ^{#§}
	Subendo	-0.12 ± 0.04	-0.10 ± 0.04	-0.03 ± 0.06 ^{#§}
E _{RR}	Subepi	0.17 ± 0.06	0.13 ± 0.05	0.10 ± 0.06
	Midwall	0.34 ± 0.09	0.26 ± 0.11	0.17 ± 0.09 ^{#§}
	Subendo	0.54 ± 0.19	0.42 ± 0.22[#]	0.25 ± 0.13^{#§}

N=10, data mean ± SD. ANT, anterior wall; PAP, LV over the papillary muscle; LAT, lateral wall on the equatorial level. $P < 0.05$ # vs. ANT, § vs. PAP by 2-way RM ANOVA with Bonferroni correction. Significant transmural gradients (bold) were observed in E_{CC} (ANT, PAP, and LAT) and E_{RR} (ANT and PAP). Significant partial gradients (subepi vs. subendo, in bold) were observed in ANT and PAP in E_{LL}, and LAT in E_{RR}.

Shear strains were small in magnitude and largely not significantly different between regions (Table 25-3). Transmural gradients were also largely not evident in the various regions.

Table 25-3. Shear Strains.

Shear Strain		ANT	PAP	LAT
E _{CL}	Subepi	0.01 ± 0.03	0.00 ± 0.03	0.00 ± 0.03
	Midwall	0.01 ± 0.03	0.01 ± 0.02	-0.01 ± 0.03
	Subendo	0.01 ± 0.02	0.02 ± 0.03	0.01 ± 0.04
E _{LR}	Subepi	0.03 ± 0.03	0.03 ± 0.03	0.06 ± 0.06
	Midwall	0.05 ± 0.05	0.05 ± 0.04	0.06 ± 0.08
	Subendo	0.07 ± 0.08	0.07 ± 0.08	0.04 ± 0.11
E _{CR}	Subepi	0.01 ± 0.04	0.02 ± 0.05	0.03 ± 0.02
	Midwall	-0.01 ± 0.04	0.04 ± 0.04	0.01 ± 0.02
	Subendo	-0.04 ± 0.08	0.05 ± 0.07 [#]	0.01 ± 0.04

N=10, data mean ± SD. [#]P<0.05 vs. ANT by 2-way RM ANOVA with Bonferroni correction.

Principal strains in LAT were significantly smaller in magnitude than ANT for the major (E₁) and minor (E₃) principal strains at the subendocardial and midwall depths (Table 25-4). PAP principal strains largely appeared intermediate between those of ANT and LAT (i.e., magnitude of ANT>PAP>LAT). Transmural gradients were evident in the major (E₁) principal strains of ANT and PAP and a partial transmural gradient in E₁ was evident in LAT.

Table 25-4. Principal Strains.

Principal Strain		ANT	PAP	LAT
E ₁ (Major)	Subepi	0.19 ± 0.06	0.16 ± 0.06	0.16 ± 0.06
	Midwall	0.35 ± 0.10	0.29 ± 0.13	0.23 ± 0.09 [#]
	Subendo	0.54 ± 0.21	0.45 ± 0.26[#]	0.26 ± 0.14^{#§}
E ₂	Subepi	0.10 ± 0.05	0.06 ± 0.04[#]	0.08 ± 0.04
	Midwall	0.14 ± 0.04	0.10 ± 0.05[#]	0.11 ± 0.03[#]
	Subendo	0.00 ± 0.02	0.01 ± 0.03	0.02 ± 0.04
E ₃ (Minor)	Subepi	-0.18 ± 0.03	-0.16 ± 0.05	-0.15 ± 0.04
	Midwall	-0.25 ± 0.05	-0.22 ± 0.06	-0.20 ± 0.05[#]
	Subendo	-0.14 ± 0.04	-0.13 ± 0.04	-0.08 ± 0.04^{#§}

N=10, data mean ± SD. $P < 0.05$ # vs. ANT, § vs. PAP by 2-way RM ANOVA with Bonferroni correction. Significant transmural gradients (bold) were observed in E₁ ANT and PAP. Partial gradients (bold) were seen in: E₁ LAT (subepi<subendo), E₂ LAT (subepi<midwall, subendo), and E₂ ANT and PAP (midwall>subepi>subendo). All regions in E₃ presented significant differences between depths (subendo<subepi<midwall).

Myofiber angles in LAT were not significantly different from those of ANT at any transmural depth (Fig. 25-2), nor were the myofiber angles of PAP significantly different from ANT or LAT at the subepicardial or midwall depths. However, the PAP subendocardial myofiber angle was significantly higher (i.e., more radial orientation, as opposed to circumferential) than ANT and LAT. All regions displayed a transmural gradient with myofiber angle increasing from the subepicardium to the subendocardium.

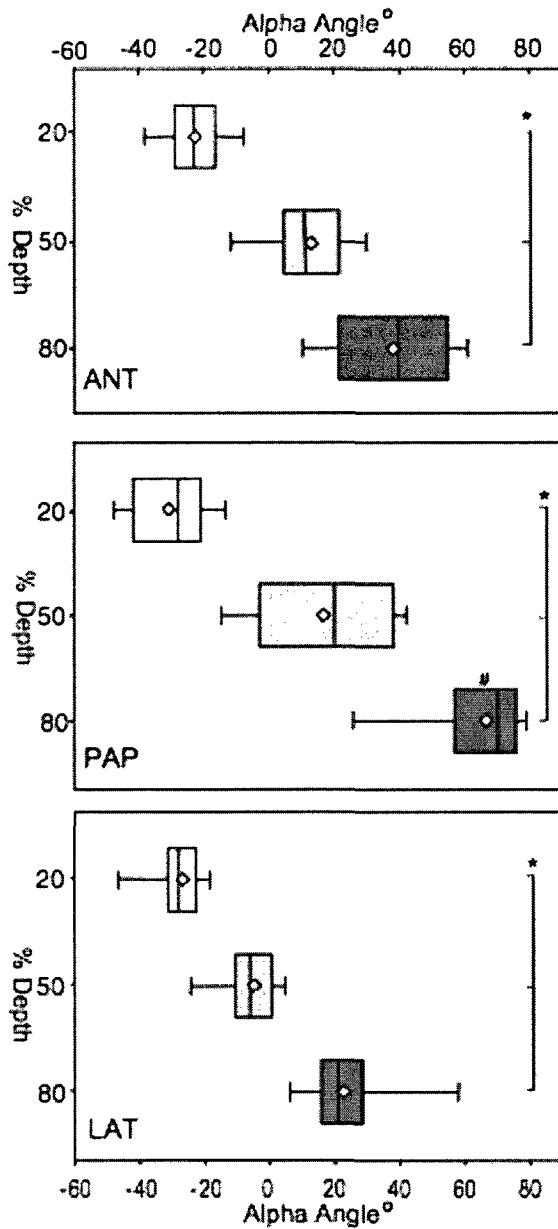


Fig. 25-2: Box plot illustrating myofiber angles in ANT, PAP, and LAT on the equatorial level in subepicardium (20% depth), midwall (50% depth) and subendocardium (80% depth). Diamond indicates group mean ($N=10$), left side of box indicates lower 25%, right side of box indicates 75%, central line indicates median, left whisker indicates lowest value, and right whisker indicates highest value. *Transmurals gradient (i.e., depths are significantly different, $P < 0.001$). # $P < 0.02$ vs. ANT and LAT by 2-way RM ANOVA with Bonferroni correction.

Myofiber strains (E_{fiber}) were not significantly different between ANT and LAT at any transmurals depth (Table 25-5). PAP E_{fiber} at the subepicardial and midwall depths were not significantly different than either ANT or LAT, but PAP E_{fiber} at the subendocardial depth was significantly less than both ANT and LAT. Cross-fiber strains (E_{cross}) in ANT were significantly greater than LAT at all transmurals depths. PAP E_{cross}

were also greater than LAT at all transmural depths. Partial transmural gradients (subendocardium>subepicardium) were evident for E_{cross} in all regions, as well as for E_{fiber} in the ANT and LAT regions.

Table 25-5. Fiber and Cross-fiber Strains.

		ANT	PAP	LAT
E_{fiber}	Subepi	-0.09 ± 0.04	-0.08 ± 0.04	-0.08 ± 0.04
	Midwall	-0.14 ± 0.03	-0.11 ± 0.03	-0.12 ± 0.03
	Subendo	-0.15 ± 0.05	-0.11 ± 0.05 [#]	-0.17 ± 0.02
E_{cross}	Subepi	-0.08 ± 0.03[‡]	-0.07 ± 0.03[‡]	-0.03 ± 0.04
	Midwall	-0.10 ± 0.02[‡]	-0.12 ± 0.04[‡]	-0.04 ± 0.02
	Subendo	-0.17 ± 0.04[‡]	-0.18 ± 0.04[‡]	-0.09 ± 0.06

N=10, data mean ± SD. $P < 0.05$ [#]vs. ANT and LAT, [‡]vs. LAT by 2-way RM ANOVA with Bonferroni correction. Significant transmural gradients (bold) were observed in E_{cross} in all regions and partial gradients (subepi vs. subendo, in bold) were observed in E_{fiber} in ANT and LAT.

DISCUSSION

The three main findings of this study were: 1) the myocardium overlying the papillary muscles displayed a transmural strain profile that is not unique, but rather consistent with adjacent free wall regions, 2) there was a continuum of transmural strain profiles across the anterolateral equatorial LV despite similarities in myofibers, and 3) a transmural strain gradient was evident in all regions. When measured at the same transverse plane in the same animals during the same heartbeats, transmural strains in the anterior LV (ANT) were greater than those of the lateral region (LAT); strains in the myocardium overlying the antero-lateral papillary (PAP) were largely intermediate between those of ANT and LAT, consistent with its location within this continuum.

LV Myocardium Overlying Antero-Lateral Papillary is Not Unique

The myocardium overlying the antero-lateral papillary muscle (PAP) displayed normal and major principal strains that were largely intermediate between those of the anterior (ANT) and lateral (LAT) regions of the LV. Similarly, the shear strains in PAP were largely not different from those of ANT or LAT, nor were myofiber angles or strains. These results suggest that PAP is not functionally unique relative to adjacent regions of the LV.

The few instances in which PAP displayed unique strains all were found in the subendocardium, and largely can be explained by the greater PAP subendocardial myofiber angle relative to that of the other regions. For instance, the subendocardial E_{fiber} in PAP, which was less than that of ANT and LAT, is derived from the subendocardial strain tensor \mathbf{E} by the cosine of α . Therefore, for similar strains, regions with higher myofiber angles (i.e., PAP) will have lower E_{fiber} . E_{CC} and E_{CR} were both slightly, but significantly, different in PAP subendocardium relative to LAT and ANT. These differences may also relate to the difference in PAP subendocardial myofiber angle given that myofibers in the adjacent regions were predominantly circumferentially oriented.

Others have noted an abrupt increase in myofiber angle within 1-2 mm of the junction between the myocardium and antero-lateral papillary muscle.^{30,31} Given that the myofibers within the papillary muscle are highly aligned at an acute angle to the LV myocardium,^{30,31} it is logical that the myofiber angle in the subendocardium bordering the papillary muscle would greatly increase to dovetail with the fibers in the papillary muscle itself.

In light of these results, it appears that the myocardium overlying the antero-lateral papillary muscle may not be severely depressed relative to other regions of the LV, as previously proposed.^{30, 41} It should be noted that in these previous studies the myocardium overlying the papillary muscles was compared to regions located more anteriorly and in different hearts. Based on the results of the present study, the previously observed decreased deformation of the myocardium overlying the papillary muscle could, at least in part, be explained by the antero-lateral continuum found here, where the anterior region displays strains of greater magnitude than regions located more laterally.

A number of other limitations may have influenced the conclusions of Holmes et al. Compared to the normal and principal strains reported in this study and similar studies,^{33, 34, 39, 42} the anterior LV strains reported by Holmes were significantly less (~half) for both transmural depths measured (“inner wall” and “outer wall”),³⁰ suggesting overall decreased myocardial function in their animals. It also is worth noting that in their study the majority of the animals underwent mitral valve replacement.³⁰ Based on studies demonstrating mitral valve annuloplasty alters transmural strains,⁴³ the mitral valve replacements likely affected their results. The study by Holmes was further limited because comparisons were made between the two regions from different animals during different heart beats.³⁰

Antero-Lateral Continuum of LV Transmural Strains Despite Similarities in Myofibers

A continuum of LV transmural strains in which strains decreased moving from the anterior to lateral equatorial LV, is supported by greater E_{RR} and E_{LL} , greater major and minor principal strains, and greater E_{cross} , in ANT compared to LAT. These differences were evident in the subendocardium and midwall, but were not always statistically significant at the subepicardium. E_{CC} was not significantly different between regions, nor were shear strains. Surprisingly, myofiber angles and E_{fiber} were not significantly different between regions. This suggests that regional differences in normal and principal strains were not due to inherent differences in myofibers.

The finding of ~2x greater wall thickening (E_{RR}) in ANT than LAT is consistent with the findings of Cheng et al.,⁴² although in that study the lateral and anterior regions were at different transverse planes (lateral equatorial vs. anterior basal). As in the present study, Cheng et al.⁴² found no significant differences in myofiber angles or myofiber strains between the two locations despite differences in wall thickening. The results of these two studies, suggest that differences in coupling between these fundamental contractile units (myofibers) within the macrostructure of the myocardium likely accounts for the observed macroscopic differences in wall thickening. Possible mechanisms related to differences in coupling were studied in detail by Cheng et al.⁴² Regional differences in LV geometry may also relate to these differences in strain. According to Bogeaert et al.,⁴⁴ the anterior portion of the LV has a larger radius of curvature compared to the lateral LV in the same transverse plane. This greater radius of curvature in the anterior LV would yield less pressure development for a given amount of

wall thickening, therefore greater wall thickening in ANT may be a compensatory mechanism to develop greater force to overcome its geometric shortcoming. Even with greater wall thickening in the anterior LV, however, Bogeart et al.⁴⁴ found that the anterior LV region contributed less to the ejection fraction relative to the lateral LV. In this study, ED thicknesses between the different regions were chosen to be comparable, therefore differences in strain can not be attributed to differences in thickness, but rather must be due to fundamental differences in the mechanics of the different regions.

Longitudinal strains (E_{LL}) were also found to be greater in ANT than LAT. Given that Bogeart et al.⁴⁴ found the radius of curvature in both the circumferential and longitudinal directions to be greater in ANT compared to LAT, greater E_{LL} in ANT may again be a compensatory mechanism. It is also interesting to note that in LAT E_{LL} was significantly less than E_{CC} , whereas in ANT E_{CC} and E_{LL} were comparable. While the finding of comparable E_{CC} and E_{LL} in ANT is consistent with that of Costa et al.,⁴⁵ this finding is in contrast to the work of Villarreal et al.⁴⁶ who found that, at least in the midwall of dogs using a triangular array of three piezoelectric crystals, E_{CC} was greater than E_{LL} in the anterior equatorial LV, whereas E_{CC} and E_{LL} were comparable in the lateral equatorial LV.

Transmural Gradients Evident throughout Regions

All three regions demonstrated significant transmural gradients (in which all three transmural depths were statistically different) or partial transmural gradients (in which subendocardium and subepicardium depths were different) in E_{CC} and E_{RR} , and ANT and PAP demonstrated partial gradients in E_{LL} . Similarly, all regions demonstrated

transmural or partial transmural gradients in the major principal strain (E_1). Transmural gradients in myofiber angles were also noted in all regions, and myofiber strains demonstrated a partial gradient in ANT and LAT.

Transmural gradients in normal strains have been demonstrated in a number of previous studies using various modalities. Transmural gradients in radial strains (wall thickening) have been particularly well characterized in a variety of species using a number of imaging modalities.^{45, 47-53} Transmural gradients in E_{CC} have also been previously demonstrated.^{30, 44, 45} Given that the LV myocardium is a constant volume system with a roughly cylindrical shape, mechanically there must be a transmural gradient in wall thickening during contraction, as reasoned by Gallagher et al.⁴⁹ While this is true theoretically, the LV is not homogeneous and displaced volume during contraction does not necessarily need to accumulate in the subendocardium in all regions of the LV. In fact, previous studies of transmural strains 8 weeks after bead set implantation showed a loss of the transmural E_{RR} gradient despite maintained cardiac function.³⁴ Nevertheless, globally the LV must have a transmural gradient in wall thickening, as well as in E_{CC} and E_{LL} , for systolic contraction to occur.

The transmural gradient in myofiber angle has been well characterized and appears conserved across species.^{45, 54-56} This gradient is fundamental to LV torsion,⁵⁷⁻⁵⁹ which in turn is key to LV force development, as well as minimization of transmural gradients of myofiber work and O_2 consumption.^{58, 60, 61} Indeed, computational modeling has shown that myofiber orientation dramatically affects LV wall stress.⁶²⁻⁶⁴ The partial transmural gradient in myofiber strain (subendocardium significantly greater than subepicardium) found in this study is consistent with studies in the LV lateral equatorial

region using the same transmural beadset technique^{33, 65} and in humans using MRI,⁶⁶ although others have not found evidence for such a transmural gradient.^{42, 45}

Transmural Strains of Myocardium Overlying Papillary Implicate Robust Cardiac Structure

Based on what is known regarding papillary muscle mechanics, the finding of this study that the myocardial muscle overlying the antero-lateral papillary muscle displays transmural strains consistent with those of adjacent regions is rather surprising. The papillary muscles undergo considerable motion and contraction throughout the cardiac cycle,^{32, 67} and given that the papillary muscles are mechanically contiguous with the overlying myocardium, one might expect the myocardium in that region to experience distinct forces relative to adjacent regions, and therefore demonstrate unique transmural strain profiles. The lack of the distinction in transmural strains of the myocardium overlying the papillary muscles, however, can be seen as evidence for the robust nature of the cardiac structure. That is, the complex helical myofiber structure is built able to withstand these forces of the papillary muscles, and when these forces are removed LV function in that area that delicate balance of forces is altered and that region's contractile properties do appear to change.^{22, 23, 68}

Implications

The main findings of this study have a number of implications for our understanding of cardiac physiology and pathology. The finding that the myocardium overlying the papillary muscle is not unique despite the complex dynamics of the

attached papillary muscle, points to a finely tuned, complex system. The heterogeneity of the LV, as demonstrated by the anterolateral continuum in strains and transmural strain gradients, further points to the complexity of the LV and suggests that strategies such as engineered cardiac patches should optimally be designed to be regionally and depth-specific. Lastly, the importance of coupling between the fundamental contractile unit of the myocyte suggested by the results of this study, similarly points to the complexity of the LV, specifically the importance of the configuration of myocytes within the macrostructure of the myocardium: their orientation, interconnections with one another, and interaction with the ECM. These aspects of myocyte configuration should optimally be taken into account in clinical interventions such as engineered cardiac patches or the introduction of stem cells. Furthermore, the importance of this coupling points to the significant role of the extracellular matrix in cardiac function,^{69, 70} and provides a mechanism for decreased cardiac function in disease states in which matrix components such as collagen are abnormal.⁷¹⁻⁷³ Potentially interventions preventing or reversing such matrix changes could improve cardiac function in these patients, although this remains to be demonstrated.

Limitations

While the transmural beadset technique and accompanying analysis used in this study provides substantial insight into myocardial strains at different transmural depths in the beating heart, several limitations to this technique should be noted. First, while beadset implantation does not require cardiopulmonary bypass and the markers are relatively small, it is likely that the markers themselves and the process of implantation

may subtly affect overall cardiac function as well as myofiber mechanics in the localized region of implantation. Second, this study was performed in anesthetized ovine, therefore some of the results may be altered by anesthesia and be species specific, although certainly some characteristics of myocardial architecture and mechanics (i.e., gradient of myofiber angle across the LV wall^{45, 54-56}) appear to be conserved across species. Third, there are inherent uncertainties in myofiber angle measurements, variability in final depth of bead placement, limitations in the number of beads that can be placed transmurally, uncertainty in computational fitting to bead data and the videographic imaging modality itself. However, these uncertainties are relatively small and would not account for the regional differences found in this study. Fourth, this study included analysis at three equatorial locations spanning from the anterior LV to the lateral LV; analysis of transmural myocardial strains at more locations would be necessary to confirm a true anterolateral gradient in transmural myocardial strains as suggested by the results of this study. While previous studies have analyzed transmural strains in terms of laminar sheets utilizing β angles, considerable controversy remains about the usefulness of such measurements. These measurements are also technically difficult and subject to multiple errors. For instance, while the major β is used for calculations at a given depth, there are multiple β s evident at each depth, especially at the subendocardium, and it is not appropriate to average them.^{42, 74} Furthermore, β measurements are subject to artifacts in tissue preparation and assume tissue homogeneity, whereby measurements from very small areas are taken to be representative of much larger regions. Clearly, laminar sheets severely oversimplify the complexity of myocyte arrangement in the myocardium.⁷⁵ Because of these limitations, laminar sheet analysis was not performed in this study.

CONCLUSIONS

In summary, in this study we have demonstrated that the LV myocardium overlying the antero-lateral papillary muscle is not unique relative to adjacent equatorial regions, but rather is consistent with an antero-lateral gradient in strains with transmural strains greatest in the anterior region and least in the lateral region. Furthermore, these differences in transmural strains were demonstrated despite similar myofiber strains, suggesting that while the contracting myofiber units in the different regions are similar, their coupling is distinct leading to differences in normal strains. The findings contained in this study add to our understanding of LV function, as well as contain potential implications regarding the role of the extracellular matrix in contributing to LV function by connecting myofibers and potential clinical implications for interventions involving the implantation of myocytes with or without scaffolds.

This chapter, which demonstrated an antero-lateral continuum in transmural strain profiles of the left ventricle, is the first of two chapters (Chapters 25 and 26) on left ventricle myocardial mechanics. In the next chapter, analysis of transmural myocardial strains throughout the cardiac cycle reveal significant temporal and regional heterogeneity in left ventricular strain development.

REFERENCES

1. Sarris GE, Cahill PD, Hansen DE, Derby GC, Miller DC. Restoration of left ventricular systolic performance after reattachment of the mitral chordae tendineae. The importance of valvular-ventricular interaction. *J Thorac Cardiovasc Surg.* 1988;95(6):969-979.
2. Hansen DE, Cahill PD, Derby GC, Miller DC. Relative contributions of the anterior and posterior mitral chordae tendineae to canine global left ventricular systolic function. *J Thorac Cardiovasc Surg.* 1987;93(1):45-55.
3. Hansen DE, Cahill PD, DeCampi WM, Harrison DC, Derby GC, Mitchell RS, Miller DC. Valvular-ventricular interaction: importance of the mitral apparatus in canine left ventricular systolic performance. *Circulation.* 1986;73(6):1310-1320.
4. Yun KL, Fann JI, Rayhill SC, Nasserbakht F, Derby GC, Handen CE, Bolger AF, Miller DC. Importance of the mitral subvalvular apparatus for left ventricular segmental systolic mechanics. *Circulation.* 1990;82(5 Suppl):IV89-104.
5. Moon MR, DeAnda A, Jr., Daughters GT, 2nd, Ingels NB, Jr., Miller DC. Effects of mitral valve replacement on regional left ventricular systolic strain. *Ann Thorac Surg.* 1999;68(3):894-902.
6. Sarris GE, Miller DC. Valvular-ventricular interaction: the importance of the mitral chordae tendineae in terms of global left ventricular systolic function. *J Card Surg.* 1988;3(3):215-234.
7. Aikawa K, Sheehan F, Otto C, Coady K, Bashein G, Bolson E. The severity of functional mitral regurgitation depends on the shape of the mitral apparatus: a three-dimensional echo analysis. *J Heart Valve Dis.* 2002;11(5):627-636.
8. He S, Lemmon JJ, Weston M, Jensen M, Levine R, Yoganathan A. Mitral valve compensation for annular dilatation: in vitro study into the mechanisms of functional mitral regurgitation with an adjustable annulus model. *J Heart Valve Dis.* 1999;8(3):294-302.
9. Messas E, Guerrero JL, Handschumacher MD, Chow CM, Sullivan S, Schwammenthal E, Levine RA. Paradoxical decrease in ischemic mitral regurgitation with papillary muscle dysfunction: insights from three-dimensional and contrast echocardiography with strain rate measurement. *Circulation.* 2001;104(16):1952-1957.
10. Kisanuki A, Otsuji Y, Kuroiwa R, Murayama T, Matsushita R, Shibata K, Yutsudo T, Nakao S, Nomoto K, Tomari T, et al. Two-dimensional echocardiographic assessment of papillary muscle contractility in patients with prior myocardial infarction. *J Am Coll Cardiol.* 1993;21(4):932-938.
11. Kaul S, Spotnitz WD, Glasheen WP, Touchstone DA. Mechanism of ischemic mitral regurgitation. An experimental evaluation. *Circulation.* 1991;84(5):2167-2180.
12. Khankirawatana B, Khankirawatana S, Mahrous H, Porter TR. Assessment of papillary muscle function using myocardial velocity gradient derived from tissue Doppler echocardiography. *Am J Cardiol.* 2004;94(1):45-49.

13. Hider CF, Taylor DE, Wade JD. The Effect of Papillary Muscle Damage on Atrioventricular Valve Function in the Left Heart. *Q J Exp Physiol Cogn Med Sci.* 1965;50:15-22.
14. Burch GE, De Pasquale NP, Phillips JH. Clinical manifestations of papillary muscle dysfunction. *Arch Intern Med.* 1963;112:112-117.
15. Godley RW, Wann LS, Rogers EW, Feigenbaum H, Weyman AE. Incomplete mitral leaflet closure in patients with papillary muscle dysfunction. *Circulation.* 1981;63(3):565-571.
16. Okita Y, Miki S, Ueda Y, Tahata T, Sakai T. Left ventricular function after mitral valve replacement with or without chordal preservation. *J Heart Valve Dis.* 1995;4 Suppl 2:S181-192; discussion S192-183.
17. Lee EM, Shapiro LM, Wells FC. Importance of subvalvular preservation and early operation in mitral valve surgery. *Circulation.* 1996;94(9):2117-2123.
18. Hennein HA, Swain JA, McIntosh CL, Bonow RO, Stone CD, Clark RE. Comparative assessment of chordal preservation versus chordal resection during mitral valve replacement. *J Thorac Cardiovasc Surg.* 1990;99(5):828-836; discussion 836-827.
19. Rozich JD, Carabello BA, Usher BW, Kratz JM, Bell AE, Zile MR. Mitral valve replacement with and without chordal preservation in patients with chronic mitral regurgitation. Mechanisms for differences in postoperative ejection performance. *Circulation.* 1992;86(6):1718-1726.
20. Horskotte D, Schulte HD, Bircks W, Strauer BE. The effect of chordal preservation on late outcome after mitral valve replacement: a randomized study. *J Heart Valve Dis.* 1993;2(2):150-158.
21. Athanasiou T, Chow A, Rao C, Aziz O, Siannis F, Ali A, Darzi A, Wells F. Preservation of the mitral valve apparatus: evidence synthesis and critical reappraisal of surgical techniques. *Eur J Cardiothorac Surg.* 2008;33(3):391-401.
22. Pitarys CJ, 2nd, Forman MB, Panayiotou H, Hansen DE. Long-term effects of excision of the mitral apparatus on global and regional ventricular function in humans. *J Am Coll Cardiol.* 1990;15(3):557-563.
23. Corin WJ, Sutsch G, Murakami T, Krogmann ON, Turina M, Hess OM. Left ventricular function in chronic mitral regurgitation: preoperative and postoperative comparison. *J Am Coll Cardiol.* 1995;25(1):113-121.
24. Langer F, Schafers HJ. RING plus STRING: papillary muscle repositioning as an adjunctive repair technique for ischemic mitral regurgitation. *J Thorac Cardiovasc Surg.* 2007;133(1):247-249.
25. Hvass U, Tapia M, Baron F, Pouzet B, Shafy A. Papillary muscle sling: a new functional approach to mitral repair in patients with ischemic left ventricular dysfunction and functional mitral regurgitation. *Ann Thorac Surg.* 2003;75(3):809-811.

26. Rama A, Praschker L, Barreda E, Gandjbakhch I. Papillary muscle approximation for functional ischemic mitral regurgitation. *Ann Thorac Surg.* 2007;84(6):2130-2131.
27. Kron IL, Green GR, Cope JT. Surgical relocation of the posterior papillary muscle in chronic ischemic mitral regurgitation. *Ann Thorac Surg.* 2002;74(2):600-601.
28. Streeter DD, Jr., Spotnitz HM, Patel DP, Ross J, Jr., Sonnenblick EH. Fiber orientation in the canine left ventricle during diastole and systole. *Circ Res.* 1969;24(3):339-347.
29. Greenbaum RA, Ho SY, Gibson DG, Becker AE, Anderson RH. Left ventricular fibre architecture in man. *Br Heart J.* 1981;45(3):248-263.
30. Holmes JW, Takayama Y, LeGrice I, Covell JW. Depressed regional deformation near anterior papillary muscle. *Am J Physiol.* 1995;269(1 Pt 2):H262-270.
31. Armour JA, Randall WC. Structural basis for cardiac function. *Am J Physiol.* 1970;218(6):1517-1523.
32. Rayhill SC, Daughters GT, Castro LJ, Niczyporuk MA, Moon MR, Ingels NB, Jr., Stadius ML, Derby GC, Bolger AF, Miller DC. Dynamics of normal and ischemic canine papillary muscles. *Circ Res.* 1994;74(6):1179-1187.
33. Cheng A, Langer F, Rodriguez F, Criscione JC, Daughters GT, Miller DC, Ingels NB, Jr. Transmural sheet strains in the lateral wall of the ovine left ventricle. *Am J Physiol Heart Circ Physiol.* 2005;289(3):H1234-1241.
34. Cheng A, Langer F, Rodriguez F, Criscione JC, Daughters GT, Miller DC, Ingels NB, Jr. Transmural cardiac strains in the lateral wall of the ovine left ventricle. *Am J Physiol Heart Circ Physiol.* 2005;288(4):H1546-1556.
35. Kindberg K, Carlhall C, Karlsson M, Nguyen TC, Cheng A, Langer F, Rodriguez F, Daughters GT, Miller DC, Ingels NB, Jr. Transmural strains in the ovine left ventricular lateral wall during diastolic filling. *J Biomech Eng.* 2009;131(6):061004.
36. Waldman LK, Nosan D, Villarreal F, Covell JW. Relation between transmural deformation and local myofiber direction in canine left ventricle. *Circ Res.* 1988;63(3):550-562.
37. Niczyporuk MA, Miller DC. Automatic tracking and digitization of multiple radiopaque myocardial markers. *Comput Biomed Res.* 1991;24(2):129-142.
38. Daughters GT, Sanders WJ, Miller DC, Schwarzkopf A, Mead CW, Ingels NB, Jr. A comparison of two analytical systems for 3-D reconstruction from biplane videoradiograms. *IEEE Comput Cardiol.* 1989;15:79-82.
39. Harrington KB, Rodriguez F, Cheng A, Langer F, Ashikaga H, Daughters GT, Criscione JC, Ingels NB, Miller DC. Direct measurement of transmural laminar architecture in the anterolateral wall of the ovine left ventricle: new implications for wall thickening mechanics. *Am J Physiol Heart Circ Physiol.* 2005;288(3):H1324-1330.

40. Kindberg K, Karlsson M, Ingels NB, Jr., Criscione JC. Nonhomogeneous strain from sparse marker arrays for analysis of transmural myocardial mechanics. *J Biomech Eng.* 2007;129(4):603-610.
41. Miyoshi H, Takayama Y, Tamura T, Kitashiro S, Izuoka T, Saito D, Imuro Y, Iwasaka T. Regional myocardial function at the papillary muscle insertion site. *Jpn J Physiol.* 2001;51(1):109-114.
42. Cheng A, Nguyen TC, Malinowski M, Daughters GT, Miller DC, Ingels NB, Jr. Heterogeneity of left ventricular wall thickening mechanisms. *Circulation.* 2008;118(7):713-721.
43. Cheng A, Nguyen TC, Malinowski M, Liang D, Daughters GT, Ingels NB, Jr., Miller DC. Undersized mitral annuloplasty inhibits left ventricular basal wall thickening but does not affect equatorial wall cardiac strains. *J Heart Valve Dis.* 2007;16(4):349-358.
44. Bogaert J, Rademakers FE. Regional nonuniformity of normal adult human left ventricle. *Am J Physiol Heart Circ Physiol.* 2001;280(2):H610-620.
45. Costa KD, Takayama Y, McCulloch AD, Covell JW. Laminar fiber architecture and three-dimensional systolic mechanics in canine ventricular myocardium. *Am J Physiol.* 1999;276(2 Pt 2):H595-607.
46. Villarreal FJ, Lew WY. Finite strains in anterior and posterior wall of canine left ventricle. *Am J Physiol.* 1990;259(5 Pt 2):H1409-1418.
47. Gascho JA, Copenhaver GL, Heitjan DF. Systolic thickening increases from subepicardium to subendocardium. *Cardiovasc Res.* 1990;24(10):777-780.
48. Bolli R, Patel BS, Hartley CJ, Thornby JI, Jeroudi MO, Roberts R. Nonuniform transmural recovery of contractile function in stunned myocardium. *Am J Physiol.* 1989;257(2 Pt 2):H375-385.
49. Gallagher KP, Osakada G, Matsuzaki M, Miller M, Kemper WS, Ross J, Jr. Nonuniformity of inner and outer systolic wall thickening in conscious dogs. *Am J Physiol.* 1985;249(2 Pt 2):H241-248.
50. LeGrice IJ, Takayama Y, Holmes JW, Covell JW. Impaired subendocardial function in tachycardia-induced cardiac failure. *Am J Physiol.* 1995;268(5 Pt 2):H1788-1794.
51. Myers JH, Stirling MC, Choy M, Buda AJ, Gallagher KP. Direct measurement of inner and outer wall thickening dynamics with epicardial echocardiography. *Circulation.* 1986;74(1):164-172.
52. McCulloch AD, Omens JH. Non-homogeneous analysis of three-dimensional transmural finite deformation in canine ventricular myocardium. *J Biomech.* 1991;24(7):539-548.
53. Rademakers FE, Rogers WJ, Guier WH, Hutchins GM, Siu CO, Weisfeldt ML, Weiss JL, Shapiro EP. Relation of regional cross-fiber shortening to wall thickening in the intact

- heart. Three-dimensional strain analysis by NMR tagging. *Circulation*. 1994;89(3):1174-1182.
54. Weis SM, Emery JL, Becker KD, McBride DJ, Jr., Omens JH, McCulloch AD. Myocardial mechanics and collagen structure in the osteogenesis imperfecta murine (oim). *Circ Res*. 2000;87(8):663-669.
 55. Takayama Y, Costa KD, Covell JW. Contribution of laminar myofiber architecture to load-dependent changes in mechanics of LV myocardium. *Am J Physiol Heart Circ Physiol*. 2002;282(4):H1510-1520.
 56. Knisley SB, Baynham TC. Line stimulation parallel to myofibers enhances regional uniformity of transmembrane voltage changes in rabbit hearts. *Circ Res*. 1997;81(2):229-241.
 57. Buchalter MB, Rademakers FE, Weiss JL, Rogers WJ, Weisfeldt ML, Shapiro EP. Rotational deformation of the canine left ventricle measured by magnetic resonance tagging: effects of catecholamines, ischaemia, and pacing. *Cardiovasc Res*. 1994;28(5):629-635.
 58. Ingels NB, Jr. Myocardial fiber architecture and left ventricular function. *Technol Health Care*. 1997;5(1-2):45-52.
 59. Ingels NB, Jr., Daughters GT, 2nd, Stinson EB, Alderman EL. Measurement of midwall myocardial dynamics in intact man by radiography of surgically implanted markers. *Circulation*. 1975;52(5):859-867.
 60. Arts T, Reneman RS, Veenstra PC. A model of the mechanics of the left ventricle. *Ann Biomed Eng*. 1979;7(3-4):299-318.
 61. Arts T, Veenstra PC, Reneman RS. Epicardial deformation and left ventricular wall mechanisms during ejection in the dog. *Am J Physiol*. 1982;243(3):H379-390.
 62. Rijcken J, Bovendeerd PH, Schoofs AJ, van Campen DH, Arts T. Optimization of cardiac fiber orientation for homogeneous fiber strain during ejection. *Ann Biomed Eng*. 1999;27(3):289-297.
 63. Rijcken J, Arts T, Bovendeerd P, Schoofs B, van Campen D. Optimization of left ventricular fibre orientation of the normal heart for homogeneous sarcomere length during ejection. *Eur J Morphol*. 1996;34(1):39-46.
 64. Bovendeerd PH, Arts T, Huyghe JM, van Campen DH, Reneman RS. Dependence of local left ventricular wall mechanics on myocardial fiber orientation: a model study. *J Biomech*. 1992;25(10):1129-1140.
 65. Ashikaga H, Criscione JC, Omens JH, Covell JW, Ingels NB, Jr. Transmural left ventricular mechanics underlying torsional recoil during relaxation. *Am J Physiol Heart Circ Physiol*. 2004;286(2):H640-647.
 66. MacGowan GA, Shapiro EP, Azhari H, Siu CO, Hees PS, Hutchins GM, Weiss JL, Rademakers FE. Noninvasive measurement of shortening in the fiber and cross-fiber

directions in the normal human left ventricle and in idiopathic dilated cardiomyopathy. *Circulation*. 1997;96(2):535-541.

67. Komeda M, Glasson JR, Bolger AF, Daughters GT, 2nd, Ingels NB, Jr., Miller DC. Papillary muscle-left ventricular wall "complex". *J Thorac Cardiovasc Surg*. 1997;113(2):292-300; discussion 300-291.
68. Takayama Y, Holmes JW, LeGrice I, Covell JW. Enhanced regional deformation at the anterior papillary muscle insertion site after chordal transection. *Circulation*. 1996;93(3):585-593.
69. Fomovsky GM, Thomopoulos S, Holmes JW. Contribution of extracellular matrix to the mechanical properties of the heart. *J Mol Cell Cardiol*. 2009.
70. Weber KT. Cardiac interstitium in health and disease: the fibrillar collagen network. *J Am Coll Cardiol*. 1989;13(7):1637-1652.
71. Weber KT, Pick R, Janicki JS, Gadodia G, Lakier JB. Inadequate collagen tethers in dilated cardiopathy. *Am Heart J*. 1988;116(6 Pt 1):1641-1646.
72. Marijianowski MM, Teeling P, Mann J, Becker AE. Dilated cardiomyopathy is associated with an increase in the type I/type III collagen ratio: a quantitative assessment. *J Am Coll Cardiol*. 1995;25(6):1263-1272.
73. Villari B, Campbell SE, Hess OM, Mall G, Vassalli G, Weber KT, Krayenbuehl HP. Influence of collagen network on left ventricular systolic and diastolic function in aortic valve disease. *J Am Coll Cardiol*. 1993;22(5):1477-1484.
74. Covell JW. Tissue structure and ventricular wall mechanics. *Circulation*. 2008;118(7):699-701.
75. Anderson RH, Sanchez-Quintana D, Niederer P, Lunkenheimer PP. Structural-functional correlates of the 3-dimensional arrangement of the myocytes making up the ventricular walls. *J Thorac Cardiovasc Surg*. 2008;136(1):10-18.

Chapter 26: Temporal and Regional Heterogeneity in Left Ventricular Deformation: Implications for Myofiber Coupling

This chapter is the second in a series of two chapters (Chapters 25 and 26) that investigate left ventricular myocardial mechanics using transmural beadsets. While these chapters provide important insight into cardiac mechanics and left ventricular heterogeneity in transmural strains in particular, these studies do not directly relate to the overarching goals of this thesis. Therefore, these studies have been included in the Appendix. In this second study, analysis of transmural strains at different left ventricular sites throughout the cardiac cycle demonstrates significant temporal and regional heterogeneity in left ventricular strain development.

ABSTRACT

Background: Given the constant volume constraint of the isovolumic contraction (IVC) portion of the cardiac cycle, it was commonly believed that little myocardial strain or shear developed during this time period. However, a recent study demonstrated significant myocardial deformation during IVC. In light of known regional heterogeneity in transmural LV myocardial strain at end-systole, we investigated regional heterogeneity in transmural strains in different anterolateral equatorial LV locations (anterior (ANT), myocardium overlying the anterolateral papillary muscle (PAP), and lateral (LAT)) throughout the cardiac cycle, with particular attention paid to IVC and early ejection.

Methods: Transmural radiopaque beadsets were placed into ten sheep in three locations (ANT, LAT, and PAP) along the equatorial LV wall. Biplane videofluoroscopy was performed allowing the *in vivo* measurement of radial, circumferential, and longitudinal strains at each of three LV wall depths (subepicardial, midwall, and subendocardial) in the three locations for each heart beat. Myofiber angle measurements at each depth in each location from histological sections post-mortem allowed transformation of these strains into fiber and cross-fiber strains.

Results: While transmural thickening clearly dominated the radial strain curve throughout the cardiac cycle, initially transmural thinning was noted that was greater in LAT compared to the other regions. The longitudinal strain profile of LAT throughout the cardiac cycle was also substantially different than the other regions, with LAT lengthening during early ejection while the other regions contracted. During IVC circumferential lengthening was noted, particularly in ANT and PAP. Fiber strains during throughout the cardiac cycle were equivalent across regions, despite substantial regional differences in transmural strain development.

Conclusions: Therefore, the three principal findings of this study were: 1) regional heterogeneity in transmural strains throughout the cardiac cycle, 2) relative regional differences varied within the cardiac cycle, and 3) regional differences occurred despite similarities in myofibers, which not only suggests underlying static regional differences in myofiber coupling, but a temporal component to this coupling. These findings have

implications for the mechanism of pressure development in the LV, as well as myofiber coupling and related myocardial and myofiber clinical interventions.

The work contained in this chapter is under preparation for submission to *American Journal of Physiology-Heart and Circulatory Physiology*.

INTRODUCTION

During isovolumic contraction (IVC) the left ventricular (LV) volume remains constant; therefore it was commonly believed that during IVC the LV myocardium developed little strain or shear, but rather underwent isometric contraction in preparation for the rapid, complex LV deformation that occurs during ejection. However, a recent study by Ashikaga et al.¹ demonstrated that the canine anterior LV myocardium undergoes significant transmural deformations during IVC. Considering known regional^{2, 3} variability in myocardial strains, the aim of this study was to investigate regional heterogeneity in transmural strains and shears in different anterolateral equatorial LV locations throughout the cardiac cycle, with particular attention paid to IVC and early ejection. To accomplish this aim, transmural beadsets were inserted without cardiopulmonary bypass into normal ovine hearts in three sites across the anterolateral LV at the same transverse equatorial plane, allowing analysis of transmural strains developed simultaneously throughout the cardiac cycle in the same heart during the same heartbeats.

METHODS

The methods for surgical transmural beadset placement, data acquisition, analysis of fiber angles, and quantification of strains have been described in Chapter 25 of this thesis.

Analysis of Strain Development Throughout the Cardiac Cycle

For assessment of regional and transmural differences during IVC and early ejection, comparisons between strains in each region and transmural depth were made for the time points of mid-IVC (33.3 msec), end-IVC (66.7 msec), and early ejection (100 msec). Analysis was also performed on the magnitude of strain peaks (maximum or minimum), irrespective of when it occurred within the cardiac cycle, as the timing of that peak relative to end diastole.

Statistical Analysis

Data are reported as mean \pm SEM. Comparisons between groups (LV location: ANT, LAT, PAP; transmural depth: subepicardium, midwall, subendocardium) were performed using 2 way repeated measures (RM) ANOVA with a Bonferroni correction using SigmaStat (version 3.5, SPSS, Inc. Chicago, IL). Significance level was set at $p=0.017$ for analysis of strains at mid-IVC, end-IVC, and early ejection time points (since 3 time points were analyzed) and $p=0.05$ for analysis of strain peaks throughout the cardiac cycle.

RESULTS

Transmural Thickening (Radial Normal Strain)

Maximum transmural thickening (E_{RR}) for all regions occurred substantially after end systole (Fig. 26-2). The magnitude of the maximum E_{RR} peak was greatest for ANT,

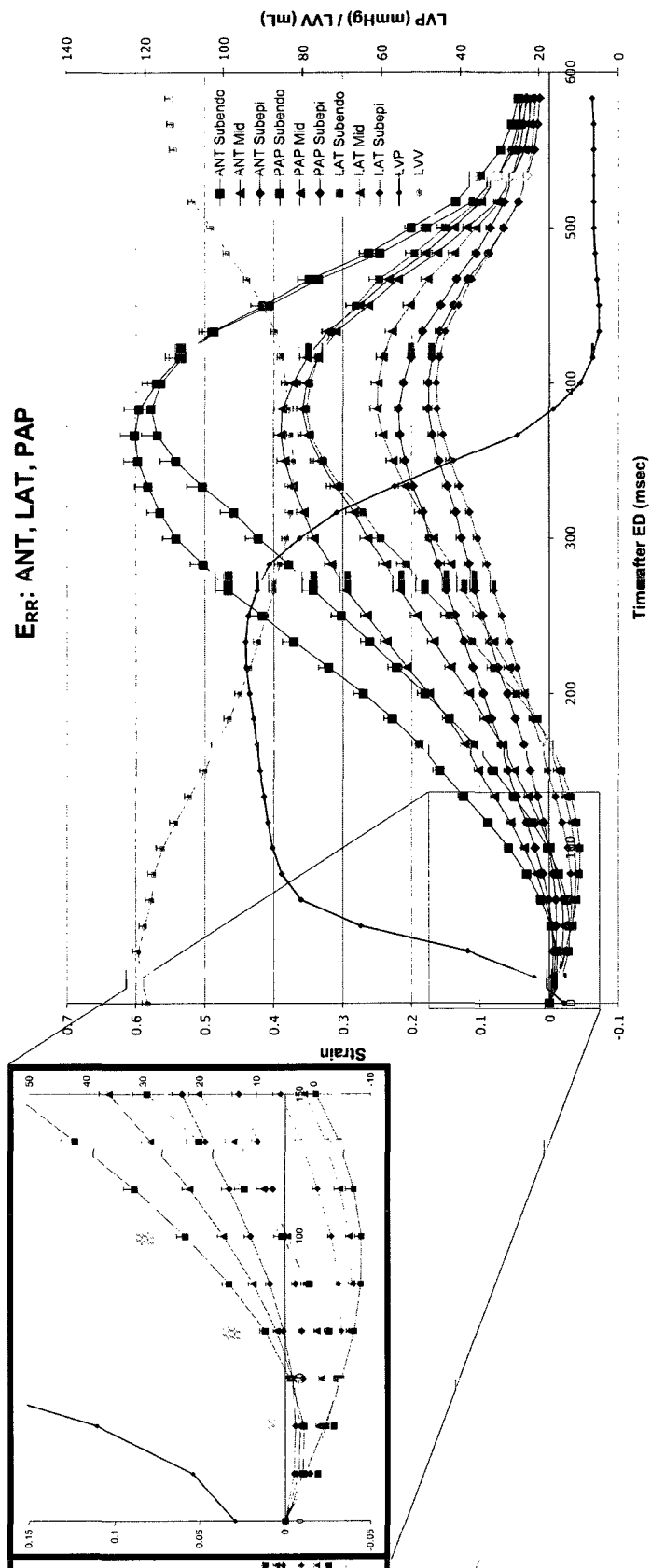


Fig 26-1: E_{RR} in ANT, PAP, and LAT regions plotted throughout the cardiac cycle. Inset illustrates the same data on magnified scales during IVC and early ejection. $*p < 0.05$ ANT vs. LAT, # $p < 0.05$ all significantly different, by 2-way RM ANOVA with Bonferroni all pairwise multiple comparison.

followed by PAP, and then LAT ($p < 0.001$). A transmural gradient in the magnitude of this maximum peak was also evident with subendo>midwall>subepi ($p < 0.001$).

While clearly transmural wall thickening dominated E_{RR} throughout the cardiac cycle, transmural thinning was evident during IVC. Overall during IVC there appeared to be an anterolateral gradient in this transmural thinning, with LAT thinning the most and the peak of this thinning occurring the latest. Specifically, at mid-IVC LAT E_{RR} was significantly less than ANT ($p = 0.007$), and ANT was significantly different from LAT and PAP at end-IVC and early ejection (each $p < 0.01$). A partial transmural gradient (subendo>subepi) in E_{RR} was evident in ANT at the early ejection time point ($p < 0.001$), and ANT and LAT were significantly different within the subepicardium at this time point ($p = 0.002$), while ANT was significantly different from LAT and PAP in the midwall and subendocardium (each $p \leq 0.016$). Analysis of the magnitude and timing of the minimum peak of this transmural thinning revealed that the transmural thinning peak of LAT was greater than and occurred later than that of ANT and PAP (each $p < 0.001$), and the magnitude of thinning peak of the subendocardium was greater than midwall and subepicardium ($p < 0.001$).

Longitudinal Normal Strains

The overall shape of the transmural longitudinal normal strain (E_{LL}) throughout the cardiac cycle was substantially different in LAT compared to ANT and PAP (Fig. 26-2). During the first portion of systole LAT E_{LL} was straining, while ANT and PAP E_{LL} were contracting. Analysis of the magnitude and timing of the E_{LL} minimum peak

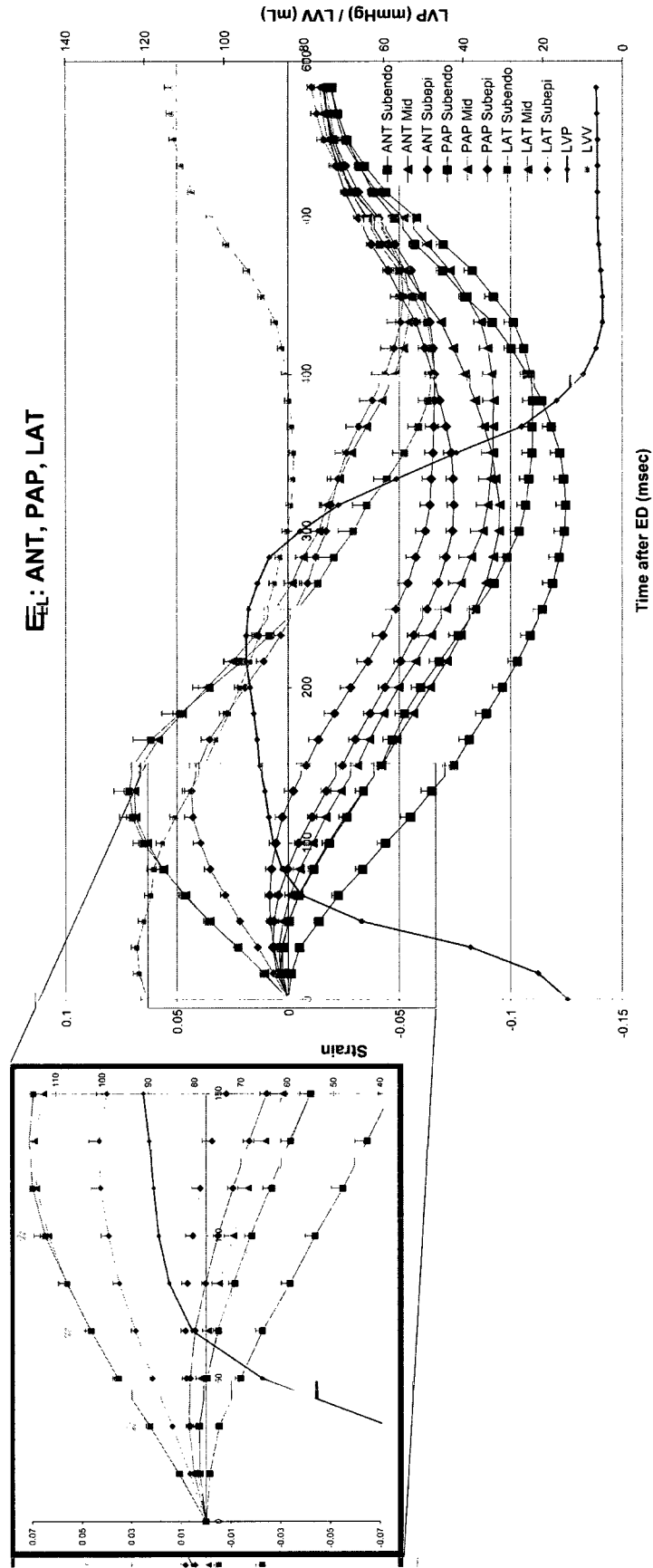


Fig. 26-2: E_{LL} in ANT, PAP, and LAT regions plotted throughout the cardiac cycle. Inset illustrates the same data on magnified scales during IVC and early ejection. $\hat{p} < 0.05$ PAP and ANT vs. LAT, by 2-way RM ANOVA with Bonferroni all pairwise multiple comparison.

revealed regional differences in magnitude with LAT less than ANT and PAP ($p=0.047$), and that the minimum peak of subendo>midwall>subepi ($p<0.001$). This minimum peak in LAT midwall and subepicardial layers also occurred significantly later than the same layers in ANT (each ~ 100 msec later, each $p\leq 0.07$).

The curves of E_{LL} during IVC and early ejection for each region also showed significantly different strain patterns in LAT compared to ANT and PAP; while ANT and PAP E_{LL} began to contract during this period, LAT E_{LL} lengthened. Indeed statistical analysis revealed that LAT E_{LL} was significantly greater than ANT and PAP at mid-IVC, end-IVC, and the early ejection time points (each $p<0.001$ for each time point). Transmural gradients were also evident in LAT and ANT including LAT subepicardium E_{LL} significantly different from the other LAT layers at end-IVC (each $p\leq 0.014$). Transmural gradients in ANT E_{LL} included subendocardium less than subepicardium at mid-IVC ($p=0.003$), subendocardium less than midwall and subepicardium at end-IVC (each $p\leq 0.013$), and subendocardium less than subepicardium ($p<0.001$) at early ejection. In terms of regional differences within individual layers, LAT was significantly greater than ANT and PAP in the subendocardium and midwall at mid-IVC, end-IVC, and early ejection (each $p<0.001$ for each time point for each layer) and in the subepicardium LAT was greater than ANT ($p=0.010$) at end-IVC and LAT was greater than ANT ($p=0.002$) at early ejection.

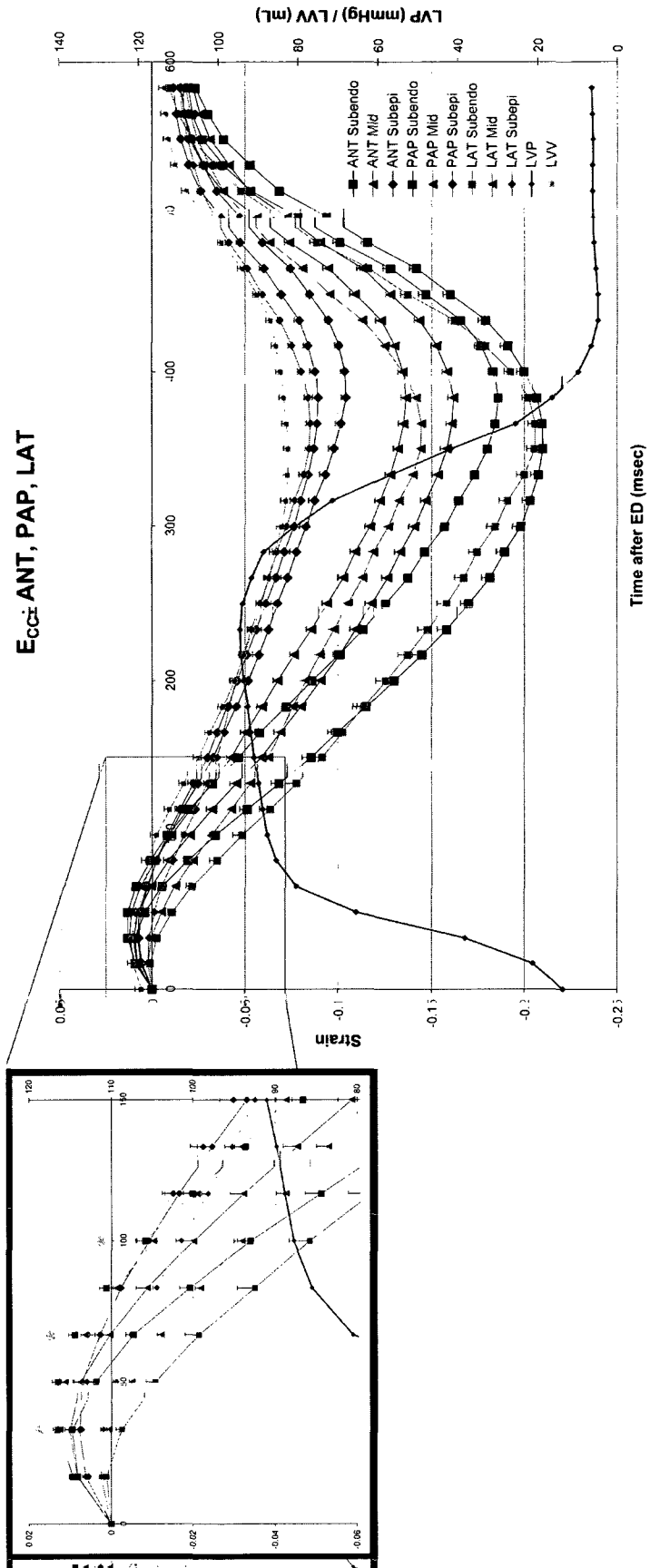


Fig. 26-3: E_{cc} in ANT, PAP, and LAT regions plotted throughout the cardiac cycle. Inset illustrates the same data on magnified scales during IVC and early ejection. * $p < 0.05$ PAP vs. LAT, $\wedge p < 0.05$ PAP and ANT vs. LAT, by 2-way RM ANOVA with Bonferroni all pairwise multiple comparison.

Circumferential Normal Strains

Circumferential normal strains became minimum (contraction) during isovolumic relaxation (Fig. 26-3). Only a slight trend in regional differences between the magnitudes of the circumferential strain peaks was evident ($p=0.076$). However, during IVC circumferential lengthening was evident, particularly in ANT and PAP. Also, significant regional differences were evident during IVC; these included LAT E_{CC} was significantly less than PAP at mid-IVC ($p=0.015$) and LAT E_{CC} was significantly less than PAP at end-IVC ($p=0.010$). No transmural differences were evident.

Myofiber Fiber and Cross-fiber Strains

Transmural fiber strains (E_f) of the different regions throughout the cardiac cycle appeared similar (Fig. 26-4A), each with a transmural gradient. While the magnitude of the minimum E_f peak of ANT and LAT were not different, that of PAP was less than LAT and ANT (each $p\leq 0.025$). A transmural gradient in the magnitude of the minimum E_f peak was also statistically significant, with subendo>midwall>subepi ($p<0.001$). The similarity in ANT and LAT E_f strains contrasted with substantial differences in transmural strain development during the same time periods (Fig. 26-4B). During IVC and early ejection E_f of the different regions displayed no significant differences at any of the time points analyzed. However, transmural differences were noted. During IVC

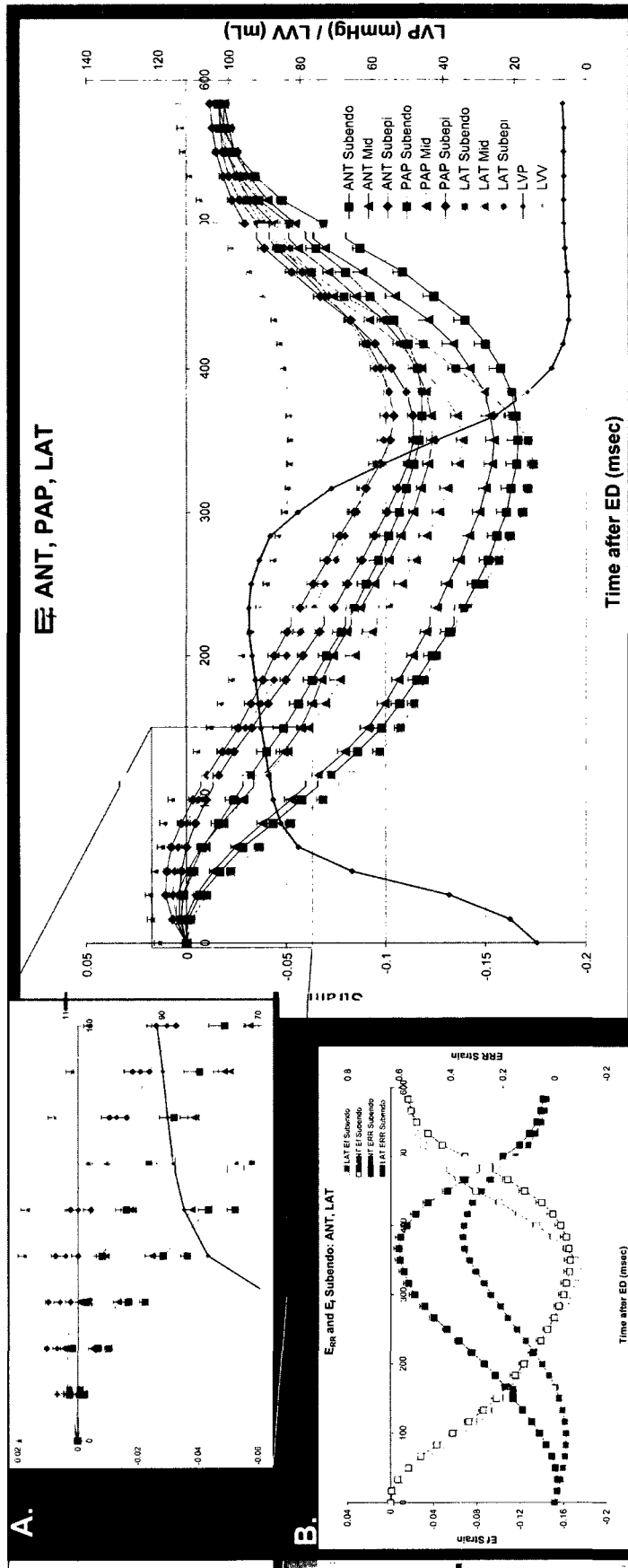


Fig. 26-4: A) E_f in ANT, PAP, and LAT regions plotted throughout the cardiac cycle. Inset illustrates the same data on magnified scales during IVC and early ejection. $p < 0.05$ subepi v subendo; $p < 0.05$ subepi different from mid and subendo, by 2-way RM ANOVA with Bonferroni all pairwise multiple comparison. B) Plot of E_f and E_{RR} in ANT and LAT subendocardium demonstrating similar strains in E_f , but dramatically different E_{RR} .

subepicardial myofibers of LAT and PAP in particular were stretching while subendocardial myofibers were simultaneously contracting. The subepicardial E_f for the different regions were significantly different from subendocardial E_f at end-IVC ($p=0.004$) and early ejection ($p=0.002$).

Transmural cross fiber strains (E_{cross}) throughout the cardiac cycle (Fig. 26-5) displayed significant regional and transmural differences. The magnitude of the E_{cross} minimum peak of LAT was significantly less than ANT and PAP (each $p\leq 0.025$) and an anterolateral gradient in the timing of E_{cross} minimum peak was evident ($p<0.001$), with the peak of ANT first, followed by PAP and then LAT. A transmural gradient in the magnitude of the E_{cross} minimum peak was also evident with subendo>midwall>subepi ($p<0.001$). Regional and transmural differences were also noted in E_{cross} during IVC and early ejection. While LAT E_{cross} stretched, E_{cross} in ANT and PAP contracted. Statistical analysis revealed that LAT E_{cross} was greater than ANT and PAP at mid-IVC (each $p\leq 0.002$), and LAT was different from ANT and PAP at end-IVC and early ejection (each $p\leq 0.001$ for each time point).

Of note was the difference in the interrelationship between E_{cross} and E_f in LAT compared to ANT and PAP (Fig. 26-6). While in both ANT and PAP (PAP not shown, but similar to ANT) E_{cross} and E_f strain curves were comparable in shape and magnitude, in LAT E_{cross} was significantly greater than E_f during IVC and early ejection. In all the regions E_{cross} generally mirrored E_{RR} throughout the cardiac cycle. Interestingly, LAT E_{cross} during IVC continued to mirror E_{RR} despite E_{RR} being negative during that time period (Fig. 26-7).

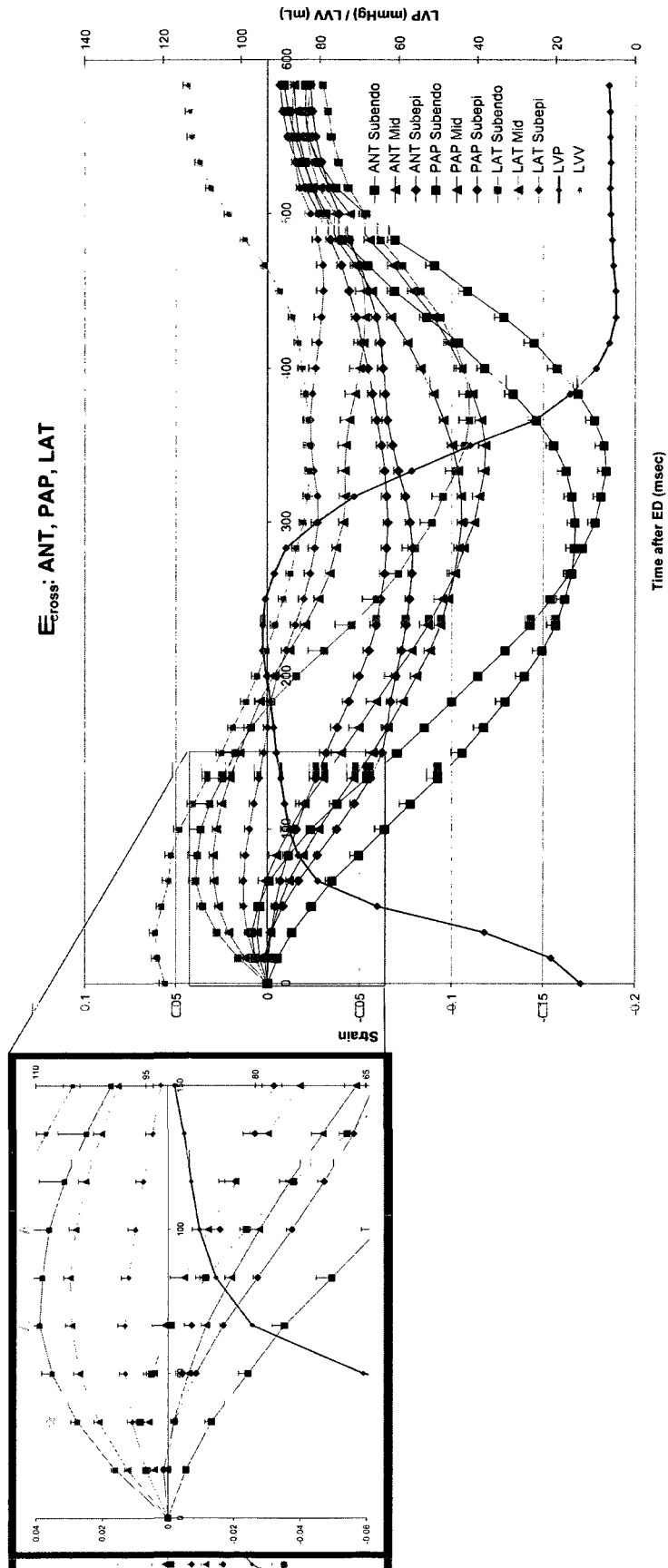


Fig. 26-5: E_{cross} in ANT, PAP, and LAT regions plotted throughout the cardiac cycle. Inset illustrates the same data on magnified scales during IVC and early ejection. * $p < 0.05$ PAP and ANT vs. LAT, $\wedge p < 0.05$ all three regions different, by 2-way RM ANOVA with Bonferroni all pairwise multiple comparison.

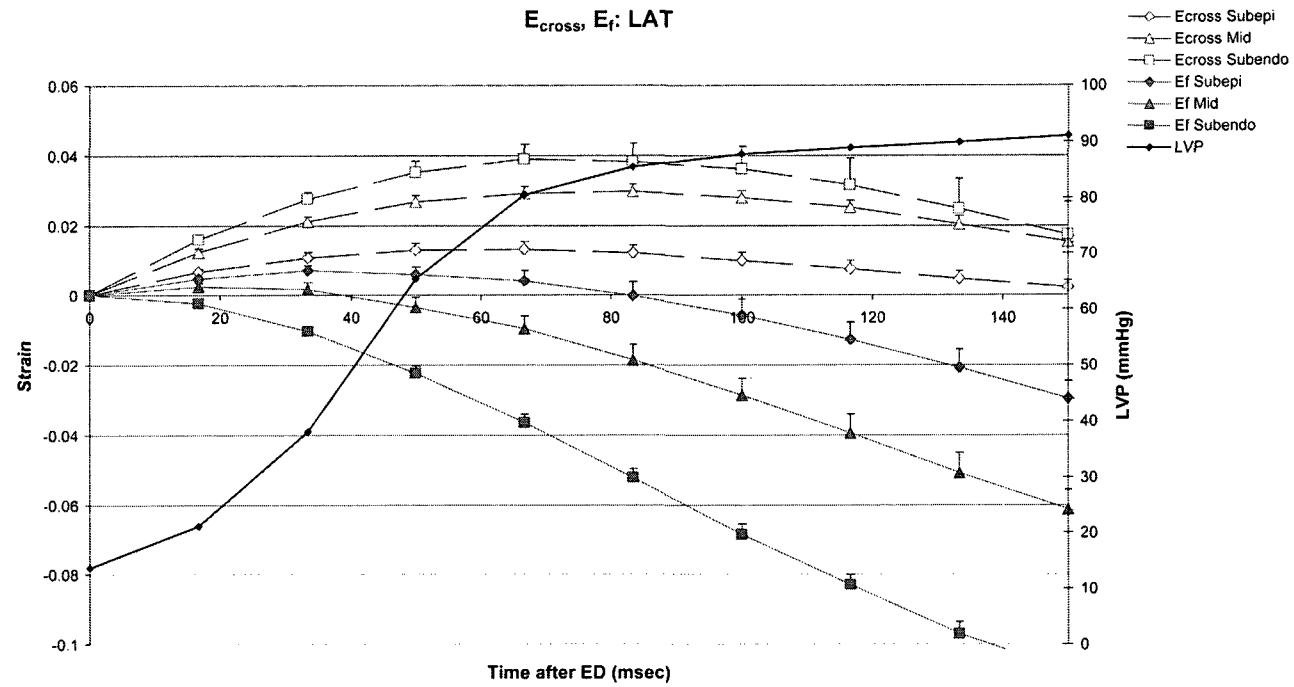


Fig. 26-6: E_{cross} and E_f during IVC and early ejection demonstrating significant differences between E_{cross} and E_f in LAT (left plot) that were not evident in ANT (right plot). * $p < 0.05$ E_f vs. E_{cross} , by 2-way RM ANOVA with Bonferroni all pairwise multiple comparison.

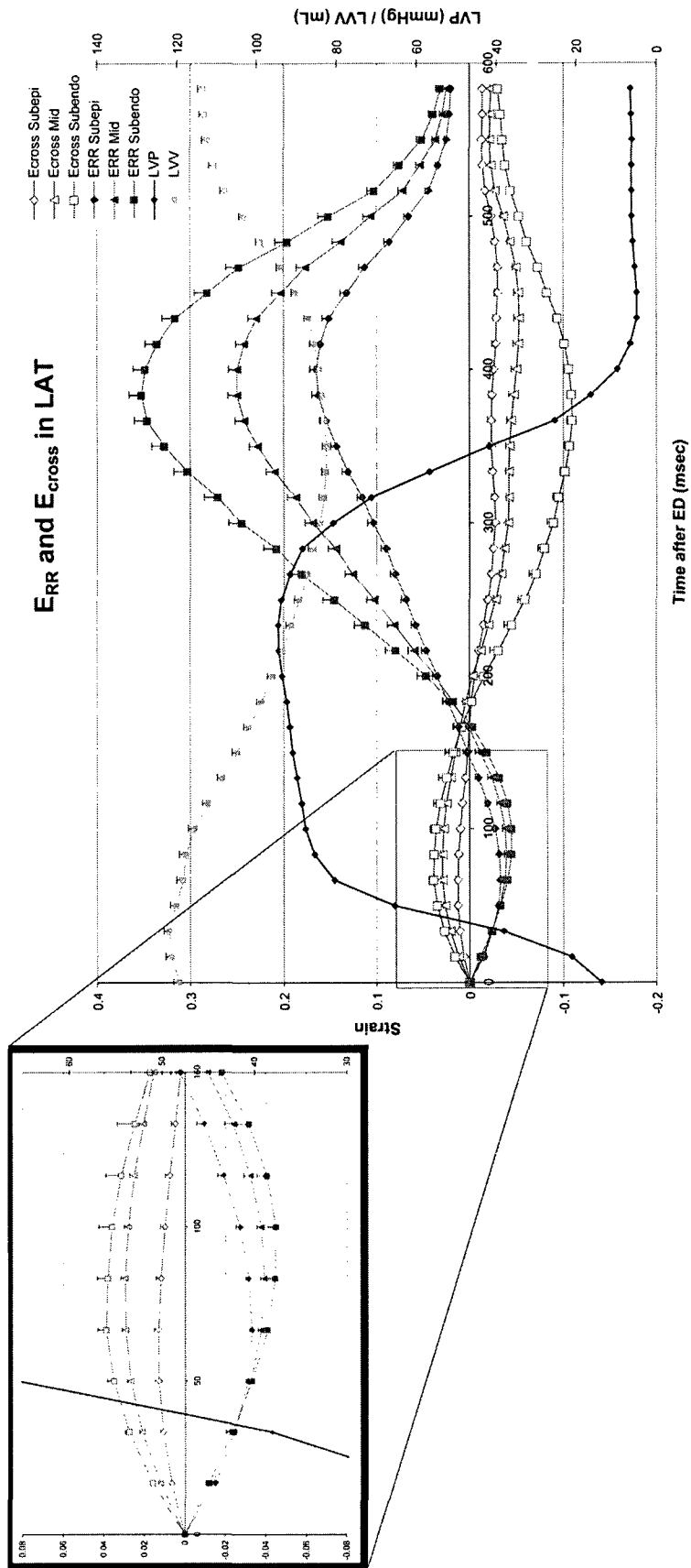


Fig. 26-7: E_{cross} and E_{RR} in LAT plotted throughout the cardiac cycle. Inset illustrates the same data on magnified scales during IVC and early ejection.

DISCUSSION

The three principal findings of this study were: 1) regional heterogeneity in transmural strains was evident throughout the cardiac cycle, 2) regional differences varied within the cardiac cycle, and 3) regional differences occurred despite similarities in myofibers, which not only suggests underlying static regional differences in myofiber coupling, but a temporal component to this coupling. When measured at the same equatorial transverse plane, in the same heart, during the same heart beats the anterior (ANT), lateral (LAT), and myocardium overlying the anterolateral papillary muscle (PAP), displayed transmural normal strains that varied substantially throughout the cardiac cycle and relative to one another. This regional and temporal heterogeneity in LV strain is of particular interest with respect to the mechanism of pressure development in the LV, as well as implications for myofiber coupling and related myocardial and myofiber clinical interventions.

Temporal and Regional Heterogeneity in Transmural Thickening

While transmural thickening clearly dominated the E_{RR} strain curve throughout the cardiac cycle, initially transmural thinning was noted. While this early transmural thinning has been visually apparent in curves of transmural thickening throughout the cardiac cycle included in other studies,^{1, 4} this finding has largely been overlooked. It is also interesting to note that the maximum transmural thickening occurs substantially after systole. This could be due to the decrease in the afterload that the fibers must contract against as the pressure drops.

Regional differences in transmural thickening were evident throughout the cardiac cycle, not just at end systole as previously reported (see Chapter 25). There was an anterolateral gradient in the magnitude of maximum transmural thickening (ANT>PAP>LAT), which occurred after end systole, but this gradient was not evident during IVC. Instead, during IVC LAT was significantly different from the other two regions, displaying the greater transmural thinning whose peak occurred later than the other two regions. Therefore, while regional differences were evident throughout various parts of the cardiac cycle, these differences varied, with LAT appearing part of an anterolateral gradient after systole, but appearing distinct from the other regions during IVC and systole.

Temporal and Regional Heterogeneity in Longitudinal Strain

Significant variability in longitudinal strain was noted throughout the cardiac cycle particularly in the LAT region, which lengthened during IVC and a large portion of systole, and then contracted during the remainder of the cardiac cycle. Substantial regional heterogeneity was apparent, including lengthening in LAT which was not evident in the other regions, as well as differences in the magnitude and timing of the longitudinal contraction peak (the LAT peak had a lower magnitude and occurred later than ANT and PAP). However, this regional heterogeneity also varied within the cardiac cycle; while the longitudinal transmural strain curves of LAT were drastically different from that of ANT and PAP during the early part of the cardiac cycle, late in the cardiac cycle LAT longitudinal transmural strain curves appeared quite similar to those of ANT and PAP.

Temporal and Regional Heterogeneity in Circumferential Strain

As was found for the transmural thickening peak, the peak of circumferential contraction occurred after end systole. This again could be because the fibers, that are already contracting and are largely oriented circumferentially, experience a decrease in afterload as the pressure drops. In fact the E_f strain curves display a similar peak after end systole. In terms of regional heterogeneity, unlike the other normal strains circumferential strains did not display significant regional differences in their strain peaks. However, during IVC regional differences were noted including a significant lengthening in ANT and PAP that was not evident in LAT. As noted by Ashikaga et al.,¹ the ANT subepicardium at end-IVC was straining while the subendocardium was contracting. The data from our curves suggest that this is a brief phenomenon related to timing as the subepicardial layer took longer to move from initial lengthening to contracting compared to the subendocardium. As in the other normal strains, a temporal component to regional heterogeneity was evident in circumferential strain, with the circumferential strains in LAT significantly different from the other regions during IVC, but similar to the other regions during the remainder of the cardiac cycle.

Temporal and Regional Strain Heterogeneity Despite Similarities in Myofibers

While regional differences were noted in all the normal strains curves, and these relative regional differences even varied within the cardiac cycle, the myofibers of the different regions (ANT and LAT in particular) remained remarkably similar throughout the cardiac cycle. The myofiber angles of ANT and LAT were not significantly different

at any transmural depth, nor were there any differences between ANT and LAT in terms of E_f strains during IVC and early ejection, or in the magnitude of the E_f peak throughout the cardiac cycle. Subtle differences in PAP E_f from that of ANT and LAT likely reflect differences in myofiber angle as the papillary muscle fibers connect to the myocardium in that region, as discussed previously (see Chapter 25). All regions during IVC displayed subepicardial fibers stretching and subendocardial fibers contracting, which Ashikaga noted in ANT and attributed to IVC “untwisting.”¹

Yet despite the myofibers of ANT and LAT behaving the same, the strains generated in each region were substantially different, and these relative differences varied throughout the cardiac cycle. For instance, late in the cardiac cycle after systole LAT E_{LL} appeared to have the same, albeit lower magnitude, transmural strain profile as ANT E_{LL} , whereas early in systole ANT and LAT E_{LL} demonstrated completely opposite strain behavior: ANT was contracting while LAT was lengthening. Meanwhile, E_f of both regions were contracting to the same degree. These results suggest that the observed regional heterogeneity is not due to inherent regional differences in myofiber contraction, but regional differences in how the myofibers are coupled. The hypothesis that regional differences in coupling of myofibers account for regional differences in normal strains is also supported by the observed regional differences in E_{cross} .

Furthermore, the observed temporal variation to this regional heterogeneity suggests that there is some temporal component to myofiber coupling. This idea of temporal myofiber coupling is further supported by the dramatic differences in strain behavior in a given region despite relatively uniform fiber contraction. As discussed

above, LAT longitudinal strain changes dramatically during late systole, from lengthening to contraction, while the fibers continue to contract.

Additionally it is interesting to note that while E_f and E_{cross} demonstrate similar strain profiles throughout the cardiac cycle in ANT, E_f and E_{cross} strain profiles are distinct in LAT. This difference between ANT and LAT could reflect differences in coupling between E_f and E_{cross} in ANT and LAT and/or differences in transmural coupling.

Components Contributing to Early Rise in LV Pressure

While the various regions and strains displayed different behavior throughout the cardiac cycle, only some of those regions and normal strains appeared to be contributing significantly to the functionally important steep rise in LV pressure during IVC. Examining which regions and strains were contributing to the development of LV pressure in the normal heart also has important implications for disease. Transmural thickening (or radial normal strain) did not appear to be contributing significantly, but rather all regions displayed transmural thinning during IVC and only ANT E_{RR} was even positive by end-IVC. The subendocardial layer of ANT was contracting in the longitudinal direction during IVC, and therefore could have been contributing to LV pressure development during that time period. The PAP subendocardial layer may have been contributing somewhat at end-IVC, but the remaining layers and all the layers of LAT were lengthening and therefore were not contributing to pressure development. Circumferential strain in all the layers of LAT (but most particularly the subendocardial layer), as well as the subendocardial layer of ANT did appear to be contracting

significantly during IVC, and therefore could have been contributing to the pressure rise; but the remaining layers were lengthening. Meanwhile, the subendocardial and midwall fibers were contracting during IVC. These results are consistent with those of Bogaert et al.⁵ using MRI tagging who found that circumferential shortening, as opposed to wall thickening or longitudinal shortening, correlated well with different regions' contribution to the ejection fraction. It is particularly interesting that transmural thickening does not appear to be a major factor in early pressure development, as LV wall thickening is a commonly utilized metric for LV function and when the entire cardiac cycle is considered E_{RR} dominates the other normal strains in terms of magnitude. It also should be noted that some of this pressure rise may be the result of the contraction of the apical LV which occurs before these equatorial regions, or the posterior wall that was not assessed in this study. Nonetheless, these results suggest that certain regions and layers may be functionally important to the development of LV pressure, which may have clinical relevance.

Relationship of Results to Previous Studies of End Systole LV Transmural Strain Heterogeneity

We previously reported regional heterogeneity based on the strains calculated at end systole relative to the undeformed state of end diastole (see Chapter 25). One of the findings of that study was that LAT displayed depressed E_{LL} deformation relative to the other regions. However, in examining LAT E_{LL} throughout the cardiac cycle, we see that in only analyzing the strain at end systole some of the LAT E_{LL} contraction was not accounted for because it occurs after end systole. LAT E_{LL} contraction also was delayed

relative to the other regions, therefore analysis of E_{LL} strain of the various regions at end systole made that of LAT appear less than the other regions. Nevertheless, when analysis was performed on the minimum E_{LL} peak throughout the cardiac cycle, as done in the present study, LAT E_{LL} strain was still less than the other regions. The other normal strains, E_{RR} and E_{CC} , peak after end systole, therefore in studies in which analysis is performed of the strain at end systole relative to end diastole, some of this strain is missed.

Implications

The findings of this study suggesting that myofiber coupling underlies regional and temporal transmural strain heterogeneity raise important implications. Given increasing interest in the use of stem cells and other myocyte progenitors to aid cardiac function, the importance of the scaffolding and the manner by which myofibers are coupled to properly develop cardiac strain should be taken into account. The obvious heterogeneity in the LV should also be considered in the design of myocardial patches. This evidence supporting the importance of myofiber coupling also draws attention to the importance of the extracellular matrix to proper myocardial function, and conversely extracellular matrix dysfunction as potentially contributing to various cardiomyopathies. In cardiomyopathies in which study of the affected myocytes have not revealed myocyte abnormalities, future research may reveal that the extracellular matrix coupling these myocytes actually causes the myocardial dysfunction.

Furthermore, the finding that equatorial transmural wall thickening does not appear to be a key contributor to the rapid LV pressure rise during IVC has important

clinical implications. While transmural wall thickening is a commonly utilized, easy to measure parameter to clinically assess LV function and identify pathology, the results of this study suggest that circumferential shortening may be more important to the ability of the LV to develop pressure during early ejection. As imaging modalities in use clinically continue to be refined, measures of circumferential shortening may become more useful in assessing the functional impact of LV lesions.

Limitations

While the transmural beadset technique and accompanying analysis used in this study provides substantial insight into myocardial strains at different transmural depths in the beating heart, several limitations to this technique should be noted. First, while beadset implantation does not require cardiopulmonary bypass and the markers are relatively small, it is likely that the markers themselves and the process of implantation may subtly affect overall cardiac function as well as myofiber mechanics in the localized region of implantation. Second, this study was performed in anesthetized ovine, therefore some of the results may be altered by anesthesia and be species specific, although certainly some characteristics of myocardial architecture and mechanics (i.e., gradient of myofiber angle across the LV wall^{2, 6-8}) appear to be conserved across species. Third, there are inherent uncertainties in myofiber angle measurements, variability in final depth of bead placement, limitations in the number of beads that can be placed transmurally, uncertainty in computational fitting to bead data and the videographic imaging modality itself. However, these uncertainties are relatively small and would not account for the regional differences found in this study. While previous studies have

analyzed transmural strains in terms of laminar sheets utilizing β angles, considerable controversy remains about the usefulness of such measurements. These measurements are also technically difficult and subject to multiple errors. For instance, while the major β is used for calculations at a given depth, there are multiple β s evident at each depth, especially at the subendocardium, and it is not appropriate to average them.^{3, 9} Furthermore, β measurements are subject to artifacts in tissue preparation and assume tissue homogeneity, whereby measurements from very small areas are taken to be representative of much larger regions. Clearly, laminar sheets severely oversimplify the complexity of myocyte arrangement in the myocardium.¹⁰ Because of their limitations, laminar sheet analysis was not performed in this study.

CONCLUSIONS

In summary, in this study we have demonstrated regional variation in LV transmural strain profiles throughout the cardiac cycle. Furthermore, these differences in regional transmural strains changed relative to one another throughout the cardiac cycle while myofiber contraction in the different regions remained similar. These findings suggest regional differences in myofiber coupling, such that contractile units that function similarly can be interconnected in distinct manners resulting in regional differences in normal strains. Furthermore, these results suggest a temporal component to this coupling. These findings have potential implications for understanding myofiber coupling and its contribution to cardiac function, as well as clinical interventions involving implantation of myocytes with or without connecting scaffolds.

This chapter, which demonstrated substantial temporal and regional heterogeneity in transmural strain development in the left ventricle, is the second of two chapters (Chapters 25 and 26) addressing left ventricle myocardial mechanics. As stated in the preface of this chapter, these studies provide important insight into cardiac mechanics, but do not directly relate to the goals of this thesis and, therefore, have been included in the Appendix.

REFERENCES

1. Ashikaga H, van der Spoel TI, Coppola BA, Omens JH. Transmural myocardial mechanics during isovolumic contraction. *JACC Cardiovasc Imaging*. 2009;2(2):202-211.
2. Costa KD, Takayama Y, McCulloch AD, Covell JW. Laminar fiber architecture and three-dimensional systolic mechanics in canine ventricular myocardium. *Am J Physiol*. 1999;276(2 Pt 2):H595-607.
3. Cheng A, Nguyen TC, Malinowski M, Daughters GT, Miller DC, Ingels NB, Jr. Heterogeneity of left ventricular wall thickening mechanisms. *Circulation*. 2008;118(7):713-721.
4. Rodriguez F, Langer F, Harrington KB, Cheng A, Daughters GT, Criscione JC, Ingels NB, Miller DC. Alterations in transmural strains adjacent to ischemic myocardium during acute midcircumflex occlusion. *J Thorac Cardiovasc Surg*. 2005;129(4):791-803.
5. Bogaert J, Rademakers FE. Regional nonuniformity of normal adult human left ventricle. *Am J Physiol Heart Circ Physiol*. 2001;280(2):H610-620.
6. Weis SM, Emery JL, Becker KD, McBride DJ, Jr., Omens JH, McCulloch AD. Myocardial mechanics and collagen structure in the osteogenesis imperfecta murine (oim). *Circ Res*. 2000;87(8):663-669.
7. Takayama Y, Costa KD, Covell JW. Contribution of laminar myofiber architecture to load-dependent changes in mechanics of LV myocardium. *Am J Physiol Heart Circ Physiol*. 2002;282(4):H1510-1520.
8. Knisley SB, Baynham TC. Line stimulation parallel to myofibers enhances regional uniformity of transmembrane voltage changes in rabbit hearts. *Circ Res*. 1997;81(2):229-241.
9. Covell JW. Tissue structure and ventricular wall mechanics. *Circulation*. 2008;118(7):699-701.
10. Anderson RH, Sanchez-Quintana D, Niederer P, Lunkenheimer PP. Structural-functional correlates of the 3-dimensional arrangement of the myocytes making up the ventricular walls. *J Thorac Cardiovasc Surg*. 2008;136(1):10-18.